JOURNAL OF AGRICULTURAL SCIENCES

TARIM BİLİMLERİ DERGİSİ

ANKARA UNIVERSITY FACULTY OF AGRICULTURE

e-ISSN 2148-9297

JAS

Year 25

Volume 31

Issue 02

Ankara University
Faculty of Agriculture

JOURNAL OF AGRICULTURAL SCIENCES

TARIM BILIMLERI DERGISI

e-ISSN: 2148-9297

Ankara - TÜRKİYE

Year **2025** Volume **31** Issue **2**

JOURNAL OF AGRICULTURAL SCIENCES
TARIM BİLİMLERİ DERGİSİ
ANKARA UNIVERSITY FACULTY OF AGRICULTURE
e-ISSN 2148-9297

Product Information

Publisher	Ankara University, Faculty of Agriculture
Owner (On Behalf of Faculty)	Prof. Dr. Hasan Huseyin ATAR
Editor-in-Chief	Prof. Dr. Halit APAYDIN
Journal Administrator	Salih OZAYDIN
Library Coordinator	Dr. Can BESIMOGLU
IT Coordinator	Lecturer Murat KOSECAVUS
Graphic Design	Ismet KARAASLAN
Date of Online Publication	25.03.2025
Frequency	Published four times a year
Type of Publication	Double-blind peer-reviewed, widely distributed periodical
Aims and Scope	JAS publishes high quality original research articles that contain innovation or emerging technology in all fields of agricultural sciences for the development of agriculture.
Indexed and Abstracted in	Clarivate Science Citation Index Expanded (SCIE) Elsevier Scopus TUBITAK-ULAKBIM-TRDizin CAB International EBSCO FAO-AGRIS SOBIAD OpenAire BASE IFIS CNKI

Management Addres

Journal of Agricultural Sciences - Tarım Bilimleri Dergisi
Ankara University Faculty of Agriculture Publication Department 06110 Diskapi/Ankara-Türkiye
Telephone : +90 312 596 14 24 | Fax : +90 312 317 67 24
E-mail: tbdeditor@ankara.edu.tr | http://jas.ankara.edu.tr/

JOURNAL OF AGRICULTURAL SCIENCES
TARIM BİLİMLERİ DERGİSİ
ANKARA UNIVERSITY FACULTY OF AGRICULTURE
e-ISSN 2148-9297

JOURNAL OF AGRICULTURAL SCIENCES
TARIM BİLİMLERİ DERGİSİ
ANKARA UNIVERSITY FACULTY OF AGRICULTURE
e-ISSN 2148-9297

CONTENTS **2025, 31(2)**

Research articles:

Journal of Agricultural Sciences
(Tarim Bilimleri Dergisi)

J Agr Sci-Tarim Bili
e-ISSN: 2148-9297
jas.ankara.edu.tr

JAS

Studying the Genetic Gain of Traits Related to Remobilization and Photosynthesis in Bread Wheat Cultivars Released During Five Decades in Golestan Province of Iran

Hossein Avarsaji[a], Manoochehr Khodarahmi[b*], Marjan Diyanat[a], Islam Majidi Heravan[a], Habiballah Soughi[c]

[a]*Department of Horticultural Sciences and Agronomy, Science and Research Branch, Islamic Azad University, Tehran, IRAN*
[b]*Seed and Plant Improvement Institute, Agricultural Research, Education and Extension Organization (AREEO), Karaj, IRAN*
[c]*Horticulture Crops Research Department, Golestan Agricultural and Natural Resources Research and Education Center, AREEO, Gorgan, IRAN*

ARTICLE INFO
Research Article
Corresponding Author: Manoochehr Khodarahmi, E-mail: khodarahmi_m@yahoo.com
Received: 12 December 2023 / Revised: 30 August 2024 / Accepted: 09 October 2024 / Online: 25 March 2025

Cite this article
Avarsaji H, Khodarahmi M, Diyanat M, Heravan I M, Soughi H (2025). Studying the Genetic Gain of Traits Related to Remobilization and Photosynthesis in Bread Wheat Cultivars Released During Five Decades in Golestan Province of Iran. *Journal of Agricultural Sciences (Tarim Bilimleri Dergisi),* 30(2):252-279. DOI: 10.15832/ankutbd.1403339

ABSTRACT
In order to determine the trend of breeding progress and the genetic gain in the Iran's Golestan province, twenty registered spring wheat cultivars, which had been widely cultivated from 1968 to 2018, were investigated. A randomized complete block design with three replications was conducted to study these cultivars in the research stations of Gorgan and Gonbad during three consecutive years (2015-2018). Different morphological characteristics, grain yield and yield components, and some important traits related to remobilization and photosynthesis were measured. Morphological traits including plant height, peduncle length, and spike length did not show any significant trend during the 50-year of breeding improvement in these regions; whereas significant increases were observed for grain yield, biological yield, harvest index, thousand kernel weight, and grain filling rate in the both areas. During the period of breeding investigated, the total contribution of remobilization has decreased, in particular that from stem's, showed a significant decrease. In contrast, the amount, efficiency, and contribution of photosynthesis revealed to play a significant role in genetic improvement obtained for the cultivars' successful performances in the regions. Based on the results obtained from the study of different parts of the plants, in addition to being an important photosynthetic source for wheat, over the time, as compared to the other wheat organs, spike showed an increasing potential for the amount of remobilization. It is expected that genotypes selected for higher levels of remobilization abilities with increased photosynthesis, could result in breeding superior high-yielding cultivars in future of the national wheat programs.

Keywords: Genetic gain, Photosynthesis, Registered cultivars, Remobilization, Spring wheat

1. Introduction

Wheat (*Triticum aestivum* L.) with an annual production of more than 600 million tons across all the continents is the major crop cultivated worldwide (Goel et al. 2018). Wheat production has increased significantly from 222 million tons in 1961 until now (FAO 2021). However, there is still a long gap between the demand and the annual genetic gain of wheat. The average annual increase in wheat genetic gain has been reported to be 1%, while the demand for wheat has increased by 1.7% annually and will reach to one billion tons in 2050 (Tadesse et al. 2019).

The carbon required for grain filling in wheat comes from three sources: current assimilates, remobilization of assimilates stored in the stem and other parts of the plant before the anthesis stage, and remobilization of temporary assimilates stored in the stem after this stage (Bahrani et al. 2011). Photosynthesis is the most important source for providing photosynthetic assimilates needed for grain growth under favorable environmental conditions, but the contribution of remobilization of photosynthetic assimilates to the grain development of wheat increases under stress conditions (Mojtabaie Zamani et al. 2013; Ma et al. 2015).

According to the results of the study of Sun et al. (2021), by replacing cultivars improved between 1940 and 2010 in Shaanxi Province, China, the amount of dry matter mobilization from the stem has increased significantly under normal irrigation conditions. It was shown that, leaves and spikes were considered the most important photosynthetic resources in wheat, and the role of spike assimilates had been increased significantly during the years of wheat breeding under rainfed conditions. These researchers stated that the accumulation of assimilates in the stem and the photosynthesis of the spike, both caused the increase in the grain weight potential. In another study, it was reported that a higher yield can be due to a higher level of assimilation

during grain filling and remobilization of stored photosynthetic assimilates from stem and leaves to the sink (grain). Also, significant correlations between remobilization from spike and stem with grain yield were reported (Baral et al. 2020).

The warm and humid climate of northern Iran encompasses the provinces of Mazandaran, Guilan, Golestan and parts of Ardabil (Moghan). The Golestan province with about 350 000 hectares cultivation of wheat is the most important province in the northern region of Iran. This province with production of about one million ton per year (Agricultural Statistics Booklet 2021). However, in the current cropping season (2022-23) due to the occurrence of severe drought in this province, the production decreased greatly. Hence, limited number of cultivars have been released for this climate. In fact, only the investigated cultivars in this research have had the chance to perform under aforesaid stress conditions.

2. Material and Methods

In this study, 20 cultivars of wheat improved in the warm and humid climate of northern Iran between 1968 and 2018 were studied (Table 1). The cultivar, Ehsan, Tiregan and Merag were registered after the beginning of this study; which as promising breeding lines, were also investigated at the present study. The research was carried out with these cultivars using a randomized complete block design with three replications during the cropping years of 2015-2018 in the agricultural research stations of Gorgan (latitude, 36° 54′ N and longitude, 54° 25′ E) and Gonbad (latitude, 37° 16′ N and longitude, 55° 12′ E). The climate of Golestan province has several different types of sub-climates among which Gorgan's climate has been determined to reflect “Mediterranean climate” and “moderate semi-humid area”; Gonbad's climate has been classified as “cold Mediterranean” and “semi-dry area”, based on the two different climatic classification methods “Köppen” and “Emberger”, respectively. Meteorological statistics related to the rainfall and the average minimum and maximum temperatures in Gorgan and Gonbad during these three cropping years are presented in Table 2.

Table 1- Name of cultivar, pedigree and year of release of spring wheat cultivar released during 1968 to 2018 in the Gorgan and Gonbad in the northern climate of Iran

Cultivar No.	*Cultivar name*	*Year of release*	*Pedigree*
1	Inia	1968	LR64/SN64
2	Khazar1	1973	(P4160(F3)*Nr69)LR64
3	Moghan1	1974	LERMA-ROJO-64/NORIN-10-BREVOR//3*ANDES-ENANO
4	Moghan2	1976	Choti/Lerma, landrace from Indi
5	Alborz	1979	FRONTANA/MIDA//KENYA-117-A/3/2*COLLAFEN/4/SONORA-64/ KLEIN-RENDIDOR/3/CIANO-67//2*LERMA-ROJO-64/SONORA-64
6	Kaveh	1980	FORTUNA/PALOMA
7	Golestan	1986	ALONDRA ”S”
8	Rasoul	1992	Veery"s"=KAVKAZ/(SIB)BUHO//KALYANSONA/BLUEBIRD
9	Tajan	1995	BOBWHITE/NEELKANT(CM67428-GM-LR-5M-3R-LB-Y)
10	Shiroudi	1997	NORD-DESPREZ/VG-9144//KALYANSONA/BLUEBIRD/3/YACO/4/VEERY-5
11	Milan	2001	BARKAT/90ZHONG87
12	Shanghai	2001	SHANGHI
13	Arta	2006	HD2206/Hork//Bul/6/CMH80A.253/2/M2A/CML//Ald*4/5/BH1146/H56.71// BH1146/3/CMH78.390/4/Seri 82/7/Hel/3*Cno79/7/2*Seri 82
14	Darya	2006	SHA4/CHIL
15	Moghan3	2006	LUNA/3/V763.23/V879.c8//PVN/4/PICUS/5/OPATA
16	Morvarid	2009	MILAN/(SHA7)SHANGHAI-7
17	Gonbad	2011	ATRAK/WANG-SHUI-BAI
18	Ehsan	2016	SABUF/7/ALTAR 84/AE.SQUARROSA (224)//YACO/6/CROC_1/AE.SQUARROSA (205)/5/BR12*3/4/IAS55*4/CI14123/3/IAS55*4/EG,AUS//IAS55*4/ALD
19	Tiregan	2017	PFAU/MILAN/5/CHEN/AEGILOPS SQUARROSA (TAUS)//BCN/3/VEE#7/BOW/4/PASTOR
20	Merag	2018	PFAU/MILAN/3/SKAUZ/KS94U215//SKAUZ

Table 2- Meteorological statistics in Gorgan and Gonbad

	Year	*2016*				*2017*			
	Month	Dec	Jan	Feb	Mar	Apr	May	June	July
	Total rainfall (mm)	26.2	2.5	79.5	18.5	40.4	37.1	2.2	5
	Ave. min. temp (ºC)	1.7	2.5	1.6	4.5	8.5	14.3	18.4	22.5
	Ave. max. temp (ºC)	13.1	13.5	10.7	16.6	19.6	26.3	31.9	34.4
	Year	2017				2018			
	Month	Dec	Jan	Feb	Mar	Apr	May	June	July
Gorgan	Total rainfall (mm)	71.8	60	41.5	31.7	35.5	23.5	10.5	15
	Ave. min. temp (ºC)	4.8	5.2	4.4	7.3	9.6	14.1	19.7	25.1
	Ave. max. temp (ºC)	15.1	14	12.7	17.8	21.3	27.1	31.8	37.5
	Year	2018				2019			
	Month	Dec	Jan	Feb	Mar	Apr	May	June	July
	Total rainfall (mm)	48.8	126.3	127.3	121.4	69.8	41	3.0	24.7
	Ave. min. temp (ºC)	7.2	3.6	4.2	5.6	10	13.6	19.8	23.9
	Ave. max. temp (ºC)	16.3	14.5	14.5	17.4	19.2	26.6	34.2	34.1
	Year	2016				2017			
	Month	Dec	Jan	Feb	Mar	Apr	May	June	July
	Total rainfall (mm)	37.5	9	94.6	35.6	37.2	30.4	0.3	7.1
	Ave. min. temp (ºC)	1.4	2.5	1.8	4.7	8	14	18	22
	Ave. max. temp (ºC)	15	14.3	7.6	11.7	21.5	28.8	35.5	37.7
	Year	2017				2018			
	Month	Dec	Jan	Feb	Mar	Apr	May	June	July
Gonbad	Total rainfall (mm)	45.4	65.8	72.4	33.9	41.4	40.4	8.2	0.2
	Ave. min. temp (ºC)	4.7	4.5	4.6	7.6	9.2	13.1	18.5	24.6
	Ave. max. temp (ºC)	16.4	16.1	13.5	18	22	27.5	34.4	41.2
	Year	2018				2019			
	Month	Dec	Jan	Feb	Mar	Apr	May	June	July
	Total rainfall (mm)	63.7	81.2	152.3	163.8	51.2	41.5	6.3	7.1
	Ave. min. temp (ºC)	7.7	4.9	4.3	5.2	10.3	13.5	20.1	24.6
	Ave. max. temp (ºC)	17	15.9	15.2	19.4	20.7	28.2	36.3	36.9

Wheat cultivars were planted with a density of 350 grains per square meter in plots of 6.66 meters long, and 1.2 meters wide with 20 cm planting row spacing by a Wintersteiger planter on the November 22. The amount of chemical fertilizers used was determined based on the soil test (Table 3). Potash fertilizer (from the source of potassium sulfate at the rate of 100 kg/ha) and phosphate fertilizer (phosphate from the source of ammonium phosphate at the rate of 150 kg/ha) were added to the soil at the

time of cultivation, and nitrogen fertilizer (from the source of urea) was added twice (at the rate of 100 kg/ha at the time of cultivation, and at the rate of 100 kg/ha at the beginning of spring growth) were dispersed on to the soil. To manage broad- and narrow-leaf weeds, the herbicide Granstar (Tribenuron methyl DF 75%) at the rate of 20 grams per hectare (gr/ha), and the herbicide Puma Super (Fenoxaprop-p -ethyl) at the rate of 1.2 liters per hectare was used after the tillering and before stem elongation stage, respectively. In order to control rusts and other leaf spot diseases, the Folicur fungicide was sprayed once before spike swelling and then at the spike emergence stage, another same dose of this fungicide was applied. Also, to prevent and control Fusarium head blight at the flowering stage, Rex Duo fungicide was used.

Table 3- Soil characteristics of Gorgan and Gonbad farms (depth 0-30 cm)

Location	*Texture*	*Specific gravity (g/cm^3)*	*Absorbable potassium (ppm)*	*Absorbable phosphorus (ppm)*	*Absorbable nitrogen (%)*	*Organic carbon (%)*	*pH*	*Electrical conductivity Ec*10^3*	*Saturation (%)*
Gorgan	Silty loam	1.3	296	13.7	0.13	1.3	7.1	1.1	43.6
Gonbad	Silty loam	1.3	700	14	0.14	1.4	7.6	3.8	52.1

During the growing season and after harvesting, various traits including the plant height (PLH), peduncle length (PDL), spike length (SPL), grain yield (YLD), biological yield (BYD), number of grains per spike (G/S), number of spikes per square meter (S/M^2), thousand kernel weight (TKW), harvest index (HI) grain filling period (GFP) and grain filling rate (GFR) were measured. The harvest index was calculated by dividing the grain yield by the biological yield. The method of Cox et al. 1990 and Papakosta & Gayians 1991 was used to calculate the traits related to remobilization and photosynthesis. Data analysis was done after checking the assumption of homogeneity of experimental errors' variances using Bartlett's test. The data obtained through the combined analysis based on a randomized complete block design was then analyzed using the SAS software ver. 9.2. Linear regression analyses between the evaluated traits and the year of cultivar release were done using the software SPSS ver. 21 and the graphs were generated by an Excel software.

3. Results

The variance analysis of the studied traits revealed a significant difference among the cultivars improved during different years in terms of the most morphological, phenological and yield traits and yield components (Table 4). Also, there was a significant difference for the year of cultivars release in terms of the efficiency of remobilization from the spike and other leaves and the contribution of remobilization from other leaves, stem and total remobilization, at the probability level of one percent (P<0.01). For the trait remobilization from the other leaves, there was a significant difference at the probability level of five percent (P<0.05 (Table 5).

Table 4- Combined variance analysis of investigated traits based on the year of release in 20 historically most important wheat cultivars released in Gorgan and Gonbad in the north climate of Iran during 1968–2018

S.O.V	*df*	*Mean Squares*										
		PLH	*PDL*	*SPL*	*YLD*	*BYD*	*G/S*	*S/M^2*	*TKW*	*HI*	*GFP*	*GFR*
Year	2	392.41^{ns}	395.11^{ns}	5.89^{ns}	6.38^{ns}	67.19^{ns}	753.02^{ns}	69673.73^{ns}	390.52^{ns}	328.95^{ns}	1629.27^{ns}	0.85^{ns}
Region	1	2773.03^{ns}	71.97^{ns}	7.32^{ns}	33.94^{ns}	16.60^{ns}	30.51^{ns}	548109.85*	352.65^{ns}	647.08^{ns}	8623.13^{ns}	4.62^{ns}
Year Region ×	2	3254.27**	81.98^{ns}	11.56**	9.84**	60.46**	424.38**	8197.06^{ns}	44.27^{ns}	259.98**	299.71*	0.45**
(Year× Region) Rep	12	37.24	72.04	0.12	0.39	6.74	18.96	3362.35	17.17	13.64	5.74	0.01
Year of release	16	224.61**	44.17**	3.45**	10.42**	14.32**	154.65*	4057.27^{ns}	234.68**	203.62**	67.85**	0.18**
× Year of release Region	16	16.46^{ns}	14.18^{ns}	0.74^{ns}	1.21^{ns}	3.81^{ns}	37.57^{ns}	3273.28^{ns}	8.18^{ns}	39.43^{ns}	4.78^{ns}	0.01^{ns}
Year× Year of release	32	23.60^{ns}	10.025^{ns}	0.63^{ns}	0.34^{ns}	2.37^{ns}	66.93^{ns}	3462.74^{ns}	15.54^{ns}	27.51^{ns}	3.22^{ns}	0.02^{ns}
× Year of release Year× Region	32	44.61**	11.74^{ns}	0.78*	0.79**	2.78^{ns}	68.95**	2610.84^{ns}	13.76**	20.29^{ns}	6.69**	0.01**
Error	192	13.30	8.33	0.49	0.21	1.96	38.16	1847.04	5.38	14.20	2.93	0.006
CV (%)	-	3.64	7.95	7.32	10.83	10.84	16.02	11.11	5.90	13.44	4.53	7.08

* and ** significantly at 5 and 1 % probability levels, respectively; Plant height (PLH), Peduncle length (PDL), Spike length (SPL), Grain yield (YLD), Biological yield (BYD), Number of grains per spike (G/S), Number of spikes per square meter (S/M^2), Thousand kernel weight (TKW), Harvest index (HI) Grain filling period (GFP) and Grain filling rate (GFR)

Table 5- Combined variance analysis of investigated traits related to the amount and efficiency remobilization of based on the year of release in 20 historically most important wheat cultivars released in Gorgan and Gonbad in the north climate of Iran during 1968–2018

S.O.V	df	Mean Squares									
		Amount of remobilization					Remobilization efficiency				
		Spike	Flag leaf	Other leaves	Stem	Total	Spike	Flag leaf	Other leaves	Stem	Total
Year	2	2.73	1.94^{ns}	56.32**	0.04^{ns}	784.6^{ns}	39.97**	0.54	0.013^{ns}	0.008^{ns}	7017.65^{ns}
Region	1	0.20	282.19	12932.11	15166.31	47.77	0.0043**	0.123	0.034	0.001	0.830
Region × Year	2	28.46**	1896.07**	10218.47**	3710.11**	1421.2^{ns}	15.94**	0.39	61.24**	0.006	5761.07**
Rep (Region× Year)	12	7.58	569.74	2134.59	6981.42	18492.91	0.0001	0.30	0.074	0.005	0.240
Year of release	16	21.72	223.96	807.69*	5292.61	5227.18	0.0005**	0.010	0.0149**	0.005	0.023
Year of release× Region	16	2.76**	217.04	1118.39**	3617.69	6215.36	0.0003	0.013	0.018**	0.0023	0.0337
Year of release× Year	32	23.04	267.10	312.71	2500.02^{ns}	5924.17^{ns}	0.0002	0.018	0.007	0.005	0.018
Year of release× Region× Year	32	17.45**	384.98	179.76	3741.02^{ns}	6873.42^{ns}	0.0003	0.014	0.070**	1.95**	0.12**
Error	192	4.68	206.99	378.73	5026.19	6535.84	0.0002	0.010	0.006	0.004	0.031
CV (%)	-	11.78	52.17	46.23	30.14	25.01	20.51	40	39.60	29.65	23.66

* and ** significantly at 5 and 1 % probability levels, respectively

Table (Continued) 5- Combined variance analysis of investigated traits related to contribution of remobilization based on the year of release in 20 historically most important wheat cultivars released in Gorgan and Gonbad in the north climate of Iran during 1968–2018

S.O.V	df	Mean Squares				
		Remobilization contributions				
		Spike	Flag leaf	Other leaves	Stem	Total
Year	2	0.77	1.91	0.74	1141.79	3847.16
Region	1	8.741	34.97	0.763	12161.34**	11678.02*
Region× Year	2	0.52	1.23	0.89	212.24	4547.04*
Rep (Region× Year)	12	6.996	27.98	97.577	547.240	1131.53
Year of release	16	5.063	20.25	70.443**	1222.67**	1904.70**
Year of release× Region	16	7.399	29.60	62.587**	874.92**	1648.23**
Year of release× Year	32	0.30	0.64	0.12**	267.04	1407.67**
Year of release× Region× Year	32	10.46**	15.49	17.15**	219.74	622.01**
Error	192	2.693	10.774	9.951	339.43	484.48
CV (%)	-	51.79	51.79	47.43	33.87	30.02

* and ** significantly at 5 and 1 % probability levels, respectively

There was a significant difference between the year of cultivar release in terms of all the traits related to the amount, efficiency and contribution of photosynthesis except for the amount of photosynthesis from other leaves (Table 6). The interaction effect of the region by year of release of the cultivar also for the traits of remobilization amount of spike and other leaves, remobilization efficiency from other leaves, contribution of remobilization from other leaves, stem and total remobilization, all traits related to photosynthesis except flag leaf photosynthesis efficiency and stem contribution of photosynthesis was significant at a probability level of one percentage. Linear regression graphs for the traits were drawn for each region separately where the interaction of

year of release was significant in the region. In contrast, for the traits where the interaction of year of release was not significant in the region, linear regression graphs were plotted using the average of data for the two regions (Table 7).

Table 6- Combined variance analysis of investigated traits related to the amount and efficiency of photosynthesis based on the year of release in 20 historically most important wheat cultivars released in Gorgan and Gonbad in the north climate of Iran during 1968–2018

S.O.V	*df*	*Mean Squares*									
		Amount of Photosynthesis					*Photosynthesis efficiency*				
		Spike	*Flag leaf*	*Other leaves*	*Stem*	*Total*	*Spike*	*Flag leaf*	*Other leaves*	*Stem*	*Total*
Year	1	241682.75**	225.33**	142459.52*	243.66**	35506.62**	48.91**	6.72	7.97^{ns}	0.09	8987.70**
Region	2	22031.87	2110.86	54321.19**	0.06^{ns}	1226.4^{ns}	0.170	95.43**	10.14	0.337**	194.616**
Region × Year	2	19352.21**	1473.57	2714.06	18.14**	4317.8	5.47**	9.81**	21.41**	0.035	54.18**
Rep(Region× Year)	12	2492.08	2837.93	3911.88	3.50	42394.75	0.462	1.94	0.557	0.005	5.946
Year of release	19	31115.44**	30549.95**	34413.72	29169.02**	473208.70	1.065**	3.43**	0.878**	0.023**	13.756**
Year of release× Region	19	13911.73**	15906.10**	15173.62**	13376.33*	214931.10**	0.577**	2.28	0.4596*	0.010	7.902**
Year of release× Year	38	1544.41**	1266.04	1921.86	0.07*	7467.65	0.51	1.54	0.21	1.18^{ns}	845.97**
Year of release× Region× Year	38	1170.66	2185.81^{ns}	2218.09	0.03	6490.34	0.47	0.97	0.65**	1.02**	3.37
Error	228	2514.97	2880.96	3163.28	7093.29	47293.98	0.161	1.50	0.182	0.007	3.103
CV (%)	-	11.23	12.27	13.30	35.67	14.09	20.97	27.47	21.24	39.58	20.47

* and ** significantly at 5 and 1 % probability levels, respectively

Table (Continued) 6- Combined variance analysis of investigated traits related to contribution of photosynthesis based on the year of release in 20 historically most important wheat cultivars released in Gorgan and Gonbad in the north climate of Iran during 1968–2018

S.O.V	*df*	*Mean Squares*				
		Photosynthesis contributions				
		Spike	*Flag leaf*	*Other leaves*	*Stem*	*Total*
Year	1	1.14	25.51	193.97	226.44	9807.36**
Region	2	8.74	34.98	122.68	5140.544**	4827.889
Region × Year	2	1.07	20.94	242.71**	279.71**	2647.01*
Rep (Region× Year)	12	6.996	27.97	97.573	135.331	859.264
Year of release	19	5.0635*	20.257*	70.429**	513.750*	840.726*
Year of release× Region	19	7.399**	29.605**	62.602**	332.700	725.734*
Year of release× Year	38	0.74	10.677	70.10**	411.24	1377.21**
Year of release× Region× Year	38	0.21	8.38	10.06	121.08	292.48^{ns}
Error	228	2.693	10.775	19.950	241.836	377.422
CV (%)	-	1.69	3.50	4.93	31.90	5.89

* and ** significantly at 5 and 1 % probability levels, respectively

Table 7– Mean of investigated traits based on the year of release in 20 historically most important wheat cultivars released in Gorgan and Gonbad in the north climate of Iran during 1968–2018

Cultivar No.	*Cultivar name*	*Year of release*	*Grain yield*	*Plant height*	*Thousand kernel weight*	*Biological yield*	*Harvest index*	*Spikes/M²*	*Peduncle length*	*Spike length*	*Grains/spike*	*Grain filling period*	*Grain filling rate*
Inia	1	1968	3.854	99.111	36.706	12.508	27.676	386.343	37.789	9.339	38.858	40.630	0.926
Khazar1	2	1973	3.918	98.667	35.672	12.021	27.333	375.130	34.011	9.782	37.072	40.333	0.912
Moghan1	3	1974	3.332	95.389	31.667	12.267	22.452	382.722	36.150	9.504	37.506	37.241	0.878
Moghan2	4	1976	3.989	96.778	35.278	12.545	27.570	411.398	35.868	9.814	42.422	35.389	1.021
Alborz	5	1979	3.710	100.444	41.894	13.023	26.435	393.426	37.078	10.611	36.692	40.519	1.066
Kaveh	6	1980	2.944	108.333	34.967	11.204	23.247	378.880	36.369	9.436	40.014	35.167	1.015
Golestan	7	1986	2.884	100.278	39.117	12.212	21.217	374.704	37.569	10.061	34.083	38.417	1.075
Rasoul	8	1992	4.580	99.222	41.306	12.981	30.334	396.444	35.724	9.806	37.700	37.083	1.144
Tajan	9	1995	4.995	95.389	39.939	12.458	31.991	374.944	36.231	9.725	39.519	38.630	1.055
Shiroudi	10	1997	4.717	96.389	41.867	12.416	29.990	373.870	34.503	9.483	38.083	40.065	1.070
Milan, Shanghai	11, 12	2001	4.863	98.694	42.444	12.961	31.009	387.368	34.540	9.047	34.950	37.833	1.151
Arta, Darya, Moghan3	13, 14, 15	2006	4.795	99.611	39.552	13.422	29.386	393.559	35.323	9.590	40.469	36.556	1.106
Morvarid	16	2009	5.186	102.111	39.222	13.596	32.808	387.370	39.579	8.972	42.511	37.417	1.067
Gonbad	17	2011	4.652	98.667	39.128	13.086	29.561	350.306	34.311	9.921	42.333	33.972	1.177
Ehsan	18	2016	4.510	105.389	45.344	14.395	25.885	392.769	36.213	10.043	34.625	36.778	1.267
Tiregan	19	2017	5.411	101.722	44.883	14.201	31.350	410.509	36.221	9.675	35.419	38.944	1.178
Merag	20	2018	4.752	104.556	38.850	14.567	28.330	401.750	38.963	8.828	43.028	37.528	1.057

Table (Continued) 7– Mean of investigated traits based on the year of release in 20 historically most important wheat cultivars released in Gorgan and Gonbad in the north climate of Iran during 1968–2018

Cultivar No.	*Cultivar name*	*Year of release*	*Spike dry matter remobilization*	*Flag leaf dry matter remobilization*	*Other leaves dry matter remobilization*	*Stem dry matter remobilization*	*Total dry matter remobilization*	*Spike dry matter remobilization efficiency*	*Flag leaf dry matter remobilization*	*Other leaves dry matter remobilization*	*Stem dry matter remobilization efficiency*	*Total dry matter remobilization efficiency*
Inia	1	1968	17.508	28.833	52.050	225.667	324.058	0.069	0.290	0.245	0.204	0.809
Khazar1	2	1973	17.717	17.167	32.167	260.000	327.050	0.078	0.209	0.172	0.227	0.686
Moghan1	3	1974	15.350	26.667	36.000	228.333	306.350	0.065	0.264	0.190	0.242	0.760
Moghan2	4	1976	17.017	21.167	64.333	218.333	320.850	0.070	0.219	0.300	0.198	0.788
Alborz	5	1979	16.567	27.000	47.833	250.000	341.400	0.075	0.301	0.241	0.237	0.855
Kaveh	6	1980	16.783	30.500	31.000	229.667	307.950	0.081	0.311	0.151	0.204	0.747
Golestan	7	1986	16.567	23.000	56.333	213.333	309.233	0.059	0.226	0.240	0.193	0.718
Rasoul	8	1992	18.608	25.667	58.333	285.000	387.608	0.084	0.236	0.256	0.266	0.843
Tajan	9	1995	17.608	24.833	51.667	254.333	348.442	0.078	0.266	0.230	0.227	0.801
Shiroudi	10	1997	19.817	32.867	42.333	210.000	305.017	0.090	0.313	0.223	0.197	0.823
Milan, Shanghai	11, 12	2001	17.017	25.417	38.833	260.000	341.267	0.078	0.248	0.191	0.249	0.766
Arta, Darya, Moghan3	13, 14, 15	2006	19.592	28.117	30.222	252.833	330.764	0.081	0.248	0.146	0.229	0.705
Morvarid	16	2009	19.100	32.667	33.833	188.167	273.767	0.095	0.298	0.159	0.164	0.716
Gonbad	17	2011	22.833	35.333	47.167	248.833	354.167	0.080	0.273	0.191	0.190	0.733
Ehsan	18	2016	19.667	26.500	38.383	235.000	319.550	0.072	0.201	0.161	0.211	0.644
Tiregan	19	2017	19.650	43.000	32.167	195.000	289.817	0.096	0.332	0.143	0.172	0.743
Merag	20	2018	19.833	21.167	49.833	183.333	274.167	0.078	0.205	0.217	0.172	0.673

Table (Continued) 7– Mean of investigated traits based on the year of release in 20 historically most important wheat cultivars released in Gorgan and Gonbad in the north climate of Iran during 1968–2018

Cultivar No.	*Cultivar name*	*Year of release*	*Contribution of spike dry matter remobilization*	*Contribution of flag leaf dry matter remobilization*	*Contribution of other leaves dry matter remobilization*	*Contribution of stem dry matter remobilization*	*Total contribution of dry matter remobilization*	*Spike photosynthesis*	*Flag leaf photosynthesis*	*Other leaves photosynthesis*	*Stem photosynthesis*	*Total photosynthesis*
Inia	1	1968	3.792	7.583	14.060	59.648	85.084	377.696	366.371	343.154	169.885	1257.106
Khazar1	2	1973	2.069	4.137	7.457	66.145	79.809	391.128	391.678	376.678	151.275	1310.758
Moghan1	3	1974	5.421	10.842	11.789	87.522	115.575	306.305	294.988	285.655	148.877	1035.825
Moghan2	4	1976	2.543	5.086	14.273	51.276	73.179	427.414	423.264	380.097	226.097	1456.872
Alborz	5	1979	3.176	6.352	10.686	60.045	80.258	404.782	394.348	373.515	171.348	1343.993
Kaveh	6	1980	4.426	8.852	8.287	68.565	90.129	355.933	342.216	341.716	180.550	1220.415
Golestan	7	1986	3.941	7.882	17.496	75.655	104.974	322.004	315.571	282.237	158.215	1078.027
Rasoul	8	1992	2.726	5.452	11.432	58.084	77.694	470.527	463.468	430.802	204.135	1568.931
Tajan	9	1995	2.334	4.667	10.020	47.782	64.802	520.319	513.094	486.261	283.594	1803.269
Shiroudi	10	1997	3.301	6.603	8.694	43.220	61.819	471.793	458.743	449.277	281.610	1661.424
Milan, Shanghai	11, 12	2001	2.568	5.136	7.604	51.829	67.137	490.789	482.389	468.973	247.806	1689.958
Arta, Darya, Moghan3	13, 14, 15	2006	2.914	5.829	6.146	51.749	66.638	472.791	464.266	462.160	239.549	1638.767
Morvarid	16	2009	3.062	6.124	6.476	34.591	50.253	522.883	509.316	508.150	353.816	1894.166
Gonbad	17	2011	3.723	7.446	9.794	51.658	72.621	455.102	442.602	430.769	229.102	1557.575
Ehsan	18	2016	2.723	5.446	8.124	52.698	68.991	468.206	461.373	449.490	252.873	1631.942
Tiregan	19	2017	4.108	8.216	6.144	34.686	53.154	534.943	511.593	522.427	359.593	1928.556
Merag	20	2018	2.152	4.303	9.954	37.208	53.617	499.877	498.544	469.877	336.377	1804.675

Table (Continued) 7– Mean of investigated traits based on the year of release in 20 historically most important wheat cultivars released in Gorgan and Gonbad in the north climate of Iran during 1968–2018

Cultivar No.	*Cultivar name*	*Year of release*	*Spike photosynthesis efficiency*	*Flag leaf photosynthesis efficiency*	*Other leaves photosynthesis efficiency*	*Stem photosynthesis efficiency*	*Total photosynthesis efficiency*	*Contribution of spike photosynthesis*	*Contribution of flag leaf photosynthesis*	*Contribution of other leaves photosynthesis*	*Contribution of stem photosynthesis*	*Spike photosynthesis efficiency*
Inia	1	1968	1.465	3.836	1.639	0.157	7.097	96.208	92.417	85.940	40.468	315.033
Khazar1	2	1973	1.707	4.854	1.993	0.133	8.688	97.931	95.863	92.543	34.685	321.022
Moghan1	3	1974	1.304	3.296	1.524	0.157	6.281	94.579	89.158	88.211	45.811	317.758
Moghan2	4	1976	1.774	4.627	1.796	0.221	8.418	97.457	94.914	85.727	48.724	326.821
Alborz	5	1979	1.814	4.607	1.846	0.163	8.430	96.824	93.648	89.314	39.955	319.742
Kaveh	6	1980	1.700	3.729	1.661	0.172	7.262	95.574	91.148	91.713	47.225	325.661
Golestan	7	1986	1.135	3.305	1.216	0.139	5.796	96.059	92.118	82.504	36.950	307.631
Rasoul	8	1992	2.103	4.623	1.872	0.196	8.794	97.274	94.548	88.568	41.916	322.306
Tajan	9	1995	2.304	5.763	2.488	0.259	10.814	97.666	95.333	89.980	52.218	335.198
Shiroudi	10	1997	2.131	4.723	2.445	0.268	9.568	96.699	93.397	91.306	56.780	338.181
Milan, Shanghai	11, 12	2001	2.217	5.085	2.331	0.240	9.874	97.432	94.864	92.396	48.171	332.863
Arta, Darya, Moghan3	13, 14, 15	2006	1.962	4.683	2.179	0.227	9.051	97.086	94.171	93.854	48.251	333.362
Morvarid	16	2009	2.610	4.782	2.463	0.316	10.171	96.938	93.876	93.524	65.409	349.747
Gonbad	17	2011	1.591	3.433	1.711	0.178	6.912	96.277	92.554	90.206	48.342	327.379
Ehsan	18	2016	1.690	3.563	1.930	0.234	7.418	97.277	94.554	91.876	47.302	331.009
Tiregan	19	2017	2.594	4.701	2.348	0.325	9.968	95.892	91.784	93.856	65.314	346.846
Merag	20	2018	2.029	5.232	2.029	0.312	9.603	97.848	95.697	90.046	62.792	346.383

Based on the results of linear regression analysis between grain yield and the year of cultivar release, grain yield had a significant and increasing trend during the cultivar improvement years in both Gorgan and Gonbad regions (Figure 1a). The average genetic improvement of cultivars from the year 1968 was estimated 30 kg/ha/yr for the grain yield ($R^2 = 0.56$, $P<0.01$).

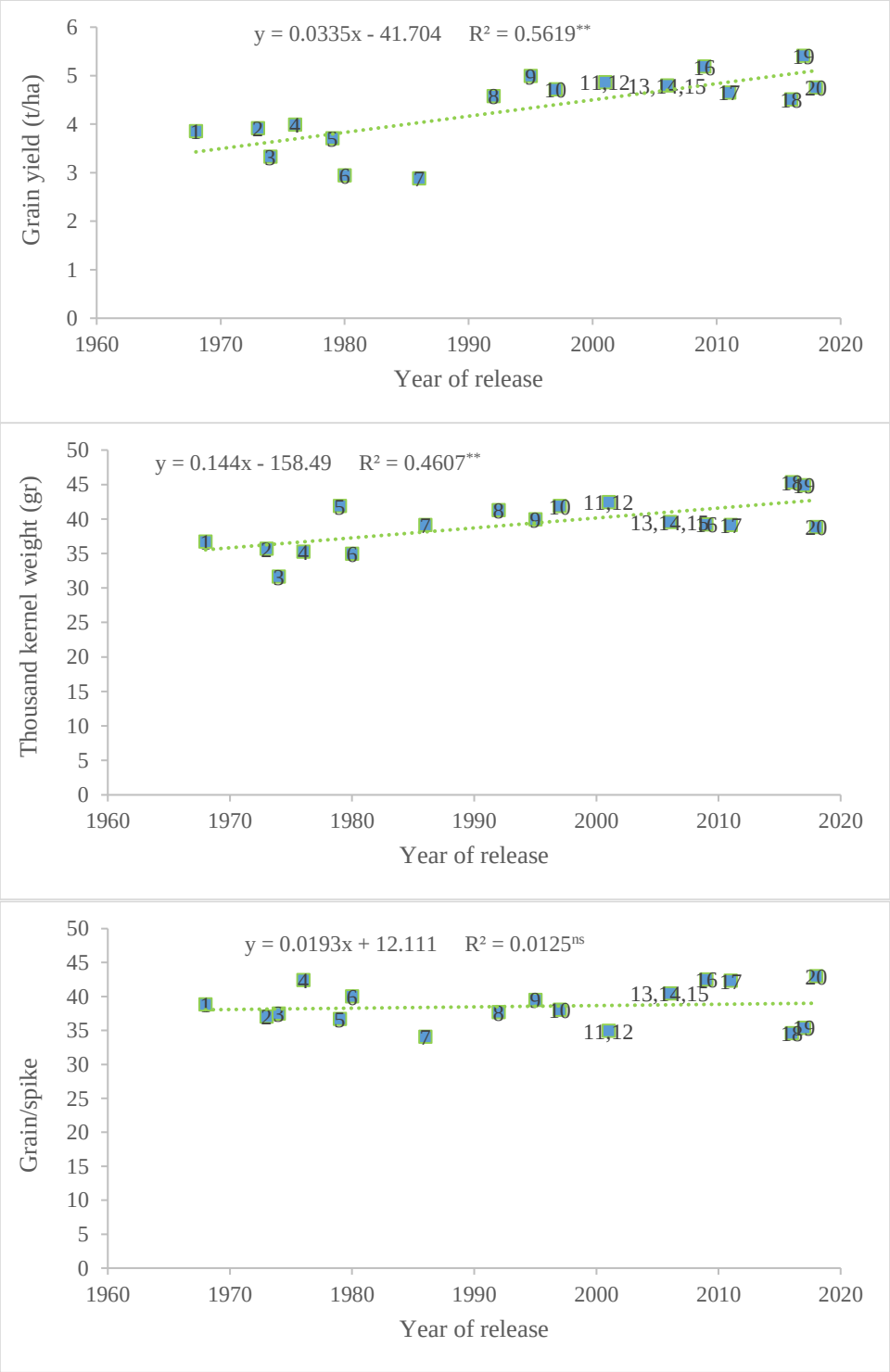

Figure 1- Liner regression equation between Grain yield (a), Thousand kernel weight (b) and Grain/spike (c) against the year of release of 20 historically most important wheat cultivars released in Gorgan and Gonbad in the north climate of Iran during 1968–2018; 1=Inia, 2=Khazar1, 3=Moghan1, 4=Moghan2, 5=Alborz, 6=Kaveh, 7=Golestan, 8=Rasoul, 9=Tajan, 10=Shiroudi, 11=Milan, 12=Shanghai, 13=Arta, 14=Darya, 15=Moghan3, 16=Morvarid, 17=Gonbad, 18=Ehsan, 19=Tiregan, 20=Merag

Based on the results of linear regression analysis, there was a significant relationship between the thousand kernel weight (TKW) and the year of cultivar release in the both regions (Figure 1b). The average genetic gain of TKW of cultivars from 1968

to 2018 in the two regions was 0.14 gr/yr (R^2 = 0.46, P<0.01). There was a positive and significant correlation between TKW and YLD (r = 0.596, P<0.05).

Although there was a significant difference in terms of the number of grains in the spike among the years of release of cultivars, it seems that during the wheat breeding program of the cultivars studied, the increase of the number of grains in none of the two regions of Gorgan and Gonbad was considered much because there was no significant trend during the years of their release. (Figure 1c). The correlation of this trait with grain yield was also not significant (r = 0.261 ns).

The trend of increasing the number of spikes per square meter, S/M^2 (with an average of 356.45) was not significant during the years of cultivar release in the two regions.

In this research, there was a no significant relationship between the spike/m^2 and the year of cultivar release in the both regions (Figure 2a). The biological yield has increased and for this trait, a significant trend was observed during the years of cultivar release (Figure 2b). On average, the genetic gain from 1968 to 2018 for biological yield was estimated to be 42 kg/ha/yr (R^2 = 0.65, P<0.01). The correlation of this trait with YLD was also positive and significant (r = 0.933, P<0.01).

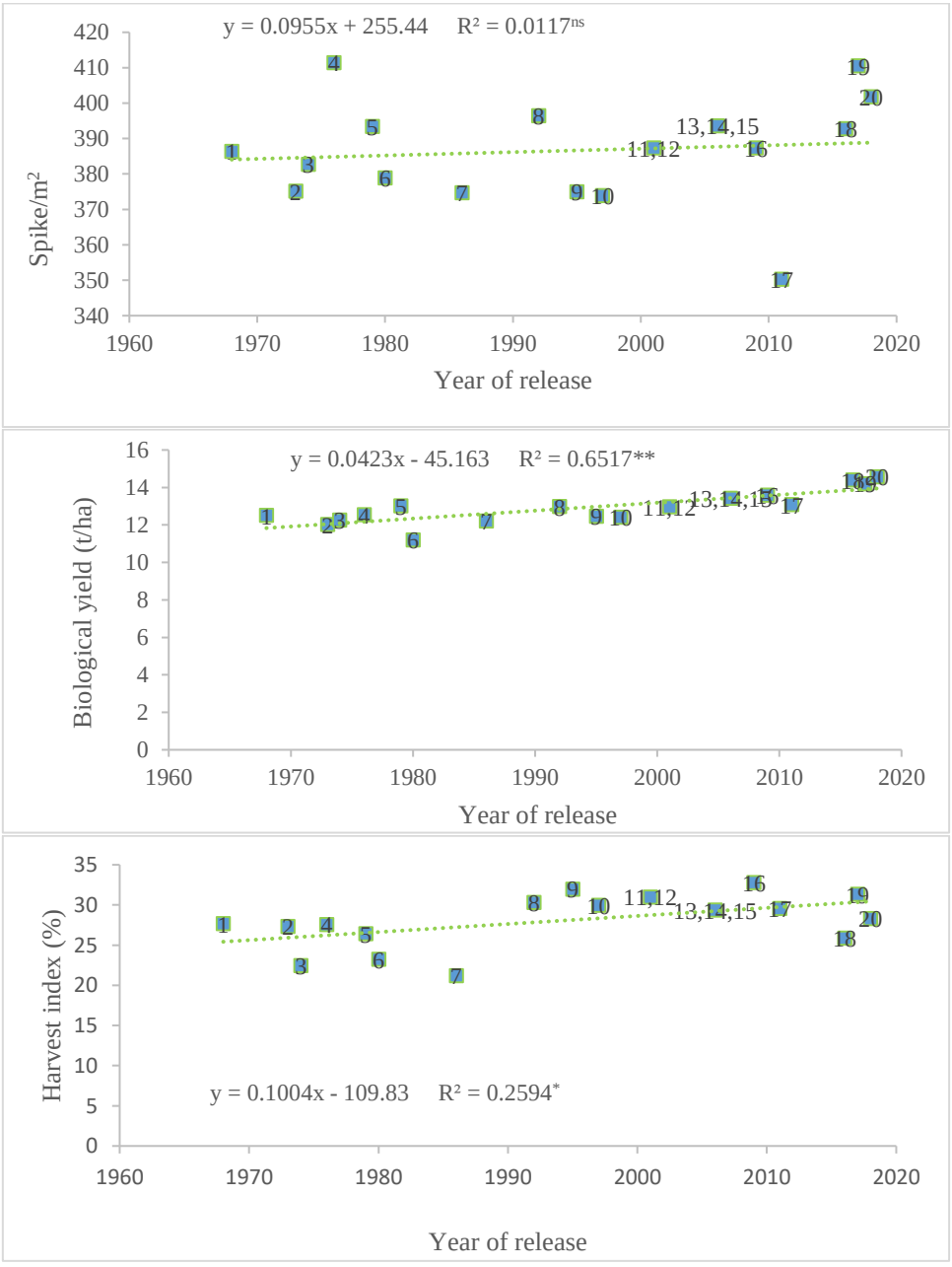

Figure 2- Liner regression equation between Spike/m^2 (a), Biological yield (b) and Grain/spike (c) against the year of release of 20 historically most important wheat cultivars released in Gorgan and Gonbad in the north climate of Iran during 1968–2018; 1=Inia, 2=Khazar1, 3=Moghan1, 4=Moghan2, 5=Alborz, 6=Kaveh, 7=Golestan, 8=Rasoul, 9=Tajan, 10=Shiroudi, 11=Milan, 12=Shanghai, 13=Arta, 14=Darya, 15=Moghan3, 16=Morvarid, 17=Gonbad, 18=Ehsan, 19=Tiregan, 20=Merag

As shown in Figure 2c, based on the results of linear regression analysis, although to some extend, the harvest index has increased in both the regions, the increase of this trait during the period of cultivar release found to be significant (P<0.05). The average genetic gain of harvest index of the cultivars investigated from 1968 to 2018 in the two regions of Gorgan was 0.1% per year (R^2 = 0.25, P<0.05). A significant and positive correlation was observed between YLD and harvest index (r = 0.941**).

Unlike the length of the grain filling period, which did not have a significant trend in any of the regions studied, the grain filling rate had significant increasing trend in the two regions (Figure 3a and 3b). The average genetic gain for grain filling rate from 1968 to 2017 in the two regions was 0.004 mg/day/yr (R^2 = 0.62, P<0.01). The correlation of yield with grain filling rate was positive and significant (r = 0.510*); where, the correlation of yield with the SFP was positive and non-significant (r = 0.038 ns).

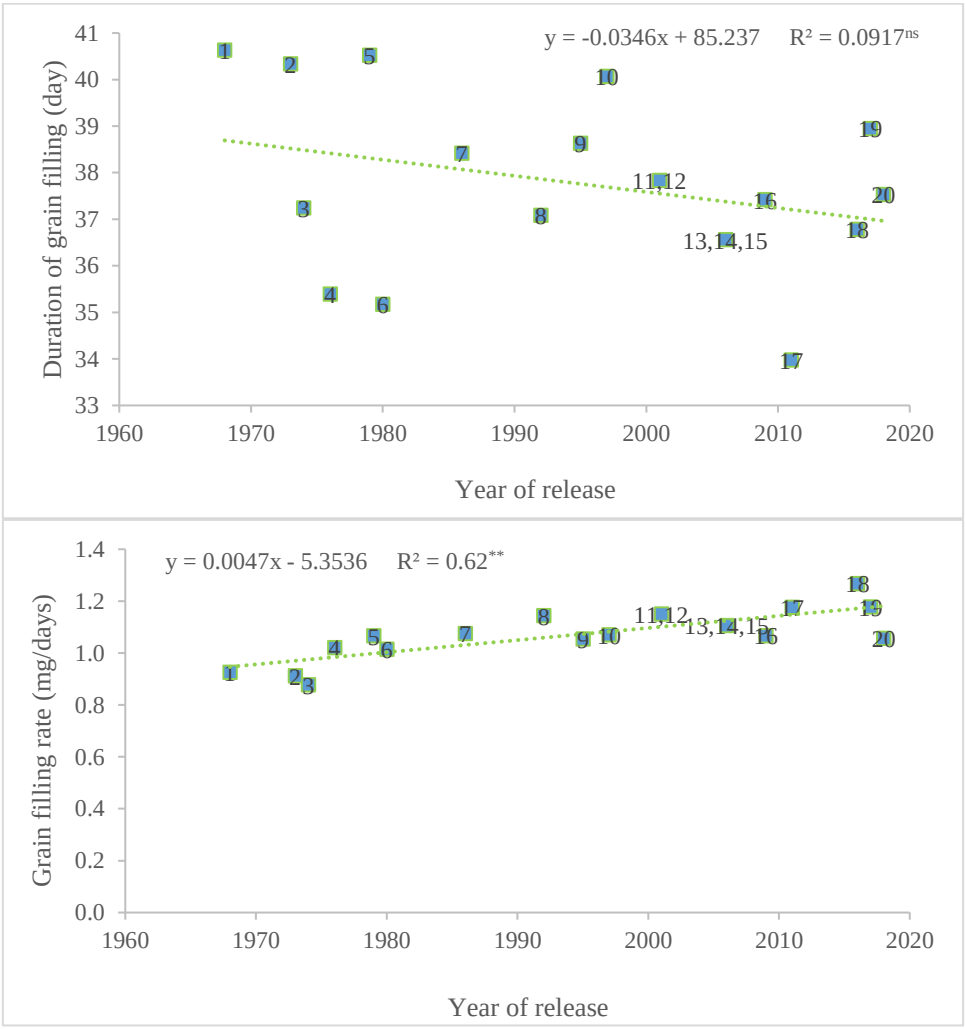

Figure 3- Liner regression equation between Duration of grain filling (a) and Grain filling rate (b) against the year of release of 20 historically most important wheat cultivars released in Gorgan and Gonbad in the north climate of Iran during 1968–2018; 1=Inia, 2=Khazar1, 3=Moghan1, 4=Moghan2, 5=Alborz, 6=Kaveh, 7=Golestan, 8=Rasoul, 9=Tajan, 10=Shiroudi, 11=Milan, 12=Shanghai, 13=Arta, 14=Darya, 15=Moghan3, 16=Morvarid, 17=Gonbad, 18=Ehsan, 19=Tiregan, 20=Merag

The results of analysis of variance showed a significant difference for plant height (PLH) in the years of release, but based on the results of linear regression analysis between the PLH and the year of release, the PLH even though not significantly, showed decreasing tend in the Gorgan region while to some extent increasing trend was observed in the Gonbad region as shown in Figure 4a. The correlation between the PLH (with an average of 101.80 cm for the all cultivars in both regions) and YLD was also negative and non-significant (r = 0.164 ns).

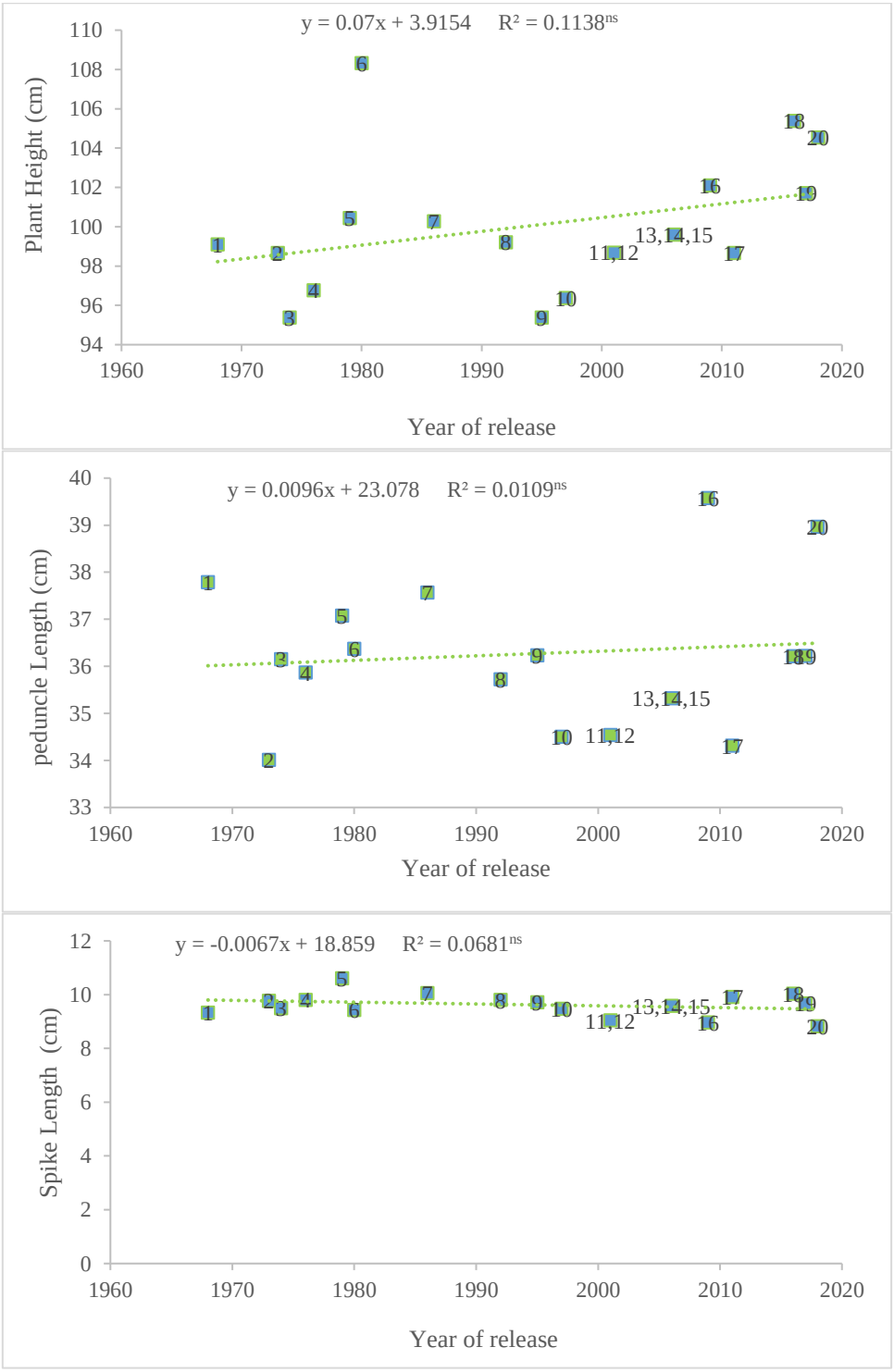

Figure 4- Liner regression equation between plant height (a), peduncle length (b) and spike length (c) against the year of release of 20 historically most important wheat cultivars released in Gorgan and Gonbad in the north climate of Iran during 1968–2018; 1=Inia, 2=Khazar1, 3=Moghan1, 4=Moghan2, 5=Alborz, 6=Kaveh, 7=Golestan, 8=Rasoul, 9=Tajan, 10=Shiroudi, 11=Milan, 12=Shanghai, 13=Arta, 14=Darya, 15=Moghan3, 16=Morvarid, 17=Gonbad, 18=Ehsan, 19=Tiregan, 20=Merag

Linear regression analysis of SPL and PDL with the year of cultivar release showed that during the years of cultivar improvement for these traits, PDL increased vs. SPL decreased. However, the changes were not statistically significant (Figure 4b and 4c). The correlation of these traits with the trait grain yield was also negative and non-significant. In this way, during the years of release, no attempt was made for selection to increase or decrease these traits.

Based on the results of the linear regression analysis of the amount of remobilization with the year of cultivar release, during the correction periods from 1968 to 2018, only the amount of remobilization from spike in both Gorgan and Gonbad regions has increased significantly, which means the selection was aimed at increasing the amount of remobilization from the spike. The amount of remobilization from the flag leaf also showed increasing but non-significant trend. On the other hand, the total amount

of remobilization showed increasing but non-significant trend, which may be due to the reduction of remobilization from other leaves of the plant and stem during the breeding years, although the trend of decreasing remobilization from other leaves (in both Gorgan and Gonbad regions) and the stem was also not significant (Figures 5 and 6).

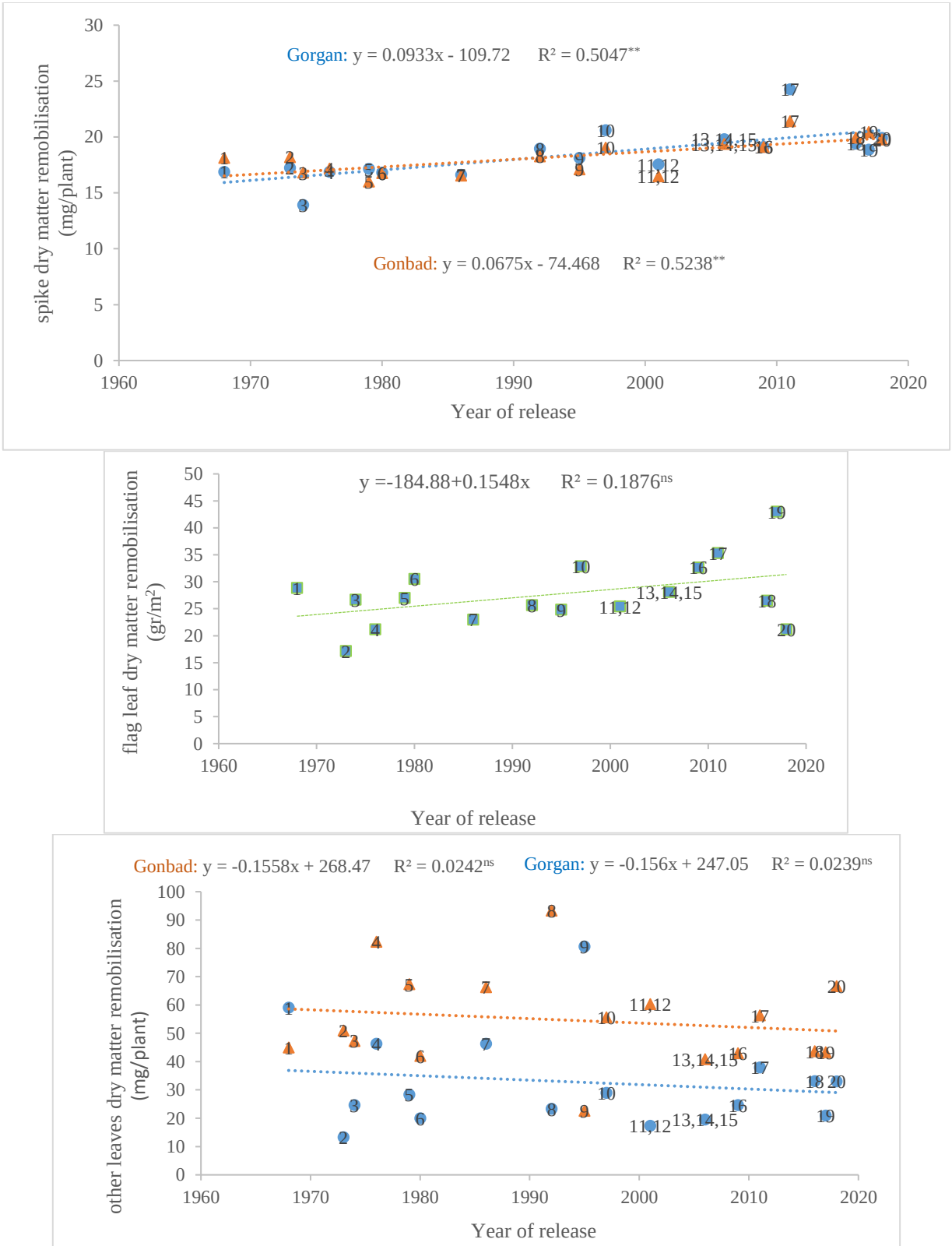

Figure 5- Liner regression equation between spike dry matter remobilization (a), flag leaf dry matter remobilization (b) and other leaves dry matter remobilization (c) against the year of release of 20 historically most important wheat cultivars released in Gorgan and Gonbad in the north climate of Iran during 1968–2018; 1=Inia, 2=Khazar1, 3=Moghan1, 4=Moghan2, 5=Alborz, 6=Kaveh, 7=Golestan, 8=Rasoul, 9=Tajan, 10=Shiroudi, 11=Milan, 12=Shanghai, 13=Arta, 14=Darya, 15=Moghan3, 16=Morvarid, 17=Gonbad, 18=Ehsan, 19=Tiregan, 20=Merag

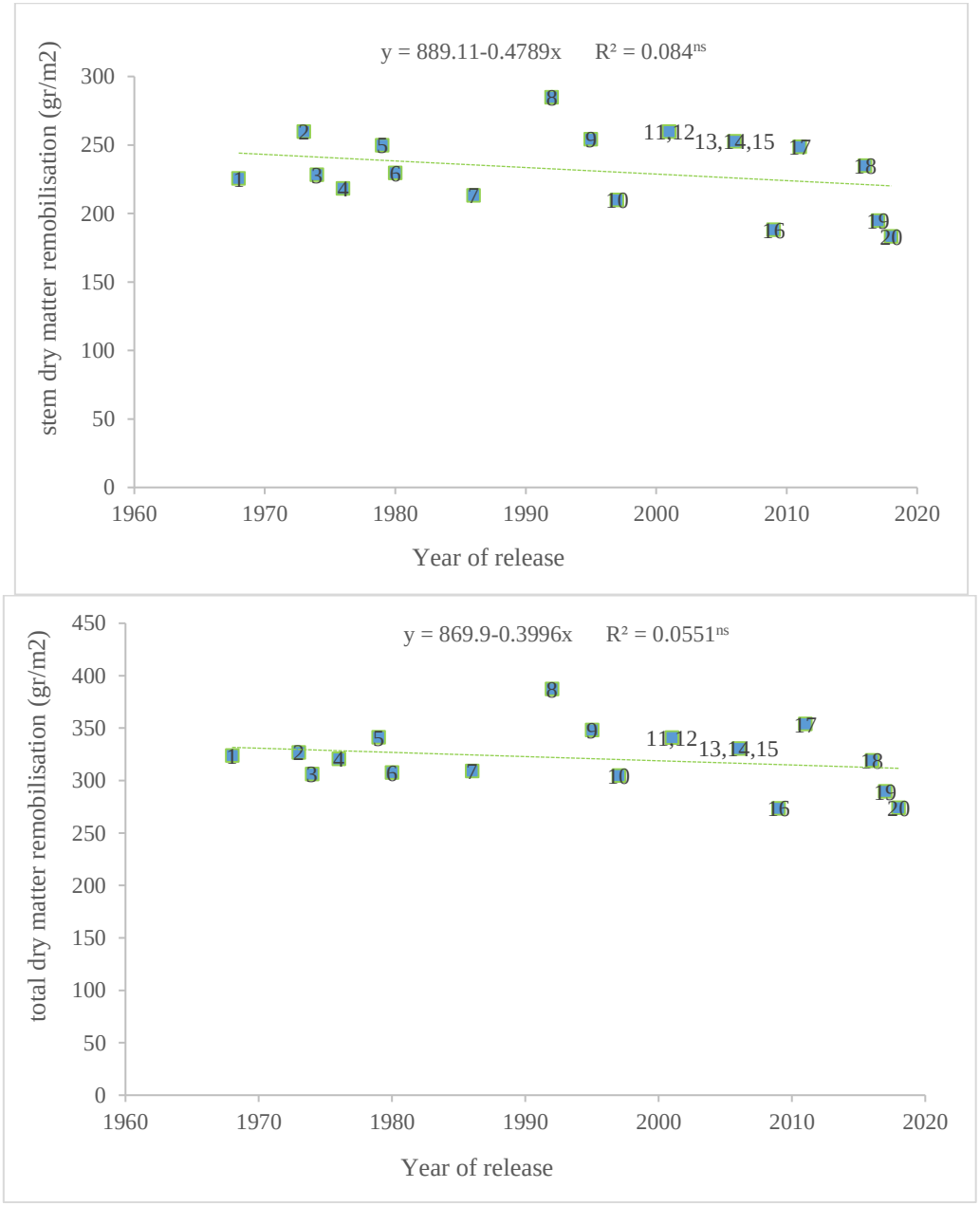

Figure 6- Liner regression equation between stem dry matter remobilization (a) and total dry matter remobilization (b) against the year of release of 20 historically most important wheat cultivars released in Gorgan and Gonbad in the north climate of Iran during 1968–2018; 1=Inia, 2=Khazar1, 3=Moghan1, 4=Moghan2, 5=Alborz, 6=Kaveh, 7=Golestan, 8=Rasoul, 9=Tajan, 10=Shiroudi, 11=Milan, 12=Shanghai, 13=Arta, 14=Darya, 15=Moghan3, 16=Morvarid, 17=Gonbad, 18=Ehsan, 19=Tiregan, 20=Merag

The average genetic gain values obtained for the trait of remobilization from spike for Gorgan and Gonbad regions were (0.093 gr/m^2/yr; R^2 = 0.51, P<0.01) and (0.067 gr/m^2/yr; R^2 = 0.52, P<0.01), respectively. The correlation of this trait with grain yield was also positive and significant (r = 0.725, P<0.05).

Spike remobilization efficiency during the years of release of cultivars had a significant increasing trend at the five percent probability level, but total remobilization efficiency and flag leaf and stem remobilization efficiency did not show a significant trend in the years of cultivar release (Figures 7 and 8). Despite the decrease in the remobilization efficiency of other leaves in the Gorgan region, the trend of changes of this trait was not significant in both Gorgan and Gonbad regions. In this way, it can be stated that during the breeding activities to improve the yield of wheat in this region, selection was made to increase the efficiency of remobilization of spike, but no effort was made to change the remobilization efficiency of other parts of the wheat cultivars. Among different parts of a plant, only spike remobilization efficiency was increased, the correlation of spike remobilization efficiency with grain yield was also positive and significant (r = 0.704, P<0.05), the correlation of total remobilization efficiency and other plant parts with yield was not significant. The percentage of genetic improvement for spike

remobilization efficiency trait was estimated to be 0.03 gr/gr per year during the 50 years of release of these cultivars (R^2 = 0.28, P<0.05).

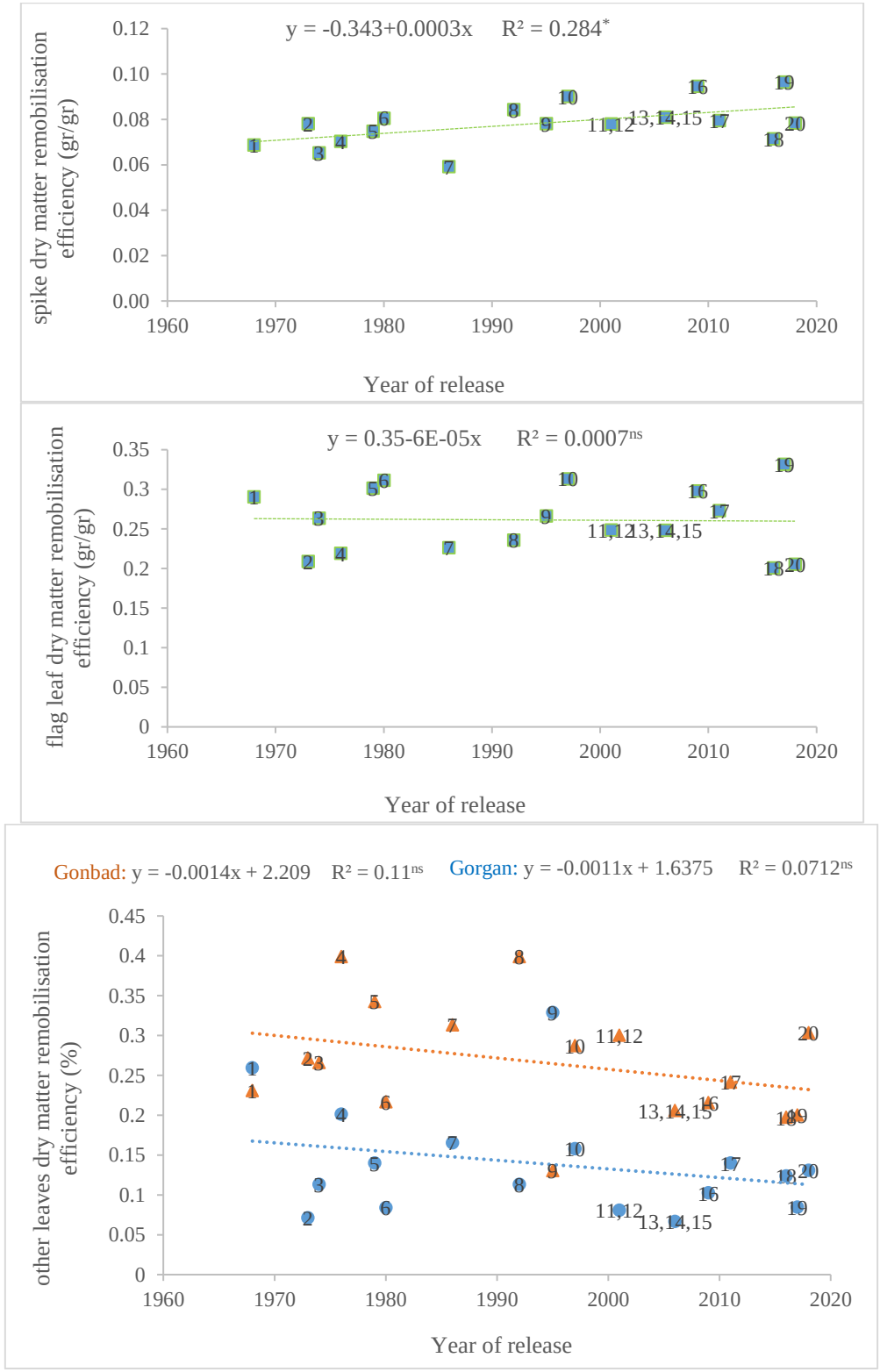

Figure 7- Liner regression equation between spike dry matter remobilization efficiency (a), flag leaf dry matter remobilization efficiency (b) and other leaves dry matter remobilization efficiency (c) against the year of release of 20 historically most important wheat cultivars released in Gorgan and Gonbad in the north climate of Iran during 1968–2018; 1=Inia, 2=Khazar1, 3=Moghan1, 4=Moghan2, 5=Alborz, 6=Kaveh, 7=Golestan, 8=Rasoul, 9=Tajan, 10=Shiroudi, 11=Milan, 12=Shanghai, 13=Arta, 14=Darya, 15=Moghan3, 16=Morvarid, 17=Gonbad, 18=Ehsan, 19=Tiregan, 20=Merag

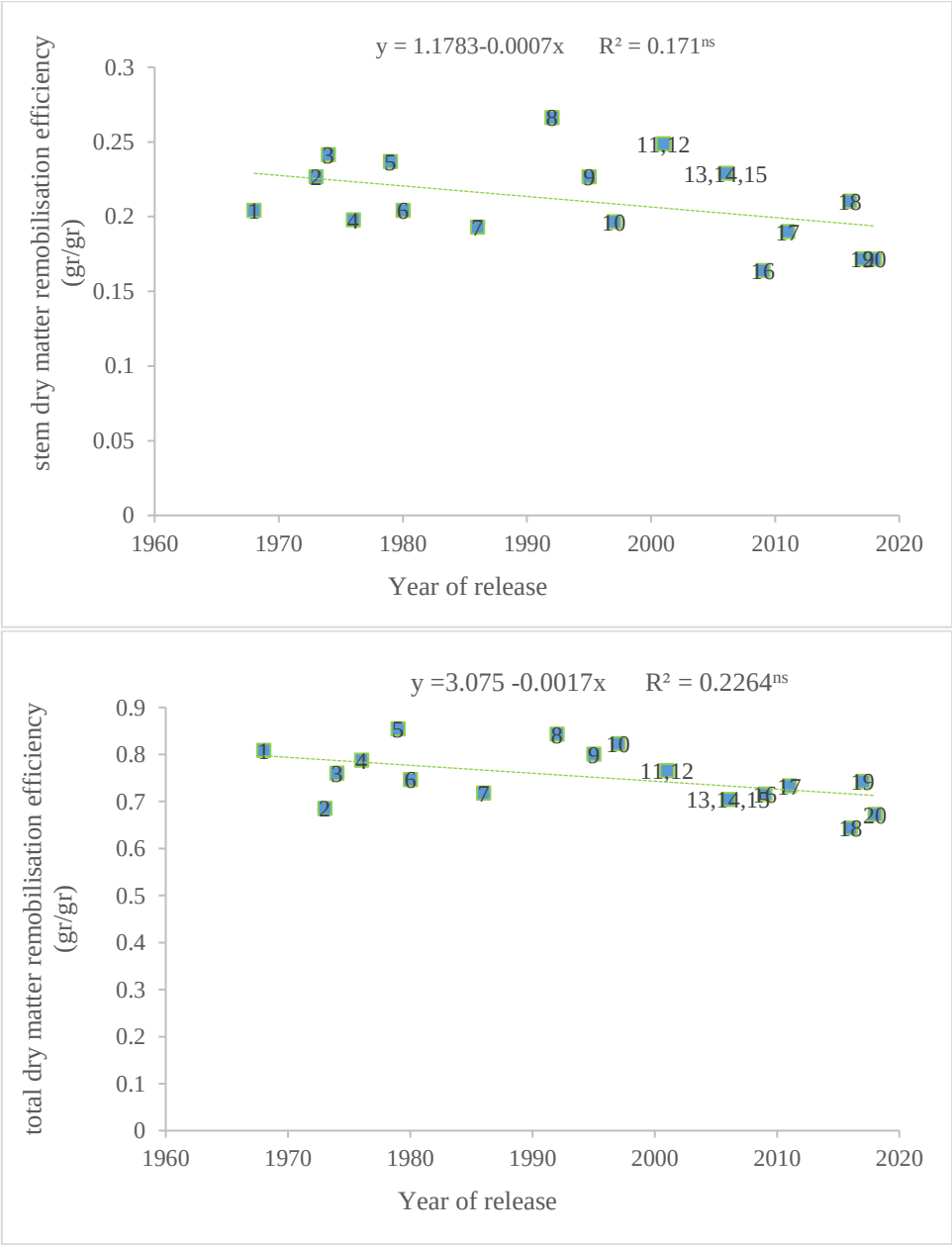

Figure 8- Liner regression equation between stem dry matter remobilization efficiency (a) and total dry matter remobilization efficiency (b) against the year of release of 20 historically most important wheat cultivars released in Gorgan and Gonbad in the north climate of Iran during 1968–2018; 1=Inia, 2=Khazar1, 3=Moghan1, 4=Moghan2, 5=Alborz, 6=Kaveh, 7=Golestan, 8=Rasoul, 9=Tajan, 10=Shiroudi, 11=Milan, 12=Shanghai, 13=Arta, 14=Darya, 15=Moghan3, 16=Morvarid, 17=Gonbad, 18=Ehsan, 19=Tiregan, 20=Merag

Based on the results of the analysis of the changes of remobilization during the years of cultivars improvement, the remobilization contributions of all parts of the plant and consequently the contribution of the total remobilization were decreased. However, this decrease was non-significant for the characteristics of the remobilization contribution of other leaves in the both regions, and significant for the total and stem remobilization contribution in both Gorgan and regions (Figures 9 and 10). The average reduction of stem and total remobilization contribution from 1968 to 2018 in the Gorgan region was -0.853%/yr (R^2 = 0.36, P<0.05) and -1.157%/yr (R^2 = 0.37, P<0.01) and in the Gonbad area, it was -0.335%/yr (R^2 = 0.42, P<0.01) and -0.314%/yr (R^2 = 0.31, P<0.05), respectively. It seems that with the decrease in the amount and efficiency of remobilization of other leaves of the plant except the flag leaf and stem, the contribution of these parts of the plant in remobilization had shown decreases during the breeding periods, and the selection to increase the amount and efficiency of remobilization of the spike had not been able to reduce the remobilization of the other parts. To compensate, the plant in this way, the amount, efficiency and contribution of total remobilization of the yield had been decreased during the cultivar breeding program. The correlation coefficient of the remobilization contribution of different plant parts and the total remobilization with grain yield was negative. This coefficient for the flag leaf remobilization contribution was r = 0.595, P<0.05. The correlations for the remobilization contribution of other leaves (r = -0.876), stem (r = -0.882), and the contribution of total remobilization (r = -0.928) were all significant at the probability level of one percent.

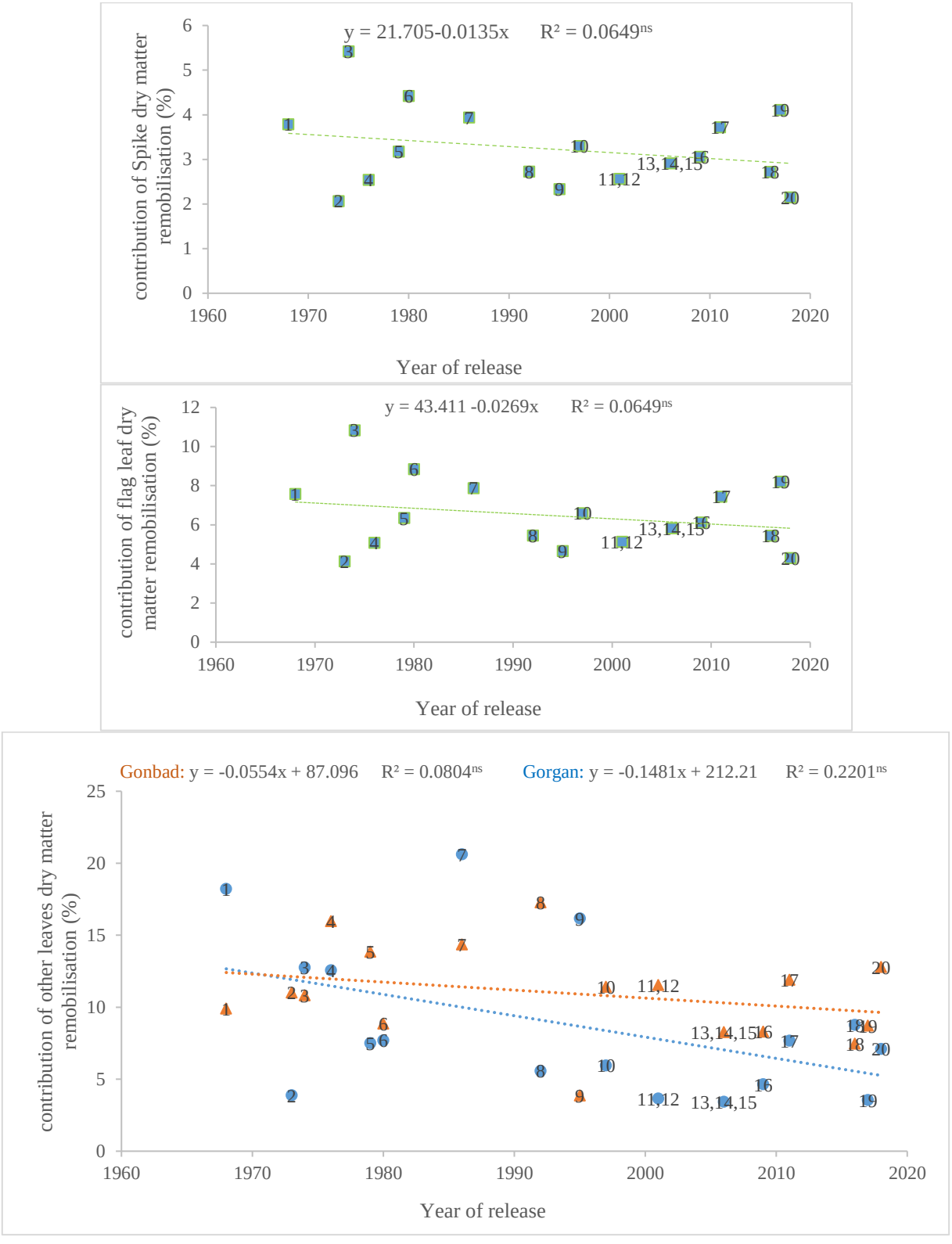

Figure 9- Liner regression equation between contribution of spike dry matter remobilization (a), contribution of flag leaf dry matter remobilization (b) and contribution of other leaves dry matter remobilization (c) against the year of release of 20 historically most important wheat cultivars released in Gorgan and Gonbad in the north climate of Iran during 1968–2018; 1=Inia, 2=Khazar1, 3=Moghan1, 4=Moghan2, 5=Alborz, 6=Kaveh, 7=Golestan, 8=Rasoul, 9=Tajan, 10=Shiroudi, 11=Milan, 12=Shanghai, 13=Arta, 14=Darya, 15=Moghan3, 16=Morvarid, 17=Gonbad, 18=Ehsan, 19=Tiregan, 20=Merag

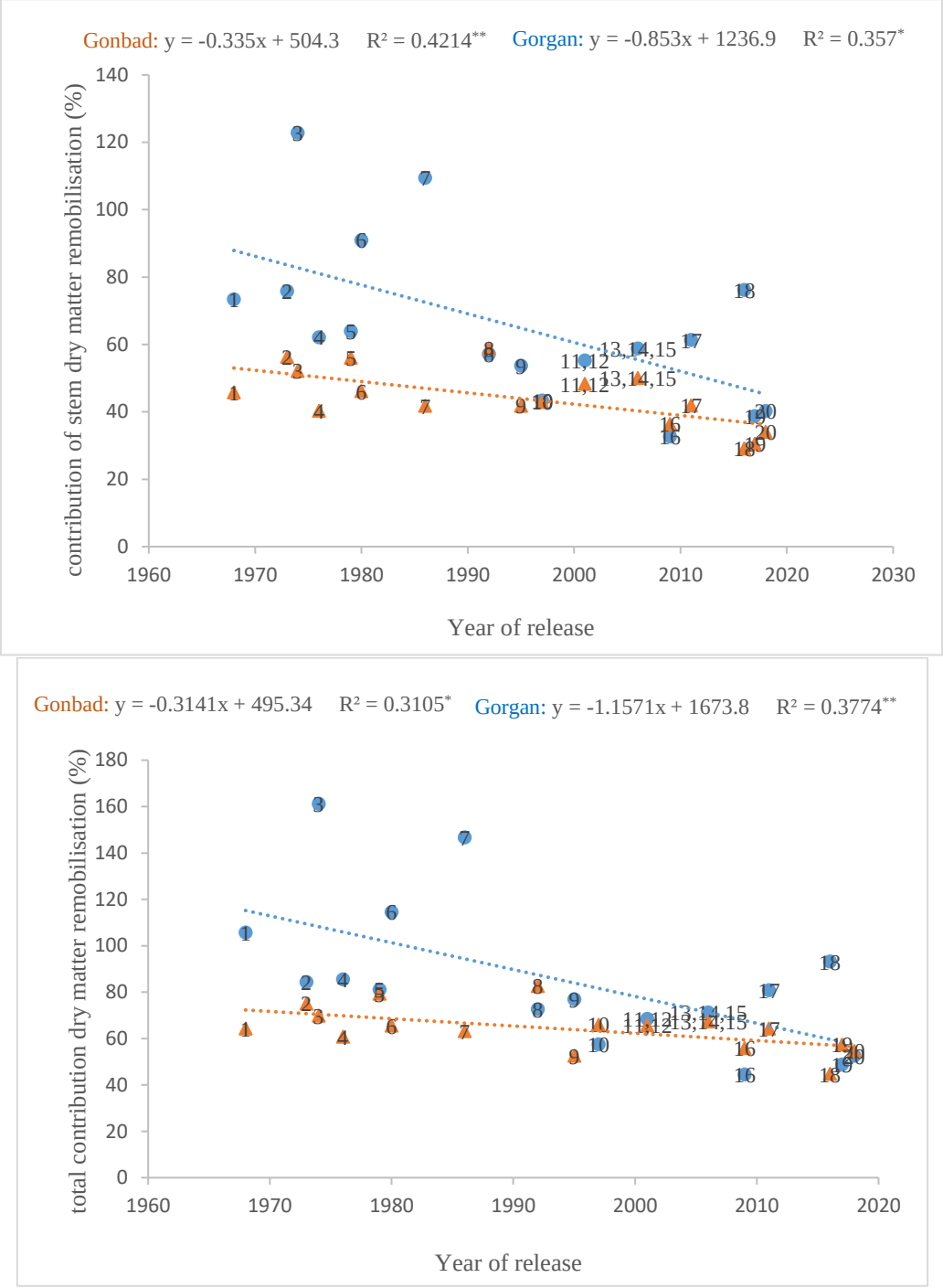

Figure 10- Liner regression equation between contribution of stem dry matter remobilization (a) and total contribution of dry matter remobilization (b) against the year of release of 20 historically most important wheat cultivars released in Gorgan and Gonbad in the north climate of Iran during 1968–2018; 1=Inia, 2=Khazar1, 3=Moghan1, 4=Moghan2, 5=Alborz, 6=Kaveh, 7=Golestan, 8=Rasoul, 9=Tajan, 10=Shiroudi, 11=Milan, 12=Shanghai, 13=Arta, 14=Darya, 15=Moghan3, 16=Morvarid, 17=Gonbad, 18=Ehsan, 19=Tiregan, 20=Merag

During the years of release of cultivars, the selections made for increasing the amount of photosynthesis from different parts of the plant and the overall increase of the amount of photosynthesis in wheat, so that these traits showed a significant increasing trend during the years of release of cultivars (Figures 11 and 12). The percentages of genetic gain for these traits in the Gorgan region 4.76 gr/m^2/yr (R^2 = 0.54, P<0.01), 4.86 (R^2 = 0.54, P<0.01), 5.02 (R^2 = 0.56, P<0.01), 3.89 (R^2 = 0.45, P<0.01) and 18.53 (R^2 = 0.54, P<0.01) and in the Gonbad area, 1.64 gr/m^2/yr (R^2 = 0.38, P<0.01), 1.38 (R^2 = 0.26, P<0.05), 1.86 (R^2 = 0.42, P<0.01), 2.72 (R^2 = 0.54, P<0.01) and 7.61 (R^2 = 0.47, P<0.01) were estimated. These traits showed a positive and highly significant correlation coefficient with YLD (r = 0.928, r = 0.918, r = 0.931, r = 0.929 and r = 0.925, respectively).

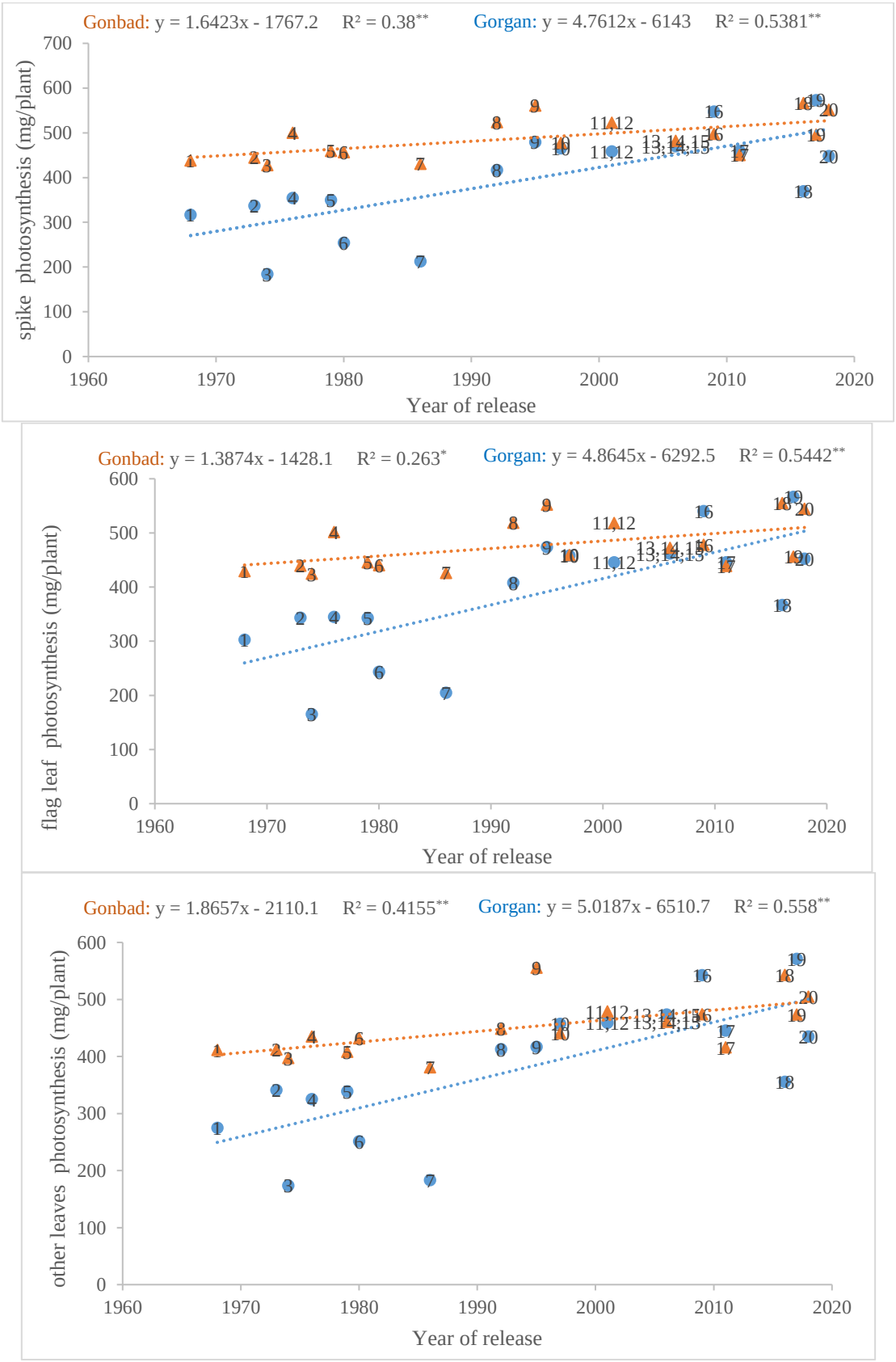

Figure 11- Liner regression equation between spike photosynthesis (a), flag leaf photosynthesis (b) and other leaves photosynthesis (c) against the year of release of 20 historically most important wheat cultivars released in Gorgan and Gonbad in the north climate of Iran during 1968–2018; 1=Inia, 2=Khazar1, 3=Moghan1, 4=Moghan2, 5=Alborz, 6=Kaveh, 7=Golestan, 8=Rasoul, 9=Tajan, 10=Shiroudi, 11=Milan, 12=Shanghai, 13=Arta, 14=Darya, 15=Moghan3, 16=Morvarid, 17=Gonbad, 18=Ehsan, 19=Tiregan, 20=Merag

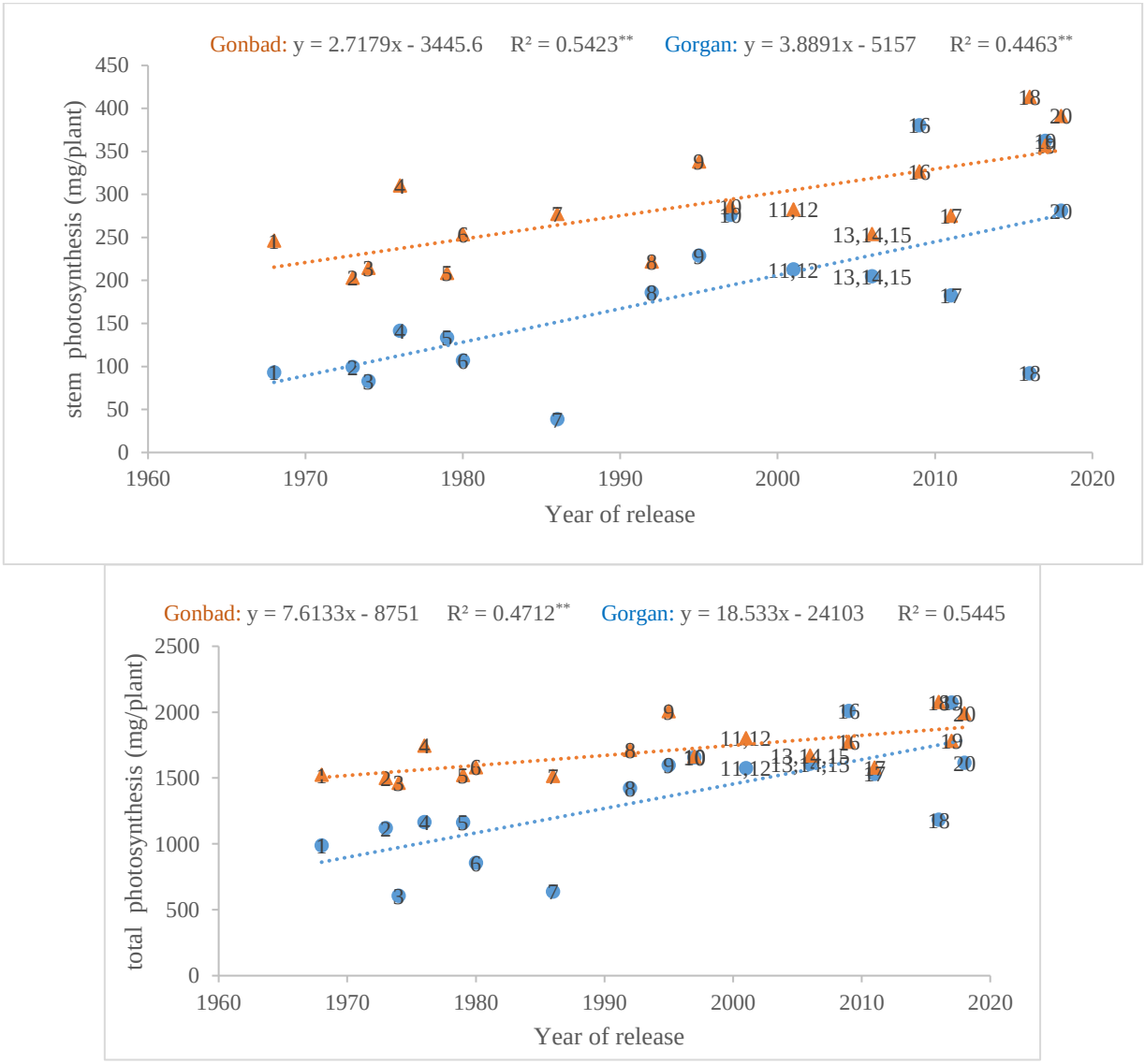

Figure 12- Liner regression equation between stem photosynthesis (a) and total photosynthesis (b) against the year of release of 20 historically most important wheat cultivars released in Gorgan and Gonbad in the north climate of Iran during 1968–2018; 1=Inia, 2=Khazar1, 3=Moghan1, 4=Moghan2, 5=Alborz, 6=Kaveh, 7=Golestan, 8=Rasoul, 9=Tajan, 10=Shiroudi, 11=Milan, 12=Shanghai, 13=Arta, 14=Darya, 15=Moghan3, 16=Morvarid, 17=Gonbad, 18=Ehsan, 19=Tiregan, 20=Merag

The photosynthesis efficiency of different parts of the plant and the total photosynthesis efficiency have also had increased during the years 1968 to 2018 in released wheat cultivars. However, as shown in the Figures 13 and 14, this trend was significant only for the total photosynthesis efficiency and those of spike and other leaves in the Gorgan region ($P<0.05$) and for the photosynthetic efficiency of the stem in both the Gorgan and Gonbad regions ($P<0.01$).

The genetic gain during the 50 years of breeding in the Gorgan region for the photosynthesis efficiency of spike and other leaves were 0.023 gr/gr/yr ($R^2 = 0.35$, $P<0.05$) and 0.017 gr/gr/yr ($R^2 = 0.28$, $P<0.05$), respectively. In this area, the genetic gain for total photosynthesis and for stem photosynthesis were estimated 0.075 gr/gr/yr ($R^2 = 0.31$, $P<0.05$) and 0.003 gr/gr/yr ($R^2 = 0.40$, $P<0.01$), respectively. The photosynthesis efficiency for stem was estimated 0.002 gr/gr/yr ($R^2 = 0.44$, $P<0.05$) in the Gonbad area. However, the photosynthesis efficiency of spike ($r = 0.722$), flag leaf ($r = 0.540$), other leaves ($r = 0.784$), stem ($r = 0.786$) and total photosynthesis efficiency ($r = 0.718$) had a positive and significant correlation with grain yield.

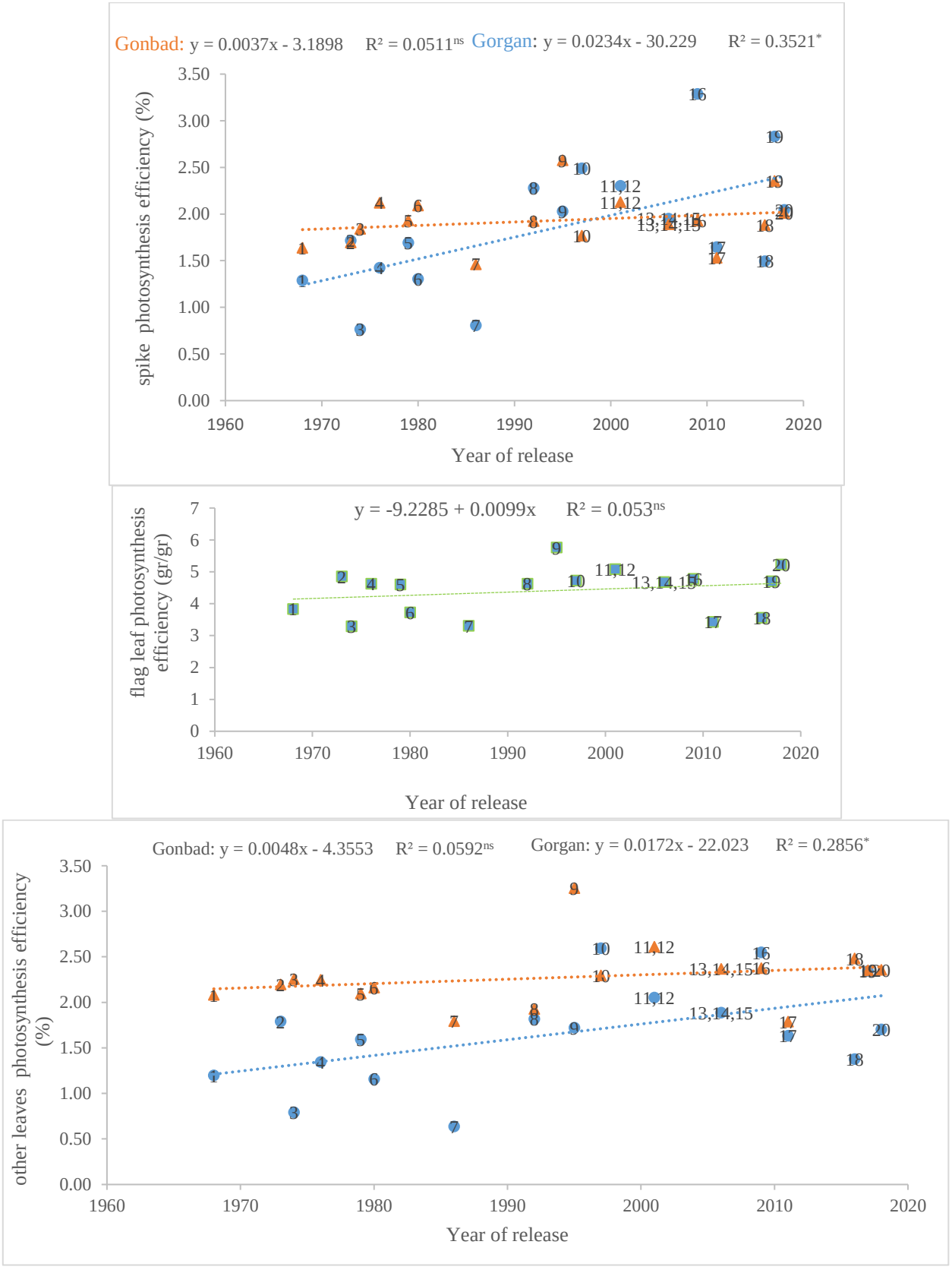

Figure 13- Liner regression equation between spike photosynthesis efficiency (a), flag leaf photosynthesis efficiency (b) and other leaves photosynthesis efficiency (c) against the year of release of 20 historically most important wheat cultivars released in Gorgan and Gonbad in the north climate of Iran during 1968–2018;1=Inia, 2=Khazar1, 3=Moghan1, 4=Moghan2, 5=Alborz, 6=Kaveh, 7=Golestan, 8=Rasoul, 9=Tajan, 10=Shiroudi, 11=Milan, 12=Shanghai, 13=Arta, 14=Darya, 15=Moghan3, 16=Morvarid, 17=Gonbad, 18=Ehsan, 19=Tiregan, 20=Merag

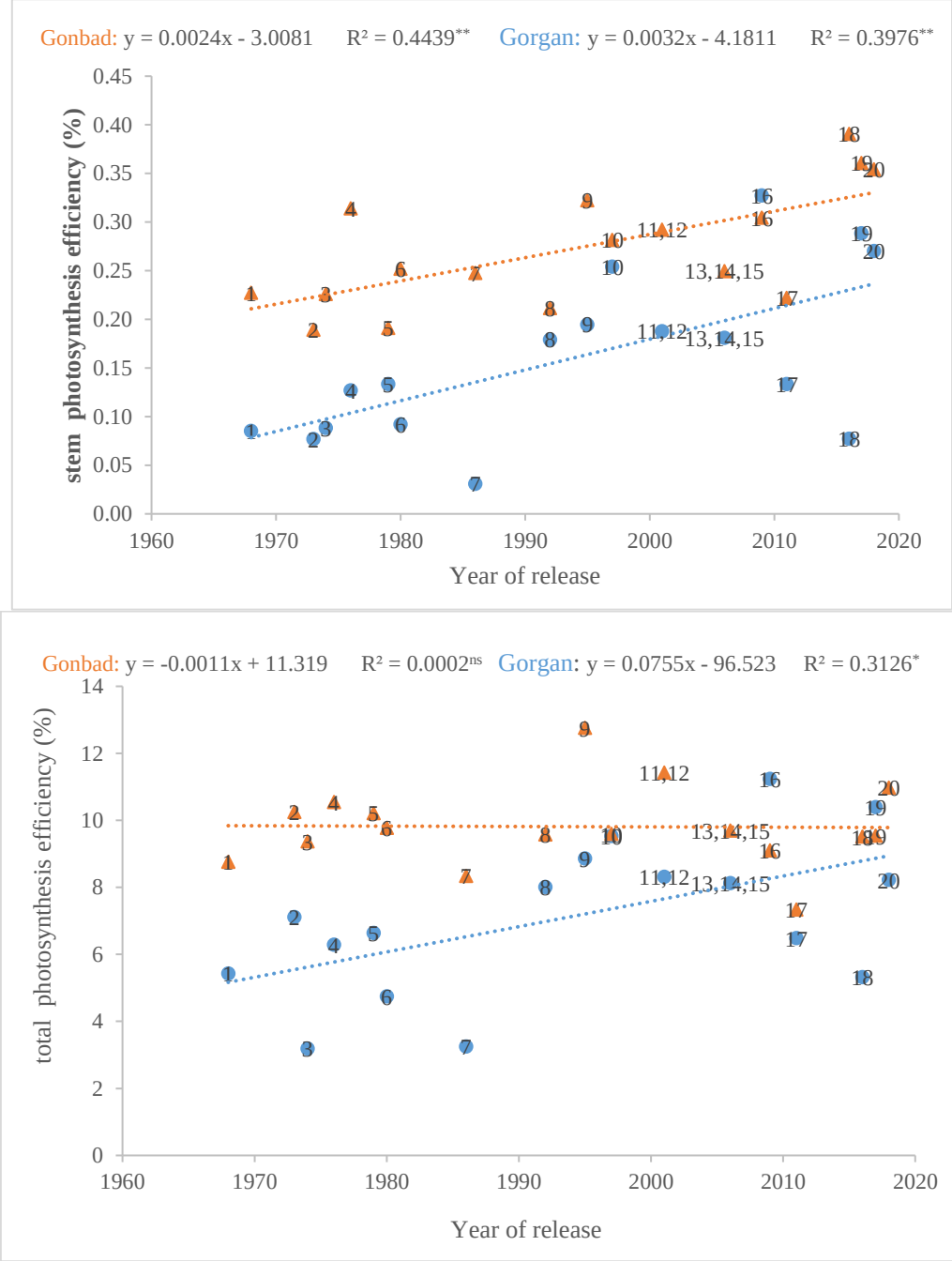

Figure 14- Liner regression equation between stem photosynthesis efficiency (a) and total photosynthesis efficiency (b) against the year of release of 20 historically most important wheat cultivars released in Gorgan and Gonbad in the north climate of Iran during 1968–2018; 1=Inia, 2=Khazar1, 3=Moghan1, 4=Moghan2, 5=Alborz, 6=Kaveh, 7=Golestan, 8=Rasoul, 9=Tajan, 10=Shiroudi, 11=Milan, 12=Shanghai, 13=Arta, 14=Darya, 15=Moghan3, 16=Morvarid, 17=Gonbad, 18=Ehsan, 19=Tiregan, 20=Merag

Considering the linear regression analysis, the contribution of photosynthesis of different parts of the plant and the contribution of total photosynthesis with the year of cultivar release were increased (Figures 15 and 16). In general, the photosynthesis had been increased in the cultivars released during recent years. The slope of the line regression of the photosynthesis, for spike and flag leaf in the Gorgan region, and for stems in the two regions showed increasing trends. The contribution of total photosynthesis was significant for Gonbad and Gorgan at the probability levels of five and one percent, respectively. The percentage of genetic gain in the Gorgan region for the contributions of the photosynthesis of the spike, the flag leaf, and the total photosynthesis were 0.052 (R^2 = 0.26, P<0.05), 0.104 (R^2 = 0.26, P<0.05), and 0.721 (R^2 = 0.37, P<0.01). The percentage of genetic gain in the Gonbad region for the contribution of the total photosynthesis was 0.314 (R^2 = 0.31, P<0.05) 0.383 (R^2 = 0.50, P<0.01). These traits had positive and significant correlation coefficients with YLD (r = 0.595, r = 0.687 and r = 0.800, respectively).

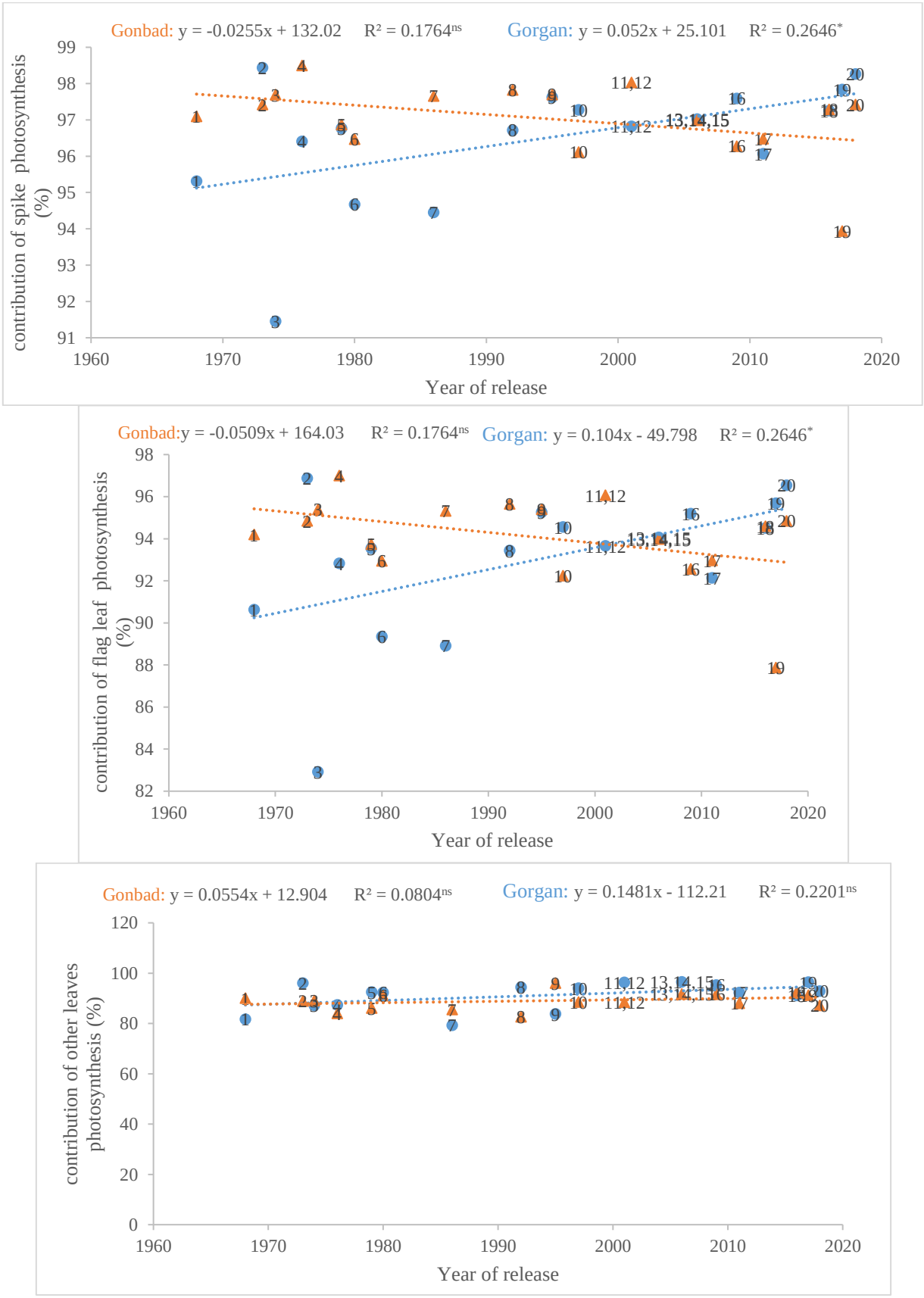

Figure 15- Liner regression equation between contribution of spike photosynthesis (a), contribution of flag leaf photosynthesis (b) and contribution of other leaves photosynthesis (c) against the year of release of 20 historically most important wheat cultivars released in Gorgan and Gonbad in the north climate of Iran during 1968–2018; 1=Inia, 2=Khazar1, 3=Moghan1, 4=Moghan2, 5=Alborz, 6=Kaveh, 7=Golestan, 8=Rasoul, 9=Tajan, 10=Shiroudi, 11=Milan, 12=Shanghai, 13=Arta, 14=Darya, 15=Moghan3, 16=Morvarid, 17=Gonbad, 18=Ehsan, 19=Tiregan, 20=Merag

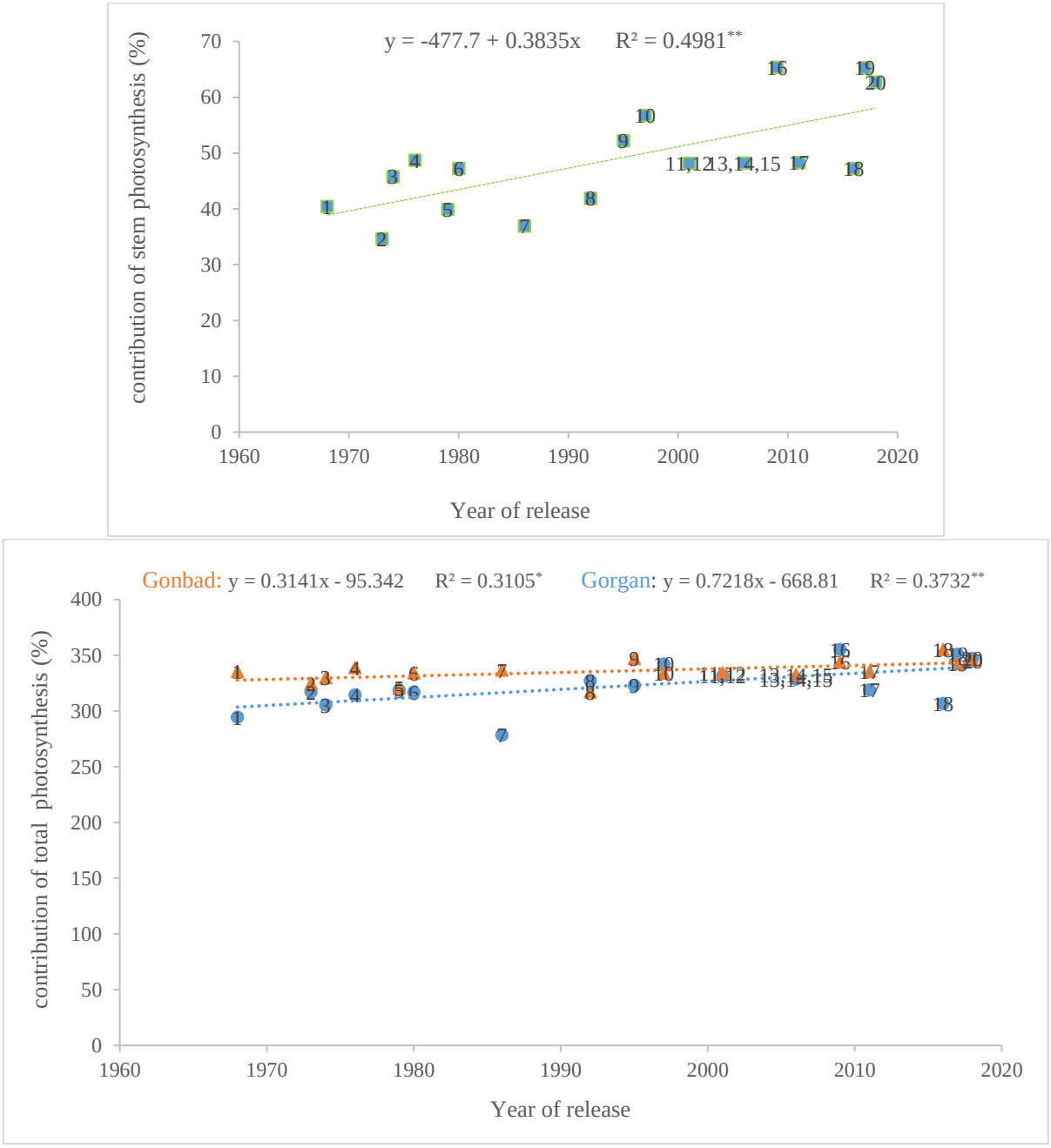

Figure 16- Liner regression equation between contribution of stem photosynthesis (a) and contribution of total photosynthesis (b) against the year of release of 20 historically most important wheat cultivars released in Gorgan and Gonbad in the north climate of Iran during 1968–2018; 1=Inia, 2=Khazar1, 3=Moghan1, 4=Moghan2, 5=Alborz, 6=Kaveh, 7=Golestan, 8=Rasoul, 9=Tajan, 10=Shiroudi, 11=Milan, 12=Shanghai, 13=Arta, 14=Darya, 15=Moghan3, 16=Morvarid, 17=Gonbad, 18=Ehsan, 19=Tiregan, 20=Merag

4. Discussion

In recent decades, the increase in wheat grain yield has decreased or even stopped. Meanwhile, increasing food production seems necessary due to the exponential growth of the population (Achilli et al. 2022). Awareness of the increase in the yield over the years due to the change of traits affecting it is necessary to understand the limiting factors of yield performance (Yadav et al. 2021). The source, sink and mobilization of assimilates are the three key factors that affect the formation of grain yield in wheat. The abundance of the source, the size of the sink and the unobstructed mobilization of assimilates increase the grain yield (Sun et al. 2021).

In this study, we investigated some morphological, phenological and physiological traits related to yield and its yield components in a set of cultivars released during the last 50 years in the warm and humid climate of northern Iran. For this purpose, field experiments were carried out in the Gorgan and Gonbad regions, the main wheat cultivation areas in the warm and humid northern climate of Iran. The results of our experiments showed that the morphological traits including PLH, PDL and

SPL did not show any significant changes during the years of cultivar release in the Gorgan and Gonbad regions. This is despite the fact that in a large number of previous studies, including those conducted in the temperate and cold climates of Iran, the results showed a decrease in the PLH of the new cultivars (Zand et al. 2002; Ant et al. 2013; Zarebayati et al. al., 2014; Alipour et al. 2019; Achilli et al. 2022; del Pozo et al. 2022; Yadav et al. 2021). The reason for not observing a significant trend in the trait of PLH in the northern climate may be the positive correlation of this trait with resistance to diseases such as FHB and foliar *Septoria*. The reason for this can be attributed to the proximity of the spikes of sensitive cultivars to the soil surface. Basically, genotypes with a PLH of less than 100 cm are closer to the plant remains on the soil surface, which increases the probability of contamination of the spikes and increases the sensitivity to the disease (Klar et al. 2007; Khodarahmi et al. 2023). It is likely that further PLH reduction in new cultivars will not occur in the future unless the correlation between PLH genes and *Fusarium* head blight resistance genes are broken by selection among numerous recombinant breeding lines made by the backcross method.

Rife et al. 2019 also reported a non-significant decreasing trend for the PLH of wheat cultivars released between 1992 and 2014 in the central plains.

The grain yield of cultivars released between 1968 and 2018 in the two regions of Gorgan and Gonbad showed a significant linear regression trend during the years of cultivar improvement and release. The yield increase of these cultivars was 30 kg/ha per year. The increase in biological yield, TKW and harvest index also had a significant linear trend in both regions, despite the increase in the S/M^2 and the number of grains per spike in both the regions, but none of these traits have had a significant progressive trend during the years of cultivar release. Increasing grain yield is the most important target of wheat breeding programs in the world, including Iran. The increase in annual bread wheat yield has been reported in many studies (Khodarahmi et al. 2023; Khan et al. 2022; Hanif et al. 2022; Yadav et al. 2021; Gerard et al. 2020; Rife et al. al. 2019). However, there is still a big gap between the demand and the annual genetic achievements of this crop in the world.

Grain yield in wheat is caused by the cumulative effects of its components, so identifying these components and their relationship with grain yield can be effective in selecting high-yielding cultivars (Tshikunde et al. 2019). The yield components in wheat include the number of grains per spike, the number of spikes per spike, the S/M^2 and TKW. Therefore, to increase grain yield, one or more of its components should be changed (Gibson & Paulsen 1999). Based on the results obtained in this study, there was a positive and significant correlation between YLD with the S/M^2 and TKW, which indicates the importance of selecting such traits for achieving genetic gain in grain yield during wheat breeding programs. Many other researchers have also reported an increase in yield and the yield components over the years of breeding wheat cultivars (Aisawi et al. 2015; Crespo-Herrera et al. 2018; Sadrjahani et al. 2017; Gerard et al. 2020; Yadav et al. 2021). It seems that the breeders in the Gorgan and Gonbad regions made their selection to increase the grain yield by increasing the TKW. The increase in TKW during a breeding process of cultivars had also been previously reported by Yao et al. (2019) and Yadav et al. (2021).

The number of grains per spike had an increasing but non-significant trend during the years of cultivar release. The correlation between this trait and YLD was positive and non-significant. Khodarahmi et al. (2023) and Alipour et al. (2019) also stated that the number of spike's grains did not have a significant change during the breeding programs, but the increase in the TKW had a significant trend in the breeding programs of the wheat cultivars in Iran, which may be due to a greater Farmers' tendency for choosing large grain wheats (with more TKW) for its better marketability.

The number of grains per spike is one of the traits affecting YLD (Esmailzadeh Moghadam et al. 2014; Khodarahmi & Vazan 2019; Qain et al. 2015; Tian et al. 2011; Philipp et al. 2018). Contrary to the results obtained in this study, Achilli et al. 2022 reported a significant increase in the number of grains per spike and no significant changes in TKW in the durum wheat cultivars released from 1934 to 2015.

The significant increasing trend of biological yield and harvest index in both the Gorgan and Gonbad regions can indicate the role of vegetative organs in increasing the photosynthesis or the remobilization of nutrients from these organs to the grain. The results obtained in this study are in accordance with the results obtained by Mróz et al. (2022), del Pozo et al. (2022), Hanif et al. (2021), Gao et al. (2017).

In wheat, an increase in a cultivar's yield depends on the increase in its biological yield while maintaining or improving its harvest index (Beche et al. 2014). Reynolds et al. (2011) and Blum (2016) believed that increasing biological performance in plants is the result of increasing the capacity or efficiency of photosynthesis. On the other hand, the yield of a crop is determined by the assimilates produced through photosynthesis in the grain filling stage, along with the mobilization of the assimilates from different parts of the plant before the flowering stage (Yang et al. 2022).

Contrary to the grain filling rate, which had a significant increase in both the Gorgan and Gonbad regions, the length of the grain filling period had a decreasing and non-significant trend, and the results obtained are in accordance with the results of Rahemi Karizaki et al. (2015). In contrast, Mróz et al. (2022) reported a significant increase in grain filling period in 20 wheat cultivars released since 1975 in Norway. The correlation between the SFP and yield was also non-significant ($r = 0.038$) and the correlation of grain filling rate with yield was positive and significant ($r = 0.510$). Attarbashi et al. (2001) also found a positive

and significant correlation between grain yield and grain filling rate and stated that the grain yield of wheat genotypes was not affected by the grain filling period.

In this study, when anthesis started from early to mid-April and grain filling took 6-7 weeks, the average temperature during grain filling was about 17-19 degrees Celsius. Milka et al. (2008) showed that each 1 °C increase in daily temperature above the optimum temperature for the grain filling, caused a decrease of approximately 2.8 mg in grain weight and 1.3 days during the grain filling period. Therefore, temperatures above the optimum range will eventually decrease the length of the grain filling period, despite the fact, high temperatures would increase the grain filling rate. In wheat, grain filling depends on three main sources: current assimilates produced by photosynthesis in leaves and stems, mobilization of stored carbohydrates and nitrogen-containing compounds in these organs and their subsequent remobilization to the spike and grains, and produced assimilates by the spike (Plaut et al. 2004; Kandić et al. 2023).

During the years of cultivars improvement, the contribution of remobilization decreased, which was significant for the total remobilization and that of and stem, but from the amount and efficiency of remobilization in the plant, the contribution of spike during the years of release of cultivars had a significant increasing trend. Under favorable conditions, remobilization can potentially contribute up to 20% of grain dry weight (Wardlaw & Willenbrink 2000). Although this ratio would increase significantly under drought conditions (Ehdaie et al. 2008).

For example, Zhang et al. (2011) showed that under water stress conditions, the contribution of spike and peduncle in grain weight was up to 73%. Sun et al. (2021) also reported an increase in remobilization from the spike during the breeding process of winter wheat cultivars from 1940 to 2010, but contrary to the results obtained in this study, these researchers stated that remobilization from the stem increased during the years of cultivar release which may be due to the reduction of the PLH in the cultivars investigated. One of the reasons for the decrease in the amount of stem remobilization in cultivars released in the northern climate of the country may be the lack of PLH reduction of cultivars in this region during the years of cultivar release, according to Austin et al. (1980) and Shearman et al. et al. (2005) carbohydrate remobilization from the stem of tall cultivars is less involved in the formation of grain yield as compared to the modern shorter cultivars with shorter stem height. Maydup et al. (2010) also stated that the contribution of stem in remobilization has decreased in modern cultivars.

The amount, efficiency and contribution of photosynthesis has been increasing during the years of cultivars improvement, and among the different parts of the plant, this increase has been significant for the spike and stem. Researchers believe that in C3 cereals, shoot (particularly the flag leaf) and the ear during grain filling play the main role as sources of assimilates (Sanchez-Bragado et al. 2014). Sun et al. (2021) also reported a significant increase in spike contribution in photosynthesis in eight winter wheat cultivars released between 1940 and 2010 in Shaanxi Province, China. The importance of participation of the green structure of wheat spikes in the filling of grains due to suitable light conditions for photosynthesis, a longer photosynthetic period after pollination compared to leaves and their availability to growing grains has been confirmed by many researchers (Maydupa et al. 2010).

Demotes-Mainard & Jeuffroy (2001) believe that wheat cultivars with larger and longer spikes have the ability to allocate more photosynthetic materials to grains as compared to those with smaller and shorter spikes. The contribution of spike photosynthesis in wheat varies from 10 to almost 80 percent of the materials absorbed in the grain depending on the cultivar and growing conditions (Maydup et al. 2010; Sanchez-Bragado et al. 2014; Rivera-Amado et al. 2020). Sanchez-Bragado et al. (2014) emphasized the increase of spike contribution in grain filling from 91 to 100% in native cultivars as compared to the increase from 49 to 82% in modern cultivars. According to the results of another research, under normal irrigation conditions, photosynthesis in spikes was much higher than one in flag leaves; whereas, photosynthesis in spikes decreased less than in one in flag leaves under water stress conditions (Abbad et al. 2004).

Based on the results of this study, the amount and contribution of photosynthesis of flag leaf had increased during the years of release of the cultivars in the Gorgan region. Sun et al. (2014) also reported an increase in flag leaf photosynthesis during the replacement of new breeding cultivars from 1940 to 2010 in Shaanxi Province, China.

5. Conclusions

The study of the genetic gain of the yield showed that the grain yield has increased from 3.854 t/ha in 1968 to 4.752 t/ha in 2018. The annual yield progress was estimated to be 30 kg/ha per year. It seems that the main reason for the genetic improvement in grain yield was the focus of the breeders on increasing the yield components, including the TKW and the S/M^2, without a significant increase in the number of grains per spike. Plant morphological traits had no significant role in increasing YLD in the past 50 years.

During the years of cultivar improvement, while the amount, efficiency and contribution of the remobilization decreased which were in particular significant for the total's and stem's remobilization, the amount, efficiency and contribution of photosynthesis increased during these years. Based on the results obtained from studying different parts of the plant, spike proved to be an important photosynthetic source for wheat through which remobilization showed a significant increase over the time of

wheat improvement. Therefore, achieving a higher level of genetic improvement/gain in yield requires more efficiency enhancement in the national crop improvement programs through wider uses of genetic diversity to incorporate novel alleles expressing higher amounts of yield, taking into account a more efficient photosynthetic and remobilization from spike, as well as applying new breeding approaches such as speed breeding and genomic selection.

References

Abbad H, Jaafari S E, Bort J & Araus J L (2004). Comparison of flag leaf and ear photosynthesis with biomass and grain yield of durum wheat under various water conditions and genotypes. Agronomie 24(1):19–28. https://doi.org/10.1051/agro:2003056

Achilli A L, Roncallo P F & Echenique V (2022). Genetic Gains in Grain Yield and Agronomic Traits of Argentinian Durum Wheat from 1934 to 2015. Agronomy 12(9):2151. https://doi.org/10.3390/agronomy12092151

Agricultural Statistics Booklet (2021). Volume I: Crop production. Ministry of Jihad-e-Keshavarzi. Office of Statistics and Information Technology. Available at: http://amar.maj.ir/Portal/Home/Default.aspx?CategoryID=117564e0-507c-4565-9659 fbabfb4acb9b

Aisawi K A B, Reynolds M P, Singh R P & Foulkes M J (2015). The physiological basis of the genetic progress in yield potential of CIMMYT spring wheat cultivars from 1966 to 2009. Crop science 55:1749–1764. https://doi.org/10.2135/cropsci2014.09.0601

Alipour H, Bihamta M R, Mohammadi V & Peyghmbari S A (2019). Trends in main agronomic traits and grain yield in wheat landraces and cultivars during the last decades in Iran. Iranian Journal of Crop Sciences 49(4): 125-136. https://doi.org/10.22059/ijfcs.2017.202331.654059

Ant Z, Ismailzadeh Moghadam M, Kashani A & Moradi F (2013). Trend of changes in grain yield and some physiological traits in spring bread wheat cultivars introduced in 1952 to 2008 in Iran. Seed and Plant Production Journal 29(4): 461-483. https://doi.org/10.22092/sppj.2017.110525

Austin R B, Morgan C L, Ford M A & Blackwell R D (1980). Contribution to grain yield from pre anthesis assimilation in tall and dwarf barley genotypes in two cotrasting seasons. Annals of Botany 45:309-314. https://doi.org/10.1093/oxfordjournals.aob.a085826

Bahrani A, Abad H H S, Sarvestani Z T, Moafpourian G H & Band A A (2011). Remobilization of dry matter in wheat: effects of nitrogen application and post-anthesis water deficit during grain filling. International Proceedings of Chemical, Biological and Environmental Engineering. https://doi.org/10.1080/01140671.2011.599397

Baral B R, Pande K R, Gaihre Y K, Baral K R, Sah S K, Thapa Y B & Singh U (2020). Increasing nitrogen use efficiency in rice through fertilizer application method under rainfed drought conditions in Nepal. Nutrient Cycling in Agroecosystems 118(1):103-114. https://doi.org/10.1007/s10705-020-10086-6.

Beche E, Benin G, Lemes C, Munaro L & Marchese J (2014). Genetic gain in yield and changes associated with physiological traits in Brazilian wheat during the 20th century. European Journal of Agronomy 61:49-59. https://doi.org/1010.1016/j.eja.2014.08.005

Blum A (2016). Osmotic adjustment is a prime drought stress adaptive engine in support of plant production. Plant. Cell 128:1-7. https://doi.org/10.1111/pce.12800

Cox MC, Qualset, CO & Rains, DW (1990). Genetic variation for nitrogen assimilation and translocation in wheat. III: nitrogen translocation in relation to grain yield and protein. Crop Science 26: 737 – 740. https://doi.org/10.2135/cropsci1986.0011183X002600040022x

Crespo-Herrera LA, Crossa J, Huerta-Espino J, Vargas M, Mondal S, Velu G, Payne TS, Braun H & Singh RP (2018). Genetic gains for grain yield in CIMMYT's semi-arid wheat yield trials grown in suboptimal environments. Crop Science 58:1890– 1898. https://doi.org/10.2135/cropsci2018.01.0017

del Pozo A, Jobet C, Matus I, Méndez-Espinoza A M, Garriga M, Castillo D & Elazab A (2022). Genetic Yield Gains and Changes in Morphophysiological-Related Traits of Winter Wheat in Southern Chilean High-Yielding Environments. Front Plant Science 12:732988. https://doi: 10.3389/fpls.2021.732988

Demotes-Mainard S & Jeuffroy M H (2001). Partioning of dry matter and nitrogen to the spike growth period in wheat crops subjected to nitrogen deficiency. Field Crops Res. 70: 153-165. https://doi.org/10.1016/S0378-4290(01)00133-2

Ehdaie B, Alloush G A & Waines J G (2008). Genotypic variation in linear rate of grain growth and contribution of stem reserves to grain yield in wheat. Field Crops Research 106:34–43. https://doi.org/10.1016/j.fcr.2007.10.012

FAO organization (2021) FAOSTAT Online Statistical Service. Rome: FAO. Available online at: http://apps.fao.org

Gao F, Ma D, Yin G, Rasheed A, Dong Y, Xiao Y, Xia X, Wu X, He Z (2017). Genetic progress in grain yield and physiological traits in Chinese wheat cultivars of southern Yellow and Huai Valley since 1950. Crop Science 57:760–773. https://doi.org/10.2135/cropsci2016.05.0362

Gerard G S, Crespo-Herrera L A, Crossa J, Mondal S, Velu G, Juliana P, Huerta-Espino J, Vargas M, Rhandawa M S, Bhavani S, Braun H & Singh R P (2020). Grain yield genetic gains and changes in physiological related traits for CIMMYT's high rainfall wheat screening nursery tested across international environments. Field Crops Research 249: 107742. https://doi.org/10.1016/j.fcr.2020.107742

Gibson L R & Paulsen G M (1999). Yield components of wheat grown under high temperature stress during reproductive growth. Science 39:1841–1846. https://doi.org/10.2135/cropsci1999.3961841x

Hanif U, Gul A, Amir R, Munir F, Sorrells M E, Gauch H G, Mahmood Z, Subhani A, Imtiaz M, Alipour H, Rasheed A & He Z (2022). Genetic gain and G×E interaction in bread wheat cultivars representing 105 years of breeding in Pakistan. Crop Science 62 (1):178. https://doi.org/10.1002/csc2.20655

Kandić V, Savić J, Rančić D & Dodig D (2023) Contribution of Agro-Physiological and Morpho-Anatomical Traits to Grain Yield of Wheat Genotypes under Post-Anthesis Stress Induced by Defoliation. Agriculture 13(3):673. https://doi.org/10.3390/agriculture13030673

Khan H, Krishnappa G, Kumar S, Nath Mishra C, Parkash O, Rathore A, Rani Das R, Yadav R, Krishna H, Parkash Bishnoi O, Singh Sohu V, Sendhil R, Singh Yadav S, Singh G & Pratap Singh G (2022). Genetic gains in grain yield in wheat (*Triticum aestivum* L.) cultivars developed from 1965 to 2020 for irrigated production conditions of northwestern plains zone of India. Cereal Research Communication https://doi.org/10.1007/s42976-022-00293-y

Khodarahmi M, Soughi H, Shahbazi K Jafarby J & Khavarinejad MS (2023). Trends in important agronomic traits, grain yield and its components in bread wheat cultivars released in northern warm and humid climate of Iran, 1968–2018. Cereal Research Communication 1-12. https://doi.org/10.1007/s42976-023-00353-x

Maydup M L, Antonietta M, Guiamet J J, Graciano C, López J R & Tambussi E A (2010). The contribution of ear photosynthesis to grain filling in bread wheat (*Triticum aestivum* L.). Field Crop Research 119:48–58. https://doi.org/10.1016/j.fcr.2010.06.014

Milka D B, Marija M, Balalic K & Kobiljski B D (2008). The parameters of grain filling and yield components in common wheat (triticum aestivum l) and durum wheat (*triticum turgidum* l. *Var Durum).* Central European Journal of Biology 3:75–82. https://doi.org/10.2478/s11535-007-0050-x

Mróz T, Dieseth JA & Lillemo M (2022). Historical grain yield genetic gains in Norwegian spring wheat under contrasting fertilization regimes. Crop Science 62(3):997-1010. https://doi.org/10.1002/csc2.20714

Papakosta D K & Gayians A A (1991). Nitrogen and dry matter accumulation, remobilization and losses for Mediterranean wheat during grain filling. Agronomy Journal 83: 864 – 870. https://doi.org/10.2134/agronj1991.00021962008300050018x

Philipp N, Weichert H, Bohra U, Weschke W, Schulthess A W & Weber H (2018). Grain number and grain yield distribution along the spike remain stable despite breeding for high yield in winter wheat. PLoS One 10: 13(10): e0205452. https://doi.org/10.1371/journal.pone.0205452

Plaut Z, Butow B J, Blumenthal C S & Wrigley C W (2004). Transport of dry matter into developing wheat kernels and its contribution to grain yield under post-anthesis water deficit and elevated temperature. Field Crops Research 86:185–198. https://doi.org/10.1016/j.fcr.2003.08.005

Rahemi Karizaki A, Galeshi S & Soltani A (2015). Evaluation of improvement of rate and duration of grain filling duration inbreeding processes in wheat cultivars. Journal of Plant Production 22 (1): 23-38. https://doi.org/20.1001.1.23222050.1394.22.1.2.9

Reynolds M, Bonnett D, Chapman SC, Furbank R T, Manès Y, Mather D E & Parry M A J (2011). Raising yield potential of wheat. I. Overview of a consortium approach and breeding strategies. Journal of Experimental Botany 62:439–452. https://doi.org/10.1093/jxb/erq311

Rife T W, Graybosch R A & Poland J A (2019). A field-based analysis of genetic improvement for grain yield in winter wheat cultivars developed in the us central plains from 1992 to 2014. Crop Science 59:905–910. https://doi.org/10.2135/cropsci2018.01.0073

Rivera-Amado C, Molero G, Trujillo-Negrellos E, Reynolds M & Foulkes J (2020) Estimating Organ Contribution to Grain Filling and Potential for Source Upregulation in Wheat Cultivars with a Contrasting Source–Sink Balance. Agronomy 10(10):1527. https://doi.org/10.3390/agronomy10101527

Sadrjahani S, Esmaeilzadeh Moghaddam M, Nemati N, Bloorian M & Norzad AR (2017). Evaluation of trend changes in grain yield and characteristics physiology in 15 varietie facultative and winter bread wheat. Agronomic Research in Semi Desert Regions 15(1):35-53.

Sanchez-Bragado R, Molero G, Reynolds M P & Araus J L (2014). Relative contribution of shoot and ear photosynthesis to grain filling in wheat under good agronomical conditions assessed by differential organ 13C. Journal of Experimental Botany 65:5401–5413. https://doi.org/10.1093/jxb/eru298.

Shearman V J, Sylvester-Bradley R, Scott R K &Foulkes M J (2005). Physiological processes associated with wheat yield progress in the UK. Crop Science 45:175-185. https://doi.org/10.2135/cropsci2005.0175a

Sun Y, Wang X, Wang N, Chen Y & Zhang S (2014). Changes in the yield and associated photosynthetic traits of dry-land winter wheat (*Triticum aestivum* L.) from the 1940s to the 2010s in Shaanxi Province of China. Field Crops Research 167:1–10. https://doi.org/10.1016/j.fcr.2014.07.002

Sun Y, Zhang S & Yan J (2021). Contribution of green organs to grain weight in dryland wheat from the 1940s to the 2010s in Shaanxi Province, China. Scientific Reports 11: 3377. https://doi.org/10.1038/s41598-021-82718-y

Tadesse W, Sanchez-Garcia M, Gizaw Assefa S, Amri A, Bishaw Z, Ogbonnaya FC & Baum M (2019). Genetic Gains in Wheat Breeding and Its Role in Feeding the World. Crop Breeding,Genetics and Genomics 1:e190005. https://doi.org/10.20900/cbgg20190005

Tshikunde N, Mashilo J, Shimelis H & Odindo A (2019). Agronomic and physiological traits and associated quantitative trait loci (QTL) affecting yield response in wheat (*Triticum aestivum* L.): a review. Front Plant Science 10:1428. https://doi.org/10.3389/fpls.2019.01428

Wardlaw IF & Willenbrink J (2000). Mobilization of fructan reserves and changes in enzyme activities in wheat stems correlate with water stress during kernel filling. New Phytologist 148:413–422. https://doi.org/10.1046/j.1469-8137.2000.00777.x

Yadav R, Gupta S, Gaikwad K B, Bainsla N K, Kumar M, Babu P, Ansari R, Dhar N, Dharmateja P & Prasad R (2021) Genetic Gain in Yield and Associated Changes in Agronomic Traits in Wheat Cultivars Developed Between 1900 and 2016 for Irrigated Ecosystems of Northwestern Plain Zone of India. Frontiers in Plant Science 12: 719394. https://doi.org/10.3389/fpls.2021.719394

Yang J, Shi W, Xiao G, Zhang X, Wang D, Xu H, Wu J, Yang Z, Lai Y, Duan M & Zhang J (2022). Optimum total nitrogen application is required to reduce the yield loss of hybrid rice to high temperature, Field Crops Research 288: 108696. https://doi.org/10.1016/j.fcr.2022.108696.

Yao Y, Lv L, Zhang L, Yao H, Dong Z, Zhang J, Ji J, Jia X & Wang H (2019). Genetic gains in grain yield and physiological traits of winter wheat in Hebei Province of China, from 1964 to 2007. Field Crops Research 239: 114–123. https://doi.org/10.1016/j.fcr.2019.03.011

Zand E, Kouchaki A, Rahimian Mashhadi H & Nasiri Mahallati M (2002). Study of 50-year changes in morphological and physiological characteristics of some Iranian wheat. Agricultural sciences and industries 16(1): 161-171.

Zarebayati A, Khodarahmi M & Mostavavi K (2014) Genetic gain of agronomic traits of bread wheat cultivars released for cold regions of Iran from 1930 to 2010. 13th Iranian Conference on Crop Science and Plant Breeding and 3rd Iranian Conference on Seed Science and Technology. Karaj. Iran.

Zhang Y, Zhang Y, Wang Z & Wang Z (2011). Characteristics of canopy structure and contributions of non-leaf organs to yield in winter wheat under different irrigated conditions. Field Crops Research. 123:187–195. https://doi.org/10.1016/j.fcr.2011.04.014

Journal of Agricultural Sciences
(Tarim Bilimleri Dergisi)

J Agr Sci-Tarim Bili
e-ISSN: 2148-9297
jas.ankara.edu.tr

JAS

Effects of Four Different Media from Selected Agricultural Wastes on the Total Production and Nutrient Profile of Vermicompost

Damrongrak Issariyaporn[a], Huck Ywih Ch'ng[b*], On-thong Jumpen[c]

[a]*Faculty of Science Technology and Agriculture, Yala Rajabhat University, Yala, 95000 THAILAND*

[b]*Faculty of Agro-Based Industry, University Malaysia Kelantan Jeli Campus, 17600 Jeli, Kelantan MALAYSIA*

[c]*Faculty of Natural Resources, Prince of Songkhla University, Hat Yai, Songkhla, 90110 THAILAND*

ARTICLE INFO

Research Article

Corresponding Author: Huck Ywih Ch'ng, E-mail: huckywih@umk.edu.my

Received: 25 June 2024 / Revised: 05 September 2024 / Accepted: 10 October 2024 / Online: 25 March 2025

Cite this article

Issariyaporn D, Ch'ng HY, Jumpen O (2005). Effects of Four Different Media from Selected Agricultural Wastes on the Total Production and Nutrient Profile of Vermicompost. *Journal of Agricultural Sciences (Tarim Bilimleri Dergisi),* 31(2):280-287. DOI: 10.15832/ankutbd.1504615

ABSTRACT

Large volumes of agricultural waste and residue are produced by agricultural activities in the tropics annually. Burning is still a common method of disposal, although it pollutes the environment. Vermicomposting is an alternate technique for managing agricultural waste. This study was conducted to ascertain the yield and particular chemical characteristics of vermicompost produced by earthworm breeding in various agricultural wastes. Agricultural waste including mushroom culture by-products, cow dung, oil palm branch residue, and sugarcane bagasse were used as raising base of African Nightcrawler earthworms (*Eudrillus eugeniae*). The completed vermicompost yields and selected chemical properties were determined. Earthworms in cow dung produced the maximum amount of vermicompost in terms of dry weight, followed by those in mushroom culture by-products, oil palm branch residue, and bagasse. The largest amounts of humic acid, nitrogen (N), and potassium (K) were found in vermicompost from cow dung. The maximum electrical conductivity (EC), organic matter, magnesium (Mg), and manganese (Mn) were found in vermicompost from oil palm branch residue. Bagasse vermicompost had the greatest pH, phosphorus (P), iron (Fe), zinc (Zn), and copper (Cu) values. Vermicompost derived from different feedstocks will produce different total nutrients contents and vermicompost quality. As a result, cow dung is recommended to be used as the primary material and mixed with specific other agricultural waste products as raising base materials to generate high grade vermicompost.

Keywords: Vermicompost, Nutrient Profile, Mushroom Culture By Product, Cow Dung, Oil Palm Branch Residue, Bagasse

1. Introduction

Vermicompost is defined as peat-like, finely broken-down materials produced by a non-thermophilic process that involves the biodegradation and stabilization of organic materials through interactions between earthworms and microorganisms. Utilizing specific earthworm species might fasten the conversion of organic waste and result in a better-quality end product (Ndegwa & Thompson 2001). Within 30 days, 5 kg of worms or an estimated 10 000 worms) can convert around 1 tonne of garbage into vermicompost at the optimal temperature (20–30 °C) and moisture (60–70%) (Singh et al. 2008; Joshi et al. 2013). The plants receive essential nutrients from the vermicompost in a form that they can readily absorb (Wang et al. 2017). Vermiculture is therefore considered a practice that may benefit both soil health and agricultural productivity.

Vermicompost has been shown to benefit a variety of crops, including vegetables, grains, legumes, flowering plants, and field crops (Atiyeh et al. 2000; Blouin et al. 2019). Vermicompost is said to have a much higher nutritional content and bioavailability than composts made under traditional thermophilic conditions (Lazcano et al. 2009; Joshi et al. 2013). Vermicompost use as organic fertilizer significantly improved crop production, soil physico-chemical characteristics, and microbial biological activity (Rekha et al. 2018). In addition to being nutrient-rich, vermicompost also has high-quality humus, plant growth hormones, enzymes, and compounds that can shield plants from pests and diseases (Dhanuja et al. 2020).

Vermicompost can be created from a variety of agricultural wastes, including straw, husk, leaves, stalks, weeds, and more. In addition to the more popular aeration composting, the digestive system of an earthworm may also compost manures such those from cows, goats, and sheep. The source of the raw materials used as bedding and feed, as well as the type of earthworm used, affect the amount of nutrients in vermicompost (Bisen et al. 2011; Manaig 2016; Hitinayake et al. 2018; Zarei et al. 2018;). Using diverse earth worm species (*Eisenia fetida* and local collections), vermicomposting of

various feedstocks in Ethiopia, such as sorghum straw, tef straw, industrial waste, fruit waste, and khat waste, demonstrated difference amongst earthworms for their reproduction and vermicast production.

There are significant amounts of agricultural residues and trash produced by agricultural activities such as the production of plants and animals as well as in the agroindustry. According to a report by Prasertsan & Sajjakulnukit (2006), Thailand produced 28 026 711 and 4 099 859 metric tonnes of bagasse and oil palm branch residue, respectively, while 13 998 196 and 19 005 628.14 metric tonnes of waste from animal manure and rice straw were produced, respectively. Additionally, one of the agricultural wastes that is widely distributed and is burned to prevent excessive accumulation is rice residues like rice husk and straw. In order to maintain good soil for high fertility, a high content of organic matter in the soil must be maintained.

One promising management approach is to convert the agricultural wastes into a vermicompost. Vermicomposting is able to decompose residues that are difficult to decompose such as mushroom culture by-products in which the main constituents are sawdust, bagasse, oil palm branch residue and so on. Besides, converting such residues by conventional composting process is very time consuming. Vermicompost contains considerable levels of organic carbon, nitrates, phosphates, exchangeable calcium, and other vital plant nutrients (Lim et al. 2015; Song et al. 2015). Vermicompost typically has notable positive benefits on plant growth, according to most of these studies. However, there have been very few experimental investigations exploring effects of different media on the total production and nutrient profile of vermicompost. Hence, the objective of this research was to investigate the yield and selected chemical properties of vermicompost produced by African Nightcrawler earthworms (*Eudrillus eugeniae*) raised in various materials, namely mushroom culture by-products (MBP), oil palm branch residue (OP), and sugarcane bagasse (B) as the raising base materials in comparison to using cow dung (CD).

2. Material and Methods

2.1 Sampling and preparation of MBP, CD, OP, and B

Dry CD and MBP were collected from the animal farm and mushroom houses in Mealand Agricultural Center, Rajabahat Yala University, Thailand. Sugarcane bagasse was collected from sugarcane juicing sites around the suburban areas of Yala province, Thailand. The OP was collected from palm oil mill factories in Pattani province, Thailand. Total N, P, K, Ca, Mg, Fe, Mn, Zn, and Cu of the aforementioned samples were analyzed by standard methods described in Section 3 of Materials and Methods. These materials were allowed to decompose under shading for one month.

2.2 Medium preparation and earthworm raising

The earthworm raising base materials was prepared by mixing pre-decomposed materials with loamy soil at a ratio of 9:1, based on volume basis (v/v). The loamy soil mixed with these organic materials have the following chemical properties: pH value of 7.3 (1:1 soil: water), 4.60% organic matter, 0.23% total N, 58 mg/kg available P, and 148 mg/kg exchangeable K. Water was added to raise the moisture to around 60% of the water holding capacity. The materials were placed into round black plastic containers (27 cm in diameter and 23 cm in height) which have small holes for drainage and aeration. Before putting in the raising base material, the hole was closed with small plastic net. After two weeks of incubation under shading, a total of 60 individual mature African Nightcrawler earthworms (*Eudrillus eugeniae*) were embedded onto the surface of the media which consists of four different raising base materials. The earthworms were fed with cucumber, Chinese cabbage, and convolvulus. The moisture content of the media was monitored and maintained at an appropriate level. The experiment consisted of 4 treatments, namely MBP, CD, OP, and B. Each treatment was replicated with 5 replications.

2.3 Vermicompost collection and analysis of selected chemical properties and total nutrients

Vermicompost from each experimental unit was collected on the 60th day. During collection, the fresh weight from each experimental unit was recorded. After that, the vermicompost from each experimental unit were air dried for two weeks, and the dry weight was determined after constant weight was attained for each experimental unit. Next, the air-dried vermicompost from each experimental unit was ground with a mortar. The pH and electrical conductivity (EC), humic acid, organic matter and total carbon (C) were determined by using a pH and EC meter (1:5 vermicompost: water) (Tan 2016), gravimetric analysis (Tan 2014), and the Walkley and Black method (Walkley & Black 1934; Tan 2016), respectively.

Plant nutrients in the total form was analyzed. The total N was determined by the Micro Kjeldahl method (Tan 2016). After the determination of total C and total N, C:N ratio values were calculated. Other elements were determined after wet digestion of the vermicompost by an acidic mixture of nitric and perchloric (5:1v/v). Total P was detected with the molybdate blue method and total K with a flame photometer, whereas total Ca, Mg, Fe, Mn, Zn, and Cu were detected with an Atomic Absorption Spectrophotometer (Tan 2016).

2.4 Data analysis

The total dry weight of the finished vermicomposts, as well as the selected chemical properties and total nutrients in the vermicomposts from all treatments were subjected to Analysis of Variance (ANOVA) to detect the treatment effects, and the means were separated by using Duncan's Multiple Range Test (DMRT) at P≤0.05.

3. Results and Discussions

3.1 Dry weight of finished vermicomposts produced under different raising base materials

Earthworms in CD generated the significant highest dry weight of vermicompost followed by those in MBP, OP and B. Their dry weights were 744.58, 387.58, 270.05, and 14.27 g, respectively. The dry weights were significantly different among treatments (P≤0.05) (Figure 1). The earthworms raised in CD produced similar amounts of vermicompost to that of earthworms raised in composted fresh plant in a study by Nuchnoon et al. (2017). Sirithanakorn et al. (2014) reported that earthworms (*Eudrilus eugeniae*) raised in CD produce egg sacks, new earthworms, and increase the weight of vermicompost compared to those raised in composted water lily, composted banana leaf sheet, and coco-peat. Vodounnou et al. (2016) also revealed that earthworms (*Eisenia fetida*) raised in cow dung had the best growth rate and could produce new earthworms followed by pig, rabbit, poultry and sheep dung.

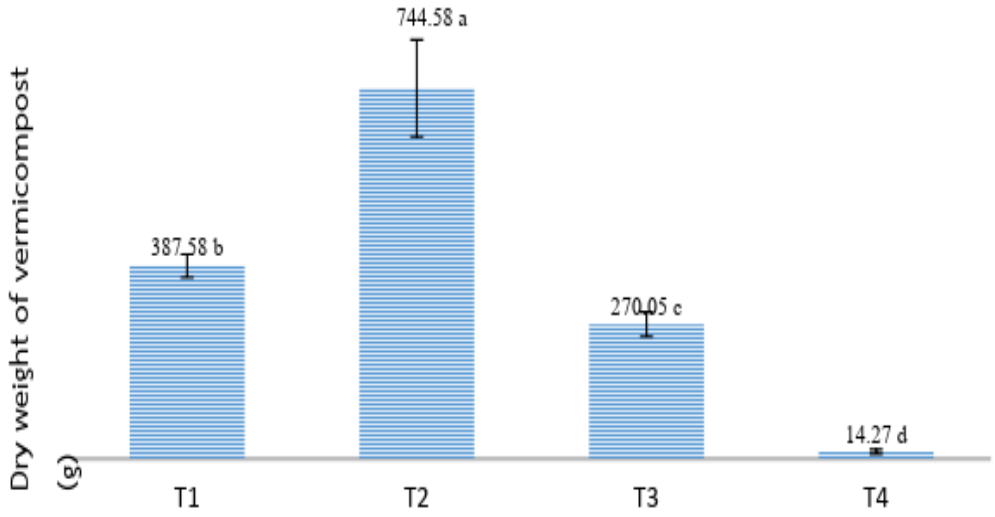

Figure 1- Dry weight of finished vermicomposts produced under different raising base materials.
Means between columns with different letter(s) indicate significant difference between treatments by Duncan Multiple Range Test at P≤0.05. Bars represent the mean values ± standard error

The B treatment yielded the least vermicompost, because the very hard texture was difficult to consume by the earthworms. Normally, earthworms eat decayed or rotten organic materials. Thus, it is better to allow more time for the pre-decomposition process to allow the material to properly decay before using for this purpose. The other advantage of pre-decomposition is to improve the vermicompost quality by killing pathogens *via* heat from the composting process (Ndegwa & Thomson 2001). The vermicompost produced from African Nightcrawler raised in CD bedding was darker in color and softer in texture than those in other bedding materials. Vermicomposts from MBP and OP showed dark brown in color and a little bit hard granule (figure 2)

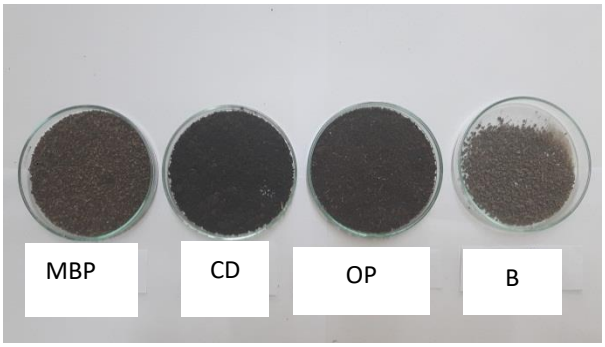

Figure 2- Vermicomposts from different raising base materials

3.2 Chemical properties of finished vermicomposts produced from different raising base materials

Vermicompost from B and CD showed significantly higher pH than those of MBP and OP. The pH level is one of the indices for assessing the vermicompost quality. The pH range of all the produced vermicomposts was between 6.33 and 7.65. When organic matter is broken down by microorganisms during vermicomposting, organic acids are produced, which causes the pH to change to almost neutral (Das et al. 2012). The increase in the vermicomposts pH also could be due to the earthworm's calciferous glands in the internal digestive track which secrete calcium carbonate ($CaCO_3$) to eliminate carbon dioxide (CO_2) produced from breathing (Dores-Silva et al. 2014). Additionally, the elevated pH during the vermicomposting process may be caused by the primary substrate's increased mineral N content. The release of their nitrogen content as ammonia volatilization during the vermicomposting process resulted in an elevation in pH in these beds with regard to the brief period of decomposition of bigger molecules such proteins, amino acids, and lipids. The results in this study corroborate with those of Sodaei et al. (2007) and Velasco-Velasco et al. (2011).

In terms of EC, vermicompost from OP showed the significant highest EC (985.33 µS/cm). The EC of vermicomposts from other raising base materials were not significantly different. The findings show that all of the vermicompost samples had salinity levels below 2 dS/m, indicating that they are appropriate for application to crop cultivation without endangering the soil and plants (Ofusu-Budu et al. 2010). This result could be explained by the simpler leaching in vermicompost and, to a lesser extent, by the ion consumption and buildup in the earthworm biomass (Rahman et al. 2017).

Vermicompost from CD yielded the highest amount of humic acid (45.86%) followed by those from MBP (34.26%), OP (25.47%), and B (12.53%). This might be as a result of the earthworms' greatest capacity to digest cow dung in comparison to other materials, which are more difficult to do since they contain lignin. According to Malherbe & Cloete (2002), the lignin portion of lignocellulose, which is the most resistant to biodegradation, is the reason why it is difficult to degrade lignocellulose during composting. This polymer's composition affects both its own decomposition and the decomposition of hemicelluloses in addition to determining how quickly it breaks down. Biodegradation is challenging because of the structural and macromolecular features of lignin, especially when the lignin content is high (generally greater than 20%) (Vikman et al. 2002). In the study by Vichaivit et al. (2012), the humic acid was equivalent to vermicomposts made from pig manure and peat coir mixtures in the ratio of 1:1 v/v fed with various kinds of fresh organic materials such plant leaves, fruit peels, tubers, and food scraps. Organic matter and total C in the OP vermicompost was significantly higher than CD, MBP, and B vermicomposts. The values were much lower than that of the standard organic fertilizer criteria of 30% announced by the Department of Agriculture, Ministry of Agriculture and Cooperatives, Thailand (Table 1). This could be due to the higher rate of decomposition facilitated by the earthworms. Earthworms consume the organic material while microbial degradation occurs during the vermicomposting process. Table 1 shows that MBP, CD, and B vermicomposts had lower percentages of total C than OP vermicompost, indicating that earthworms hastened the decomposition of the organic matter, which had less lignin than oil palm branch debris. Since carbon is a significant component of organic molecules, the foundation of all living things, these molecules are also the source of energy for the composting process (Ansari & Sukhraj 2010).

Table 1- Selected chemical properties of finished vermicomposts produced from different raising base materials

Raising base materials	*pH (1:5, V:water)*	*EC (1:5, V:water) (µS/cm)*	*Humic acid (%)*	*Organic matter (%)*	*Total C (%)*	*C:N ratio*
MBP	6.51^{b}	384.00^{b}	34.26^{b}	7.54^{b}	4.37^{b}	6.1:1^{a}
CD	7.44^{a}	451.00^{b}	45.86^{a}	5.56^{b}	3.21^{b}	2.5:1^{b}
OP	6.33^{b}	985.33^{a}	25.47^{c}	9.14^{a}	5.30^{a}	4.4:1^{a}
B	7.65^{a}	491.00^{b}	12.53^{d}	6.94^{b}	4.03^{b}	7.75:1^{a}

Means within column with different letter(s) indicate significant difference between treatments by Duncan Multiple Range Test at P≤0.05

In terms of C:N ratio, the values for all vermicomposts from four different raising base materials were below 20 (Table 1). The C:N ratio, one of the most commonly used indices of the maturity of organic waste, decreased during the vermicomposting process, which was acceptable according to Dominguez and Edwards (2011). The rapid decomposition of organic waste, as well as the mineralization and stabilisation throughout the vermicomposting process, caused the drop in the C:N ratio (Kaushik & Garg 2003). According to Majlessi et al. (2012), organic waste has reached an advanced stage of maturation when the C:N ratio falls to less than 20. The reduction of substrate's C:N value is due to nitrogenous excretion and microbial respiration during the decomposition process (Solis-Mejia et al. 2012).

3.3 Macronutrients and micronutrients of raw feedstocks and finished vermicomposts produced from different raising base materials

The total N in the raw feedstock was the highest (2.33%) in OP, followed by CD (1.76%), MBP (0.43%), and B (0.28%) (Figure 3). The total N in the finished vermicomposts from CD (1.26%) and OP (1.20%) were not significantly different, and both were distinctly higher than in those from MBP (0.72%) and B (0.52%) (Figure 3). The higher amounts of N in vermicomposts from

CD and OP may be caused by the reduction of organic matter, mineralization of organic compounds including protein and amino acids that contain N, and conversion of ammonia-N to nitrate-N (Pramanik et al. 2007). The N level of the vermicomposts from CD and OP might be due to mucus release, nitrogen-containing compounds, growth-stimulating hormones, and enzymes generated by earthworms (Tripathi et al. 2015). In comparison to Warma & Anglopez (2002) and Suthar (2006), the outcomes of the current investigation were relatively less significant. The final N content in the vermicomposts mostly depended on the starting N in the raw feedstock and the degree of decomposition. The total N concentration in the completed vermicomposts (Figure 3) was lower than the total N concentrations in the raw feedstock, which may be related to the rise in pH in the vermicomposts (Table 1) and the N lost by ammonia volatilization (Figure 3). As observed in Figure 3, the total P in the raw feedstock was 0.44%, 0.39%, 0.35%, and 0.15% in B, OP, CD, and MBP, respectively.

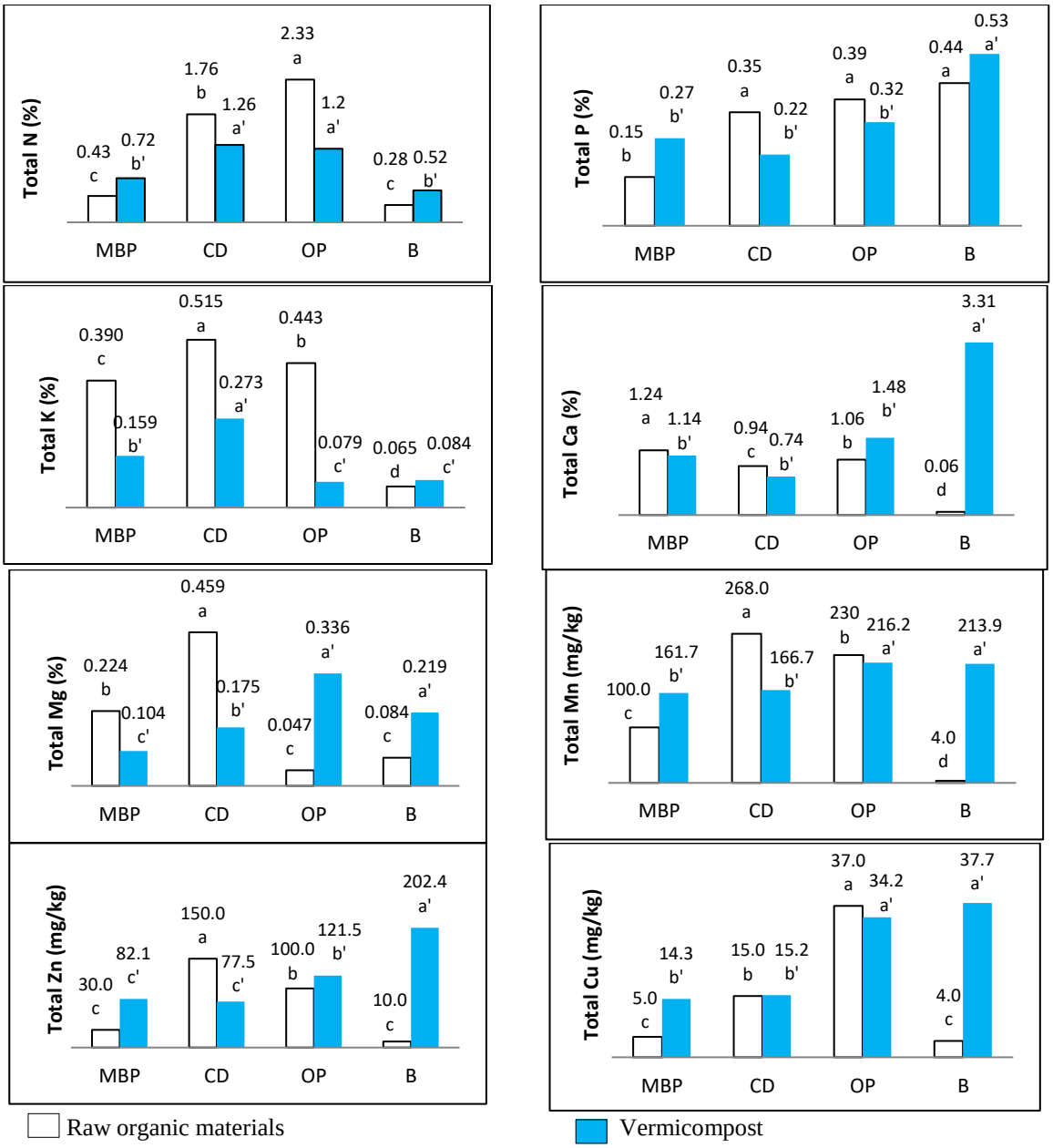

Figure 3- Comparison of total macronutrients and micronutrients between raw feedstock and finished vermicomposts produced from different raisin base materials. Means between columns with different letter(s) indicate significant difference between treatments by Duncan's Multiple Range Test (DMRT) at P≤0.05

The total P in the finished vermicompost from B (0.53%) was significantly higher than that in OP (0.32%), MBP (0.27%), and CD (0.32%) (Figure 3). The total P content in the finished B and MBP vermicompost varied between 0.27% and 0.53%, which was higher than in the raw feedstock. The primary process for the solubilization of insoluble P is the generation of acid by microbes during the decomposition of organic waste. Additionally, the earthworm gut's phosphatases and P-solubilizing bacteria found in the worm casts both contribute to the release of accessible P content from organic waste during vermicomposting, converting P into forms that are more bio-available to plants (Goswami et al. 2013).

As seen in Figure 3, the total K in the raw feedstock was 0.515%, 0.443%, 0.390%, and 0.065% in CD, OP, MBP, and B, respectively (Figure 3). The total K in finished CD vermicompost (0.273%) was significantly higher than those from the other organic materials (Figure 3). The total K in OP vermicompost (0.079%) and from B (0.084%) were not significantly different. Greater enzymatic and bacterial activity in the earthworm's digestive system results in increased mineralization of organic compounds containing K and other elements, as seen by the increased total K in vermicomposts (Garg et al. 2006). The primary cause causing an elevated K level during the vermicomposting process was the earthworm's intestine's rich bacteria (Pramanik et al. 2007).

Figure 3 displays that the total Ca in the raw feedstock was 1.24%, 1.06%, 0.94%, and 0.06% in MBP, OP, CD, and B, respectively. Vermicompost produced from B had Ca levels that were noticeably greater (3.31%) than those from other treatments (Figure 3). The increased level of inorganic C in the vermicompost was predominantly caused by gastrointestinal mechanisms connected to calcium metabolism (Suthar 2008). The total Mg in the raw feedstock was 0.459%, 0.224%, 0.084%, and 0.047% in CD, MBP, B, and OP, respectively (Figure 3). The total Mg in OP vermicompost (0.336%) and B vermicompost (0.219%) were significantly higher than those from MBP (0.104 %) and CD (0.175 %) vermicomposts (Figure 3).

Total N-P_2O_5-K_2O of MBP, CD, OP and B vermicompost were 0.72-0.62-0.19, 1.26-0.50-0.33, 1.20-0.73-0.10, and 0.52-1.21-0.10, respectively. Overall, the macronutrient values reported in this study were lower than the organic fertilizer quality criteria announced by the Department of Agriculture, Ministry of Agriculture and Cooperatives, Thailand (Total N $\geq$ 1, $P_2O_5 \geq$ 0.5, $K_2O \geq$ 0.5% w/w). Thus, it should be further studied for enrichment of primary plant nutrients, especially K_2O. Cassava peels may be an interesting material that yields a high amount of total K after digestion by *Eisenia fetida* (Saravanan & Wesely 2018).

The amount of total micronutrients in the raw feedstock and finished vermicomposts produced from different raising base materials are presented in Figure 3. Total Mn concentrations in all vermicomposts were not significantly different they showed in the range of 161.68-216.21 mg/kg. The B vermicompost showed the highest concentration of total Zn (202.38 mg/kg), followed by that of OP (121.53 mg/kg), MBP (82.13 mg/kg), and CD (77.46 mg/kg). The total Zn concentration in OP was significantly higher than those in other vermicomposts. On the other hand, total Zn concentration in the vermicompost from MBP and CD were not significantly difference. The B and OP vermcomposts showed the highest concentration of total Cu (37.73 mg/kg and 34.20 mg/kg, respectively) (Figure 3). Earlier studies reported values 2.00–37.70 mg/kg for Cu, 5.70–120.00 mg/kg for Zn and 10.00–105.00 mg/kg for Mn (Chaudhuri et al. 2000; Kitturmath et al. 2007; Giraddi 2007; 2011; Waseem et al. 2013). According to Dominguez & Edwards (2011), vermicompost typically contains adequate amounts of micronutrients, which have been substantiated by our results for total Fe, Mn, Zn, and Cu concentrations in the finished CD, MBP, B, and OP vermicomposts.

4. Conclusions

The vermicompost produced by African Nightcrawler earthworms (*Eudillus eugeniae*) raised in CD gave significant higher dry weight. The vermicompost from CD also had a neutral pH (7.44) and highest yield of humic acid. However, vermicompost made from several agricultural waste products showed varying levels of each plant nutrient element's greatest concentration. Thus, CD should be used as the main material and mixed with other agricultural waste products as raising base materials or enriched specific the purpose minerals to make high grade vermicompost.

References

Ansari A & Sukhraj K (2010). Effect of vermiwash and vermicompost on soil parameters and productivity of okra (*Abelmoschus esculentus*) in Guyana. *African Journal of Agricultural Research* 5(14):1794–1798. https://doi.org/10.5897/AJAR09.107

Atiyeh R M, Subler S, Edwards C A, Bachman G, Metzger J & Shuster W (2000). Effects of vermicomposts and composts on plant growth in horticultural container media and soil. Pedobiologia 44:579-590. https://doi.org/10.1078/S0031-4056(04)70073-6

Bisen J S, Singh A K, Kumar R, Bora D K & Bera B (2011). Vermicompost quality as influenced by different species of earthworm and bedding material. Two and Bud 58:137-140

Blouin M, Barrere J, Meyer N, Lartigue S, Barot S & Mathieu J (2019). Vermicompost significantly affects plant growth. A meta-analysis. Agronomy for Sustainable Development 39:34. https://doi/10.1007/s13593-019-0579-x. hal-02164337f

Chaudhuri P S, Pal TK, Bhattacharjee G & Dey S K (2000). Chemical changes during vermicomposting (*Perionyx excavatus*) of kitchen waste. Tropical Ecology 41(1):107–110

Das D, Bhattacharyya P, Ghosh B C & Banik P (2012). Effect of vermicomposting on calcium, sulphur and some heavy metal content of different biodegradable organic wastes under liming and microbial inoculation. *Journal of Environmental Science and Health* 47(3):205–211. https://doi.org/10.1080/03601234.2012.634346

Dhanuja C, Abbasi T & Abbasi S A (2020). Fertilization of paddy cultivation with vermicompost: A critical mini review. Organic Agriculture 10: 309–325. https://doi.org/10.1007/s13165-019-00274-2

Dores-Silva P R, Da Silva B M, Zozolotto T C, Landgraf M D & Rezende M O O (2014). Understanding the vermicompost process in sewage sludge: A humic fraction study. *International Journal of Agriculture and Forestry* 4(2): 94-99. https://doi.org/10.5923/j.ijaf.20140402.08

Garg P, Gupta A & Satya S (2006). Vermicomposting of different types of waste using *Eisenia foetida*: a comparative study. Bioresource Technology 97(3): 391–395. https://doi.org/10.1016/j.biortech.2005.03.009.

Giraddi R S (2007). Vermitechnologies (in Kannada). University of Agricultural Sciences, Dharwad, 62 pp

Giraddi R S (2011). Research priorities in vermitechnologies. Final report submitted to NABARD, Mumbai, 106 pp

Goswami L, Patel A K, Dutta G, Bhattacharyya P, Gogoi N & Bhattacharya S S (2013). Hazard remediation and recycling of tea industry and paper mill bottom ash through vermiconversion. Chemosphere 92(6): 708–713. https://doi.org/10.1016/j.chemosphere.2013.04.066

Hitinayake H M G S B, Ubayapala K G K C, Samaranayake J K S & Weerasekera W A T H (2018). Evaluation of earthworm species and bedding material collected from tea plantations for vermicomposting in Sri Lanka. *International Journal of Environment*, Agriculture and Biotechnology 3(5): 1935-1939. https://doi.org/10.22161/ijeab/3.5.47

Joshi R, Vig A P & Singh J (2013). Vermicompost as soil supplement to enhance growth, yield and quality of *Triticum aestivum* L.: A field study. International Journal of Recycling Organic Waste in Agriculture 2(1):16. https://doi.org/10.1186/2251-7715-2-16

Kaushik P & Garg V K (2003). Vermicomposting of mixed textile mill sludge and cow dung with epigeic earthworm *Eisenia foetida*. Bioresource Technology 90(3): 311–316. https://doi.org/10.1016/s0960-8524(03)00146-9

Kitturmath M S, Giraddi R S & Basavaraj B (2007). Nutrient changes during earthworm, *Eudrilus eugeniae* (Kinberg) mediated vermicomposting of agro industrial wastes, Karnataka. *Journal of Agricultural Sciences* 20(3): 653–654

Lazcano C, Arnold J, Tato A, Zaller J G & Dominguez J (2009). Compost and vermicompost as nursery pot components: effects on tomato plant growth and morphology. *Spanish Journal of Agricultural Research* 7(4): 944-951

Lim S L, Yeong W T, Lim P & Shak K P Y (2015). The use of vermicompost in organic farming: Overview, effects on soil and economics. Journal of the Science of Food and Agriculture 95: 1143–1156. https://doi.org/10.1002/jsfa.6849

Malherbe S & Cloete T E (2002). Lignocellulose biodegradation: fundamentals and applications. Reviews in Environmental Science and Biotechnology 1:105–14. https://doi.org/10.1023/A:1020858910646

Manaig E M (2016). Vermicomposting efficiency and quality of vermicompost with different bedding materials and worm food sources as substrate. *Research Journal of Agriculture and Forestry Sciences* 4(1): 1-13. Corpus ID: 138080469

Ndegwa P M & Thompson S A (2001). Integrating composting and vermicomposting in treatment and bioconversion of biosolids. Bioresource Technology 76:107-112. https://doi.org/10.1016/s0960-8524(00)00104-8

Nuchnoon J, Lertpanich A & Popan A (2017). Effect of bedding toward number of cocoons, baby weight and vermicompost production of African night crawler (*Eudrilus eugeniae*). *King Mongkut' Agricultural Journal* 35(2): 41-48

Pramanik P, Ghosh G K, Ghosal P K & Banik P (2007). Changes in organic-C, N, P and K and enzyme activities in vermicompost of biodegradable organic waste under liming and microbial inoculants. Bioresource Technology 98: 2485–2494. https://doi.org/10.1016/j.biortech.2006.09.017

Prasertsan S & Sajjakulnukit B (2006). Biomass and biogas energy in Thailand: Potential, opportunity and barriers. *Renewable Energy* 31(5): 599-610. https://doi.org/10.1016/j.renene.2005.08.005

Rahman A, Mehrdad J, Elahe K & Mohammad P (2017). Effects on raw materials on vermicompost qualities. *Journal of Plant Nutrition* 40(11):1635-1643. https://doi.org/10.1080/01904167.2016.1270319

Rekha G S, Kaleena P K, Elumalai D, Srikumaran M P & Maheswari V N (2018). Effects of vermicompost and plant growth enhancers on the exo-morphological features of Capsicum annum (Linn.) Hepper. *International Journal of Recycling Organic Waste in Agriculture* 7: 83–88. https://doi.org/10.1007/s40093-017-0191-5

Saravanan A K & Wesely E G (2018). Vermicompost production by *Eisenia fetida* on cassava peel waste compost (periderm). International Journal of Creative Research Thoughts 6(1): 2320-2882

Majlessi M, Eslami A, Najafi Saleh H, Mirshafieean S & Babaii S (2012). Vermicomposting of food waste: assessing the stability and maturity. Iranian Journal of Environmental Health, Science 9(1): 25. https://doi.org/10.1186/1735-2746-9-25

Singh R, Sharma R R, Kumar S, Gupta R K & Patil R T (2008). Vermicompost substitution influences growth, physiological disorders, fruit yield and quality of strawberry (*Fragaria x ananassa* Duch.). Bioresource Technology 99: 8507–8511. https://doi.org/10.1016/j.biortech.2008.03.034

Sirithanakorn P, Pharam K & Sanusan S (2014). Different of bedding on growth of earthworms and vermicompost productions. *Khon Kaen Agriculture Journal* 42 Suppl.1: 714-721

Sodaei M S, Aliasgharzadeh N & Oustan S H (2007). Mineralization kinetic of nitrogen in an attended soil by com-post, vermicompost and animal manure. *Journal of Science and Technology of Agriculture and Natural Resources* 11: 405–414

Solis-Mejia L, Islas-Espinoza M & Estellar M V (2012). Vermicomposting of sewage sludge: earthworm population and agronomic advantages. Compost Science & Utilization 20(1):11–17. https://doi.org/10.1080/1065657X.2012.10737016

Song X, Liu M, Wu D, Griffiths B S, Jiao J, Li H & Hu F (2015). Interaction matters: Synergy between vermicompost and PGPR agents improves soil quality, crop quality and crop yield in the field. Applied Soil Ecology 89: 25–34. https://doi.org/10.1016/j.apsoil.2015.01.005

Suthar S (2006). Potential utilization of guar gum industrial waste in vermicompost production. Bioresource Technology 97: 2474–2477. https://doi.org/10.1016/j.biortech.2005.10.018

Suthar S (2008). Development of a novel epigeic-anecic-based polyculture-vermi-reactor for efficient treatment of municipal sewage water sludge. *International Journal of Environment and Waste Management* 2(½): 84–101. https://doi.org/10.1504/IJEWM.2008.016994

Tan H K (2016). Soil Sampling, Preparation, and Analysis, 2nd Edition. Taylor and Francis Group. ISBN: 9781138627567

Tan H K (2014). Humic Matter in Soil and the Environment: Principles and Controversies, Second Edition. CRC Press. ISBN: 9781482234459

Tripathi K M, Dhakal D D, Baral D R & Sharma M D (2015). Effect of feeding materials on yield and quality of vermicompost and municipalization of *Eisenia fetida* in subtropical environment of Napal. *International Journal of Research* 2: 23-28. https://doi.org/10.3126/KUSET.V13I2.21280

Velasco-Velasco J, Parkinson R & Kuri V (2011). Ammonia emissions during vermicomposting of sheep manure. Bioresource Technology 102: 10959-64. https://doi.org/10.1016/j.biortech.2011.09.047

Vichaivit V, Rodsopa B & Sajjapan K (2012). Qualities of vermicompost of different types of waste using *Perionyx excavates*. *King Mongkut' Agricultural Journal* 30(2): 86-96

Vikman M, Karjomaa S, Kapanen A, Wallenius K & Itävaara M (2002). The influence of lignin content and temperature on the biodegradation of lignocellulose in composting conditions. Applied Microbiology and Biotechnology 59(4-5): 591-8. https://doi.org/10.1007/s00253-002-1029-1

Vodounnou D S J V, Kpogue D N S, Tossavi C E, Mennsah G A & Fiogbe E D (2016). Effect of animal waste and vegetable compost on production and growth of eartworm (*Eisenia fetida*) during vermiculture. *International Journal of Recycling of Organic Waste in Agriculture* 5:87-92. https://doi.org/10.1007/s40093-016-0119-5

Walkley A & Black I A (1934). Estimation of soil organic carbon by the chromic acid titration method. Soil Science 34:29-38. https://doi.org/10.1097/00010694-193401000-00003

Wang X, Zhao F, Zhang G, Zhang Y & Yang L (2017). Vermicompost improves tomato yield and quality and the biochemical properties of soils with different tomato planting history in a greenhouse study. Frontiers in Plant Science 8: 1978. https://doi.org/10.3389/fpls.2017.01978

Warma P R & Anglopez M J (2002). The chemical properties of vermicompost derived from different feed stocks. In: Proceeding of the International Composting and Compost Science Symposium, Columbus, Ohio, CD Rom.

Waseem M A, Giraddi R S & Math K K (2013). Assessment of nutrients and micro fora in vermicompost enriched with various organics. *Journal of Experimental Zoology India* 16: 697–703

Zarei M, Jahandideh Mahjen Abadi V A & Moridi A (2018). Comparison of vermiwash and vermicompost tea properties produced from different organic beds under greenhouse conditions. *International Journal of Recycling of Organic Waste in Agriculture* 7: 25–32 https://doi.org/10.1007/s40093-017-0186-2

Journal of Agricultural Sciences
(Tarim Bilimleri Dergisi)

J Agr Sci-Tarim Bili
e-ISSN: 2148-9297
jas.ankara.edu.tr

Effect of Varying Biochar Particle Sizes and Concentrations on Soil Nutrient Retention and Microbial Activity

Khasifah Muhamad[a*], Uchenna Ogbonnaya[b], Kirk Semple[c], John Quinton[c]

[a]*Malaysian Agricultural Research and Development Institute, Cameron Highlands Pahang, MALAYSIA*

[b]*Hong Kong Baptist University, HONG KONG*

[c]*Lancaster University, LA1 4YW, Lancaster, UNITED KINGDOM*

ARTICLE INFO

Research Article

Corresponding Author: Khasifah Muhamad, E-mail: khasifah@mardi.gov.my

Received: 21 May 2024 / Revised: 12 September 2024 / Accepted: 10 October 2024 / Online: 25 March 2025

Cite this article

Muhamad K, Ogbonnaya U, Semple K, Quinton J (2025). Effect of Varying Biochar Particle Sizes and Concentrations on Soil Nutrient Retention and Microbial Activity. *Journal of Agricultural Sciences (Tarim Bilimleri Dergisi),* 31(2):288-301. DOI: 10.15832/ankutbd.1487379

ABSTRACT

This study aims to determine the effect of adding biochar to soil under different management systems, as well as soil nutrient availability in a temperate environment. We tested whether biochar could enhance the chemical and biological properties of soil and reduce nutrient leaching. There were two parts of the study. These two studies were not related with each other, but the only similar study approach was the ageing effect of biochar (incubated of soil mixture for up to 300 days and 30 days). In the first part of the study, 2% of biochar by weight with a <5 mm particle size was produced from hardwood and incorporated into three different types of soil. The three types are an arable loam soil, an arable sandy soil and a grassland soil. The soils with and without biochar (control) were incubated for up to 300 days. In the second part of the study, different dosages of hardwood biochar (2% and 5%) with various particle sizes (2, 1, 0.5 and 0.1 mm) were incorporated into soils with different nutrient status (fertilised and unfertilised soils) and incubated for up to 30 days. The findings from the study exhibited that hardwood biochar significantly increased the mineralisation of ^{14}C-glucose at 5% biochar dosage and at finer particle size. The pH of soil and carbon and the microbial biomass in unfertilised soil also increased after biochar addition. Adding biochar to soil had no major change on the ageing effect of the biochar and the leaching of nitrate ions, but reduced the ammonium ion leaching. The efficacy of biochar application depends on soil type, nutrient availability, biochar application rate and particle size.

Keywords: Temperate soil, Biochar, Carbon, Leaching, Mineralization

1. Introduction

Research suggests that adding rich organic material with recalcitrant carbon (C) results in increased C content in the soil (Zhang et al. 2017). Charred organic matter usually contains significant levels of recalcitrant C resistant to microbial degradation and can reside in soils for a long time, whilst influencing soil properties that improve the agronomy (Lehmann et al. 2003). Terra preta soils have demonstrated the potential to improve and sustain soil fertility by interacting with inherent colloids, nutrients and soil organic carbon to create conditions that lead to sustainability (Busch & Glaser 2015). This is of particular importance to soil due to the trends in degradation and the sensitivity of extractable organic matter and nutrients (Chen et al. 2018). The sustainability of soil fertility through agronomic practices has been a challenge to scientists owing to changing climatic conditions, changes in land use, and the availability and applicability of soil amendment measures (Paroissien et al. 2015). It has been estimated that an average of 60% of nitrogen that is applied to soils for crop production globally is either leached or undergoes surface runoff due to irrigation, whilst only the residual fraction is utilized by crops (Zhou et al. 2019). Hence, improving crop nutrient utilization rates and eliminating nutrient loss following irrigation regimes is essential (Zhou et al. 2019).

The efficacy of several soil amendments to alleviate nutrient leaching to the environment has been tested, either alone or in mixtures (Wang et al. 2016). Biochar, a form of soil amendment, can readily be made from various organic materials, such as wood, food waste, plant debris by pyrolysis. The resistant aromatic C structure of biochar supports soil aeration, aggregation, water holding capacity, compaction resistance and slow decomposition of soil carbon (Wong et al. 2019). Naturally, pyrogenic carbon in top soils represents the highly stabilized and recalcitrant carbon content of soils (Dynarski et al. 2020). Hence, the systematic application of biochar as a stable organic carbon moiety into agricultural soils can contribute to the naturally-stabilized organic carbon sinks. Due to the biochar's potential as a soil ameliorant, this study tests fertility increases in well-managed soils amended with biochar. How particle size and dosage of biochar influence the efficacy of biological activity and reduction of soil nutrient leaching were also investigated. Our hypotheses are that biochar will greatly improve the fertility of unfertilised soil to

a greater extent than fertilised soil. The finer particles of biochar will hold more nutrients than the coarser particles and 5% of biochar application will enhance the quality of soils in both fertilised and unfertilised soils compared to the lower dosage (2% application rate of biochar).

2. Material and Methods

This research consisted of two sets of experiments. The soils were collected from two sites in the UK and the biochar used in these studies were similar.

2.1. Chemicals and biochar

^{14}C glucose was obtained from Sigma Aldrich Co. Ltd. UK. Goldstar multipurpose liquid scintillation cocktail, carbo trap and carbo count were obtained from Meridian, UK. Combust aid was obtained from Perkin Elmer, USA, while the chloroform ($CHCl_3$), potassium sulphate and sodium hydroxide were supplied by Fisher Scientific, UK.

The biochar used in this study was the combinations of hardwoods which are primarily beech (Fagus spp.), and to a lesser extent ash (Fraxinus excelsior), oak (Quercus spp.), birch (Betula spp.) and cherry (Prunus spp.). Biochar was obtained from (Bodfari Environmental, St. Asaph, UK). Harwood biochar was chosen from the source because such biochar exhibit higher surface area, pore volume, liming effect and cation exchange capacity than most other biochar feedstocks (Jiang et al. 2017; Ippolito et al. 2020). Such properties are critical for nutrient retention. The method by which this biochar was produced was slow pyrolysis for 24 hours in a ring-kiln at 400 °C. Some of the biochar characterisation was conducted in the similar method with the soil characterisation. The properties of biochar used in these experiments are shown in Table 1.

2.2. Soils

Soils were collected from five various locations with similar environmental conditions, depths, as well as similar soil texture, but in the United Kingdom. However, three of the soils were from the same local area (Dundee), whilst two were from another site (Penrith), thus divided into two experimental conditions. Nevertheless, all soils were incubated with the same biochar at different conditions to investigate substrate respiration and leachability.

2.3. Experiment 1

Arable loam, arable sandy and grassland (Brown Earth) soils from Dundee, United Kingdom were collected. An arable sandy and an arable sandy loam – both in crop rotation, whereas a grassland soil was from managed, perennially grassed land. All soils were obtained from the top 20 cm of the soil profile, from the James Hutton Institute in Dundee, UK (56° 27’ N, 3° 4’ W, 29 m.a.s.l). To study the effects of aged biochar associated in soil, the biochar was added and mixed into the soils and left several months in the pots (approximately 10 months). Pots had a capacity of 38 L, with dimensions of 38 x 38 x 30 cm. Soils were mixed and placed into pots and biochar was sieved to remove particles > 2 cm in size, and mixed with half of each soil type equivalent to 2.0% of soil dry weight. Soil that did not contain biochar was also added in the pot as a control treatment. The wet-weight of each pot was approximately 25.2 kg dry soil, thus 2% biochar-treated weighed 25.7 kg total substrate. Soil or soil-biochar mix was added to pots in four equal portions and compacted by hand between each addition to ensure similar compaction.

Approximately 10 months later, a 15-cm cylindrical core was used to collect the mixture (biochar + soil) and non-mixture (no biochar) of soil samples from the pot. Composited soil samples were obtained from 4 random points in each pot. In the laboratory, the samples (soil from non-biochar treatment pots) were mixed with 2% of fresh hardwood (HW) biochar by weight, with < 5 mm particle size in thriplicate. This is to differentiate the aging effects of previously added biochar in the pot, with fresly added biochar in the laboratory. Whereas, soil with no biochar acted as a control treatment with three replications. All soil samples were then incubated for 0, 60, 180, and 300 days and kept in screw-capped jars. At each contact time and before analysis, soils were dried and sieved with a 2-mm mesh for soil aggregates suitable for soil analysis (Kandeler 2007). Table 2 displayed soil characteristics determined in this study.

2.4. Experiment 2

In this experiment, brown earth soils were collected from Penrith, Cumbria UK. These soils were chosen based on differences in soil management. The first soil was from oilseed rape-area which was properly managed i.e. well-fertilised. The second soil was collected from grassland which was not properly managed. No fertiliser had been applied for approximately 50 years. The texture of all soils was sandy clay loam. The soil samples were obtained with a shovel from the field to a depth of up to 15 cm. The soil samples were sieved through a 5-mm mesh, and amended with 2% and 5% of HW biochar with various particle sizes (2, 1, 0.5 and 0.1 mm). Unamended soil acted as a control treatment. The samples were placed in screw-capped glass jars and incubated for a month. The amounts of soil samples placed in each jar was estimated based on the total chemical and biological analyses tests. 2% and 5% of HW biochar with different parrticle sizes were then added in relative to the weight of the soil in

each jar. Lastly, soils were dried and sieved with a 2-mm mesh to achieve appropriate soil aggregates for the soil biological and chemical analyses (Kandeler 2007). The soil's physical and chemical properties are presented in Table 2.

2.5. Biological and chemical analyses of soil

Substrate-induced respiration was employed for the biological respirometry experiments (Reid et al. 2001). This experiment was carried out in order to measure the activity of microbes in the soil (respiration and biomass). Therefore, ^{14}C-glucose is used as a carbon source for microbes to utilise for respiration (release of $^{14}CO_2$) and ^{14}C- carbon incorporation into microbial biomass (Boucard et al. 2008). To assess the microbial respiration and biomass, the methods are explained as follows.

In experiment 1, at 0 and 60 days contact time, 20 g wet weight of soil was collected from jars and added to respirometry flasks with 3 mM ^{14}C-glucose solution (radioactivity of 1086 Bq) added to the soil samples, whilst 654 Bq glucose was used on days 180 and 300 (contact time). Meanwhile, in experiment 2, 3 mM of glucose solution was added to the soil samples, with radioactivity of 1051 Bq on days 0 and 30 (contact time). Both experiments followed a modified method of Doick & Semple (2003). Then, a 7-mL vial containing 1 mL NaOH (1 M) solution CO_2 trap was suspended from the lid of each respirator for the glucose mineralization. Samples were then shaken on an orbital shaker at 100 rpm. The rates of ^{14}C-glucose mineralization were measured hourly within four hours, then every two hours for another four hours in 24 hours. Rates of mineralization were also measured each day within 5 days. During the period of sampling, the NaOH vial was removed and well wiped with blue roll tissue soaked in acetone to dissolve residual ^{14}C on the surface. Afterwards, 5 mL of liquid scintillant cocktail was added into the vial and incubated in the dark overnight prior to measuring ^{14}C-activity using a liquid scintillation analyser (Canberra Packard Tri-Carb 2250A).

To determine the biomass, 4 g of soil slurry from the respirometer was collected on the last substrate sampling day, when extraction of non-fumigation sample was done with 20 mL of 0.5 M K_2SO_4. The samples collected were shaken on an orbital shaker for 30 minutes at 100 rpm, the supernatant was filtered and an aliquot (5 mL) of the supernatant was incorporated into a 20-mL vial. For liquid scintillation counting, 15 mL of liquid scintillant cocktail was also added into each vial and the samples were kept in the dark overnight. Simultaneously, the remaining samples were fumigated using a desiccator lined with soaked blue roll tissue, whilst at the centre of the desiccator, 75 mL of ethanol-free chloroform ($CHCl_3$) was placed. After vigorous boiling of $CHCl_3$ within 2 minutes, the desiccator was evacuated. After 24 hours, repeated five- or six-fold evacuation was done to ensure residual $CHCl_3$ vapour was removed. Subsequently, the soils were similarly extracted and counted as with the non-fumigation extraction method. The amounts of ^{14}C left in the soil treatments were assessed through dry combustion of 1 g of soil. The associated residual ^{14}C-glucose activity of the soils was then determined via a 3-minute combustion on the Packard, Model 307 sample oxidiser.

For chemical soil analyses, 10 g of air dried soil was used to analyze pH. pH was then measured using a pH meter model PHM 220 which was calibrated using buffers at pH 4.0 and 7.0. In addition, samples of approximately 30 mg were used for determination of total carbon. Total carbon (C) was determined by dry combustion and measured with an elemental analyser (Elementar Vario EL).

2.6. Nutrient leaching (experiments 1 and 2)

In experiment 1, the hardwood biochar that was previously added in the arable loam, arable sandy soil and grassland soil for more than 10 months was used, as well as freshly-added biochar amended in the same types of soil. Soils with no biochar acted as controls. Soils with and without biochar (2%; <5 mm particle size) were adjusted to a 1.2 g cm^{-3} bulk density and packed into 27 PVC columns in triplicate. Each column has a diameter of 5 cm and is 20 cm long. Subsequently, at the bottom of the PVC column, 40 g of sand was poured to avoid the clay particles from being lost during the leaching experiment. At the end of the column used, two layers of nylon mesh were placed, lined and secured with cable ties.

In experiment 2, hardwood biochar with various particle sizes i.e. 2, 1, 0.5 and 0.1 mm were used. The samples of fertilised and unfertilised soils were amended at two different application rates (2% and 5%). Soils amended with biochar and un-amended soil were adjusted to approximately 1.2 g cm^{-3} bulk density. Then the samples were filled into a glass column of diameter 5 cm and length 20 cm. Due to the lack of glass columns, the samples were in duplicate. All of the leaching processes commenced by pouring 100 mL of deionised water through each of the soil columns. An Erlenmeyer flask was used to collect leachates and then stored at 4 ^{O}C for two to three days before analysis. Ammonia and nitrate leachates were analysed using a Bran + Luebbe Autoanalyzer 3.

2.7. Analyses of statistics

The mean values of maximum rate, ^{14}C mineralization, ^{14}C biomass, pH, total carbon and leachate nutrient concentration amongst treatments and during contact time, were tested using a one-way analysis of variance (ANOVA) ($P<0.05$). The Holm-Sidek procedure ($P<0.05$) was used for comparison of multiple means. Statistically insignificant values were further tested by the non-parametric Kruskal-Wallis test based on ranks. In addition, the significant differences amongst treatments for non-distributed

values were tested by Tukey's test ($P<0.05$). All statistical tests were performed using the SigmaStat v. 3.5 (Systat Software Inc.).

3. Results and Discussion

3.1. Soil chemical characteristics (experiments 1 and 2)

The carbon contents of amended grassland, arable loam and arable sandy soil with fresh and aged biochar samples increased (Figures 1a, b and c). Also, fresh and aged biochar application to soil significantly increased the soil pH ($P<0.05$) (Figures 1d, e and f). This is due to the high pH of biochar (9.05) used in this study (Table 2).

Furthermore, the results also show that the smaller sizes (1, 0.5 and 0.1 mm) of biochar increased C content ($P<0.05$) more than the coarser particle sizes (2 mm) and in the treatment with no biochar (Figures 2a and b). This is because of the higher tendency of biochar to interact with soil microbes, as well as soil organic matter (de Jesus Duarte et al. 2019). In the meantime, the smaller particle sizes (0.5 and 0.1 mm) had the greatest value of soil pH ($P<0.05$) in contrast to the bigger particle sizes (1 and 2 mm) and control (Figures 3a and b). This is due to the bigger surface area of the smaller particle size of biochar.

Table 1- Biochar chemical characteristics

Parameter	***Hardwood Biochar***
% Carbon	71.38
% Nitrogen	0.45
C/N Ratio	158.68
CEC (meq 100 g^{-1})	34.36
pH	9.05
Inorganic P (mg g^{-1})	0.41

Table 2- Soils physical and chemical characteristics

Parameter	***Experiment 1***			***Experiment 2***	
	Grassland	*Arable Loam*	*Arable Sandy*	*Fertilised*	*Unfertilised*
% Clay	34.90	34.41	27.54	28.29	28.12
% Silt	17.44	16.06	6.36	11.96	9.00
% Sand	47.67	49.53	66.10	59.75	62.88
Texture	Sandy Clay	Sandy Clay Loam	Sandy Clay Loam	Sandy Clay Loam	Sandy Clay Loam
% Carbon	2.39	3.79	2.06	2.14	3.40
% Nitrogen	0.14	0.21	0.16	0.19	0.19
C/N Ratio	16.45	17.75	12.68	11.26	17.89
CEC (meq 100 g^{-1})	13.49	13.86	9.24	-	-
pH	6.08	6.53	5.81	6.16	6.15
Inorganic P (mg g^{-1})	1.15	1.57	1.15	-	-

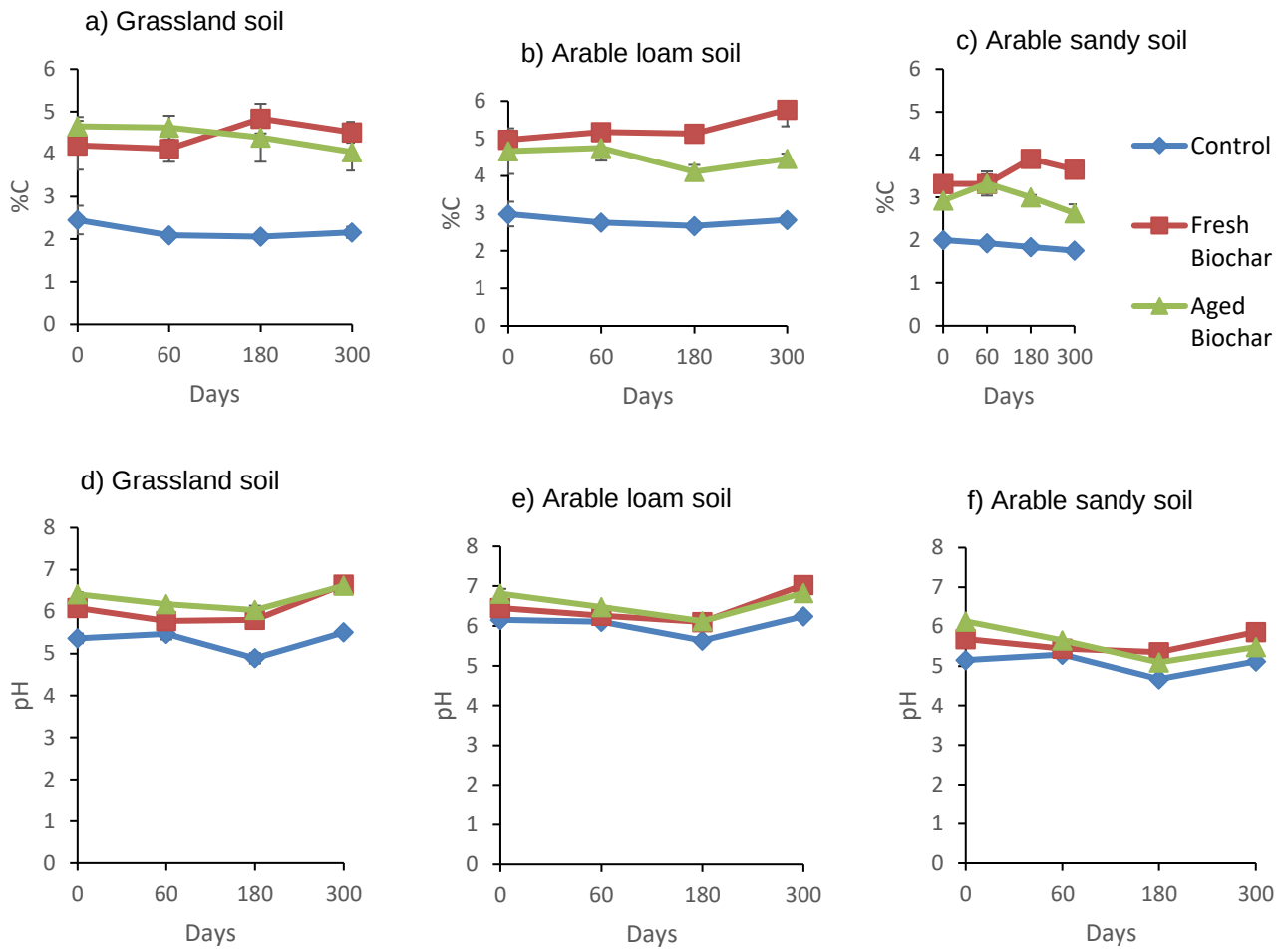

Figure 1- The carbon and pH content in the a) and d) grassland, b) and e) arable loam and c) and f) arable sandy soils treated with fresh and aged biochar; and with no biochar over 300 days. Error bars are SEM (n=3)

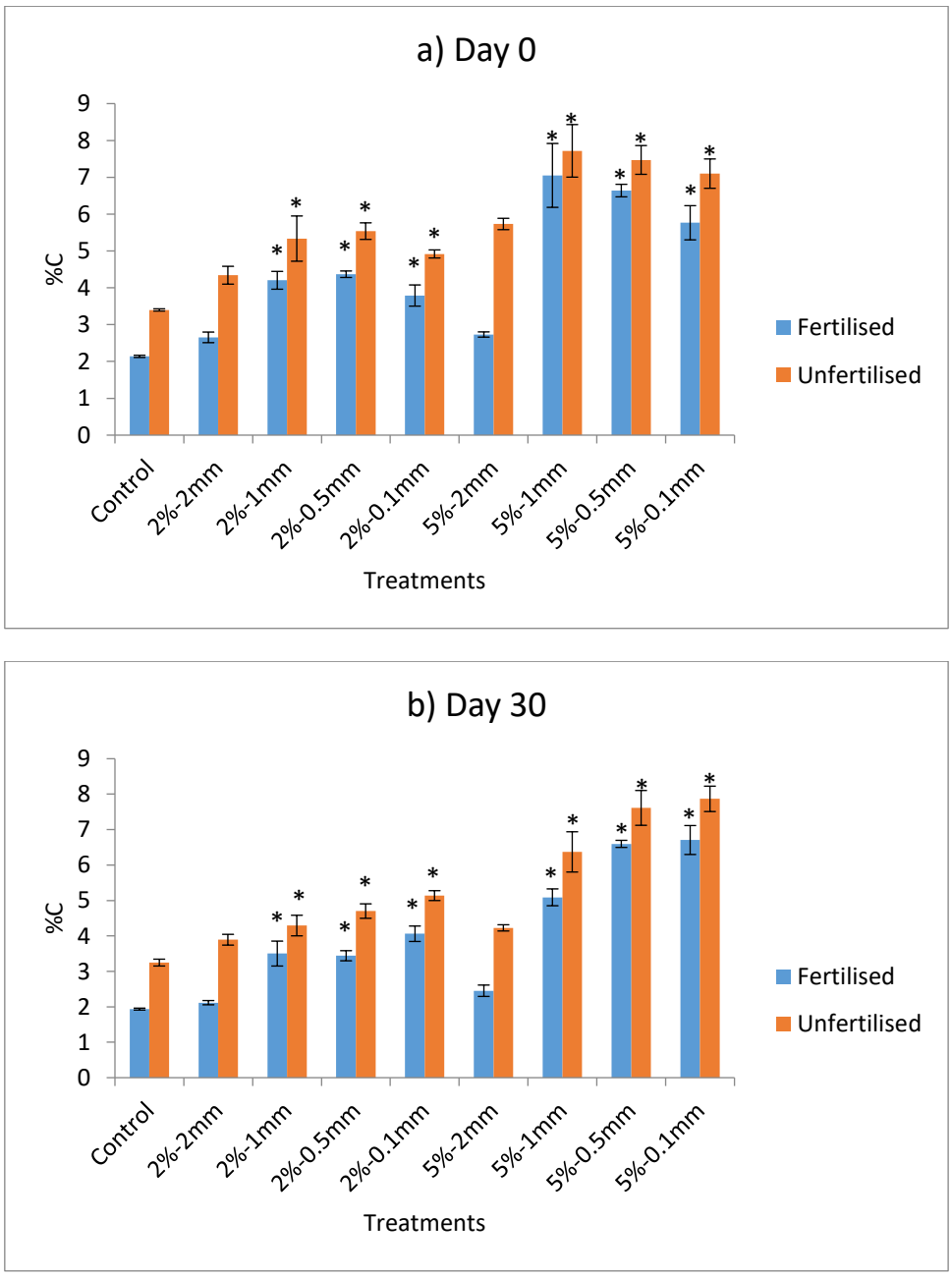

Figure 2- Carbon in fertilised and unfertilised soils in the a) Day 0 and b) Day 30, treated with 2% and 5% of biochar; and no biochar (control). Error bars are SEM (n=3). Values in asterisk indicate significance at P<0.05

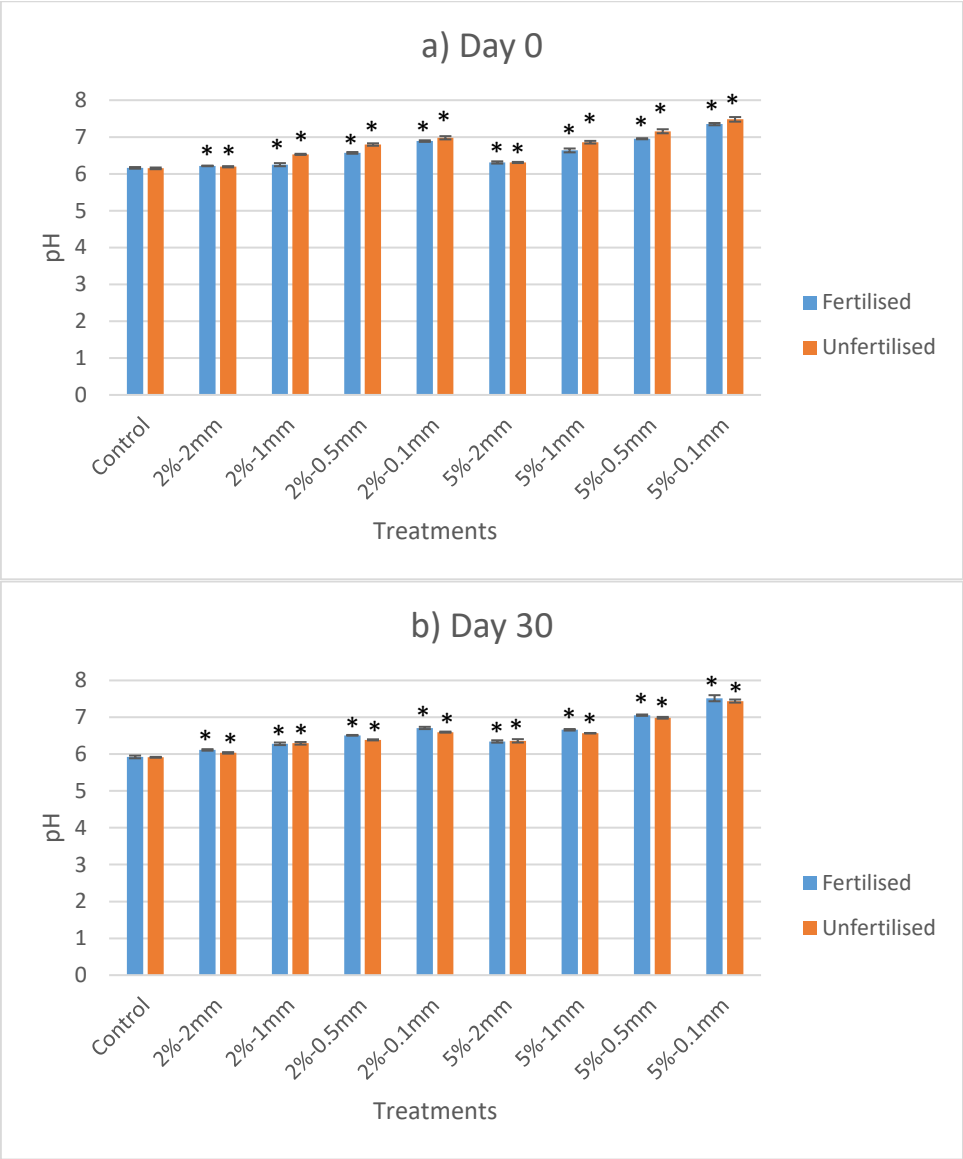

Figure 3- pH in fertilised and unfertilised soils in the a) Day 0 and b) Day 30, treated with 2% and 5% of biochar; and no biochar (control). Error bars are SEM (n=3). Values in asterisk indicate significance at P<0.05

3.2. Mineralisation of ^{14}C-glucose to $^{14}CO_2$ and incorporation of ^{14}C-glucose into microbial biomass

3.2.1. Experiment 1

During the period of incubation, the extents of mineralisation of ^{14}C-glucose in the three contrasting soils (grassland, arable loam and arable sandy soils) were constant. In addition, fresh and aged biochar application to soils did not show any major change during the incubation time. Just after 180 days of incubation it was seen that the extent of ^{14}C-glucose mineralisation in grassland soil amended with the aged biochar (74.86%) was significantly higher ($P<0.05$) than in the treatment of fresh biochar-amended soils (62.83%) (Figure 4c and Table 1). The maximum rates of ^{14}C-glucose mineralization were observed to have no significant differences in the arable loam and arable sandy soils (Tables 2 and 3). The significant effect on the maximum rates was only observed on day 180 in the aged biochar incorporated in grassland soils (4.46% h^{-1}), in comparison with the rates of fresh biochar (3.51% h^{-1}) and with no biochar (3.80% h^{-1}) in the same soil (Table 1).

Table 1- Maximum rate, ^{14}C extent mineralisation, ^{14}C biomass uptake and ^{14}C activity remaining for grassland soil amended with and without fresh biochar (FB); and aged biochar (AB), over 300 days. Error bars are SEM (n=3)

Treatment	Day	Maximum rate (% h^{-1})	^{14}C extents mineralisation (%)	^{14}C biomass uptake (%) fixed k_{EC}	^{14}C activity remaining in soil (%)
Grassland	0	2.32 ± 0.15	42.54 ± 2.46	7.99 ± 0.54	49.47 ± 2.46
Control	60	3.68 ± 0.28	75.91 ± 2.61	20.28 ± 5.07	3.81 ± 4.61
	180	3.80 ± 0.15	67.18 ± 0.45	11.32 ± 0.24	21.49 ± 0.35
	300	3.39 ± 0.11	76.39 ± 3.99*	20.77 ± 1.89	2.83 ± 4.82
FB	0	2.35 ± 0.24	41.37 ± 3.09	10.73 ± 2.25	47.90 ± 3.92
	60	3.43 ± 0.49	71.95 ± 5.28	25.30 ± 3.51	2.74 ± 6.26
	180	3.51 ± 0.20	62.83 ± 2.24	11.02 ± 0.90	26.15 ± 1.35
	300	2.84 ± 0.21	71.14 ± 2.74*	25.20 ± 2.56*	3.66 ± 4.45
AB	0	2.17 ± 0.43	42.72 ± 5.27	12.96 ± 4.21	44.31 ± 2.67
	60	3.21 ± 0.40	75.44 ± 5.17	22.73 ± 0.06	1.83 ± 5.18
	180	4.46 ± 0.20*	74.86 ± 2.07*	9.77 ± 1.75	15.37 ± 1.68
	300	5.37 ± 1.30	93.59 ± 16.09*	11.36 ± 2.90	0.00 ± 0.00

Values in asterisk indicate significance at P<0.05

Generally, biochar addition to soil did not have a great effect on the microbial biomass in the soil. On day 0, the uptake of ^{14}C-carbon into the microbial biomass in arable loam soil amended with aged biochar was significantly higher (P<0.05) than fresh biochar amended with the same soil (12.56% and 7.68%, respectively) (Table 2). However, after 60 days of incubation, the mineralisation of ^{14}C-carbon in arable loam soil amended with aged biochar was significantly (P<0.05) higher (88.12%) in comparison with the fresh biochar-amended soil (68.33%), and in the treatment with no biochar in the same soil (69.91%) (Figure 4f and Table 2). Furthermore, incorporation of ^{14}C-carbon into microbial biomass after 300 days contact time showed higher uptake in grassland soil amended with fresh biochar (25.20%) (P<0.05) compared to the uptake in the same soil amended with the aged biochar (11.36%) (Table 1). Also, the maximum rates were higher in the treatment with no biochar (control) (4.77 h^{-1}), then in the treatment with fresh biochar (3.00 h^{-1}) and aged biochar (3.44 h^{-1}) after 300 days of incubation in arable loam soil (P>0.05) (Table 2).

Table 2- Maximum rate, ^{14}C extent mineralisation, ^{14}C biomass uptake and ^{14}C activity remaining for arable loam soil amended with and without fresh biochar (FB); and aged biochar (AB), over 300 days. Error bars are SEM (n=3).

Treatment	Day	Maximum rate (% h^{-1})	^{14}C extents mineralisation (%)	^{14}C biomass uptake (%) fixed k_{EC}	^{14}C activity remaining in soil (%)
Arable loam	0	3.08 ± 0.58	54.76 ± 7.56	11.23 ± 0.57	34.01 ± 7.23
Control	60	3.09 ± 0.22	69.91 ± 3.25	21.00 ± 3.03	9.09 ± 5.87
	180	4.01 ± 0.21	71.94 ± 2.75	8.72 ± 0.41	19.34 ± 2.42
	300	4.77 ± 0.77	85.66 ± 10.72*	15.15 ± 1.68	0.00 ± 0.00
FB	0	2.80 ± 0.31	52.47 ± 4.24	7.68 ± 0.19	39.85 ± 4.43
	60	2.88 ± 0.32	68.33 ± 0.82	19.74 ± 2.33	11.93 ± 2.05
	180	3.39 ± 0.24	63.99 ± 3.75	10.05 ± 1.27	25.95 ± 4.95
	300	3.00 ± 0.14	69.88 ± 0.72*	18.19 ± 1.92	11.91 ± 2.47
AB	0	2.24 ± 0.05	46.94 ± 1.35	12.56 ± 0.09*	40.49 ± 1.44
	60	3.79 ± 0.47	88.12 ± 7.15*	18.61 ± 1.91	0.00 ± 0.00
	180	3.76 ± 0.12	70.29 ± 0.55	8.96 ± 0.09	20.75 ± 0.48
	300	3.44 ± 0.18	75.52 ± 2.93	15.68 ± 2.21	8.81 ± 1.53

Values in asterisk indicate significance at P<0.05

The variations in the extent of ^{14}C-glucose mineralisation had a small effect in the soil amended with both fresh and aged biochar. The major change only occurred after 60 and 180 days, when the aged biochar increased the extent of ^{14}C-glucose mineralisation in the arable loam and grassland soils (Figures 4f and c). Whereas, the extent of ^{14}C-glucose mineralisation in the arable sandy soil demonstrated significant effect only on the final period of incubation (day 300) (Figure 4l and Table 3). These results are in disagreement with Jones et al. (2012), who revealed that biochar enhanced the activity of microbes in the second year of the study more than in the first and in the third years of study. In addition, the researchers claimed that application of biochar to soil only led to a little impact on the turnover of ^{14}C-labelled soil organic carbon and sugars. Also, Quilliam et al. (2012) claimed that there was no major change on microbial growth after three years of biochar application to soil. These findings are in agreement with the notion that adding biochar exerts an insignificant contribution to highly fertile temperate soils.

Table 3- Maximum rate, ^{14}C extent mineralisation, ^{14}C biomass uptake and ^{14}C activity remaining for arable sandy soil amended with and without fresh biochar (FB); and aged biochar (AB), over 300 days. Error bars are SEM (n=3)

Treatment	Day	Maximum rate (% h^{-1})	^{14}C extents mineralisation (%)	^{14}C biomass uptake (%) fixed k_{EC}	^{14}C activity remaining in soil (%)
Arable sandy	0	2.08 ± 0.04	44.40 ± 1.18	8.98 ± 3.64	46.61 ± 4.15
Control	60	2.89 ± 0.24	77.67 ± 11.19	27.95 ± 7.73	0.00 ± 0.00
	180	2.40 ± 0.15	66.92 ± 1.31	13.21 ± 3.45	19.87 ± 4.63
	300	1.64 ± 0.06	75.79 ± 10.41*	13.71 ± 2.54	10.50 ± 8.43
FB	0	2.18 ± 0.10	45.97 ± 3.66	9.20 ± 0.98	44.83 ± 3.72
	60	4.23 ± 1.03	87.26 ± 11.36	4.28 ± 1.51	0.00 ± 0.00
	180	3.37 ± 0.48	72.51 ± 6.20	6.94 ± 1.42	20.55 ± 6.25
	300	2.40 ± 0.51	73.60 ± 7.53*	16.41 ± 3.64	9.98 ± 10.23
AB	0	2.13 ± 0.41	42.17 ± 2.13	10.70 ± 1.16	47.13 ± 2.21
	60	3.42 ± 0.46	78.27 ± 7.43	27.29 ± 1.15	0.00 ± 0.00
	180	3.54 ± 0.55	73.83 ± 4.60	8.99 ± 1.63	17.17 ± 4.44
	300	3.23 ± 0.57	84.30 ± 5.12*	14.65 ± 1.80	1.04 ± 6.80

Values in asterisk indicate significance at P<0.05

The incorporation of ^{14}C-glucose into the microbial biomass also did not show any changes in the biomass. In addition, the mineralisation of ^{14}C-glucose in all treatments was constantly higher than the uptake of ^{14}C-glucose into the microbial biomass. Amending soil with fresh and aged biochar increased the amounts of both oxidizable and recalcitrant carbon in the soils, which would have influenced microbial activity. Therefore, the ^{14}C-glucose mineralisation increased, resulting in a decrease in ^{14}C-uptake. In contrast, positive priming effects of the activity of microbes in degraded/stressed soils following addition of peanut shell and sugarcane-bagasse-derived biochar was observed by Nie et al. (2018). The high sand content (66%) and lower CEC (9.24 meq 100 g^{-1}) of the arable sandy soil were unfavourable for the wood biochar to interact with to ensure any significant change in microbial activities.

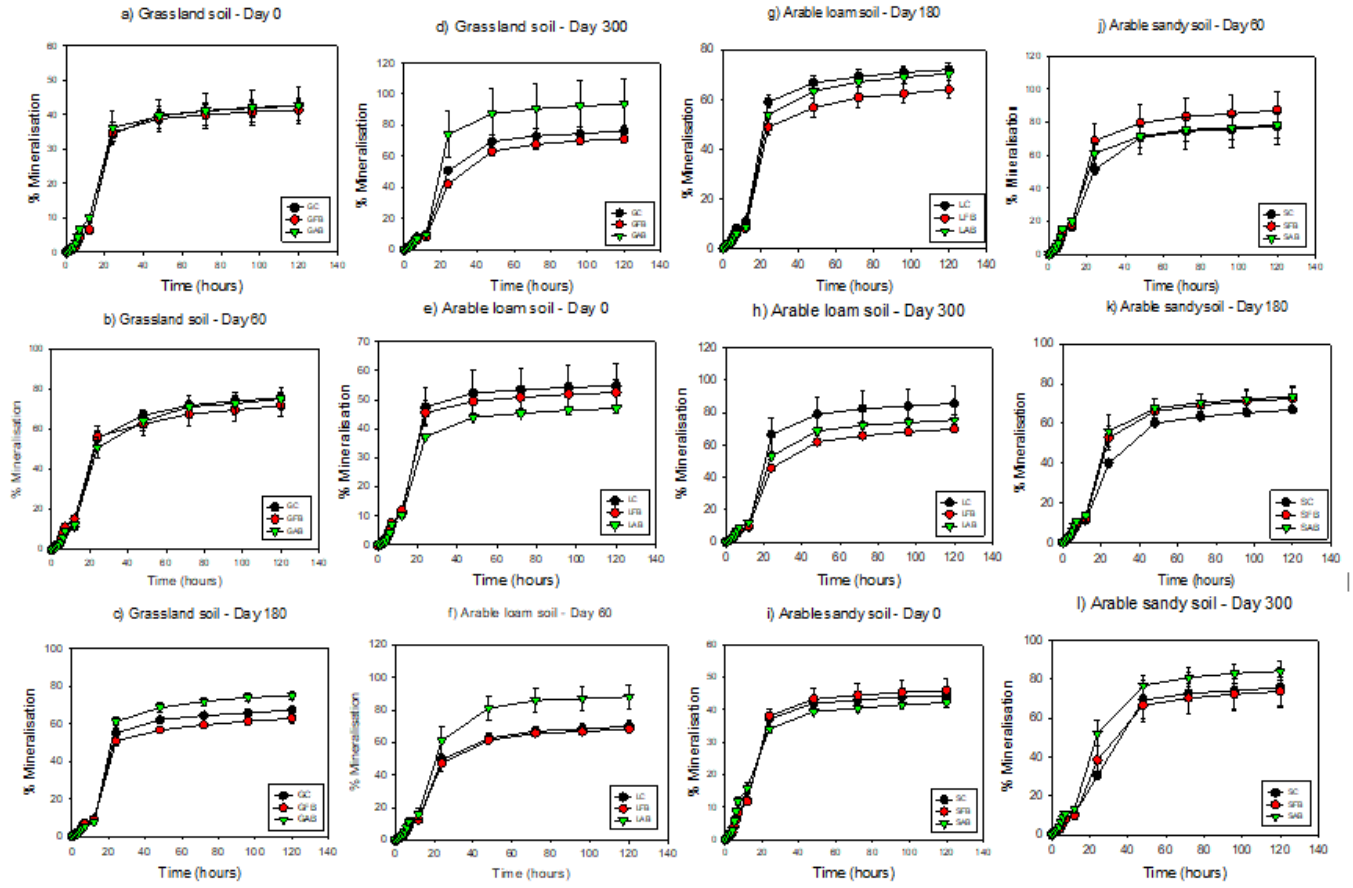

Figure 4- Mineralisation of ^{14}C-glucose of the a, b, c, d) grassland; e, f, g, h) arable loam and i, j, k, l) arable sandy soils on days 0, 60, 180 and 300, amended with fresh biochar (FB) and aged biochar (AB); and with no biochar. Error bars are SEM (n=3)

3.2.2. Experiment 2

The mineralisation of ^{14}C-glucose was low in the well-managed soil (fertilised soil) (Table 3 and Table 4) over a month. This result contrasted with the findings of experiment one, where the mineralisation of ^{14}C-glucose was higher. Moreover, the maximum rates of ^{14}C-glucose mineralisation did not show a constant pattern. Generally, with a higher application rate of biochar (5%) and finer particle size of biochar (1 and 0.1 mm) the highest and lowest maximum rates of mineralisation were observed on day 0 (1.20% h^{-1} and 0.47% h^{-1}) respectively ($P<0.05$), (Table 3). Nevertheless, the finer particle size (0.1 mm) significantly increased ($P<0.05$) mineralisation of ^{14}C-glucose at the higher dosage of biochar (5%) on the final day of incubation. In terms of the ^{14}C-glucose incorporation into the microbial biomass, the findings exhibit that at both dosages (2% and 5%), soil amended with biochar decreased the microbial biomass ($P<0.05$) in comparison with the un-amended soil (Tables 3 and 4).

Table 3- Maximum rates, ^{14}C extent mineralisation, ^{14}C biomass uptake and ^{14}C activity remaining for the fertilised soil (F) and unfertilised soil (UF) amended with 5% biochar and with no biochar (Control) over a month. Error bars are SEM (n=3). Values in asterisk indicate significance at P<0.05.

Treatment (mm)	*Day*	*Maximum rate (% h^{-1})*	*^{14}C extents mineralisation (%)*	*^{14}C biomass uptake (%)fixed k_{EC}*	*^{14}C activity remaining in soil (%)*
F Control	0	1.01 ± 0.10*	12.02 ± 1.23	93.22 ± 11.34	0.00 ± 0.00
	30	0.76 ± 0.12	10.34 ± 0.84	47.67 ± 5.45	37.78 ± 7.78
F 5% (2)	0	0.99 ± 0.08*	9.84 ± 0.47	23.54 ± 1.57*	62.91 ± 2.33
	30	0.97 ± 0.18	12.31 ± 1.15	29.04 ± 3.06*	53.50 ± 6.80
F 5% (1)	0	1.20 ± 0.19*	9.66 ± 0.18	27.17 ± 4.80*	59.80 ± 3.11
	30	0.86 ± 0.08	13.09 ± 1.13	41.19 ± 2.21*	40.33 ± 2.92
F 5% (0.5)	0	0.76 ± 0.03	8.08 ± 0.22	31.65 ± 7.49*	57.39 ± 8.45
	30	0.82 ± 0.12	13.32 ± 0.5	37.08 ± 4.50*	44.70 ± 7.56
F 5% (0.1)	0	0.47 ± 0.02	7.97 ± 0.94	30.05 ± 2.53*	58.47 ± 3.37
	30	0.85 ± 0.09	16.15 ± 0.52*	42.65 ± 2.05*	35.35 ± 7.59
UF Control	0	0.94 ± 0.15*	11.55 ± 0.39	41.20 ± 5.40	43.04 ± 7.20
	30	1.36 ± 0.08	19.09 ± 1.22	38.31 ± 4.13	35.12 ± 11.47
UF 5% (2)	0	0.88 ± 0.06	10.27 ± 1.15	6.05 ± 0.89*	79.21 ± 5.73
	30	2.12 ± 0.01	24.20 ± 0.17	26.80 ± 1.90*	40.78 ± 6.83
UF 5% (1)	0	0.74 ± 0.15	12.19 ± 0.51	9.15 ± 4.21*	74.13 ± 4.71
	30	1.95 ± 0.30	22.26 ± 1.01	31.28 ± 2.84*	38.12 ± 10.72
UF 5% (0.5)	0	0.63 ± 0.05	11.83 ± 1.49	4.37 ± 1.39*	78.49 ± 3.38
	30	1.86 ± 0.28	25.37 ± 1.26	31.59 ± 1.89*	33.44 ± 10.71
UF 5% (0.1)	0	0.36 ± 0.03	11.96 ± 0.09	8.17 ± 1.56*	75.79 ± 4.47
	30	1.51 ± 0.05	30.92 ± 0.73*	21.40 ± 1.97*	36.70 ± 8.71

Table 4- Maximum rates, ^{14}C extent mineralisation, ^{14}C biomass uptake and ^{14}C activity remaining for the fertilised soil (F) and unfertilised soil (UF) amended with 2% biochar and with no biochar (Control) over a month. Error bars are SEM (n=3). Values in asterisk indicate significance at P<0.05

Treatment (mm)	*Day*	*Maximum rate (% h^{-1})*	*^{14}C extents mineralisation (%)*	*^{14}C biomass uptake (%) fixed k_{EC}*	*^{14}C activity remaining in soil (%)*
F Control	0	1.01 ± 0.10*	12.02 ± 1.23	93.22 ± 11.34	0.00 ± 0.00
	30	0.76 ± 0.12	10.34 ± 0.84	47.67 ± 5.45	37.78 ± 7.78
F 2% (2)	0	1.05 ± 0.32	11.30 ± 1.18	72.25 ± 6.55*	11.61 ± 11.60
	30	1.10 ± 0.07	12.89 ± 0.96	61.61 ± 12.30	20.33 ± 15.47
F 2% (1)	0	0.82 ± 0.16	9.80 ± 0.40	73.49 ± 11.18*	13.08 ± 13.58
	30	0.73 ± 0.03	12.78 ± 0.64	39.63 ± 2.23*	42.75 ± 6.79
F 2% (0.5)	0	1.19 ± 0.11	9.66 ± 0.22	45.65 ± 0.86*	41.28 ± 3.39
	30	1.07 ± 0.27	13.77 ± 1.72	46.90 ± 6.51*	33.17 ± 11.27
F 2% (0.1)	0	1.07 ± 0.13	9.68 ± 0.24	48.92 ± 4.70*	37.96 ± 7.72
	30	1.02 ± 0.10	13.79 ± 1.41	43.48 ± 7.70*	36.84 ± 8.81
UF Control	0	0.94 ± 0.15*	11.55 ± 0.39	41.20 ± 5.40	43.04 ± 7.20
	30	1.36 ± 0.08	19.09 ± 1.22	38.31 ± 4.13	35.12 ± 11.47
UF 2% (2)	0	0.79 ± 0.07	10.87 ± 0.59	11.62 ± 2.88*	73.35 ± 2.26
	30	1.26 ± 0.17	22.26 ± 2.06	30.31 ± 3.85*	38.14 ± 7.82
UF 2% (1)	0	0.81 ± 0.09	11.65 ± 1.12	13.40 ± 0.97*	70.04 ± 5.82
	30	1.31 ± 0.20	26.04 ± 3.44	24.12 ± 5.61*	38.03 ± 17.72
UF 2% (0.5)	0	0.56 ± 0.05	13.39 ± 0.59	14.45 ± 0.27*	67.15 ± 5.44
	30	1.43 ± 0.17	23.43 ± 1.49	36.02 ± 2.44*	31.37 ± 11.68
UF 2% (0.1)	0	0.95 ± 0.01	11.98 ± 1.16	13.67 ± 1.43*	69.30 ± 4.36
	30	1.86 ± 0.35	29.75 ± 2.80	23.34 ± 3.45*	34.44 ± 15.64

In comparison to the mineralisation of ^{14}C-glucose the unmanaged soil (unfertilised soil) displayed the same pattern as the well-managed soil (fertilised soil) (Tables 3 and 4). The mineralisation of ^{14}C-glucose was relatively lower than the incorporation of ^{14}C-glucose into the biomass. The smallest particle size (0.1 mm) increased the ^{14}C-glucose mineralisation ($P<0.05$) after a month (30 days) contact time at a higher dosage (5%) (Table 3). Meanwhile, the maximum rates of mineralisation constantly increased over the course of the study. For instance, on days 0 and 30 the maximum rate of ^{14}C-glucose mineralisation ranged from 0.36 to 0.95 (% h^{-1}) and 1.26 to 2.12 (% h^{-1}), respectively (Tables 3 and 4). In addition, the maximum rate in the untreated soil on day 0 (Table 4) was significantly higher ($P<0.05$) than at 5% dosage, as well as at 0.1 mm of particle size (Table 3). Also, the biomass uptake of ^{14}C-glucose had a similar pattern as fertilised soil where the value of the biomass uptake decreased at the higher application rate (5%) of biochar compared to the un-amended soil ($P<0.05$). Mineralisation and biomass uptake of ^{14}C-glucose in both soils (fertilised and unfertilised soils) did not significantly affect lower rate of biochar application (2%), as well as various particle sizes of biochar (Table 4). This finding is in agreement with Jones et al. (2012) and Quilliam et al. (2012). Though, at 5% application rate of biochar, the extent of mineralisation of ^{14}C-glucose increased over the period of the study and also in both well-managed and unmanaged soils ($P<0.05$). These results indicate that the effect of amending soil with biochar exhibited an increase in microbial activity at higher application rates. Likewise, the improvement in the mineralisation of ^{14}C-carbon proves that there was a positive priming and degradation of the labile carbon fractions of biochar in soil (Hamer et al. 2004). Furthermore, Quilliam et al. (2012) observed that there was a major change in the quality of soil and microbial biomass in the treatments with higher application rates of biochar (25+25t ha^{-1} and 50+50t ha^{-1}) in contrast to the treatments with lower rates of biochar application (25t ha^{-1} and 50t ha^{-1}) after a longer period of biochar application (more than 3 years). The authors stated that soil nutrient status and soil structure improved, making it suitable for microbial habitation when higher dosages of biochar were applied.

In addition, our findings reveal that smaller particle sizes stimulated more ^{14}C-glucose mineralization than the greater sizes in fertilised and unfertilised soils. The results are in agreement with Sigua et al. (2014), where, finer particle size of biochar (<0.42 mm) increased the mineralisation rate and amount of CO_2 evolution compared to the larger particle size of biochar (>2 mm) due to higher surface area of the former. Similarly, finer-particle, spent mushroom-derived biochar (<0.5 mm) produced at 700 ^{o}C accelerated the release of phosphates and improved bacterial species richness in soils, compared to larger particle sizes (>0.5 mm) (Sarfraz et al. 2020). In support, Zhao et al. (2020) further attributed enhanced microbial activity and biomass by finer-particle (<1 mm) wood biochar (450 ^{o}C) to higher N nutrient release and degradation. Generally, uptake of ^{14}C-glucose in the control soils (fertilised and unfertilised) of this study were much higher than in soils amended with biochar. However, fertilisation increased the ^{14}C-glucose uptake by 50%, indicating the necessity of nutrient availability for glucose uptake and carbon turnover by microorganisms (Table 3) (Liang et al. 2019). The availability of nutrients and glucose in soils thus encourages microbial cellular development and carbon sequestration, but as time increases, the uptake rate decreases markedly. In fertilised soils, increases in biochar concentration significantly ($P<0.05$) reduced ^{14}C-glucose uptake and it was observed that at 2% concentration, the finer-particle biochars (0.1 and 0.5 mm) further reduced ^{14}C-glucose uptake significantly compared to larger particle sized biochars (1 and 2 mm). It seems that larger surface area and glucose adsorption sites of the finer particles inhibited glucose availability for microbial uptake and utilization.

On the contrary, lower nutrient content in unmanaged (fertilised) soil resulted in a reduction in microbial biomass uptake and a higher mineralisation rate of ^{14}C-carbon in comparison to the well-managed (fertilised) soil (Table 3). The scarce source of nutrients in unmanaged soil limits microbial ^{14}C-glucose uptake and further growth of microbes in the soils. This interpretation is supported by Zhang et al. (2014), in which the authors demonstrated that inadequate nutrients and a lack of available carbon in a larger-textured soil make the soil unsuitable for microbial growth. As biochar concentration increased, there was also a corresponding decrease in ^{14}C-glucose biomass uptake, but as incubation time increased to 30 days, ^{14}C-glucose uptake increased remarkably in the unfertilised soils. This shows that despite adsorption of glucose in soils, the extent of adsorption is reversible and in support of biochar oxidation, carbon sequestration and turnover rate regulation over time.

3.2.3. Effect of biochar on ammonium and nitrate ion loss through leaching in the arable loam, arable sandy and grassland soils (experiment 1).

The amount of ammonium ions leached increased consistently in all of the soils over the course of the study ($P<0.05$) (Figures 5a, b and c). However, the concentration of ammonium ions in all soils treated with fresh and aged biochar significantly decreased compared to untreated soils. Furthermore, in the first leaching experiment there was no change in the concentration of ammonium ions between the treatments with biochar and with no biochar ($P>0.05$). But, in the final leaching experiment the biochar treatment decreased ammonium leaching significantly ($P<0.05$) from 0.34 mgL^{-1} (control) to 0.06 mg/L (fresh biochar) and 0.14 mg/L (aged biochar) (Figure 5a); and the amount of ammonium leachate in the grassland soil peaked. In addition, the concentration of ammonium ions in the arable loam soil decreased from 0.25 to 0.09 mg/L in fresh biochar treatment and 0.15 mg/L in aged biochar treatment (Figure 5b). Meanwhile, the arable sandy soil ammonium leaching also reduced significantly ($P<0.05$) from 0.88 to 0.27 mg/L in aged biochar treatment and 0.13 mg/L in fresh biochar treatment (Figure 5c). Yao et al. (2012), demonstrated that nine various types of biochar can adsorb ammonium ions ranging from 1.8% to 15.7% owing to the high cation exchange capacity of biochar.

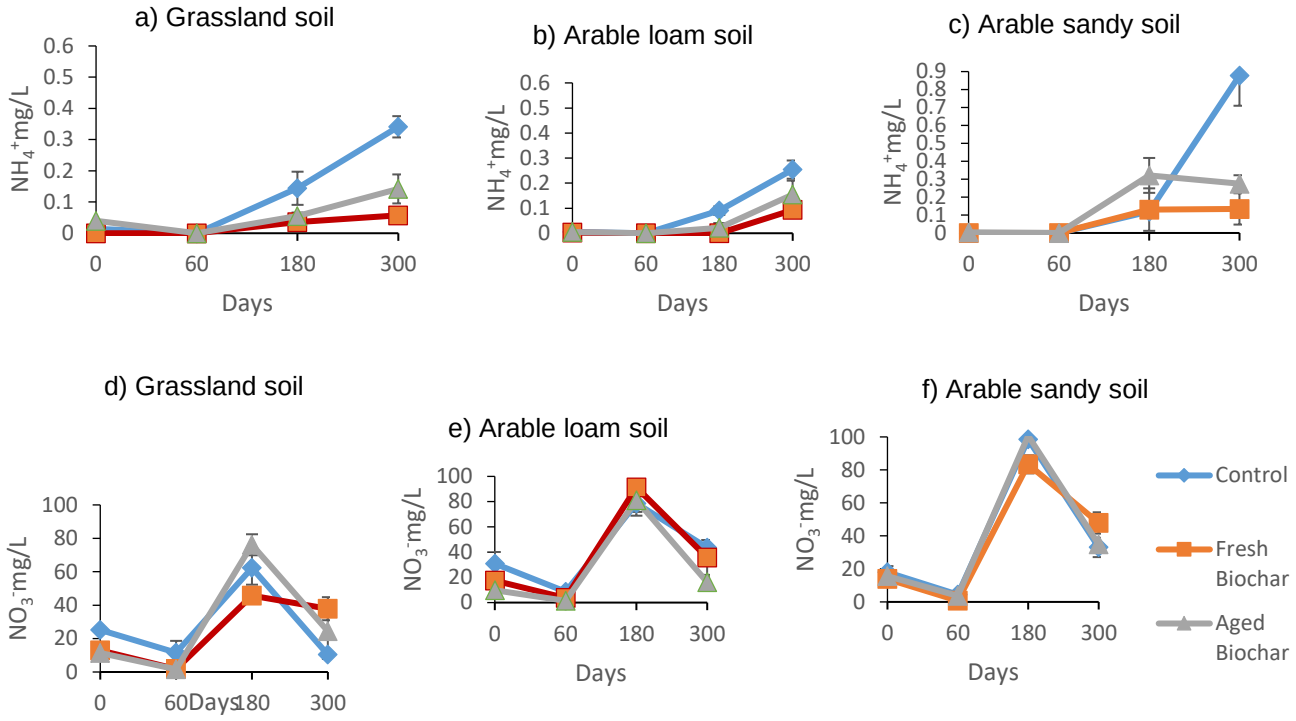

Figure 5- Concentration of ammonium (NH_4^+) and nitrate (NO_3^-) ions in the leachate of the a) and d) grassland, b) and e) arable loam and c) and f) arable sandy soils treated with fresh and aged biochar; and with no biochar, over 300 days. Error bars are SEM (n=3)

Nitrate ion concentration in the soil leachates fluctuated over the course of the study. The trend of nitrate leaching in biochar treatments did not display a consistent pattern and the differences were also insignificant (P>0.05). For example, in the first leaching experiment the concentration of nitrate ions was low. Then it increased in the middle of the leaching event and then decreased at the end of the leaching experiment (Figures 5d, e and f). This indicates that the nitrification process and reversible sorption happened, whereas the inhibition of nitrification took place at the end of the leaching experiment. Nevertheless, the mechanisms behind this process are unclear. Moreover, biochar treatments in the arable sandy soil did not show any effect, though biochar treatments were observed only to decrease the concentration of nitrate ions leached on days 0 and 60 in the arable loam and grassland soils (Figures 5d, e and f).

3.2.4. Effect of biochar on ammonium and nitrate ion loss through leaching in fertilised and unfertilised soils (experiment 2)

The amount of ammonium ions leached from both well-managed (fertilised) soil and unmanaged (unfertilised) soil was very small; and ranged from 0.00 to 0.07 mg/L. In the beginning of the leaching process, the concentration of ammonium ions in the untreated fertilised soil was higher compared to the soils with biochar treatments. However, the leaching of ammonium ions was observed to be really low and the differences were insignificant in the final leaching event which was on day 30 (Table 5). In addition, the concentration was too low to be observed in this study. However, the amount of nitrate ions leached was higher than that of ammonium ions in both soils (Table 5). Results show that biochar treatments affected nitrate leaching only in the early stage of a leaching event. For instance, the concentration of nitrate ions slightly increased at the higher application rate of biochar (5%) with 0.1 mm particle size on day 0, though at the final leaching event (day 30) the biochar did not show any effect (Table 5). An increase in nitrate leaching is not uncommon for biochar-amended soils. Since ammonium ion concentration was significantly low, we rule out nitrification occurrence. Rather it is partly due to vertical transport of smaller particles of biochar upon moisture addition (Wang et al. 2013) and electrostatic repulsion due to more negative charges of O-containing functional groups on biochar surfaces (Zhang et al. 2020). This would have been more obvious in the finer-particle-sized and high-dosage of biochar. Nevertheless, during the final leaching process, unmanaged soil (unfertilised) treated with (2, 1, 0.5 and 0.1 mm) biochar reduced the concentration of nitrate ions in the leachate at both higher and lower application rates in comparison to the control treatment (Table 5). But in fertilised soils, 2, 1 and 0.5 mm biochars (5%) either increased or had no effect on leachate formation after 30 days of incubation. Obviously, this shows reversible nitrate adsorption capacities of the biochars and microbial influence to enhance availability of the nitrates following increase in contact time.

Table 5- Effect of ammonium (NH_4^+) and nitrate (NO_3^-) leaching, in fertilised and unfertilised soils treated with 2% and 5% biochar; and with no biochar, over a month. Error bars are SEM (n=2). Values in asterisk indicate significance at P<0.05

Variable	*Treatments (mm)*	*Fertilised Day 0 (mg/L)*	*Fertilised Day 30 (mg/L)*	*Unfertilised Day 0 (mg/L)*	*Unfertilised Day 30 (mg/L)*
Ammonium (NH_4^+) Leaching	Control	0.07 ± 0.05	0.00 ± 0.00	0.01 ± 0.01	0.00 ± 0.00
	2% (2)	0.00 ± 0.00	0.00 ± 0.00	0.03 ± 0.00	0.01 ± 0.01
	2% (1)	0.00 ± 0.00	0.00 ± 0.00	0.00 ± 0.00*	0.00 ± 0.00
	2% (0.5)	0.00 ± 0.00	0.00 ± 0.00	0.00 ± 0.00	0.00 ± 0.00
	2% (0.1)	0.00 ± 0.00	0.00 ± 0.00	0.00 ± 0.00*	0.00 ± 0.00
	5% (2)	0.00 ± 0.00	0.00 ± 0.00	0.00 ± 0.00	0.01 ± 0.01
	5% (1)	0.00 ± 0.00	0.00 ± 0.00	0.00 ± 0.00	0.00 ± 0.00
	5% (0.5)	0.00 ± 0.00	0.00 ± 0.00	0.01 ± 0.01	0.00 ± 0.00
	5% (0.1)	0.00 ± 0.00	0.00 ± 0.00	0.00 ± 0.00	0.00 ± 0.00
Nitrate (NO_3^-) Leaching	Control	19.70 ± 0.45	15.92 ± 2.42	11.48 ± 0.63	15.04 ± 0.92
	2% (2)	16.60 ± 3.50	15.81 ± 2.54	12.08 ± 0.88	7.04 ± 4.58
	2% (1)	16.28 ± 0.33	9.72 ± 4.36	10.45 ± 0.30	9.38 ± 0.11
	2% (0.5)	17.70 ± 0.55	5.29 ± 2.87	10.48 ± 0.63	12.11 ± 2.93
	2% (0.1)	18.83 ± 0.88	4.47 ± 0.76	10.90 ± 0.05	8.03 ± 0.54
	5% (2)	17.53 ± 2.63	17.11 ± 6.01	10.83 ± 0.08	4.88 ± 0.20*
	5% (1)	11.55 ± 1.60	22.08 ± 3.64	9.28 ± 0.43	3.66 ± 0.62*
	5% (0.5)	15.30 ± 1.15	14.15 ± 2.34	9.63 ± 0.73	2.18 ± 0.12*
	5% (0.1)	22.30 ± 1.75*	6.00 ± 3.47	12.53 ± 0.13*	5.25 ± 0.37*

4. Conclusions

Pyrolysis of biomass to produce biochar sustainably stabilizes carbon and can enhance soil and agronomic properties upon application. This study revealed that smaller particle sizes and higher application rate of biochar mineralised more ^{14}C-carbon than greater sizes. Soils with poor nutrient contents have more advantages than soils which are rich in nutrients with respect to the microbial growth. These benefits were further enhanced when higher application rates were applied. Finer particle sizes of biochar were also more beneficial. In addition, biochar had a higher preference to adsorb ammonium ions rather than nitrate ions. This can minimise the loss of ammonium ions through leaching and reduces the potential for eutrophication. The soils investigated in this study are temperate soils. This study provides vital information with regards to the use of biochar in the temperate region to sequester carbon, ameliorate acidic soils and manage ammonium ion inputs. The effects of biochar are dependent on various factors, such as the kind of soils used, the dosage, as well as the particle size of biochar. Consequently, the results of this study are useful for understanding the factors that influence the application of biochar in agricultural fields. These factors need to be further assessed prior to the application of biochar on a broader and wider scale.

Acknowledgements

We would like to thank Prof Nick Ostle, Mr James Turner, Dr Vassil Karloukovski and Lakam Mejus for their help with soil and biochar collection from Edinburgh and Penrith, UK. Also, we would like to thank Anne Wilkinson, Helen Quirk, Dave Hugh and Dr Annette Ryan for their technical assistance in the laboratory.

References

Busch D & Glaser B (2015). Stability of co-composted hydrochar and biochar under field conditions in a temperate soil. *Soil Use and Management* 31(2): 251-258. https://doi.org/10.1111/sum.12180

Boucard T K, McNeill C, Bardgett R D, Paynter C D & Semple K T (2008). The impact of synthetic pyrethroid and organophosphate sheep dip formulations on microbial activity in soil. *Environmental Pollution* 153: 207 – 214. https://doi:10.1016/j.envpol.2007.07.027

Chen H, Yang Z, Chu R K, Tolic N, Liang , Graham D E, Wullschleger S D & Gu B (2018). Molecular insights into arctic soil organic matter degradation under warming. *Environmental Science & Technology* 52(8): 4555-4564. https://doi.org/10.1021/acs.est.7b05469

Dynarski K A, Bossio D A & Scow K M (2020). Dynamic Stability of Soil Carbon: Reassessing the "Permanence" of Soil Carbon Sequestration. *Frontiers in Environmental Science* 8: 218. https://doi.org/10.3389/fenvs.2020.514701

de Jesus Duarte S, Glaser B & Pellegrino Cerri C E (2019). Effect of biochar particle size on physical, hydrological and chemical properties of loamy and sandy tropical soils. *Agronomy* 9(4): 165. https://doi.org/10.3390/agronomy9040165

Doick K J & Semple K T (2003). The effect of soil: water ratios on the mineralisation of phenanthrene: LNAPL mixtures in soil. *FEMS Microbiology Letters* 220(1): 29-33. https://doi.org/10.1016/S0378-1097(03)00056-9

Hamer U, Marschner B, Brodowski S & Amelung W (2004). Interactive priming of black carbon and glucose mineralisation. *Organic Geochemistry* 35(7): 823-830. https://doi.org/10.1016/j.orggeochem.2004.03.003

Ippolito J A, Cui L, Kammann C, Wrage-Mönnig N, Estavillo J M, Fuertes-Mendizabal T, Cayuela M L, Sigua G, Novak J, Spokas K & Borchard N (2020). Feedstock choice, pyrolysis temperature and type influence biochar characteristics: a comprehensive meta-data analysis review. Biochar 2: 421-438. https://doi.org/10.1007/s42773-020-00067-x

Jiang S, Nguyen T A, Rudolph V, Yang H, Zhang D, Ok Y S & Huang L (2017). Characterization of hard-and softwood biochars pyrolyzed at high temperature. *Environmental geochemistry and Health* 39: 403-415. DOI 10.1007/s10653-016-9873-6

Jones D L, Rousk J, Edwards-Jones G, DeLuca T H & Murphy D V (2012). Biochar-mediated changes in soil quality and plant growth in a three year field trial. *Soil Biology and Biochemistry* 45: 113-124. https://doi.org/10.1016/j.soilbio.2011.10.012

Kandeler E (2007). Physiological and biochemical methods for studying soil biota and their function. *Soil Microbiology, Ecology, and Biochemistry* pp. 53-83. https://doi.org/10.1016/B978-0-08-047514-1.50007-X

Lehmann J, da Silva Jr J P, Steiner C, Nehls T, Zech W & Glaser B (2003). Nutrient availability and leaching in an archaeological Anthrosol and a Ferralsol of the Central Amazon basin: fertilizer, manure and charcoal amendments. *Plant and Soil* 249(2): 343-357. https://doi.org/10.1023/A:1022833116184

Liang Z, Olesen J E, Jensen J L & Elsgaard L (2019). Nutrient availability affects carbon turnover and microbial physiology differently in topsoil and subsoil under a temperate grassland. *Geoderma* 336: 22-30. https://doi.org/10.1016/j.geoderma.2018.08.021

Nie C, Yang X, Niazi N K, Xu X, Wen Y, Rinklebe J, Ok Y S, Xu S & Wang H (2018). Impact of sugarcane bagasse-derived biochar on heavy metal availability and microbial activity: a field study. *Chemosphere* 200: 274-282. https://doi.org/10.1016/j.chemosphere.2018.02.134

Quilliam R S, Marsden Karina A, Gertler C, Rousk J, DeLuca T H & Jones D L (2012). Nutrient dynamics, microbial growth and weed emergence in biochar amended soil are influenced by time since applicatioan and reapplication rate. *Agriculture, Ecosystem and Environment* 158: 192-199. https://doi.org/10.1016/j.agee.2012.06.011

Paroissien J B, Darboux F, Couturier A, Devillers B, Mouillot F, Raclot D & Le Bissonnais Y (2015). A method for modeling the effects of climate and land use changes on erosion and sustainability of soil in a Mediterranean watershed (Languedoc, France). *Journal of Environmental Management* 150: 57-68. https://doi.org/10.1016/j.jenvman.2014.10.034

Reid B J, MacLeod C J, Lee P H, Morriss A W, Stokes J D & Semple K T (2001). A simple 14C-respirometric method for assessing microbial catabolic potential and contaminant bioavailability. *FEMS Microbiology Letters* 196(2): 141-146. https://doi.org/10.1111/j.1574-6968.2001.tb10555.x

Sarfraz R, Yang W, Wang S, Zhou B & Xing S (2020). Short term effects of biochar with different particle sizes on phosphorous availability and microbial communities. *Chemosphere*, 256, 126862. pp https://doi.org/10.1016/j.chemosphere.2020.126862

Sigua G, Novak J, Watts D, Cantrell K, Shumaker P, Szögi A & Johnson M (2014). Carbon mineralization in two ultisols amended with different sources and particle sizes of pyrolyzed biochar. *Chemosphere* 103: 313-321. https://doi.org/10.1016/j.chemosphere.2013.12.024

Wang D, Zhang W, Hao X & Zhou D (2013). Transport of biochar particles in saturated granular media: effects of pyrolysis temperature and particle size. *Environmental Science & Technology* 47(2): 821-828. https://doi.org/10.1021/es303794d

Wang W, Zeng C, Sardans J, Wang C, Zeng D & Peñuelas J (2016). Amendment with industrial and agricultural wastes reduces surface-water nutrient loss and storage of dissolved greenhouse gases in a subtropical paddy field. *Agriculture, Ecosystems & Environment* 231: 296-303. https://doi.org/10.1016/j.agee.2016.07.012

Wong J W C, Webber J B W & Ogbonnaya U O (2019). Characteristics of biochar porosity by NMR and study of ammonium ion adsorption. *Journal of Analytical and Applied Pyrolysis*, 143, 104687 pp. https://doi.org/10.1016/j.jaap.2019.104687

Yao Y, Gao B, Zhang M, Inyang M & Zimmerman A R (2012). Effect of biochar amendment on sorption and leaching of nitrate, ammonium, and phosphate in a sandy soil. *Chemosphere* 89: 1467-1471. https://doi.org/10.1016/j.chemosphere.2012.06.002

Zhang Q.-z, Dijkstra F A, Liu X.-r, Wang Y.-d, Huang J & Lu N (2014). Effects of biochar on soil microbial biomass after four years of consecutive application in the north China plain. *PloS One* 9(7): p.e102062. https://doi.org/10.1371/journal.pone.0102062

Zhang J, Tang X, Zhong S, Yin G, Gao Y & He X (2017). Recalcitrant carbon components in glomalin-related soil protein facilitate soil organic carbon preservation in tropical forests. *Scientific Reports* 7(1): 1-9. DOI:10.1038/s41598-017-02486-6

Zhang M, Song G, Gelardi D L, Huang L, Khan E, Mašek O, Parikh S J & Ok Y S (2020). Evaluating biochar and its modifications for the removal of ammonium, nitrate, and phosphate in water. *Water Research*, 116303 pp. https://doi.org/10.1016/j.watres.2020.116303

Zhao R, Wu J, Jiang C & Liu F (2020). Effects of biochar particle size and concomitant nitrogen fertilization on soil microbial community structure during the maize seedling stage. *Environmental Science and Pollution Research* 27(12): 13095-13104. https://doi.org/10.1007/s11356-020-07888-0

Zhou J, Liang X, Shan S, Yan D, Chen Y, Yang C, Lu Y, Niyungeko C & Tian G (2019). Nutrient retention by different substrates from an improved low impact development system. *Journal of Environmental Management* 238: 331-340. https://doi.org/10.1016/j.jenvman.2019.03.019

Journal of Agricultural Sciences
(Tarim Bilimleri Dergisi)

J Agr Sci-Tarim Bili
e-ISSN: 2148-9297
jas.ankara.edu.tr

Mobile Device-Based Detection System of Diseases and Pests in Rose Plants Using Deep Convolutional Neural Networks and Quantization

Burhan Duman[a]

[a]*Department of Computer Engineering, Isparta University of Applied Sciences, Isparta, TURKEY*

ARTICLE INFO
Research Article
Corresponding Author: Burhan Duman, E-mail: burhanduman@isparta.edu.tr
Received: 12 July 2024 / Revised: 13 October 2024 / Accepted: 27 October 2024 / Online: 25 March 2025

Cite this article
Duman B (2025). Mobile Device-Based Detection System of Diseases and Pests in Rose Plants Using Deep Convolutional Neural Networks and Quantization. *Journal of Agricultural Sciences (Tarim Bilimleri Dergisi),* 31(2):302-318. DOI: 10.15832/ankutbd.1514972

ABSTRACT
In agriculture, the rapid and accurate identification of plant diseases and pests is crucial for maintaining the quality and yield of agricultural products. This study focuses on detecting diseases and pests affecting *Rosa damascena* Mill. plants through an ensemble learning approach and deploying the model in an Android mobile application-a rarity in similar research. A new dataset was created using images from the natural habitat and season of *Rosa damascena* Mill., covering seven different diseases and pests.

For this approach, pre-training was performed with mixed-Convolutional Neural Network (CNN) models DenseNet169, ResNet152, MobileNetV2, VGG19, and NasNet. DenseNet169 and MobileNetV2, which are the models with the highest classification success obtained from mixed-CNN models, were combined in the new model by fine-tuning with the ensemble learning method. In the performance tests of the model, an accuracy of 95.17% was obtained.

In addition, this study introduces an Android mobile application integrating these models, a distinctive feature compared to other similar studies. The best performances of these models, DenseNet169 and MobileNetV2 in both flat buffered and quantized forms, were performed separately on a computer, a physical mobile device, and an Android emulator. MobileNetV2 outperformed DenseNet169 (2271 ms) by having the lowest average inference time (301 ms) on mobile devices. These results demonstrate the effectiveness of using a mobile device to detect rose plant diseases and pests efficiently in natural environments.

Keywords: Mobile application, Image classification, Deep ~~l~~earning, Plant disease and pests, *Rosa damascena* Mill

1. Introduction

Agriculture is one of the most important and significant resources for the country's economy. However, agricultural products are severely affected by plant diseases. These challenges can be addressed by using modern agricultural technologies (Sharma & Singh 2015). These technologies, which are considered costly compared to traditional methods, can be made cost-effective by applying machine learning and deep learning approaches in image processing applications. Additionally, learning about leaf diseases can yield better results than traditional methods (Khitthuk et al. 2018).

Foliar diseases in plants depend on factors such as survival and climate, but most arise from attacks by viruses, bacteria, and fungi. Pathological diseases cause 85% of foliar diseases and most farmers in developing countries rely on traditional methods such as visual observation, physiological observation, manual inspection, laboratory tests and tissue analysis, which are more labor and time consuming. Typically, manual detection of foliar diseases is considered to be specialized and unsatisfactory due to the human factor. Therefore, it is becoming increasingly common to introduce a modern, deep learning-based approach to disease detection (Mutka & Bart 2015; Mahlein 2016; Weerakoon et al. 2017; Ferentinos 2018).

Rosa damascena Mill., which is called the “Isparta Rose” in Turkey, is a valuable industrial plant used in the food, medicine, cosmetics, and various other sectors. Introduced to Isparta from the Kazanlık region of Bulgaria in the late 19th century, *Rosa damascena* Mill. is now cultivated in the provinces of Isparta, Burdur, Afyon, and Denizli. This plant is generally harvested in May and June, with regional and seasonal variations, and should be harvested early in the morning to optimize oil production (Ersan & Başayiğit 2022). *Rosa damascena* Mill. thrives in temperate climates and is a shrub-type industrial plant known for its pink color, intense fragrance, and flowers that measure an average diameter of 7 cm and weigh 2-3 grams (see Figure 1).

Figure 1- *Rosa damascena* Mill

Products such as oil obtained from the Isparta oil rose have applications in various fields, particularly in the cosmetics and pharmaceutical sectors. Turkey generates an income of approximately 10 million dollars from rose products annually (Bıtrak & Hatırlı 2022). As with every plant species, the rose plant can also be affected by diseases and pests. These infections can lead to a reduction in flower yield and quality (Karanfil 2021). Managing various diseases and pests on *Rosa damascena* Mill. is essential. Of the numerous diseases, the main ones are rose rust (*Phragmidium mucronatum*) and rose powdery mildew (*Sphaerotheca rosae*). The most significant pests include cochlea (*Rhodococcus perornatus*), proboscis (*Mecorhis umgaricus*), sprout wasp (*Syrista parreyssi*), sprout aphid (*Ardis brunniventris*), scissors beetle (*Perotis chlorana*), rose moth (*Cnaemidophorus rhododactyla*), comma aphid (*Leulmidosa*), rose aphid (*Macrosiphum rosae*), spider mite (*Tetranychus urticae Koch*), and leafhopper (Thrips meridionalis Priesner) (Baydar 2016).

Poor timing of control against diseases and pests in *Rosa damascena* Mill. results in biomass losses and a decrease in the oil content, hence poor quality products with lower yields (Yılmaz 2015). Therefore, early detection of diseases and pests in RDM and prompt application of spraying will help prevent adverse outcomes as much as possible. Failure to do so may result in the spread of these diseases and pests to other rose plants, causing significant damage (Fazili et al. 2024).

Farmers typically rely on traditional methods, primarily visual observation, to identify diseases in *Rosa damascena* Mill. Visual classification with the naked eye requires prior knowledge and experience, especially in diagnosing leaf-based diseases. This manual process can be time-consuming, and diseases found in plants may be misidentified. Inaccurate disease detection can lead to incorrect treatment.

In the literature, academic studies on rose plants can be classified into two categories: cut rose and oil rose. Cut roses are often grown for landscaping and commercial sales. The main characteristic that distinguishes oil rose from cut rose is its ability to be industrially processed and converted into various commercial products. Deep learning methods play a significant role in academic studies on cut roses. For instance, Swetharani & Prasad (2021) used Convolutional Neural Networks to classify leaf diseases with an accuracy of 97.30% using images from cut rose leaves. Rajbongshi et al. (2020) utilized the MobileNet architecture to classify four rose disease types with 95.63% accuracy, using 400 images. Ma et al. (2020) applied CNN-based Alexnet, VGG16, and neural discriminative dimensionality reduction (NDDR) methods to detect Black Spot in roses in China. They found that the NDDR-CNN model yielded the best results. Khaleel et al. (2022) employed a Deep Learning-based CNN model to detect four diseases in rose plant leaves, achieving an accuracy rate of 64.35%. Yin et al. (2021) distinguished between the early, middle, and advanced stages of Black Spot disease in the leaves of Chinese roses and healthy leaves, achieving a success rate of 84.16% with the Faster R-CNN technique.

In recent years, many computer vision and deep learning methods have been developed to address the challenges arising from manual techniques (Chen et al. 2020). These methods focus on creating an image database, performing feature extraction, and conducting classification analysis. Fuentes et al. (2018) using a database of 5,000 images and deep convolutional neural networks, achieved a 96% success rate in tomato disease and pest identification. Zhong & Zhao (2020) achieved a 93.30% F1-Score classification success with the DenseNet-121 deep convolution network using 2,462 apple leaf images across six different diseases. Sethy et al. (2020) used a database of 5,932 rice leaf images covering four diseases in their study. The study, which employed thirteen different CNN models, reached an F1-Score of 97.96% with MobileNetV2 feature extraction and SVM classification.

In this study, a system is presented to address the above-mentioned disadvantages and enable quicker, more accurate classification performance. The system, which includes computer vision and a mobile application, offers an accessible solution that aims to detect diseases faster and more accurately without the need for prior knowledge and experience. As a result, more

precise measures can be taken in a short period. Timely spraying will reduce pesticide residues that can negatively impact the export of other products, especially rose oil, and prevent economic losses due to decreased harvests.

The main contributions of this study to the literature are:

- The creation of a new dataset on plant diseases and pests affecting the oil rose, which is one of the most important economic products in Turkey and the world.
- Transfer learning and fine-tuning methods were applied to the CNN models to achieve optimal results in classification-based CNN models
- An ensemble method using mixed-CNN models was used to improve the classification performance of the detecting system.
- A mobile application was developed that integrates flatbuffered and quantized versions of the models to utilize the performance of the best models in real-time and without network access in the field.

The second section of the paper describes the characteristics of the dataset created, the deep learning algorithms used in the study, ensemble learning, and the performance evaluation criteria. The third section examines the results of the algorithms used in the experimental study, while the fourth section discusses the conclusions of the study and future research directions.

2. Development of the Proposed System

The architecture for the proposed disease and plant pest classification approach, including the model training, refinement, and testing processes, is given in Figure 2. For the training and testing of the models, a study-specific original dataset from the rose field was created and labeled. Classification performances of the prepared dataset were observed in a mixed manner with CNN-based approaches. After the obtained classification predictions, the mixed CNN-based model was selected by applying the ensemble learning method on CNN-based algorithms to ensure maximum accuracy performance. During this process, the weights of each model were saved separately in a .h5 file format. The weight file of the models was converted to *.tflite* format and transferred to the developed mobile application.

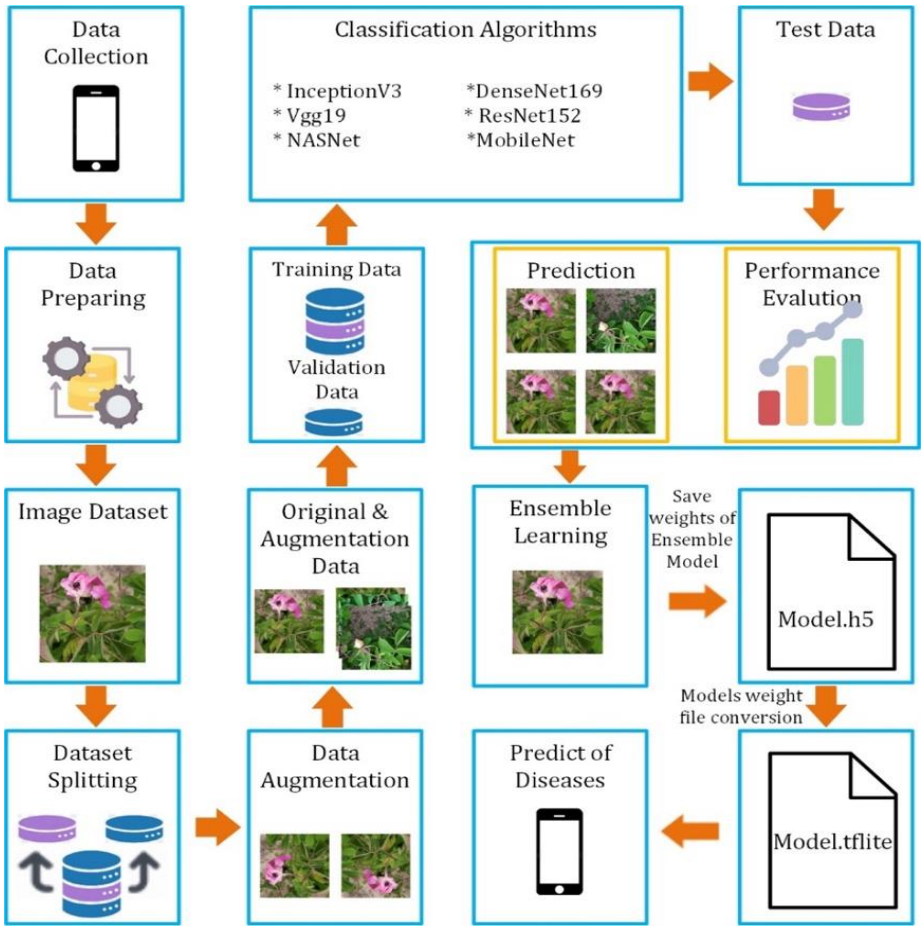

Figure 2- Schematic illustration of proposed system architecture

2.1 Image datasets

The dataset for this study consists of images collected from various rose gardens located in different districts and villages in the Isparta province between May & July 2022. In total, 567 images were captured under natural conditions using a Samsung SM-M317F mobile phone. The dataset includes images of rose plant diseases and pests, such as *Botrytis spp.*, *Ardis brunniventris*, *Mecorhis umgaricus*, *Rhodococcus perornatus*, *Sphaerotheca rosae*, *Phragmidium mucronatum*, and *Macrosiphum rosae*, as well as healthy rose plants. The images were labeled with the assistance of an expert agricultural engineer and by referencing relevant literature. A selection of these images is shown in Figure 3.

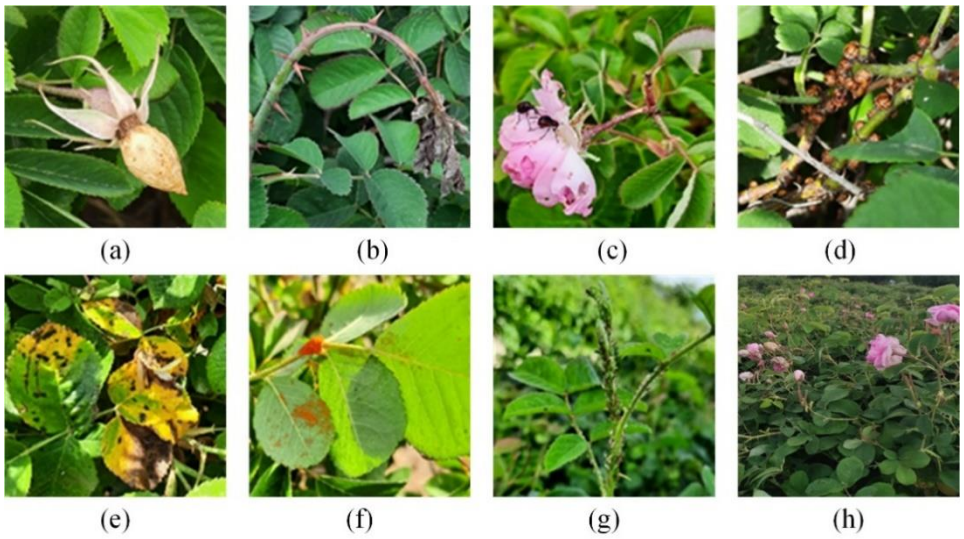

Figure 3- Healthy and diseased variants in the dataset (a) *Botrytis spp.*, (b) *Ardis brunniventris*, (c) *Mecorhis ungarica*, (d) *Rhodococcus perornatus*, (e) *Sphaerotheca rosae*, (f) *Phragmidium mucronatum*, (g) *Macrosiphum rosae*, (h) Healthy

2.2. Data preparing

For the experimental study on the deep learning-based classification of Isparta oil rose diseases, a dataset was created using leaf images from seven diseased plants and one healthy plant. Images collected from the natural environment and labeled according to disease types were carefully reviewed to exclude unsuitable images; these images were subsequently excluded from the dataset. To optimize processing speed, the high file size images in the dataset, originally sized at 3 456 × 3 456 pixels, were resized to 600 × 600 pixels. These images were not cropped. The 567 images in the dataset were randomly selected and divided into training (65%), validation (15%), and test (20%) datasets. In the training and testing processes of mixed CNN models, each image was extracted using Equations 1 - 5 to create ideal images and visual diversity.

$$area = X_{height}\ x\ Y_{width} \tag{1}$$

$$X_{height} = picture.boundingRect(first\_pic) \tag{2}$$

$$Y_{width} = picture.boundingRect(first\_pic) \tag{3}$$

$$Aspect_{ratio} = \frac{X_{height}}{Y_{width}} \tag{4}$$

$$extent = \frac{object\_area}{bounding\_rectange\_area} \tag{5}$$

These formulas calculate ratios between an object and its surrounding rectangle in dataset images, hence enabling the detection of the size. This is especially useful in resizing images that don't fit the 600×600 target size. The advantage of this is that the method will preserve the visual integrity of the objects without degrading image resolution. Stretching images while preserving aspect ratios will keep pictures from deforming through the processing. These operations increase the consistency of data and results for more reliable analysis. This ensures that all the images in the dataset are homogeneous before feeding into any CNN model.

Data augmentation techniques were applied to the images within the dataset to increase the variety. In total, 2 633 images were generated for training and testing, utilizing seven different augmentation techniques: shear_range, fill_mode, horizontal_flip, height_shift_range, width_shift_range, rotation_range, and zoom_range. Table 1 illustrates the disease

categories used in the study, their labels, and the number of training, validation, and test images in the original and augmented data.

Table 1- Labels, disease categories and the count of images in these categories

		Image counts (without data augmentation)			*Image counts (with data augmentation)*		
Label	*Category*	***Train***	***Validation***	***Test***	***Train***	***Validation***	***Test***
0	Healthy	25	6	6	115	29	28
1	Ardis brunniventris	38	9	9	176	42	42
2	Botrytis spp.	44	11	11	204	51	51
3	Macrosiphum rosae	41	10	10	187	48	48
4	Phragmidium mucronatum	51	13	12	236	59	58
5	Rhodococcus perornatus	61	16	15	282	73	72
6	Mecorhis ungarica	70	18	17	325	82	81
7	Sphaerotheca rosae	50	12	12	234	55	55
	Total	380	95	92	1759	439	435
		567			**2633**		

The dataset categories show an unbalanced distribution of images due to the uneven prevalence of diseases and pests during the time period when the dataset images were collected from the natural environment.

2.3. Integrating Mixed-CNN models to system

The disease detection model utilizes transfer learning. Knowledge gained from CNN algorithms, previously trained with large datasets and proven effective, was fine-tuned for new datasets and different classes by adjusting network parameters.

In the algorithm of the system, the dataset and hyperparameters serve as input variables for each designed CNN model. The base CNN model, with initial parameters (weights, input shape, pooling, etc.), is loaded from the Keras applications library. Since the prior learning dataset differs from the dataset used in the target task, the first layers are not trained, allowing prior knowledge to be preserved.

Subsequent layers in the base model and newly added layers (pooling, dropout, dense) are trained with the dataset and hyperparameters specific to the target task. As a result, the model parameters are updated and learning occurs based on the new dataset. The weights providing the best performance during training are saved. Performance metrics are derived from evaluating the trained model with test data it has not seen before. Performance can be gauged by assessing the metrics obtained for each model.

At this point, ensemble learning was applied using basic deep learning models. Through the majority voting method, $C(n,r) = n!/((r!\,(n-r)!))\,p$ predictions from *n* deep learning models with different combinations of *r* elements ($1 < r \leq n$) were combined and the accuracy of the ensemble model was measured. This process led to the ensemble model achieving the highest classification performance.

2.3.1. Deep convolutional neural networks

Deep learning models are widely applied across various research domains, including agriculture, health, and space studies, for tasks such as object detection and classification. In agriculture, they are used for predicting crop yield, while in health, they aid in the early detection of diseases. Moreover, deep learning models contribute to space studies through the classification of constellations (Jung et al. 2021; Oikonomidis et al. 2023; Yu et al. 2023).

These algorithms, which contain multiple hidden layers, excel at tasks such as prediction, classification, speech recognition, visual object recognition, object detection, and drug discovery. Notable deep learning algorithms include Convolutional Neural Networks (CNNs), Generative Adversarial Networks (GANs), Long-Short Term Memory (LSTM) networks, Multilayer Perceptrons (MLPs), and Self-Organizing Maps (SOMs). Among these, pre-trained CNN algorithms, in particular, have demonstrated substantial success in classification tasks (Abulwafa 2022; Dewangan 2023).

The use of pre-trained CNN algorithms for classification is often referred to as transfer learning. This approach facilitates the rapid achievement of successful results with relatively small datasets. By utilizing knowledge gained from models trained on different datasets, transfer learning enables prediction, feature extraction, and fine-tuning in new applications (Iman et al. 2023; Vrbančič & Podgorelec 2020).

Researchers use different pre-trained CNN architectures to train models with their own data in classification applications. In this experimental study, InceptionV3, DenseNet169, ResNet152, VGG19, MobileNet, and NASNet, which are popular pre-trained CNN models in this field, were used to classify the disease and health status of oil rose in Isparta province.

DenseNet

DenseNet (Dense Convolutional Network) has been brought to the literature by Cornwell University, Tsinghua University and Facebook AI Research (FAIR). It received the best article award at the 2017 CVPR with more than 2000 citations. It is a network architecture where each layer is connected to every other layer immediately (Huang et al. 2017). The feature maps of all preceding layers are handled as separate inputs for each layer, while the feature maps of each subsequent layer are passed as input to each layer's own feature maps. This connection model provides the most advanced accuracies. DenseNet-121, DenseNet-169, DenseNet-201, and DenseNet-264 models are used where DenseNet's different Dense Blocks are used (Pan et al. 2019).

InceptionV3

Szegedy et al. (2015) confirmed that InceptionV3 is the Winner of the ILSVRC 2014 image classification competition. In the model of this network, there are symmetrical and asymmetrical blocks. Each block has different convolution, mean or maximum pooling, and concats layers. On the last side of the network, there is the Softmax layer for convolution, average pooling, forgetting, full coupling, and classification, respectively.

MobileNet

TensorFlow's first mobile computer vision model is the MobileNet design, which was put forth in 2017. Deeply separable convolutions are used by MobileNet. As a result, compared to a network with regular convolutions of the same depth, the number of parameters is considerably reduced. A neural network called MobileNet is made up of highly separable convolution from existing convolution. A concept called "deeply separable convolution" is used to factor an existing convolution and entails two steps; point convolution conducts the sum processing, while deep convolution filters the convolution. Deep convolution applies a single filter to every channel of incoming data and then outputs the final product (Lee 2020).

NASNet

Neural Architecture Search (NAS) was developed by Google Brain and, in 2017, achieved a classification accuracy on ImageNet that was 1.2% higher than that of previously published studies (Zoph & Le 2016). NAS algorithm, which consists of three components: Search Space, Search Strategy, Performance Estimation Strategy, are scalable CNN architectures and consists of reinforcing learning method and separable convolution and reduction blocks. In addition, NAS algorithms can be classified into three different categories: Evolutionary Computation (EC), gradient, and Reinforcement Learning (RL) (Liu et al. 2021).

ResNet

ResNet was introduced to the literature in 2015 by Kaiming He, Xiangyu Zhang, Shaoqing Ren and Jian Sun. More layers have been added over the years for deep learning architectures to solve more complex tasks. Adding more layers causes accuracy saturation, rapid drops, and increase in the training error. The reason for this is the degradation/optimization problem encountered in the optimization of deep models. To solve this problem, ResNet architecture, which uses a 34-layer flat network architecture with less filters and lower complexity than VGG networks based on VGG-19 architecture, has been developed. The architecture was then converted into a residual mesh by adding jump links or residual blocks to this flat mesh (Reddy et al. 2021).

VGG19

The VGG19 architecture is a 19-layer version of the VGG (Visual Geometry Group) architecture, consisting of 16 convolutional layers and three fully connected layers. The input image is a fixed-size 224×224 RGB image. The VGG19 architecture includes similar layers which have weight sharing. This architecture uses 3×3 convolutional filters and usually contains 5 convolutional layers with filter numbers 64, 128, 256, 512 and 512 respectively. In addition, the VGG19 architecture includes 3 fully connected layers and uses the SoftMax function for multiclassification (Simonyan & Zisserman 2014).

2.3.2. Ensemble learning

Ensemble learning is a machine learning technique used across various artificial intelligence applications to improve generalization by combining multiple base learners. This method enhances average model predictions by incorporating diverse training data and models, with the final prediction based on majority voting among the classifiers (Yang et al. 2023). Ensemble learning seeks to surpass traditional single learning methods, benefiting from factors such as mitigating overfitting, computational advantages, and enhanced representativeness. Additionally, ensemble methods address challenges in machine learning, such as class imbalance, concept drift, and high-dimensional data. Ensemble classifiers combine the outputs of multiple

base models using distribution aggregation methods, such as summing conditional probability vectors, to arrive at the final class prediction. Mathematical formulations for ensemble classifiers are described, with Equation 6 defining the final class prediction and Equation 7 detailing the aggregation process (Sagi & Rokach 2018).

$$\hat{y} = argmax(\varphi(x_i)) \quad (6)$$

$$\varphi(x_i) = \sum_{k=1}^{K} f_k(x_i) \quad (7)$$

Where; x_i represents the input features of a single example, $\hat{y} \in R$ for regression problems and $\hat{y} \in Z$ for classification problems.

In Equation 6, the model assigns a class label corresponding to the maximum score $\varphi(x_i)$returned by the function $\varphi(x_i)$.The function $\varphi(x_i)$ is further elaborated in Equation 7 as the sum of individual contributions from different classifiers or feature functions. This allows us to view the final prediction as a sum of many feature-specific evaluations; hence, more robust decision-making is achieved.

2.3.3. Adding transfer learning to fine-tunning

Fine-tuning is the process of retraining a pre-trained model for a specific task, typically trained on a larger dataset. The model is adjusted to perform better on a different task by using the general features it has learned. The convolutional layers of the model are frozen, allowing training to be conducted solely on the newly added dense layers.

Due to the small size of the dataset and the necessity of achieving high performance with faster training, state-of-the-art deep learning models were implemented using the transfer learning method. As part of the fine-tuning process, the base convolutional layers of models pre-trained on large-scale image datasets were frozen. These layers have learned to extract general features, such as edges and textures, from input images, which can be utilized for various classification tasks. The weights of these frozen layers remain unchanged during the new training process, thereby reducing the computational cost of the training.

Since the labels from the original classification task differ from the class labels used for disease and pest detection, new dense layers that are specific to the dataset have been added in place of the original classification layers. As shown in Table 2, this new model architecture has been redesigned to include *global average pooling*, *dropout*, *dense* and *batch normalization* layers sequentially. The ReLU activation function was employed in the intermediate layers, while *softmax* was used in the output layer. The number of classes in the output layer was adjusted according to the number of diseases and pests (Figure 4).

Table 2- New layers and parameters added for fine-tuning

Modified Model Architecture	
Basemodel (trainable = False)	*DenseNet169, MobileNetV2, VGG19, NASNet, InceptionV3, ResNet152*
New added layers and their parameters	keras.layers.*GlobalAveragePooling2D(),* keras.layers.*Dropout(0.4),* keras.layers.*Dense(256, activation='relu'),* keras.layers.*BatchNormalization(),* keras.layers.*Dropout(0.3),* keras.layers.*Dense(128, activation='relu'),* keras.layers.*BatchNormalization(),* keras.layers.*Dropout(0.2),* keras.layers.*Dense(8, activation='softmax')*

Fine-tuned models were tested using the Adam and SGD optimization algorithms. The categorical cross-entropy loss function was employed, and accuracy was selected as the metric to evaluate the model's performance. Various epoch values were tested to determine the most suitable model. Controls such as *reduce_lr_on_plateau*, *early_stopping*, and *model_checkpoint* were incorporated into the model to update the learning rate and prevent overfitting. While the new layers were updated during the training process, the frozen convolutional layers continued to extract general features from the input images. After assessing the training and validation accuracy, the classification performance was measured using test data. A confusion matrix was generated, and metrics such as precision, recall, and F1-score were calculated.

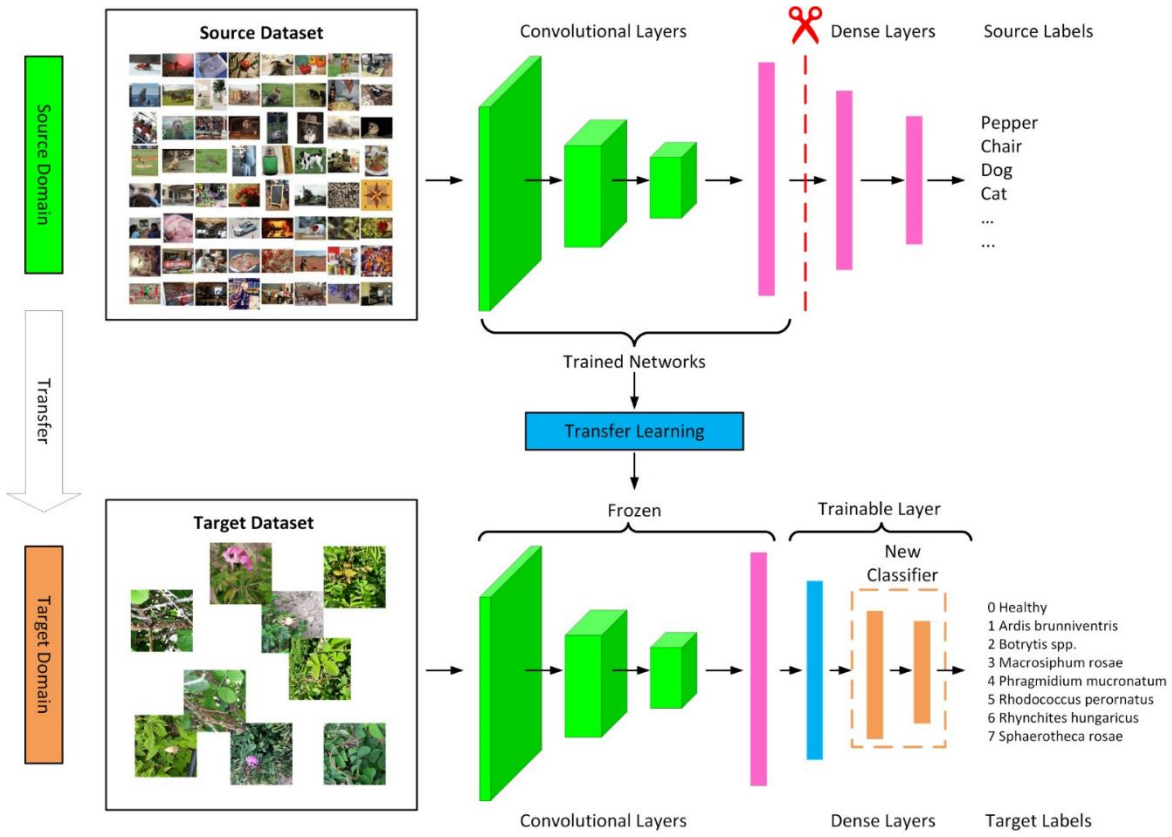

Figure 4- Demonstration of the application of the transfer learning (adopted from Tao et al. 2020)

2.3.4. Quantization

Quantization is an essential technique used in Deep Neural Network (DNN) models to reduce computational and storage requirements, making them suitable for resource-constrained mobile and embedded devices. By reducing the precision of numerical data, weights, deviations, and activations, quantization allows for the use of lower precision representations, such as 8-bit integers instead of 32-bit floating point values (Chen et al. 2020). This optimization technique is crucial for adapting deep neural networks for deployment in resource-constrained environments, but it involves trade-offs in model accuracy (Ahn et al. 2023). Quantization can be achieved through Quantization-Aware Training (QAT) or Post-Training Quantization (PTQ) methods. QAT, which involves retraining the model, preserves accuracy but is computationally expensive. In contrast, PTQ, applied after training, is faster but often less accurate (Gholami et al. 2022). Various options for PTQ include dynamic range, integer, and float16 quantization. This study focuses on dynamic range post-training quantization.

2.4. Performance evaluation

The metrics outlined in Equations 8-11 were used to calculate the performance values of the eight deep learning models employed in the study. Accuracy measures the proportion of correctly classified samples within the classified sample data. Precision quantifies how many of the sample data classified as positive are actually positive. Recall indicates how much of the sample data that should be predicted as positive was actually classified as positive. The F1-Score represents the harmonic mean of the precision and recall metrics.

$$\gamma_{accuracy} = \frac{TP + TN}{TP + TN + FP + FN} \quad (8)$$

$$\gamma_{precision} = \frac{TP}{TP + FP} \quad (9)$$

$$\gamma_{recall} = \frac{TP}{TP + FN} \quad (10)$$

$$\gamma_{f1score} = 2 \times \left(\frac{\gamma_{precision} \times \gamma_{recall}}{\gamma_{precision} + \gamma_{recall}} \right) \quad (11)$$

- **True Positive (TP):** A correct prediction that a plant is diseased or not diseased.

- **True Negative (TN)**: A prediction that a healthy plant is not diseased.

- **False Positive (FP):** A prediction of a healthy plant as diseased.

- **False Negative (FN)**: A prediction state indicating that a diseased plant is healthy.

2.5. Mobile application

A mobile application has been developed, which performs classification for the detection of diseases and plant pests, for real-time use. In this way, it will be possible to classify plants taken with a mobile phone or tablet instantly. In the Flutter-based application, TensorFlow Lite library was preferred for efficient use of deep learning tools. Here TensorFlow Lite is used to convert the models into FlatBuffer files (*.tflite*). These converted models were then integrated into the application's folder using TensorFlow version 2.4.1.

For mobile application development, the Android Studio Graffe and Visual Studio Code environments were used, alongside Flutter 2.3.0 -a popular cross platform framework- supported in these environments. Dart, an object-oriented programming language, was employed for coding in the Visual Studio Code environment. The code underwent thorough testing for performance and functionality on the Pixel 2 Android x86 emulator, after which an APK was generated and installed on a smartphone. Figure 5 shows the developed mobile application and the implementation of the models.

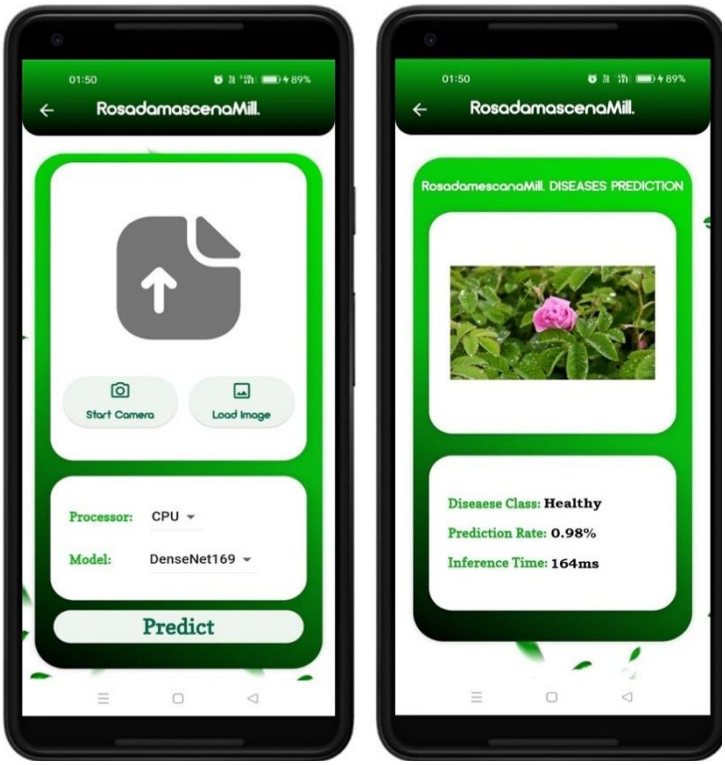

Figure 5- Representative screenshot of the developed mobile application

3. Results and Discussion

3.1 Experimental procedure

Experimental studies were conducted on a virtual machine in a cloud environment. A Tesla T4 GPU with CUDA 11.4 and TensorFlow 2.4.1 deep learning library were used alongside the Python programming language.

The hyperparameters used for model training in the experimental study, which employed six deep learning models to classify oil rose diseases, are provided in Table 3.

Table 3- Train hyperparameters

Parameter	*Setting*
Image size	224×224×3
Batch size	40
Optimizer	Adam
Loss function	Categorical Cross Entropy
Epochs	10, 20, 30, ….,150
Output Activation	Softmax
Learning rate	0.00001 - 0.01

3.2. Comparison performance of CNN-based models

With the dataset created for the study, the InceptionV3, DenseNet169, ResNet152, VGG19, MobileNet, and NASNet deep learning models were trained both with and without data augmentation. The training results, including loss and accuracy graphs based on incremental data are presented in Figure 6.

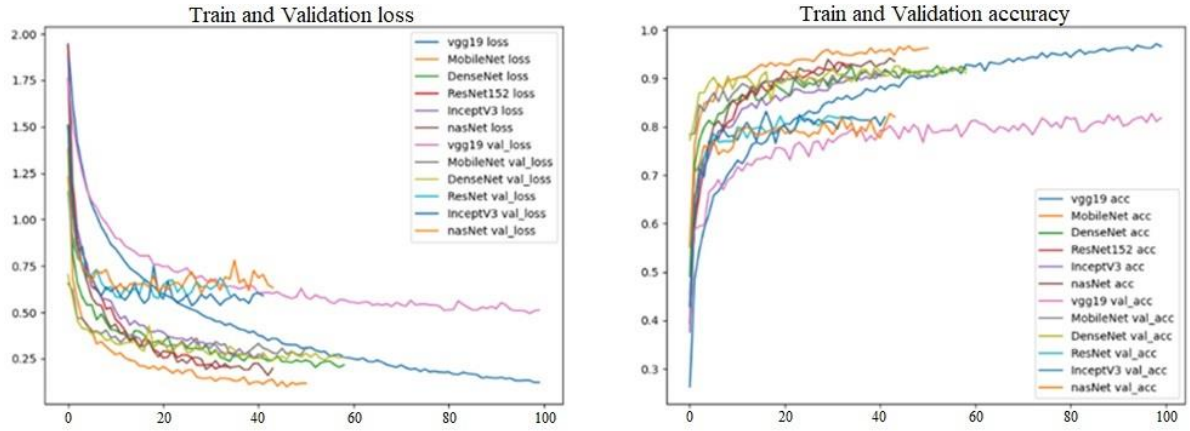

Figure 6- Training and validation loss-accuracy graphs of deep learning models after data augmentation

During model training, the training process is automatically terminated when the validation loss rate fails to improve due to adjustments in the *learning rate (lr)* applied to the model with the *reduce_lr_loss* and *early_stop* parameters. As a result, the maximum number of epochs specified as a model parameter may not be reached, causing the number of epochs in the graphs to vary.

The minimum validation loss during model training with non-augmented data was obtained as follows: 0.74 for the VGG19 model, 0.67 for the DenseNet169 model, 0.81 for the NASNet model, 0.83 for the InceptionV3 model, 0.86 for the ResNet152 model, and 0.70 for the MobileNet model. The minimum validation loss results from training with augmented data are as follows: 0.51 for the VGG19 model, 0.25 for the DenseNet169 model, 0.63 for the NASNet model, 0.58 for the InceptionV3 model, 0.59 for the ResNet152 model, and 0.31 for the MobileNet model.

When training the VGG19, DenseNet169, NASNet, InceptionV3, ResNet152, and MobileNet models with non-augmented data, the highest validation accuracies achieved were 0.81, 0.86, 0.81, 0.80, 0.75, and 0.83 respectively. In contrast, when training with augmented data, the validation accuracies were as follows: 0.82 for VGG19, 0.93 for DenseNet169, 0.82 for NASNet, 0.83 for InceptionV3, 0.91 for ResNet152, and 0.83 for MobileNet.

The precision, recall, and F1-score metrics from the test results are presented in Table 4 to identify the model with the best performance. The highest score from the test results was achieved with the DenseNet169 model. The lowest performance was observed with the InceptionV3 model. All six models achieved the highest accuracy in predicting the healthy class with label 0.

Table 5 presents the data for six different deep learning models designed for the study, including both original and augmented data, as well as the corresponding accuracy rates achieved during the training and testing phases. Among the pre-trained models trained with the original data, the InceptionV3 model attained a training accuracy of 98%, while the DenseNet169 model achieved validation and test accuracies of 86% and 80%, respectively.

When trained with augmented data, the InceptionV3 model yielded the lowest training accuracy, while the VGG19 model achieved the highest. An average validation accuracy of 85% was observed, with the DenseNet169 model achieving the highest validation accuracy of 93%, while other models ranged between 82% and 93%. During evaluation with the test data, the fine-tuned DenseNet169 model exhibited the highest performance at 93%, followed by the fine-tuned MobileNetV2 model with a performance of 90% (see Figure 7).

Table 4- Precision, recall and f1-score values of test results

Models and metrics		***Disease Label***							
		0	*1*	*2*	*3*	*4*	*5*	*6*	*7*
InceptionV3	precision	0.93	0.70	0.73	0.81	0.81	**0.98**	0.70	0.82
	recall	0.93	0.84	0.80	0.73	0.60	0.88	0.78	0.85
	f1-score	0.93	0.76	0.77	0.77	0.69	0.92	0.74	0.84
DenseNet169	precision	**1.00**	**0.93**	0.90	**0.90**	**0.98**	**0.98**	**0.90**	**0.96**
	recall	**1.00**	0.90	**0.98**	**0.97**	**0.90**	**0.94**	**0.82**	**1.00**
	f1-score	**1.00**	**0.92**	**0.94**	**0.93**	**0.94**	**0.96**	**0.86**	**0.98**
ResNet152	precision	0.98	0.82	0.67	0.89	0.70	0.89	0.69	0.88
	recall	0.98	0.87	0.85	0.74	0.64	0.86	0.64	0.90
	f1-score	0.98	0.85	0.75	0.81	0.67	0.88	0.67	0.89
VGG19	precision	0.92	0.81	0.80	0.89	0.71	0.90	0.76	0.92
	recall	0.98	0.87	0.85	0.83	0.68	0.88	0.64	0.94
	f1-score	0.95	0.84	0.82	0.86	0.69	0.89	0.70	0.93
MobileNet	precision	0.97	0.84	**0.92**	0.88	0.93	**0.98**	0.80	**0.96**
	recall	**1.00**	**0.97**	0.87	0.88	0.82	0.92	0.80	0.96
	f1-score	0.98	0.90	0.90	0.88	0.87	0.95	0.80	0.96
NasNet	precision	0.88	0.74	0.83	0.81	0.73	0.95	0.64	0.93
	recall	**1.00**	0.86	0.82	0.76	0.66	0.78	0.76	0.79
	f1-score	0.94	0.79	0.83	0.78	0.69	0.85	0.69	0.85

Table 5- Accuracy values of models for Training, Validation, and Testing

Dataset	***Accuracy***	***InceptionV3***	***DenseNet169***	***ResNet152***	***VGG19***	***MobileNet***	***NasNet***	***Average***
Original	Train	**0.98**	0.96	0.95	0.96	0.97	0.95	0.96
	Validation	0.80	**0.86**	0.75	0.81	0.83	0.81	0.82
	Test	0.70	**0.80**	0.73	0.75	0.78	0.67	0.75
Augmentation	Train	0.91	0.93	0.93	**0.97**	0.96	0.94	0.94
	Validation	0.83	**0.93**	0.82	0.82	0.91	0.82	0.85
	Test	0.80	**0.93**	0.81	0.84	0.90	0.80	0.85

In the confusion matrix, the main diagonal shows correctly predicted images, while the off-diagonal entries represent incorrectly predicted images. Looking at the normalized confusion matrix in Figure 8, it is evident that classification is successful for nearly all classes. However, the images labeled as class 6 show a relatively lower classification performance compared to those labeled with other categories, and there are examples of misclassification. In the row where the true classification label is 6, it can be observed that misclassification occurs more frequently for label 2 (normalized value 0.13).

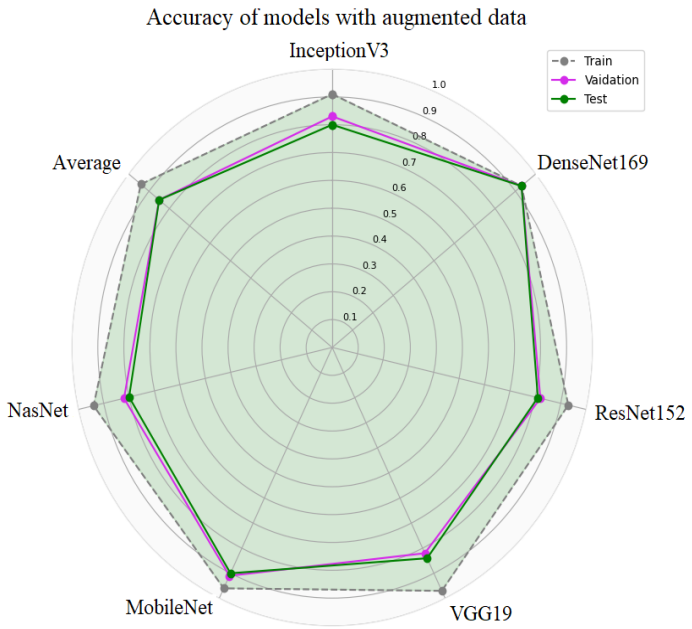

Figure 7- Training, validation and testing performances of models with augmented data

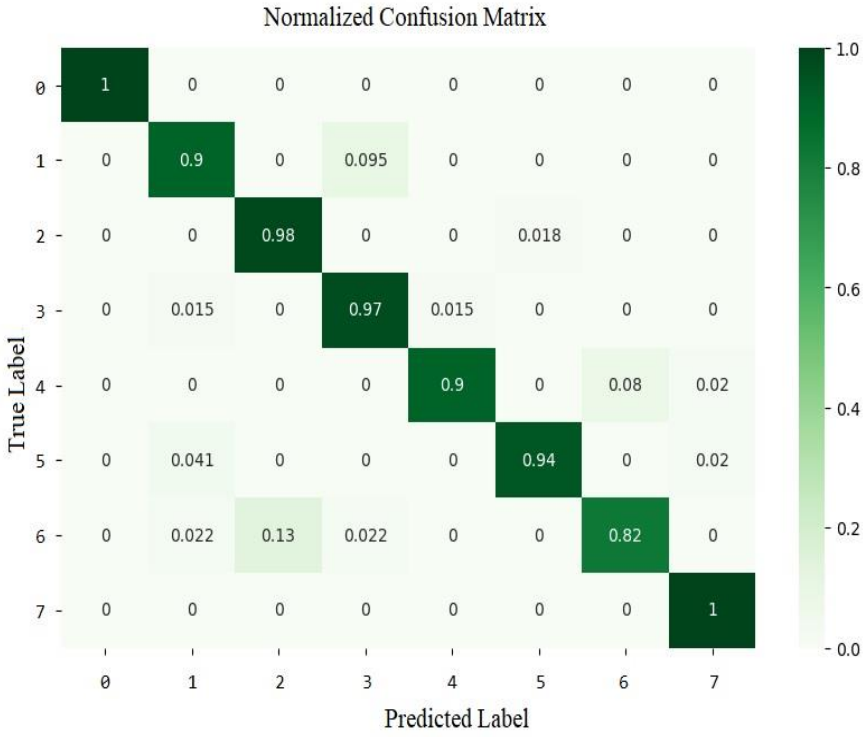

Figure 8- Confusion matrix of the DenseNet169 model

This may be attributed to the presence of both *Botrytis_spp* and *Mecorhis ungarica* diseases in the images of the dataset. In Figure 9, the images corresponding to both of these diseases are presented together.

The ensemble test accuracy was determined by combining the predictions of deep learning models using various combinations in the ensemble learning approach employed in the study to improve classification performance. Among these combinations, the combination of DenseNet169, ResNet152, MobileNet, VGG19, and NASNet models produced the best performance using the maximum voting method. The classification success rate of the deep learning model, which was 93%, increased to 95.17% with ensemble learning.

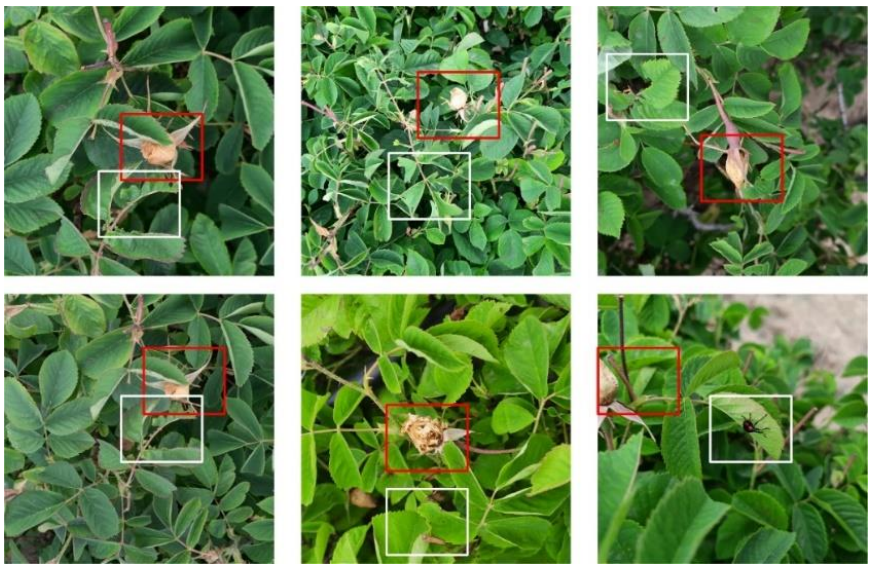

Figure 9- Images of *Botrytis_spp* (red rectangle) and *Mecorhis ungarica* (white rectangle) diseases together

3.3. Performance of mobile application

DenseNet169 and MobileNetV2 emerged as the top-performing models among the six models that were trained and tested on a desktop computer. The performances of these models were evaluated in the mobile application developed for disease and pest detection in the natural environment of the oil rose.

Given the limited hardware resources available on mobile devices, it is essential for inference models to be resource-efficient. Furthermore, these models are expected to deliver satisfactory processing times during inference.

If one examines the file sizes of the two models both before and after conversion to flatbuffer files, it becomes apparent that TensorFlow Lite inherently reduces the file size. The DenseNet169 model had a file size of 55.4MB in .h5 format, which was reduced to 50MB after conversion to *.tflite* format, and further reduced to 13.3MB after post-quantization. The MobileNetV2 model, originally 13MB, was reduced to 9.9MB after conversion to *.tflite* format, and further down to 2.77MB after post-quantization.

To evaluate the inference time and confidence in the developed mobile application, a test was conducted using 10 images from each class. The values were obtained by running the mobile application in the Visual Studio Code environment using an Android emulator and on a physical device.

When using the DenseNet169 model for predictions on the emulator, the inference time ranged from 1 266 ms to 1 577 ms, yielding confidence values between 50.1% and 98.4% for complete accuracy. When evaluated with the quantized DenseNet169 model, the inference time ranged from 21875 ms to 24087 ms, resulting in confidence values between 56.5% and 99.7% for full accuracy. Predictions made with the MobileNetV2 model showed inference times ranging from 137 ms to 225 ms, with confidence values between 88.3% and 99.3% for complete accuracy. For the tests conducted with the quantized MobileNetV2 model, the inference time varied between 2 842 ms and 3 591 ms, yielding confidence values between 62.3% and 99.9% for full accuracy.

The same tests were carried out on the physical mobile device. With the DenseNet169 model, the inference time ranged from 2 113 ms to 2 238 ms, and the confidence value was between 88.1% and 99.9%. For tests with the quantized DenseNet169 model, the inference time ranged from 2 485 ms to 2 932 ms, with the confidence value ranging from 80.8% to 99.9% for full accuracy. Predictions made using the MobileNetV2 model showed inference times ranging from 293 ms to 303 ms, yielding confidence values between 99.7% and 99.9% for full accuracy. In tests conducted with the quantized MobileNetV2 model, the inference time varied between 404 ms and 530 ms, generating confidence values ranging from 89.7% to 99.9% for full accuracy.

3.4. Overall evaluation

Table 6 illustrates the utilization of various algorithms for classifying diseases in different plant species. Deep learning algorithms and ensemble learning notably demonstrate substantial success in this area. The performance of these algorithms seems to be influenced by factors such as the number of classes in the dataset and the volume of images available. In many studies, established datasets such as the PlantVillage dataset were used, while others curated their datasets by collecting images from the internet. A significant portion of dataset images was obtained under controlled environmental conditions. Additionally, some studies

included an image enhancement process to refine the dataset further. The highest performance was achieved by the models developed by Vallabhajosyula et al. (2022) and Ma et al. (2020), which used datasets with two classes and a relatively high number of images. Ma et al. (2022) concentrated solely on black spot disease.

Unlike the proposals by Harbola et al. (2024) and Prathiksha et al. (2024), this paper adopts an ensemble learning approach, where the accuracy rates are high but fails to put into consideration the realization on a mobile application, and the images are mostly taken in a controlled environment.

When comparing the performance of the study with other studies on rose plants, particularly those involving similar species and a comparable number of classes, it becomes apparent that the study's performance is relatively higher. Despite using data augmentation, the small size of the original dataset and the fact that the images were obtained in an uncontrolled environment limit the model performance from reaching nearly 100%. While other studies focus on detection from single-leaf images taken in controlled environments, this study conducts detection from plant images in their natural environment.

In addition, there have been no deep learning-based studies focused on disease detection in *Rosa damascena* Mill. plants. Moreover, this study deployed the deep learning model with the highest classification performance in a mobile application, a rare occurrence in similar studies. In their study on a mobile application, Hemalatha et al. (2022) implemented only a single model within the mobile application and did not perform a comparative analysis of inference times across different platforms or with various model configurations.

Table 6- Comparison of similar studies in the literature

Ref.	*Types of Plant*	*Num. of class*	*Base algorithm used for classification*	*Image count*	*Accuracy (%)*	*Deployment to any environment*
Vallabhajosyula et al. (2022)	14 crops	38	Ensemble (Deep learn.)	54305 (plant village)	100	-
Fuentes et al. (2018)	Tomato	10	CNN	5000	96	-
Astani et al. (2022)	Tomato	13	Ensemble (Machine learn.)	23811	95.98	-
Zhong & Zhao (2020)	Apple	6	DenseNet-121	2462	93.30	-
Sethy et al. (2020)	Rice	4	MobileNet+SVM	5932	97.96	-
Hemalatha et al. (2022)	Sugarcane	6	LeNet-5	2940	96	Android application
Ahila et al. (2019)	Maize	4	LeNet	4365	97.89	-
Wang et al. (2021)	Cucumber	4	DUNet(DeepLabV3 + and U-Net)	1000	92.85	-
Uğuz & Uysal (2021)	Olive leaf	3	Custom CNN	3400	95	Web app.
Swetharani & Prasad (2021)	Rose	-	CNN	-	97.3	-
Nuanmeesri (2021)	Rose	15	Vgg16+SVM	4032	88.33	-
Rajbongshi et al. (2020)	Rose	4	MobileNet	400	95.63	-
Ma et al. (2020)	Rose	2	AlexNet-VGG16-NDDR	900	99.10	-
Khaleel et al. (2022)	Rose	4	CNN	(not known)	64.35	-
Yin et al. (2021)	Rose	2	FasterR-CNN	650	84.16	-
This Study	*Rosa damascena* Mill.	8	DenseNet169 Ensemble model	567	93 95.1	Mobile application (with and without quantization)

In this study, the performance of the models was evaluated based on inference time across different environments, such as a personal computer, a mobile phone emulator, and a mobile device. In the computer environment, the designed DenseNet169 and MobileNetV2 models were tested, while in the mobile environment, the post-quantized models were also tested. The obtained results are shown in Table 7 as average values.

Table 7- Inference time of deep learning models in different environments

Model	*Average Inference Time (ms)*		
	Computer*	***Emulator****	***Physical Mobile Device****
MobileNetV2	71	182	301
DenseNet169	119	1394	2271
Quantized MobileNetV2	NA	3303	434
Quantized DenseNet169	NA	22491	2624

*** Intel(R) Core(TM) i9-10920X CPU 3.50GHz 32GB, Win 10 Pro**
**** Pixel 2 API**
***** Samsung A6+: Cortex A53 CPU 1.8GHz 4GB, Android 10**

An examination of the inference times shows that the designed MobileNetV2 model has the lowest inference times in both virtual and physical environments. The fastest inference time is obtained on a desktop computer, followed by the emulator and then the physical mobile device. The post-quantized MobileNetV2 model shows slightly slower inference times in mobile environments compared to the MobileNetV2 base model but is significantly faster than the DenseNet169 models. Both the post-quantized MobileNetV2 model and the DenseNet169 model show slower inference times compared to their base models.

Rakib et al. (2024) proposed a model that is even independent of an internet connection, but it works with a very small dataset and a trivial application process. Adebisi et al. (2024) studied on the efficiency of multiple deep learning models on FPGA hardware, but failed to delve into finding an actual solution for mobile application or real-time usage. While the work of Padeiro et al. (2024) developed certain techniques of improvement for quantized models, their work did not include the integration of mobile applications. Actually, Katumba et al. (2024) studied on the quantization of models such as EfficientNetv2B0 and BeanWatchNet, integrated them in a mobile application, but they did not use real natural environment data, with accuracy rates not high but only up to 90-91%.

4. Conclusions and Future Work

Detecting plant diseases is challenging due to the large variety of diseases and the similarities between some of them. A mixed-CNN approach for disease and pest detection is presented using the new dataset created in the study. Six different newly designed deep learning models were trained with the new dataset. All models achieved training accuracies over 90%, with the VGG19 model performing best at 97%. Validation accuracies ranged from 82% to 93%, with DenseNet169 emerging as the best-performing model. Testing accuracies ranged from 80% to 93%, with the DenseNet169 model achieving a classification accuracy of 93%. Ensemble deep learning further improved test accuracy to 95.17%. Nevertheless, the small size and uncontrolled nature of the dataset may have limited test accuracy.

A comparative study was conducted on different platforms with the DenseNet169 and MobileNetV2 models using tflite and quantized variants. The results show that the MobileNetV2 model achieved the lowest inference times: 71 ms on a desktop computer, 182 ms on an emulator, and 301 ms on a physical mobile device. In contrast, inference times increased in mobile environments with the post-quantization of the models. However, the size of the post-quantized MobileNetV2 model decreased from 9.9MB to 2.77MB, and the size of the DenseNet169 model from 50MB to 13.3MB. In scenarios where inference time is critical, the tflite-converted MobileNetV2 model or the quantized MobileNetV2 model are better options for optimizing memory usage and power consumption.

The evidence supports the claim that the developed detection system can effectively diagnose rose diseases and pests with high accuracy. The system's real-time disease classification on smartphones suggests that the resulting mobile application could be a valuable and cost-effective tool for growers.

In future studies, the dataset will be expanded by collecting more images through the mobile application developed and a higher accuracy will be achieved. The second state will explore detecting multiple diseases in a single image and recommending appropriate treatments. Additionally, plans include transferring inference models embedded in the mobile application to cloud environments for broader accessibility via API.

Acknowledgements

I would like to thank Assist. Prof. Sinan Demir, member of the Faculty of Agriculture, Isparta University of Applied Sciences for his support in the systematic classification of diseases and pests. I am also thankful to Kaggle and Google for supplying free GPU computation platform.

Funding

This research did not receive any specific grant from funding agencies in the public, commercial, or not-for-profit sectors.

Declaration of competing interest

The authors report no conflict of interest.

Data availability

The dataset is publicly available on the Mendeley data platform and can be referenced as "Duman, Burhan (2023), 'ISPGULDataset8C,' Mendeley Data, V1, doi: 10.17632/8ptzbtryhj.1."

Code availability

To access the source code of the mobile application, please visit the following link:
https://github.com/burhanduman/RosaDamascenaMillDiseasesV1.git

References

Abulwafa A E (2022). A Survey of Deep Learning Algorithms and its Applications. *Nile Journal of Communication and Computer Science* 3(1): 28-49

Adebisi J, Srinu S & Mitonga V (2024). Deep Learning Algorithm Analysis of Potato Disease Classification for System on Chip Implementation. *Journal of Digital Food, Energy & Water Systems* 5(1)

Ahila P, Arivazhagan R S, Arun M & Mirnalini A (2019). Maize leaf disease classification using deep convolutional neural networks. *Neural Comput. Appl.* 31: 8887-8895

Ahn H, Chen T, Alnaasan N, Shafi A, Abduljabbar M & Subramoni H (2023). Performance Characterization of using Quantization for DNN Inference on Edge Devices: Extended Version arXiv preprint arXiv:2303.05016

Astani M, Hasheminejad M & Vaghefi M (2022). A diverse ensemble classifier for tomato disease recognition. *Computers and Electronics in Agriculture* 198: 107054

Baydar H (2016). Oil Rose Cultivation and Industry. Science and Technology of Medicinal and Aromatic Plants (5th Expanded Edition). Süleyman Demirel University Press, 51: 290-325 (In Turkish)

Bıtrak O O & Hatırlı S A (2022). Global Oil Rose Market and Turkey's Role. *Selçuk University Akşehir Vocational School Journal of Social Sciences* 13: 85-94 (In Turkish)

Chen J, Chen J, Zhang D, Sun Y & Nanehkaran Y A (2020). Using deep transfer learning for image-based plant disease identification. *Computers and Electronics in Agriculture* 173: 105393

Chen Y, Zheng B, Zhang Z, Wang Q, Shen C & Zhang Q (2020). Deep learning on mobile and embedded devices: State-of-the-art, challenges, and future directions. ACM Computing Surveys (CSUR) 53(4): 1-37

Dewangan O (2023). Study and Innovative Approach of Deep Learning Algorithms and Architecture. In Exploring Future Opportunities of Brain-Inspired Artificial Intelligence (pp. 28-45). IGI Global

Ersan R & Başayiğit L (2022). Ecological modelling of potential Isparta Rosa areas (*Rosa damascena* Mill.). *Industrial Crops and Products* 176: 114427

Fazili M A, Ganie I B & Hassan Q P (2024). Studies on pharmacological aspects, integrated pest management and economic importance of Rosa damascena L. *South African Journal of Botany* 174: 534-541

Ferentinos K P (2018). Deep learning models for plant disease detection and diagnosis. *Computers and Electronics in Agriculture* 145: 311-318

Fuentes A F, Yoon S, Lee J & Park D S (2018). High-performance deep neural network-based tomato plant diseases and pests diagnosis system with refinement filter bank. *Frontiers in Plant Science* 9: 1162

Gholami A, Kim S, Dong Z, Yao Z, Mahoney M W & Keutzer K (2022). A survey of quantization methods for efficient neural network inference. In Low-Power Computer Vision (pp. 291-326). Chapman and Hall/CRC

Harbola G, Rawat M S, Gupta A & Gupta R (2024, May). Intelligent Diagnosis of Potato Leaf Diseases using Deep Learning. In 2024 4th International Conference on Pervasive Computing and Social Networking (ICPCSN) 372-377 IEEE

Hemalatha N K, Brunda R N, Prakruthi G S, Prabhu B V B, Shukla A & Narasipura O S J (2022). Sugarcane leaf disease detection through deep learning. In Deep Learning for Sustainable Agriculture, 297-323 https://doi.org/10.1016/B978-0-323-85214-2.00003-3

Huang G, Liu Z, Van Der Maaten L & Weinberger K Q (2017). Densely connected convolutional networks. Proceedings of the IEEE Conference on Computer Vision and Pattern Recognition, 4700-4708

Iman M, Arabnia H R & Rasheed K (2023). A review of deep transfer learning and recent advancements. *Technologies* 11(2): 40

Jung K, Lee J I, Kim N, Oh S & Seo D W (2021). Classification of space objects by using deep learning with micro-Doppler signature images. *Sensors* 21(13): 4365

Karanfil A (2021). Prevalence and molecular characterization of Turkish isolates of the rose viruses. *Crop Protection* 143: 105565

Katumba A, Okello W S, Murindanyi S, Nakatumba-Nabende J, Bomera M, Mugalu B W & Acur A (2024). Leveraging edge computing and deep learning for the real-time identification of bean plant pathologies. *Smart Agricultural Technology* 9: 100627. https://doi.org/10.1016/j.atech.2024.100627

Khaleel M I, Sai P G, Kumar A U R, Raja P & Hoang V T (2022). Rose Plant Leaves: Disease Detection and Pesticide Management using CNN. 2022 6th International Conference on Trends in Electronics and Informatics (ICOEI), 1067-1072

Khitthuk C, Srikaew A, Attakitmongcol K & Kumsawat P (2018). Plant leaf disease diagnosis from color imagery using co-occurrence matrix and artificial intelligence system. 2018 International Electrical Engineering Congress (IEECON), 1-4

Lee S H (2020). Deep learning based face mask recognition for access control. *Journal of the Korea Academia-Industrial Cooperation Society* 21(8): 395-400

Liu Y, Sun Y, Xue B, Zhang M, Yen G G & Tan, K C (2021). A survey on evolutionary neural architecture search. IEEE Transactions on Neural Networks and Learning Systems.

Ma J, Pang L, Yan L & Xiao J (2020). Detection of black spot of rose based on hyperspectral imaging and convolutional neural network. *AgriEngineering* 2(4): 556-567

Mahlein AK (2016). Plant disease detection by imaging sensors–parallels and specific demands for precision agriculture and plant phenotyping. *Plant Disease* 100(2): 241-251

Mutka A M & Bart R S (2015). Image-based phenotyping of plant disease symptoms. *Frontiers in Plant Science* 5: 734

Nuanmeesri S (2021). A hybrid deep learning and optimized machine learning approach for rose leaf disease classification. *Eng. Technol. Appl. Sci. Res.* 11(5): 7678-7683

Oikonomidis A, Catal C & Kassahun A (2023). Deep learning for crop yield prediction: a systematic literature review. *New Zealand Journal of Crop and Horticultural Science* 51(1): 1-26

Pan W, Qin J, Xiang X, Wu Y, Tan Y & Xiang L (2019). A smart mobile diagnosis system for citrus diseases based on densely connected convolutional networks. *IEEE Access* 7: 87534-87542

Prathiksha B J, Kumar V, Krishnamoorthi M, Poovizhi P, Sowmiya D & Thrishaa, B. (2024, April). Early Accurate Identification of Grape leaf Disease Detection using CNN based VGG-19 model. In 2024 International Conference on Cognitive Robotics and Intelligent Systems (ICC-ROBINS) (pp. 263-269). IEEE

Rajbongshi A, Sarker T, Ahamad M M & Rahman M M (2020). Rose diseases recognition using MobileNet. 2020 4th International Symposium on Multidisciplinary Studies and Innovative Technologies (ISMSIT) 1-7

Rakib A F, Rahman R, Razi A A & Hasan A T (2024). A lightweight quantized CNN model for plant disease recognition. Arabian *Journal for Science and Engineering* 49(3): 4097-4108

Reddy D S, Rajalakshmi P & Mateen M A (2021). A deep learning based approach for classification of abdominal organs using ultrasound images. *Biocybernetics and Biomedical Engineering* 41(2): 779-791

Sagi O & Rokach L (2018). Ensemble learning: A survey. *Wiley Interdisciplinary Reviews: Data Mining and Knowledge Discovery* 8(4): e1249

Sethy P K, Barpanda N K, Rath A K & Behera S K (2020). Deep feature based rice leaf disease identification using support vector machine. *Computers and Electronics in Agriculture* 175: 105527

Sharma R & Singh G (2015). Access to modern agricultural technologies and farmer household welfare: Evidence from India. *Millennial Asia* 6(1): 19-43

Simonyan K & Zisserman A (2014). Very deep convolutional networks for large-scale image recognition. *arXiv preprint* arXiv:1409.1556

Swetharani K & Prasad G V (2021). Design and implementation of an efficient rose leaf disease detection and classification using convolutional neural network. *International Journal of Image Mining* 4(1): 98-113

Szegedy C, Liu W, Jia Y, Sermanet P, Reed S, Anguelov D, Erhan D, Vanhoucke V & Rabinovich A (2015). Going deeper with convolutions. Proceedings of the IEEE Conference on Computer Vision and Pattern Recognition, 1-9

Tao W, Al-Amin M, Chen H, Leu M C, Yin Z & Qin R (2020). Real-time assembly operation recognition with fog computing and transfer learning for human-centered intelligent manufacturing. *Procedia Manufacturing* 48: 926-931

Uğuz S & Uysal N (2021). Classification of olive leaf diseases using deep convolutional neural networks. *Neural Comput. & Applic.* 33: 4133–4149.https://doi.org/10.1007/s00521-020-05235-5

Vallabhajosyula S, Sistla V & Kolli V K K (2022). Transfer learning-based deep ensemble neural network for plant leaf disease detection. *J. Plant Dis. Prot.* 129: 545-558. https://doi.org/10.1007/s41348-021-00465-8

Vrbančič G & Podgorelec V (2020). Transfer learning with adaptive fine-tuning. *IEEE Access* 8: 196197-196211

Wang C, Du P, Wu H, Li J, Zhao C & Zhu H (2021). A cucumber leaf disease severity classification method based on the fusion of DeepLabV3+ and U-Net. *Computers and Electronics in Agriculture* 189: 106373

Weerakoon W M W et al. (2017). Effect of leaf color chart based nitrogen management on the performance of rice crop. *Field Crops Research* 151: 15-23

Yang Y, Lv H & Chen N (2023). A survey on ensemble learning under the era of deep learning. *Artificial Intelligence Review* 56(6): 5545-5589

Yilmaz H (2015). Estimating the economic costs and level of pesticide use in oil rose (Rosa damascena Mill.) orchards: evidence from a survey for the lakes region of Turkey. *Erwerbs-obstbau* 57(4): 195-202

Yin J, Yu D, Li Z, Guo W & Zhu H (2021). Chinese Rose flower disease recognition method based on deep learning. Frontier Computing: Proceedings of FC 2020, 1309-1319

Yu Z, Wang K, Wan Z, Xie S & Lv Z (2023). Popular deep learning algorithms for disease prediction: a review. *Cluster Computing* 26(2): 1231-1251

Zhong Y & Zhao M (2020). Research on deep learning in apple leaf disease recognition. *Computers and Electronics in Agriculture* 168: 105146

Zoph B & Le Q V (2016). Neural architecture search with reinforcement learning. ArXiv Preprint, ArXiv:1611.01578

Journal of Agricultural Sciences
(Tarim Bilimleri Dergisi)

J Agr Sci-Tarim Bili
e-ISSN: 2148-9297
jas.ankara.edu.tr

JAS

Cell Suspension Cultures and High Frequency Shoot Regeneration of Some Hypericum species

Hussein Abdullah Ahmed Ahmed[a,b,c*], Serkan Uranbey[b], Terezia Salaj[c], Veronika Mistrikova[c]

[a]*Department of Field Crops, College of Agriculture, University of Kirkuk, 36001, KIRKUK, IRAQ*

[b]*Department of Field Crops, Faculty of Agriculture, Ankara University, 06110, ANKARA, TÜRKİYE*

[c]*Plant Science and Biodiversity Center, Slovak Academy of Sciences, Institute of Plant Genetics and Biotechnology, 95007, NITRA, SLOVAK REPUBLIC*

ARTICLE INFO

Research Article
Corresponding Author: Hussein Abdullah Ahmed Ahmed, E-mail: husseinabdullah@uokirkuk.edu.iq
Received: 19 August 2024 / Revised: 20 September 2024 / Accepted: 29 October 2024 / Online: 25 March 2025

Cite this article

Ahmed H A A, Uranbey S, Salaj T, Mistrikova V (2025). Cell Suspension Cultures and High Frequency Shoot Regeneration of Some Hypericum species. *Journal of Agricultural Sciences (Tarim Bilimleri Dergisi),* 31(2):319-331. DOI: 10.15832/ankutbd.1535826

ABSTRACT

The *Hypericum* genus is significant both medically and economically due to its bioactive compounds. This study utilized plant biotechnology techniques to develop an efficient and reliable adventitious shoot regeneration and suitable cell suspension culture system for various *Hypericum* species, including *Hypericum perforatum* L., *Hypericum leptophyllum* Hochst, *Hypericum heterophyllum* L., *Hypericum humifusum* L., and *Hypericum athoum* Boiss. & Orph. High frequency of callus induction using leaf explants on MS medium containing 1.0 mg/L BAP and 0.1 mg/L 2,4-D for *Hypericum perforatum* L. (100%), *Hypericum humifusum* L. (90%), and *Hypericum leptophyllum* Hochst (90%). The best shoot regeneration was also achieved in *Hypericum humifusum* L. (86.3%), *Hypericum perforatum* L. (73.0%), *Hypericum leptophyllum* Hochst (45.67%) and *Hypericum athoum* Boiss. & Orph. (18.33%) on MS medium with 1.0 mg/L BAP and 0.1 mg/L 2,4-D. Calli clusters obtained on callus induction medium were cultured on cell suspension culture MS basal media with B5 vitamins containing 2 mg/L glycine, 1 mg/L 2,4-D, 0.1 mg/L KIN, and 0.1 mg/L BAP. The friable calli developed in the suspension culture and plated on the medium. The proembryogenic structures formed turned to embryonic structures. These globular embryos further transformed into heart and cotyledonary stage and germinated. The maximum number of shoot/callus or percentage of germination of somatic embryo were respectively recorded for H. *perforatum* L. (15.37/callus), H. *leptophyllum* Hochst (6.9/callus), H. *heterophyllum* L. (9.6/callus), H. *humifusum* L. (16.8/callus) and H. athoum Boiss. & Orph. (11.7/callus). H. perforatum L. and H. humifusum L. showed the best shoot regeneration capacity as recorded in adventitious shoot regeneration studies. The plants were acclimatized with 85-100 % survival rat, H. perforatum and H. humifusum L. had also the highest survival rate (100%) as having regeneration capacity.

Keywords: Cell suspension culture, Shoot regeneration, *Hypericum* species, Medicinal plant

1. Introduction

Hypericum species belong to the Clusiaceae (Guttiferae, Hypericaceae) family and are distributed worldwide with around 500 species (Crockett & Robson 2011; Henzelyová & Čellárová 2018). *Hypericum* genus, used in the treatment of numerous diseases, is an important taxonomic group for its invaluable source of natural compounds with therapeutic properties (Alahmad et al. 2021; Shasmita et al. 2023). The some of these natural compounds has rich bioactive properties. Therefore, *Hypericum* species are also characterized by the presence of different types of secretory tissues such as dark glands and secretory ducts in their structures. These secretory structures are areas where bioactive substances are accumulated or synthesized and can be located in different places depending on the plant tissue. The most important of metabolites are hypericin and pseudohypericin known as compounds of the naphthodiantrone group, hyperforin and adhyperforin, known as phloroglucinol derivatives, flavonoids, xanthones, and procyanidin compounds (Barnes et al. 2001; Greeson et al. 2001; Dall'Agnol et al. 2003; Radusiene et al. 2004; Hong et al. 2004; Tanaka & Takaishi 2006; Smelcerovic et al. 2006; Medina et al. 2006; Uzbay 2008; Zubrická et al. 2015; Jendželovská et al. 2016). These compounds can only be synthesized by plants of the *Hypericum* genus and have important biological activities, including antiviral, anticancer, antiretroviral, antibacterial and antidepressant properties (Ciccarelli et al. 2001; Guedes & Eriksson 2005; Griffith et al. 2010; Crockett & Robson 2011). Due to the high medicinal and economic value of *Hypericum* species, the demand for biotechnological methods has increased. Many of the endemic *Hypericum* species are to be preserved and the production of secondary metabolites is possible in a short time and in large quantities using biotechnological methods (Simic et al. 2014; Hussain et al. 2022). Plant tissue, organ and cell culture applications focus on the presence of bioactive compounds and these techniques are employed under controlled environmental conditions to generate plant-specific metabolites used in medicinal and cosmetics industry (Eibl et al. 2018; Al-Atrakchii et al. 2019; Gubser et al. 2021; Faizy at al. 2022; Murthy et al. 2023; Abdulkareem et al. 2024). Cell suspension methods maybe

important tools for the extraction of secondary metabolites from medicinal plants. These techniques have been also becoming increasingly popular as a host system to produce recombinant proteins (Tekoah et al. 2015; Yue et al. 2016). Cell suspension methods can be used to produce virus-free, low-cost in plant and stable secondary metabolites production. In addition, they are effective on post-translational modifications and cost efficiency over bacterial expression systems (Santos et al. 2016; Zagorskaya & Deineko 2017; Permyakova et al. 2019). There are many factors influencing cell suspension culture and the size of cell aggregates such as plant species, explant source, type of explant, phytochemicals, dark/light conditions, temperature, nutrient composition, pH of the culture medium and sucrose concentration (Buter et al. 1998; Bais et al. 2002; Parveen & Shahzad 2014; Saad et al. 2016).

Tissue culture applications are an alternative method for the micropropagation of *Hypericum* species such as H. *perforatum* (Santarem & Astarita 2003; Karpinen et al. 2006; Wójcik & Podstolki 2007; Palmer & Keller 2011; Banerjee et al. 2012; Afsharzaleh et al. 2021; Mikhovich et al. 2021; Ravindran et al. 2022), H. *heterophyllum* (Ayan & Cirak 2006), H. *humifusum* L. (Selvakesavan & Gregory 2021), H. *foliosum* Aiton, H. *hirsutum* L. and H. *maculatum* Crantz (Moura 1998; Coste et al. 2011). H. *perforatum*, H. *angustifolium* and H. *triquetrifolium* have been studied under *in vitro* conditions and they have been produced in large quantities (Pretto & Santarem, 2000; Mulinacci et al. 2008; Karakaş et al. 2009). Moreover, there are only a few reports on cell suspension cultures on *Hypericum* species (Selvakesavan & Gregory 2021; Kruszka et al. 2022). This study also aimed to improve callus induction and regeneration suitable for *in vitro* secondary metabolite production using cell suspension culture method in different *Hypericum* species (H. *perforatum* L, H. *leptophyllum* Hochst, H. *heterophyllum* L, H. *humifusum* L. and H. *athoum* Boiss. & Orph.) and to develop high frequency adventitious shoot regeneration system by organogenesis or somatic embryogenesis.

2. Material and Methods

2.1. Hypericum species

The seeds of H. *perforatum* L, H. *leptophyllum* Hochst, H. *heterophyllum* L. were collected from various agro-ecological regions in Türkiye. H. *humifusum* L. and H. *athoum* Boiss. & Orph. were also obtained from the laboratory of the Pavol Jozef Šafárik University, Faculty of Science, Institute of Biology and Ecology, Department of Genetics, Košice-Slovak Republic.

2.2. Surface sterilization and germination condition

The seeds of *Hypericum* species were kept at +4 ºC for 24 hours, and surface sterilization was carried out by soaking the seeds in 1% $AgNO_3$ for 15 min. The seeds were then washed five times in sterilized water for 5 minutes. Thereafter, the seeds were cultured on MS (Murashige & Skoog 1962) with Gamborg's B5 vitamins (Gamborg et al. 1968) containing 30 g/L sucrose, 7 g/L agar and 2 mg/L glycine in a growth cabinet at 24°C with 8/16 h dark/ fluorescent light.

2.3. Culture conditions and callus initiation from leaf explants of Hypericum species

The seeds of different *Hypericum species* were germinated, 7-10 old days of with length of 6-8.5 cm and then isolated and used to initiate callus and regenerate shoots. Various combinations and concentrations of 6-benzylaminopurine (BAP), Kinetin (KIN) and dichlorophenoxyacetic acid (2,4-D) were utilized to start callus induction and shoot regeneration. Culture on MS/Gamborg B5 vitamins medium with stable concentrations of growth regulators was conducted using *in vitro* seedlings of *Hypericum.* The effects of 2,4-D (0.1 mg/L and 1.0 mg/L) in combination with BAP (0.1 mg/L and 1.0 mg/L) and Kinetin (0.1 mg/L and 1.0 mg/L) were tested. The culture medium was supplemented with 30 g/L sucrose and solidified with 7 g/L agar. The pH of the medium was adjusted to 5.6 before autoclaving. All explants were cultured in the dark at a temperature of 24 ± 2 °C. The embryonic white, healthy, friable, lightly dispersed and granular calli were weighed in a sterile cabinet and on sterile blotting paper.

2.4. Initiation of cell suspension cultures

After germination of *Hypericum* species, 7-10 old days of leaf were used to initiate callus on MS medium supplemented with 1 mg/L 2,4-D, 0.1 mg/L BAP and 7 g/L agar. They were then transferred to 250 mL Erlenmeyer flasks containing 100 mL liquid medium. This medium consisted of MS basal media, Gamborg's B5 vitamins, 30 g/L sucrose, and 2 mg/L glycine. The medium was supplemented with 1 mg/L 2,4-D, 0.1 mg/L KIN, and 0.1 mg/L BAP.

The cell suspensions were then shaken at 120 rpm on an orbital shaker and cultured at 24 ± 1 °C under 40% relative humidity and continuous darkness, as this culture conditions promotes biomass production. The growth of the suspension cultures was assessed using sedimented cell volume (SCV) as a non-destructive quantitative measure. Every two weeks, subcultures were performed by transferring 3 mL of SCV from each sample into 22 mL of fresh liquid medium. This process was repeated three times with five Erlenmeyer flasks in each repetition. Erlenmeyer flasks were tightly sealed with sterile aluminium foil and wrapped with parafilm on the outermost part. To ensure proper dispersion and separation of the cells within

the suspension medium, the cell suspension culture media were kept in a growth chamber. Developed massive cell aggregates were transferred to the same media solidified with agar.

2.5. Light microscopy analysis

Microscopic analysis techniques were employed for shape assessment, facilitating the evaluation of cultured cell quality (the quality of cultured cells). Suspension cultures were observed with a Leica DM5500B microscope, equipped with a LEICA DFC450 C camera (Pragolab s.r.o., Slovak Republic); and calluses were observed with a LEICA MZ10F stereo microscope equipped with a LEICA DFC 420C camera (Pragolab s.r.o., Slovak Republic). This parameter is of particular importance, especially in scenarios involving size-able cell aggregates such as those found in somatic embryo cultures. Shape analysis facilitates the identification and elimination of aberrant somatic embryos during developmental stages, allowing the selection of somatic embryos demonstrating fitting attributes. Furthermore, investigations were conducted on samples derived from cell suspension cultures of Hypericum. The progression and growth of somatic embryos were examined.

2.6. Maturation of the somatic embryos and plant regeneration

Globular somatic embryos were cultured using different media formulations, including half strength basal medium solidified with agar without PGRs or with various doses of BAP (0.1 mg/L and 1.0 mg/L) and 2,4-D (0.1 mg/L and 1.0 mg/L). The cultures were kept in the dark at a temperature of 25± ◦C for 9 weeks, with regular transfers to fresh medium every 2 weeks. Each Petri dish (10 cm diameter) contained 4 globular somatic embryos as one replication. Once callus formation occurred, the embryos were conveyed to maturation medium MS + BAP 0.1 mg/L + sucrose 30 g/L and agar 7 g/L for shoot regeneration. Subcultures were performed every two weeks.

2.7. Rooting and acclimatization

Shoots developed adventitiously on calli were carefully excised using forceps and scalpels, and then carried to a MS medium containing 0.2 mg/L IBA for rooting. The cultures were placed under white fluorescent light with a photoperiod of 16 hours of light and 8 hours of darkness, at a controlled temperature of 25±2 °C. Once the plantlets had developed roots, any agar residues were gently washed off without causing damage to the roots. The rooted plantlets were then transplanted into a substrate consisting of peat and perlite mixed with field soil. To prevent moisture loss, all transplanted plants were covered with polyethylene bags. After 10 days, the bags were gradually opened to gradually expose the plants to the greenhouse environment and acclimatize them.

2.8. Experimental design

Regeneration trials were designed according to the completely randomised design with three replicates, using 90 mm disposable Petri dishes in which 10 explants were cultured in each replicate. The data obtained were analysed using the JMP-13 statistical package (SAS 2017). The mean values of the applications were compared using the Duncan test. Percentages were subjected to arcsine transformation before statistical analysis (Snedecor & Cochran 1967).

3. Results and Discussion

The seeds of *Hypericum* species were germinated on MS medium with a success rate ranging from 40% to 100%, and no contamination was observed. (Figure 1). H. *perforatum* L. and H. *athoum* Boiss. & Orph. showed high germination capacity. This germination variation of the species could be due to the provision of seeds from natural environments or different culture conditions. Germinated seeds were subcultured from auxiliary buds after 4-5 weeks. Developed plantlets produced mass branches and formed thick roots as shown (Figure 2). The leaf explants were isolated from these new plantlets in all species.

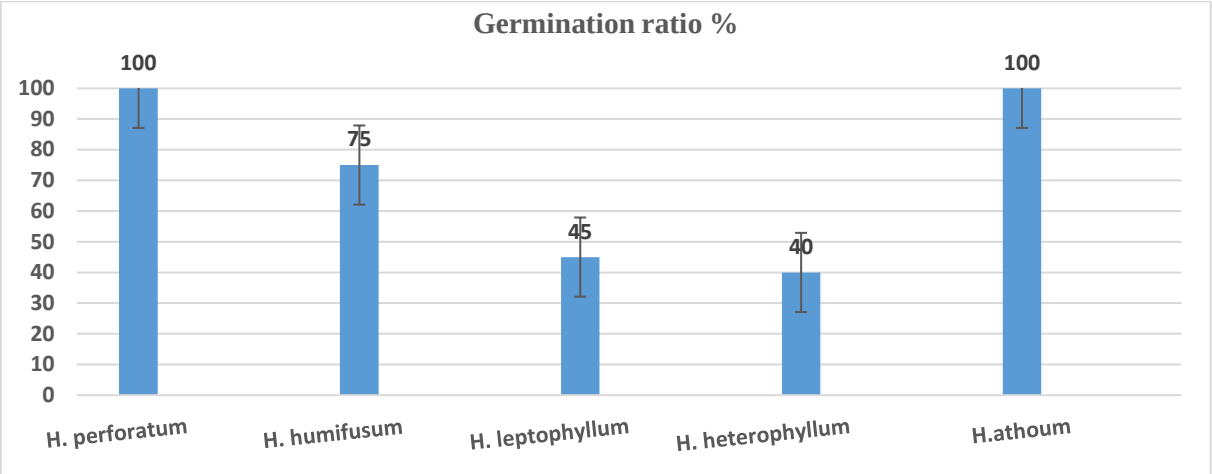

Figure 1- *In vitro* germination ratio of *Hyericum* species

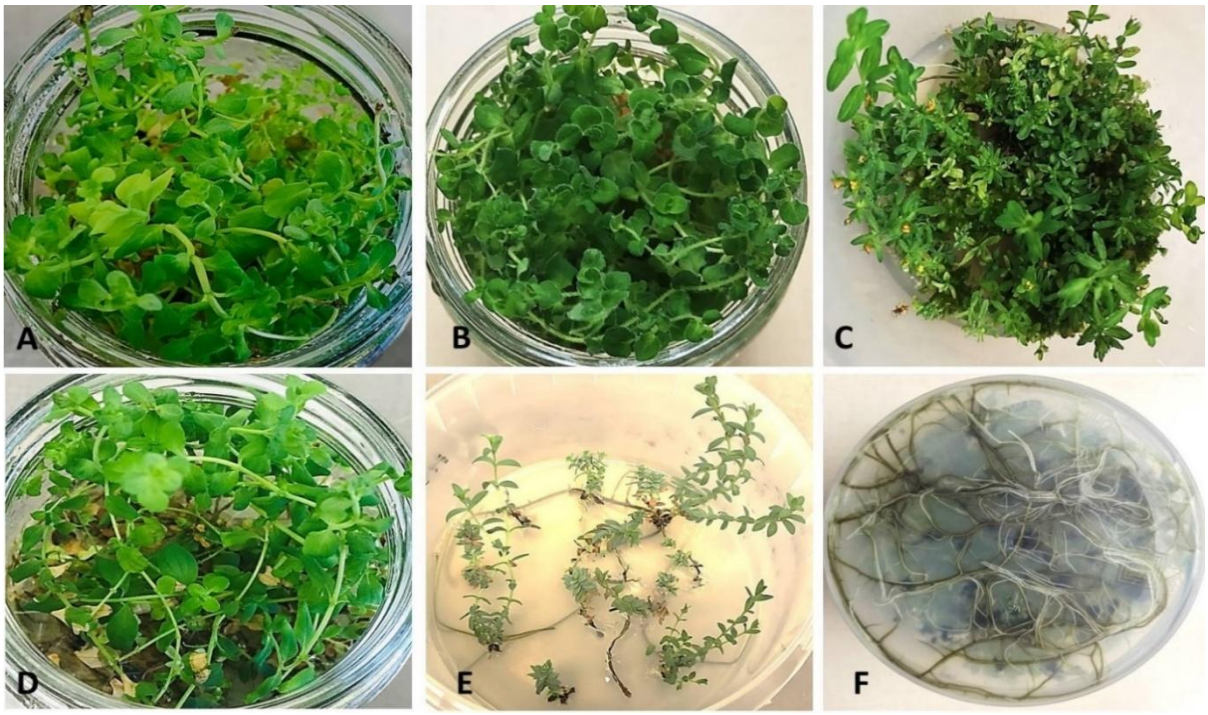

Figure 2- The leaf explants derived from the plantlets developing from auxiliary buds of germinated seeds after 4-5 weeks culture initiation (A*)* H. *perforatum* L. (B) H. *athoum* Boiss. & Orph. (C) H. *humifusum* L. (D) H. *leptophyllum* Hochst. (E) H. *heterophyllum* L. (F)Formation of thick and mass roots of germinated seeds of H. *perforatum* L

3.1. Adventitious shoot regeneration of Hypericum ssp

In the study, the effects of 2,4-D and two cytokinins (BAP and KIN) on the organogenesis of five *Hypericum* species cells were investigated. The leaf explants of all species were enlarged within 10 days. Callus formation and the induction of loose cell masses in all *Hypericum* species derived from leaf explants were also observed after two-four weeks of culture initation in all species under dark conditions. Clusters of calli started to emerge from the incisions of leaf and afterwards calli consistently developed from the cut zone of the petiole of the whole species. The embryonic white, healthy, friable, lightly dispersed and granular calli developed on leaf explants of the whole species (Figure 3). 2,4-D concentration of 0.1-1.0 mg/L with BAP or KIN on the media promoted the callus initiation responses of the whole species. The doses of 2,4-D drastically affected callus regeneration in many plant species (Zheng & Konzak 1999; Niazian et al. 2019). The best callus induction was seen on MS medium containing 1.0 mg/L BAP and 0.1 mg/L 2,4-D for H. *perforatum* L. (100%), H. *humifusum L.* (90.0%) and H. *leptophyllum* Hochst (90.0%). The highest callus weight was also determined on the same medium for three species Tables 1-3. However, 1.0 mg/L KIN and 0.1-1.0 mg/L 2,4-D promoted callus formation and callus weight for H. *athoum* Boiss. & Orph. and H. *heterophyllum* L. Tables 4-5. Similarly, combinations of KIN X 2,4-D were reported for suitable callus induction and MS medium including 0.90 µM of 2,4-D and 0.11 µM of KN showed the best callus induction from leaf explants of H. *perforatum* L. (Bais et al. 2002). Leaf, leaf discs and leaf axil derived from *in vitro* conditions for is generally the best source

for efficient and high frequency callus formation and shoot regeneration for *Hypericum* species (Pretto & Santarem 2000; Xu et al. 2001; Mccoy & Camper 2002; Pasqua et al. 2003; Ayan et al. 2005; Wójcik & Podstolki 2007; Mulinacci et al. 2008; Bais et al. 2002; Karakaş et al. 2015; Afsharzaleh et al. 2021; Ravindran et al. 2022). But limited studies were reported different organs and tissues such as mature leaf disc, seeds, mature stem segments, anthers of mature flower and *in vitro* nodal segments could be utilized for organogenesis via callus culture (Kirakosyan et al. 2000; Ayan et al. 2005; Mañero et al. 2012; Savio et al. 2012). In our study leaf explants also derived from *in vitro* responded well callus formation and shoot regeneration.

Then 4 weeks later globular calli with somatic embryos were transferred to the first same medium supplemented with 2,4-D BAP and KIN for shoot regeneration. Shoot primordia's initials occurred after 4-8 weeks of culture for all species tested. Number of shoots was recorded after 8 weeks of culture for each basic media and all species tested. The frequency of shoot regeneration was statistically influenced (P<0.01) for each basal media in all *Hypericum* species Table 1-5.

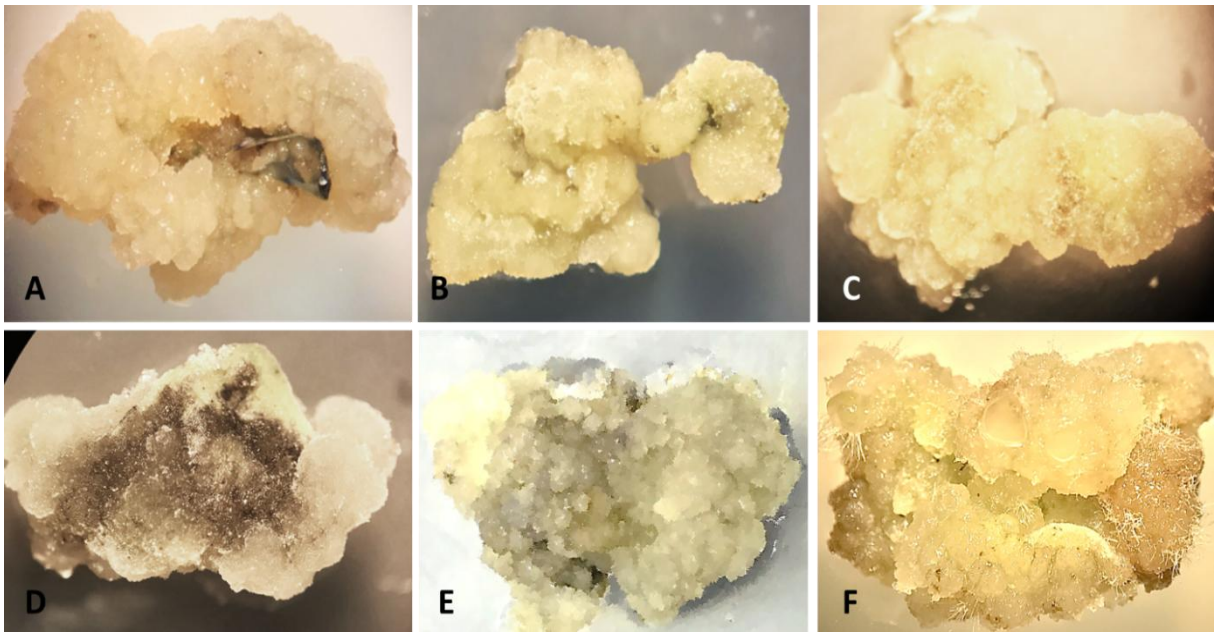

Figure 3- Callus formation and the induction of cell masses in all *Hypericum* species derived from leaf explants under dark conditions (A-B) H. *perforatum* L., (C) H. *athoum* Boiss. & Orph., (D) H. *humifusum* L. (E) H. *leptophyllum* Hochst, (F) H. *heterophyllum* L

Table 1- Effect of PGRs on callus and shoot induction from leaf explants of *Hypericum perforatum* L

PGR (mg/L)			*Leaf explants*			
BAP	***KIN***	***2,4-D***	***Callus induction (%)***	***Callus weight (g)***	***% Shoot Induction***	***Number of shoots/explants***
0.1		1.0	90.0 a*	2.103 ab*	57.33 b*	5.73 b*
1.0		0.1	90.0 a	2.750 ab	73.00 a	7.30 a
1.0		1.0	83.9 ab	3.043 ab	58.33 b	6.03 b
	0.1	1.0	70.8 abc	3.593 a	54.33 b	6.20 b
	1.0	0.1	59.7 c	1.427 b	23.67 c	3.31 c
	1.0	1.0	68.1 bc	1.613 b	32.67 c	4.02 c

BAP 6-benzylaminopurine, KIN: Kinetin, 2,4-D: dichlorophenoxyacetic acid; * Different letters in a column are significant at P<0.01 level

Table 2- Effect of PGRs on callus and shoot induction from leaf explants of *Hypericum humifusum* L

PGR (mg/L)			*Leaf explants*			
BAP	***KIN***	***2,4-D***	***Callus induction (%)***	***Callus weight (g)***	***% Shoot Induction***	***Number of shoots/explants***
0.1		1.0	75.00	0.873 b*	34.67 b*	4.57 c*
1.0		0.1	90.00	3.070 a	86.33 a	8.63 a
1.0		1.0	77.73	1.107 b	43.67 b	5.48 b
	0.1	1.0	63.87	0.038 c	17.33 c	2.73 d
	1.0	0.1	63.93	0.051 c	16.67 c	2.66 d
	1.0	1.0	71.60	0.036 c	13.67 c	2.57 d

BAP 6-benzylaminopurine, KIN: Kinetin, 2,4-D: dichlorophenoxyacetic acid; * Different letters in a column are significant at P<0.01 level

Table 3- Effect of PGRs on callus and shoot induction from leaf explants of *Hypericum leptophyllum* Hochst

PGR (mg/L)			*Leaf explants*			
BAP	***KIN***	***2,4-D***	***Callus induction (%)***	***Callus weight (g)***	***% Shoot Induction***	***Number of shoots/explants***
0.1		1.0	90.00 a*	2.83 c*	50.00 a*	5.00 ab*
1.0		0.1	90.00 a	5.95 a	45.67 ab	5.30 a
1.0		1.0	72.27 b	4.01 b	41.67 b	4.17 bc
	0.1	1.0	90.00 a	1.05 d	17.67 d	2.97 d
	1.0	0.1	81.13 ab	2.87 c	19.67 d	3.46 cd
	1.0	1.0	90.00 a	2.66 c	27.00 c	4.05 c

BAP 6-benzylaminopurine, KIN: Kinetin, 2,4-D: dichlorophenoxyacetic acid; * Different letters in a column are significant at P<0.01 level

Table 4- Effect of PGRs on callus and shoot induction from leaf explants of *Hypericum heterophyllum* L

PGR (mg/L)			*Leaf explants*			
BAP	***KIN***	***2,4-D***	***Callus induction (%)***	***Callus weight (g)***	***% Shoot Induction***	***Number of shoots/explants***
0.1		1.0	90.00 a*	0.037 c*	8.67 c*	2.17 b*
1.0		0.1	59.00 b	0.104 b	13.00 b	2.58 b
1.0		1.0	60.00 b	0.036 c	12.00 bc	2.57 b
	0.1	1.0	53.07 b	0.036 c	12.00 bc	2.57 b
	1.0	0.1	76.93 ab	0.081 b	18.33 a	3.25 a
	1.0	1.0	77.73 ab	0.293 a	14.00 b	2.80 ab

BAP 6-benzylaminopurine, KIN: Kinetin, 2,4-D: dichlorophenoxyacetic acid; * Different letters in a column are significant at P<0.01 level

Table 5- Effect of PGRs on callus and shoot induction from leaf explants of *Hypericum athoum* Boiss. & Orph

PGR (mg/L)			*Leaf explants*			
BAP	***KIN***	***2,4-D***	***Callus induction (%)***	***Callus weight (g)***	***% Shoot Induction***	***Number of shoots/explants***
0.1		1.0	61.93 b*	0.650 b*	15.00 b*	3.22 abc*
1.0		0.1	65.87 b	0.287 b	16.67 ab	3.82 a
1.0		1.0	61.93 b	0.553 b	7.67 c	2.61 d
	0.1	1.0	90.00 a	0.790 b	14.67 b	2.99 cd
	1.0	0.1	78.93 ab	0.847 b	14.67 b	3.33 abc
	1.0	1.0	90.00 a	3.523 a	23.00 a	3.65 ab

BAP 6-benzylaminopurine, KIN: Kinetin, 2,4-D: dichlorophenoxyacetic acid; * Different letters in a column are significant at P<P<0.01 level

All species formed high frequency shoot proliferation all media tested. H. *perforatum* L., H. *humifusum* L. and H. *leptophyllum* Hochst, showed high regeneration capacity in all media tested compared to H. *heterophyllum* L. and H. *athoum* Boiss. & Orph. The maximum shoot regeneration frequency (86.3 %, 73.0 %, 45.67 %, 18.33 % and 16.67 %) was respectively recorded in H. *humifusum* L., H. *perforatum* L., H. *leptophyllum* Hochst, and H. *athoum* Boiss. & Orph. on MS medium supplemented with 1.0 mg/L BAP and 0.1 mg/L 2,4-D. The highest number of shoots per explant (8.33, 7.30, 5.30, 3.82) was also respectively found on the same medium in H. *humifusum* L., H. *perforatum* L., H. *leptophyllum* Hochst, and H. *athoum* Boiss. & Orph. (Figure 4). However, the best regeneration frequency (18.33 %) and the maximum of shoots per explants (3.25) were determined on MS basal medium containing 1.0 mg/L Kinetin and 0.1 mg/L 2,4-D for H. *heterophyllum* Hochst.

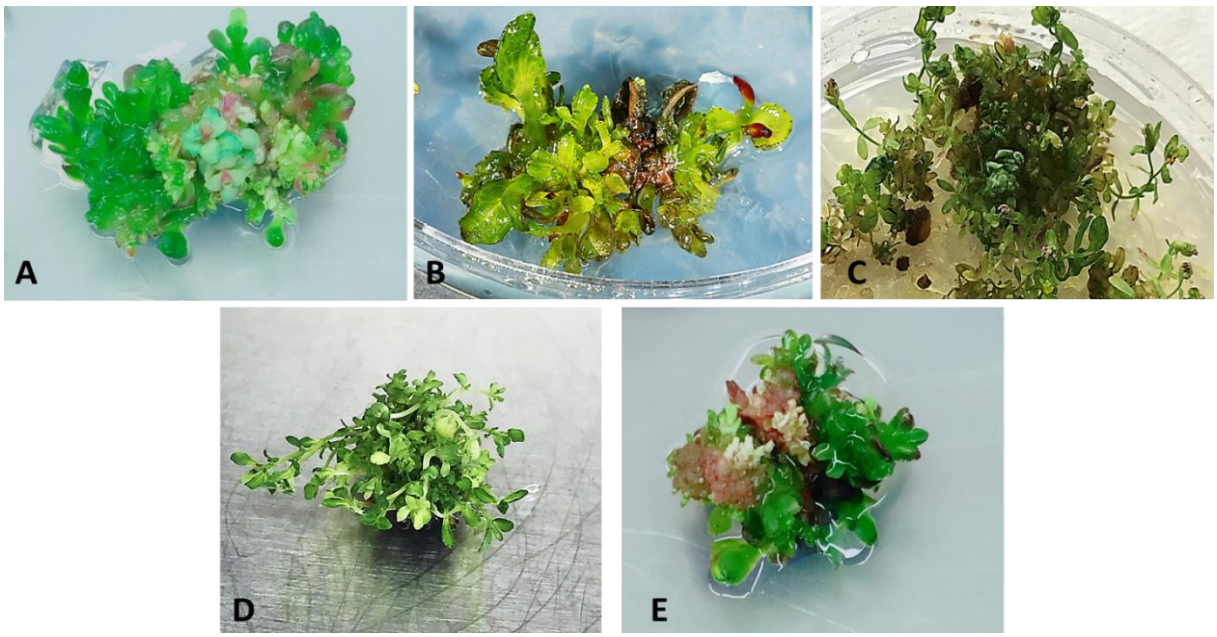

Figure 4- Development of shoot primordias and adventitious shoot regeneration of *Hypericum* species on MS medium supplemented with 1.0 mg/L BAP and 0.1 mg/L 2,4-D. (A) H. *perforatum* L. (B) H. *athoum* Boiss. & Orph. (C) H. *humifusum* L. (D) H. *leptophyllum* Hochst. (E) H. *heterophyllum* L

Comparing cytokinine types included in MS media, four species responded better to BAP in our study. High levels of BAP combined with low levels of 2,4-D comparatively induced regeneration frequency four genotypes. Recent studies have shown that many efficient adventitious callus/shoot regenerations and micropropagation methods of different *Hypericum* ssp were reported until date (Cellarova et al. 1992; Moura 1998; Pretto & Santarem 2000; Mccoy & Camper 2002; Karpinen et al. 2006; Ayan & Cirak 2006; Mulinacci et al. 2008; Karakaş et al. 2009; Coste et al. 2011; Banerjee et al. 2012; Afsharzaleh et al. 2021; Mikhovich et al. 2021; Selvakesavan & Gregory 2021; Ravindran et al. 2022). Similarly, in previous studies conducted with H. *foliosum* Aiton, H. *perforatum* L., H. *maculatum*, H. *angustifolium*, H. *hirsutum* L., and H. *triquetrifolium*, it was stated that the combined use of BAP and NAA as a cytokinin/auxin source significantly promoted adventitious shoot regeneration (Moura 1998, Pretto & Santarem 2000; Mulinacci et al. 2008; Karakaş et al. 2009; Coste et al. 2011). BAP also has critical a role in hypericin production in *Hypericum in vitro* conditions (Karakaş et al. 2009). Moreover, basal media containing high concentrations of BAP produced shoots with more branched as indicated other studies (Cellarova et al. 1992; Koperd´akova, et al. 2009). Our results also revealed that high BAP concentration and low concentration of 2,4-D promoted callus and regeneration with well-developed shoots (Figure 4).

3.2. Regeneration of Hypericum ssp. using cell suspension culture techniques

Cell suspension cultures was derived from inducing callus in leaf explants of *Hypericum* species seedlings on MS medium supplemented with 1 mg/L 2,4-D, 0.1 mg/L BAP and 7 g/L agar. Callus development and suspension cultures were induced as reported previous studies developed using leaf explants *in vitro* grown seedlings of *Hyperium* species (Bais et al. 2002; Gadzovska et al. 2007; Walker et al. 2002; Wang et al. 2015; Zubrick´a et al. 2015; Afsharzadeh et al. 2021; Ravindran et al. 2022).

These clusters were detached from the basal and transferred to cell suspension culture medium. This medium MS basal media with Gamborg's B5 vitamins containing 30 g/L sucrose, and 2 mg/L glycine, 1 mg/L 2,4-D, 0.1 mg/L KIN, and 0.1 mg/L BAP. BAP either alone or in combination with NAA is the most preferred plant growth regulators for enhanced production of secondary metabolites in *in vitro* shoot cultures of H. *perforatum* (Karppinen et al. 2007; Gadzovska et al. 2014; Kwiecień et al. 2015; Kwiecień et al. 2018). However, we added KIN and 2,4-D to suspension culture as KIN and 2,4-D promoted suitable globular calli formation and shoot regeneration for some *Hyperium* species.

The friable calli in the suspension culture began to grow within 2-4 weeks and all species formed white, healthy, friable, lightly dispersed and granular calli clusters. Percentage of volumetric callus growth of the species was fluctuated between 45-223%. The highest callus growth ratio was respectively observed in H. *perforatum* (223%) and H. *humusifum* (212%). However, H. *leptophyllum* (45%) responded the minimum callus proliferation in (Figure 5).

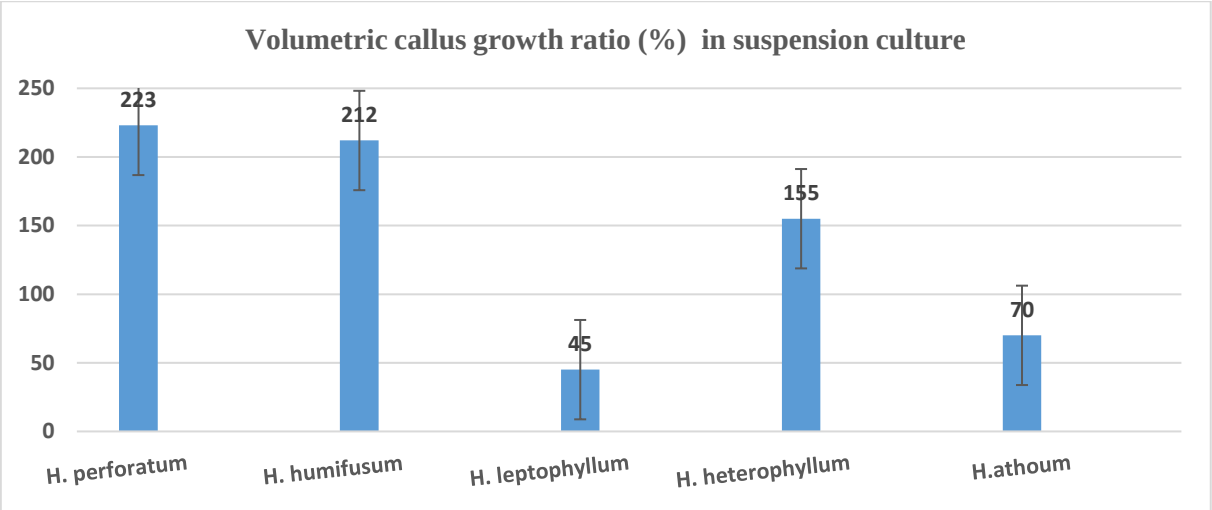

Figure 5- Volumetric callus growth ratio of *Hypericum* species on callus induction medium

The colour of cell suspension turned into different light and dark brown colour tones for each *Hypericum* species after 2-3 weeks later. We observed that phenol synthesis of the species was at the different level and death of tissue and cells (Figure 6). To provide culture conditions more stable subcultures were performed every 2 weeks. Subculturing of calli affected the formation and quality of embryonic cells as well as the sustainability of the suspension cultures. Subculturing the suspensions every 2 weeks considerably was observed to increase biomass production and number of aggregates. Homogenous cell suspensions and subculture interval provide uniform access to nutrition precursors and growth regulators and facilitate to determine critical stage of competent suspension cells (Mustafa et al. 2011; Kong et al. 2020).

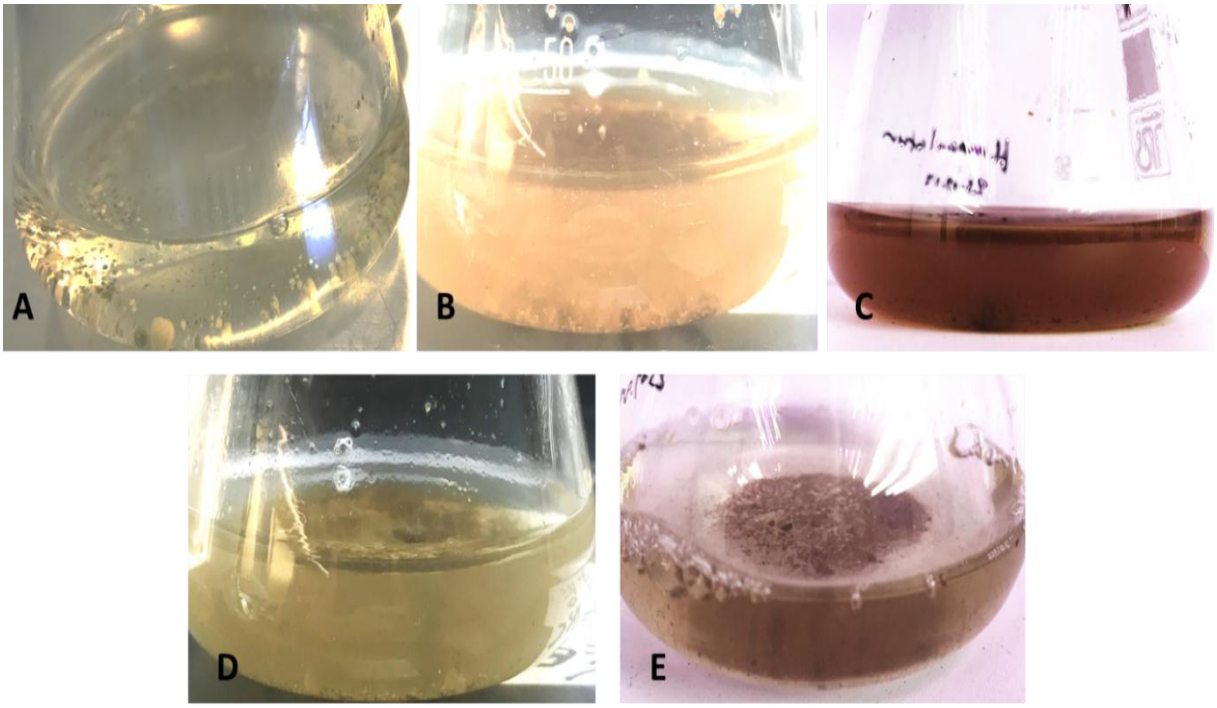

Figure 6- Suspension cell cultures of *Hypericum* species (A) H. *perforatum* (B) H. *athoum* Boiss. & Orph. (C) H. *humifusum* L. (D) H. *leptophyllum* Hochst. (E) H. *heterophyllum*

The cells isolated from calli developed in suspension culture were separatable for each species examined under a light microscope. It was observed that the cells were generally homogeneous for each species (Figure 7)

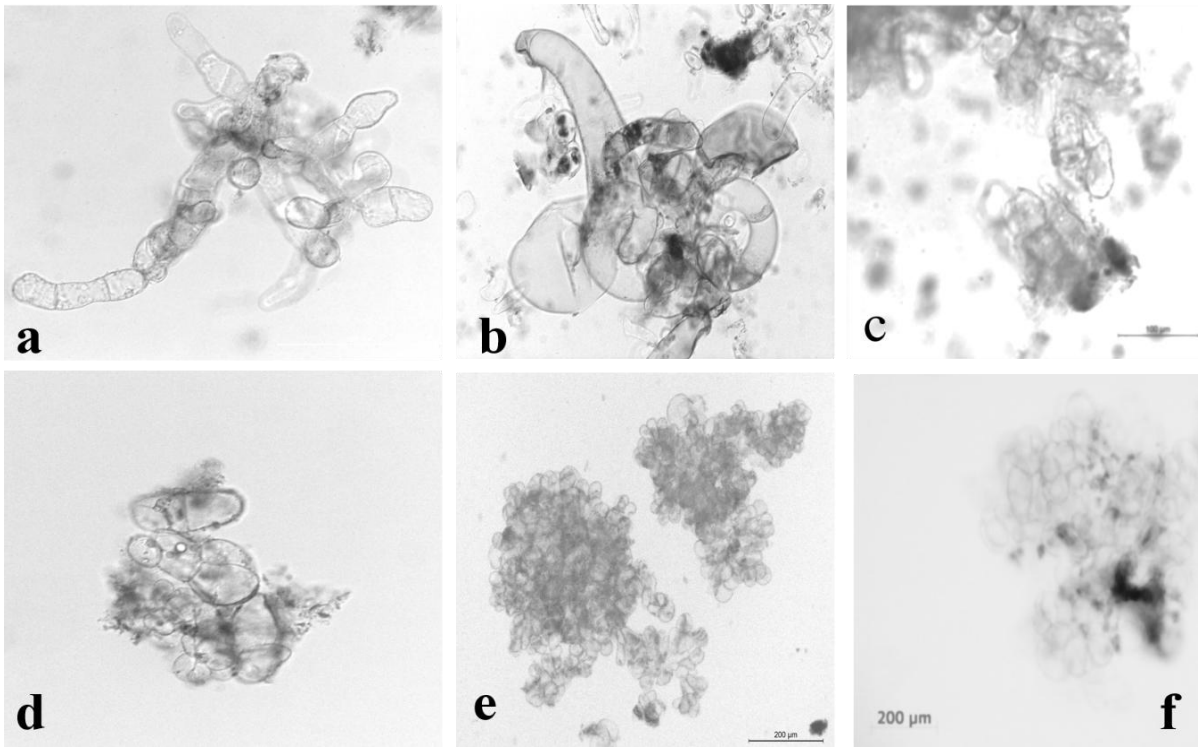

Figure 7- Light microscopic view of cells from the established suspension cultures of different *Hypericum* spp. such as (A) H. *leptophyllum* Hochst., (B) H. *humifusum* L., (C) H. *perforatum* L., H. *athom* Boiss. & Orph. and (E-F) H. *heterophyllum* L. (scale bar=200 µm)

Cell suspension cultures were plated a single globular structure after plating on agar-solidified basal media. The proembryogenic masses of suspension enlarged and formed globular, translucent, whitish separable aggregates. Protuberances were observed and turned to embryonic structures within 2-4 weeks (Figure 8). Differentiation time of somatic embryos for each species was different. Formation of somatic embryos was 1-2 weeks earlier for H. *humifusum* L., H. *heterophyllum* L. and H. *perforatum* L. species. These globular embryos further transformed into heart and cotyledonary stage. Then 2-4 weeks later, mature cotyledonary stage started, and cotyledons thickened and enlarged.

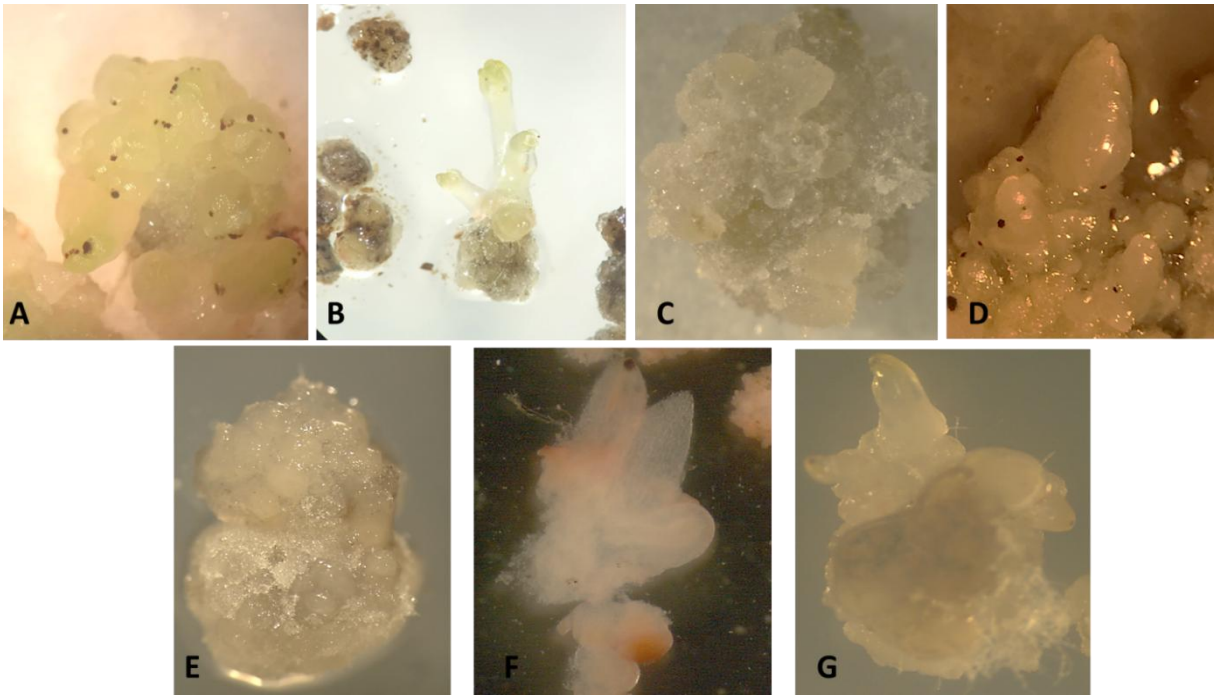

Figure 8- Embryonic callus induction and embryo proliferation after plating on agar-solidified medium in *Hypericum* species (A-B) H. *perforatum* L. *(*C) H. *athoum* Boiss. & Orph., *(*D) H. *humifusum* L., (E.) H. *heterophyllum* L. *(*F-G) H. *leptophyllum* Hochst.

Mature cotyledonary stage embryos were transferred to MS supplemented with 1 mg/L 2,4-D, 0.1 mg/L KIN, and 0.1 mg/L BAP and 7g/L agar. Germination of somatic embryos was visible for all *Hypericum* species within 3-5 weeks. The highest mean number of shoot per callus or percentage of germination of somatic embryo were respectively recorded for H. *perforatum* L. (15.37/callus), H. *leptophyllum* Hochst (6.9/callus), H. *heterophyllum* L. (9.6/callus), H. *humifusum* L. (16.8/callus) and H. *athoum* Boiss. & Orph.(11.7/callus). H. *perforatum* L. and H. *humifusum* L. showed the best shoot regeneration capacity as recorded in adventitious shoot regeneration studies (Figure 9). When germinated embryos were cultured in the same medium for more 7-8 weeks, shoot development weakened and leave began to turn yellow. Germination of mature somatic embryos decreased if they were continuously cultured on a maturation medium. All germinated somatic embryos of all species were successfully rooted. Cotyledonary stage somatic embryos germinated were rooted on MS medium containing 30 g/L sucrose with agar 7 g/L. More than 70 % of somatic embryos of all species germinated and produced thick and branched shoots. Percentage of rooting of these germinated embryos was fluctuated between average 90-100 % for each species (Figure 9). Long, mass, white and healthy roots were observed on full strength MS medium. Root growth was optimized in full strength MS medium supplemented with 0.2 mg/L IBA. Most of the embryos of all species converted to whole plants with all their organs fully developed after 2-5 weeks later on germination medium. Rooted plantlets were carried to pots including a turf and vermiculite (in a 1:1 proportion) mixture. The plants were acclimatized with 85-100 % survival rate 4-5 weeks later after transferring the greenhouse (Figure 9). H. *perforatum* and H. *humifusum* L. had also the highest survival rate (100%) as having regeneration capacity.

Recently, a few cell suspension cultures techniques of *Hyperium* ssp. have been also used for H. *androsaemum* L. (Dias et al. 2000), H. *perforatum* L. (Dias et al. 2001; Bais et al. 2002; Cui X-H et al. 2010; Gadzovska et al. 2013; Wang et al. 2015), H. *calycinum* L. (Klingauf et al. 2005), H. *triquetrifolium* (Karakaş et al. 2015), H. *androsaemum* L., H. *linariifolium* Vahl, H. *elodes* L., H. *pulchrum* L., H. *humifusum* L., H. *undulatum* Schousb. ex Willd, H. *perfoliatum* L., H. *canariense* L., H. *tomentosum* L., H. *perforatum* L. and H. *maculatum* Crantz (Selvakesavan & Gregory 2021). In our study, H. *perforatum* L., H. *leptophyllum* Hochst, H. *heterophyllum* L. H. *humifusum* L. and H. *athoum* Boiss. & Orph. were also successfully propagated using cell suspension cultures techniques.

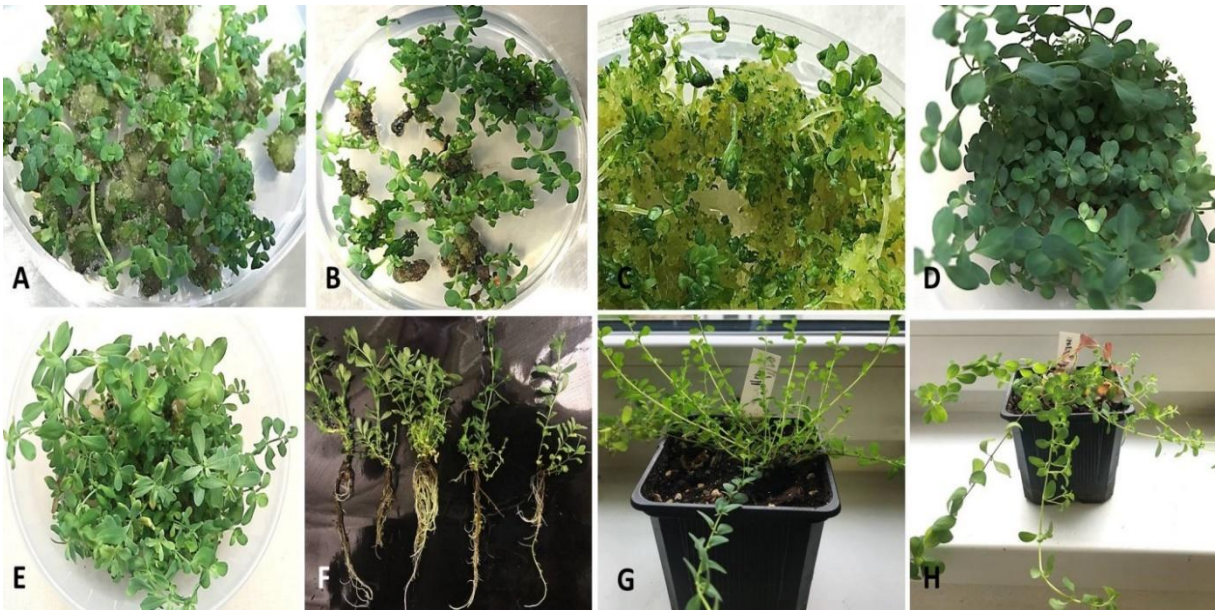

Figure 9- Germination of cell suspension-derived embryos, shoot regeneration, rooting and acclimatization of *Hypericum* species cultured suspension culture (A) H. *perforatum* L. (B) H. *humifusum* L. (C) H. *leptophyllum* Hochst, (D) H. *athoum* Boiss. & Orph (E) H. *heterophyllum* (F) Rooting of *Hypericum* spp. MS medium containing 0.2 mg/L IBA (G-H) Well-acclimatized 10-12 weeks old plantlets of H. *humifusum* and H. *perforatum* L.

4. Conclusions

Plant tissue culture methods are an important and efficient effective tool for multiplying of the species in short time, pathogen free production and providing availability of desired quantity of bioactive compounds as being in *Hypericum* species containing rich and valuable secondary metabolites. The field cultivation of *Hypericum* species may be time consuming and labour intensive and there are many biotic and abiotic obstacles that prevent high secondary metabolite yields from plants exposed to different environmental conditions (Coste et al. 2021; Tavakoli et al. 2020; Shasmita et al. 2023). Since these barriers have resulted in insufficient production of metabolites from H. *perforatum* L. we need a large-scale production system for plant and its bioactive compounds (Shasmita et al. 2023). Therefore, efficient and reliable tissue and organ culture, callus

culture, cell suspension techniques for each *Hyperium* species must be improved. In this study, it was developed high frequency regeneration protocol for five *Hypericum* species and efficient and homogenous suspension culture was established for initiation H. *perforatum* L, H. *athoum* Boiss. & Orph, H. *humifusum* L., H. *leptophyllum* Hochst, H. *heterophyllum* L. using leaf-derived calli. H. *perforatum* L. and H. *humifusum* L. had high callus and shoot regeneration capacity and positively responded to suspension cultures compared to other species.

Acknowledgements

Thankful to Inst. of Plant Gen. and Bio. Plant Sci. and Biodiv. Center, Slovak Academy of Sci. Nitra, Slovak Republic for providing facility and supporting the present research work. Distinguished thanks are due to Prof. Dr. Eva Čellárová (UPJS, Fac. of Sci. Inst. of Bio. and Eco. Dept. of Gen. Košice-Slovak Republic) for their kindly gift of *Hypericum humifusum* and *Hypericum athoum* seeds.

Funding

The authors declare that the study is funded by the Slovak Academic Information Agency / Slovak Republic.

References

Afsharzadeh N, Azizi M & Samiei L (2021). Medium optimization for callus induction, shoot regeneration and rooting of *Hypericum perforatum* from stem and leaf explants. *Journal of Horticulture Science* 34:1-3 https://doi.org/10.22067/jhs.2021.60331.0

Alahmad A, Feldhoff A, Bigall N C, Rusch P, Scheper T & Walter J G (2021). *Hypericum perforatum* L.-mediated green synthesis of silver nanoparticles exhibiting antioxidant and anticancer activities *Nanomaterials* 11(2): 487 *https://doi.org/*10.3390/nano11020487

Al-Atrakchii A O A, Yousif H H & Al-Barwari A O M (2019). Effect of altitude and nitrogen fertilization on some vegetative and flowering parameters and essential oil percentage of lavender plant (Lavandula angustifolia). *Kirkuk University Journal For Agricultural Sciences* 10(2): 40-47 http://doi.org/ 10.58928/ku19.10205

Abdulkareem A A, Ghaffoori A T & Alsabte A A (2024). *In vitro* propagation of date Palm using bioreactor technology. *Kirkuk University Journal for Agricultural Sciences* 15(1): 98-106 http://doi.org/ 10.58928/ku24.15110

Ayan A K & Cirak C (2006). *In vitro* Multiplication of *Hypericum heterophyllum*, an Endemic Turkish species. *American Journal of Plant Physiology* 1(1): 76-81 https://doi.org/ 10.3923/ajpp.2006.76.81

Ayan A, Cirak C, Kevseroglu K & Sokmen A (2005). Effects of explant types and different concentrations of sucrose and phytohormones on plant regeneration and hypericin content in *Hypericum perforatum* L. *Turkish Journal of Agriculture and Forestry* 29(3): 197-204

Bais H P, Walker T S, Mcgrew J J & Vivanco J M (2002). factors affecting growth of cell suspension cultures of *Hypericum perforatum* L. (st. john's wort) and production of hypericin. *In Vitro Cellular & Developmental Biology-Plant* 38: 58–65 https://doi.org/10.1079/IVP2001253

Barnes J, Anderson L A & Phillipson J D (2001). St John's wort (*Hypericum perforatum* L.): A review of its chemistry, pharmacology and clinical properties. Journal of Pharm Pharmacology 53(5): 583-600 https://doi.org/10.1211/0022357011775910

Banerjee A, Bandyopadhyay S & Raychaudhuri S S (2012). *In vitro* regeneration of *Hypericum perforatum* L. using thidiazuron and analysis of genetic stability of regenerants. *Indian Journal Biotechnology* 11: 92–98

Behera S S, Mishra P, Samal M, Mohapatra D, Monalisa K & Naik K S (2023). Recent advances in tissue culture and secondary metabolite production in *Hypericum perforatum* L.. *Plant Cell, Tissue and Organ Culture* 154: 13–28 https://doi.org/10.1007/s11240-023-02525-3

Buter B, Orlacchio C, Soldati A & Berger K (1998). Significance of genetic and environmental aspects in the field cultivation of *Hypericum perforatum*. *Planta Medica*. 64(5): 431-437 https://doi.org/10.1055/s-2006-957475

Cellarova E, Kimakova K & Brutovska R (1992). Multiple shoot formation in *Hypericum perforatum* L. and variability of R_0. *Engineering* 12(6): 445-452 https://doi.org/10.1002/abio.370120602Citations

Ciccarelli D, Andreucci A C & Pagni A M (2001). Translucent glands and secretory canals in *Hypericum perforatum* L. (Hypericaceae): morphological, anatomical and histochemical studies during the course of ontogenesis. *Annals of Botany* 88(4): 637-644 https://doi.org/10.1006/anbo.2001.1514

Coste A, Pop C, Halmagyi A & Butiuc-Keul A (2021). Secondary metabolites in shoot cultures of Hypericum. In: Ramawat K G, Ekiert H M & Goyal S (eds) Plant Cell and Tissue Differentiation and Secondary Metabolites. Springer, Cham, pp 273–307

Coste A, Vlase L, Halmagyi A, Deliu C & Coldea G (2011). Effects of plant growth regulators and elicitors on production of secondary metabolites in shoot cultures of *Hypericum hirsutum* and *Hypericum maculatum*. Plant Cell, Tissue and Organ Culture 106: 279–288 https://doi.org/10.1007/s11240-011-9919-5

Crockett S L & Robson N K (2011). Taxonomy and chemotaxonomy of the genus *Hypericum*. *Medicinal and Aromatic Plant Science and Biotechnology* 5(Special Issue 1): 1-13

Dall'Agnol R, Ferraz A, Bernardi AP, Albring D, Nör C, Sarmento L, Lamb L, Hass M, von Poser G & Schapoval E E (2003). Antimicrobial activity of some Hypericum species. *Phytomedicine* 10(6-7): 511-516 https://doi.org/ 10.1078/094471103322331476

Dias A C P, Seabra R M, Andrade P B, Ferreres F & Fernandes-Ferreira M (2001). Xanthone production in calli and suspended cells of *Hypericum perforatum*. *Journal of Plant Physiology* 158(7): 821-827 https://doi.org/10.1078/0176-1617-00195

Dias A C P, Seabra R M, Andrade P B, Ferreres F & Fernandes-Ferreira M (2000). Xanthone biosynthesis and accumulation in calli and suspended cells of *Hypericum androsaemum*. *Plant Science* 150(1): 93–101 https://doi.org/10.1016/S0168-9452(99)00178-8

Eibl R, Meier P, Stutz I, Schildberger D, Huhn T & Eibl D (2018). Plant cell culture technology in the cosmetics and food industries: current state and future trends. *Applied Microbiology and Biotechnology* 102(20): 8661-8675 https://doi.org/10.1007/s00253-018-9279-8

Faizy WS, Toma RS & Tamer YS (2022). *In vitro* propagation of Pyracantha coccinea as affected by growth regulators and different carbon sources. *Kirkuk University Journal for Agricultural Sciences* 13(4): 244-252 http://doi.org/10.58928/KU22.13421

Gadzovska S, Maury S, Delaunay A, Spasenoski M, Hagège D, Cour tois D & Joseph C (2013). The influence of salicylic acid elicitation of shoots, callus, and cell suspension cultures on production of naphtodianthrones and phenylpropanoids in *Hypericum perforatum* L. *Plant Cell, Tissue and Organ Culture* 113(1): 25-39 https://doi.org/ 10.1007/s11240-012-0248-0

Gadzovska S, Maury S, Delaunay A, Spasenoski M, Joseph C & Hag`ege D (2007). Jasmonic acid elicitation of *Hypericum perforatum* L. cell suspensions and effects on the production of phenylpropanoids and naphtodianthrones. *Plant Cell, Tissue and Organ Culture* 89: 1–13 https://doi.org/10.1007/s11240-007-9203-x

Gamborg O L, Miller R A & Ojima K (1968). Nutrient requirements of suspension cultures soybean root cells. *Experimental Cell Research* 50(1): 151-158 https://doi.org/ 10.1016/0014-4827(68)90403-5

Greeson J, Sanford B & Monti D A (2001). St. John's wort (*Hypericum perforatum* L.) A review of the current pharmacological, toxicological and clinical literature. *Psychopharmacology* 153(4): 402-214 https://doi.org/10.1007/s002130000625

Griffith T N, Varela-Nallar L, Dinamarca M C & Inestrosa N C (2010). Neurobiological effects of Hyperforin and its potential in Alzheimer's disease therapy. *Current Medicinal Chemistry* 17(5): 391-406 https://doi.org/10.2174/092986710790226156

Gubser G, Vollenweider S, Eibl D & Eibl R (2021). Food ingredients and food made with plant cell and tissue cultures: State-of-the art and future trends. Engineering in Life Scince 21: 87–98 https://doi.org/10.1002/elsc.202000077

Guedes R C & Eriksson L A (2005). Theoretical Study of Hypericin. *Journal of Photochemistry and Photobiology A: Chemistry* 172(3): 293-299 https://doi.org/10.1016/j.jphotochem

Henzelyová J & Čellárová E (2018). Modulation of naphthodianthrone biosynthesis in hairy root-derived Hypericum tomentosum regenerants. *Acta Physiologiae Plantarum* 40: 82 https://doi.org/10.1007/s11738-018-2664-1

Hong D, Yin F, Hu L H & Lu P (2004). Sulfonated xanthones from *Hypericum sampsonii*, *Phytochemistry*, 65(18): 2595-2598 https://doi.org/ 10.1016/j.phytochem

Hussain M J, Abbas Y, Nazli N, Fatima S, Drouet S, Hano C & Abbasi B H (2022). Root cultures, a boon for the production of valuable compounds: A comparative review. *Plants* 11(3): 439 https://doi.org/ 10.3390/plants11030439. PMID: 35161423

Jendželovská Z, Jendželovský R, Kuchárová B & Fedoročko P (2016). Hypericin in the light and in the dark: two sides of the same coin. *Frontiers in Plant Science* 7: 560 https://doi.org/10.3389/fpls.2016.00560

Karakaş Ö, Özen H Ç & Onay A (2015). Determination of hypericin con tent in callus and cell suspension cultures of *Hypericum triquetrifolium* Turra. *Advances in Zoology and Botany* 3(4): 184-189 https://doi.org/10.13189/azb.2015.030404

Karakaş O, Toker Z, Tilkat E, Ozen H C & Onay A (2009). Effects of different concentrations of benzylaminopurine on shoot regenera tion and hypericin content in *Hypericum Triquetrifolium* Turra. *Natural Product Research* 23(16): 1459-1465 https://doi.org/10.1080/14786410701664528

Karppinen K, Hokkanen J, Tolonen A, Mattila S & Hohtola A (2007). Biosynthesis of hyperforin and adhyperforin from amino acid pre cursors in shoot cultures of *Hypericum perforatum*. *Phytochemistry* 68(7): 1038-1045 https://doi: 10.1016/j.phytochem.2007.01.001

Karppinen K, György Z, Kauppinen M, Tolonen A, Jalonen J, Neubauer P, Hohtola A & Häggman H (2006). *In vitro* propagation of *Hypericum perforatum* L. and accumulation of hypercins, pseudohypericins and phloroglucinols. *Propagation of Ornamental Plants* 6(4): 170-179

Kirakosyan A, Hayashi H, Inoue K, Charchoglyan A & Vardapetyan H (2000). Stimulation of the production of hypericins by man nan in *Hypericum perforatum* shoot cultures. Phytochemistry 53(3): 345-348. https://doi.org/ 10.1016/s0031-9422(99)00496-3

Klingauf P, Beuerle T, Mellenthin A, El-Moghazy S A M, Boubakir Z & Beerhues L (2005). Biosynthesis of the hyperforin skeleton in *Hypericum calycinum* cell cultures. *Phytochemistry* 66(2): 139–145 https://doi.org/10.1016

Kong E Y Y, Biddle J, Foale M & Adkins S W (2020). Cell suspension culture: a potential in vitro culture method for clonal propagation of coconut plantlets via somatic embryogenesis. *Industrial Crops and Products* 147: 112125 https://doi.org/10.1016

Koperdáková J, Katkovèınová Z, Košuth J, Giovannini A & Cèllárová E (2009). Morphogenetic response to plant growth regulators in transformed and untransformed *Hypericum perforatum* L. clones. *Acta Biologica Cracovıensia Series Botanica* 51(1): 61–70

Kruszka D, Selvakesavan R K, Kachlicki P & Franklin G (2022). Untargeted metabolomics analysis reveals the elicitation of important secondary metabolites upon treatment with various metal and metal oxide nanoparticles in *Hypericum perforatum* L. cell suspension cultures. *Industrial Crops and Products* 178: 114561 https://doi.org/10.1016/j.indcrop

Kwiecień I, Szydlowska A, Kawka B, Beerhues L & Ekiert H (2015). Accumulation of biologically active phenolic acids in agitated shoot cultures of three *Hypericum perforatum* L. cultivars 'Elixir', 'Helos', and 'Topas'. *Plant Cell, Tissue and Organ Culture* 123: 273–281 https://doi.org/10.1007/s11240-015-0830-3

Mañero F J, Algar E, Gómez M S M, Sierra M D S & Solano B R (2012). Elicitation of secondary metabolism in *Hypericum perforatum* by rhizosphere bacteria and derived elicitors in seedlings and shoot cultures. *Pharmaceutical Biology* 50(10): 1201-1209 https://doi.org/ 10.3109/13880209.2012.664150

Mccoy J & Camper N D (2002). Development of a micropropagation protocol for St. John' s wort (*Hypericum perforatum* L.). *Horticultural Science* 37(6): 978–980 https://doi.org/10.21273/HORTSCI.37.6.978

Medina M A, Martínez-Poveda B, Amores-Sánchez M I & Quesada A R (2006). Hyperforin: More than an antidepressant bioactive compound? *Life Sciences* 79(2): 105-111 https://doi.org/10.1016/j.lfs

Mikhovich Z E, Echishvili E E, Portnyagina N V & Skrotskaya O V (2021). Peculiarities of *Hypericum perforatum* L. reproduction in vitro culture and development of plants in the open field. *Samara Journal of Science* 10(4): 79–86 https://doi.org/10.17816/snv2021104112

Moura M (1998). Conservation of *Hypericum foliosum* Aiton, an endemic azorean species, by micropropagation. *In Vitro Cellular & Developmental Biology-Plant* 34(3): 244-248

Murashige T & Skoog F (1962). A revised medium for rapid growth and bioassays with tobacco tissue cultures. *Plant Physiology* 15: 473-497 https://doi.org/10.1111/j.1399-3054.1962.tb08052.x

Murthy H N, Joseph K S, Paek K Y & Park S Y (2023). Anthraquinone production from cell and organ cultures of Rubia species: an overview. *Metabolites* 13(1):39 https://doi.org/ 10.3390/metabo13010039

Mulinacci M, Giaccherini C, Santamaria A R, Caniato R, Ferrari F, Valletta A, Vincieri F F & Pasqua G (2008). Anthocyanins and xanthones in the calli and regenerated shoots of *Hypericum perforatum* var angustifolium (sin. Fröhlich) Borkh. *Plant Physiology and Biochemistry* 46(4): 414-420 https://doi.org/10.1016/j.plaphy

Mustafa N R, Winter W D, Iren F V & Verpoorte R (2011). Initiation, growth and cryopreservation of plant cell suspension cultures. *Nature Protocols* 6: 715–742 https://doi.org/10.1038/nprot.2010.144

Niazian M, Shariatpanahi M E, Abdipour M & Oroojloo M (2019). Modeling callus induction and regeneration in an anther culture of tomato (*Lycopersicon esculentum* L.) using image processing and artificial neural network method. *Protoplasma* 256(5): 1317-1332 https://doi.org/10.1007/s00709-019-01379-x

Palmer C D & Keller W A (2011). Plant regeneration from petal explants of *Hypericum perforatum* L. *Plant Cell, Tissue and Organ Culture* 105: 129–134 https://doi.org/10.1007/s11240-010-9839-9

Parveen S & Shahzad A (2014). Factors affecting *in vitro* plant regeneration from cotyledonary node explant of (L.) Roxb. A highly medicinal legume. *African Journal of Biotechnology* 13(3): 413-422 https://doi.org/10.5897/AJB2013.13126

Permyakova N V, Sidorchuk Y V, Marenkova T V, Khozeeva S A, Kuznetsov V V, Zagorskaya A A, Rozov S M & Deineko E V (2019). CRISPR/Cas9-mediated gfp gene inactivation in Arabidopsis suspension cells. *Molecular Biology Reports* 46(6): 5735-5743 https://doi.org/10.1007/s11033-019-05007-y

Pretto F R & Santarém E R (2000). Callus formation and plant regeneration from *Hypericum perforatum* leaves. *Plant Cell, Tissue and Organ Culture* 62: 107–113 https://doi.org/10.1023/A:1026534818574

Radusiene J, Bagdonaite E & Kazlauskas S (2004). Morphological and chemical evaluation on *Hypericum perforatum* and H. *maculatum* in Lithuania. *Acta Horticulturae* 629: 55-62 https://doi.org/10.17660/ActaHortic

Ravindran B M, Rizzo P, Franke K, Fuchs J & D'Auria J (2022). Simple and robust multiple shoot regeneration and root induction cycle from different explants of *Hypericum perforatum* L. genotypes. *Plant Cell, Tissue and Organ Culture* 152(1): 1–15 https://doi.org/10.1007/s11240-022-02370-w

Saad C N, Mazlan F I & Karim A K (2016). Factors affecting the establishment and growth of Pogostemon cablin cell suspension cultures. *International Journal of Advanced Research in Science, Engineering and Technology* 3(10): 2790-2796

Santarem E R & Astarita L V (2003). Multiple shoot formation in Hyperi cum perforatum L. and hypericin production. *Brazilian Journal of Plant Physiology* 15(1): 43–47 https://doi.org/10.1590/S1677-04202003000100006

Santos R B, Abranches R, Fischer R, Sack M & Holland T (2016). Putting the spotlight back on plant suspension cultures. *Frontiers in Plant Science* 7: 297 https://doi.org/ 10.3389/fpls.2016.00297

Savio L E B, Astarita L V & Santarém E R (2012). Secondary metabolism in micropropagated *Hypericum perforatum* L. grown in non-aerated liquid medium. *Plant Cell, Tissue and Organ Culture* 108: 465–472 https://doi.org/10.1007/s11240-011-0058-9

SAS Institute Inc (2017). JMP® Statistical Discovery Software, version 13.0; – SAS Institute Inc., Cary, NC

Selvakesavan R K & Gregory F (2021). Robust in vitro culture tools suitable for sustainable bioprospecting of the genus Hypericum. *Industrial Crops and Products* 170: 113715 https://doi.org/10.1016/j.indcrop.2021.113715

Shasmita B S, Mishra P, Samal M, Mohapatra D, Monalisa K & Naik S K (2023). Recent advances in tissue culture and secondary metabolite production in *Hypericum perforatum* L. *Plant Cell, Tissue and Organ Culture* 154: 13–28 https://doi.org/10.1007/s11240-023-02525-3

Simic S G, Tusevski O, Maury S, Delaunay A, Joseph C & Hagège D (2014). Effects of polysaccharide elicitors on secondary metabolite production and antioxidant response in *Hypericum perforatum* L. shoot cultures. *The Scientific World Journal* ID 609649 https://doi.org/10.1155/2014/609649

Smelcerovic A, Verma V, Spiteller M, Ahmad M S, Puri S C & Qazi G N (2006). Phytochemical analysis and genetic characterization of six *Hypericum* species from Serbia. *Phytochemistry* 67(2): 171-177 https://doi.org/10.1016/j.phytochem

Snedecor G W & Cochran W G (1967). Statistical methods. 6th Edition, Ames, Iowa, the Iowa state University

Tanaka N & Takaishi Y (2006). Xanthones from *Hypericum* chinense. *Phytochemistry* 67(19): 2146-2151 https://doi.org/10.1016/j.phytochem

Tavakoli F, Rafieiolhossaini M, Ravash R & Ebrahimi M (2020). UV-B radiation and low temperature promoted hypericin biosynthesis in adventitious root culture of *Hypericum perforatum*. *Plant Signaling & Behavior* 15(7): 15:1559–2324 https://doi.org/ 10.1080/15592324.2020.1764184

Tekoah Y, Shulman A, Kizhner T, Ruderfer I, Fux L, Nataf Y, Bartfeld D, Ariel T, Gingis-Velitski S, Hanania U & Shaaltiel Y (2015). Large-scale production of pharmaceutical proteins in plant cell culture-the Protalix experience. *Plant Biotechnology Journal* 13(8):1199-1208 https://doi.org/10.1111/pbi.12428

Uzbay T I (2008). *Hypericum perforatum* and substance dependence: a review. *Phytotherapy Research* 22(5): 578-582 https://doi.org/10.1002/ptr.2420

Walker T S, Bais H P & Vivanco J M (2002) Jasmonic acid-induced hypericin production in cell suspension cultures of *Hypericum perforatum* L. (St. John's wort). *Phytochemistry* 60(30): 289-293 https://doi.org/10.1016/S0031-9422(02)00074-2

Wang J, Qian J, Yao L & Lu Y (2015). Enhanced production of flavonoids by methyl jasmonate elicitation in cell suspension culture of *Hypericum perforatum*. *Bioresources and Bioprocessing* 2(1): 1-9 https://doi.org/10.1186/s40643-014-0033-5

Wójcik A & Podstolski, A (2007). Leaf explant response in in vitro culture of St. John's wort (*Hypericum perforatum* L.). *Acta Physiologiae Plantarum* 29: 151–156 https://doi.org/10.1007/s11738-006-0019-9

Yue W, Ming QL, Lin B, Rahman K, Zheng CJ, Han T & Qin L P (2016). Medicinal plant cell suspension cultures: pharmaceutical applications and high-yielding strategies for the desired secondary metabolites. *Critical Reviews in Biotechnology* 36(2): 215-232 https://doi.org/ 10.3109/07388551.2014.923986

Zagorskaya A A & Deineko E V (2017). Suspension-cultured plant cells as a platform for obtaining recombinant proteins. *Russian Journal of Plant Physiology* 64: 795–807 https://doi.org/10.1134/S102144371705017X

Zheng M Y & Konzak C F, (1999). Effect of 2,4-dichlorophenoxyacetic acid on callus induction and plant regeneration in anther culture of wheat (*Triticum aestivum* L.). Plant Cell Reports 19(1):69-73 https://doi.org/ 10.1007/s002990050712

Zubrická D, Mišianiková A, Henzelyová J, Valletta A, De Angelis G, D'Auria FD, Simonetti G, Pasqua G & Čellárová E (2015). Xanthones from roots, hairy roots and cell suspension cultures of selected *Hypericum* species and their antifungal activity against Candida albicans. *Plant Cell Reports* 34(11): 1953-1962 https://doi.org/ 10.1007/s00299-015-1842-5

Journal of Agricultural Sciences
(Tarim Bilimleri Dergisi)

J Agr Sci-Tarim Bili
e-ISSN: 2148-9297
jas.ankara.edu.tr

JAS

The Effect of Male Broiler Parent Live Weight Differences during the Growing Period on Progeny Broiler Performance

Ahmet Uçar[a*], Okan Elibol[a], Mesut Türkoğlu[a]

[a]*Ankara University, Faculty of Agriculture, Department of Animal Science, 06110, Ankara, TÜRKIYE*

ARTICLE INFO
Research Article
Corresponding Author: Ahmet Uçar, E-mail: ucara@ankara.edu.tr
Received: 17 June 2024 / Revised: 18 September 2024 / Accepted: 04 November 2024 / Online: 25 March 2025

Cite this article
Uçar A, Elibol O, Türkoğlu M (2025). The Effect of Male Broiler Parent Live Weight Differences during the Growing Period on Progeny Broiler Performance. *Journal of Agricultural Sciences (Tarim Bilimleri Dergisi),* 31(2):332-343. DOI: 10.15832/ankutbd.1502100

ABSTRACT
With the increase in demand for broilers, breeds that provide rapid weight gain, efficient use of feed and high carcass yield have been selected for chicken meat production. The trial was carried out to determine the effect of broiler male parent's body weights of growing period (six and eighteen weeks) on progeny broiler performance traits. Cockerels in the study were allocated into 5 groups as Light Standard (LS), Light Light (LL), Standard Standard (SS), Heavy Heavy (HH) and Heavy Standard (HS) according to the live weight at the 6th and 18th weeks. When these cocks were young (24 weeks of age), prime (35 weeks of age) and old (48 weeks of age), the broiler performance of the offspring obtained from them by artificial insemination was evaluated. In terms of sire body weights during the study, the HH group had the highest live weight. In terms of the 35th d body weights of broilers, HH group reached the highest average in all periods, while the LS group had the lowest average and LL, SS and HS were close to each other. The average European Production Efficiency Index (EPEI) values of LL, LS, SS, HS and HH groups were found to be 434, 423, 429, 422 and 460, in three broiler trials average, respectively. The heritability for the body weight trait was found as for the 7th d= 0.18, 14th d= 0.21, 21st d= 0.31, 28th d= 0.30 and 35th d= 0.37. In conclusion, it was determined that the highest broiler performance was observed in the offspring of HH cock (heavy at the 6th and 18th week). In addition, it was determined that changes in live weight of sires after the 6th week (efforts to bring them to standard weight) would negatively affect the broiler performance of the offspring. Considering the EPEI, in which feed conversion rate and liveability are also included in the formula in addition to live weight it is suggested that HH group sires should be preferred for heavier broiler and more economical meat production.

Keywords: Parent stock, Body weight, Heritability, Broiler performance, Rearing period

1. Introduction

Chicken was the first animal species for which Mendelian inheritance was proven nearly a century ago, and also the first animal whose genome was sequenced in 2004 among farm animals (International Chicken Genome Sequencing Consortium 2004). Industrial production has made it easy to replace dual-purpose chicken with stocks grown specifically for meat or eggs. With the increase in demand for broilers, breeds that provide rapid weight gain, efficient use of feed and high carcass yield have been selected for chicken meat production (Eitan & Soller 2002; Thiruvenkadan et al. 2011). Poultry genetics has entered a new era with the contribution of a century of research on poultry genetics, chicken genome sequencing and the application of molecular genetic information in commercial breeding programs, especially on body weight gain (Mebratie et al. 2019).

Live weight gain has been the first and most significant trait in the breeding of meat-type chickens, and it will continue to be significant (Emmerson 1997; Nyalala et al. 2021). Improvement in body weight has consistently been the primary selection trait for decades because of its ease of selection, high heritability, and major impact on the overall cost of meat production (Arthur & Albers 2003). After evaluating the quantity of meat obtained from broilers at slaughter age for many years, it was concluded that meat quantity obtained per breeder should also be taken into consideration in genetic selection programs (Pollock 1999). Unlike layer breeders, uniformity and live weight control are more important in rearing broiler breeders (Sweeney et al. 2022).

A female broiler parent can produce approximately 150-160 chicks in a production period lasting 40 weeks. Broilers reach 2.3-2.8 kg slaughter weight and 1.5-1.7 feed conversion ratio with high viability during the 5th-6th week of fattening period (Sarıca et al. 2018; Türkoğlu & Sarıca 2018a). Considering the reproductive performance of the parents and the performance of their offspring, it is clear that more than 300 kg meat per female parent and about 3 tons of meat per male parent can be produced, indicating why the financial values of the broiler parents are higher (Uçar et al. 2017). Each rooster is of great importance in order to get the greatest benefit from the broiler chicken lines with superior genetic structure created by primary breeding companies through very laborious and challenging processes (Emmerson 2003).

In natural mating flocks, which are usually housed in mixed male-females, the structure of production is planned according to the female. Under these conditions, there is less interest in male reproductive performance. However, the fact that economic value of males cannot be ignored shows the necessity of increasing their reproductive capacity (Sexton 1983). Efforts are mainly made to keep male parent weights at standard level in order to optimize reproductive performance (Burke & Mauldin 1985; Ingram et al. 1987; Hocking & Duff 1989; Beer 2009). While breeding companies place great emphasis on selecting the heaviest males in their sire line populations to produce heavier broilers, parent-stock firms rarely use this information, considering this selection to be complete. Although selection has been made during the breeding phase, there is still enough genetic variation in the parent stocks obtained from the selected birds to allow selection for heavier males (Leeson & Summers 2010). It has been reported that there is a low but positive correlation between the body weights of male parents at 3 and 20 weeks of age, and a significant correlation at the level of 0.42 between 5 and 20 weeks of body weights. Likewise, it is stated that there is a strong positive relationship between parental weights and the body weights of their offspring, and that the offspring of heavy males are heavier than other males (Van Wambeke et al. 1979; Van Wambeke et al. 1981). When we selected 20% and 50% of the parent males starting from the heaviest at 3-4 weeks of age, an increase of approximately 2% and 1% in the average live weight of broilers is expected, respectively. It is reported that if we choose 50% of the parent males, about 4 times the extra expense that will be made can be returned from the slaughter of broilers (Leeson & Summers 2010).

Breeding companies provide guidance to companies that raise parent stock with care and management guides. It is known that the main task is to reach a standard weight suitable for genotypes in field conditions. However, our knowledge about the extent to which this is achieved is limited. Furthermore, there is no information about the performance of broilers obtained from sires that have been brought to standard weight or not. Our study was designed to shed light on this uncertainty, at least partially. This trial was carried out to determine the effect of broiler male parent's body weights of growing period (six and eighteen weeks) on progeny broiler performance traits.

2. Material and Methods

All procedures were carried out in accordance with the rules declared by the Ankara University Experimental Animals Ethics Committee (2020-1547).

2.1. Selection and rearing of male parents

Male parents, which are the main animal material used in the experiment, were provided by a broiler parent breeding farm of Erpiliç (Türkiye) company. At the five week of age, when the Ross 308 male chicks were classified according to their weight, the birds were assigned into 3 separate pens, each with a capacity of 1200 birds, as light, standard and heavy males in the same pens. In the 6th week of the growth period, which is accepted as the beginning of the experiment, all young roosters were weighed individually and wing tags were attached to 100 birds of the same weight from each pen (300 in total). The average live weights according to the pens were determined as 850 g (light), 1150 g (standard) and 1450 g (heavy), indicating a 300 g BW difference among them. The backs of these 300 selected roosters were painted blue to distinguish them from those that were not selected. All cockerels were weighed individually on the same day of each week between weeks 6 and 18 of the rearing period. The descriptive statistics of the 6th and 18th week weight data of selected males are presented in Table 1.

Thus, the roosters were divided into five groups as a result of their live weight values at the 6th and 18th weeks: Light Light (LL), Light Standard (LS), Standard Standard (SS), Heavy Standard (HS) and Heavy Heavy (HH). A total of 25 roosters (5 from each group) were determined in these five groups, with average weights of 2230 g, 2715 g, 2740 g, 2760 g and 3260 g, respectively (Table 1).

Table 1- BW mean of the selected males from pens according to groups (g)

Week	*LL*	*LS*	*SS*	*HS*	*HH*	*SEM*[1]
6	851 ^{c}	851 ^{c}	1151 ^{b}	1453 ^{a}	1453 ^{a}	2.06
18	2230 ^{c}	2715 ^{b}	2740 ^{b}	2760 ^{b}	3260 ^{a}	18.50

[1]SEM: Standard Error of Mean; a,b,c: Differences between means indicated with different letters in the same row are significant (P<0.05)

During the rearing period, a total of 17.0, 15.5 and 15.5 kg of feed per male was provided in light, standard and heavy pen, respectively. A total of 25 males were randomly placed in individual male cages in the Poultry House of Ankara University. Each cage was arranged to have 1 bowl feeder and 1 nipple drinker. The size of each cage compartment was 47x50x55 cm.

2.2. Selection and rearing of female parents

220 female breeders at the age of 45 weeks were selected from the production farm belonging to the company from which the roosters were selected. These were determined to be egg laying by physical checks and were weighed and those within the range of 3800-3900 g were selected. Afterwards, these females were transferred to Ankara University. The hens were weighed again a week after their arrival at the university, and the average weight of the females placed to each group was determined to be 3919

g. For each female, 1 feeder and 1 nipple drinker were arranged per cage, and there was a specific code based on the rooster on the front of their cages. Individual cages measured 55x45x40.

2.3. Egg production period

Males and females were randomly distributed in cages on floors and rows, thus ensuring that males and females belonging to each group were present in every part of the house. A total of 25 cocks and 220 hens were placed in individual cages and the production period continued. At the bird level, the house temperature was tried to be kept between 24-26 ºC. Plastic wire mesh (chick carpet) was laid on the cage floor wire to minimize foot-leg, breast and eggshell problems due to the heavy weight of the broiler parents. The diagram of the males and females assigned to them at the beginning of egg-laying period, determined as 5 cocks in each group and 44 hens per cock group (Figure 1).

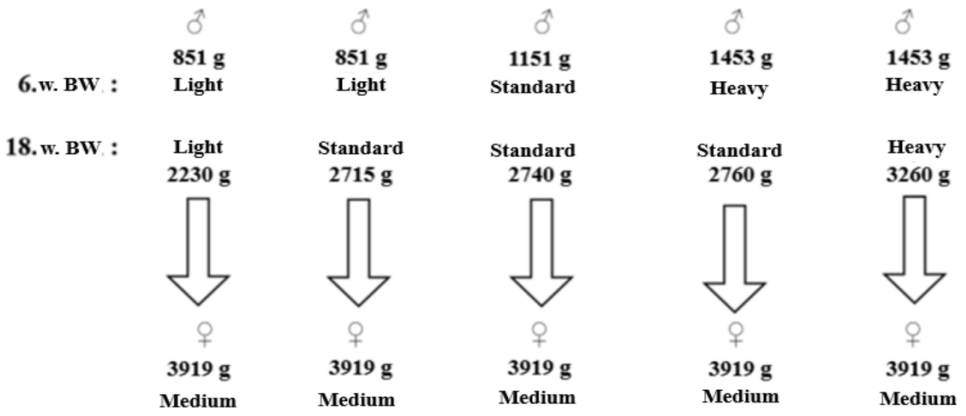

Figure 1- Group of cockerels and scheme of given hens

A total of 3 broiler studies were conducted according to the age groups of the sires (young, prime and old). In the first broiler experiment, chicks obtained from 24-week-old males and 47-week-old females were used. In the second and last broiler experiments, 35 and 48-week-old males with 58 and 71-week-old females were used, respectively.

2.4. Lighting and feeding program

The 8-hour daily lighting period applied to the roosters during the growing period was continued after they were transferred to the house. In males, first light stimulation was increased to 10 hours per week on 21st and that week it was increased to 12 hours. When the cocks were 22 weeks old, the hens were brought to the house and the lighting was fixed at 14 hours/daily this week. A homogeneous lighting of 60-80 lux was provided at bird level.

Feedig of the parents was carried out once a day between 8-9 am (once a week after insemination around 7 pm). Feed prepared in granule form, obtained from a commercial company, with a content of 2800 kcal/kg ME, 14% CP and 3.2% Ca, was provided throughout the entire production period. Considering that the birds were reared in cages, less feed quantity was calculated compared to when reared them on the floor. This calculation was made by following the egg production and BW gains.

2.5. Preparation of the males and artificial insemination

The males were accustomed to the massage method for ejaculate within 3 weeks of their arrival at the Poultry House. In order to obtain clean semen, feed was not provided on the morning of the insemination day and cloaca circumference of males were shaved. Artificial insemination was carried out once a week between 17:30-19:00 pm. The semen obtained from 5 cocks in each group was mixed undiluted and calculated according to the number of hens per group.

2.6. Storage and hatching of eggs

Eggs were collected 4 times a day (at 9, 12 a.m. and 3, 6 p.m.). After the hen and cock group code were permanently noted on the eggs, they were kept in two storage cabinets (Çimuka, Turkey) with a total capacity of 1400 eggs. These cabinets were adjusted to 18 ºC temperature and 70% relative humidity (RH), and eggs were stored for a maximum 10 d. The incubation was carried out in 2 fully automatic Çimuka (T960C) combined type incubators, each of which can hold 882 eggs.

During the incubation, the machine temperature value was arranged according to the shell temperature. For this purpose, the shell temperatures of 10 eggs from different layers were measured at the same time every day with a thermometer (Braun, ThermoScan 5), and the machine temperature set value was adjusted so that the average shell temperature was 100.0 ºF (37.8 ºC). The eggs were

arranged in a mixed order according to the groups in order to eliminate the differences that may occur between the floors, especially the temperature, in the storage and development machines. In the hatch machine, each group was placed in their own baskets separately. During the incubation, the humidity was set at 50-55% RH in the machines. Turning was performed once an hour at a 45 º angle during the 18 d setter machine. On the 18th d of incubation, the eggs that were found to be infertile or the embryos were dead by candling were separated and the eggs with continued development were transferred to the hatching baskets. A total of 3 incubations were carried out for broiler trials. Approximately 1300, 1450 and 1100 eggs were used for each of the 3 incubations.

2.7. Determination of broiler performance

In order to minimize the effect of incubation time in broiler experiments, chicks hatched between 490-500 hours of incubation period were used. After the gender of chicks were determined, they were weighed and raised separately according to the sire groups. The weighed chicks were then reared in the Broiler Research House at the university, with equal numbers of male and female chicks per pen. The house had a total area of 120 m^2 (10x12 m), and the required number of 1 m^2 pens were prepared according to the number of groups and replications in the trials (Table 2).

Table 2- Number of pens and chicks used in broiler experiments

Experiments	*Pens per group*	*Total Number of Pens*	*Broilers per Pen*	*Broilers per Group*	*Total Number of Broilers*
1	7	35	14	98	490
2	9	45	14	126	630
3	5	25	16	80	400

During the broiler rearing period, 55 lux light intensity illumination was provided in the chicken coop 24 hours a day. Starter feed (3,000 kcal ME/kg and 23.5% CP) was provided between days 0-10 and grower feed (3,200 kcal ME/kg and 22.0% CP) was offered between days 11-28. Finisher feed (3,300 kcal ME/kg and 20.0% CP) was provided between 29 and 35 days. Feeds were formulated to meet National Research Council (1994) recommendations. Feed and water were ad libitum offered to the chickens during all rearing periods. Water was provided to broilers in each pen via a nipple drinker line (3 nipples per pen). For the first 4 days, enough graph paper was laid to cover 2/3 of the pen, and a chick feeder was used until weight measurement in the first week. After the first week of the experiment, a hanging feeder (15 kg capacity) was used in each pen. The average feed intake (FI) per pen was calculated by adding weighed feed in front of each pen, and by weighing the remaining feed in the feeders weekly (with a scale with a sensitivity of 2 g). Feed conversion ratio (FCR) was also calculated from the sum of feed intake per pen and live weight per pen. The chicks were weighed in a scale with an accuracy of 0.01 g on the first day they were placed in the pen, and the average body weight (BW) was determined by weighing them individually with an accuracy of 2 g on the 7th, 14th, 21st, 28th and 35th days.

2.8. Statistical analyses

In the trials, feed intake per broiler (FI), feed conversion ratio (FCR; dead broiler weights were also taken into account when calculating FCR), mortality rate (MR), liveability (LV) and European Production Efficiency Index (EPEI) were calculated. EPEI group averages were also calculated, allowing broiler performance criteria such as BW, FCR and LV to be evaluated together.

The data were stored and organized in the MS Excel program, and randomness was taken into consideration in the design of the experiments. Variation between paternal half-siblings was used to calculate heritability levels. While the SAS (2015) package program was used to calculate heritability levels, the relevant procedures of the SPSS (2011) 20.0 package program were used for all other statistical analyses. Differences between groups were analyzed by DUNCAN multiple comparison test, and statements of statistical significance were based on $P \leq 0.05$ unless otherwise stated.

According to the body weight averages of each of the 5 males in the sire groups (5 males in each group were considered as a single male because they were inseminated by mixing the semen of the males), the heritability degree was calculated from the weights of 568 broilers (276 females + 292 males). The model was arranged according to gender and weight of the chicks at the time of placement in the house. The effect of the storage day of the eggs and the pen in which the animals were reared were not included in the model because they were not significant.

Heritability estimates were obtained for each trait separately using within group correlation (dams nested within sires) by *Proc Mixed* procedure with REML algorithm in SAS (2015). Model included Sire, Dam (Sire) and residual as Random effects. After obtaining variance component estimates, heritability was estimated as:

$$\boldsymbol{h^2 = 4\frac{\sigma^2_{sire}}{\sigma^2_{Total}}}$$

3. Results

3.1. Body weight

Average BW of 0, 7, 14, 21, 28 and 35 d of broiler experiments are shown in Table 3.

Table 3- Broiler BW Averages according to Sire BW Groups in 3 Experiments

Experiments / Sire Ages	*Broiler Rearing Days*					
	0	*7*	*14*	*21*	*28*	*35*
Experiment 1 / Young	---------- g ----------					
Light Light (LL)	46.0^{ab}	196.6^{b}	530.8^{cd}	1091.4^{cd}	1799.2^{b}	2456.7^{b}
Light Standard (LS)	45.6^{b}	200.4^{ab}	523.1^{d}	1070.4^{d}	1744.7^{c}	2396.7^{c}
Standard Standard (SS)	44.8^{c}	200.8^{ab}	538.0^{bc}	1105.1^{bc}	1817.2^{b}	2489.8^{b}
Heavy Standard (HS)	45.8^{b}	203.8^{a}	552.3^{a}	1122.8^{ab}	1870.3^{a}	2562.2^{a}
Heavy Heavy (HH)	46.5^{a}	197.8^{b}	547.5^{ab}	1131.8^{a}	1875.6^{a}	2578.1^{a}
SEM	*0.23*	*1.76*	*4.11*	*8.24*	*11.23*	*13.75*
Experiment 2 / Prime	---------- g ----------					
Light Light (LL)	46.9^{a}	155.9^{c}	433.4^{b}	923.9^{b}	1566.4^{bc}	2126.4^{b}
Light Standard (LS)	45.8^{b}	158.0^{c}	418.3^{c}	867.9^{c}	1502.7^{d}	2029.0^{c}
Standard Standard (SS)	45.3^{b}	163.1^{b}	441.9^{b}	931.9^{b}	1576.2^{b}	2127.7^{b}
Heavy Standard (HS)	45.6^{b}	163.4^{b}	442.2^{b}	927.9^{b}	1563.8^{c}	2125.3^{b}
Heavy Heavy (HH)	47.0^{a}	168.7^{a}	453.6^{a}	966.5^{a}	1644.4^{a}	2256.3^{a}
SEM	*0.32*	*1.43*	*3.53*	*7.56*	*11.21*	*15.73*
Experiment 3 / Old	---------- g ----------					
Light Light (LL)	45.8^{c}	159.6	432.1^{b}	946.3^{b}	1653.2^{a}	2395.3^{b}
Light Standard (LS)	47.5^{ab}	161.3	437.0^{b}	949.0^{b}	1622.4^{ab}	2431.5^{b}
Standard Standard (SS)	48.4^{a}	163.3	430.4^{b}	944.5^{b}	1641.4^{a}	2409.2^{b}
Heavy Standard (HS)	46.5^{bc}	161.4	440.7^{b}	950.0^{b}	1611.4^{b}	2386.0^{b}
Heavy Heavy (HH)	48.1^{a}	167.2	462.7^{a}	1012.5^{a}	1703.5^{a}	2523.4^{a}
SEM	*0.39*	*3.19*	*5.45*	*10.45*	*32.59*	*23.06*

a,b: According to Duncan's test, there is a difference between means with different letters in the same column (P<0.05)

Experiment 1: Although the lightest group was HH in the first week, the heaviest chick weight was also measured in this group at the end (P<0.05). In detail, in the following week, HH group chicks accelerated their live weight gain and reached the highest weight in the 3rd week. When an average of live weight for the last two weeks is considered, it is observed that the LS group had the lowest, the SS and LL groups had the middle, and the HH and HS groups had the highest live weight (P<0.05).

Experiment 2: HH and LL group chicks had a higher weight than the other groups on the first day. In the first week, the HH group was followed by the SS and HS groups, while the LL and LS groups remained at the lowest average. After the seventh day, the LL group reached a similar weight with the SS and HS groups in terms of live weight gain. The highest live weight average was found in the HH group, while the lowest average was determined in the LS group (P<0.05). Similar to the first experiment, the LS group had the lowest mean, while the LL, SS and HS groups had a medium level and the HH group had the highest mean. In general, the reason why the live weight was lower in this trial compared to the 1st and 3rd trials was that it was carried out in the hot summer months. Because the cooling systems in the house in the university research unit did not work effectively during this extremely hot period.

Experiment 3: In terms of live weight on the first day, HH and SS groups reached the highest average, followed by LS and HS, while the LL group had the lowest live weight average (P<0.05). While there was no difference between the groups in the first week (P>0.05), it was determined that the HH group was 90 g heavier than the closest group and the other groups had similar averages (P<0.05).

3.2. Feed conversion ratio

The averages of FCR between 0-7, 0-14, 0-21, 0-28 and 0-35 d in the broiler studies are presented in Table 4.

Table 4- Broiler FCR Averages according to Sire BW Groups in 3 Experiments

Experiments / Sire Ages	*Broiler Rearing Days*				
	0 - 7	*0 - 14*	*0 - 21*	*0 - 28*	*0 - 35*
Experiment 1 / Young	---------- g / g ----------				
Light Light (LL)	1.018	1.165^{ab}	1.241^{b}	1.327^{b}	1.459^{ab}
Light Standard (LS)	1.006	1.160^{b}	1.237^{b}	1.353^{ab}	1.472^{ab}
Standard Standard (SS)	1.044	1.184^{a}	1.266^{a}	1.357^{a}	1.454^{ab}
Heavy Standard (HS)	1.045	1.173^{ab}	1.259^{a}	1.360^{a}	1.486^{a}
Heavy Heavy (HH)	1.004	1.153^{b}	1.243^{b}	1.330^{b}	1.438^{b}
SEM	*0.014*	*0.007*	*0.005*	*0.009*	*0.013*
Experiment 2 / Prime	---------- g / g ----------				
Light Light (LL)	1.213	1.269^{a}	1.337	1.390	1.563^{bc}
Light Standard (LS)	1.199	1.233^{c}	1.333	1.400	1.572^{bc}
Standard Standard (SS)	1.159	1.253^{abc}	1.338	1.410	1.579^{ab}
Heavy Standard (HS)	1.204	1.264^{ab}	1.325	1.414	1.611^{a}
Heavy Heavy (HH)	1.194	1.237^{bc}	1.314	1.383	1.540^{c}
SEM	*0.019*	*0.009*	*0.009*	*0.009*	*0.012*
Experiment 3 / Old	---------- g / g ----------				
Light Light (LL)	1.180	1.319	1.358	1.417	1.510
Light Standard (LS)	1.119	1.270	1.324	1.403	1.486
Standard Standard (SS)	1.176	1.325	1.363	1.431	1.500
Heavy Standard (HS)	1.205	1.320	1.360	1.449	1.513
Heavy Heavy (HH)	1.120	1.329	1.345	1.425	1.510
SEM	*0.031*	*0.029*	*0.024*	*0.012*	*0.016*

a, b: According to Duncan's test, there is a difference between means with different letters in the same column (P<0.05)

Experiment 1: While there was no significant difference in the first week, a difference began to emerge between the groups after the 2nd week, and it was determined that the SS group, which had low values until the last week, showed improvement in the last week, while the HS group had the worst average (P<0.05).

Experiment 2: While a difference was observed among groups in the second week of the experiment, there was no significant difference among them in the 1st, 3rd and 4th week. While the HS group had the worst feed conversion ratio in the last week, the HH group reached the best value (P<0.05).

Experiment 3: Differences among groups were not significant in any week of the trial (P>0.05).

3.3. Mortality

The mean mortality rates between d 0-7, 0-14, 0-21, 0-28 and 0-35 in the broiler studies are provided in Table 5.

Experiment 1: SS, LS and HS groups had a higher mean than LL and HH groups. The increase in mortality rate in the broiler chicken groups whose sires later reached the standard weight was higher than in the SS group whose sires always reached the standard weight (P<0.05).

Experiment 2: Mortality rate at week 2 in the SS group was significantly different compared to the other groups (P<0.05). In other weeks, there were only numerical differences.

Experiment 3: Although the mortality rates in the HS group were significantly higher (P<0.05) than the other groups in the 2nd, 3rd and 4th weeks of the trial, this difference was not significant in the whole period (P>0.05).

General Evaluation

In terms of sire body weights (Table 6), while the HS group approached the HH group at the age of 48 weeks, broilers belonging to the HH group had the heaviest live weight in all periods (P<0.05).

Table 5- Broiler Mortality Rate Means according to Sire BW Groups in 3 Experiments

Experiments / Sire Ages	*Broiler Rearing Days*				
	0 - 7	*0 - 14*	*0 - 21*	*0 - 28*	*0 - 35*
Experiment 1 / Young	---------- % ----------				
Light Light (LL)	0.00	0.00	0.00[b]	0.00[b]	1.02[b]
Light Standard (LS)	1.02	1.02	1.02[b]	2.04[b]	5.10[a]
Standard Standard (SS)	0.00	1.02	1.02[b]	2.04[b]	4.08[ab]
Heavy Standard (HS)	1.02	2.04	3.06[a]	5.10[a]	6.12[a]
Heavy Heavy (HH)	0.00	0.00	0.00[b]	0.00[b]	0.00[b]
SEM	*0.47*	*0.64*	*0.67*	*0.94*	*1.65*
Experiment 2 / Prime	---------- % ----------				
Light Light (LL)	2.38	2.38[ab]	2.38	2.38	2.38
Light Standard (LS)	0.00	0.00[b]	1.58	1.58	1.58
Standard Standard (SS)	3.17	4.76[a]	4.76	4.76	4.76
Heavy Standard (HS)	0.79	1.58[b]	2.38	2.38	3.17
Heavy Heavy (HH)	0.00	1.58[b]	1.58	2.38	2.38
SEM	*1.13*	*1.27*	*1.33*	*1.35*	*1.35*
Experiment 3 / Old	---------- % ----------				
Light Light (LL)	0.00	0.00[b]	0.00[b]	0.00[b]	1.25
Light Standard (LS)	0.00	0.00[b]	0.00[b]	0.00[b]	1.25
Standard Standard (SS)	0.00	0.00[b]	0.00[b]	0.00[b]	1.25
Heavy Standard (HS)	2.50	3.75[a]	5.00[a]	5.00[a]	5.00
Heavy Heavy (HH)	1.25	1.25[b]	1.25[b]	1.25[b]	3.75
SEM	*0.94*	*0.96*	*0.98*	*0.98*	*1.35*

a, b: According to Duncan's test, there is a difference between means with different letters in the same column (P<0.05)

Table 6- Sire Body Weight Averages (selection and insemination weeks for broiler studies)

Sires BW Groups	*Periods and Weeks*				
	Rearing		*Production*		
	Beginning	*Finish*	*Young*	*Prime*	*Old*
	6	*18*	*24*	*35*	*48*
	---------- g ----------				
Light Light (LL)	851[c]	2230[c]	3321[c]	4781[b]	5268[b]
Light Standard (LS)	851[c]	2715[b]	3742[b]	4782[b]	5566[b]
Standard Standard (SS)	1151[b]	2740[b]	3733[b]	4765[b]	5460[b]
Heavy Standard (HS)	1453[a]	2760[b]	3698[b]	4789[b]	5675[b]
Heavy Heavy (HH)	1453[a]	3260[a]	4134[a]	5253[a]	6174[a]
SEM	*2.06*	*18.53*	*24.19*	*63.69*	*104.22*

a,b: According to Duncan's test, there is a difference between means with different letters in the same column (P<0.05)

While the LL, SS and HS groups had similar averages in all periods in terms of the 35th day live weight of the broilers, the lowest average was weighed in the LS group and the highest average was weighed in the HH group (Table 7). In the whole experiment's average, 35th d BW of the LL, LS, SS, HS and HH groups were 2320, 2250, 2320, 2319 and 2431 g, respectively (Table 7).

Table 7- Average 35th d BW of Broilers according to Sire BW Groups 3 Experiments

BW Groups	*Sire Ages (Week) / Experiments*			
	Young (24)	*Prime (35)*	*Old (48)*	*Average*
	1	*2*	*3*	
	---------- g ----------			
Light Light (LL)	2465[b]	2126[b]	2395[b]	2320[b]
Light Standard (LS)	2397[c]	2029[c]	2432[b]	2250[c]
Standard Standard (SS)	2492[b]	2128[b]	2409[b]	2320[b]
Heavy Standard (HS)	2562[a]	2125[b]	2386[b]	2319[b]
Heavy Heavy (HH)	2574[a]	2256[a]	2523[a]	2431[a]
SEM	*13.75*	*15.73*	*23.06*	*18.65*

a, b: According to Duncan's test, there is a difference between means with different letters in the same column (P<0.05)

In terms of the FCR, a better performance had been achieved than the current catalogue values of the breeding companies (Cobb 2018; Aviagen 2019a; Aviagen 2019b). As indicated in Table 8, the HH group has sufficient values not only for live weight but also for feed conversion ratio.

Table 8- Average 0-35th d FCR in Broilers according to Sire BW Groups 3 Experiments

BW Groups	*Sire Ages (Week) / Experiments*			
	Young (24)	*Prime (35)*	*Old (48)*	*Average*
	1	*2*	*3*	
	---------- *g/g* ----------			
Light Light (LL)	1.459[ab]	1.563[bc]	1.510	1.511[b]
Light Standard (LS)	1.472[ab]	1.572[bc]	1.486	1.510[b]
Standard Standard (SS)	1.454[ab]	1.579[ab]	1.500	1.511[b]
Heavy Standard (HS)	1.486[a]	1.611[a]	1.513	1.537[a]
Heavy Heavy (HH)	1.438[b]	1.540[c]	1.510	1.496[c]
SEM	*0.013*	*0.012*	*0.016*	*0.008*

a, b: According to Duncan's test, there is a difference between means with different letters in the same column (P<0.05)

In the whole experiment's average, 35th d mortality of the LL, LS, SS, HS and HH was 1.71, 3.05, 3.88, 5.30 and 2.25%, respectively (Table 9). Only the differences between the first study results were significant (P<0.05), while the differences in terms of other studies and overall mean remained numerical.

Table 9- Average 0-35th d Mortality in Broilers according to Sire BW Groups 3 Experiments

BW Groups	*Sire Ages (Week) / Experiments*			
	Young (24)	*Prime (35)*	*Old (48)*	*Average*
	1	*2*	*3*	
	---------- % ----------			
Light Light (LL)	1.02[b]	2.38	1.25	1.71
Light Standard (LS)	5.10[a]	1.58	1.25	3.05
Standard Standard (SS)	4.08[ab]	4.76	1.25	3.88
Heavy Standard (HS)	6.12[a]	3.17	5.00	5.30
Heavy Heavy (HH)	0.00[b]	2.38	3.75	2.25
SEM	*1.65*	*1.35*	*1.35*	*1.306*

a, b: According to Duncan's test, there is a difference between means with different letters in the same column (P<0.05)

In the first experiment, the LS group had the lowest and the HH group had the highest index in terms of EPEI (P<0.05). In the second experiment, while all groups except HH had similar averages, the HH group again reached the highest average (P<0.05). In the last experiment, the LS group had the greatest value, followed by the HH, LL and SS groups, and the HS group had the lowest index value (P<0.05). In the average of 3 broiler experiments, the mean EPEI values of the LL, LS, SS, HS and HH groups were found to be 434, 423, 429, 422 and 460, respectively (P<0.05). When we consider the differences in these values in the general average, it can be concluded that the HH group reached the highest EPEI, while the other groups had values close to each other (Table 10).

Table 10- Average 35th d EPEI in Broilers according to Sire BW Groups 3 Experiments

BW Groups	*Sire Ages (Week) / Experiments*			
	Young (24)	*Prime (35)*	*Old (48)*	*Average*
	1	*2*	*3*	
	---------- EPEI ----------			
Light Light (LL)	476^{ab}	382^{b}	447^{ab}	434^{b}
Light Standard (LS)	445^{d}	363^{b}	464^{a}	423^{b}
Standard Standard (SS)	470^{cd}	363^{b}	453^{ab}	429^{b}
Heavy Standard (HS)	472^{bc}	363^{b}	425^{b}	422^{b}
Heavy Heavy (HH)	513^{a}	409^{a}	449^{ab}	460^{a}
SEM	*8.93*	*6.65*	*9.12*	*4.79*

a, b: According to Duncan's test, there is a difference between means with different letters in the same column (P<0.05)

According to the calculations, the heritability for the body weight trait was found as h^2 = 0.18 for the 7th day, h^2 = 0.21 for the 14th day, h^2 = 0.31 for the 21st day, h^2 = 0.30 for the 28th day and h^2 = 0.37 for the 35th day.

4. Discussion

According to the experiments conducted, it has been reported that the share of genetics rather than environmental conditions in improving broiler performance characteristics is higher and this rate is approximately 85% (Havenstein et al. 2003a; Havenstein et al. 2003b). FCR, breast meat ratio and slaughter weight come to the fore compared to reproductive traits in terms of contributing to the profit increase rate of integrated firms (Emmerson 2003). However, the basis of the factors affecting the profit increase of companies is the broiler meat production per parent (Decuypere et al. 2010). Generally, studies have shown that the broiler performance of the offspring of heavy and light male parents varies (Van Wambeke et al. 1979; Van Wambeke et al. 1981; Leeson & Summers 2010). Our experiments differ from other trials due to the comparison of groups consisting of both heavy and light sires as a result of standard weighting during the rearing period.

In broiler experiments, HH group had the highest body weight in terms of placement time. In the first two trials, LL group approached the HH group, while in the last trial it had the lowest weight. The SS group, on the other hand, showed the opposite result of LL group. In order to eliminate the effect of hatching time (Özlü et al. 2018), chicks obtained between 490-500 h of hatch were used. There was no difference between egg weight averages of hens according to the cock groups. However, there was a difference between the groups in terms of placement time weight. As reported by Tahir et al. (2011) despite the high positive relationship between egg and chick weights, and between chick and slaughter weight, our results indicate that the first-day BW of groups, except for the HH group, were not reflected in the final weight means.

It has been reported that there is a low but significant relationship between the 3-week and 20-week age weights of male parents, and the 3-week-old weights have a positive, albeit low, relationship with the broiler performance of their offspring (Van Wambeke et al. 1979). In another study, a positive and significant correlation of 0.42 was calculated between the BW of male parents at 5 and 20 weeks of age (P<0.01). In this study, the 6th week BW performance of heavy ones and the offspring from other sires at the ages of 31, 41 and 51 weeks were 1671 and 1605 g, 1688 and 1573 g and 1727 and 1636 g, respectively, and the average of the whole period was determined as 1695 and 1604 g. In conclusion, heavy sires were reported to have approximately 90 g heavier progenies (Van Wambeke et al. 1981). When we consider the differences with the HH group and others, the results of the latter study are similar to our results. As a result of selection of male individuals in terms of body weight at the pure line level, variation in the performance characteristics of their offspring continues (Sarica et al. 2021). When selection is made at the parental level, serious variations are observed in the performance of the offspring, as in our study.

In our study, the levels of muscle and fat ratios in body of males were not measured. The extra feed given to the light pen after grading may have increased the fat ratio of LS group males after the 6th week of rearing period (Lin 1981; Leenstra 1986). It has been reported that there is a high positive relationship between abdominal fat and carcass fat and a negative effect on FCR. It is also reported that the heritability of abdominal fat is as high as 0.40-0.82 (Griffiths et al. 1978; Becker et al. 1981; Cahaner

& Nitsan 1985; Leenstra & Pit 1988; Gaya et al. 2006). It is considered that this factor may be effective in the low performance of the offspring of the LS group.

Van Emous (2015) showed that the growth period BW values influence broiler performance, as indicated in our study, while body composition at the end of the rearing period has a direct effect on hatchability results and broiler performance. Control of BW of male parents is very important in broiler strains (Türkoğlu & Sarıca 2018a). However, it has been demonstrated by our results that these practices should be questioned and different breeding strategies should be applied. It is thought that BW is very important not only during rearing period but also during the production period. According to the results of the present study, it was determined that bringing the standard weight in both heavy and light pens negatively affected broiler performance. In order to obtain positive results, standard weighting process can be slower or instead of bringing it to standard weight, it can be ensured that each pen is on its own average weight. Looking at the 1, 2, 3 and general averages in terms of live weight in the last week, it is observed that the HH group is ahead of the average of the other four groups by 88, 129, 92 g and 111 g, respectively. According to Leeson & Summers (2010), selecting the heaviest 20% or the heaviest 50% of the sires at the age of 3-4 weeks will increase the broiler performance by approximately 2 and 1%, respectively. If we take the 2320 g value after the HH group as a basis in the general averages, the difference of 111 g in the BB group reaches a higher value by about 5%.

Assuming that the breeding companies have completed selection, the integrated firms select the cockerels to be sent from rearing houses to the production houses phenotypically according to their general appearance. However, as stated similarly to our findings, the individual genetic variations of the prospective parent cocks are still at a level to allow selection (Leeson & Summers 2010). If we take into account 15% of female parent chicks given by the breeding companies to the integrated companies, half of them will be used during the production period. Therefore, it may be possible to select the heavier 50% of male parents. In broiler parents, hatching eggs are generally obtained from natural mating flocks (Pollock 1999). However, artificial insemination may be a more effective application as the BW of the genotypes increase further in the following years as a result of reduced success of cocks in natural mating (as in the commercial turkey parents). In addition, artificial insemination provides effective use of heavier sires (Brillard 2001). Considering body condition and composition, and male body weight (Leeson & Summers 2010; Van Emous 2015), rearing and feeding practices should be preferred to ensure success in natural mating. Since artificial insemination was used in our study, the results of this study obtained through natural mating are also important, since in a study comparing broiler chickens obtained by natural mating and artificial insemination, those with artificial insemination showed worse results in terms of both performance and immunity-related characteristics (Shaheen et al. 2020).

Body weight of the broiler parents at maturity affects carcass composition and carcass protein ratio (Salas et al. 2019). Not only body weight differences but also broiler parents' nutritional differences during the rearing period can affect the broiler performance of their offspring (Araújo et al. 2019; Moraes et al. 2019).

Since artificial insemination in roosters could not be followed individually, it was not possible to calculate heritability separately for groups. In our study, the calculated heritability of body weight between 1 and 5 weeks of age was 0.18-0.37, similar to some studies reported in the literature (Leenstra & Pit 1988; Koerhuis & Thompson 1997), but it seems to be lower than generally reported (Leenstra & Pit 1988; Mignon-Grasteau 1999; Gaya et al. 2006; Leeson & Summers 2010; Türkoğlu & Sarıca 2018b).

While it is aimed to maintain high fertility in production by reaching the standard weight, the effect of male parent BW on broiler performance is offen overlooked. Although reproductive performance is important, it is known that the main profit of integrated companies is the characteristics related to BW as the final product. Therefore, the aim is to achieve BW gain in the most effective way. The HH group had the highest mean in regards of EPEI (EPEI is a formula in which the most important parameters in broiler production such as BW, Liveability and FCR are evaluated together).

Contrary to the belief that standard weight roosters will perform better, the HH group comes to the fore when more and economical meat production is aimed. However, in order to make clearer interpretations, there is a need for studies to reveal the economic analysis of the productivity parameters of the offspring obtained from all groups of roosters. While higher meat production could be made from HH cocks, lower body weight gain was not achieved in the LL group compared to the others, and this was achieved more effectively with less feed.

Leeson & Summers (2010) stated that the most active cocks in the flock are those with standart weights. Although higher performance was obtained from the HH group, the reproductive performance of these heavy roosters under natural mating conditions is another subject worth investigating. Social relations between cocks are also a very important factor in flocks (Ottinger 1983; Ottinger 1989). In some studies, it has been reported that the frequency of the offspring of the cocks in the flock is variable and as a matter of fact, the indiviaual genetic contribution of the cocks to broilers can vary between 7 and 77% (Jones & Mench 1991; Bilcik et al. 2005).

5. Conclusions

In conclusion, it has been determined that breeding parentstock (PS) cannot be selected only based on 6th week rooster weight. It was determined that the performance of the offspring of these roosters decreased when they reached standard weight at 18 weeks. Especially when light cocks at 6 weeks of age reached the standard weight at 18 weeks, the broiler performance of their offspring was at its lowest level. In summary, it was determined that the offspring of roosters with high live weights at both 6 and 18 weeks of age showed the best broiler performance. In other words, it was determined that changes in body weight after the 6th week did not have a positive effect. Considering the EPEI formula, which includes feed conversion ratio and livability as well as live weight, HH group roosters should be preferred for heavier and more economical broiler production.

Acknowledgments

We would like to thank Erpiliç company for their contributions. This article was summarized from the first author's PhD thesis.

References

Aviagen (2019a). Ross 308 / Ross 308 FF Broiler Performance Objectives. Aviagen.

Aviagen (2019b). Ross 708 Broiler Performance Objectives. Aviagen.

Araújo C S S, Hermes R G, Bittencourt L C, Silva C C, Araújo L F, Granghelli C A, Roque F A & Leite B G S (2019). Different dietary trace mineral sources for broiler breeders and their progenies. Poult. Sci. 98(10): 4716-4721

Arthur J A & Albers G A (2003). Industrial perspective on problems and issues associated with poultry breeding. Poultry genetics, breeding and biotechnology 1- 12. Book: CABI Publishing

Becker W A, Spencer J V, Mirosh A & Verstrate J A (1981). Abdominal and carcass fat in five broiler strains. Poult. Sci. 60:693-697

Beer M D (2009). Current approaches to feeding broiler breeders. Proc. World Poultry Science Association (WPSA), 17th European Symposium on Poultry Nutrition, Edinburgh, UK, 23-27 August, 2009

Bilcik B, Estevez I & Russek-cohen E (2005). Reproductive success of broiler breeders in natural mating systems: the effect of male-male competition, sperm quality, and morphological characteristics. Poult. Sci. 84:1453-1462

Brillard J (2001). Future strategies for broiler breeders: an international perspective. World's Poult. Sci. J. 57:243-250

Burke W & Mauldin J (1985). Reproductive characteristics of broiler breeder males from flocks with low fertility. Poult. Sci. 64 (Suppl 1), 73.

Cahaner A & Nitsan Z (1985). Evaluation of simultaneous selection for live body weight and against abdominal fat in broilers. Poult. Sci. 64:1257-1263

COBB (2018). Broiler Performance & Nutrition Supplement. Cobb Vantress Inc. Siloam Springs, AR.

Decuypere E, Bruggeman V, Everaert N, Li Y, Boonen R, De Tavernier J, Janssens S & Buys N (2010). The Broiler Breeder Paradox: ethical, genetic and physiological perspectives, and suggestions for solutions. Brit. Poult. Sci. 51:569-579. doi 10.1080/00071668.2010.519121

Eitan Y & Soller M (2002). Associated effects of sixty years of commercial selection for juvenile growth rate in broiler chickens: Endo/exophysiological, or genetic?. Proc. 7th World Congress on Genetics Applied to Livestock Production, Montpellier, France, August 19-23, 2002.

Emmerson D (1997). Commercial approaches to genetic selection for growth and feed conversion in domestic poultry. Poult. Sci., 76:1121-1125. doi 10.1093/ps/76.8.1121

Emmerson D (2003). Breeding objectives and selection strategies for broiler production. Poultry Genetics, Breeding and Biotechnology:133-136. Book: CABI Publishing

Gaya L G, Ferraz J B S, Rezende F M, Mourão G B, Mattos E C, Eler J P & Michelan F T (2006). Heritability and Genetic Correlation Estimates for Performance and Carcass and Body Composition Traits in a Male Broiler Line. Poult. Sci., 85:837-843. doi 10.1093/ps/85.5.837

Griffiths L, Leeson S & Summers J (1978). Studies on abdominal fat with four commercial strains of male broiler chicken. Poult. Sci. 57:1198-1203

Havenstein G, Ferket P & Qureshi M (2003a). Carcass composition and yield of 1957 versus 2001 broilers when fed representative 1957 and 2001 broiler diets. Poult. Sci., 82:1509-1518. doi 10.1093/ps/82.10.1509

Havenstein G, Ferket P & Qureshi M (2003b). Growth, livability, and feed conversion of 1957 versus 2001 broilers when fed representative 1957 and 2001 broiler diets. Poult. Sci. 82:1500-1508. doi 10.1093/ps/82.10.1500

Hocking P & Duff S (1989). Musculo-Skeletal lesions in adult male broiler breeder fowls and their relationships with body weight and fertility at 60 weeks of age. Brit. Poult. Sci. 30:777-784

Ingram D R, Biron T R, Wilson H R & Mather F B (1987). Lighting of End of Lay Broiler Breeders: Fluorescent Versus Incandescent. Poult. Sci., 66:215-217. doi 10.3382/ps.0660215

International Chicken Genome Sequencing Consortium (2004). Sequence and comparative analysis of the chicken genome provide unique perspectives on vertebrate evolution. Nature 432(7018): 695-716

Jones M & Mench J (1991). Behavioral correlates of male mating success in a multisire flock as determined by DNA fingerprinting. Poult. Sci. 70:1493-1498

Koerhuis A & Thompson R (1997). Models to estimate maternal effects for juvenile body weight in broiler chickens. Genetics Selection Evolution 29:225

Leenstra F (1986). Effect of age, sex, genotype and environment on fat deposition in broiler chickens—a review. *World's Poult. Sci. J.* 42:12-25

Leenstra F & Pit R (1988). Fat deposition in a broiler sire strain. 3. Heritability of and genetic correlations among body weight, abdominal fat, and feed conversion. Poult. Sci., 67:1-9

Leeson S & Summers J D (2010). Broiler breeder production. Book: Nottingham University Press.

Lin C (1981). Relationship between increased body weight and fat deposition in broilers. World's Poult. Sci. J. 37:106-110

Mebratie W, Reyer H, Wimmers K, Bovenhuis H & Jensen J (2019). Genome wide association study of body weight and feed efficiency traits in a commercial broiler chicken population, a re-visitation. Sci. Repo. 9(1): 922

Mignon-Grasteau S (1999). Genetic parameters of growth curve parameters in male and female chickens. *Brit. Poult. Sci.* 40:44-51

Moraes T G V, Pishnamazi A, Wenger I I, Renema R A & Zuidhof M J (2019). Energy and protein dilution in broiler breeder pullet diets reduced offspring body weight and yield. Poult. Sci. 98(6): 2555-2561

Nyalala I, Okinda C, Kunjie C, Korohou T, Nyalala L & Chao Q (2021). Weight and volume estimation of poultry and products based on computer vision systems: a review. Poult. Sci., 100.5: 101072.

Ottinger M A (1983). Hormonal Control of Reproductive Behavior in the Avian Male1. Poult. Sci. 62:1690-1699. doi 10.3382/ps.0621690

Ottinger M A (1989). Sexual Differentiation of Neuroendocrine Systems and Behavior1,2. Poult. Sci. 68:979-989. doi 10.3382/ps.0680979

Özlü S, Shiranjang R, Elibol O & Brake J (2018). Effect of hatching time on yolk sac percentage and broiler live performance. Braz. J. Poult. Sci. 20: 231-236

Pollock D (1999). A geneticist's perspective from within a broiler primary breeder company. Poult. Sci. 78:414-418. doi 10.1093/ps/78.3.414

Salas C, Ekmay R D, England J, Cerrate S & Coon C N (2019). Effect of body weight and energy intake on body composition analysis of broiler breeder hens. Poult. Sci. 98(2): 796-802

Sarıca M, Türkoğlu M & Yamak U S (2018). Developments in Poultry Breeding and Türkiye Poultry Breeding. Book: Poultry Science (Raising, Feeding, Diseases) (In Turkish), pp. 1-39

Sarıca M, Erensoy K, Oğuzhan E, Yeter B & Camci Ö (2021). Effects of Male Selection for Body Weight on Performance of Offsprings in Broiler Pure-Lines. Braz. J. Poult. Sci., 23.

SAS I (2015). Base SAS 9.4 procedures guide: SAS Institute.

Shaheen M S, Mehmood S, Mahmud A & Riaz A (2020). Effects of different mating strategies in broiler breeder during peak and postpeak phase on subsequent broiler performance. Poult. Sci. 99(7): 3501-3510

Sexton T J (1983). Maximizing the Utilization of the Male Breeder: A Review. Poult. Sci., 62:1700-1710. doi 10.3382/ps.0621700

SPSS I (2011). "IBM SPSS statistics for Windows, version 20.0." New York: IBM Corp 440.

Sweeney K M, Aranibar C D, Kim W K, Williams S M, Avila L P, Starkey J D & Wilson J L (2022). Impact of every-day versus skip-a-day feeding of broiler breeder pullets during rearing on body weight uniformity and reproductive performance. Poult. Sci. 101(8): 101959

Tahir M, Cervantes H, Farmer C W, Shim M Y & Pesti G M (2011). Broiler performance, hatching egg, and age relationships of progeny from standard and dwarf broiler dams. Poult. Sci., 90:1364-1370. doi 10.3382/ps.2010-01165

Thiruvenkadan A K, Prabakaran R & Panneerselvam S (2011). Broiler breeding strategies over the decades: an overview. World's Poult. Sci. J. 67(2): 309-336

Türkoğlu M & Sarıca M (2018a). Breeder Chicken Rearing. Book: Poultry Science (Raising, Feeding, Diseases) (In Turkish), pp. 344-353

Türkoğlu M & Sarıca M (2018b). Chicken Genetics and Breeding.Book: Poultry Science (Raising, Feeding, Diseases) (In Turkish), pp. 354-404

Uçar A, Özlü S & Türkoğlu M (2017). Developments in broiler performance characteristic. 8th Balkan Animal Science Conference, Balnimalcon, 6-8 September, Prizren, Kosova. 31 pp

Van Emous R (2015). Body composition and reproduction in broiler breeders: impact of feeding strategies. PhD thesis, Wageningen University and Research.

Van Wambeke F, Moermans R & De Groote G (1979). Early body-weight selection of broiler breeder males in relation to reproductive and growth performance of their offspring. Brit. Poult. Sci. 20:565-570

Van Wambeke F, Moermans R & De Groote G (1981). A comparison of the reproductive and growth performances of offspring from broiler breeder males selected for early growth rate using artificial insemination and unselected males kept on deep litter. Reproduction Nutrition Développement 21:1059-1065

Journal of Agricultural Sciences (Tarim Bilimleri Dergisi) 2025, 31 (2) : 344 – 358 DOI: 10.15832/ankutbd.1521005

Journal of Agricultural Sciences
(Tarim Bilimleri Dergisi)

J Agr Sci-Tarim Bili
e-ISSN: 2148-9297
jas.ankara.edu.tr

Regional Analysis of Organic Agriculture, Husbandry, and Beekeeping Efficiency in Türkiye

Melike Kübra Ekiz Bozdemir[a*], Selen Avci Azkeskin[a]

[a]*Department of Industrial Engineering, Kocaeli University, Kocaeli, TÜRKİYE*

ARTICLE INFO
Research Article
Corresponding Author: Melike Kübra Ekiz Bozdemir, E-mail: melike.ekiz@kocaeli.edu.tr
Received: 23 July 2024 / Revised: 10 October 2024 / Accepted: 05 November 2024 / Online: 25 March 2025

Cite this article
Bozdemir Ekiz M K, Azkeskin Avci S (2025). The Effect of Good Agricultural Practices on Yield Characteristics of Black Cumin Genotypes. *Journal of Agricultural Sciences (Tarim Bilimleri Dergisi),* 31(2):344-358. DOI: 10.15832/ankutbd.1521005

ABSTRACT
Organic production enhances soil fertility, preserves biodiversity, and reduces pollution by avoiding from chemical pesticides and genetically modified organisms. Moreover, the increasing consumer demand for organic foods has encouraged producers to prioritize soil health and sustainable agricultural practices. The objective of this study is to analyze the development of organic agriculture, husbandry, and beekeeping, which contribute to biodiversity and ecosystem preservation through pollination, in Türkiye. Additionally, the study aims to offer insights for policy makers to establish a well-balanced production network. In this study, Türkiye's provinces were classified according to The Nomenclature of Territorial Units for Statistics (NUTS)-Level 1 (12 regions) and evaluated with Data Envelopment Analysis (DEA). Organic agriculture was evaluated Super Efficiency (SE) model while organic husbandry-beekeeping was evaluated Lee and Zu model which is taken into account zero data. Moreover, to derive a final ranking of organic agriculture and organic husbandry-beekeeping, the Copeland method, based on superiority comparison and not requiring normalization, was used. This study is noteworthy as the first of its kind to comprehensively consider organic agriculture, animal husbandry, and beekeeping collectively.

Keywords: Organic agriculture, Organic husbandry, Organic beekeping, Sustainability, Data Envelopment Analysis

1. Introduction

Chemical fertilizers, pesticides, and fungicides are widely used to meet the growing global food demand, aiming to boost crop yields in agriculture. However, their excessive application leads to soil pollution and poses risks to biodiversity, potentially threatening various species. Additionally, they have detrimental effects on the health of both producers and consumers, causing chronic illnesses and, in severe cases, fatalities (Durán-Lara et al.2020). Organic agriculture emerges as a prominent alternative to conventional farming, seeking to address the adverse impacts of traditional agricultural practices on the environment and human health. Unlike conventional methods, organic agriculture avoids synthetic fertilizers, pesticides, and genetically modified organisms to enhance crop yields. Instead, it relies on biofertilizers, natural pathogens, and pest control mechanisms to maintain soil fertility, promote biodiversity, and manage pests. Consequently, organic agriculture supports biodiversity, yields healthier products, and reduces water, soil, and air pollution (Zor et al. 2023). Over the long term, it significantly contributes to enhancing the sustainability of food systems (Sapbamrer & Thammachai, 2021). In recent years, interest in organic production has surged, driven by increasing consumer demand for organic foods and producers' efforts to safeguard soil health and promote sustainable agricultural practices (Sink et al. 2017; Aghasafari et al. 2020).

The transition from conventional agriculture to organic agriculture is mirrored in traditional animal husbandry practices. In recent years, significant advancements have been made in enhancing farm animal performance and reducing production costs in husbandry. However, concerns regarding animal health, welfare, and environmentally sustainable practices have been overshadowed by heightened production demands (Sundrum, 2001). In response to this case, organic husbandry has emerged, prioritizing animal welfare, reduced number of animals per unit area, limited use of pesticides and pharmaceuticals, and environmentally sustainable production methods. Organic husbandry is grounded in principles ensuring that animals can express natural behaviours, are not subjected to undue stress, are fed organic feed, and possess enhanced resilience to infections compared to conventionally raised animals (Åkerfeldt et al.2021).

Türkiye has considerable potential in terms of animal population, yet its utilization of this potential for organic animal production remains inadequate. Regions with vast meadow and pasture areas, devoid of industrial pollution, offer great potential for organic beekeeping, as well as the husbandry of both large and small ruminants, such as sheep and cattle. However, for

various reasons, this potential has not been fully realized. For instance, animal breeders in these regions often operate as small family businesses, and organic farming and animal husbandry are subject to certification systems, with many breeders lacking sufficient knowledge and training in these areas. Additionally, the lack of consumer awareness and low purchasing power in the domestic market hinder the development of organic animal husbandry, despite significant increases in the number of organic animals, as well as milk, meat, and particularly egg production over the past decade. Moreover, the proportion of organic animal products in total animal production remains low and inadequate despite the rise in organic animal husbandry (Ak, 2017).

The potential for a country or region/regions to be self-sufficient in terms of both agricultural and animal production has become a necessity in today's world. In this context, the necessity of both ensuring economic development and minimizing logistics needs (increasing oil prices, transportation problems due to epidemics such as COVID-19, global threats, etc.) has emerged. Türkiye is a country that is diverse in terms of its climate, soil and water wealth and socio-economic characteristics due to its geographical location. For this reason, instead of considering Türkiye as a whole, the study preferred The Nomenclature of Territorial Units for Statistics (NUTS)-Level 1 (12 regions) classification based on population, geography, regional development plans, basic statistical indicators, and socio-economic development ranking.

The aim of this study is to analyse the development and current situation of organic agriculture, husbandry and beekeeping in Türkiye on a regional basis and to give ideas to policy makers in order to provide a regionally balanced production network. In addition to organic agriculture and husbandry, beekeeping, which contributes to biodiversity and the ecosystem through pollination and supports the maintenance of rural employment, has also been taken into consideration. A review of the literature reveals that this study is the first to evaluate organic agriculture, husbandry, and beekeeping collectively. The work proceeds as follows. In Chapter 2, a very detailed literature analysis is presented on studies evaluating the efficiency of organic agriculture, husbandry and beekeeping with Data Envelopment Analysis (DEA). The study also stands out in this respect. In Chapter 3, the methodology consisting of DEA, one of the most preferred methods in relative efficiency, and Copeland, which is based on superiority and offers full ranking without normalization, is presented. Finally, Chapter 4 contains Results and Analysis, and Chapter 5 contains Conclusion.

2. Literature Review

In this part of the study, we first evaluated papers on the efficiency of organic agriculture using DEA. These papers are grouped into the following categories: (i) Comparisons of institutions and organizations involved in both traditional and organic agriculture, (ii) evaluations of the efficiency of enterprises in organic agriculture, and (iii) assessments of the performance of organic agriculture in various regions and countries. Additionally, we examined papers on organic husbandry using DEA, but found that these studies are quite limited. Furthermore, no papers on organic beekeeping were found. Therefore, we also evaluated papers on DEA in traditional husbandry and beekeeping.

In the previous section, the reasons for the transition from traditional agriculture to organic agriculture, as well as the process itself, were explained. When examining the papers on organic agriculture in the literature, we identify a group of studies that compare traditional and organic agriculture, which we refer to as the first group. Table 1 includes the input and output variables, as well as the models used in papers comparing traditional and organic agriculture. Kuosmanen et al. (2021) evaluated the efficiency of organic farms from 2010 to 2017 to analyse the changes and progress of organic agriculture in Finland over the years. The study found that, although there is a significant performance difference between organic and conventional agriculture, the difference in production performance between farms has decreased over the years.

Table 1- Papers comparing traditional agriculture and organic agriculture

	DMUs	*Inputs*	*Outputs*	*Model*
Koner & Laha 2024	- organic and conventional farms	- average marketing costs	- average farm gate price	- VRS
Kuosmanen et al. 2021	- 2010-2017 years	- labor - the farm capital - the utilized agricultural area - energy	- total output of crops and crop products and livestock and livestock products	- DEA
Charyulu & Biswas 2010	- organic and conventional cotton farm - organic and conventional sugarcane farm - organic and conventional paddy farm - organic and conventional wheat farm	- per acre cost on seeds -fertilizers -pesticides -inter culture/weeding	-gross value of production per acre	- Super Efficiency
Uzundumlu et al. 2021	- organic and conventional wheat farms	- land amount - fixed costs - variable costs - fertilizer	- wheat production	- Input-Oriented Two-Stage Bootstrapped DEA
Riar et al. 2020	- organic and conventional cotton farms	- seed rate - irrigation - nutrient inputs	- cotton yield	- CCR
Poudel et al. 2015	- organic and conventional coffee farms	- farm size - labor - fertilizer - capital - coffee tree - labor cost - plant protection	- production product market value	- Constant Return to Scale (CRS) - Decreasing Return to Scale (DRS) - Increasing Return to Scale (IRS)
Basavalingaiah et al. 2022	- conventional, integrated and organic coffee-pepper farms	- labour - machinery - diesel - farmyard manure - greenleaf manure - nitrogen - phosphorus - potassium - micronutrient - herbicides - fungicides - pesticides - lime	- coffee	- DEA and Life cycle Assessment (LCA)
Zhen et al. 2023	- conventional, organic conversion and organic tea farm	- nitrogen (N) fertilizer - phosphorus (P2O5) - potassium (K2O) - labor - fuel - pesticide cost	- net income	- Super Efficiency
Artukoglu et al. 2010	- organic and conventional olive farms	- land - fertilizer costs - organic control costs for disease and pests - pesticide costs for disease and pests - fuel oil costs - labour costs - other costs	- conventional olive gross production value - organic olive gross production value	- CRS and Variable Returns to Scale (VRS)
Kashiwagi & Kamiyama 2023	- organic and conventional olive farms	- labor - paid cost - tree	- olive production	- Metafrontier DEA
Sintori et al. 2023	- organic, conservation, low-input, and standard olive farms	- variable capital - capital - labour - land	- revenues	- DEA

Charyulu & Biswas (2010) evaluated the efficiency of conventional and organic farms producing cotton, sugarcane, rice, and wheat in four states of India. They concluded that organic agriculture is more efficient on farms producing cotton and sugarcane, while conventional agriculture is more efficient on farms producing rice and wheat. Uzundumlu et al. (2021) assessed the efficiency of companies producing organic and conventional wheat in Erzurum province, Türkiye, and found that enterprises

with medium-sized land are more efficient than those with small and large land. However, they also concluded that although organic production enterprises are more efficient, their variable costs are higher. Riar et al. (2020) evaluated organic and conventional cotton farms according to their size.

Poudel et al. (2015) evaluated the efficiency of organic and conventional coffee farms in Nepal and determined changes in efficiency using Tobit regression. They found that efficiency was associated with education, farm experience, and access to credit. Basavalingaiah et al. (2022) assessed the efficiency of conventional, integrated, and organic coffee-pepper farms using DEA and Life Cycle Assessment (LCA) methodology. Zhen et al. (2023) evaluated the environmental, economic, and technical efficiency of conventional, organic-conversion, and organic tea farms. They concluded that while there were no significant differences in the technical efficiency of the farm types, the environmental efficiency of organic-conversion and organic tea farms was significantly higher than that of conventional tea farms.

Kashiwagi & Kamiyama (2023) analysed the transition process of olive farms in the West Bank region of Palestine to organic agriculture using a meta frontier with directional distance function approach, taking into account the heterogeneity in agricultural technology. They concluded that organic farming is not cost-efficient, but empirical evidence also showed that the performance gap decreases over time. Artukoğlu et al. (2010) found that the technical efficiency of organic farms is higher than that of conventional farms, although the efficiency values are generally low. Raimondo et al. (2021) examined the efficiency of organic and conventional olive farms using Stochastic Frontier Analysis (SFA). Sintori et al. (2023) classified olive farms as organic, conservation, low-input, and standard.

Table 2- Papers evaluating farms or companies in organic agriculture

	DMUs	Inputs	Outputs	Model
Casolani et al. 2021	- organic conversion and organic farm that are subsidized from european union	- agriculture area - fixed cost, - variable cost	- total farm revenue	- CCR
Nastis et al. 2019	- organic farms that are subsidized from european union	- capital - land - labor - variable inputs	- profit	- Fuzzy CRS model of (Saati & Memariani, 2005)
Ersoy et al. 2021	first model: - 2009-2018 years second model: - organic tea farms	first model: - farms - tea area - fresh tea second model: - fresh tea - production cost	first model: - organic dry black tea - share of organic tea in dried tea second model: - organic dry black tea	- Super Efficiency
Melo 2021	- organic rice farms	- land area - seed preparation - seeds - labor - organic fertilizer	- total yield	- SFA and SBM

In the second group, we viewed the efficiency of farms or companies in organic agriculture as shown in Table 2. Some of these papers were conducted to analyse the contribution of support programs for the transition to organic agriculture (Nastis et al. 2019; Casolani et al.2021). Additionally, we assessed the efficiency of businesses producing organic tea (Ersoy et al.2021), organic rice farms (Melo 2021), and export-oriented organic rice farms. Koner & Laha (2024) examined the marketing efficiency of organic farms in three regions of India, revealing that marketing efficiency is influenced by factors such as the economic situation, education level, farming experience, land size of the farmer household, and type of marketing arrangement.

In the final part of organic agriculture, we viewed the efficiency of organic agriculture in regions, states, or countries as shown in Table 3. Manta et al. (2023) evaluated 27 countries of the European Union using data from 2000 to 2017 to investigate the connection between national culture and organic agriculture efficiency. Menten et al. (2023) analysed the change in organic agriculture efficiency of 32 OECD countries between 2011 and 2020. They clustered countries according to their efficiency levels on a yearly basis using context-dependent DEA. Efficiency changes between periods were examined with the Malmquist total factor productivity index. Yadava & Komaraiah (2021) and Yadava (2024) evaluated the organic farming performance of 21 and 22 states in India, respectively.

Table 3- Papers on the efficiency of organic agriculture in regions, states, or countries

	DMUs	Inputs	Outputs	Model
Yadava & Komaraiah 2021	- 21 Indian States	first model: - organic land - farmers - biofertilizers - manure second model: - organic land - farmers - biofertilizers - manure - land in conversion period	first model: - pure organic production second model: - pure organic production - production in the conversion period	- DEA and Bootstrap DEA
Manta et al. 2023	- 27 countries of the European union	- area of organic cultivation - number of producers of organic products	- total amount of sales	- DEA
Menten et al. 2023	- 32 countries of the OECD	- land - farmers	- organic product sales	- CRS, VRS and Context- Dependent and Malmquist

In this section, we reviewed papers using DEA on organic husbandry, an area of increasing interest (Manuelian et al., 2020). However, we found that the number of papers on this topic was quite limited. Therefore, we also analyzed traditional husbandry. Table 4 presents traditional husbandry with DEA, including input and output variables, and models.

Table 4- Papers on traditional husbandry

	DMUs	Inputs	Outputs	Model
Kuhna et al. 2020	- 371 Chinese hog farms	- Labor - Feed - Other cost	- Weight gain Undesirable/Bad Output - COD - Ammonia	- Slack-based DEA model (SBM)
Pandey & Singh 2021	- European farms	Agriculture Input - Forage land - Agricultural land - Fertilizer Animal farming Input - Forage - Grassland - Dairy Cow - Cattle feed	Agriculture Output - Cereal - Protein crops - Potato - SugerBeet - Oil-seed - Industrial crops - Vegetables - Forage Animal farming Output - Meat - Milk	- Network DEA
He et al.2022	- Counties of Tongliao	- Capital - Labor - Land - Public - Infrastructure	- Output value of grass-based livestock husbandry	-Malmquist index
Gomes et al.2015	- 21 beef cattle production systems	Economic Model Input - labor - area of pasture - spending on buying animals - other expenses Socio-environmental Model Input - area of pasture - spending on buying animals	Economic Model Output - area for native forest - livestock gross revenue Socio-environmental Model Output - labor - area for native forest - livestock gross revenue	-BCC

Considering animal husbandry, undesirable outputs such as greenhouse gases, chemical oxygen demand (COD), nitrogen, phosphorus, and ammonia are generated. Kuhn et al. (2020) categorized pig farms into large, medium, and small and identified COD and ammonia as undesirable outputs for evaluating environmental efficiency. They concluded that medium-sized farms, particularly those in transition, face challenges of low environmental efficiency and high pollution abatement costs due to limited waste disposal options. It is recommended to enhance waste management through projects for biogas production. Yan & Zhang (2023) accounted for carbon emissions from husbandry, a significant source of greenhouse gases. Pandey & Singh (2021)

assessed the technical and environmental efficiency of European farms concerning both plant and animal production. Gomes et al. (2015) constrained the weighting of output variables in their study to evaluate whether capital costs yield economic, environmental, and social benefits.

Table 5- Papers on traditional beekeeping

	DMUs	*Inputs*	*Outputs*	*Model*
Makri et al. 2015	- beekeeping farms in Greece	- Fixed capital - Variable capital - Labour wages	- Gross return	- CRS and VRS
Aydın et al.2020	-beekeeping farms in Çanakkale	- labor - variable costs - fixed costs - number of frame	- Total income	- CRS and VRS
Dogan & Adanacioglu 2021	-beekeeping farms in Gümüşhane	- Number of bee hives - Feed costs - Medication costs - Labour costs - Other variable costs	- Gross Product Value	- CRS and VRS
Aşkan 2023	-beekeeping farms in Erzincan and Van	- Labor - Fixed costs - Variable costs - Number of hives	- Total honey production amount	- CRS and VRS
Angón et al2021	-beekeeping farms in La Pampa	- Investment - Feed costs - Labour costs - Number of hives	- Honey production	- CRS

In this section, no papers on organic beekeeping with DEA were found; therefore, traditional beekeeping studies were reviewed, as presented in Table 5. Particularly noteworthy is that most of the studies were conducted in Türkiye and its provinces. Aydin et al. (2020) divided beekeeping farms into three groups based on the number of hives and found that the efficiency values of the group with a higher number of hives were significantly higher than those of the other groups. Ceyhan et al. (2017) assessed the efficiency of beekeepers' unions and honey producers' unions in Türkiye. Additionally, Dogan & Adanacioglu (2021) evaluated the efficiency of beekeeping farms in Gümüşhane. Aşkan (2023) conducted a similar study in Erzincan and Van provinces, which are important representatives of local and gastronomy tourism. In Greece, Makri et al. (2015) investigated beekeeping farm efficiency, while Ferenczi et al.(2023) evaluated the efficiency of beekeeping farms in Hungary. Angón et al. (2021) evaluated beekeeping farms in Argentina and concluded that factors such as marital status, educational level, primary family income, source information usage, planning, and health area positively affected efficiency.

Upon examining the literature, it becomes apparent that there is a greater abundance of papers focusing on the efficiency of both traditional and organic agriculture at a product level. Furthermore, studies evaluating countries to analyse the impact of support programs for transitioning to organic agriculture are also prevalent. However, when reviewing the literature on organic husbandry and beekeeping, it is noted that studies in these areas are limited, with a preference for examining traditional husbandry and beekeeping instead. Many studies on traditional husbandry tend to focus on farms specific to certain animal species (such as beef, sheep, or poultry). Similarly, provincial analyses are predominant in traditional beekeeping studies. Moreover, Pandey & Singh (2021) conducted an evaluation of organic agriculture and husbandry together. Nevertheless, no study has been identified that evaluates organic agriculture, husbandry, and beekeeping collectively. Incorporating beekeeping alongside organic agriculture and husbandry in our study introduces a novel perspective compared to existing literature, offering a more comprehensive understanding of these practices.

3. Materials and Method

3.1. Data Gathering

The data in our study was obtained from the organic agriculture statistics section of the website of the Ministry of Agriculture of the Republic of Türkiye and was taken as basis for 2022, which contains the most up-to-date (TR Ministry of Agriculture & Forestry, 2024). In organic agriculture, products (number), farmer (number) and area (da) are determined as inputs, and the production (tons) is determined as output. Organic husbandry and beekeeping were evaluated together and poultry (number), small cattle (number), cattle (number), hive (number), and farmer (number) were selected as inputs. Outputs are meat (tons), milk (tons), egg (number) and honey (tons).

3.2. Methodology

In our study, Türkiye 's provinces were classified according to NUTS-Level 1 and each region evaluated as a Decision Making Unit (DMU). While the SE model was used for the organic agriculture of the regions, the Lee and Zu model, where zero data was taken into account, was used for organic husbandry and beekeeping. A noteworthy observation from the literature in Chapter 2 is the absence of models that account for zero data. Therefore, introducing a methodology that considers zero data for assessing the efficiency of farms, businesses, states, or countries has contributed a novel approach to the literature. Furthermore, to generate a unified ranking of efficiency for organic agriculture and organic husbandry-beekeeping, the Copeland method, which relies on superiority comparison and does not necessitate normalization, was adopted (Saari & Merlin , 1996). The proposed methodology is illustrated in Figure 1.

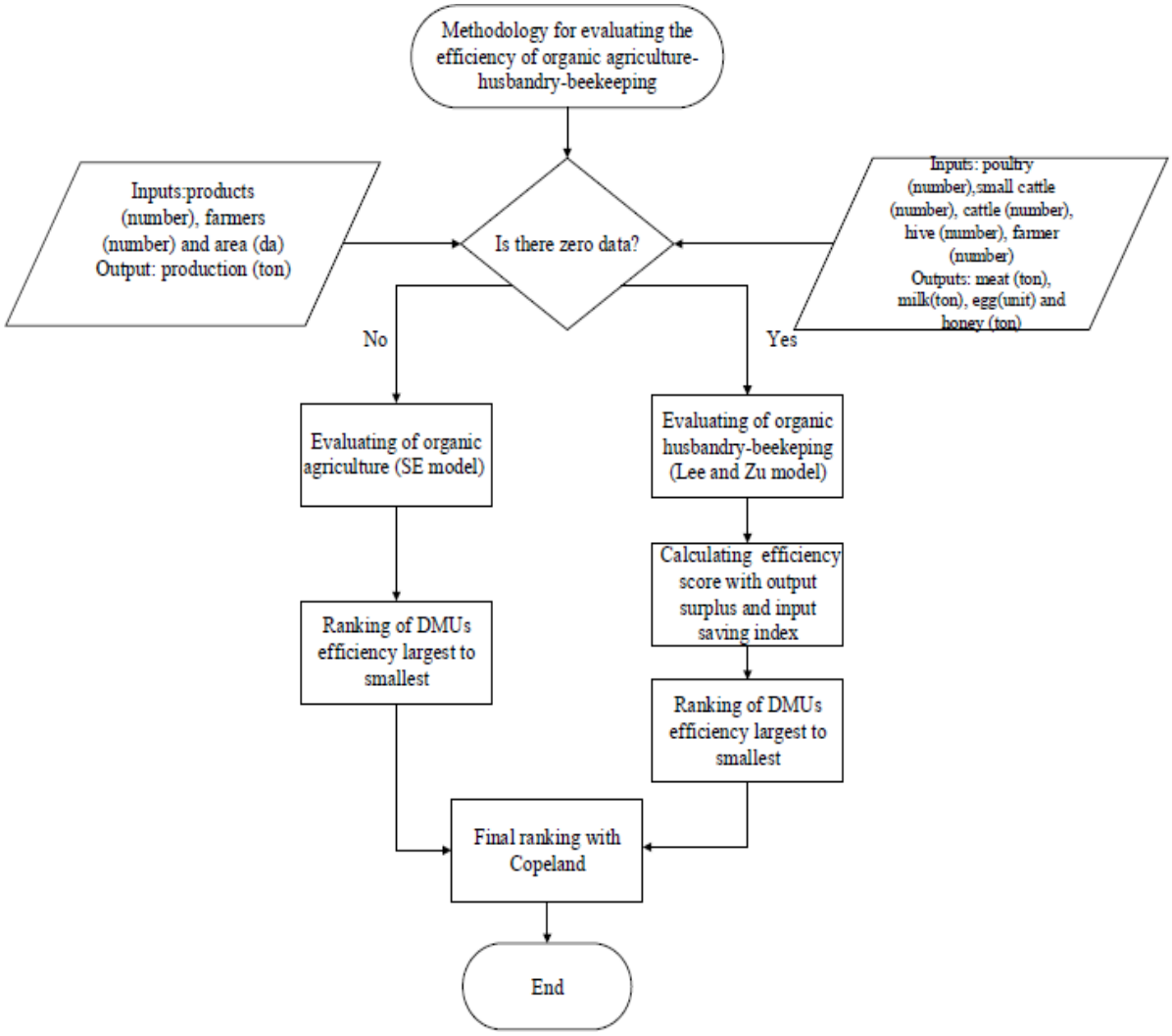

Figure 1- Steps for recommended methodology

3.2.1. Data Envelopment Analysis

DEA, a method based on linear programming and non-parametric assumptions, serves to evaluate the relative efficiencies of units producing similar outputs using similar inputs. The pioneering DEA model, the CCR was introduced by Charnes, Cooper, and Rhodes, enables the differentiation between efficient and inefficient DMUs, with efficient DMUs delineating the efficiency frontier and providing a preference ranking for inefficient ones (Charnes et al. 1978). However, the classical DEA models, the CCR model under the assumption of CRS and the BCC model under the assumption of VRS as proposed by Banker et al.(1984), fail to rank efficient DMUs. Consequently, numerous methodologies have been proposed to enhance DEA's discriminatory power, such as the Super-Efficiency (SE) model proposed by Andersen & Petersen (1993).

Initially, the parameters and decision variables for the SE model are delineated below, followed by the exposition of the input-oriented SE model (Andersen & Petersen, 1993). The primary objective of this model is to ascertain the efficiency score of DMU_0, which denotes the DMUS under assessment. In this context, θ_k symbolizes the efficiency score, with k representing the total number of DMUs.

Parameters:

N cluster of DMU
M cluster of input
S cluster of output
x_{ik} i-th input value of DMU k
y_{rk} r-th output value of DMU k
Decision Variables:
θ_k Efficiency score of DMU k
λ_k Matrix containing the weights of inputs and outputs for DMU k

(SE Model)

$$\text{Min } \theta_0 \tag{1}$$

$$\sum_{k \in N-\{0\}} \lambda_k x_{ik} \leq \theta_0 x_{i0} \qquad \forall i \in M \tag{2}$$

$$\sum_{k \in N-\{0\}} \lambda_k y_{rk} \geq y_{r0} \qquad \forall r \in S \tag{3}$$

$$\sum_{k \in N-\{0\}} \lambda_k = 1 \tag{4}$$

$$\lambda_k \geq 0 \qquad \forall k \in N \tag{5}$$

In the SE model, DMUs are omitted from the dataset, thereby disrupting the existing efficient frontier and establishing a new one. The DMU under evaluation for efficiency is positioned beyond this newly established efficient frontier, yielding an efficiency score equal to or greater than 1. A higher efficiency score for an efficient DMU is indicative of greater desirability. In contrast, inefficient DMUs are unable to lie on the efficient frontier, resulting in their efficiency score as same as the classical models.

In the VRS assumption, the SE model may face infeasibility issues when evaluating certain efficient DMUs. Seiford & Zhu (1999) outline the necessary and sufficient conditions for the infeasibility of SE models, demonstrating that infeasibility is inevitable in the context of the VRS assumption in SE model. Various studies have attempted to address the challenge of infeasibility associated with the VRS assumption in SE model (Lovell & Rouse, 2003; Chen, 2005; Cook et al. 2009). Lee et al. (2011) propose a two-stage process to mitigate the issue of VRS infeasibility, producing a score that encompasses in both inputs and outputs. Additionally, Chen & Liang (2011) establish that the two-stage process can be resolved through a single linear program. Lee et al. (2011) illustrate that infeasibility arises in the input-oriented (output-oriented) model when there is any output surplus (input saving). In such cases, this novel approach identifies radial efficiency and output surplus (input saving) concurrently, yielding a SE score that encompasses both radial efficiency and output surplus (input saving) if present. However, these new SE model may still face infeasibility when dealing with positive data. In an extension of the research by Lee et al. (2011), Lee & Zu (2012) refine the model to ensure feasibility even in the presence of zero data in inputs. They assert that zero output data does not lead to infeasibility in the output-oriented SE models proposed in previous studies by Lee et al. (2011), Chen & Liang (2011), and Cook et al. (2009). The reason behind this is that the constraints on the output side can always be satisfied. Lee & Zu model is presented below (Lee & Zhu 2012):

(*Lee &Zu model)*

$$Min\ \tau + M\left(\sum_r \beta_r + \sum_i t_i\right) \tag{6}$$

$$\sum_{k \in N-\{0\}} \lambda_k x_{ik} - t_i x_{imax} \leq (1+\tau)\, x_{i0} \qquad \forall i \in M \tag{7}$$

$$\sum_{k \in N-\{0\}} \lambda_k y_{rk} \geq (1-\beta_r)\, y_{r0} \qquad \forall r \in S \tag{8}$$

$$\sum_{k \in N-\{0\}} \lambda_k = 1 \tag{9}$$

$$\lambda_k \geq 0,\ \beta_r \geq 0,\ t_i \geq 0,\ \tau \text{ is unlimited} \tag{10}$$

Where; $x_{imax} = max_{k=1}^{1}\{x_{ik}\}$, t_i is input saving and β_r output surplus, input saving index and output surplus index are calculated as follows with $I = \{i|\, t_i^* > 0\}$ and $R = \{r|\, \beta_r^* > 0\}$.

$$\hat{\imath} = \begin{Bmatrix} 0 & if\ I = \emptyset \\ \frac{\sum_{i\in I}\left(\frac{1+t_i^*}{1}\right)}{|I|} & if\ I \neq \emptyset \end{Bmatrix} \qquad o = \begin{Bmatrix} 0 & if\ R = \emptyset \\ \frac{\sum_{r\in R}\left(\frac{1}{1-\beta_r^*}\right)}{|R|} & if\ R \neq \emptyset \end{Bmatrix}$$

Then, the SE with zero data can be defined as $\breve{\theta} = 1 + \tau^* + o + \hat{\imath}$.

Consider a simple numerical example in Table 6 includes with 5 DMUs, two inputs (x_1 , x_2) and a single output (y_1). Here, $x_{1max} = max_{k=1}^{1}\{x_{1k}\} = 3$ and $x_{2max} = max_{k=1}^{1}\{x_{2k}\} = 4$. Table 7 shows the optimal values ($\tau^*, t_1^*, t_2^*, \beta_1^*$) from the Lee and Zhu model and input saving index ($\hat{\imath}$), output surplus index (o), SE with zero data ($\breve{\theta}$) from the formulas.

Table 6- Sample data set

DMUs	*Inputs*		*Output*
	x_1	x_2	y_1
1	2	1	1
2	1	2	1
3	1	4	2
4	2	3	1
5	3	0	1

Table 7- Lee and Zu model results of the sample data set in Table 6

DMUs	$1+\tau^*$	t_1^*	t_2^*	β_1^*	$\frac{t_1^{**}}{x_{1max}}$	$\frac{t_2^{**}}{x_{2max}}$	$\beta_1^* * y_{1k}$	Input saving index ($\hat{\imath}$)	Output surplus index (o)	SE with zero data score ($\breve{\theta}$)
1	1	0	0	0	0	0	0	0	0	1
2	1.4	0	0	0	0	0	0	0	0	1.4
3	1	0	0	0.5	0	0	1	0	2	3
4	0.6	0	0	0	0	0	0	0	0	0.6
5	0.67	0	0.25	0	0	1	0	1.25	0	1.92

3.2.2. Copeland

The results from multi-criteria decision-making techniques can differ based on the evaluation methods utilized. This variance poses challenges for decision-makers, leaving them unsure when selecting the method and determining the best alternative. To resolve this issue, presenting alternative rankings obtained through multi-criteria decision-making methods using an integrative approach aids decision-making. Hence, the Copeland method serves as an integrative tool for this purpose (Saari & Merlin, 1996).

Step 1: The comparative superiorities are calculated according to Equation (11), where *i* represents the rank value of an alternative in the row, *j* represents the rank value of an alternative in the column, $f_k(i, j)$ denotes the superiority of alternative *i* over alternative *j*, and $r_k(A_i)$ signifies the rank value of alternative *i* with respect to method *k*.

$$f_k(i,j) = \begin{cases} r_k(A_i) < r_k(A_j) \wedge\ i \neq j \implies 1 \\ r_k(A_i) > r_k(A_j) \wedge\ i \neq j \implies 0 \\ r_k(A_i) = r_k(A_j) \vee\ i \neq j \implies 0 \end{cases} \tag{11}$$

Step 2: The total comparative superiorities are computed using Equation (12), where $S(i, j)$ represents the overall superiority of alternative *i* to alternative *j*, *k* denotes the rank value according to the MCDM method, and *m* signifies the total number of MCDM methods.

$$S(i,j) = \sum_{k=1}^{m} f_k\,(i,j), \quad i \neq j \tag{12}$$

Step 3: The conditions for winning, tying, and losing are provided sequentially in Equation (13).

$$G(i,j) = \begin{cases} S(i,j) > S(j,i) \wedge\ i \neq j \Longrightarrow 1 \\ S(i,j) = S(j,i) \wedge\ i \neq j \Longrightarrow 1/2 \\ S(i,j) < S(j,i) \wedge\ i \neq j \Longrightarrow -1 \end{cases} \quad (13)$$

Step 4: Where GP_i represents the winnig score of alternative i, BP_i represents the tying score of alternative i, and YP_i represents the losing score of alternative i, the Copeland score CP_i is calculated using Equation (14).

$$\begin{aligned} GP_i &= \sum_{i=1}^{n} G(i,j)\ , G(i,j) > 0,\ n \\ BP_i &= \sum_{i=1}^{n} G(i,j)\ , G(i,j) = 1/2,\ n \\ YP_i &= \sum_{i=1}^{n} G(i,j)\ , G(i,j) < 0,\ n \\ CP_i &= GP_i + BP_i - YP_i \end{aligned} \quad (14)$$

3. Results and Analysis

In this study, to assess the efficiency of organic agriculture and organic husbandry-beekeeping, Türkiye's provinces were categorized according to NUTS-Level 1, with each region being treated as a DMU. Figure 2 illustrates the division of the 81 provinces into 12 groups on the map of Türkiye. Data pertaining to organic agriculture for these 12 groups were sourced from the website of the Ministry of Agriculture of the Republic of Türkiye and are presented in Table 8. Similarly, data concerning organic husbandry-beekeeping are provided in Table 9 (TR Ministry of Agriculture & Forestry, 2024). Figure 3 presents density maps for the selected outputs and inputs in our evaluation of organic agriculture and husbandry and beekeeping. Panel (a) shows the density of organic crop production (tons), one of the outputs in our analysis of organic agriculture. Panel (b) illustrates the total number of poultry, sheep, and cattle, which represent the inputs used in the evaluation of organic husbandry. Finally, panel (c) displays organic honey production (tons), representing the output of organic beekeeping.

Figure 2- The Nomenclature of Territorial Units for Statistics (NUTS)-Level 1 classification

Table 8- Organic agriculture data of the regions

DMUs	*Level 1 Zone Name*	*Inputs*		*Output*
		Products (number)	*Farmer (number)*	*Area (da)*	*Production (ton)*
1	Istanbul	105	14	605.29	431.41
2	West Marmara	259	436	42,943.94	12,444.86
3	Aegean	505	11,060	697,436.73	389,127.34
4	East Marmara	480	808	28,483.95	23,793.90
5	West Anatolia	222	553	59,941.72	41,351.56
6	Mediterrenian	319	452	155,184.36	55,962.33
7	Central Anatolia	311	724	155,093.64	190,318.48
8	West Blacksea	260	2,434	149,715.22	36,778.42
9	East Blacksea	50	15,472	118,044.17	62,034.75
10	Northeast Anatolia	87	1,936	403,189.93	149,383.18
11	Central East Anatolia	128	1,639	145,919.50	88,822.95
12	Southeast Anatolia	90	903	184,457.90	102,711.94

Table 9- Organic husbandry-beekeeping data of the regions

Level 1 Zone Name	*Inputs*					*Outputs*			
	Poultry (number)	*Small cattle (number)*	*Cattle (number)*	*Hive (number)*	*farmer (number)*	*Meat (ton)*	*Milk (ton)*	*Egg (number)*	*Honey (ton)*
Istanbul	0	0	0	35	1	0	0	0	0.71
West Marmara	17,814	1,172	2,844	1,287	62	27.54	2,572.5	2,155,630	10.85
Aegean	352,662	22	2,762	664	28	78.00	16,054	41,117,289	13.15
East Marmara	139,044	0	232	289	17	0.99	959.50	27,407,376	4.96
West Anatolia	420	1,651	116	438	6	0	0	54,000	8.71
Mediterranean	17,000	2,485	60	12,477	42	0	264.00	3,517,867	481.53
Central Anatolia	0	0	1,206	4,709	60	0	6,910.8	0	88.20
West Black sea	0	0	0	74	1	0	0	0	0.74
East Black sea	113,500	0	0	12,143	100	0	0	2,000	132.11
Northeast Anatolia	0	0	0	11,310	34	0	0	0	183.49
Central East Anatolia	43,968	0	0	24,478	88	0	0	13,190,400	386.89
Southeast Anatolia	0	0	0	5,033	22	0	0	0	40.85

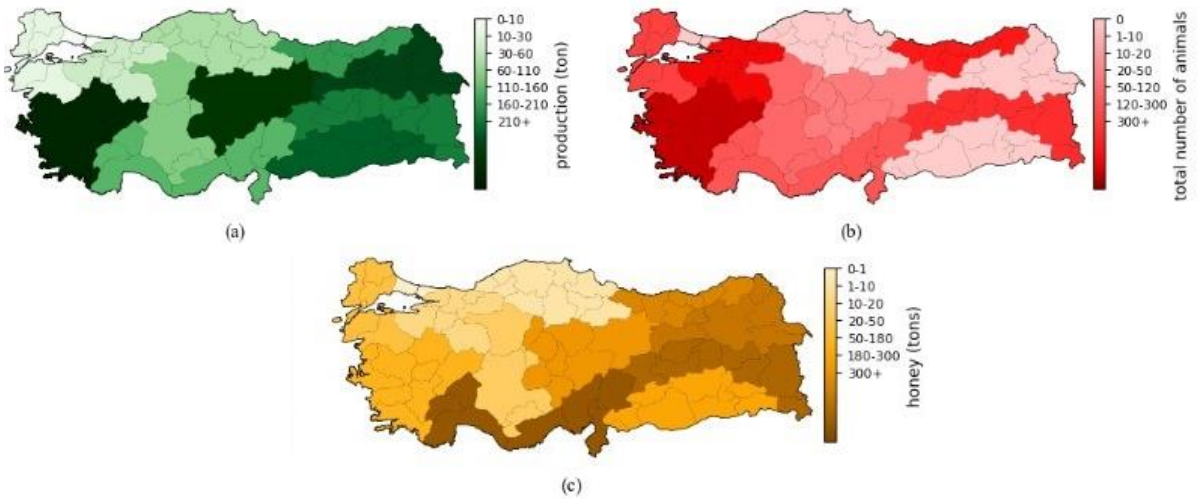

Figure 3- By region (a) organic agricultural production (b) number of poultry, sheep, and cattle (c) organic honey production

According to Figure 3 map (a), Istanbul exhibits the lowest agricultural production. However, as depicted in Figure 4, Istanbul possesses 14% of the authorized organizations with organic production certificates, trailing behind Izmir (TR. Ministry of Agriculture & Forestry, 2024). Moreover, the quantity of organic agricultural production is notably low in the Marmara Region (encompassing Istanbul, Western Marmara, and East Marmara), despite its significant population and high demand for organic products based on socio-economic characteristics. Conversely, the Aegean region, home to Izmir, boasts the highest agricultural production. Examining the number of organic animals illustrated in map (b), similar trends are evident for Istanbul and the Aegean region. Furthermore, while East Marmara, primarily focused on the poultry sector, stands out, Northeast and Southeast Anatolia, prominent in organic animal feed production, fall behind. Lastly, concerning map (c), the Mediterranean and Central East Anatolia regions lead in honey production.

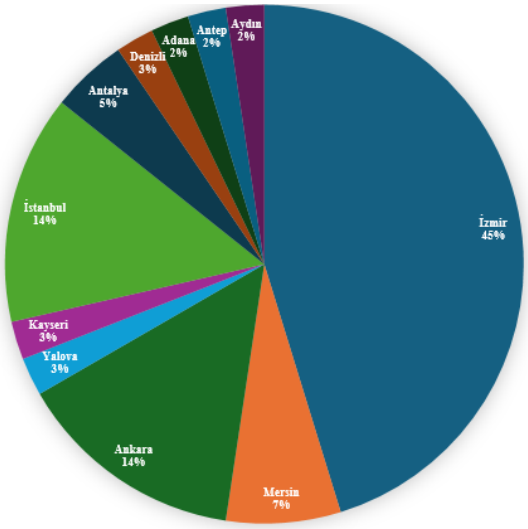

Figure 4- Authorized organizations for organic agriculture and husbandry

Table 10- Efficiency scores and final rankings

		Organic Crop		*Organic Husbandry-Beekeeping*		*Final Ranking*	
DMUs	***Level 1 Zone Name***	***Super efficiency score***	***Ranking***	***Super efficiency with zero data***	***Ranking***	***Borda count***	***Copeland***
1	Istanbul	2.1	3	2.11	8	5	6
2	West Marmara	0.42	11	6.99	3	7	7
3	Aegean	2.77	2	40.61	1	1	1
4	East Marmara	0.69	8	8.67	2	3	3
5	West Anatolia	0.64	9	0.61	11	11	11
6	Mediterranean	0.51	10	4.15	5	8	9
7	Central Anatolia	4.83	1	2.55	7	2	2
8	West Black Sea	0.4	12	1.01	9	12	12
9	East Black Sea	1.79	5	0.67	10	8	8
10	Northeast Anatolia	1.81	4	2.55	6	3	3
11	Central East Anatolia	0.93	7	6.56	4	5	5
12	Southeast Anatolia	1.29	6	0.50	12	10	10

In our study, we evaluated the efficiency of organic agriculture using the SE model and the efficiency of organic husbandry-beekeeping using Lee and Zu's model, which accounts for zero data. According to the organic crop efficiency scores derived from the SE model, Central Anatolia ranks first, with the Aegean Region in second place. Although the Aegean Region has the highest output, its second-place ranking is attributed to its significantly higher inputs compared to Central Anatolia. Additionally, despite having the lowest output, the Istanbul region ranks third due to its relatively low inputs. Finally, the West Black Sea Region, while not having a particularly low output, ranks last because of the high number of farmers considered as an input. According to the organic husbandry and beekeeping efficiency scores obtained from the Lee and Zhu model, the Aegean, East Marmara, and West Marmara regions rank in the top three, respectively. These regions engage in all activities (poultry, cattle, sheep, and beekeeping) and their outputs are higher than those of other regions. Additionally, despite having the highest output in honey production, the Mediterranean Region ranks fifth due to having zero data for meat production.

According to Table 10, the Aegean Region ranks second in organic crop and first in organic husbandry and beekeeping, indicating that it has a balanced production network. Although Central Anatolia ranks first in organic crop, it only ranks seventh in organic husbandry and beekeeping, primarily due to the zero data on poultry and small cattle in this region. As mentioned earlier, Istanbul has a favourable ranking in organic crop due to its low input and output, yet it ranks eighth in organic husbandry and beekeeping. Considering its population, Istanbul needs to further enhance its organic production capabilities. Northeast Anatolia ranks fourth and sixth, respectively. In this region, where the geographical features are known to be suitable, support for husbandry should be prioritized. Similar observations can be made for other regions as well. In conclusion, to establish a

balanced production network across all regions, existing farms should be integrated into the certification system, or organic agriculture should be promoted through grant support.

Since the efficiency scores from these models can vary greatly, summing them may lead to misleading results. Additionally, due to extreme values in the efficiency scores from Lee and Zu's model, normalizing the scores does not effectively differentiate between DMUs with low efficiency scores. To obtain a single final ranking from these two sets of rankings, we employed the Borda count method, widely used in the literature, and the Copeland method, which is based on superiority comparison and does not require normalization. As shown in Table 10, the rankings are similar in both methods. The Aegean region, which ranks first in organic husbandry-beekeeping and second in organic agriculture, ranked first overall. According to Figure 3 (a, b, c), Central Anatolia, which has average values, ranks first in organic agriculture efficiency score based on the weighted input and output ratio. However, since it ranks seventh in organic husbandry-beekeeping, it comes in second in the final rankings.

East Marmara and North Anatolia are ranked third according to the Borda count method. Istanbul, which were last in terms of organic agriculture production, number of animals, and honey production, and Central East Anatolia ranked fifth. Istanbul is in the middle ranks due to its low inputs as well as outputs. In the Copeland method, Central East Anatolia ranked fifth, while Istanbul ranked sixth, thus resolving the tie. Finally, West Anatolia and West Black Sea ranked in the bottom two according to both methods.

4. Conclusions

Türkiye, with approximately half of its total land area being agricultural, is a significant producer and exporter of agricultural products. It is the largest producer and one of the leading exporters of various grain products, oilseeds, hazelnuts, raisins, figs, and tea. Thanks to its favourable geography, fertile soil, abundant water resources, and suitable climatic conditions, a wide variety of products such as fruits, vegetables, and grains are cultivated. These features make Türkiye naturally conducive to organic agriculture. However, organic product production and consumption rates remain low, comprising only 0.1% of the global organic agriculture market. To address this, many projects have been initiated to popularize organic agriculture, support the production of organic products accessible to all income groups, establish traceability, implement an effective control and certification system, and increase consumer awareness about organic products. As a result, the number of organic farming enterprises and the total organic farming land area have significantly increased over the last decade. However, certain challenges negatively impact organic agriculture in Türkiye. For instance, farms in the country are generally fragmented and small-scale family businesses. Approximately 65% of farms in Türkiye cover only 0-5 hectares, while lands under 10 hectares constitute about 83% of the total agricultural land. In our study, we handled the number of farmers as an input; however, due to the lack of scaling for the size of the farming, could not include in the evaluation. Therefore, if the ministry or policymakers scale these enterprises according to their size and share the data accordingly, more accurate analyses can be conducted, and can be assessed more effectively.

Türkiye has significant potential in terms of animal numbers, and although its potential for organic animal production is very high, it is not fully utilized. Regions with extensive meadow and pasture areas and no industrial pollution have great potential for organic sheep and cattle breeding and beekeeping. However, animal breeders in these regions are mostly small family businesses. Despite the need for a certification system to follow organic husbandry and beekeeping, some regions, such as the East and the Black Sea, lack certification bodies. Additionally, animal breeders' knowledge and training regarding both the certification system and organic husbandry are inadequate. For these reasons, this potential has not been fully realized. Furthermore, although the number of organic animals, and the production of milk, meat, and especially eggs, have increased considerably in the last decade, the lack of sufficient consumer awareness and low purchasing power in the domestic market negatively impact the development of organic husbandry. In this context, policymakers can create organizations to support organic production, particularly in regions with low performance. This includes providing farmers with necessary training, developing grant-based support programs, and expanding institutions that offer organic production certification systems in other regions as well as the Aegean Region. In the Eastern Anatolia and Black Sea Region, where husbandry and beekeeping are intensively practiced, farms can be encouraged to join the certification system. Furthermore, the marketing and promotion network for organic products can be enhanced, leading to greater branding and distribution of registered local products across various regions of Türkiye. Thus, interest in organic production can increase in alignment with the rising demand in both domestic and international markets.

In conclusion, Türkiye has regions that vary significantly in terms of natural, climatic, and socio-economic conditions. Therefore, analysing the development of organic agriculture, husbandry, and beekeeping on a regional basis in our study can provide a better understanding of the current situation and guide policy makers in formulating the necessary strategies.

References

Aghasafari H, Karbasi A, Mohammadi H & Calisti R (2020). Determination of the best strategies for development of organic farming: A SWOT–Fuzzy Analytic Network Process approach. *Journal of Cleaner Production* 277: 124039. doi:https://doi.org/10.1016/j.jclepro.2020.124039

Ak İ (2017). Organic Livestock in Turkey. *Proceeding of The Eurasian Agriculture and Natural Sciences Congress,*, (pp. 190-192). Bishkek, Kyrgzstan

Åkerfeldt M P, Gunnarsson S, Bernes G & Blanco-Penedo I (2021). Health and welfare in organic livestock production systems—a systematic mapping of current knowledge. *Organic Agriculture* 11(1): 105-132

Andersen P & Petersen N C (1993). A procedure for ranking efficient units in Data Envelopment Analysis. *Management Science* 39: 1261-1264

Angón E, Bragulat T, García A, Giorgis A & Perea J (2021). Key factors affecting the technical efficiency of bee farms in the province of La Pampa (Argentina): A two-stage DEA approach. *Revista de la Facultad De Ciencias Agrarias UNCuyo* 55(1): 150-163

Artukoglu M M, Olgun A & Adanacioglu H (2010). The efficiency analysis of organic and conventional olive farms: Case of Turkey. *Agricultural Economics* 56(2): 89 - 96

Aşkan E (2023). Increasing Honey Production Effectiveness in Erzincan and Van Provinces. *Sustainability* 15(9): 7524

Aydın B, Aktürk D & Arsoy D (2020). Economic and efficiency analysis of beekeeping activity in Turkey: Case of Çanakkale Province. *Ankara Üniv Vet Fak Derg* 67: 23-32

Banker R, Charnes A & Cooper W (1984). Some models for estimating techical and scale inefficiencies in Data Envelopment Analysis. *Management Science* 30: 1078-1092

Basavalingaiah K, Paramesh V, Parajuli R, Girisha H, Shivaprasad M, Vidyashree G & Rajanna G (2022). Energy flow and life cycle impact assessment of coffee-pepper production systems: An evaluation of conventional, integrated and organic farms in India. *Environmental Impact Assessment Review 92*(January): 106687

Casolani N, Nissi E, Giampaolo A & Liberato L (2021). Evaluating the effects of European support measures for Italian organic farms. *Land use policy* 102: 105225

Ceyhan V, Canan S, Yıldırım Ç & Türkten H. (2017). Economic Structure and Services Efficiency of Turkish Beekeepers' Association. *European Journal of Sustainable Development* 6(4): 53-64

Charnes A, Cooper W & Rhodes E. (1978). Measuring the efficiency of decision-making units. *European Journal of Operational Research* 2: 429-444

Charyulu D K & Biswas S (2010). Economics and efficiency of organic farming vis-à-vis conventional farming in India. Ahmedabad, India: Indian Institute of Management

Chen Y (2005). Measuring super-efficiency in DEA in the presence of infeasibility. *European Journal of Operational Research* 161(2): 545-551

Chen Y & Liang L (2011). Super-efficiency DEA in the presence of infeasibility: One model approach. *European Journal of Operational Research* 213(1): 359-360

Cook W, Liang L, Zha Y & Zhu J (2009). A modified super-efficiency DEA model for infeasibility. *Journal of the Operational Research Society* 60(2): 276-281

Dogan N & Adanacioglu H (2021). Performance Evaluation of Beekeeping Farms: A Case Study from Gümüşhane, Turkey. *Pakistan J. Zool* 53(5): 1837-1846

Durán-Lara E F, Valderrama A & Marican A (2020). Natural organic compounds for application in organic farming. *Agriculture* 10(2): 41. doi:https://doi.org/10.3390/agriculture10020041

Ersoy Y, Tehci A & Yıldız S (2021). Efficiency measurement in businesses producing organic products within the scope of ecological marketing: The example of a tea business. *Akademia Journal of Nature and Human Sciences* 7(1): 19-31, (In Turkish).

Ferenczi A, Szucs I & Gáthy A (2023). Economic Sustainability Assessment of a Beekeeping Farm in Hungary. *Agriculture* 13(6): 1262

Gomes E, Abreu U, Mello J, Carvalho T & Zen S (2015). Economic and socio-environmental performance assessment of beef cattle production systems: a data envelopment analysis (DEA) approach with weight restrictions. *Revista Brasileira de Zootecnia* 44(6): 219-225

He D, Deng X, Jin G, Wang X, Zhang Y, Sun Z & Zhao Z (2022). Ecological efficiency of grass-based livestock husbandry under the background of rural revitalization: An empirical study of agro-pastoral ecotone. *Frontiers in Environmental Science* 10(848134): 1-12

Kashiwagi K & Kamiyama H (2023). Effect of adoption of organic farming on technical efficiency of olive-growing farms: empirical evidence from West Bank of Palestine. *Agricultural and Food Economics* 11(26): 1-28

Koner N & Laha A (2024). Estimating Marketing Efficiency of Organic Farmers: Evidence from Districts of West Bengal India. *International Journal of Rural Management* 20(3): 335-352. https://doi.org/10.1177/09730052241229685

Kuhna L, Balezentis T, Hou L & Wang D (2020). Technical and environmental efficiency of livestock farms in China: A slacks-based DEA approach. *China Economic Review* 62: 101213

Kuosmanen N, Yli-Heikkilä M, Väre M & Kuosmanen T (2021). Productive performance of organic crop farms in Finland 2010–2017. *Organic Agriculture* 11: 1-14

Lee H S, & Zhu J (2012). Super-efficiency infeasibility and zero data in DEA. *European Journal of Operational Research* 216(2): 429-433

Lee H S, Chu CW & Zhu J (2011). Super-efficiency DEA in the presence of infeasibility. *European Journal of Operational Research* 212(1): 141-147

Lovell C & Rouse A (2003). Equivalent standard DEA models to provide super-efficiency scores. *Journal of the Operational Research Society* 54: 101–108

Makri P, Papanagiotou P & Papanagiotou E (2015). Efficiency and economic Analysis of Greek Beekeeping Farms. *Bulgarian Journal of Agricultural Science* 21(3): 479-484

Manta F, Morrone D, Toma P & Campobasso F (2023). Determining paths of innovation: The role of culture on the adoption on organic farming management. *Business Strategy and the Environment* 32(1): 96-109

Manuelian C, Penasa M, Costa L, Burbi S, Righi F & Marchi M (2020). Organic Livestock Production: A Bibliometric Review. *Animals* 10(4): 618

Melo M (2021). Organic Rice Production and Consumption to Sustain Food Security in Oriental Mindoro, Philippines. *Review of Integrative Business and Economics Research* 10(3): 338-354

Menten C, Çekiç B & Özal Saraç N. (2023). Evaluation of Organic Agriculture Production Efficiency in OECD Countries within the Framework of Sustainable Development Goals. *Hacettepe University Journal of Faculty of Economics and Administrative Sciences* 41(Special issue on Agriculture): 77-97. (In Turkish)

Nastis S A, Bournaris T & Karpouzos D (2019). Fuzzy data envelopment analysis of organic farms. *Operational Research* 19: 571-584

Pandey U & Singh S (2021). Environmental performance evaluation of European farms by assessing polluting factors in joint production. *Journal of Cleaner Production* 328: 129457

Poudel K L, Johnson T G, Yamamoto N, Gautam S & Mishra B (2015). Comparing technical efficiency of organic and conventional coffee farms in rural hill region of Nepal using data envelopment analysis (DEA) approach. *Organic Agriculture* 5: 263-275

Raimondo M, Caracciolo F, Nazzaro C & Marotta G (2021). Organic Farming Increases the Technical Efficiency of Olive Farms in Italy. *Agriculture* 11(3): 209

Riar A, Mandloi L, Sendhil R, Poswal R, Messmer M & Bhullar G (2020). Technical efficiencies and yield variability are comparable across organic and conventional farms. *Sustainability* 12(10): 4271

Saari D. & Merlin V (1996). The Copeland method. *Economic Theory 8*: 51-76. doi:https://doi.org/10.1007/BF01212012

Saati S & Memariani A (2005). Reducing weight flexibility in fuzzy dea. *Appl Math Comput* 161(2): 611–622

Sapbamrer R & Thammachai A (2021). A systematic review of factors influencing farmers' adoption of organic farming. *Sustainability* 13(7): 3842. doi:https://doi.org/10.3390/su13073842

Seiford L & Zhu J (1999). Infeasibility Of Super-Efficiency Data Envelopment Analysis Models. *INFOR: Information Systems and Operational Research* 37(2): 174-187

Sink N, Petkovsek M M, Veberic R & Marsic N K (2017). Chemical composition and morphometric traits and yield ofcarrots grown in organic and integrated farming systems. *Turkish Journal of Agriculture and Forestry 41*(6): 452-462. doi:https://doi.org/10.3906/tar-1705-8

Sintori A, Konstantidelli V, Gouta P & Tzouramani I (2023). Profitability, Productivity, and Technical Efficiency of Cretan Olive Groves across Alternative Ecological Farm Types. *Agriculture* 13(12): 2194

Sundrum A (2001). Organic livestock farming: a critical review. *Livestock Production Science* 67(3): 207-215. doi:https://doi.org/10.1016/S0301-6226(00)00188-3

T.R. Ministry of Agriculture and Forestry. (2024, May 16). Retrieved from T.R. Ministry of Agriculture and Forestry: https://www.tarimorman.gov.tr/Konular/Bitkisel-Uretim/Organik-Tarim/Yetkili-Kuruluslar-KSK

TR Ministry of Agriculture and Forestry. (2024, May 9). Retrieved from 2022 Organic Agriculture Statistics: https://www.tarimorman.gov.tr/Konular/Bitkisel-Uretim/Organik-Tarim/Istatistikler

Uzundumlu A S, Tamşen M & Bilgiç A (2021). Comparison of organic and conventional wheat in terms of efficiency and cost in Turkey: a case study of Erzurum Province. *Custos e@ gronegócio online* 17: 217-238

Yadava A K (2024). Macroeconomic determinants of organic farming efficiency: Double bootstrap DEA estimates from the Indian states. *Regional Science Policy & Practice Regional Science Policy & Practice* 16(6): 100036

Yadava A K & Komaraiah J B (2021). Benchmarking the performance of organic farming in India. *Journal of Public Affairs* 21(2): e2208

Yan J & Zhang Y (2023). Quantitative assessment, spatial and temporal characteristics, and dynamic evolution of carbon emissions from animal husbandry in China: 2001–2020. *Environmental Science and Pollution Research* 30: 116186–116201

Zhen H, Qiao Y, Ju X, Hashemi F & Knudsen M T (2023). Organic conversion tea farms can have comparable economic benefits and less environmental impacts than conventional ones—A case study in China. *Science of The Total Environment* 877: 162698

Zor M, Özüpek B, Pekacar S & Deliorman D (2023). Antioxidants, enzyme inhibitory activities, and phytochemical profiles of seven medicinal plants grown with organic farming techniques. *Journal of Agriculture and Forestry* 47(6): 918-930. doi:https://doi.org/10.55730/1300-011X.3137

Journal of Agricultural Sciences
(Tarim Bilimleri Dergisi)

J Agr Sci-Tarim Bili
e-ISSN: 2148-9297
jas.ankara.edu.tr

JAS

Optimization of Bioactive Compound Extraction from Propolis by Reflux, Maceration and Ultrasound-assisted Methods and Characterization of the Extracts

Sevde Nur Şenol Yazkan[a], Müge Hendek Ertop[b*]

[a]*Kastamonu University, Graduate School of Natural and Applied Sciences, Department of Food Engineering, Kastamonu, TÜRKIYE*
[b]*Kastamonu University, Faculty of Engineering and Architecture, Department of Food Engineering, Kastamonu, TÜRKIYE*

ARTICLE INFO
Research Article
Corresponding Author: Müge Hendek Ertop, E-mail: mugeertop@kastamonu.edu.tr
Received: 28 August 2024 / Revised: 13 October 2024 / Accepted: 11 November 2024 / Online: 25 March 2025

Cite this article
Yazkan Şenol S N, Ertop Hendek M (2025). Optimization of Bioactive Compound Extraction from Propolis by Reflux, Maceration and Ultrasound-assisted Methods and Characterization of the Extracts. *Journal of Agricultural Sciences (Tarim Bilimleri Dergisi),* 31(2):359-372. DOI: 10.15832/ankutbd.1540221

ABSTRACT
The region, botanical origin, and bee species influence the raw propolis content and its bioactive properties. Additionally, the extraction methods, solvents, and various process parameters significantly affect the bioactive properties of propolis extract, which is consumed as a food supplement or pharmaceutical product. In this study, propolis with a chestnut botanical origin, obtained from the Black Sea region in Turkey, was used as the raw material. The process parameters of three basic extraction methods—maceration (M), reflux (R), and ultrasound-assisted (UA)—were optimised using response surface methodology. Antioxidant activity (AA) and total phenolic content (TPC) were used as response parameters. The optimised levels for M were 78.46% ethanol concentration and 71.05 hours for extraction time; for R, 80.64% ethanol concentration, 117.44 minutes for extraction time, and 38.38°C for temperature; and for UA, 82.49% ethanol concentration, 59.12 minutes for extraction time, and 40.53°C for temperature. The results were statistically validated using the t-test. The AA, TPC, and phenolic, volatile, and mineral contents were compared among the optimised chestnut propolis extracts. Chrysin, a flavone, and pinocembrin, a flavanone, along with ferulic and ellagic acid, among the phenolic acids, were identified as the most abundant phenolic compounds. Among the 11 elements, the highest macro elements were Na, K, and Ca, while the trace elements were Fe and Zn. The phenolic, volatile, and mineral compositions of the optimised propolis extracts exhibited heterogeneous distributions. However, fatty acids (e.g., 18:0, 18:1) were present at relatively high levels only in R; phenolic compounds were obtained in relatively high amounts via M extraction. Some minor volatiles were detected only by UA extraction. Following the characterisation of the optimised extracts, it was determined that each extraction method has its own unique advantages. The results indicate that all three methods should be optimised and used together to achieve the highest component composition and bioactivity.

Keywords: Food supplement, Bee products, Response surface methodology, Bioactivity

1. Introduction

Propolis is a bee product with resinous material collected from the exudates and buds of plants mixed with pollen, wax, and bee enzymes. It is known to be used in complementary medicine because of its anti-inflammatory, antimicrobial, immunomodulatory, antioxidant, and immunostimulating activities from ancient times (Mele 2023; Bankova et al. 2021; Asem et al. 2019). The content of propolis, which is rich in bioactive components, varies depending on its botanical and geographical origin and harvest time (Kasote et al. 2022). The chemical composition of propolis varies depending on the plant source of the resin and balsam collected by bees (Al Dreini et al. 2023). Propolis is basically composed of 50% vegetable balsam and resin, 30% wax, 10% aromatic and essential oils, 5% pollen, and some other organic compounds, such as polyphenols and terpenoids, in nature (Rocha et al. 2023). Overall, more than 300 different bioactive compounds, such as phenolic aldehydes, ketones and polyphenols (phenolic acids, flavonoids, and esters) have been identified in propolis. The flavonoid group included chrysin, pinocembrin, apigenin, galangin, kaempferol, quercetin, tectocrisin, and pinostrobin, among others (El-Guendouz et al. 2019). The flavonoids that had the highest concentrations were pinosembrin (~4.7%), pinobencin (~3.1%), galangin (~2.2%), and chrysin (~2.1%). Another important group of identified bioactive compounds comprises phenolic acids, which also exhibit aromatic properties; these compounds include ferulic, cinnamic, caffeic, benzoic, salicylic, and p-coumaric acids (Do Nascimento Araújo et al. 2020).

Since the plant flora in which the hives are located determines the dominant primary, secondary, and minor pollen contents of bee products, the product characteristics and bioactive properties differ. For example, since the dominant pollen content of bee products such as honey, propolis, and pollen obtained from beekeeping activities carried out in locations where chestnut trees are dense in the Black Sea region of Turkey is chestnut, these products are called as "chestnut propolis, chestnut honey and

chestnut pollen". The color, composition, and related bioactive properties of propolis vary among countries worldwide and of different botanical origins (Özdal et al. 2023).

Raw propolis cannot be consumed directly due to its wax, resin, herbal balsam content, and bioactive compounds; therefore, it must be extracted appropriately. There are different extraction methods for the preparation of propolis extracts. The maceration method is the most basic method for extracting a sample by reducing it to the appropriate size and then maintaining it at room temperature for a certain period of time in a suitable solvent and a closed container (Silici & Kutluca 2005). In reflux extraction, heat is applied to the prepared solution during extraction, and the solution is kept in a water bath at a specific temperature and time (Margeretha et al. 2012). Ultrasound-assisted extraction aims to increase extraction efficiency with the help of sound waves during extraction processes. Many studies on extraction methods, solvent types, extraction times, and temperatures are available in the literature. Several of these studies examined the extraction yield, and several examined the extraction efficiency via total phenolic (TPC) and/or flavonoid (TFC) contents. Some studies include evaluations of the extraction of specific components (Özdal et al. 2023). Increasing the number of studies in which different solvents, temperatures, times, extraction methods, and their combinations are optimized will benefit both scientific and industrial users in eliminating deficiencies in this field. This study aimed to optimize the process parameters of three basic extraction methods (maceration, reflux, and ultrasound-assisted) for producing chestnut propolis ethanolic extracts. For this purpose, the response surface methodology was used, and the bioactive qualities of the optimized chestnut propolis extracts obtained were compared.

2. Material and Methods

2.1. Materials

Chestnut propolis samples were obtained from the apiaries of the Azdavay, Bozkurt, Cide, Doğanyurt, İnebolu and Küre districts, which include the borders of the Kastamonu chestnut forest region, during the 2021 harvest period, through the Kastamonu Beekeepers Association. The raw propolis samples were divided into small pieces and milled into powder then kept in a deep freezer at -18 °C until extraction.

2.2. Chemicals

1,1-Diphenyl-2-picrylhydrazyl (DPPH) and Folin–Ciocalteu's reagent were obtained from Sigma-Aldrich Co. (Munich, Germany). Acetonitrile, sodium carbonate, ethanol and methanol were supplied by Merck KGaA (Darmstadt Germany). All phenolic standards as pure HPLC grade were purchased Sigma-Aldrich Co. (Munich, Germany).

This study consisted of 3 stages: optimization of the extraction conditions according to the experimental design, validation of the optimization results and characterization of the extracts which were produced at optimum extraction conditions.

2.3. Optimization of the extraction conditions

Experimental design: The ethanol concentration, extraction time, and temperature parameters were chosen as three independent variables. Antioxidant Activity (AA) (inhibition %) and TPC (mg GAE/100 mL) were two dependent variables. Response surface methodology (RSM) – The central composite rotatable design (CCRD) desirability function was used to evaluate the effect of the three independent factors on the two responses (Design Expert 7.0.0, Stat-Ease, Inc., Minneapolis, MN, USA). The experimental design involved 13 design points for maceration, 20 for reflux, and 20 for ultrasound-assisted extraction, including three replicates of the central point. Probability values (P) at a 95% confidence level were used to determine the significance and effectiveness of the response. Lack of fit test and Analysis of variance (ANOVA) was carried out using the software. For reflux extraction, a temperature of 70 °C and a duration of 2 hours have been recommended (Cottica et al. 2011; Abduh et al. 2023). Studies in the literature show that for maceration, a wide range from 3 hours to 7 days has been used. For ultrasound-assisted extraction, an average duration of 30 minutes has been suggested. While the generally accepted ethanol concentration for propolis extraction is 70% absolute ethanol (Pobiega et al. 2019), studies in the literature report concentrations ranging from 50% to 98% (Kim et al. 2009; Margeretha et al. 2012; Kara et al. 2022). The selection of minimum and maximum variable ranges for the extraction parameters of all three methods in this study was based on data from the literature. The experimental levels of independent variables were given in Table 1.

According to the experimental design of each extraction method, the ethanol concentration was applied. The mixture of ethanol and propolis was homogenized (Ultra-Turrax IKA T25, Staufenim Breisgau, Germany) at 10000 rpm for 30 s. Then, the extraction time and temperature parameters were applied according to the design. After centrifugation (Nüve, Germany) at 10000 rpm for 5 min, the extracts were filtered and stored at + 4 °C.

Maceration extraction: Propolis (5 g) was extracted with 50 mL of ethanol for 6-72 hours (at 25 ºC) at concentrations (50-90% v/v) specified in the experimental design, with periodic mixing at room temperature.

Reflux extraction: Propolis (5 g) was extracted with 50 mL of ethanol for 10-160 min at various temperatures (30-90 °C) and concentrations (50-90% v/v) specified in the experimental design.

Ultrasound-assisted extraction: Propolis (5 g) was extracted in an ultrasonic bath (Mikrotest, MUB12, Türkiye) (Operating frequence 28 KHz; dimension: 255*310*400 mm) with 50 mL of ethanol for 5-60 min at various temperatures (30-70 °C) and concentrations (50-90% v/v), as specified in the experimental design.

Table 1- The experimental levels of independent variables

Independent variables	*Levels*				
	-1.414	-1	0	+1	+1.414
Ethanol conc. (%)	**50**	55.86	**70**	84.14	**90**
Extraction time (hour)	**6**	15.67	**39**	62.33	**72**

a

Independent variables	*Levels*				
	-1.681	-1	0	+1	-1.681
Ethanol conc. (%)	**50**	58.11	**70**	81.89	**90**
Extraction time (min)	**10**	40.40	**85**	129.60	**160**
Temperature (°C)	**30**	42.16	**60**	77.84	**90**

b

Independent variables	*Levels*				
	-1.681	-1	0	+1	+1.681
Ethanol conc. (%)	**50**	58.11	**70**	81.89	**90**
Extraction time (min)	**5**	16.15	**32.50**	48.85	**60**
Temperature (°C)	**30**	38.11	**50**	61.89	**70**

c

** a: Maceration extraction, b: Reflux extraction, c: Ultrasound-assisted extraction methods*

2.4. Validation of the optimization results

Validation was performed by triplicate extraction under optimum conditions for each method. The average values of the responses were calculated. The estimated values from the model and averages were compared by using one-sample *t*-test. The lack of a statistically significant difference ($P>0.05$) between the results obtained from the validation test indicated that the model obtained via optimization was experimentally successful.

2.5. Analysis methods

2.5.1. Total phenolic content (TPC)

TPC of the propolis extracts was determined according to the Folin–Ciocalteu assay (Shahidi & Naczk 1995). Briefly, 0.5 mL of Folin–Ciocalteu's reagent (0.2 N) was added to 0.1 mL of extract (100 times diluted with ethanol). Then mixing the tube using a vortex, 0.4 mL of Na_2CO_3 solution and 4 mL of distilled water were added to the reaction mixture.

The absorbance readings were taken at 760 nm after incubation at room temperature for 1 hour using a UV–VIS spectrophotometer (Shimadzu Corporation, Japan) against the blank prepared using ethanol instead of extracts. Results were

expressed as gallic acid equivalent (mg GAE/100 mL) using the calibration curve [concentration = (Abs + 0.041)/0.002] obtained using gallic acid standard solutions.

2.5.2. Antioxidant activity

The antioxidant activity (inhibition %) of the propolis extracts was determined using the 2,2-diphenyl-1-picrylhydrazyl (DPPH) radical scavenging procedure. 1500 µL of DPPH solution was added to 75 µL of diluted (100 times) extracts, and the mixture was vortexed. After the mixture was incubated for 30 min, the absorbance readings were taken at 517 nm using a UV–VIS spectrophotometer. Inhibition % value was calculated with the following equation:

$$\text{Inhibition \%} = [\ 1 - (\frac{Abs\ Sample}{Abs\ Control})]*100 \quad (1)$$

2.5.3. Phenolic compounds

Phenolic content analysis was performed on a reversed-phase (RP) column. HPLC-PDA was carried out according to a validated method using 25 polyphenols (Kara et al. 2022). The ethanolic propolis sample was concentrated using the diethyl ether/ethyl acetate liquid–liquid extraction technique and subsequently passed through a C18 column (20 µL). For HPLC analysis (Shimadzu Corporation LC 20AT), a gradient phase was applied using 70–30% acetonitrile-ultrapure water and 2% acetic acid-ultrapure water mobile phases. The column oven temperature was 30 °C, and the mobile flow rate was 1.0 mL/min. Results were expressed as µg standard phenolic substance per mL extract sample.

2.5.4. Volatile compounds

Head-space solid-phase microextraction (SPME) method was used to determine the volatile compounds. The homogenized propolis extract was placed in a 125 mL flask with a magnetic stirring bar to extract the volatile compounds. The flask was then sealed with silicone septa and immersed in a water bath at 50 °C. After 5 min of equilibration, a 65 mm DCP (divinylbenzene/carboxen/polydimethylsiloxane (DVB/CAR/PDMS) fiber was exposed to the sample headspace for 15 min. The sample was stirred continuously using a magnetic stir bar throughout the extraction process. After extraction, the fiber was placed into the injector port of a gas chromatograph for 5 minutes to desorb volatiles thermally. The volatile compounds were identified and quantified with a gas chromatograph coupled to a quadrupole mass detector (Shimadzu GCMS QP 2010 Ultra, Japan). Volatile compounds were separated on an RXİ-5MS capillary column (30 m; 0.25 mm; 0.25 μm). Helium was used as the carrier gas with a flow rate of 1 mL/min (pressure: 100 kPa). The injector temperature was set at 250 °C. The oven temperature program was held for 5 min at 50 °C, after which the temperature was increased by 5 °C/min to 270 °C. The temperature was maintained at 270 °C for 5 minutes, resulting in a total runtime of 54 minutes. The mass detector operated at 250 °C in scan mode with electron impact ionization (ion source temperature: 200 °C).

2.5.5. Mineral contents

The mineral content of the samples was assessed using a microwave-assisted nitric acid digestion procedure (CEM MARS6, USA) followed by analysis with inductively coupled plasma–optical emission spectrometry (ICP–OES) (Spectro Blue, Germany). Approximately 1 mL of each sample was mixed with 1 mL of H_2O_2 (30% v/v) and 10 mL of HNO_3 (67% v/v) in PTFE flasks. The digestion program included heating to 200 °C for 15 min, followed by a 15-min hold at 200 °C. After cooling to room temperature, the solutions were transferred to 50 mL polyethylene flasks and diluted with ultrapure water. The digested samples were filtered through microfilters and analyzed by ICP–OES (Al Khalifa & Ahmad 2010). Calibration standards were prepared using a multi-element standard stock solution (Merck, Germany). All measurements were performed in triplicate.

2.5.6. Statistical analysis

Analysis of variance (ANOVA) (IBM SPSS 1.0.0.781) was used to statistical evaluation of the results. After optimization, the obtained results were validated experimentally. For comparison ($P<0.05$) of the results, one-sample *t*-test (SPSS 17.0.1, Chicago, IL, USA) was used. The data were given as the mean ± standard deviation.

3. Results

3.1. Optimization of extraction parameters

Based on the experimental design, the software subsequently analyzed the results of the AA and TPC values. “Lack of fit” and “Sequential model sum of squares” tests were carried out (Table 2) for AA and TPC. R-squared (R^2), adjusted R^2, and the standard deviation were calculated for each function. After a comparison of the values subsequently, the suggested functions were ascertained.

Table 2- Statistical parameters of optimization; P values for model selection and lack of fit tests; model and independent variable factors; variance analysis results of functions (a); Selected solutions determined by desirability function and comparison of the results obtained from optimum point verification tests with the estimated values from model (b)

Statistical parameters		*Maceration extraction*		*Ultrasound-assisted extraction*		*Reflux extraction*	
		TPC	***AA***	***TPC***	***AA***	***TPC***	***AA***
Model selection and lack of fit test	Quadratic	**0.0277**	**0.0006**	**0.0104**	**0.0073**	**0.0037**	**0.0002**
	Lineer	0.1147	0.0075	0.0216	0.0199	0.2144	0.0501
	Cubic	0.1658	0.3557	0.3172	0.4388	0.1861	0.0876
	Lack of fit	0.1497	0.6065	0.3738	0.3976	0.1093	0.0676
Model and independent variable factors	Model	**0.0294**	**0.0001**	**0.0077**	**0.0055**	**0.0098**	**0.0002**
	A-Ethanol conc.	**0.0130**	**<0.0001**	**0.0084**	**0.0011**	**0.0496**	**0.0007**
	B-Extraction time	0.6552	0.3173	**0.0106**	**0.0207**	0.5489	0.1657
	C-Temperature	-	-	**0.0465**	0.6566	**0.0199**	**0.0006**
	AB	0.3297	0.1202	0.1725	0.2570	0.2064	0.6488
	AC	-	-	0.5199	0.4636	0.2239	0.0067
	BC	-	-	0.7049	0.4530	0.1997	**0.0311**
	A^2	**0.0316**	**0.0019**	**0.0054**	0.0022	**0.0008**	**<0.0001**
	B^2	0.0933	**0.0023**	0.1035	0.0366	0.3890	0.6390
	C^2	-	-	**0.0243**	0.7046	0.1104	**0.0309**
R^2		0.78	**0.96**	0.83	0.84	0.82	**0.92**
Adjusted R^2		0.62	0.93	0.67	0.70	0.65	0.86
Variation coefficient (%)		11.81	3.98	10.17	8.82	12.11	7.04

**TPC: Total phenolic content, AA: Antioxidant activity; ** The values P<0.05 are statistically significant*

(a)

Extraction type	*Independent factors*			*AA (%)*	*TPC (mg/100 mL)*
	A (%)	*B (time)*	*C (℃)*		
Maceration	78.46	71.05 (h)	-	84.16	980.39
Reflux	80.64	117.44 (min)	38.38	79.76	788.55
Ultrasound-assisted	82.49	59.12 (min)	40.53	80.68	695.91

(b)

Extraction type	*Response*	*Estimated value*	*Average experimental result**	*Difference*	*P-value**
Maceration	AA	84.16	88.61 ± 2.05^{A}	-4.45	0.275
	TPC	980.39	977.5 ± 4.11^{a}	-2.89	0.610
Reflux	AA	79.76	79.50 ± 1.95^{AB}	+0.26	0.916
	TPC	788.56	917.5 ± 11.02^{b}	+128.94	0.054
Ultrasound-assisted	AA	80.68	75.22 ± 2.17^{B}	-5.46	0.241
	TPC	695.91	812.5 ± 10.18^{c}	+116.59	0.055

** Average ± standard deviation; Values P<0.05 indicate statistical significance*
AA: Antioxidant activity; TPC: Total phenolic content; A: Ethanol concentration; B: Extraction time; C: Temperature

The quadratic function was accepted for AA and TPC for all extraction methods (P<0.05). 'Lack of fit' was not significant (P>0.05) for both properties. The influence of the ethanol concentration, which is one of the independent factors on the TPC and AA, was statistically significant (P<0.05) for all extraction types. However, the influence of extraction time was statistically significant (P<0.05) for only ultrasound-assisted extraction. The temperature factor had a statistically significant effect (P<0.05) on the TPC for reflux and ultrasound-assisted extractions and AA for only ultrasound-assisted extraction. The model was approved to be statistically significant (P<0.05) for all the extraction types and responses. The results of the ANOVA for the quadratic function were presented in Table 2. Final equations were coded with the following factors:

For maceration extraction;

$TPC= +768+104.07*A+14.66*B+46.59*AB-90.32*A^2 + 65.49B^2$
$AA= +67.84+9.59*A+1.03*B+2.38*AB-4.92*A^2 + 4.76B^2$

For ultrasound-assisted extraction;

$TPC=+621.74+48.87*A+46.85*B-33.92*C+28.67*AB-13.01*AC-7.61*BC-51.44*A^2-26.04*B^2 - 38.53*C^2$
$AA=+74.51+7.31*A+4.45*B-0.74*C+2.55*AB+1.61*AC-1.65*BC-6.44*A^2-3.80B^2 +0.62*C^2$

For reflux extraction;

$TPC=+710.94+46.38*A-12.89*B-57.50*C+36.68*AB-35.19*AC-37.27*BC-95.80*A^2-18.21*B^2-35.42*C^2$
$AA=+70.32+5.69*A-1.78*B-5.88*C+0.73*AB-5.29*AC-3.89*BC-8.21*A^2-0.56*B^2-2.90*C^2$

Figure 1a shows the response of the interaction effect of the ethanol concentration and extraction time on the AA concentration (a) and on the TPC (b) for maceration extraction. AA and TPC increased with increasing ethanol concentration. However, both responses tended to decrease after the central point with increasing ethanol concentration. The opposite was true for the extraction time.

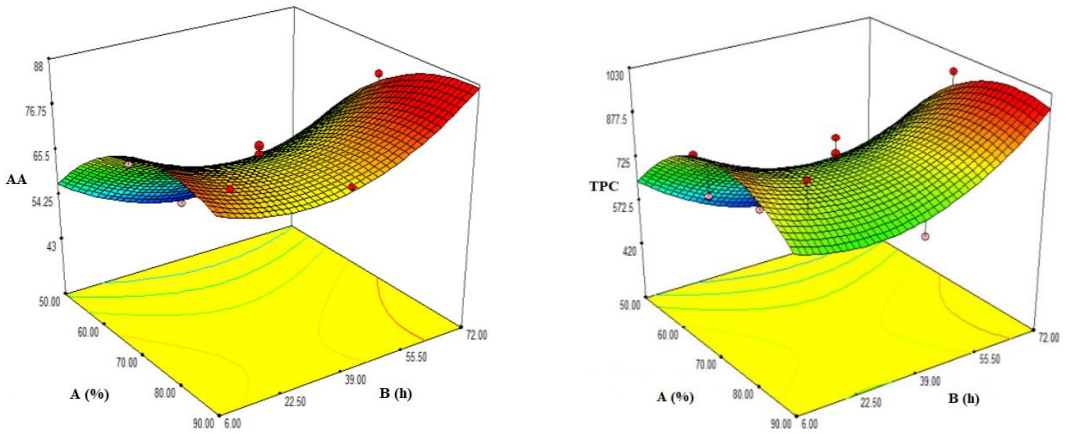

(a)

The TPC and AA exhibited quadratic functions for ultrasound-assisted extraction. Figure 1b shows the response of the interaction effect on the ethanol concentration (A), extraction time (B), and temperature (C) on AA (a) and the TPC (b) for ultrasound-assisted extraction. AA and TPC increased with ethanol concentration, extraction time, and temperature. However, both responses tended to decrease after the central point with increasing independent factors (except for temperature for AA).

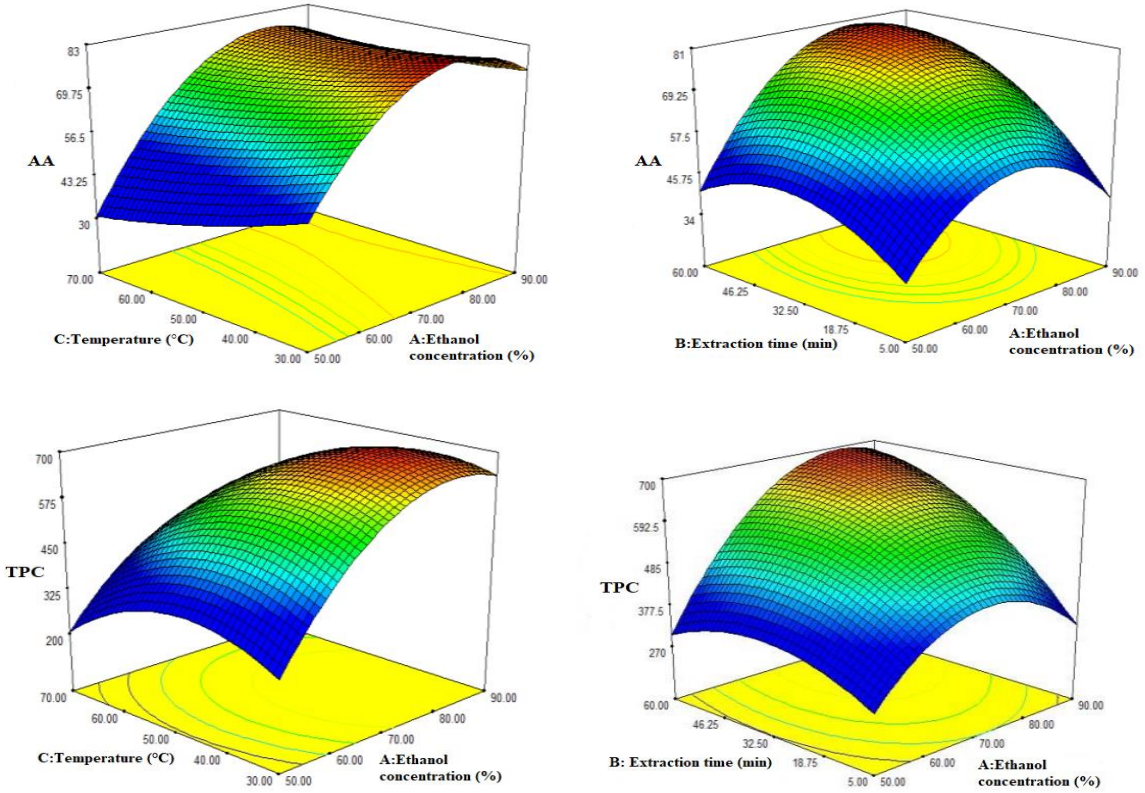

(b)

The TPC and AA exhibited a quadratic function for reflux extraction. Figure 1c shows the response of the interaction effect of ethanol concentration (A), extraction time (B), and temperature (C) on the AA concentration (a) and on the TPC (b) for reflux extraction. AA and TPC increased with increasing ethanol concentration and temperature. However, both responses tended to decrease after the central point with the increase in both independent factors. The opposite trend was observed for the extraction time.

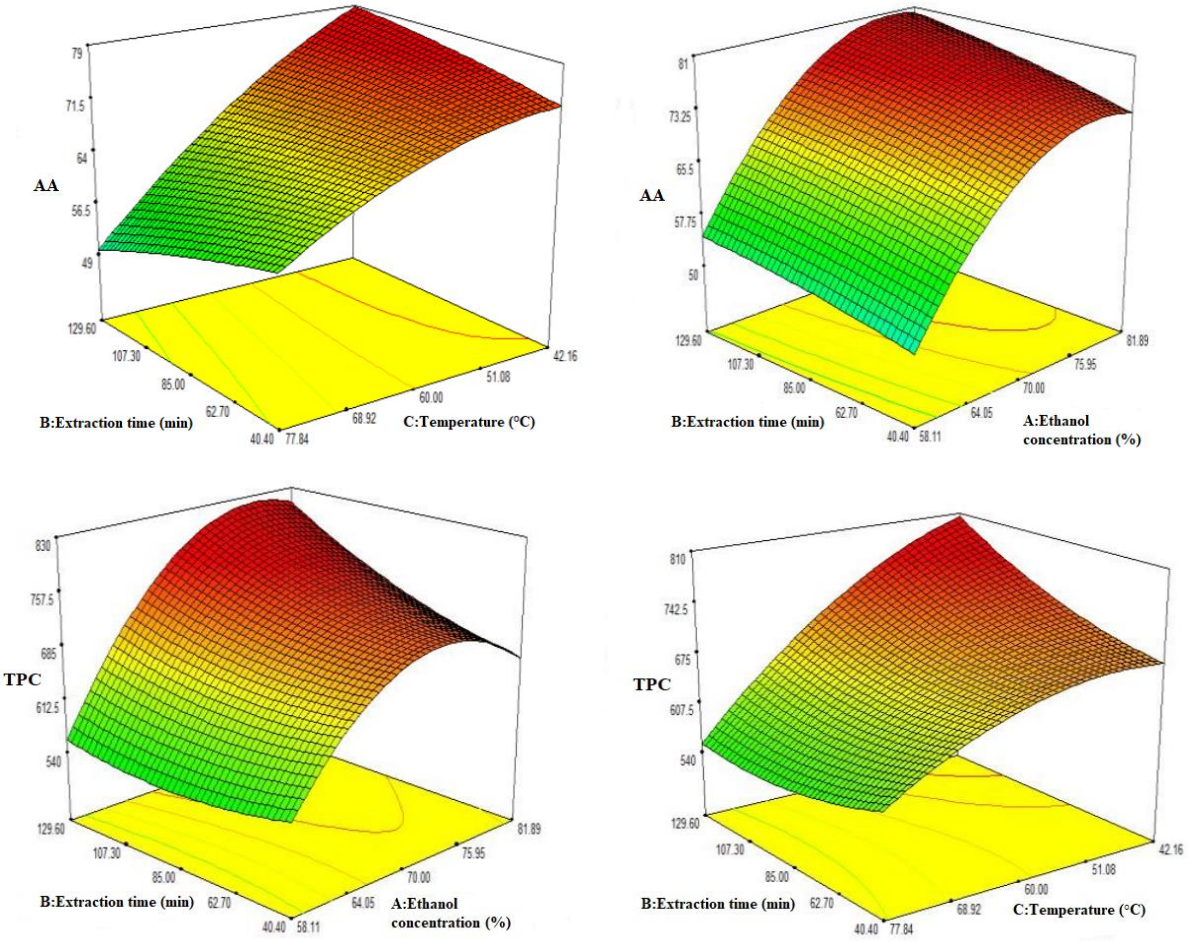

(c)

Figure 1- Response surface plots showing the mutual effects of the ethanol concentration (A), extraction time (B) and temperature (C) on the AA concentration and TPC for maceration (a), ultrasound-assisted extraction (b) and reflux extraction (c)

The AA and TPC were evaluated according to the desirability function which was based on the idea that the ‘‘quality’’ of a product or process has multiple quality characteristics. The first solution had a desirability value (100%) from the suggested solutions by the software. This solution was selected as the optimum point and applied in the study (Table 2b).

3.2. Experimental validation of the optimization results

The optimized levels given in Table 2b were used for the preparation of the extracts in triplicate. The AA and TPC contents of the optimized extracts were analyzed for all extraction types, and the average values of the results were determined. Whether there was a statistically significant ($P<0.05$) difference between the average and estimated values from the model by applying the one-sample *t*-test, was evaluated. One-sample *t*-test results for each response were given in Table 2b. There was not detected any statistical significance ($P>0.05$) between the results obtained from the validation test. This result indicates that the model obtained via optimization was experimentally successful.

3.3. Characterization of optimized chestnut propolis extracts

The propolis extracts produced by the optimized extraction models were compared in terms of bioactive properties, volatile compounds, and mineral contents.

3.3.1. Bioactive properties

TPC and AA values of the chestnut propolis extracts obtained by maceration, reflux and ultrasound-assisted extraction optimization are shown in Table 2b. The highest TPC and AA were achieved by maceration extraction ($P<0.05$).

In this study, the phenolic compounds in optimized chestnut propolis extracts obtained by three extraction methods were characterized via RP-HPLC-PDA. Chromatograms were presented in the Supplementary Material file, and the results were given in Table 3.

Among 25 phenolic substances, chlorogenic acid, protocatechuic acid, epicatechin, m-OH benzoic acid, syringic acid, routine, myricetin, resveratrol, daidzein, luteolin, rhamnetin, and curcumin could not be detected in any chestnut propolis extract in the present study. Gallic acid was detected only in samples prepared by reflux and ultrasound-assisted extraction. Chrysin, a flavone, was determined to be the most abundant compound, followed by pinocembrin. In addition, chestnut propolis extracts were rich in other phenolics, such as ferulic acid, ellagic acid, and caffeic acid phenyl ester (CAPE). The extract obtained by maceration had a higher content of polyphenols, especially CAPE.

Table 3-Phenolic compounds in chestnut propolis extracts identified via HPLC

	Maceration extraction		*Reflux extraction*		*Ultrasound-assisted extraction*	
	µg phenolic/mL	*Retention time*	*µg phenolic/mL*	*Retention time*	*µg phenolic/mL*	*Retention time*
Phenolic acids (%)	51.62		52.19		51.21	
Gallic acid	-		4.47	7.24	4.67	7.10
Protocatechuic acid	-		-		-	
Chlorogenic acid	-		-		-	
p-OH benzoic acid	6.63	16.13	7.15	15.57	6.23	15.45
m-OH benzoic acid	-		-		-	
Ellagic acid	432.40	19.70	416.04	19.27	400.67	19.22
p-coumaric acid	194.36	19.98	174.40	19.51	216.03	19.43
Ferulic acid	453.41	20.74	412.56	20.29	424.05	20.23
CAPE	292.89	43.08	263.70	42.18	283.46	42.44
Caffeic acid	210.72	17.17	190.69	16.64	208.94	16.52
Syringic acid	-		-		-	
t-cinnamic acid	117.87	28.02	106.72	27.41	111.90	27.35
Flavonoids (%)	48.38		47.81		48.79	
Flavonol						
Rhamnetin	-		-		-	
Quercetin	32.03	26.43	31.87	25.83	31.94	25.74
Rutin	-		-		-	
Myricetin	-		-		-	
Flavan–3–ols						
Epicatechin	-		-		-	
Flavones						
Chrysin	763.85	41.76	668.45	40.83	764.67	41.07
Daidzein	-		-		-	
Apigenin	41.11	30.17	38.40	29.43	38.69	29.41
Luteolin	-		-		-	
Flavanones						
Pinocembrin	740.35	42.60	687.05	41.66	726.41	41.9
Hesperetin	23.96	30.76	17.88	30.05	15.87	30.02
Nonflavonoid polyphenols						
Resveratrol	-		-		-	
Curcumin	-		-		-	

3.3.2. Identification of volatile compounds

The volatile compounds in the optimized chestnut propolis extracts identified via the SPME-GC/MS method were listed in Table 4.

Table 4- Volatile compounds identified in optimized chestnut propolis extracts

Compound type	*Compound*	*Maceration extraction (%)*	*Reflux extraction (%)*	*Ultrasound-assisted extraction (%)*
Benzene derivative	Styrene	-	-	0.20
Monoterpene	Trisiklen	0.23	-	0.24
Monoterpene	cis-Ocimene	47.40	36.02	-
Monoterpene	.Δ.3-Carene	-	-	60.94
Monoterpene	Kampen	2.56	0.83	1.42
Monoterpene	Verbenene	-	-	0.48
Aromatic aldehyde	Benzaldehyde	0.25	0.42	0.47
Monoterpene	Pinen	5.27	3.4	5.67
Hydrocarbon	Decane	4.73	3.47	4.43
Aliphatic hydrocarbon	Limonen	7.69	4.05	4.27
Aromatic alcohol	Benzyl alcohol	-	1.12	-
Other	p-Cresol	0.48	0.64	0.18
Alcohol	Farnesol	0.29	-	-
Aromatic hydrocarbon	Undecane, 5-methyl-	0.36	-	-
Carboxylic acid and esters	Benzoic acid	0.91	0.42	0.62
Aromatic hydrocarbon	Dodecane	2.47	1.17	2.21
Other	Bornyl acetate	-	-	0.22
Phenolic monoterpenoid	Carvacrol	4.58	2.21	2.23
Phenol	Eugenol	2.79	1.61	2.07
Sesquiterpenoid	Ylangene	-	-	1.03
Sesquiterpene	α-Cubebene	1.04	0.48	0.75
Sesquiterpene	α-Copaene	2.37	1.01	1.91
Sesquiterpene	Longifolene	0.44	-	0.44
Sesquiterpene	Caryophyllene	1.17	1.14	1.74
Sesquiterpene	Germacrene	0.47	0.38	0.51
Phenylpropene	trans-Isoeugenol	-	-	0.19
Sesquiterpene	α--Humulene	-	-	0.40
Phenol	Phenol, 2-methoxy-3-(2-propenyl)-	1.04	-	-
Sesquiterpene	Amorphene	1.89	0.64	0.94
Sesquiterpene	β.-Selinene	-	-	0.14
Sesquiterpene	α--Guaiene	1.32	-	-
Sesquiterpene	Muurolene	-	-	0.54
Sesquiterpene	Bisabolene	0.37	-	0.30
Sesquiterpene	Cadinene	0.83	0.62	0.51
Fatty acid	Myristic acid	-	3.17	-
Fatty acid	Pentadecylic acid	-	2.43	-
Ketone	Cyclopentadecanone, 2-hydroxy-	-	9.44	-
Fatty acid	Palmitic acid	-	7.69	-
Fatty acid	Oleic acid	-	3.79	-
Fatty acid	Stearic acid	-	0.48	-
Fatty acid	Arachidic acid	-	2.89	-
Other	Naphthalene, 1,2,3,5,6,8a-hexahydro-4,7-dimethyl-1-(1-methylethyl)-, (1S-cis)-	1.10	-	1.24
Other	Alloaromadendrene oxide-(1)	0.19	-	0.22
Sterol	Amyl acetate	0.43	-	-
Triterpene	Squalene	6.00	5.86	3.49
Other	Cyclooctasiloxane, hexadecamethyl-	0.43	-	-
Sterol	Stigmast-5-en-3-ol, (3.beta.)- (CAS)	0.86	-	-

The GC-MS analysis of propolis extracts revealed approximately 40 peaks, suggesting a variety of compounds. According to Table 4, these compounds are categorized into several classes: hydrocarbons, terpenoids, diterpenoids, triterpenoids, and phenols. Terpenoids were the most prevalent class among them. Among these compounds, cis-ocimene was dominant in the maceration (44.05%) and reflux (36.02%) extraction samples, while Δ-3-carene (56.60%) was predominant in the ultrasound-assisted propolis extract. A total of 47 compounds were detected in the SPME extracts isolated from the samples. Based on the results of this study, various volatile aromatic compounds, ranging from 26 to 31 in number, were determined in each extracted propolis sample.

3.3.3. Mineral composition

This study determined the concentrations of 13 individual elements (Pb, Cd, Zn, Cu, Ni, Fe, Mn, Cr, Al, P, Na, Ca, and K) in chestnut propolis extracts using ICP–OES. Heavy metals and other elements demonstrated a heterogeneous distribution in propolis extracts (Table 5).

Table 5- Mineral contents of optimized chestnut propolis extracts

	Trace elements (ppm)								
	Al	***Cr***	***Mn***	***Fe***	***Ni***	***Cu***	***Zn***	***Cd***	***Pb***
M	-	0.055±6.631^{A}	0.148±3.354^{A}	0.676±10.929^{B}	0.048±10.479^{B}	-	0.150±4.779^{B}	-	0.806±5.326^{B}
R	0.203±8.520	-	0.147±2.601^{A}	2.710±9.481^{A}	-	-	0.569±9.979^{A}	-	1.361±7.447^{A}
U	-	0.070±2.713^{B}	0.093±0.432^{B}	0.422±2.259^{C}	0.071±2.647^{A}	-	0.167±2.426^{B}	-	0.941±2.284^{B}

(a)

Macro elements (ppm)			
P	***Na***	***Ca***	***K***
7.386±33.971^{A}	12.750±0.141^{A}	10.750±0.070^{B}	78.550±417^{A}
7.998±36.452^{A}	12.625±0.368^{A}	49.250±0.043^{A}	-
6.160±60.032^{B}	11.400±0.062^{B}	7.000±0.071^{C}	56.800±0.317^{B}

(b)

*-: Non-determined; * Different letters (A-C) in the same column indicate the statistical significance (P<0.05) of the difference between extraction methods*
**M: Maceration extraction, R: Reflux extraction, U: Ultrasound-assisted extraction

Generally, the element levels detected in reflux extraction were the highest. While the K content was found to be highest after maceration (78.55 ppm) and ultrasound-assisted extraction (56.80 ppm), K could not be detected after reflux extraction. Conversely, Ca was found at the highest concentration (49.25 ppm) by the reflux method, whereas it was found at lower and similar concentrations (10.75-7.00 ppm) during maceration and ultrasound-assisted extraction. P and Na were detected via all the extraction methods. P and Na were found at similar concentrations (P>0.05) via maceration and reflux extraction and at lower concentrations (P<0.05) via ultrasound-assisted extraction. Cu and Cd could not be detected by any of the three methods. While the Al content was determined via reflux extraction, Ni and Cr could not be detected. Mn was found at similar concentrations (0.148-0.147 ppm) in chestnut propolis extracted by maceration and reflux extraction methods but at a concentration of 0.093 ppm for ultrasound-assisted extraction. Fe, Zn, and Pb were detected via all three methods, with concentrations being higher for the reflux extraction method compared to the other methods.

4. Discussion

Phenolic compounds, which are secondary metabolites of plant origin and are found in many natural products, are agents responsible for AA. In this study, the highest TPC and AA were achieved by maceration extraction. Maceration is one of the most commonly used traditional methods for extracting the active components of propolis. A study comparing maceration, soxhlet, and ultrasound-assisted extraction methods revealed that the extracts obtained with the 5-day maceration method provided the highest TPC (Zin et al. 2018). Conditions such as solvent type and extraction time also affect the extraction efficiency and final product properties. In a study conducted by Mokhtar et al. (2019), have been reported that the use of ethanol as a solvent in maceration extraction resulted in higher phenolic and flavonoid contents than did the use of water. The chemical composition and bioactivity of propolis vary according to seasonality, the flora of the region where hives are located, dominant botanical origin, bee species, and extraction types and parameters (Calegari et al. 2020).

At least 300 different propolis compounds have been identified; their biological activities are attributed mainly to phenolic components, such as flavonoids (flavonols, flavones, flavonones, dihydroflavonols, and chalcones); aromatic aldehydes; terpenes; alcohols; and beta-steroids. Phenolic compounds have biological activities, such as antioxidant potential, because they have hydroxyl groups and aromatic compounds in their chemical structures (Calegari et al. 2020). Chromatographic analyses are the most frequently used methods for determining phenolic substances in propolis. In this study, the phenolic compounds in optimized chestnut propolis extracts obtained by three extraction methods were characterized via RP-HPLC-PDA. In this study, 12 of the 25 phenolic substances were not detected in any extract.

According to different studies, the main phenolic compounds identified in propolis are hydroxycinnamic acids, hydroxybenzoic acid, chrysin, galangin, pinocembrin, quercetin, apigenin, ferulic acid, luteolin, cinnamic acid, benzoic acid, flavones, flavonols, and flavanones (Calegari et al. 2020; Woźniak et al.2020). Several studies have shown that the ethanol ratio in the solvent affects the phenolic composition of propolis extracts. While the phenolic acid content is high in solvents with high water content, no significant change is observed in solvents containing 70% or more ethyl alcohol (Kara et al. 2022). The ethanol rates (%) determined due to the optimization of all three extraction methods were very close in this study. Accordingly, it was determined that there was no significant difference in terms of the distribution of phenolic compounds. Additionally, gallic acid was found only in samples prepared by reflux and ultrasound-assisted extraction in the study. Kara et al. (2022) reported that the ethanol content is an effective parameter for determining the gallic acid content during propolis extraction. They detected gallic acid and protocatechuic acid in all extraction methods for solvents containing only 0% and 20% ethanol. When the general phenolic constituents of the optimized chestnut propolis extracts were evaluated, chrysin, a flavone, was determined to be the most abundant compound, followed by pinocembrin. A study comparing the antioxidant activities and phenolic compositions of propolis samples extracted under different extraction conditions and ethanol concentrations revealed caffeic acid as the main component in samples prepared with solvents containing 0-40% ethanol. Chrysin and pinocembrin were identified as the main components in extracts containing 60% ethanol or higher (Kara et al. 2022). In another study comparing lactic acid and ethanol solutions for propolis extraction, it was found that the Chrysin and naringenin were found as the most abundant phenolic compounds in the initial samples (Atayoglu et al. 2023)

In addition, chestnut propolis extracts were rich in other phenolics, such as ferulic acid, ellagic acid, and caffeic acid phenyl ester (CAPE). Propolis samples containing CAPE were reported to exhibit stronger radical scavenging activity (Sulaiman et al. 2014). In this study, the extract obtained by maceration had a higher content of polyphenols, especially CAPE. It was also determined to be the sample with the highest antioxidant activity (inhibition %).

The beneficial biological activities of propolis, such as antimicrobial, anti-inflammatory, anti-ulcer, and anti-cancer properties, are closely related to its bioactive compounds. Flavonoids are effective against various bacteria and protect against ulcers (Ruiz-Hurtado et al. 2021). Chrysin, which was detected in the highest amount in the chestnut propolis extracts in this study, is known to have anti-inflammatory and antineoplastic effects and functions as an important antioxidant and hepatoprotective agent (liver protector) (Shahbaz et al. 2023).

According to the Turkish Food Codex Bee Products Communiqué (Anonymous 2021), published as a draft by the Ministry of Agriculture and Forestry, "propolis extracts must contain at least 8 of the 20 phenolic compounds (ferulic acid, pinobanksin 3-acetate, chrysin, cinnamic acid, galangin, pinocembrin, kaempferol, caffeic acid, p-coumaric acid, benzoic acid, quercetin, artepilin C, rutin, catechol, naringenin, myricetin, hesperidin, apigenin, chlorogenic acid and CAPE) and at least 1 mg/L or 1 mg/kg." In this study, chestnut propolis extract prepared by maceration as a result of optimization contained 11 phenolic components specified in the draft communique, and extracts prepared by refluxing and ultrasound-assisted extraction methods contained 12 components. The optimized extracts met the requirements of draft communique limits.

The volatile compounds of propolis strongly depend on the bee species, the botanical flora at the collection site, and the solvents used in the extraction of propolis. The compounds identified in the propolis volatile fraction represent one of the primary botanical sources of propolis. Due to their flavour and biological activity, volatile compounds in propolis are beneficial for chemical characterization. The compounds detected in the extracts were categorized as hydrocarbons, terpenoids, diterpenoids, triterpenoids, and phenols in Table 4. Among these, terpenoids are the most prevalent due to their nature as volatile organic compounds. Therefore, GC–MS is the best method for their detection. Hydrocarbons are also volatile, but most of those found in propolis can be detected at moderate levels because they are long chains. In this study, the extraction method affected the detection of fatty acids (such as oleic, stearic, and palmitic acids), which were determined mainly via the reflux method. The flavonoid and phenol classes of compounds were the least common (Table 4).

Floral volatile compounds can vary greatly in their prevalence, ranging from widespread to quite rare. Many floral scents are frequently found across various plant families. These volatile compounds are highly effective at attracting pollinators. The most frequently encountered floral volatiles include benzaldehyde, limonene, β-ocimene, and linalool, which are common and dominant components in the floral aromas of numerous species (Farré-Armengol et al. 2017). Among them, ocimene is particularly notable for its significant ecological function due to its prevalence and abundance in floral scents.

β-Ocimene (3,7-dimethyl-1,3,6-octatriene), the chemical formula $C_{10}H_{16}$, is a monoterpenoid with two stereoisomers, cis- and trans-β-ocimene. The trans isomer is more common than the cis isomer. Cis-β-ocimene is less abundant than trans-β-ocimene in floral scents (Farré-Armengol et al. 2017). Since the propolis used in the present study was of chestnut origin, it is thought that the cis-isomer of ocimene is dominant (Table 4). While the percentage of Cis-Ocimen was 44.05% in maceration and 36.02% in reflux extraction samples, it could not be detected in ultrasound-assisted extraction samples.

While styrene was detected with ultrasound-assisted extraction, other methods could not obtain this compound. Stytrene is a benzene derivative and occurs naturally in small amounts in some plants and foods (cinnamon, coffee beans, balsam trees, and peanuts). Δ-3-carene, which constitutes 56.60% of the ultrasound-assisted propolis extract, is a bicyclic monoterpene found in hemp and other plants. Δ-3-carene is a natural component of turpentine. It is found in citrus, cypress, and pine trees and has a sweet, pungent, herbal, and earthy scent. Basil, rosemary, some peppers, and pine and cedar trees also naturally produce Δ-3-carene. Δ-3-carene is found in many plants essential oils and is a popular ingredient in cosmetics, fragrances, and food flavouring agents. Its presence in turpentine also makes it a powerful agent for use as an industrial-strength insect repellent. Δ-3-caren is known to have anti-inflammatory and anti-Alzheimer effects. It is effective against fungal infections and has the potential to improve bone health through increased calcium absorption into bones (Anonymous 2024). Another compound found in optimized propolis extracts obtained by all three methods is benzaldehyde, an important aromatic aldehyde. Its aroma was likened to bitter almond oil. A study on benzaldehyde indicated that it has anticancer effects and potential as an antitumor compound (Saitoh & Saya 2016). It was reported that carvacrol is a phenolic monoterpenoid found in the essential oils of some plants, especially thyme (*Thymus vulgaris*), oregano (*Origanum vulgare*), wild bergamot (*Citrus aurantium bergamia*) and pepperwort (*Lepidium flavum*). Additionally, carvacrol has a wide range of bioactivities, such as anticancer, antimicrobial, and antioxidant activities. The antimicrobial activity of carvacrol is greater than that of other volatile compounds and essential oils due to a phenol moiety, a free hydroxyl group, and hydrophobicity (Sharifi-Rad et al. 2018). Eugenol, primarily derived from clove oil, is a phenolic aromatic compound. Its well-known antibacterial, antiviral, antifungal, anticancer, anti-inflammatory, and antioxidant properties have made it valuable for many years in sectors like cosmetics, medicine, and pharmacology. Additionally, it is recognized as a natural mosquito repellent (Ulanowska & Olas 2021).

Mineral diversity is transferred to the composition of propolis by transferring the mineral composition of the soil to the plants from which propolis is obtained. Therefore, plant sources strongly influence the elemental composition of propolis (Lovakovic et al. 2018). The basic propolis content is used to develop reliable traceability methods and distinctive features of the geographical areas where it is produced to indicate environmental pollution (Golubkina et al. 2016). Propolis is an important food supplement for human nutrition because of its antibacterial, antifungal, antiviral, and antioxidant activities. Therefore, it is crucial to determine propolis's content in terms of essential minerals and heavy metals. In this study, the concentrations of 13 individual elements (Pb, Cd, Zn, Cu, Ni, Fe, Mn, Cr, Al, P, Na, Ca, and K) and heavy metals in chestnut propolis extracts demonstrated a heterogeneous distribution (Table 5). Generally, the element levels detected in reflux extraction were the highest. Parameters such as time, temperature, and applications in propolis extraction impact the elemental distribution and concentrations of the extracts.

A study conducted by Bayram (2020) revealed that K, Ca, Fe, Mg, and Na are the main elements in propolis obtained from Turkey, China, Brazil, and Ethiopia. Similarly, our study found K, Ca, Na, and P as key elements. Acun & Gül (2021) reported the Fe content of chestnut propolis to be 1.53 ppm, which aligns with our findings (0.422-2.71 ppm). While their study found the K content to be 3.11 ppm, our study found it to be in the range of 56.80-78.55 ppm. Another study examined (Arda, 2022) the mineral composition of three different commercial propolis drop products (brands A, B, and C) using the ICP-OES method. It found Ca levels of 9.28-5.53 ppm in samples B and C and Zn levels of 2.09-0.12 ppm in the same samples. Additionally, Cu was detected at 0.79 ppm in sample A but was not found in samples B or C. These findings indicate that the elemental distribution can vary widely in propolis extracts used as food supplements.

5. Conclusions

Various factors, such as region, botanical origin, and bee species, affect the raw propolis content and bioactive properties. However, propolis is not consumed in its raw form; it is consumed in its extract form as an important food supplement due to its bioactive features, such as anti-inflammatory, antimicrobial, and antioxidant properties. For this reason, extraction methods, parameters, and process parameters such as solvents and even contaminants significantly impact the bioactive properties and qualities of the final product.

In this study, three basic extraction methods, namely, maceration, reflux, and ultrasound-assisted methods were optimized, and the bioactive qualities of the obtained extracts were compared. As a result of optimization, similar values were suggested for the ethanol concentration for all three methods (min. 78.46%-max.82.49%). In this case, there was no significant difference between the predicted and validated AA and TPC values. However, considering the recommended times for maceration, reflux, and ultrasound-assisted extraction methods (71.05 h, 117.44 min, and 59.12 min, respectively), ultrasound-assisted extraction may be preferred because of its production process speed and high capacity. The reflux method may be preferred when the time factor is ignored because of the investment cost. On the other hand, the phenolic, volatile, and mineral compositions of the optimized propolis extracts showed varied distributions. Fatty acids were found to be more abundant in extracts obtained via the

reflux method, while phenolic compounds were more prevalent in the maceration method. Based on the results of this study, it was determined that different characteristics of the propolis extract emerged as a result of optimizing the parameters for the three extraction methods. In light of this conclusion, it is recommended to conduct a study where all three extraction methods are used in combination, with their parameters optimized collectively.

Abbreviations	**Full name**
Biological, Chemical and Microbiological	
AA	Antioxidant activity
ANOVA	Analysis of variance
CAPE	Caffeic acid phenyl ester
CCRD	The central composite rotatable design
DPPH	1,1-Diphenyl-2-picrylhydrazyl
DVB/CAR/PDMS	Divinylbenzene/carboxen/polydimethylsiloxane
GAE	Gallic acid equivalent
RSM	Response surface methodology
TPC	Total phenolic content
Instrumental techniques	
GC-MS	Gas chromatography/Mass spectrometry
HPLC	High pressure liquid chromatography
HS/SPME	Head-space/solid-phase microextraction
ICP–OES	Inductively coupled plasma–optical emission spectrometry
UV	Ultraviolet

Funding

This research was supported by Kastamonu University, Scientific Research Projects Coordinatorship with Project Number KÜ-BAP01/2021-14.

References

Abduh M Y, Ramdhani F, Setiawan A, Rifqialdi G, Rahmawati A & Zainudin I M (2023). Determination of productivity, yield and bioactivity of propolis extract produced by *Tetragonula* spp. Cultivated in Modular tetragonula hives. *Heliyon:* 9(6) https://doi.org/10.1016/j.heliyon.2023.e17304

Acun S & Gül H (2021). Usage of microencapsulated pine propolis in cupcake production. *Journal of the Institute of Science and Technology* 11(2): 1205-1217 (in Turkish). https://doi.org/10.21597/jist.855038

Al Khalifa A S & Ahmad D (2010). Determination of key elements by ICP-OES incommercially available infant formulae and baby foods in Saudi Arabia. *African Journal of Food Science* 4(7): 464 – 468

Al Dreini S, Fatfat Z, Abou Ibrahim N, Fatfat M Gali-Muhtasib H & Khalife H (2023). Thymoquinone enhances the antioxidant and anticancer activity of Lebanese propolis. *World Journal of Clinical Oncology* 14(5): 203–214. https://doi.org/10.5306/wjco.v14.i5.203

Anonymous (2021). Turkish Food Codex Bee Products Communiqué (draft), Ministry of Agriculture and Forestry of the Republic of Turkey, https://www.tarimorman.gov.tr/Duyuru/1346/Mevzuat-Taslagi-Turk-Gida-Kodeksi-Ari-Urunleri-Tebligi (24.11.2024).

Anonymous (2024). Delta 3 Carene: The Terpene for Healthy Bones (and Can Cause Cotton mouth), https://leafwell.com/blog/delta-3-carene (24.01.2024)

Arda G (2022). Determination of macro and micro element contents in propolis products by ICP-OES, MSc Thesis, Tekirdağ Namık Kemal University. Tekirdağ

Asem N, Abdul Gapar N A, Abd Hapit N H & Omar E A (2020). Correlation between total phenolic and flavonoid contents with antioxidant activity of Malaysian stingless bee propolis extract. *Journal of Apicultural Research*, 59(4): 437-442. https://doi.org/10.1080/00218839.2019.1684050

Atayoglu A T, Atik D S, Bölük E, Gürbüz B, Ceylan F D, Çapanoğlu E & Palabiyik I (2023). Evaluating bioactivity and bioaccessibility properties of the propolis extract prepared with l-lactic acid: An alternative solvent to ethanol for propolis extraction. *Food Bioscience*, 53: 102756 https://doi.org/10.1016/j.fbio.2023.102756

Bankova V, Trusheva B & Popova M (2021). Propolis extraction methods: A review. *Journal of Apicultural Research*, 60(5): 734-743. https://doi.org/10.1080/00218839.2021.1901426

Bayram N E (2020). A study on free-radical scavenging activity, individual phenolic compounds and element concentration of propolis. *Uludağ Arıcılık Dergisi* 20(2): 145-156 https://doi.org/10.31467/uluaricilik.778751

Calegari M A, Ayres B B, Dos Santos Tonial L M, De Alencar S M & Oldoni T L C (2020). Fourier transform near infrared spectroscopy as a tool for predicting antioxidant activity of propolis. *Journal of King Saud University* 32(1): 784-790. https://doi.org/10.1016/j.jksus.2019.02.006

Cottica S M, Sawaya A C, Eberlin M N, Franco S L, Zeoula L M & Visentainer J V (2011). Antioxidant activity and composition of propolis obtained by different methods of extraction. *Journal of the Brazilian Chemical Society* 22: 929-935. https://doi.org/10.1590/S0103-50532011000500016

Do Nascimento Araújo C, Mayworm M A S, Yatsuda R, Negri G, Salatino MLF, Salatino A & Campos G B (2020). Chemical composition and antimycoplasma activity of a brown propolis from southern Brazil. Journal of Food Science and Technology 57(11): 4228–4235. https://doi.org/10.1007/s13197-020-04461-y

El-Guendouz S, Lyoussi B & Miguel M G (2019). Insight on propolis from mediterranean countries: chemical composition, biological activities and application fields. *Chemistry & Biodiversity* 16(7): e1900094. https://doi.org/10.1002/cbdv.201900094

Farré-Armengol G, Filella I, Llusià J & Peñuelas J (2017). β-Ocimene, a key floral and foliar volatile involved in multiple interactions between plants and other organisms. *Molecules* 22(7): 1148. https://doi.org/10.3390/molecules22071148

Golubkina N A, Sheshnitsan S S, Kapitalchuk M V & Erdenotsogt E (2016). Variations of chemical element composition of bee and beekeeping products in different taxons of the biosphere. *Ecological Indicators* 66: 452-457. https://doi.org/10.1016/j.ecolind.2016.01.042

Kara Y, Can Z & Kolaylı S (2022). What should be the ideal solvent percentage and solvent propolis ratio in the preparation of ethanolic propolis extract? *Food Analytical Methods* 15:1707–1719. https://doi.org/10.1007/s12161-022-02244-z

Kim S H, Kim I H, Kang B H, Lee K H, Lee S H, Lee D S & Lee J M (2009). Optimization of ethanol extraction conditions from propolis (a bee product) using response surface methodology. *Korean Journal of Food Preservation*, 16(6): 908-914

Kasote D, Bankova V & Viljoen A M (2022). Propolis: chemical diversity and challenges in quality control. *Phytochemistry Reviews* 21(6): 1887– 1911. https://doi.org/10.1007/s11101-022-09816-1

Lovakovic B T, Lazarus M, Karaconji I B, Jurica K, Semren T Z, Lusic D & Pizent A (2018). Multi-Elemental composition and antioxidant properties of strawberry tree (*Arbutus Unedo* L.) honey from the coastal region of Croatia: risk-benefit analysis. *Journal of Trace Elements in Medicine and Biology* 45: 85-92. https://doi.org/10.1016/j.jtemb.2017.09.022

Margeretha I, Suniarti D F, Herda E M & Alim Z (2012). Optimization and comparative study of different extraction methods of biologically active components of Indonesian propolis *Trigona* spp. *Journal of Natural Products* 5: 233- 242

Mele E (2023). Electrospinning of honey and propolis for wound care. *Biotechnology and Bioengineering* 120 (5): 1229–1240. https://doi.org/10.1002/bit.28341

Mokhtar S U, Hooi H S, Lene D T T & Jayaraman S (2019). Comparison of total phenolic and flavonoids contents in Malaysian propolis extract with two different extraction solvents. *International Journal of Engineering & Technology*, 6(2): 1–11 http://dx.doi.org/10.15282/ijets.6.2.2019.1001

Özdal H R, Nakilcioğlu E & Ötleş S (2023). Effects of extraction methods and extraction variables on bioactive compounds of propolis. *Gıda*, 48(6): 1123-1131 (in Turkish). http://dx.doi.org/10.15237/gida.GD23074

Pobiega K, Kraśniewska K, Derewiaka D & Gniewosz M (2019). Comparison of the antimicrobial activity of propolis extracts obtained by means of various extraction methods. *Journal of Food Science and Technology* 56(12): 5386-5395. https://doi.org/10.1007/s13197-019-04009-9

Rocha V M, Portela R D, Dos Anjos J P, De Souza C O & Umsza-Guez M A (2023). Stingless bee propolis: composition, biological activities and its applications in the food industry. *Food Production, Processing and Nutrition* 5(29): 1-13. https://doi.org/10.1186/s43014-023-00146-z

Ruiz-Hurtado P A, Garduño-Siciliano L, Dominguez-Verano P, Martinez-Galero E, Canales-Martinez M M & Rodriguez Monroy M A (2021). Evaluation of the gastroprotective efects of Chihuahua propolis on indomethacin-induced gastric ulcers in mouse. *Biomedicine & Pharmacotherapy* 137: 111345. https://doi.org/10.1016/j.biopha.2021.111345

Saitoh J & Saya H (2016). Benzaldehyde suppresses multiple signal pathways in cancer cells by regulating 14-3-3ζ-mediated protein-protein interactions. *Cancer Research* 76(14): 4758-4758. https://doi.org/10.1158/1538-7445.am2016-4758

Shahbaz M, Naeem H, Imran M, Ul Hassan H, Alsagaby S A, Al Abdulmonem W, Waqare A B, Ghorabf A H, Abdelgawadg M A, Ghoneimh M M, Hussainj M, Jbawik E A & Ihsan A (2023). Chrysin a promising anticancer agent: recent perspectives. *International Journal of Food Properties* 26 (1): 2294-2337. https://doi.org/10.21767/2248-9215.100057

Shahidi F & Naczk M (1995). Food phenolics: Sources, chemistry, effects and applications. *Technology Publishing Company*. 44(12): 287-293

Sharifi-Rad M, Varoni E M, Iriti M, Martorell M, Setzer W N, Del Mar Contreras M, Salehi B, Soltani-Nejad A, Rajabi S, Tajbakhsh M & Sharifi-Rad J (2018). Carvacrol and human health: a comprehensive review. *Phytotherapy Research* 32: 1675–1687. https://doi.org/10.1002/ptr.6103

Silici S & Kutluca S (2005). Chemical composition and antibacterial activity of propolis collected by three different races of honeybees in the same region. *Journal of Ethnopharmacology* 99: 69–73. https://doi.org/10.1016/j.jep.2005.01.046

Sulaiman G M, Al-Amiery A A & Bagnati R (2014). Theoretical, antioxidant and cytotoxic activities of caffeic acid phenethyl esterand chrysin. *International Journal of Food Sciences and Nutrition* 65(1): 101–105. https://doi.org/10.3109/09637486.2013.832174

Ulanowska M & Olas B (2021). Biological properties and prospects for the application of eugenol-A Review. *International Journal of Molecular Sciences* 22(7): 3671. https://doi.org/10.3390/ijms22073671

Woźniak M, Mrówczyńska L, Kwaśniewska-Sip P, Waśkiewicz A, Nowak P & Ratajczak I (2020). Effect of the solvent on propolis phenolic profile and its antifungal, antioxidant, and in vitro cytoprotective activity in human erythrocytes under oxidative stress. *Molecules*, 25(18): 4266. https://doi.org/10.3390/molecules25184266

Zin N B M, Azemin A, Muslim M, Rodi M & Mohd S (2018). Chemical composition and antioxidant activity of stingless bee propolis from different extraction methods. *International Journal of Engineering & Technology* 7 (4.43): 90–95. https://doi.org/10.14419/ijet.v7i4.43.25825

Journal of Agricultural Sciences
(Tarim Bilimleri Dergisi)

J Agr Sci-Tarim Bili
e-ISSN: 2148-9297
jas.ankara.edu.tr

JAS

Antioxidant, Antidiabetic, and Antimicrobial Potentials of Silver Nanoparticles Synthesized from *Viscum album*

Ebru Coteli[a*]

[a]*Vocational School of Health Services, Ahi Evran University, 40100, Kirsehir, TURKEY*

ARTICLE INFO
Research Article
Corresponding Author: Ebru Coteli, E-mail: e.coteli@ahievran.edu.tr
Received: 20 September 2024 / Revised: 29 October 2024 / Accepted: 17 November 2024 / Online: 25 March 2025

Cite this article
Coteli E (2025). Antioxidant, Antidiabetic, and Antimicrobial Potentials of Silver Nanoparticles Synthesized from *Viscum album*. *Journal of Agricultural Sciences (Tarim Bilimleri Dergisi)*, 31(2):373-391. DOI: 10.15832/ankutbd.1553350

ABSTRACT
Substances smaller than 100 nm in size are called nanoparticles. In this study silver nanoparticle synthesis was carried out by using $AgNO_3$ from leaf, fruit, and branch aqueous extracts of the mistletoe (*Viscum album* ssp. *austriacum*) plant. It was determined whether silver nanoparticles were formed using the UV-Vis method. As a result of UV-Vis analysis of plant parts, peaks were observed at 425, 427, and 430 nm, indicating the surface plasmon resonance of AgNPs. Specific functional groups involved in the formation of AgNPs and reduction of Ag were determined using FT-IR spectroscopy. SEM and EDS analyses determined that the synthesized silver nanoparticle samples were nanosized, and the average size was 59.91. In addition to the crystallite size calculated from XRD diffraction, it was observed that the crystallite size of all silver nanoparticles obtained was in the nanometer range, and the nanoparticle peaks were the same as the peaks of pure silver. Considering the antioxidant results of the study, it was determined that the highest total phenolic and flavonoid amounts were in the leaf extract (35.57±1.39 mg GAE/g extract) and fruit extract (23.42±1.29 mg QE), respectively. Additionally, it was determined that the highest radical scavenging activity was in the fruit AgNPs sample (IC_{50} 129.24±1.38 µg/mL). Additionally, it was determined that the highest antidiabetic activity (α-amylase inhibition) was in the fruit AgNPs sample (IC_{50} 123.59±1.44 µg/mL). As a result, it was determined that silver nanoparticles obtained from these plant parts had superior antioxidant, antidiabetic, and antimicrobial properties.

Keywords: *Viscum album*, Green synthesis, Characterization, Antioxidant, Antidiabetic, Antimicrobial

1. Introduction

One of the most important fields of modern science is nanotechnology. Less than 100 nanometers in size, nanoparticles have properties that are considered to be much different and superior to those of bulky materials. Because of these features, they are used effectively in many fields today, such as medicine, cosmetology, biotechnology, and the chemistry sector (Nartop 2016). Recently, plant extracts and microorganisms have begun to be frequently used for metal nanoparticle synthesis. These biological methods have been proposed as an alternative to chemical methods. It is important to use plant extracts in the biosynthesis of nanoparticles (Kasthuri et al. 2009). The synthesis of nanoparticles from plant extracts is a highly preferred method because of its low cost, environmental friendliness, control of the reaction process, and high production rates (Ahmed et al. 2016; Nasrollahzadeh et al. 2015).

Metal nanoparticles have many important properties. Therefore, nowadays, they have wide usage areas, especially in developing new technologies such as silver nanomedicine, nanoparticles, materials science, and electronics. It especially attracts the attention of scientists (Bar et al. 2009). Silver is a good catalytic agent that will catalyze many reduction reactions very effectively (Suvith & Philip 2014; Navalon et al. 2016). But the chemical synthesis of silver nanoparticles also poses an environmental hazard. Therefore, in the last few years, the plant-derived green synthesis of silver nanoparticles has gained more importance due to its economic and environmental friendliness (Wesenberg et al. 2003; Khalilzadeh & Borzoo 2016). Among metal nanoparticles, silver nanoparticles are known to have inhibitory and bactericidal effects (Cho et al. 2005). In addition, silver nanoparticles with different chemical and physical properties have begun to be used more for industrial purposes, food, medicine, and health fields (Gurunathan et al. 2015). Due to their different and special structures, these nanoparticles are frequently used in the production of antibacterial and anticancer agents, the pharmaceutical industry, the field of orthopedics, the food industry, orthopaedics, drug release, anticancer agents, industrial, home, and health-related products, coatings of medical devices, the production of optical sensors, and the field of cosmetics. It is also used to increase the potency and performance of tumor-destroying drugs (Chernousova & Epple 2013). Silver shows great toxicity to a wide variety of microorganisms. In addition, silver nanoparticles show anti-viral, anti-inflammatory, anti-platelet, and anti-angiogenesis activity. Being effective

against cancer cells has made them very important (Stoimenov et al. 2002; Safaepour et al. 2009; Elumalai et al. 2010; Sotiriou & Pratsinis 2010; Huang & Zhan 2011; Kaviya et al. 2011; Vidhu et al. 2011).

Mistletoe has been used for medicinal purposes since ancient times reported to be used. The medicinal effects of mistletoe vary according to the type of plant it is used on (Ekhaise et al. 2010). Mistletoe (*V. album*) is a semi-parasitic plant that grows on trees such as fir, pine, spruce, pear, cherry, and pumpkin trees, belonging to the order Santalales, Loranthaceae family, and Viscum genus, which is green for four seasons. *V. album* ssp. *austriacum* species live on the trunk and branches of pines. It does not shed its leaves and is green in all seasons. Especially cardiovascular system diseases caused by this parasitic plant and has been reported to have positive effects on cancer. Additionally, this plant has antipsychotic, anti-diabetic, anti-inflammatory, and hypotensive properties (Hegde et al. 2011; Orhue et al. 2014). In addition, plant extracts, radiotherapy, and the harmful and mutagenic effects of chemotherapy reduction have been reported (Büssing et al. 1994; Kovacs 2002). Thus, these plant extracts increase the effectiveness of cancer treatment (Kienle et al. 2016). Pharmacological studies conducted with *Viscum* species have shown that the chemical structure of these plant species depends on the host tree. They especially contain active molecules such as phenolics and flavonoids, viscotoxins, lignans, phenylpropanoids, sterols, fatty acids, and terpenoids (Szurpnicka et al. 2019). A study examining the effects of *Viscum* species on the central nervous system in vivo showed that they have many properties, such as sedative and analgesic (Khatun et al. 2016), antiepileptic (Geetha et al. 2018), and antidepressant (Kumar et al. 2016). In addition, studies have shown that mistletoe has bioactive effects such as immunomodulatory and antifungal (Oei et al. 2019; Zhou et al. 2023), anti-inflammatory (Nicoletti 2023), antibacterial and antiradical (Çiftci et al. 2024), antioxidant (Nicoletti 2023). In addition, viscothionine found in mistletoe has a polypeptide structure and has been reported to increase insulin secretion. It has been stated in studies that especially mistletoe extract inhibits the α-glucosidase enzyme (Park et al. 2019).

Substances that contain unpaired electrons are called free radicals. Therefore, they are very active and easily react with biological molecules (Valko et al. 2007). These radicals are formed during the normal functioning of the cell and damage proteins, DNA, carbohydrates, enzymes, and lipids by disrupting their functioning (Shinde et al. 2012). It neutralizes and destroys these harmful radicals through metabolic antioxidant systems (Barber & Harris 1994). Antioxidant substances prevent many diseases, such as diabetes, cancer, cataracts, and cardiovascular diseases, which are thought to be caused by free radicals (Huang et al. 2005; Niki 2010). Oxidative stress has been reported to be a common pathway connecting mechanisms particularly involved in the pathogenesis of diabetic complications. Diabetes mellitus is a disorder in which there are complete or partial deficiencies in insulin secretion or function. This disorder is a chronic disease characterized by disorders in protein, carbohydrate, and fat metabolism. Oxidative stress parameters between oxidative stress and diabetes when measured it has been determined that there is a direct relationship.

Literature studies have shown that silver nanoparticles have many biological activities. Silver nanoparticles were synthesized from *Viscum orientale* plant leaf extract and it was reported that these nanoparticles have anthelmintic and antimicrobial activities. Additionally, this study reported the dose-dependent antiradical activity of silver nanoparticles (Kumar et al. 2023). It has also been reported that silver nanoparticles have antiviral, antifungal, antiparasitic, antibiofilm, and antitumor activities (Almatroudi 2020). Silver nanoparticles protect cells from this damage by preventing oxidative damage that occurs in metabolism. Therefore, they are used in the prevention and treatment of neurological diseases, diabetes, and cancer caused by oxidative stress. Because of these features, they have gained importance and hope (Bhakya et al. 2016).

In this study, it was aimed to investigate the in vitro antioxidant, antidiabetic, and antimicrobial potentials of nanoparticles by synthesizing silver nanoparticles (AgNPs) using the green synthesis method from three different aqueous extracts of *V. album* plant parts (leaf, fruit, and branch) for the first time. In addition, it was aimed to determine the use potential of the plant from the results obtained from the study and to contribute to silver nanoparticle studies.

2. Material and Methods

2.1. Materials

The pine mistletoe (*Viscum album* ssp. *austriacum*) plant was collected from Kirsehir, Turkey, in October (Figure 1). The fresh plant was first cleaned of its impurities by thoroughly washing it with tap water. It was then washed twice with distilled water and filtered. It was dried for two weeks in the shade and at room temperature without exposure to sunlight. The leaves, branches, and fruits of the dried mistletoe were pulverized with the help of a mechanical grinder (Fritsch P-15, Germany).

Figure 1- The appearance of mistletoe (*V. album*)

2.2. Methods

2.2.1. Preparation of plant part aqueous extracts

10 grams of powdered plant parts were weighed and placed in a 250 mL beaker, and 100 mL of bidistilled water was added. *V. album* plant part samples were boiled at 80 °C for 30 minutes. Then, the samples were filtered with filter paper and stored at 4 °C (Chung et al. 2017).

2.2.2. Synthesis of silver nanoparticles by the green synthesis method

3 mM $AgNO_3$ (99.90%, Merck, Darmstadt, Germany), solution was prepared with distilled water (Ashraf et al. 2016). 10 mL of the *V. album* plant was taken from the aqueous extract solutions and 3 mM 90 mL $AgNO_3$ solution was added. Samples were mixed at room temperature for 45 minutes. The color changes observed in the samples indicate the emergence of silver nanoparticles (Asha et al. 2016). The samples turned a dark brown-black color after 24 hours. Thus, it was seen that silver nanoparticles were formed. Again, the formation of AgNPs was detected using the UV-Vis technique. The resulting solutions were centrifuged at 5.000 rpm for 60 min. The nanoparticles thus formed were precipitated and the supernatants were removed. The resulting nanoparticles were filtered by washing them three times with distilled water. Solid nanoparticles were placed in eppendorf tubes. After drying in an oven at 50 °C, it was weighed on a precision balance. The nanoparticles in these tubes were wrapped in aluminum foil.

2.2.3. Characterization of silver nanoparticles

2.2.3.1. UV-vis (Ultraviolet-visible spectrometry)

A reliable method for determining the surface plasmon resonance capabilities of nanoparticles is the UV-Vis spectrometry method (Bindhu & Umadevi 2013). Silver nanoparticle synthesis was carried out from different parts of the *V. album* plant. The formation of AgNPs by green synthesis was monitored by absorbance measurements at 250–600 nm in a Shimadzu UV-1800 model spectrophotometer. Distilled water was used for the blank sample.

2.2.3.2. FT-IR (Fourier transfrom infrared spectroscopy)

Determination of the functional groups of the plant extract using FT-IR spectroscopy was performed. FT-IR analyses of leaf, fruit, and branch extracts of the *V. album* plant and AgNPs obtained from these extracts were performed. Plant extracts and nanoparticles were analyzed in the range of 4000-500 cm^{-1} with the help of a Perkin Elmer Spectrum One brand device. FT-IR is a method used to determine the structure and structural properties of nanoparticles and related functional groups in biological extracts according to the wavelength of light (Shobha et al. 2014).

2.2.3.3. SEM (Scanning electron microscopy) and EDS (Energy dispersive X-ray spectroscopy)

SEM is a method that determines the shape, surface, and size of nanoparticles and reveals their images (Ali et al., 2016). The size, shape, and spatial organization of the purified AgNPs were examined by SEM. EDS is used for the analysis of the elemental composition of metal nanoparticles. It gives full information about the fundamentals of nanoparticles (Khandel & Shahi 2016). SEM-EDS (Jeol JSM 6390; scanning electron micrograph-energy dispersive x-ray spectroscopy) method was used to detect silver compounds in AgNPs.

2.2.3.4. XRD (X-ray diffraction analysis)

This method used to obtain information about the elemental composition or crystallographic structure of naturally and artificially synthesized nanoparticles (Wang 2000). The crystal structures of silver nanoparticles were studied using a RadBDMAX II computer-controlled X-ray diffractometer in the $3o \leq 2\theta \geq 80o$ range. The crystal sizes of the obtained silver nanoparticles were determined by the Debye-Scherrer equation.

2.2.4. In vitro biological activities

2.2.4.1. Antioxidant activity

2.2.4.1.1. Determination of total phenolic substance in plant samples

Total phenolic substance amounts of extracts of the *V. album* plant were determined (Slinkard & Singleton 1977). For this purpose, solutions of 1 mg/mL concentration were prepared with distilled water from plant part extracts. 0.1 mL was taken from the samples, and 4.5 mL of distilled water was added to them. Then, 0.1 mL of Folin-Ciocalteu reagent was added and vortexed. Then, 0.3 mL of 2% Na_2CO_3 was added to the samples and kept at room conditions for 2 hours. The absorbance of the samples was measured at wavelength 760 nm. For water extracts used as blanks, 0.1 mL distilled water instead of the extract was used. The same experimental procedure was used. Total phenolic substance amounts in plant samples were calculated using standard gallic acid substance. The results of the study were determined as gallic acid equivalent (mg GAE/g extract).

2.2.4.1.2. Determination of total flavonoid substances in plant samples

The total flavonoid substance amounts of *V. album* plant samples in the study were determined to be equivalent to quercetin by the modified aluminum nitrate method (Moreno et al. 2000). To evaluate the total flavonoid content, 0.5 mL of the plant extract at a concentration of 1 mg/mL was combined with 0.1 mL sodium acetate. After 1 minute, add 0.1 mL of 10% (w/v) $Al(NO_3)_3$ and shake. The volumes of the samples were completed to 5 mL using a 96% (v/v) ethanol solution. The absorbance of the samples, which were kept at room temperature for 40 minutes, was measured at a wavelength of 450 nm using a spectrophotometer device. The total flavonoid substance amounts of the samples in the study were expressed as mg quercetin equivalent (QE)/g extract. The solution prepared by adding ethanol was used as a blank instead of the sample. Analyses were performed in triplicate.

2.2.4.1.3. Determination of DPPH free radical scavenging activity of samples

This method is based on the detection of the DPPH (2,2-diphenylpicryl-1-hydrazyl, Merck) radical, which is a free radical, by the antioxidant substance and determining its purple color by measuring it in a spectrophotometer (Blois 1958). The lightening of the purple color of the radical indicates the presence of antioxidant activity. Samples of standard substances (BHT and ascorbic acid), plant extracts, and nanomolecules were prepared at concentrations of 25, 50, and 100 µg/mL. 4 mL of a 0.1 mM DPPH solution was added to 1 mL of these samples. Following the vortexing process, all samples were left for half an hour at room temperature in a dark location. At the end of the period, absorbance values of 517 nm were read in the spectrophotometer. The following formula was used to calculate the samples' DPPH radical scavenging abilities:

$$DPPH\ Radical\ scavenging\ activity\ (\%\ inhibition) = \frac{A\ control - A\ sample}{A\ control} x\ 100 \quad (1)$$

The IC_{50} value is the quantity of antioxidant material needed to scavenge 50% of the DPPH radical concentration in the samples (Deng et al. 2011; Scherer & Godoy 2009). The IC_{50} values of all samples were calculated. Inhibition-concentration graphs of the mixtures prepared at three different concentrations of 25, 50, and 100 µg/mL for each sample were drawn. IC_{50} values were calculated using the correct equation in the graphs.

2.2.4.2. Antidiabetic activities (α-amylase)

2.2.4.2.1. Determination of α-amylase enzyme inhibition of samples

In the presence and absence of *V. album* plant part extracts and silver nanoparticles, the activity of α-amylase enzyme (Merck), a carbohydrate digesting enzyme, was evaluated (Apostolidis et al. 2007). First of all, to evaluate the enzyme activity, 0.5 mL of starch and 0.5 mL of enzyme mixture were kept at 25 °C for 20 min. After that, the samples were added to 1 mL of DNS (3,5-dinitrosalicylic acid) solution and boiled for 5 minutes. The boiling samples were cooled in tap water before being mixed with 7.5 mL of distilled water. The absorbance of all samples was measured at $\lambda = 540$ nm. A control tube was created using a 0.5 mL buffer solution instead of the enzyme. To investigate the inhibitory effect of extracts and silver nanoparticles on the α-amylase enzyme, samples were prepared at concentrations of 25, 50, and 100 µg/mL. 0.5 mL of these samples were taken and placed in test tubes. 0.5 mL of enzyme was added to all tubes. The samples were kept at 37 °C for 15 minutes. 0.5 mL of starch solution was added to the samples. Then, DNS solution was added, and the boiling process was started. Sample blanks were

prepared for all the samples. A standard acarbose substance was used to compare the α-amylase enzyme inhibition of the samples. The same experimental procedure was applied to standard matter. The α-amylase enzyme inhibition values of all samples were determined using the formula below.

$$\%\ Inhibition) = \frac{[(Absorbance\ amylase - Absorbance\ Extract/Acarbose)}{Absorbance\ amylase} x\ 100 \quad (2)$$

Absorbance amylase; The absorbance of the tube is considered 100% active.
Absorbance extract; Sample absorbance-sample blank absorbance

2.2.4.3. Antimicrobial activity

2.2.4.3.1. Determination of antimicrobial activity of samples

In this study; In order to determine the antimicrobial activity of synthesized silver nanoparticles, antimicrobial activity was performed by agar well diffusion method using 11 pathogenic microorganisms for the application of AgNPs. The names of the microorganisms used are as follows: *Staphylococcus aureus* (ATCC 25923), *Bacillus cereus* (709 Roma), *Bacillus subtilis* (ATCC 6633), *Enterococcus faecalis* (ATCC 29212), *Escherichia coli* (ATCC 25922), *Aeromonas hydrophila* (ATCC7966), *Pseudomonas aeruginosa* (ATCC 27853), *Vibrio anguillarum* (ATCC 43312), *Klebsiella pneumoniae* (ATCC 13883), *Salmonella typhi* (ATCC 6539) and *Candida albicans* (ATCC 90028), Tryptic SoyAgar (TSA) medium was used in sterile petri dishes to provide growth media for microorganisms. 24-48 hour fresh cultures of pathogenic bacteria and yeast were spread on TSA Plates at a density of 10^6 cfu/mL. After sowing, the plates were opened with 6mm diameter wells, 3mM AgNP was added to 70 ml wells and after 24-48 hours of incubation, the zone diameters around the wells were measured in mm and the effect levels of AgNPs were determined. For the purposes of activity comparison, conventional antibacterial medication ampicillin was utilized (CLSI 2007).

2.2.4.3.2. Minimal inhibition concentration (MIC)

Minimum inhibition concentrations of AgNPs synthesized green by *V. album* were determined using sterile 96-well microplates. In order to carry out the study, the solutions taken from the cultures of 10 microorganisms in TSB were prepared with McFarland 0.5 turbidity test as 1x10 6 cells/ml. The concentrations determined for silver nanoparticles with green synthesis are; 512 µL/mL, 256 µL/mL, 128 µL/mL, 64 µL/mL, 32 µL/mL, 16 µL/mL, 8 µL/mL, 4 µL/mL and 2 µL/mL. The prepared microplates were incubated in an oven at 37 0 C for 24 hours. Plates taken after 24 hours were analyzed in a spectrophotometer at 600 nm (Petrus et al. 2011). In the study, the operations with AgNPs were carried out in triplicate.

2.2.4.3.3. Anti-quorum sensing analysis

In this study, Anti-quorum sensing (Anti-QS) analysis; carried out by macroscopic methods. The inhibition of violacein pigment by AgNPs indicates that nanocolloids have quorum quenching activity. In the macroscopic method, agar well diffusion method was used and *Chromobacterium violaceum* (ATCC 12472) was planted on the plates formed with TSA and the zone diameters formed by AgNPs were calculated (McLean et al. 1997).

2.2.5. Statistical analysis

The number of samples was determined to be three for the parameters examined, and The Microsoft Excel application was then used to compute the mean and standard deviations of the findings. Aqueous extracts of plant sections from the study showed significant differences in phenolic and flavonoid compounds (Kruskal-Wallis H, sig. $P<0.001$). One-sample Wilcoxon signed rank test was used to compare the antioxidant and antidiabetic results of the samples with their standards ($P<0.05$).

3. Results and Discussion

3.1. Evaluation of silver nanoparticles from V. album plant

It has been suggested that pharmacologically active compounds can pass from trees to parasitic host plants (Büssing & Schietzel 1999). The primary study was the preparation of aqueous extracts of leaf, fruit, and stem parts of *V. album* for the synthesis of AgNPs. When aqueous Ag^+ ions were subjected to *V. album* extract, they were reduced to Ag^0 state. In this study, green synthesis of AgNPs was carried out by using aqueous extracts of leaves, fruits, and stems of *V. album*. UV-Vis, FTIR, SEM, EDS, and XRD analyses were performed to characterize the synthesized AgNPs. In addition, total phenolic and flavonoid levels in plant sections were examined. The radical scavenging capabilities of plant component extracts and the AgNPs generated from them were then assessed.

The study was carried out together with samples containing silver nitrate and plant extract and control group samples without silver nitrate. Aqueous extracts of *V. album* plant parts were added to 3 mM aqueous $AgNO_3$ solution. After a short time, color

changes were observed in the silver nitrate added group samples compared to the control group samples. A brown black color change was observed over time in the extract samples to which 3 mM aqueous $AgNO_3$ solution was added (Figure 2). This color intensity increased over time. This color change is a sign that silver nanoparticles are formed. In addition, UV-Vis measurements of the samples also supported the formation of silver nanoparticles. No change was observed in the control group (plant samples without added silver nitrate).

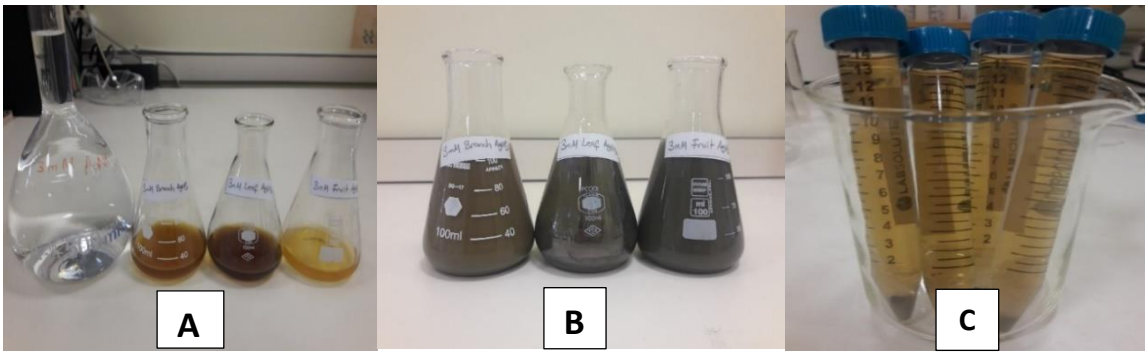

Figure 2- Aqueous solution of 3 mM $AgNO_3$ with *V. album* branch, leaf, fruit extract (A), Views of AgNPs after 24 hours of incubation (B), Appearance of AgNPs after centrifugation (C)

3.2. Characterization of silver nanoparticles (AgNPs)

3.2.1. UV-vis results

In silver nanoparticle synthesis from plant extracts, Ag^+ ions are reduced to Ag^0. Phytochemicals in the structures of plants take part in reduction reactions (Jha et al. 2009). Although the phytochemical contents of plants differ, the main mechanism is the reduction of silver ions. A color shift was noticed when silver nitrate solution was added to *V. album* extracts, suggesting the creation of silver nanoparticles. Additionally, the UV-Vis spectrophotometer method verified the creation of silver nanoparticles. UV-Vis spectroscopy method is frequently used in the characterization of the structure of nanoparticles. As a control, the absorbance values of both plant part extracts and silver nanoparticles obtained from these extracts were measured in the range of 250–600 nm on the spectrophotometer device. Silver nanoparticles were synthesized in this work utilizing extracts from *V. album* leaves, fruit, and branches. In literature studies, it has been observed that the surface plasmon resonance peaks of silver nanoparticles vary between 400 and 450 nm. As a result of the measurements made in this study, surface plasmon resonance peaks were detected in the leaf (345 nm), fruit (340 nm), and branch (345 nm) sections of the *V. album* plant. In addition, it was determined that leaf AgNPs (427 nm), fruit AgNPs (430 nm), and branch AgNPs (425 nm) obtained from these plant extracts had surface plasmon resonance peaks. The outcomes are displayed in (Figure 3).

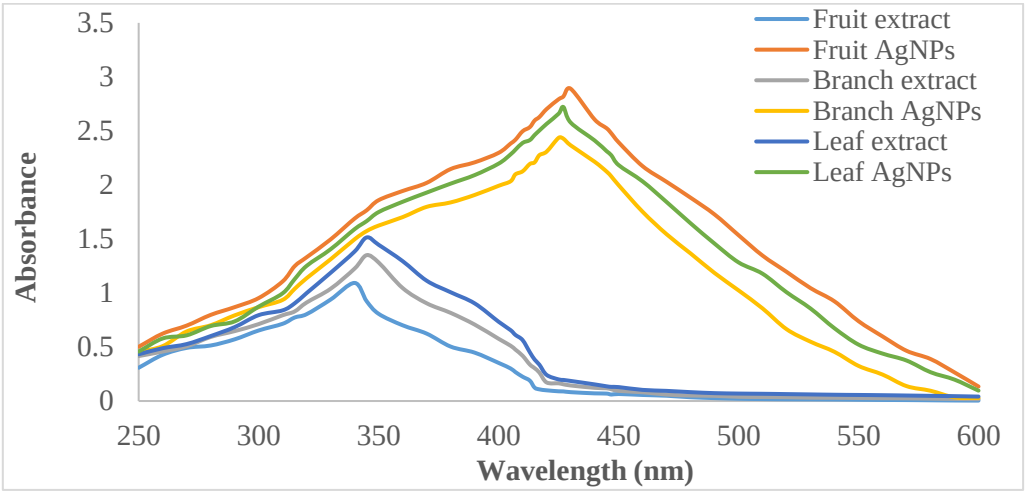

Figure 3- UV-Vis results of leaf, fruit, branch aqueous extract and silver nanoparticles

In a study, silver nanomolecules were synthesized with *V. album* fruit extract and silver nitrate solution. Surface plasmon resonance peaks were detected at 450 nm (Tahmasebi Zade Damirchi et al. 2020). In another study, the surface plasmon resonance peak wavelengths of round-shaped silver nanoparticles synthesized from different plant extracts were measured between 422 and 451nm (Akbal et al. 2016). It seems that our results are compatible with the literature.

3.2.2. FT-IR results

Fourier transform infrared (FT-IR) spectroscopy is an effective analytical technique utilized in a variety of scientific fields. It involves the measurement the plant extracts displayed a range of functional group vibrations throughout the spectral region of 4000-500 cm^{-1}. The FT-IR analysis approach was used to identify the biomolecules responsible for the reduction and stabilization of the AgNPs in this work. The FT-IR results of the study are shown in (Figure 4). FT-IR spectroscopy Plant extracts showed a variety of functional group stretching vibrations. Leaf, fruit and branch extracts of pine mistletoe showed characteristic absorption peaks corresponding to O–H stretching, C–H stretching, N–H of intramolecular hydrogen bonding. Although the peaks of the leaf extract have been observed at 3263.54 cm^{-1}, 2929.30 cm^{-1}, 1389.92 cm^{-1}, 1048.54 cm^{-1}, 1578.65 cm^{-1}, and 518.35 cm^{-1}, the peaks of the leaf AgNPs have been found at 3329.99 cm^{-1}, 1637.58 cm^{-1}, and 589.57 cm^{-1}. While the peaks of the fruit extract (3311.55 cm^{-1}, 2930.15 cm^{-1}, 1610.70 cm^{-1}, 1411.87 cm^{-1}, 1048.34 cm^{-1}, and 620.16 cm^{-1} were observed, the peaks of fruit AgNPs (3327.63 cm^{-1}, 1637.60 cm^{-1}, and 587.47 cm^{-1}) were determined. Additionally, peaks of branch extract (3301.36 cm^{-1}, 2930.97 cm^{-1}, 1589.50 cm^{-1}, 1392.43 cm^{-1}, 1047.73 cm^{-1}, 633.49 cm^{-1}) were observed, while branch AgNPs (3355.37 cm^{-1}, 2987.07 cm^{-1}, 2899.37 cm^{-1}, 2790.74 cm^{-1}, 2180.93 cm^{-1}, 2017.21 cm^{-1}, 1972.76 cm^{-1}, 1639.40 cm^{-1}, 1451.77 cm^{-1}, 1406.27 cm^{-1}, 1251.89 cm^{-1}, 1053.93 cm^{-1}, 867.83 cm^{-1}, and 656.33 cm^{-1}) peaks were determined. Our FTIR results were found to be compatible with the literature (Tahmasebi Zade Damirchi et al. 2020).

When the FT-IR spectra of the nanoparticles were examined, it was observed that there was a shift in the peaks. These shifts observed in the peaks revealed the role of functional groups in the plant in bioreduction and stabilization. In addition, FT-IR spectra of leaf and fruit extracts showed that the 1048 cm^{-1} peak disappeared, indicating that the functional group complex was good enough to form metallic oxide nanoparticles.

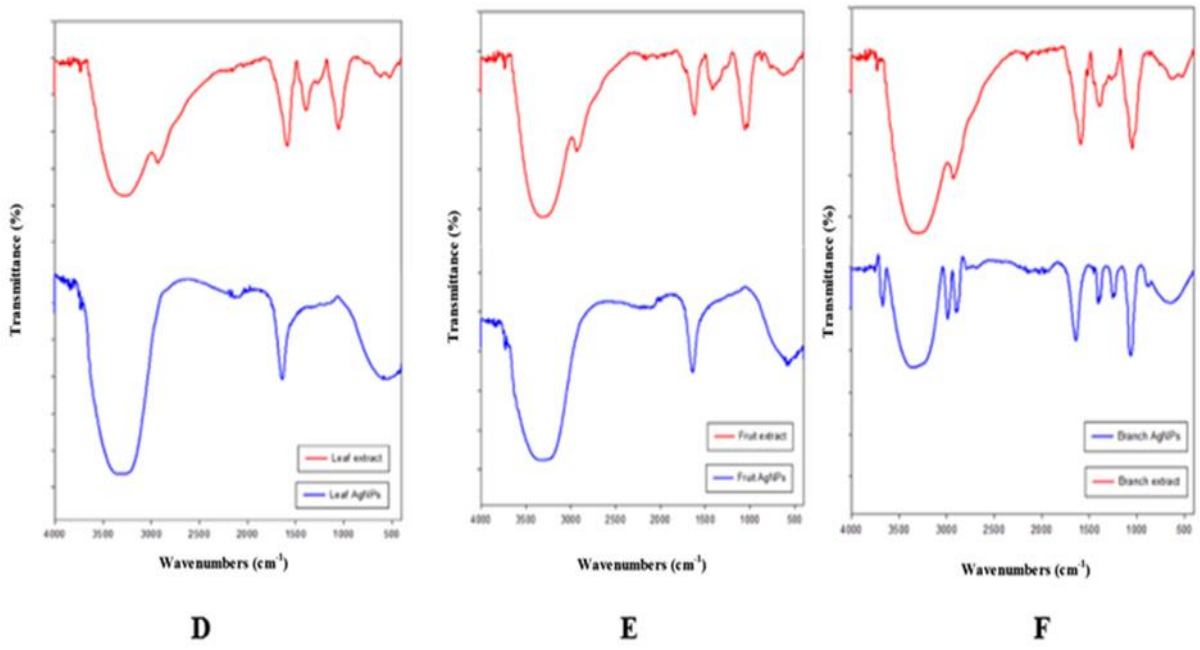

Figure- FT-IR results of leaf extract and silver nanoparticle (D), fruit extract and silver nanoparticle nanoparticle (E), branch extract and silver nanoparticle (F)

3.2.3. SEM and EDS results

AgNPs in the study were visualized by SEM analysis. The images obtained are shown in (Figures 5-7). AgNPs formation and morphological properties were determined in SEM analysis. It was noted that silver nanoparticles created from *V. album* plant parts had a spherical form. The silver nanoparticles obtained from the leaf extract are spherical in shape, and their sizes vary between 30.16 to 70.82 nm. In addition, 77% of the silver nanoparticles obtained from the leaf extract were found, and in addition to the intense silver peaks, 16% C and 7% O peaks were also observed (Figure 5).

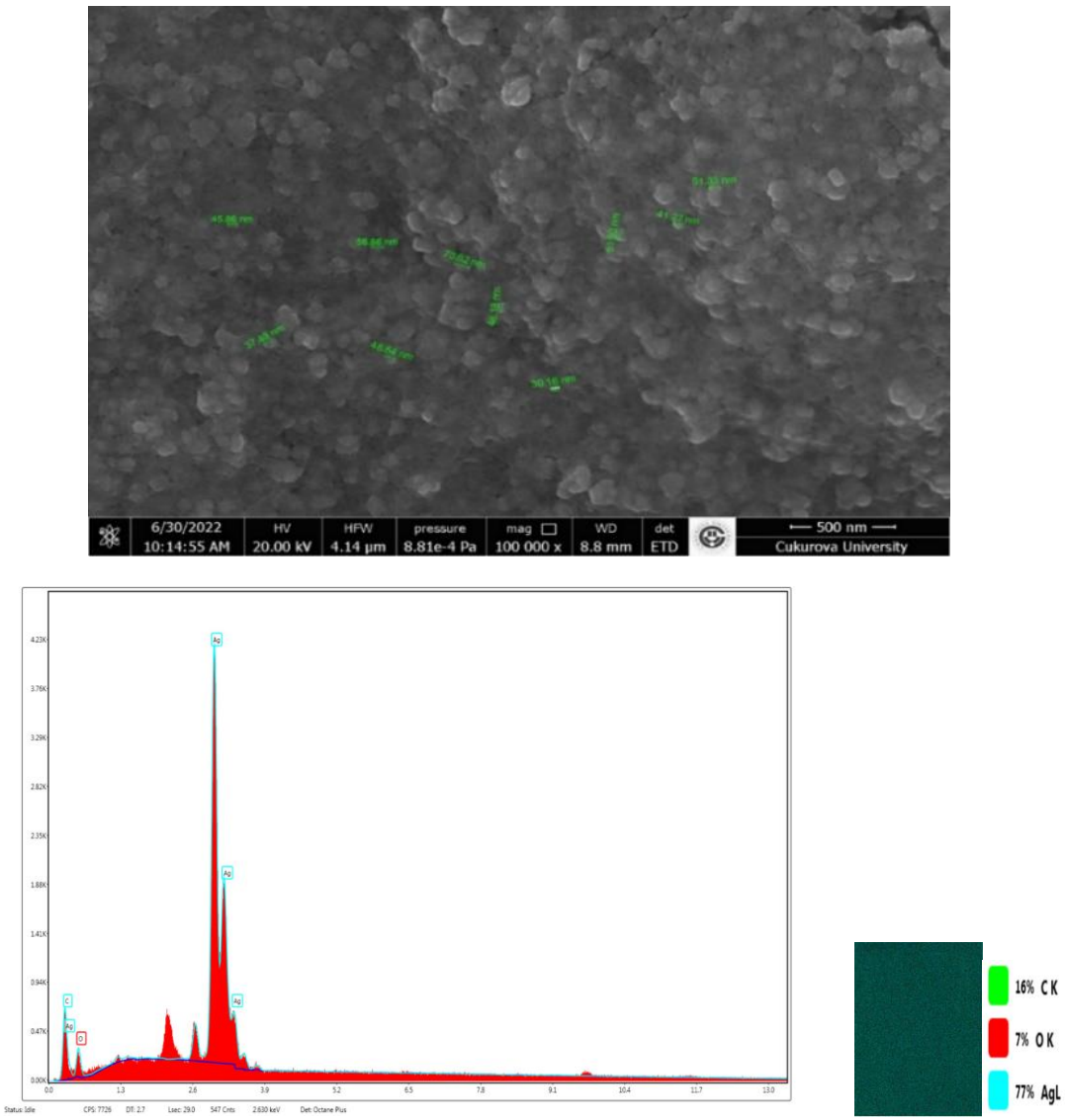

Figure 5- SEM and EDS analysis results of leaf AgNPs

In particular, it was discovered that the nanoparticles generated from the plant fruit extract were both abundant and reduced in size. Fruit silver nanoparticles range in size from 20.55 to 63.21 nm and have a spherical form. In addition, silver nanoparticles were formed at a rate of 83%, and in addition to intense silver peaks, 12% C and 6% O peaks were also observed (Figure 6).

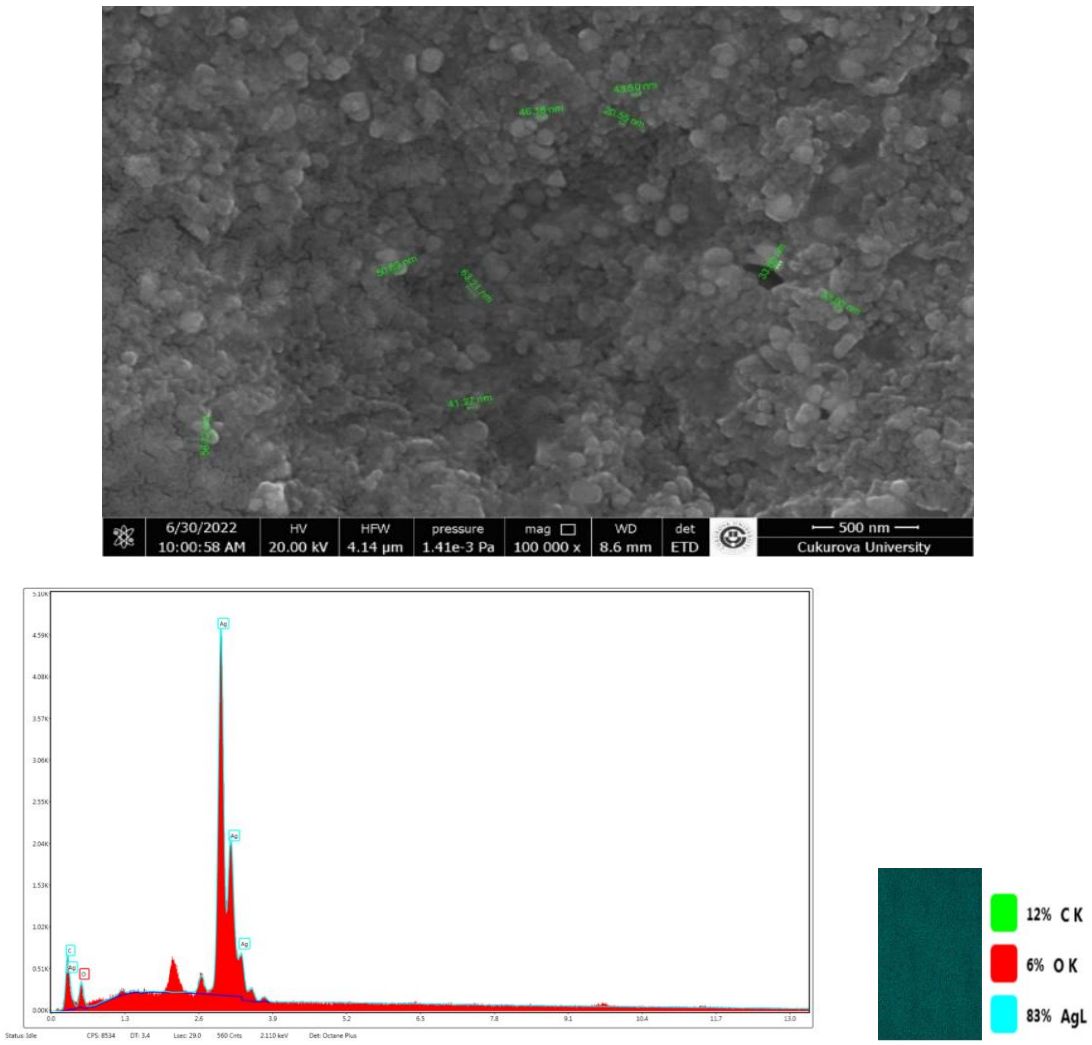

Figure 6- SEM and EDS analysis results of silver nanoparticles synthesized from fruit extract

The silver nanoparticles generated from the branch extract ranged in size from 30.16 to 99.27 nm and had a spherical shape. In particular, it was determined that 74% of the silver nanoparticles produced by the branch extract were formed. In addition to the intense silver peaks, 18% C and 8% O peaks were also observed (Figure 7).

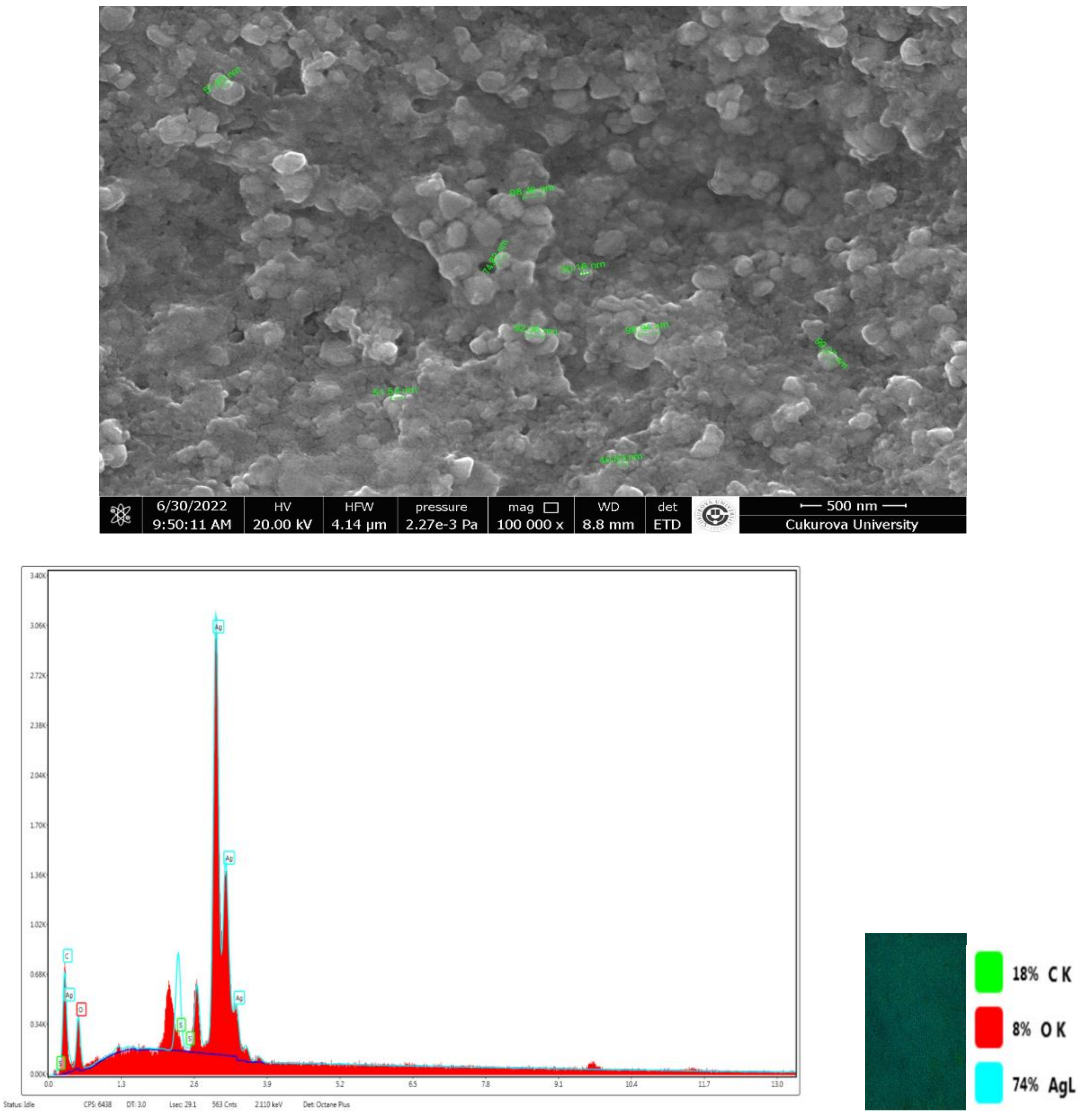

Figure 7- SEM and EDS analysis results of silver nanoparticles synthesized from branch extract

It is observed that silver nanoparticle synthesis occurs efficiently from the leaves, fruits, and branches of the *V. album* plant. SEM and EDS tests revealed that silver nanoparticles generated from *V. album* fruit aqueous extract were abundant and smaller in size. In a research, silver nanoparticles were generated from an aqueous extract of *V. album* fruit, and the silver nanoparticles obtained were spherical in form with diameters ranging from 40 to 70 nm (Tahmasebi Zade Damirchi et al. 2020). In this research, the size of silver nanoparticles produced from fruit extract was between 20.55 and 63.21 nm. Silver nanoparticles of smaller sizes were obtained compared to the literature. Additionally, it was determined that the fruit AgNPs sizes obtained from this study were smaller than the nanoparticle sizes obtained from the leaf and stem extracts.

3.2.4. XRD results

Figure 8 shows the x-ray diffractograms of silver nano particles produced by green synthesis method from the leaf, fruit and branch of *V. album* plant at room temperature. The results of X-ray measurements were indexed according to JCPDS card no: 98-042-691 and according to the literature. All silver nanoparticles exhibit a surface-centred cubic crystal structure (Awwad et al. 2013; Vigneshwaran et al. 2006; Venkatesham et al. 2012). Here, it is obvious that Ag nanoparticles were produced from three parts of the plant *V. album* (leaf, fruit, branch) with high purity, because all of them have high intensity of the peaks in the xrd graphs. The peaks (111), (200), (220), and (311) observed in the XRD results indicate the presence of pure silver nanocrystals.

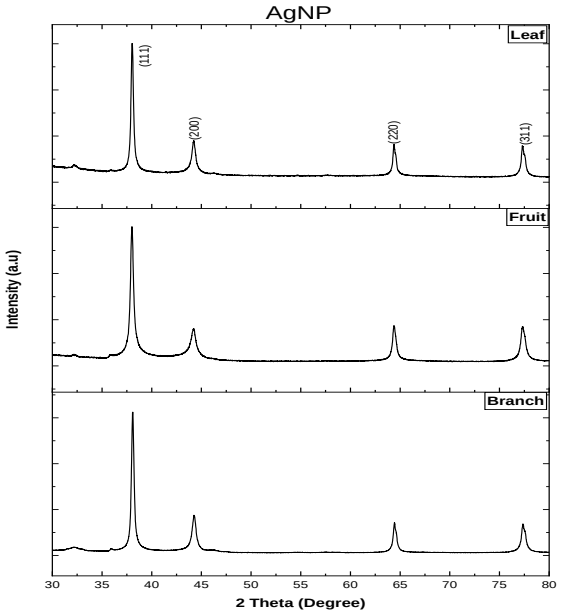

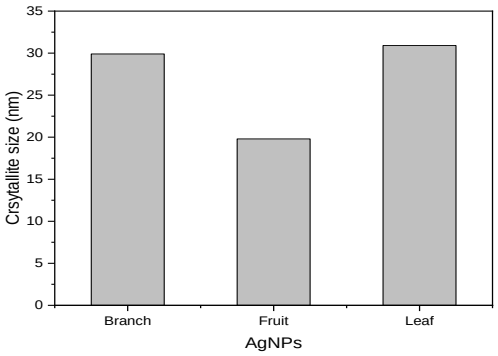

Figure 8- XRD diffractograms of AgNPs **Figure 9- Crystallite size of AgNPs**

In addition, the crystallite size of Ag nanoparticles obtained from X-ray curves was determined using the Debye-Scherrer method (Awwad et al. 2013; Qader et al. 2022).

$$D = k\lambda/\beta\cos\theta \quad (3)$$

Where; D is the crystallite size of AgNP, λ is the wavelength of the x-ray source, β is the full width at half maximum of the diffraction peak, K is the Scherrer constant with a value from 0.9 to 1, and θ is angel of maximum peak (in a radians). For this study, CuK_α X-ray is used and the wavelength value is 1.5406 A. According to these calculations, the crystallite size of the silver nanoparticles obtained from the branch and leaf was the same (~30 nm), while the crystallite size of AgNPs obtained from the fruit (19.8 nm) decreased (Figure 9).

3.3. In vitro antioxidant potential research

3.3.1. Total phenolic and flavonoid analysis results of samples

The phytochemical composition and medicinal effect of the mistletoe plant, which has been used for medicinal purposes since ancient times, vary depending on the type of plant it grows on (Jäger et al. 2021; Dash et al. 2017; Vicaş et al. 2011).

Research shows that phenolic acids and flavonoids found in the structure of plants are natural antioxidants. In particular, the antioxidant capacity of plant extracts is related to the phenolic compounds in their structure (Roman et al. 2009; Miliauskas et al. 2004). The most curious and researched chemical property of as leaves, fruits, and branches were determined as mg gallic acid equivalent (GAE)/g extract. Again, the phenolic compounds are their antioxidant activity (Materska 2008). The total phenolic substance amount (TPC) results in different parts of this plant such total flavonoid substance amount (TFC) of the plant parts was expressed as mg Quercetin equivalent (QAE)/g extract. The results of the study are shown in Table 1.

Table 1- Total phenolic and flavonoid substance amounts of *V. album* plant part extracts

Samples	***TPC (mg of GAE/g extract)***	***TFC (mg of QE/g extract)***	***sig. (p)***
Leaf-water extract (LW)	35.57±1.39	20.57±1.16	< 0.001
Fruit-water extract (FW)	34.31±1.20	23.42±1.29	< 0.001
Branch-water extract (BW)	32.24±1.44	18.95±1.04	< 0.001

(n=3, X ±SD mean of three measurements± Standard Deviation), (Kruskal-Wallis H, sig. $p < 0.001$).

Viscum album subsp. *album* growing on *Malus domestica Borkh*. total phenolic and flavonoid amounts of the plant were examined at various time intervals. The reported total phenolic amounts ranged from 33.78±1.60 to 48.62±1.31 mg GA per g of dry extract). It was also determined that total flavonoid amounts varied between 11.72±0.23 and 13.78±0.25 mg Q per g of dry extract (Pietrzak & Nowak 2021). Again, the total phenolic and flavonoid amounts of the methanol extracts of the leaves, fruits, and branches of the *Viscum album* L. plant grown on twelve different plants were calculated. Phenolic amounts of the leaves

vary between 10.18±0.58 and 16.59±0.49 mg GAE/g, and flavonoid amounts vary between 13.32±0.67 and 97.92±0.51 mg QE/g. While fruit phenolic amounts vary between 11.2±0.68 and 22.76±0.38 mg GAE/g, flavonoid amounts vary between 2.22±0.53 and 38.52±0.44 mg QE/g. Branch phenolics ranged from 9.81±0.62 to 12.83±0.51 mg GAE/g, and flavonoids from 8.52±0.48 to 74.52±0.44 mg QE/g (Korcan et al. 2023). The total phenolic results of this study are LW>FW>BW, while the total flavonoid results are FW>LW>BW (Figure 10). It has been observed that our findings are compatible with previous literature studies.

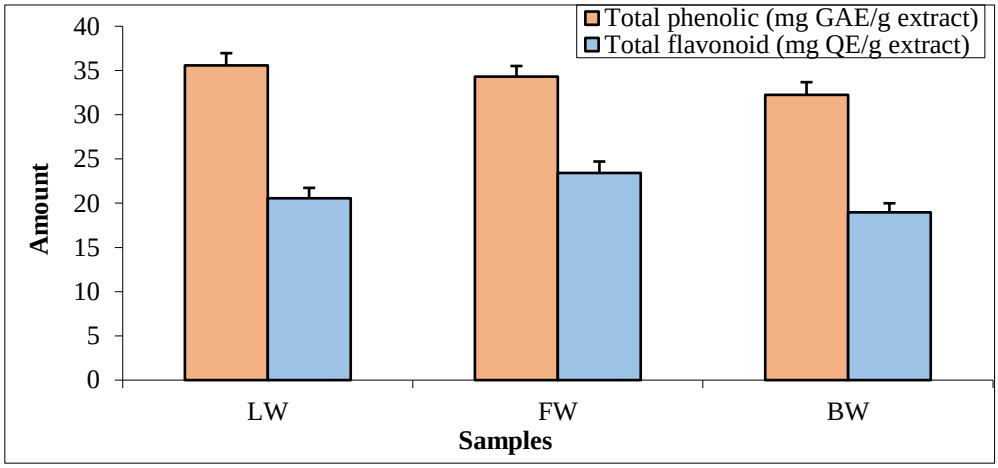

Figure 10- The total phenolic and flavonoid content of *V. album* plant extracts

3.3.2. DPPH radical scavenging activities of samples

The DPPH radical is a radical that can react with all antioxidants, including hydrophilic, lipophilic, and the weakest antioxidants. For this reason, the DPPH method is the most commonly used method in antioxidant capacity determination studies (Kedare & Singh 2011). The results of the study are shown in (Figure 11). Firstly, the inhibition percentages of the DPPH radical were calculated. The inhibition values of the samples in this study at 100 µg/mL concentration were determined as follows: Ascorbic acid (84.46)>BHT (75.63)>fruit AgNPs (42.37)> fruit extract (38.05)>leaf AgNPs (37.14)>leaf extract (35.94)>branch AgNPs (31.39)>branch extract (30.76) ($P<0.05$).

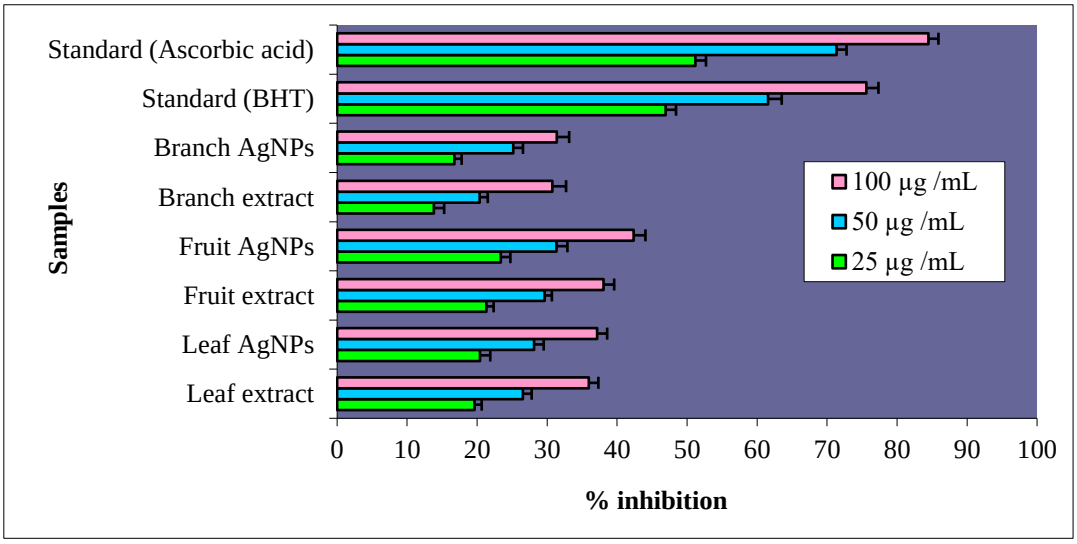

Figure 11- DPPH analysis of *V. album* plant part extracts and silver nanoparticles

In addition, in this study, the IC_{50} values of *V. album* plant part extracts (leaf, fruit, and branch) and silver nanoparticles synthesized from these extracts were also calculated. The antioxidant results of the study are expressed as both inhibition percentages and IC_{50} values. A lower IC_{50} value indicates greater antioxidant activity. For this reason, the IC_{50} values of *V. album* plant part extracts, silver nanoparticles synthesized from these extracts, and standard (BHT and Ascorbic acid) substances were calculated ($P<0.05$). The IC_{50} values for the samples in the study are shown in Table 2.

Table 2- IC_{50} values (DPPH radical scavenging activities) of *V. album* plant part extracts, silver nanoparticles and standards

Samples	*IC_{50} (µg/mL)*	*95% Confidence Interval for Mean*	
		Lower Bound	*Upper Bound*
Leaf extract	163.42±1.61	160.59	166.25
Leaf AgNPs	157.09±1.41	154.61	159.57
Fruit extract	152.88±1.85	149.63	156.13
Fruit AgNPs	129.24±1.38	126.83	131.66
Branch extract	185.29±1.27	183.06	187.51
Branch AgNPs	176.28±1.47	173.70	178.86
Standard (BHT)	27.44±1.39	25.01	29.87
Standard (Ascorbic acid)	12.83±1.26	10.62	15.04

In a study, it was found that the DPPH radical removal % inhibition values of methanol extracts of mistletoe growing on different trees were between 59.52 and 95.12 (Uçar et al. 2006). Again, DPPH radical inhibition percentages of the leaf and root parts of *V. album* growing on various trees were calculated. According to this study, the leaf parts ranged from 31.25 to 68.93, and the root parts ranged from 30.13 to 67.28 (Tahirović & Bašić 2017). The results of this study were found to be compatible with the literature. The results obtained show that AgNPs synthesized from *V. album* plant parts have significant antioxidant activity. The antioxidant capacity of the fruit aqueous extract and the silver nanoparticles produced from this extract were found to be greater than in other portions of the plant. The difference between the results may be due to the type of tree on which this plant is grown, the time of collection, the different extraction environments, and the different phytochemical contents of the plant parts (Jäger et al. 2021). Silver nanoparticles were synthesized using the leaves of *Tagetes erecta* L., one of the plants used for health purposes, and the antioxidant capacity (DPPH radical removal) of these nanoparticles was investigated. While the IC_{50} value of the plant extract was 40.0 µg/mL, the IC_{50} value of silver nanoparticles synthesized from this extract was reported to be 23.8 µg/mL. It was determined that the antioxidant capacity of silver nanoparticles was greater than that of the extract (Erenler et al. 2021). It can be concluded that these silver nanoparticles have therapeutic potential in the treatment of free radical caused illnesses.

3.4. In vitro antidiabetic potential research

3.4.1. α-amylase enzyme inhibition of samples

One of the enzymes that enables the breakdown of starch into glucose is α-amylase (Kim et al. 2014; Shim et al. 2003). Therefore, finding these enzyme inhibitors is important in the treatment of diabetes (Ibrahim et al. 2019). The α-amylase enzyme inhibition percentages values of *V. album* plant part extracts and silver nanoparticles synthesized from these extracts and standard acarbose are shown in (Figure 12).

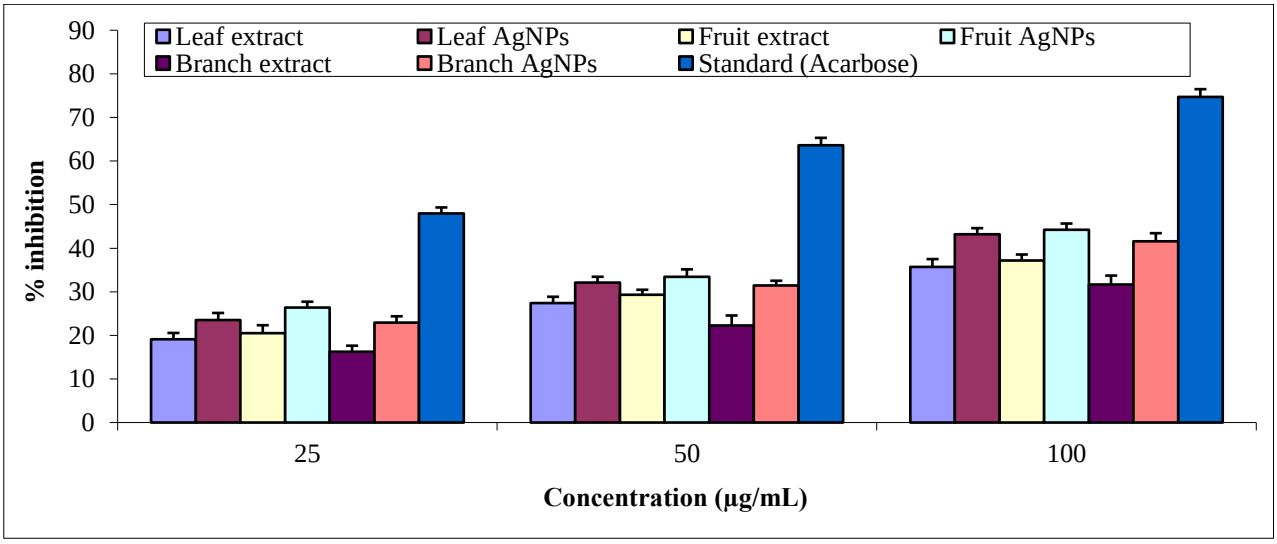

Figure 12- α-amylase enzyme inhibition percentages of the samples

The α-amylase enzyme inhibition percentages of samples at 100 µg/mL concentration are as follows: standard Acarbose (74.67±1.82), fruit AgNPs (44.21±1.45), leaf AgNPs (43.17± 1.43), branch AgNPs (41.59±1.85), fruit extract (37.16±1.39), leaf

extract (35.72±1.78) and branch extract (31.70±2.01) (P<0.05). Additionally, IC_{50} values were calculated using three different concentrations of all samples. The results are shown in Table 3.

Table 3- IC_{50} values (antidiabetic activity) of *V. album* plant part extracts, silver nanoparticles, and standard

Samples	*IC_{50} (µg/mL)*	*95% Confidence Interval for Mean*	
		Lower Bound	*Upper Bound*
Leaf extract	164.21±1.29	161.95	166.47
Leaf AgNPs	125.01±1.40	122.55	127.47
Fruit extract	156.94±1.48	154.33	159.55
Fruit AgNPs	123.59±1.44	121.06	126.12
Branch extract	189.17±2.01	185.64	192.70
Branch AgNPs	132.71±1.34	130.35	135.07
Standard (Acarbose)	22.55±1.63	19.69	25.41

Studies have shown that oxidative stress is responsible for the progression and pathogenesis of diabetes (Simmons 2006; Kaneto et al. 2007). The increase in free radicals and the weakness of the intracellular antioxidant defense system lead to an increase in diabetes complications (Gupta & Chari 2005). In a study conducted on in vivo rats, *V. album* extract was given to rats for 20 days. As a result of the study, it was determined that these extracts had radical scavenging, antioxidant, and antidiabetic activities (Ahmed et al. 2019). Studies have reported that mistletoe leaves are effective in relieving diabetes (Gray & Flatt 1999). In a study that synthesized silver nanoparticles from *Tribulus terrestris* seed extracts, which are widely used in traditional medicine, the in vitro antidiabetic activities of these nanoparticles were investigated. As a result, it was reported that silver nanoparticles at a concentration of 100 µg/mL showed high α-amylase enzyme inhibition of 75.68 ± 0.11% (Rahman et al. 2023). In this study, the α-amylase enzyme inhibition percentages of leaf, fruit, and branch silver nanoparticles at 100 µg/mL concentration were determined as leaf AgNPs (43.17± 1.43), fruit AgNPs (44.21±1.45), and branch AgNPs (41.59±1.85), respectively. It was determined that our results were lower than the *Tribulus terrestris* silver nanoparticle results. As a result of this in vitro study, it was determined that *V. album* plant parts and silver nanoparticles synthesized from these parts had antidiabetic properties.

3.5. In vitro antimicrobial potential research

Within the scope of the study, the antimicrobial activities of AgNPs (3mM) synthesized from *V. album* on pathogenic microorganisms were investigated. Zone diameters related to the antimicrobial activities of synthesized AgNPs are given in Table 4 in millimeters.

Table 4- Antimicrobial activity zone diameters of *V. album* plant extracts and silver nanoparticles

Microorganisms	*Leaf AgNPs (mm)*	*Fruit AgNPs (mm)*	*Branch AgNPs (mm)*	*V.album extract (mm)*			*Control*			
				Leaf	*Fruit*	*Branch*	*Ampicillin 10 (µL/mL)*	*Nystatin*	*$AgNO_3$ (3mM)*	*Distilled water*
S. aureus (ATCC 25923)	18	20	16	12	14	10	18	_	5	_
B. cereus (709 Roma)	12	18	17	_	13	15	17	_	4	_
E. faecalis (ATCC 29212)	12	10	15	13	12	13	15	_	5	_
B. subtilis (ATCC 6633)	_	12	_	_	_	_	_	_	4	_
E. coli (ATCC 25922)	20	10	_	12	14	_	15	_	5	_
A. hydrophila (ATCC 7966)	12	_	_	13	_	_	_	_	7	_
P. aeruginosa (ATCC 27853)	16	8	14	_	_	13	_	_	7	_
K. pneumoniae (ATCC 13883)	16	10	_	14	_	_	_	_	6	_
V. anguillarum (ATCC 43312)	12	10	_	_	13	_	15	_	5	_
S. typhi (ATCC 6539)	12	21	_	10	12	_	20		6	_
C. albicans (ATCC 90028)	_	_	_	_	_	_	_	18	_	_

After 48 hours, the inhibition zone around each well was measured in millimeters to assess the susceptibility of the test microorganisms. Antibiotic use as a control allowed for comparison of antimicrobial activity outcomes. In addition, we employed the 3 mM $AgNO_3$ solution's antibacterial activity as a control, which obscures the viewable region. The greatest inhibitory effect of the silver nanoparticle synthesized from the leaf extract was in *E. coli* with a 20 mm diameter inhibition zone, followed by *S. aureus* with an 18 mm diameter inhibition zone, and then *P. aeruginosa* and *K. pneumoniae* with a 16 mm diameter inhibition zone. Good efficacy against pneumoniae has been observed. The most inhibitory effect of the silver nanoparticle synthesized from the fruit extract was determined in *S. typhi* with a 21 mm diameter inhibition zone, followed by *S. aureus* with a 20 mm diameter inhibition zone and then *B. cereus* with an 18 mm diameter inhibition zone. The most inhibitory effect of the silver nanoparticle synthesized from the sap extract was determined in *B. cereus* with a 17 mm diameter inhibition zone, followed by *S. aureus* with a 16 mm diameter inhibition zone and then against *E. feacalis* with a 15 mm diameter inhibition zone. As can be seen in Table 4, silver nanoparticles synthesized from *V. album* leaf, fruit and branch extracts were comparable to some antibiotics in *S. aureus* and *E. coli*, *P. aeruginosa*, *K. pneumoniae*, *S. typhi*, *E. feacalis* and *B. cereus*. It has good antibacterial activity against *C. albicans* showed no antimicrobial effect with the silver nanoparticle synthesized from *V. album* (leaf, fruit and branch). Table 4 shows the widths of the inhibition zones of aqueous extracts of *V. album* leaves, fruits, and branches. Compared to ampicillin, leaf extracts of *V. album* had decreased antibacterial activity against *K. pneumoniae* (14 mm), *E. feacalis* and *A. hydrophila* (13 mm), and *E. coli* (12 mm). In contrast, compared to ampicillin and $AgNO_3$, the majority of the produced AgNPs had a better antibacterial effect on the test microorganisms. The inhibition zone diameter of 21 mm (*S. typhi*) offered the best level of antibacterial activity for AgNPs produced from *V. album* (fruit). Comparing this number to ampicillin and $AgNO_3$, it is substantially greater. The results of the antibacterial activity tests were compared to those of the control experiment. There were no zones of inhibition observed in the control, indicating that the antibacterial effect is caused by silver nanoparticles.

Nanoparticles have been used in the pharmaceutical industry as an alternative to antibiotics in recent years. As a result, it is possible that it could be a solution to the antibiotic resistance developed by pathogenic bacteria. According to reports, silver nanoparticles are being used to treat a wide range of diseases caused by both gram-negative and gram-positive bacteria. The degradation and eventual death of bacteria are brought on by AgNPs' interactions with cellular components or biomolecules. Translation and protein synthesis are impeded by denaturation, which is specifically brought on by AgNPs contact with ribosomes. Additionally, AgNPs may interact with the carboxyl and thiol groups on galactosidase, obstruct intracellular biological processes, and result in cell death (You et al. 2012). AgNPs are used in implantable technology, the treatment of wounds, medical equipment, antibacterial medications to prevent bacterial infections, and immunizations (Wang et al. 2017).

3.5.1. Minimal inhibition concentrations (MIC) of samples

Table 5 shows the minimal inhibition concentrations (MIC) of AgNPs with antimicrobial activity within the scope of the study. AgNPs derived from the leaf extract of *V. album* have a significantly higher minimum inhibitory concentration against *E. coli* and *S. aureus* than against *S. typhi* and *A. hydrophila*. The extracts MIC values against *B. cereus*, *E. faecalis*, *P. aeruginosa*, *K. pneumoniae*, and *V. anguillarum* were not significantly different.

Table 5- MIC table of *V. album* plant extracts and silver nanoparticles

Microorganisms	*Leaf (AgNPs) (µL/mL)*	*Fruit (AgNPs) (µL/mL)*	*Branch (AgNPs) (µL/mL)*	*V.album extract (µL/mL)*			*Control*			
				Leaf	*Fruit*	*Branch*	*Ampicillin 10 (µL/mL)*	*Nystatin*	*$AgNO_3$ (3mM)*	*Distilled water*
***S. aureus* (ATCC 25923)**	16	16	_	_	32	_	16	_	64	_
***B. cereus* (709 Roma)**	32	16	16	_	16	8	16	_	128	_
***E. faecalis* (ATCC29212)**	32	256	16	32	64	16	32	_	128	_
***B. subtilis* (ATCC 6633)**	_	32	_	_	--	_	_	_	256	_
***E. coli* (ATCC 25922)**	16	256	_	64	32	_	32	_	128	_
***A. hydrophila* (ATCC 7966)**	64	_	_	32	32	_	_	_	32	_
***P. aeruginosa* (ATCC 27853)**	32	256	32	_	16	16	_	_	64	_
***K. pneumoniae* (ATCC 13883)**	32	64	_	16	_	_	_	_	256	_
***V. anguillarum* (ATCC 43312)**	32	64	_	_	_	_	32	_	128	_
***S. typhi* (ATCC 6539)**	64	16	_	256	16	_	16	_	256	_
***C. albicans* (ATCC 90028)**	_	_	_	_	_	_	_	**16**	_	_

3.5.2. Anti-Quorum sensing analysis of samples

Zone diameters of AgNPs made with anti-majority detection activity (Anti-QS) agar well diffusion method was calculated in mm Table 6.

Table 6- Zone diameters of anti-quorum sensing activities of AgNPs synthesized by *V. album*

Concentration (µL/mL)	*Leaf AgNPs (mm)*	*Fruit AgNPs (mm)*	*Branch AgNPs (mm)*	*V.album extract (µL/mL)*		
				Leaf (mm)	*Fruit (mm)*	*Branch (mm)*
	3mM	3mM	3mM			
5	20	18	12	13	12	11
2.5	19	17	11	12	12	11
1.25	18	16	10	11	11	10
0.625	15	12	9	10	11	10

The loss of pigment in *C. violaceum* bacteria is an indication that the applied material (AgNPs) causes Quorum-Sensing (QS) inhibition. As stated in Table 6; it was determined that all AgNPs synthesized were effective in the agar diffusion method for anti-QS. The inhibition zones formed were determined as the regions where *C. violaceum* bacteria could not produce pigment. AgNPs are inhibit the production of acyl homoserine lactone (AHL) by *C. violaceum*, which prevent the bacteria from coming together and therefore have Anti-QS activity. AgNPs were produced from *V. album* through disc diffusion using the bioreporter strain CV12472, and varied concentrations (5, 2, 5, 1.25, and 0.625 µL/mL) were used in the *C. violaceum* experiment. In CV 12472 cultures containing exogenous AHL, the loss of purple pigment is a sign that *V. album* has inhibited quorum sensing. The amount of silver nanocolloids injected had a direct correlation with the inhibition effect on quorum sensing, as shown by the distinct halo zone of inhibition surrounding the wells of different diameter. This research establishes for the first time the quorum quenching activity of silver nanoparticles created by aqueous extracts of *V. album* (Arunkumar et al. 2022).

4. Conclusions

In traditional medicine, aqueous extracts of *V. album* have been used in cancer treatment for years. For this reason, the leaf, fruit, and branch parts of the *V. album* plant were discussed. It was determined whether silver nanoparticles could be synthesized from plant part extracts by the green method. In addition, this is the first study in which the characterization and biological activities (antioxidant, antidiabetic and antimicrobial capacities) of these plant parts and silver nanoparticles synthesized from these parts were investigated using UV-Vis, FTIR, SEM, EDS, and XRD analysis methods. The UV-Vis examination of silver nanoparticles revealed that Ag^+ ions were converted to Ag^0. Furthermore, surface plasmon resonance peaks at 427, 430, and 425 nm were observed in UV-Vis analyses, indicating the synthesis of leaf, fruit, and branch silver nanoparticles, respectively. Comparing the FTIR results of plant extracts and silver nanoparticles showed that some functional groups were involved in silver nanoparticle synthesis. When the SEM images of the plant part silver nanoparticles were examined, it was observed that the silver nanoparticles obtained from all three parts were spherical in shape. It was determined that the silver nanoparticles obtained from the fruit part extract were smaller and nanosized than the nanoparticles obtained from other parts of the plant. In addition, when the EDS results of the nanoparticles were examined, it was determined that silver nanoparticles consisting of three parts of the plant were formed in a high and pure form of 74% to 83%. XRD results of plant-part silver nanoparticles showed that the nanoparticles were formed in a pure and crystalline structure. In particular, it was determined that the crystal size of all three leaf, fruit, and branch parts was in the nanometer range. It was observed that the crystal size of the AgNPs obtained from the fruit extract was smaller. Antioxidant, antidiabetic and antimicrobial activity determinations were made to determine the biological activities of plant parts and silver nanoparticles synthesized from these parts. It has been concluded that different parts of this plant are valuable in terms of antioxidant, antidiabetic, and antimicrobial parameters. It was concluded that silver nanoparticles synthesized from the fruit extract of this plant are strong in terms of antioxidant and antidiabetic activity. It is known that the leaf and branch parts of the *V. album* plant, which is a medicinal aromatic plant, are consumed mostly, and the fruit parts are not consumed. This study showed that fruit parts thought to be poisonous are rich in both antioxidants and antidiabetics. Therefore, it was concluded that the unused fruit parts of this plant can be used in silver nanoparticle synthesis. As a result, it was concluded that leaf, fruit, and branch extracts of the *V. album* plant and silver nanoparticles synthesized from these extracts can be used as synthetic antioxidant, antidiabetic, and antimicrobial natural drug raw materials.

References

Ahmed A K, Mert H & Mert N (2019). "Investigation of the antidiabetic effects of mistletoe (*Viscum album* L.) extract in experimental diabetes in rats". *Van Veterinary Journal* 30(2): 121-125

Ahmed S, Ahmad M, Swami B L & Ikram S (2016). "A review on plants extract mediated synthesis of silver nanoparticles for antimicrobial applications: a green expertise". *J Adv Res* 7: 17–28. https://doi.org/10.1016/j.jare.2015.02.007

Akbal A, Turkdemir M H, Cicek A & Ulug B (2016). "Relation between silver nanoparticle formation rate and antioxidant capacity of aqueous plant leaf extracts". *Journal of Spectroscopy* 2016: 4083421. https://doi.org/10.1155/2016/4083421

Ali A, Zafar H, Zia M, ul Haq I, Phull A R, Ali J S & Hussain A (2016). "Synthesis, characterization, applications, and challenges of iron oxide nanoparticles". *Nanotechnol Sci Appl* 19(9): 49–67. https://doi.org/10.2147/NSA.S99986

Almatroudi A (2020). "Silver nanoparticles: synthesis, characterisation and biomedical applications". *Open Life Sciences* 15(1): 819-839. https://doi.org/10.1515/biol-2020-0094.

Apostolidis E, Kwon Y I & Shetty K (2007). "Inhibitory potential of herbal, fruit, and fungal-enriched cheese against key enzymes linked to type 2 diabetes and hypertension". *Innovative Food Science and Emerging Technologies* 8: 46-54. https://doi.org/10.1016/j.ifset.2006.06.001

Arunkumar M, Suhashini K, Mahesh N & Ravikumar R (2014). "Quorum quenching and antibacterial activity of silver nanoparticles synthesized from *Sargassum polyphyllum*". *Bangladesh Journal of Pharmacology* 9: 54-59. https://doi.org/10.3329/bjp.v9i1.17301

Asha A, Sivaranjani T, Thirunavukkarasu P & Asha S (2016). "Green synthesis of silver nanoparticle from different plants-a review". *International Journal of Pure Applied Bioscience* 4(2): 118–124. http://doi.org/10.18782/2320-7051.2221

Ashraf J M, Ansari M A, Khan H M, Alzohairy M A & Choi I (2016). "Green synthesis of silver nanoparticles and characterization of their inhibitory effects on AGEs formation using biophysical techniques". *Scientific Reports* 6: 20414. http://doi.org/10.1038/srep20414

Awwad A M, Salem N M & Abdeen A O (2013). "Green synthesis of silver nanoparticles using carob leaf extract and its antibacterial activity". *International Journal of Industrial Chemistry* 4: 29

Bar H, Bhui D K, Sahoo G P, Sarkar P, De S P & Misra A (2009). "Green synthesis of silver nanoparticles using latex of *Jatropha curcas*". *Colloids and Surfaces A: Physicochemical and Engineering Aspects* 339(1–3): 134–139. https://doi.org/10.1016/j.colsurfa.2009.02.008

Barber D & Harris S (1994). "Oxygen free radicals and antioxidants A review". *Am Pharma* 9: 26–35. https://doi.org/10.1016/s0160-3450(15)30310-x

Bhakya S, Muthukrishnan S, Sukumaran M & Muthukuma M (2016). "Biogenic synthesis of silver nanoparticles and their antioxidant and antibacterial activity". *Appl Nanosci* 6: 755-766. https://doi.org/ 10.1007/s13204-015-0473-z

Bindhu M R & Umadevi M (2013). "Synthesis of monodispersed silver nanoparticles using *Hibiscus cannabinus* leaf extract and its antimicrobial activity". *Spectrochim Acta A: Mol Biomol Spectrosc* 101: 184–190. https://doi.org/10.1016/j.saa.2012.09.031

Blois M S (1958). "Antioxidant determinations by the use of a stable free radical". *Nature* 181: 1199–1200

Büssing A, Azhari T, Ostendorp H, Lehnert A & Schweizer K (1994). "*Viscum album* L. extracts reduce sister chromatid exchanges in cultured peripheral blood mononuclear cells". *European Journal of Cancer* 30(12): 1836–1841. https://doi.org/10.1016/0959-8049(94)00299-k

Büssing A & Schietzel M (1999). "Apoptosis-inducing properties of *Viscum album* L. extracts from different host trees, correlate with their content of toxic mistletoe lectins". *Anticancer Res* 19(1A): 23–28

Chernousova S & Epple M (2013). "Silver as antibacterial agent: Ion, nanoparticle, and metal. *Angewandte Chemie International Edition* 52: 1636–1653". https://doi.org/10.1002/anie.201205923

Cho K H, Park J E, Osaka T & Park S G (2005). "The study of antimicrobial activity and preservative effects of nanosilver ingredient". *Electrochimica Acta* 51(5): 956–960. https://doi.org/10.1016/j.electacta.2005.04.071

Chung I M, Rahuman A A, Marimuthu S, Kirthi A V, Anbarasan K, Padmini P & Rajakumar G (2017). "Green synthesis of copper nanoparticles using *Eclipta Prostrata* leaves extract and their antioxidant and cytotoxic activities". *Exp Ther Med* 14(1): 18–24. https://doi.org/10.3892/etm.2017.4466

CLSI Document M100-S17 (2007). "Performance standards for antimicrobial susceptibility testing 17th Informational Supplement", Clinical and Laboratory Standards Institute, Wayne, Pennsylvania: CLSI, Table 1, 26 pp

Çiftci B, Karaman K & Kaplan M (2024). "Comparison of antioxidant, antiradical and antibacterial activities of mistletoe (*Viscum album* L.) fruits and leaves growing on diferent host tree genus". *Waste and Biomass Valorization* 15: 2819–2832. https://doi.org/10.1007/s12649-023-02307-0

Dash S P, Dixit S & Sahoo S (2017). "Phytochemical and biochemical characterizations from leaf extracts from *Azadirachta Indica*: An important medicinal plant". *Biochemistry & Analytical Biochemistry* 6: 1000323. https://doi.org/10.4172/2161-1009.1000323

Deng J, Cheng W & Yang G (2011). "A novel antioxidant activity index (AAU) for natural products using the DPPH assay". *Food Chemistry* 125(4): 1430–1435. https://doi.org/10.1016/j.foodchem.2010.10.031

Ekhaise F O, Ofoezie V G & Enobakhare D A (2010). "Antibacterial properties and preliminary phytochemical analysis of methanolic extract of mistletoe (*Tapinanthus bangwensis*)". *Bayero Journal of Pure and Applied Sciences* 3(2): 65–68. https://doi.org/10.4314/bajopas.v3i2.63223

Elumalai E K, Prasad T N V K V, Hemachandran J & Therasa S V (2010). "Extracellular synthesis of silver nanoparticles using leaves of *Euphorbia hirta* and their antibacterial activities". *Journal of Pharmaceutical Sciences and Research* 2(9): 549-554

Erenler R, Geçer E N, Genç N & Yanar D (2021). "Antioxidant activity of silver nanoparticles synthesized from *Tagetes erecta* L. leaves". *International Journal of Chemistry and Technology* 5(2): 141-146. http://dx.doi.org/10.32571/ijct.1005275

Geetha K M, Murugan V, Pavan Kumar P & Wilson B (2018). "Antiepileptic activity of *Viscum articulatum* Burm and its isolated bioactive compound in experimentally induced convulsions in rats and mice". *Eur J Biomed Pharm Sci* 5(3): 311–318

Gray A M & Flatt P R (1999). "Insulin- secreting activity of the traditional antidiabetic plant *Viscum album* (mistletoe)". *Journal of Endocrinology* 160: 409–414. https://doi.org/10.1677/joe.0.1600409

Gupta M M & Chari S (2005). "Lipid peroxidation and antioxidant status in patients with diabetic retinopathy". *Indian J Physiol Pharmacol* 49(2): 187

Gurunathan S, Park J H, Han J W & Kim J H (2015). "Comparative assessment of the apoptotic potential of silver nanoparticles synthesized by *Bacillus tequilensis* and *Calocybe indica* in MDA-MB-231 human breast cancer cells: Targeting p53 for anticancer therapy". *International Journal of Nanomedicine* 10: 4203–4223

Hegde P, Maddur M S, Friboulet A, Bayry J & Kaveri S V (2011). "*Viscum album* exerts anti-inflammatory effect by selectively inhibiting cytokine-induced expression of cyclooxygenase-2". *PLoS One* 6(10): e26312. https://doi.org/10.1371/journal.pone.0026312

Huang D, Ou B & Prior R L (2005). "The chemistry behind antioxidant capacity assays". *Journal of Agricultural and Food Chemistry* 53(6): 1841-1856. https://doi.org/10.1021/jf030723c

Huang J & Zhan G (2011). "Biogenic, silver nanoparticles by *Cacumen platycladi* extract: synthesis, formation mechanism and antibacterial activity". *Industrial Engineering Chemistry Research* 50: 9095–106. https://doi.org/10.1021/ie200858y

Ibrahim S R M, Mohamed G A, Khayat M T & Ahmed S (2019). "Mangostanaxanthone VIIII, a new xanthone from Garcinia mangostana pericarps, α-amylase inhibitory activity, and molecular docking studies". *Revista Brasileira de Farmacognosia* 29: 206-212. https://doi.org/10.1016/j.bjp.2019.02.005

Jha A K, Prasad K, Prasad K & Kulkarni A R (2009). "Plant system: nature's nanofactory". *Colloids and Surfaces B: Biointerfaces* 73(2): 219–223. https://doi.org/10.1016/j.colsurfb.2009.05.018

Jäger T, Holandino C, Melo M N D O, Peñaloza E M C, Oliveira A P, Garrett R, Glauser G, Grazi M, Ramm H, Urech K & Baumgartner S (2021). "Metabolomics by UHPLC-Q-TOF reveals host tree-dependent phytochemical variation in *Viscum album* L". *Plants* 10: 1726. https://doi.org/10.3390/plants10081726

Kaneto H, Katakami N, Kawamori D, Miyatsuka T, Sakamoto K, Matsuoka T A, Matsuhisa M &Yamasaki Y (2007). "Involvement of oxidative stress in the pathogenesis of diabetes". *Antioxid Redox Signal* 9(3): 355-366. https://doi.org/10.1089/ars.2006.1465

Kasthuri J, Veerapandian S & Rajendiran N (2009). "Biological synthesis of silver and gold nanoparticles using apiin as reducing agent". *Colloids and Surfaces B: Biointerfaces* 68: 55–60. https://doi.org/10.1016/j.colsurfb.2008.09.021

Kaviya S, Santhanalakshmi J, Viswanathan B, Muthumary J & Srinivasan K (2011). "Biosynthesis of silver nanoparticles using *Citrus sinensis* peel extract and its antibacterial activity". *Spectrochimica Acta Part A: Molecular and Biomolecular Spectroscopy* 79: 594–598. https://doi.org/10.1016/j.saa.2011.03.040

Kedare S B & Singh R P (2011). "Genesis and development of DPPH method of antioxidant assay". Journal of Food Science and Technology 48(4): 412–422. https://doi.org/10.1007/s13197-011-0251-1

Khalilzadeh M A & Borzoo M (2016). "Green synthesis of silver nanoparticles using onion extract and their application for the preparation of a modified electrode for determination of ascorbic acid". *Journal of Food and Drug Analysis* 24(4): 796–803. https://doi.org/10.1016/j.jfda.2016.05.004

Khandel P & Shahi S K (2016). "Microbes mediated synthesis of metal nanoparticles: current status and future prospects". *International Journal of Nanomaterials and Biostructures* 6(1): 1–24

Khatun A, Rahman M, Rahman M M, Hossain H, Jahan I A & Nesa L (2016). "Antioxidant, antinociceptive and CNS activities of *Viscum orientale* and high sensitive quantifcation of bioactive polyphenols by UPLC". *Front Pharmacol* 7: 176. https://doi. org/10.3389/fphar.2016.00176

Kienle G S, Mussler M, Fuchs D & Kiene H (2016). "Intravenous mistletoe treatment in integrative cancer care: a qualitative study exploring the procedures, concepts, and observations of expert doctors". *Evid Based Complement Alternat Med* 2016: 4628287. https://doi.org/10.1155/2016/4628287

Kim M, Kim E, Kwak H S & Jeong Y (2014). "The ingredients in Saengshik, a formulated health food, inhibited the activity of α-amylase and α-glucosidase as anti-diabetic function". *Nutr Res Pract* 8: 602-606. https://doi.org/10.4162/nrp.2014.8.5.602

Korcan S E, Cankaya N, Azarkan S Y & Bulduk I (2023). "Determination of antioxidant activities of *Viscum album* L.: First report on interaction of phenolics with survivin protein using in silico analysis". *Chemistry Select* 8(e202300130): 1–13. https://doi.org/10.1002/slct.202300130

Kovacs E (2002). "The in vitro effect of *Viscum album* (VA) extract on DNA repair of peripheral blood mononuclear cells (PBMC) in cancer patients". *Phytotherapy Research* 16: 143–147. https://doi.org/ 10.1002/ptr.920

Kumar P, Kumar D, Kaushik D & Kumar S (2016). "Screening of neuropharmacological activities of *Viscum album* and estimation of major favonoid constituents using TLC densitometry". *Int J Toxicol Pharmacol Res* 8: 179–186.

Kumar D G, Achar R R, Kumar J R, Amala G, Gopalakrishnan V K, Pradeep S, Shati A A, Alfaif M Y, Eldin Elbehairi S E I, Silina E, Stupin V, Manturova N, Shivamallu C & Kollur S P (2023). "Assessment of antimicrobial and anthelmintic activity of silver nanoparticles bio-synthesized from *Viscum orientale* leaf extract". *BMC Complementary Medicine and Therapies* 23: 167. https://doi.org/10.1186/s12906-023-03982-1

Materska M (2008). "Quercetin and its derivatives-a review". *Pol J Food Nutr Sci* 58(4): 407–413

McLean K, Winson M, Fish L, Taylor A, Chhabra S R, Cámara M, Daykin M, Lamb J, Swift S, Bycroft B, Stewart G & Williams P (1997). "Quorum sensing and Chromobacterium violaceum: exploitation of violacein production and inhibition for the detection of N-acyl homoserine lactones". *Microbiology* 143(12): 3703–3711. https://doi.org/10.1099/00221287-143-12-3703

Miliauskas G, Venskutonis P R & VanBeek T A (2004). "Screening of radical scavenging activity of some medicinal and aromatic plant extracts". *Food Chemistry* 85(2): 231–237. https://doi.org/10.1016/j.foodchem.2003.05.007

Moreno M I N, Isla M I, Sampietro A R & Vattuone M A (2000). "Comparison of the free radical-scavenging activity of propolis from several regions of Argentina". *J Ethnopharmacol* 71(1-2): 109–114. https://doi.org/10.1016/s0378-8741(99)00189-0

Nartop P (2016). "Use of biosynthetic silver nanoparticles in the surface sterilization of *Pyracantha coccinea* stem explants". *Pamukkale University Journal of Engineering Sciences* 23(6): 759–761. https://doi.org/ 10.5505/pajes.2016.04809

Nasrollahzadeh M, Babaei F, Fakhri P & Jaleh B (2015). "Synthesis, characterization, structural, optical properties and catalytic activity of reduced graphene oxide/ copper nanocomposites". *RSC Advances* 5: 10782–10789. https://doi.org/10.1039/C4RA12552E

Navalon S, Dhakshinamoorthy A, Alvaro M & Garcia H (2016). "Metal nanoparticles supported on two-dimensional graphenes as heterogeneous catalysts". *Coordination Chemistry Reviews* 312: 99–148. https://doi.org/10.1016/j.ccr.2015.12.005

Nicoletti M (2023). "The anti-inflammatory activity of *Viscum album*". *Plants* 12(7): 1460. https://doi.org/10.3390/plants12071460

Nicoletti M (2023). "The antioxidant activity of mistletoes (*Viscum album* and other species)". *Plants* 12: 2707. https://doi.org/10.3390/plants12142707

Niki E (2010). "Assessment of antioxidant capacity in vitro and in vivo". *Free Radic Biol Med* 49(4): 503–515. https://doi.org/ 10.1016/j.freeradbiomed.2010.04.016

Oei S L, Thronicke A & Schad F (2019). "Mistletoe and immunomodulation: insights and implications for anticancer therapies". *Evid Based Complement Altern Med* 2019: 1–6. https://doi. org/10.1155/2019/5893017

Orhue P O, Edomwande E C, Igbinosa E, Momoh A R M & Asekomhe O O (2014). "Antibacterial activity of extracts of mistletoe (Tapinanthus dodoneifollus (Dc) Dancer) from cocoa tree (Theobrama cacao)". *International Journal of Herbs and Pharmacological Research* 3(1): 24–29

Park J H, Kim Y N, Kim J K, Park H Y & Song B S (2019). "Viscothionin purifed from mistletoe (*Viscum album* var. *coloratum* Ohwi) induces insulin secretion from pancreatic beta cells". *J Ethnopharmacol* 234: 172–179. https://doi.org/10.1016/j.jep.2019.01.014

Petrus E M, Tinakumari S, Chai L C, Ubong A, Tunung R, Elexson N, Chai L F & Son R (2011). "A study on the minimum inhibitory concentration and minimum bactericidal concentration of Nano Colloidal Silver on food-borne pathogens". *International Food Research Journal* 18: 55–66

Pietrzak W & Nowak R (2021). "Impact of harvest conditions and host tree species on chemical composition and antioxidant activity of extracts from *Viscum album L*". *Molecules* 26: 3741. https://doi.org/10.3390/molecules26123741

Qader I N, Pekdemir M E, Coşkun M & Kanca M S (2022). "Biocompatible PLA/PCL blends nanocomposites doped with nanographite: Physico-chemical, and thermal behaviour". *Journal of Polymer Research* 29(7): 264. https://doi.org/ 10.1007/s10965-022-03117-z

Rahman A, Rehman G, Shah N, Hamayun M, Ali S, Ali A, Shah S K, Khan W, Shah M I A & Alrefaei A F (2023). "Biosynthesis and characterization of silver nanoparticles using *Tribulus terrestris* seeds: revealed promising antidiabetic potentials". *Molecules* 28: 4203. https://doi.org/10.3390/molecules28104203

Roman G P, Neagu E & Radu G L (2009). "Antiradical activities of *Salvia officinalis* and *Viscum album* L. extracts concentrated by ultrafiltration process". *Acta Sci Pol Technol Aliment* 8(3): 47–58.

Safaepour M, Shahverdi A R, Shahverdi H R, Khorramizadeh M R & Gohari A R (2009). "Green synthesis of small silver nanoparticles using geraniol and its cytotoxicity against Fibrosarcoma-Wehi 164". *Avicenna J Med Biotechnol* 1(2): 111–115.

Scherer R & Godoy H T (2009). "Antioxidant activity index (AAI) by the 2,2-diphenyl-1-picrylhydrazyl method". *Food Chemistry* 112(3): 654–658. https://doi.org/10.1016/j.foodchem.2008.06.026

Shim Y J, Doo H K, Ahn S Y, Kim Y S, Seong J K, Park I S & Min B H (2003). "Inhibitory effect of aqueous extract from the gall of Rhus chinensis on alpha-glucosidase activity and postprandial blood glucose". *Journal of Ethnopharmacology* 85(2–3): 283–287. https://doi.org/10.1016/S0378-8741(02)00370-7

Shinde A, Ganu J & Naik P (2012). "Effect of free radicals & Antioxidants on oxidative stress". *Journal of Dental and Allied Sciences* 1(2): 63–66

Shobha G, Moses V & Ananda S (2014). "Biological synthesis of copper nanoparticles and its impact". *International Journal of Pharmaceutical Science Invention* 3(8): 6–28

Simmons R A (2006). "Developmental origins of diabetes: the role of oxidative stress". *Free Radic Biol Med* 40(6): 917-922. https://doi.org/10.1016/j.freeradbiomed.2005.12.018

Slinkard K & Singleton V L (1977). "Total phenol analyses: Automation and comparison with manual methods". *Am J Enol Viticulture* 28: 49–55. https://doi.org/ 10.5344/ajev.1977.28.1.49

Sotiriou G A & Pratsinis S E (2010). "Antibacterial activity of nanosilver ions and particles". *Environmental Science Technology* 44(14): 5649–5654. https://doi.org/10.1021/es101072s

Stoimenov P K, Klinger R L, Marchin G L & Klabunde K J (2002). "Metal oxide nanoparticles as bactericidal agents". *Langmuir* 18(17): 6679–6686. https://doi.org/10.1021/la0202374

Suvith V S & Philip D (2014). "Catalytic degradation of methylene blue using biosynthesized gold and silver nanoparticles". *Spectrochimica Acta Part A: Molecular and Biomolecular Spectroscopy* 118: 526–532. https://doi.org/10.1016/j.saa.2013.09.016

Szurpnicka A, Zjawiony J K & Szterk A (2019). "Therapeutic potential of mistletoe in CNS-related neurological disorders and the chemical composition of *Viscum* species". *J Ethnopharmacol* 231: 241–252. https://doi.org/10.1016/j.jep.2018.11.025

Tahmasebi Zade Damirchi B, Rostami Charati F, Akbari R & Daneshvar A (2020). "Green synthesis of silver nanoparticles using the aqueous extract of *Viscum album* fruit". *Nanochem Res* 5(1): 104–110. https://doi.org/ 10.22036/ncr.2020.01.010

Tahirović A & Bašić N (2017). "Determination of phenolic content and antioxidant properties of methanolic extracts from *Viscum album* ssp. *album* Beck". *Bulletin of the Chemists and Technologists of Bosnia and Herzegovina* 49: 25–30.

Uçar E Ö, Karagöz A & Arda N (2006). "*Viscum album* ssp. it has an antioxidant effect". Fitoterapia 77(7-8): 556–560. https://doi.org/10.1016/j.fitote.2006.08.001

Valko M, Leibfritz D, Moncol J, Cronin M T D, Mazur M & Telser J (2007). "Free radicals and antioxidants in normal physiological functions and human disease". *Int J Biochem Cell Biol* 39(1): 44–84. https://doi.org/ 10.1016/j.biocel.2006.07.001

Venkatesham M, Ayodhya D, Madhusudhan A & Veerabhadram G (2012). "Synthesis of stable silver nanoparticles using gum acacia as reducing and stabilizing agent and study of its microbial properties: A novel green approach". *International Journal of Green Nanotechnology* 4(3): 199–206. https://doi.org/10.1080/19430892.2012.705999

Vicaş S I, Rugina D, Leopold L, Pintea A & Socaciu C (2011). "HPLC fingerprint of bioactive compounds and antioxidant activities of *Viscum album* from different host trees". *Not Bot Hort Agrobot Cluj* 1: 48–57. https://doi.org/10.15835/nbha3913455

Vidhu V K, Aromal S A & Philip D (2011). "Green synthesis of silver nanoparticles using Macrotyloma uniflorum". *Spectrochim Acta A Mol Biomol Spectrosc* 83(1): 392–397. https://doi.org/10.1016/j.saa.2011.08.051

Vigneshwaran N, Kathe A A, Varadarajan P V, Nachane R P & Balasubramanya R H (2006). "Biomimetics of silver nanoparticles by white rot fungus, *Phaenerochaete chrysosporium*". *Colloids Surf B: Biointerfaces* 53(1): 55–59. https://doi.org/ 10.1016/j.colsurfb.2006.07.014

Wang Z L (2000). "Transmission electron microscopy and spectroscopy of nanoparticles". *In book: characterization of nanophase materials* 3: 37–80

Wang L, Hu C & Shao L (2017). "The antimicrobial activity of nanoparticles: present situation and prospects for the future". *Int J Nanomedicine* 12: 1227-1249. https://doi.org/10.2147/IJN.S121956

Wesenberg D, Kyriakides I & Aqathos S N (2003). "White-rot fungi and their enzymes for the treatment of industrial dye effuents". *Biotechnology Adv* 22(1-2): 161–187. https://doi.org/10.1016/j.biotechadv.2003.08.011

You C, Han C, Wang X, Zheng Y, Li Q, Hu X & Sun H (2012). "The progress of silver nanoparticles in the antibacterial mechanism, clinical application and cytotoxicity". *Mol Biol Rep* 39(9): 9193–9201. https://doi.org/10.1007/s11033-012-1792-8

Zhou X, Zeng M, Huang F, Qin G, Song Z & Liu F (2023). "The potential role of plant secondary metabolites on antifungal and immunomodulatory effect". *Appl Microbiol Biotechnol* 107: 4471-4492. https://doi.org/10.1007/s00253-023-12601-5

Journal of Agricultural Sciences
(Tarim Bilimleri Dergisi)

J Agr Sci-Tarim Bili
e-ISSN: 2148-9297
jas.ankara.edu.tr

JAS

A Hybrid Lightweight Deep Neural Network Approach for Plant Disease Classification Using Self-Attention Mechanism and Transfer Learning

Thaer Sultan Darweesh Alramli[a,b], Adem Tekerek[c*]

[a]*Graduate School of Natural and Applied Sciences, Gazi University, 06570 Ankara, TURKEY*

[b]*Computer Engineering Department, University of Mosul, Mosul 41002, IRAQ*

[c]*Computer Engineering Department, Faculty of Technology, Gazi University, 06570 Ankara, TURKEY*

ARTICLE INFO

Research Article

Corresponding Author: Adem Tekerek, E-mail: atekerek@gazi.edu.tr

Received: 22 August 2024 / Revised: 29 November 2024 / Accepted: 18 November 2024 / Online: 25 March 2025

Cite this article

Alramli T S D, Tekerek A (2025). A Hybrid Lightweight Deep Neural Network Approach for Plant Disease Classification Using Self-Attention Mechanism and Transfer Learning. *Journal of Agricultural Sciences (Tarim Bilimleri Dergisi),* 31(2):392-412. DOI: 10.15832/ankutbd.1537267

ABSTRACT

Classification of plant diseases is crucial for overall food security and agricultural economies in the world. However, classification has long been challenging primarily due to the various diseases it encompasses and the different environmental factors influencing them. One of the main challenges in developing an accurate classification model is obtaining high-quality, multiclass datasets. At the same time, deep learning methods like CNN may be considered state-of-the-art in detecting complex image patterns in various applications for correct diagnoses. Still, they involve poor parameter optimizations and overfitting and have very high resource requirements. This paper introduces a combined model of classifying plant diseases in an imaging approach, which incorporates the Efficient Neural Network (ENN) with a Squeeze and Excitation Network (SEN). The architecture follows high-density feature extraction by the networks, late fusion of features, and using a cross-channel attention mechanism to boost feature representation. This work uses transfer learning to design the hyperparameter optimization scheme and early stopping scheme to avoid overfitting. We tested our model on the Plant Village Dataset and the Leaf Rose Disease Dataset with an accuracy of 96.40% for the Plant Village Dataset and 97.15% accuracy on the Leaf Rose Disease Dataset. Our model achieved higher accuracy than the traditional DNNs VGG16, Inception V3, and RESNET-50 by approximately 21.04%, 9.40%, and 4.33% on the Plant Village Dataset. It improved the classification accuracy compared to VGG16, Inception V3, and RESNET-50 by 15.80%, 11.20%, and 6.02% on the Rose leaf disease dataset, respectively. Moreover, it has the lowest times as well as space complexity: 45 minutes and 150 MB, which are less than VGG16 (50 minutes, 180 MB), Inception Net (55 minutes, 170 MB), and RESNET-50 (75 minutes, 190 MB). The global results show that our approach is superior, demonstrating enhanced performance and efficiency, which makes it well-suited for real-time applications.

Keywords: Leaf classification, Convolutional neural network, Efficient Neural Network, Squeeze and Excitation Network, Classification accuracy

1. Introduction

Plant diseases threaten global food security and sustainable agriculture, reducing crop yield, quality, and economic viability (Strange et al. 2005). Rapid and accurate diagnosis of these diseases is essential for effective prevention and management strategies. Traditional diagnostic methods rely on expert analysis, which can be time-consuming, subjective, and prone to human error (Bock et al. 2020). Deep learning methods integrated with AI have emerged as a powerful solution for automating plant disease classification, enhancing efficiency and Accuracy (Li et al. 2021). Distinguishing objects in images based solely on visual traits is complex, and traditional machine-learning approaches focused on feature extraction often struggle with Accuracy (Zhao et al. 2019). The advent of deep learning has transformed this landscape, as these methods excel at recognizing intricate data patterns and can effectively handle large datasets. They offer scalability, flexibility, and end-to-end learning capabilities (Kamilaris & Prenafeta-Boldú 2018). Deep learning has become crucial in agriculture, addressing challenges in crop monitoring, predictive modeling, harvesting, and disease detection.

Previous work has proposed several plant leaf detection frameworks based on shape, texture, and vein characteristics (Agarwal et al. 2006), along with various classification models for identifying healthy and diseased plants (Liu et al. 2016; Yanikoglu et al. 2014). Chai et al. (2010) studied four diseases of tomato leaf, including early blight and late blight leaf mildew and leaf spot, extracted 18 characteristic parameters like color and texture, and shape information on the tomato leaf spot images, using stepwise discriminant and Bayesian discriminant principal component analysis PCA, respectively. The characteristic parameters and discriminant models of methods principal component analysis and fisher discriminant were used. The precisions of the two methods were 94.71% and 98.32%, respectively. Guan et al. (2010) extracted 63 parameters, including morphology, color and texture features of spots, and diseases of the rice leaf, classified and recognized with step-based discriminant analysis

and Bayesian discriminant method, three rice diseases (blast, stripe blight, and bacterial leaf blight) into the highest recognition accuracy of 97.2%. Mohanty et al. (2016) trained a deep-learning model to recognize 14 crop species and 26 crop diseases. The trained model reached an accuracy of 99.35% on the test set. Ma et al. (2018) used a deep CNN to conduct symptom-wise recognition of four cucumber diseases, including downy mildew, anthracnose, powdery mildew, and target leaf spots. The recognition accuracy reached 93.4%. Kawasaki et al. (2015) proposed a CNN-based system for detecting cucumber leaf disease, achieving an accuracy of 94.9%. Ahmad et al. (2020) employed four pretraining convolution neural networks, VGG19, VGG16, ResNet, and Inception V3, and the models were trained by fine-tuning parameters. The experimental results demonstrated that the Inception V3 performed the best on the two datasets (the laboratory dataset and the field dataset). The average performance is superior to 10% to 15% on the laboratory dataset compared with the field dataset. Bi et al. (2022) demonstrated that the accuracy rates of recognition for two apple leaf spot and rust models obtained by agriculture experts are 77.65%, 75.59%, and 73.50% with ResNet152, Inception V3, and MobileNet, respectively.

DL approaches have outperformed classical classification accuracy for several leaf-based plant disease datasets (Reyes et al. 2015; Mehdipour-Ghazi et al. 2017). Sun et al. (2017) proposed an advanced leaf classification model using RESNET-50 architecture, which enabled the residual connection and was validated on the BJFU100 dataset. This model mitigated information loss and enhanced feature density by ensuring proper gradient flow. However, this approach was still limited by computational and memory complexities constraints. Ferentinos (2018) designed a transfer learning-based CNN model that classified 87,484 plant leave images from 58 classes with an accuracy of 99.53%. Tiwari et al. (2021) reported a mean validation accuracy of 99.58% and a mean test accuracy of 99.199% through five-fold cross-validation after training a Dense Convolutional Neural Network (DCNN) on a diverged dataset of plant leaves from 26 countries. Sai Reddy and Neeraja (2022) designed a binary classifier for distinguishing between healthy and diseased leaves that achieved 96% to 99% accuracy on the New Plant Diseases (Augmented) and Rice Leaf datasets. Most recently, Ashwinkumar et al. (2022) designed an automated model based on an optimal MobileNet-based convolutional neural network that can optimize hyperparameters via the Emperor Penguin Optimizer (EPO) and relies on an Extreme Learning Machine (ELM) classifier for final classification.

The baseline models proposed various novel DL architectures and realized high classification accuracies in leaf-based plant classification tasks. However, these approaches still have problems, such as dependency on many hyperparameters, computationally expensive, poor convergence rate, and limited accuracy. In this research, we proposed a novel hybrid classification learning model by integrating two lightweight but highly accurate DL architectures, Efficient Neural Network (ENN) with a Squeeze and Excitation Network (SEN), to resolve the mentioned challenges. Efficient Neural Network (ENN) is a popular and efficient CNN architecture that has gained equal or even better performance than other traditional CNN models on various computer vision tasks (Koonce, 2021). In addition, ENN showed exceptional skill levels on image classification tasks using fewer parameters and resources than alternative architectures. Therefore, they are beneficial when it comes to being deployed in resource-restricted situations, including mobile devices or so-called edge devices. Similarly, Squeeze and Excitation Network (SEN) architectures also come from the family of light architectures that integrate effectively with other architectures and are thus compatible with several CNN models and gain top performance across many computer vision tasks (Hu et al. 2018). In addition, these models can design adaptive recalibrating feature maps when merged with other architectures and improve feature representation.

Further, we employed transfer learning (Weiss et al. 2016) to speed up the training procedure by adopting pre-trained weights and other related hyperparameters. The proposed methodology emphasizes a process of feature extraction from the ENN and SEN models, followed by a combination of self-attention blocks (Zhao et al. 2020) and a late feature fusion technique (Akilan et al. 2017) to merge them efficiently. The performance of the proposed methodology was cross-validated using a five-fold cross-validation technique (Wong et al. 2017) on two publicly available (1) Plant Village (Hughes et al. 2015) and (2) Rose Leaf Disease (Sazzad et al. 2022) Datasets. Finally, the testing results are compared with five traditional CNNs, i.e., Inception V3, RESNET-50, and VGG16 (Theckedath et al. 2020), Conventional Inception-Visual Geometry Group Network (Pal & Kumar 2023), EffecientNetV2 (Devi et al. 2023) in terms of various performance measures and recapitulated the global findings. Our contribution can be summarised as follows:

1. Design a novel lightweight hybrid CNN architecture that integrates the ENN and SEN frameworks for multiclass plant-leaf classification while enhancing performance through self-attention blocks and a late fusion technique.
2. Performance evaluation was conducted using a five-fold cross-validation technique on two publicly available (1) Plant Village and (2) Rose Leaf Disease Datasets.
3. We compared our results with five state-of-the-art methods: (1) Inception V3, (2) RESNET-50, (3) VGG16, (4) Conventional Inception-Visual Geometry Group Network, and (5) EfficientNetV2 models, evaluating them based on classification accuracy, precision, recall, F-score, ROC, and both time and space complexity.

The structure of the rest of the paper is as follows: Section 2 includes dataset details and fundamentals of the employed DL models. In Section 3, the proposed methodology is explained. The experimental results and discussion are covered in Section 4. Finally, the conclusions and the future scope of this work are presented in Section 5.

2. Material and DL Fundamentals

2.1. Dataset description

Our study used two popular and open sources: (1) PlantVillage and (2) Rose Leaf Disease datasets for training, validation, and testing of the proposed leaf classification framework. The details of both datasets are given below:

(1) PlantVillage Dataset

The PlantVillage database is one of the most extensive and publicly available standard datasets for plant disease classification, which is often used to compare the results obtained by various methods (Hughes et al. 2015). This dataset contains 54,306 plant leaves with 12 normal and 26 disease categories that can be applied to 14 different types of plants, such as tomatoes, potatoes, apples, and Grapes. The sample collection of Plantvillage varies according to angle, light, size, noise, and so on, which is why it is among the perfect plant disease recognition databases. The samples from the Plantvillage dataset are shown in Figure 1.

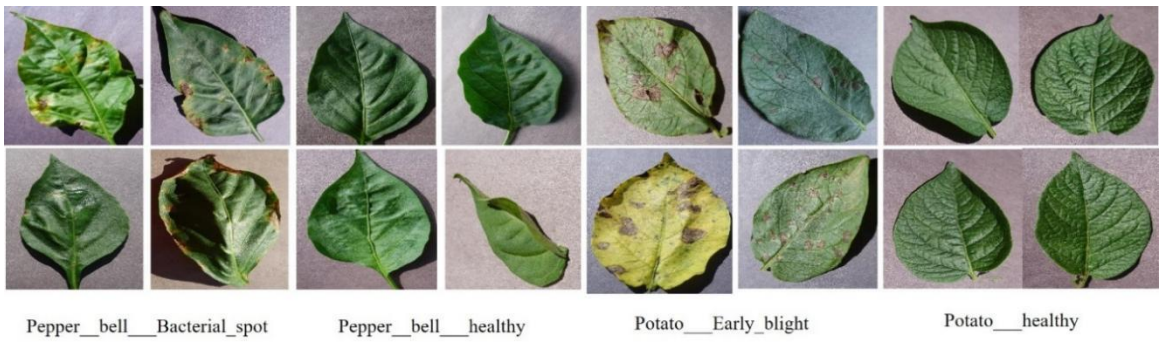

Figure 1- Visualization of leaf samples with respective classes of the PlantVillage dataset

(2) Rose Leaf Disease Dataset

The rose-leaf disease dataset is another popular and openly accessible dataset for the rose-leaf classification (Sazzad et al. 2022). It consists of 14,910 samples of rose leaves across three classes—Healthy Leaf Rose, Rose Rust, and Rose Sawfly/Rose Slug. The samples from the Rose Leaf dataset are shown in Figure 2.

Figure 2- Visualization of leaf samples with respective classes of the Rose leaf dataset

2.2. Deep learning paradigms and baseline architecture

In recent years, artificial intelligence based on deep learning has dramatically improved the most challenging tasks in computer vision, such as classification, object detection, segmentation, and generation. Deep learning models depend on artificial neural networks, which are composed of multiple layers; because of this, these models can learn complex hierarchical features independently from raw image data. Convolutional neural networks have gained widely held appeal concerning image classification; these models often outperform human performance. Due to their structure, convolutional layers may filter local patches of the input image. Thus, spatial information is not lost from these neural networks, and CNNs can capture small-scale

events and progressively learn more complex features produced by deeper networks. Recent advanced techniques such as attention mechanisms, transfer learning, generative modeling, and supervised learning have significantly improved the performance of existing CNN architectures. In our work, we employed the improvement strategies of self-attention mechanisms (Zhao et al. 2020) and transfer learning (Ghazi et al. 2017). Our proposed approach outperforms five baseline CNN architectures presented by Theckedath et al. (2020): (1) VGG-Net, (2) Inception-Net, (3) RES-Net, (4) Conventional Inception-Visual Geometry Group Network, and (5) EfficientNetV2. We describe these strategies further in the subsequent sections.

2.2.1. Self-Attention in convolution neural network

Self-attention in CNN is a mechanism that enables neural networks to detect relationships between pixels in an image. It calculates the weighted sum of each element in the sequence, with the weights changing dynamically according to how similar each element is to the others. This mechanism implies a multi-step operation including Query (Q), Key (K), and value (V) metrics to evaluate linearly transformed feature maps of input images using Eq. 1.

$$\begin{aligned} Q&=XW_Q, \\ K&=XW_K, \\ V&=XW_V \end{aligned} \quad (1)$$

Where; W_Q, W_K, and W_V are learnable weight matrices. Further, attention scores (A) are computed by considering the dot product between the Query (Q) and Key matrices (K) using Eq. 2.

$$A=\text{softmax}\left(\frac{Q*K^T}{\sqrt[2]{d}}\right) \quad (2)$$

Where; d is the dimensionality of the Key vectors. Next, Softmax normalization performs the necessary weight scaling, allowing the network to highlight contextual pixels using Eq. 3.

$$A=\text{softmax}(A) \quad (3)$$

The normalized attention ratings are utilized to generate a weighted sum of the Value matrix: $Y=AV$ represents the attended feature map. The extracted feature map is finally used in the next step.

2.2.2. Transfer learning

Transfer learning in computer vision refers to applying the experience learned by previously trained models to new vision challenges in which data is incorrectly labeled. The pre-trained models offer capabilities that are very handy for different tasks trained on massive datasets, such as ImageNet. The learned weights of the pre-trained model can be deployed as features or fine-tuned on the new dataset using intermediate layers. This way, the computational resources and time taken for training are minimized. At the same time, good performance is also realized with small or similar datasets. Let X be the input dataset with N samples, and W be the pre-trained model's weights:

The pre-trained model works as a feature extractor, and the output of one of its intermediate layers is designated as $F_{Pre}(X, W_{Pre})$. Further, the loss function L computes the discrepancy between the model's predictions and the ground truth labels (Y) using Eq. 4.

$$L=f(F_{Pre}(X,\ W_{Pre}),\ Y) \quad (4)$$

Finally, Gradient descent or its derivatives are used to optimize the model parameters (pre-trained or fine-tuned weights) to minimize the loss function. The optimization phase updates the model parameters to fit the new dataset better, leveraging the pre-trained model's knowledge.

2.2.3. Baseline CNN architectures

(1) VGG19-Net

The Visual Geometry Group at the University of Oxford proposed the VGG-Net convolutional neural network architecture. Karen Simonyan and Andrew Zisserman introduced it in their paper "Very Deep Convolutional Networks for Large-Scale Image Recognition" in 2014 (Simonyan & Zisserman, 2014). The input of the VGG neural Network is a 224x224-pixel RGB image. It gives uniform sample sizes for the ImageNet competition, and the authors subtracted 224 x 224 from the middle of every picture. Convolutional Layers use the 3×3 receptive field to scan the entire image and generate spatial patterns. The second step is the linear transformation of the output, which happens before it is ReLU-activated. The generalized VGG structure is shown in Figure 3.

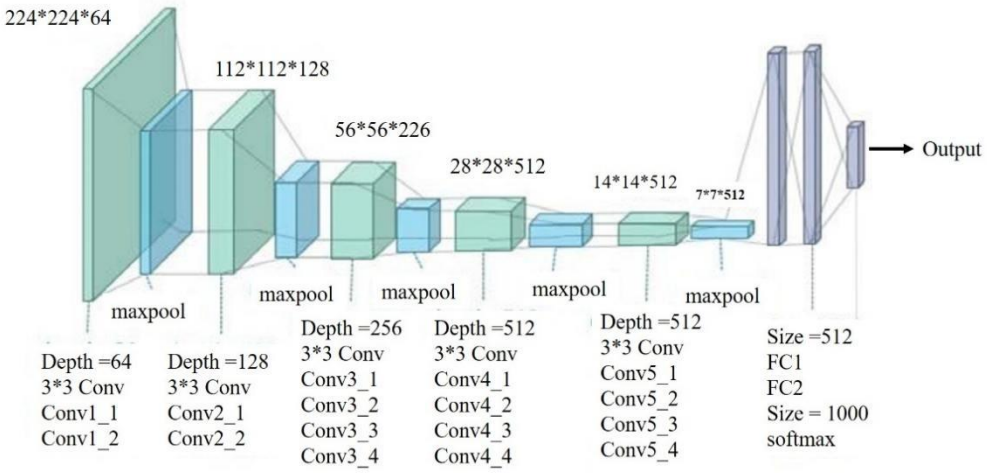

Figure 3- The generalized architecture of VGG-Net (Simonyan and Zisserman, 2014)

(2) Inception-Net

Inception-Net, also known as Google-Net, is an advanced CNN architecture that tries to overcome some of the weaknesses of VGG-Net, including overfitting and high computational cost due to its large number of hyperparameters (Szegedy et al. 2016). The convolutional network consists of 27 convolutional layers that, for instance, use a mix of kernel operations, including 1×1, 3×3, and 5×5 kernels, with the results being fed forward into the subsequent stage as feature vectors. In addition, maximum pooling is performed and concatenated before being passed on to the next inception module. These inception modules are stacked linearly to remove unnecessary and redundant image patterns for the reduction in dimension. It has 22 layers deep when not counting pooling layers and uses global average pooling right after the final inception module. Figure 4 presents Inception-Net's architecture.

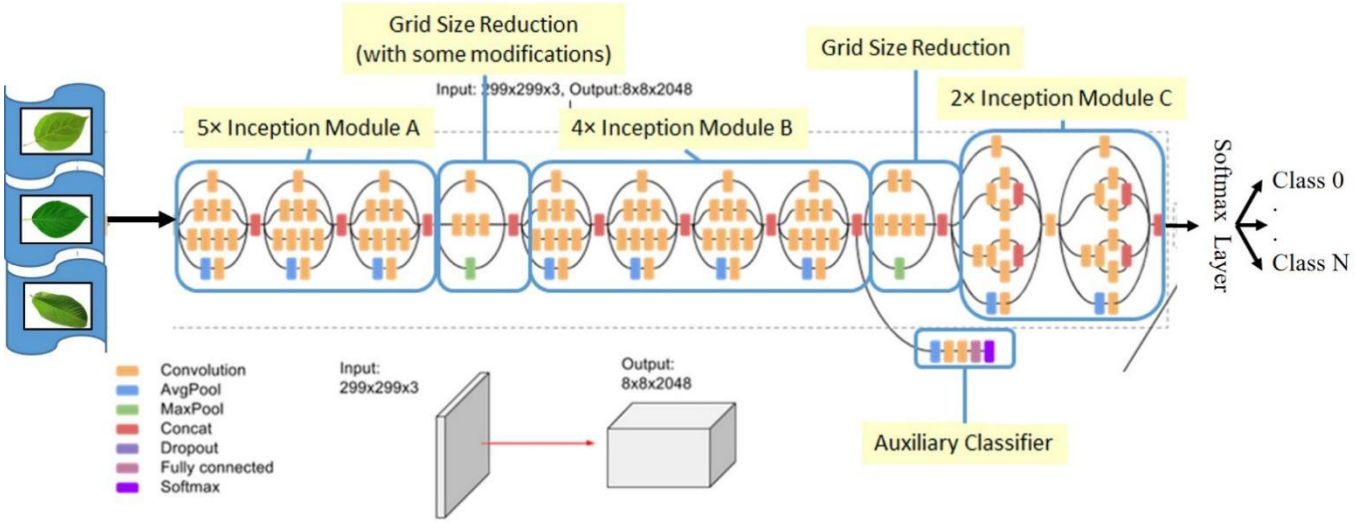

Figure 4- Inception-Net Architecture proposed in the original article (Szegedy et al. 2016)

(3) RESNET-50 Architecture

RESNET-50 is a deep neural network with 50 convolution layers within 16 blocks (He et al. 2016). It introduced skip connection to improve against the vanishing gradient problem, thus facilitating the possibility of training large deep networks. The RESNET-50 network appears as a simple bottleneck design with 1x1, 3x3, and 1x1 convolutions, which reduces the complexity of computation while preserving high representational power; instead of using fully connected layers followed by the SoftMax classifier and ReLU activation functions, it uses global average pooling (Figure 5).

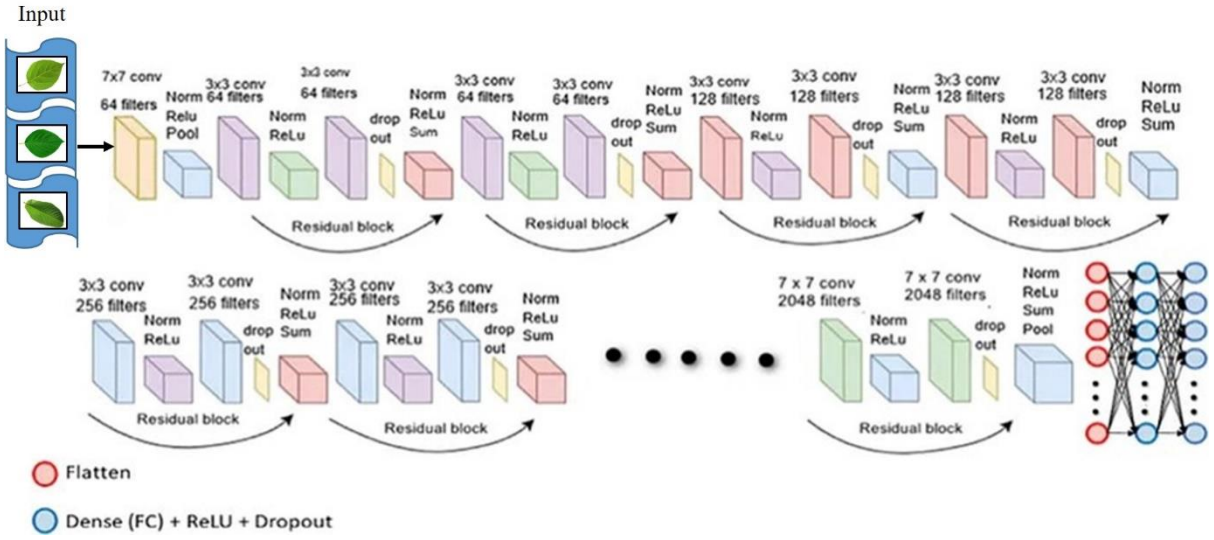

Figure 5- Original RESNET Architecture (He et al. 2016)

3. Proposed Methodology

The proposed hybrid classification framework comprises four main phases: (1) the preprocessing stage, (2) feature extraction, (3) late feature fusion, and (4) model validation, as depicted in Figure 6. In the preprocessing phase, annotations would be made to recognize the region of interest in plant images. Deep features shall be extracted from RoI using two lightweight architectures, CNNs, (1) ENN (version 1) and SEN. A self-attentive mechanism is applied on both feature sets to capture dependencies among different sub-regions in the image. These optimized features are merged using a late feature fusion technique. Finally, two dense layers are followed by a SoftMax layer, which classifies the leaves based on their imaging patterns. Five-fold cross-validation is implemented to measure the framework's performance, and the results are recorded further for analysis. The workings of each phase are discussed in detail in the subsequent subsections.

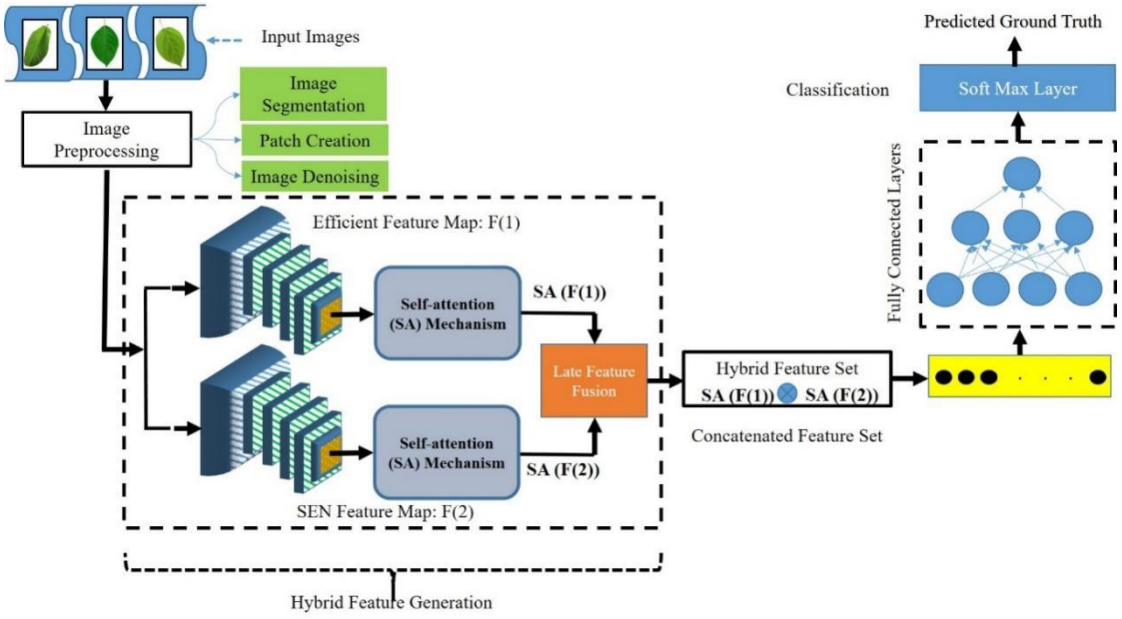

Figure 6- The proposed Leaf classification network

3.1. Data preprocessing

For the first approach, we employed the standard architecture of U-Net developed for image segmentation (Ronneberger et al. 2015) (Figure 7). Further, we fixed a suitable patch size and applied the customized BM3D filtering technique to reduce the noise level in the input leaf images (Chen et al. 2010). The method entails partitioning the input image into overlapping small blocks and continuing to scan for similar blocks within a localized neighborhood. Metrics of Euclidean distance or structural similarity index estimate the disparity of the block. In our work, we set the patch size at 224 x 224 and utilized the Gradient-Based Structural Similarity (Chen et al. 2006) Index (G-SSIM) to compute the block similarities. The G-SSIM

formula is found by calculating the similarity between the gradient distributions of the two image blocks. The mathematical definition of G-SSIM is given in Eq. 5.

$$G\text{-}SSIM\ (x,y) = \frac{2*\mu_x*\mu_y+ C_1}{\mu_x{}^2+ \mu_y{}^2+C_1} * \frac{2*\sigma_{xy}+ C_2}{\sigma_x{}^2+ \sigma_y{}^2+C_2} \quad (5)$$

Where:

- μ_x and μ_y are the means of the gradient distributions of image blocks x and y respectively.
- σ_x and σ_y are the standard deviations of the gradient distributions of image blocks x and y, respectively.
- σ_{xy} is the covariance of the gradient distributions of image blocks x and y, respectively,
- $C1$ and $C2$ are small constants added to avoid instability when the denominator is near zero.

The mean, variance, and covariance can be computed with the derivatives of the image blocks. After the process of gradient distribution, they are calculated using the formula for similarity measurement using gradients. The subsequent blocks are grouped to generate a clean waveform for the noisy signals and suppress noise. In the BM3D collaborative filtering technique, similar blocks are jointly processed, which increases denoising performance. The pseudocode of the customized BM3D algorithm is given in Algorithm 1.

(A): Original Samples

(B): Segmented Samples

Figure 7- Samples of original (A) and segmented leaves (B) using U-NET

Algorithm 1: Pseudocode for image denoising using the customized BM3D algorithm

1. **Parameter declaration**
   - PATCH_SIZE = (224, 224), C1 = 0.01, C2 = 0.03, THRESHOLD = 0.8
2. Define Functions:
   - **Noise_reduction(input_image):**
     - Apply BM3D filter to input_image.
     - Return the denoised image.
   - **Divide_into_blocks(input_image):**
     - Divide the input image into blocks of size PATCH_SIZE.
     - Return the blocks.
   - **Calculate**_similarity_index(block1, block2):
     - Calculate the Gradient-based Structural Similarity Index (G-SSIM) between block1 and block2.
     - Return the similarity index.
   - **collaborative_filtering(block1, block2):**
     - Implement BM3D Collaborative Filtering between block1 and block2.
     - Return the denoised block.
3. **Main Function:**
   - **main():**
     - Read the input image.
     - Perform noise reduction using the noise_reduction function.
     - Divide the denoised image into blocks using the divide_into_blocks function.
     - For each block in the blocks:
       - Create an empty list of similar_blocks.
       - For each other_block in the blocks:
         - If other_block is not equal to block:
           - Calculate the similarity index between block and other_block using calculate_similarity_index.
           - If the similarity index is greater than THRESHOLD:
             - Append other_block to similar_blocks.
       - For each similar_block in similar_blocks:
         - Perform collaborative filtering between block and similar_block using the collaborative_filtering function.

3.2. Hybrid feature generation

Feature hybridization is one of the most important parts of machine learning in which one looks to combine existing features or create new ones to enhance model performance. This process helps identify complex, non-linear relationships between input features and the target variable for better predictive accuracy. We have developed two lightweight yet efficient deep neural network architectures: The Efficient Neural Network (ENN) and the Squeeze and Excitation Network (SEN). These architectures correctly identify complex leaf patterns and reduce the risk of overfitting when used in applications with large feature spaces, such as the Plant Village dataset with 38 classes. Detailed descriptions for both architectures are provided in the following subsections.

3.2.1. EfficientNet (B0) architecture

EfficientNet is a state-of-the-art convolutional neural network that attempts to balance the parameters of accuracy and computational cost using compound scaling, which adjusts all dimensions-depth, width, and resolution-simultaneously (Tan et al. (2019). To achieve that, this balancing act with a compound coefficient resulted in great performance at low computational costs. The depth and complex features captured by stacked convolutional blocks include the Efficient Neural Network Version 1, which is slightly larger and better for the optimal floating-point operation per second. B0 has been chosen for its reduced computational cost and faster processing, giving it an edge in making it suitable for real-time applications. The core component of it is the use of squeeze and excitation optimization within the MBConv layer. MBConv is roughly analogous to the inverted residual blocks in MobileNet v2, allowing skip connections between convolutional blocks' input and output. It begins with a 1x1 convolution to double the number of feature maps, then depthwise and pointwise convolutions to reduce the channel numbers to 3x3. Such skip connections connect the thinner layers, and thicker layers are stacked between skips. Its architecture is shown in Figure 8.

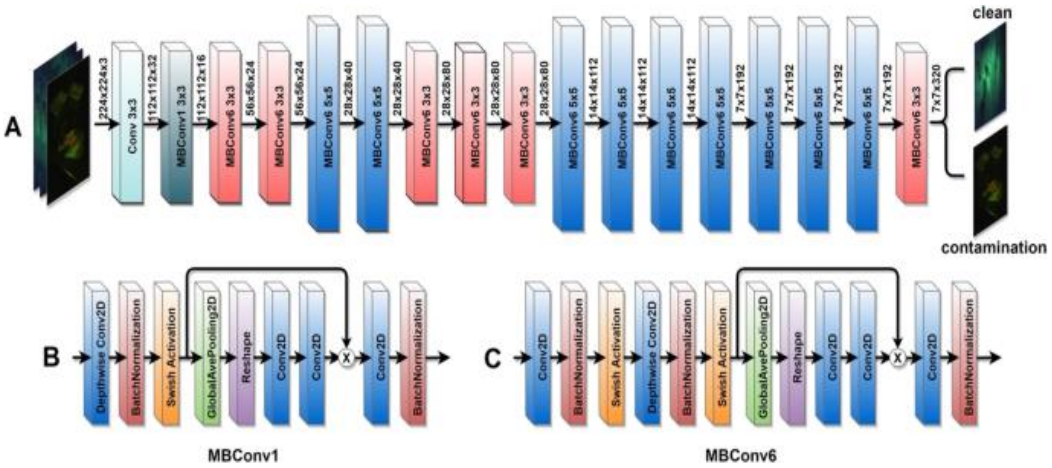

Figure 8- The concise representation of the EfficientNet-B0 model

3.2.2. Squeeze and excitation network

The SE networks introduce a novel architectural component enhancing the representative capacity of convolutional neural networks by adaptively recalibrating channel-wise feature responses (Hu et al. 2018). The SE block works under two steps: squeeze and excitation. In the squeeze step, global average pooling is applied to the feature maps; this condenses spatial information into channel descriptors, capturing the global context of feature activation. Then is the excitation step, where the squeezed outputs are passed through a fully connected layer to create channel-wise scaling factors like those of the sigmoid activation function. These scaling factors are then used to modulate the original feature maps, thus amplifying the informative features and suppressing the less relevant ones. This has enabled better learning of complex patterns by improving feature discrimination and achieved performance benefits in a large class of tasks, such as image classification, object detection, and semantic segmentation. It has been demonstrated that SE networks indeed enhance the accuracy of the model while at the same time retaining computational efficiency, making them a breakthrough improvement over deep learning methodologies. The architecture of the SE block is shown in Figure 9.

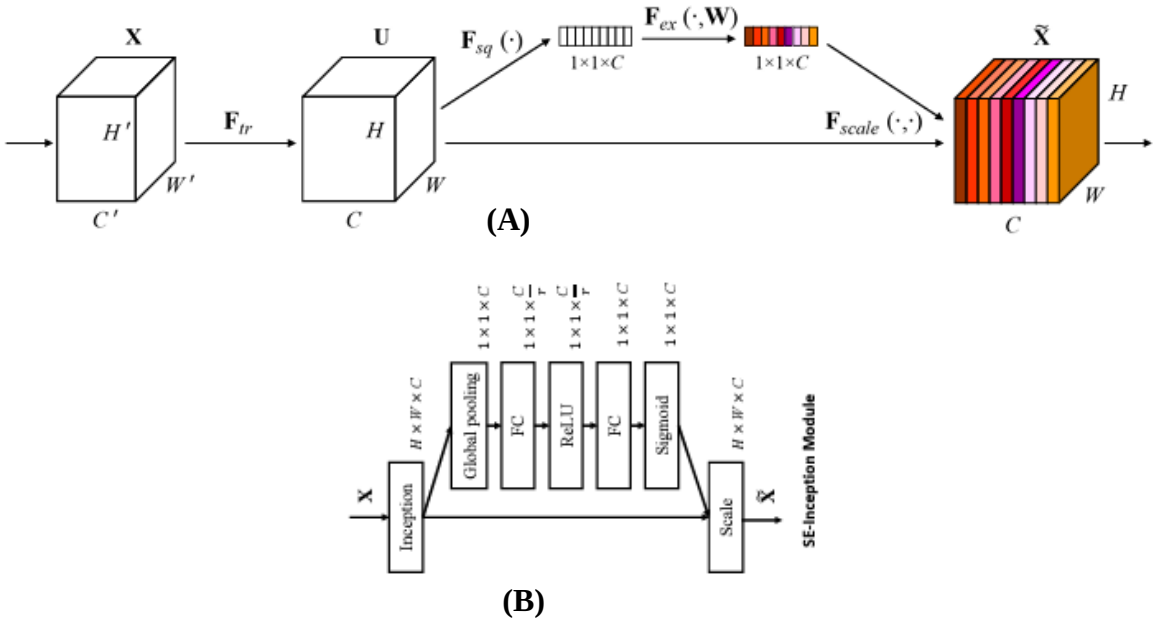

Figure 9- A Squeeze-and-Excitation block (A) and SE-Inception module (B). Both images are directly taken from the original research paper published in 2018 (Hu et al. 2018)

3.2.3. Feature hybridization

Feature hybridization forms the central module in our classification framework, utilizing two newly developed deep, dense modules: Hybrid Block 1 and Hybrid Block 2, as depicted in Figures 10 (A) and 10 (B). These modules amalgamate differently selected modules from both the Squeeze-and-Excitation architecture and EfficientNetB0 architecture to grasp the spatial locality of both diseased and healthy patterns of the leaves. This hybrid block 1 takes an input 3D tensor: 224 × 224 × 3, which interprets as an RGB image. The working of this module is initiated by using a 2D convolution layer with the kernel size 112 × 112 and 64 output channels. Then, normalization and ReLU of the non-linearity activation function apply. The spatial attention mechanism recalibrates the feature maps as added above. It gives a combined output of size 1064 ×1024×64 resulting from the Squeeze Block and the Weighted Bottleneck (WB) Conv1 block, elaborated as a parallel path of many convolution layers and concatenation.

Output from the Excitation Block is tensor size 1024 × 1024 × 64, which is processed through a 3 × 3 convolutional filter by batch normalization and followed by a non-linear activation function. It adds zeros to one side and one corner for spatial dimensions, followed by a GAP layer that reduces spatial dimensions but pools features across depth. After a BN step, a Depthwise Conv2D layer further operates on feature maps. This Depthwise Conv2D output is added to the input feature maps of size 112 × 112 × 64 and fed into another Depthwise Conv2D operation. In Hybrid Block 2, two input tensors are employed. The first is an RGB image of 224 × 224 × 3. The second is a size 112 × 112 × 64 feature map from the previous processing stage.

The main path takes an input of 224 × 224 × 3 and processes it with a 2D convolution with a 112 × 112 kernel and 64 output channels. The weighted bottleneck WB conv blocks are then utilized after batch normalization, and a ReLU activation function is used for dimensionality reduction. Finally, 56 × 56 × 128 is used, and the output from these WB blocks goes through a convolution operation of size 3 × 3. Outputs of the primary and auxiliary paths are concatenated along the channel dimension. The resulting tensor is passed through a 3 × 3 convolutional layer with a Filter Block. Another mechanism is applied, such as an attention mechanism for feature recalibration. Downsampling is done with a pooling convolution layer so that the output comes out to be a tensor of 56 × 56 × 128. GAP operation reduces the spatial dimensions while keeping the channel dimensions, followed by a batch normalization layer on GAP output. This output from the above norm-0 tensor is then merged with the 64 x 112 x 112 channel input tensor through concatenation along the channel dimension. The merged tensor is then forwarded to subsequent layers or blocks in the neural network's architecture.

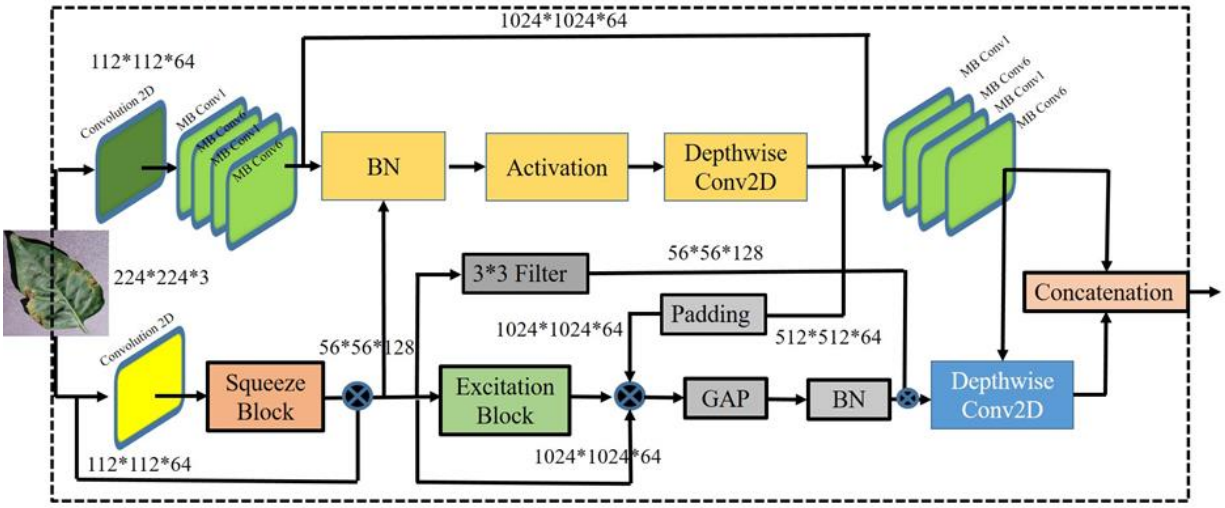

(A). Hybrid Block 1

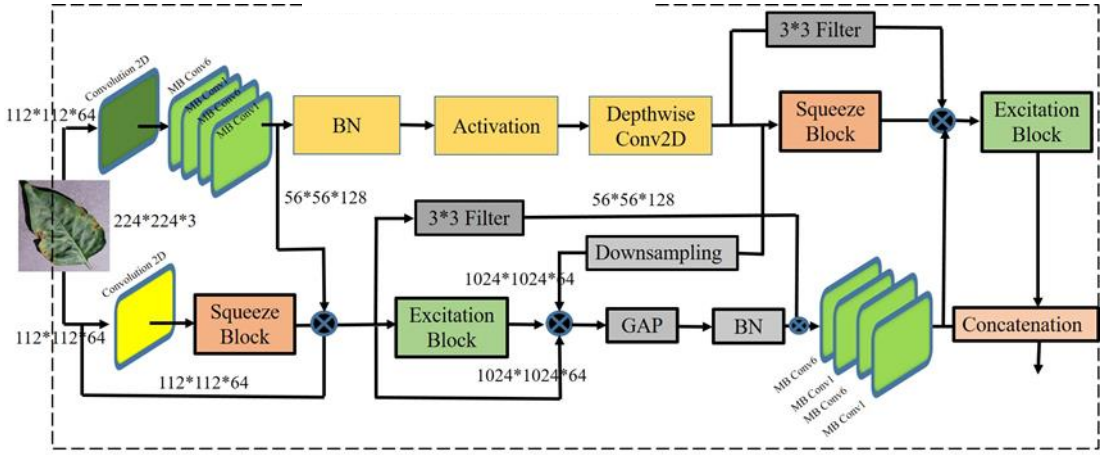

(B). Hybrid Block 2

Figure 10- The architecture of hybrid blocks 1 (A) and 2 (B). Here, BN indicates "Batch Normalization," and GAP refers to "Global Average Pooling."

3.3. Ladder-shaped CNN classification network

Our proposed multiclass classification architecture is a ladder-shaped CNN architecture with an alternating sequence of 14 modules with Hybrid Block 1 and Hybrid Block 2, as shown in Figure 11. As mentioned, these blocks comprise convolutional layers, batch normalization, activation functions, squeeze-and-excitation blocks, downsampling, and concatenations. The initial layers process the input, a set of leaf images, in parallel to be fed through the 14-module sequence: hybrid Block 1 and 2 alternates to allow multi-scale feature extraction and hierarchical representation within this architecture. The architecture alternates between consecutive Hybrid Block 2 modules with Hybrid Block 1 in between and repeats this pattern throughout all 14 modules. It improves multi-scale feature extraction and hierarchical learning, enhancing overall architecture's abilities. It follows the final module by passing information to a SoftMax layer that returns a probability distribution for multiclass classification. Hybrid blocks based on attention mechanisms, residual connections, and multi-scale processing enable critical feature usage in improving the classification of leaves as diseased or healthy. Algorithm 2 describes the pseudocode of the proposed classification algorithm.

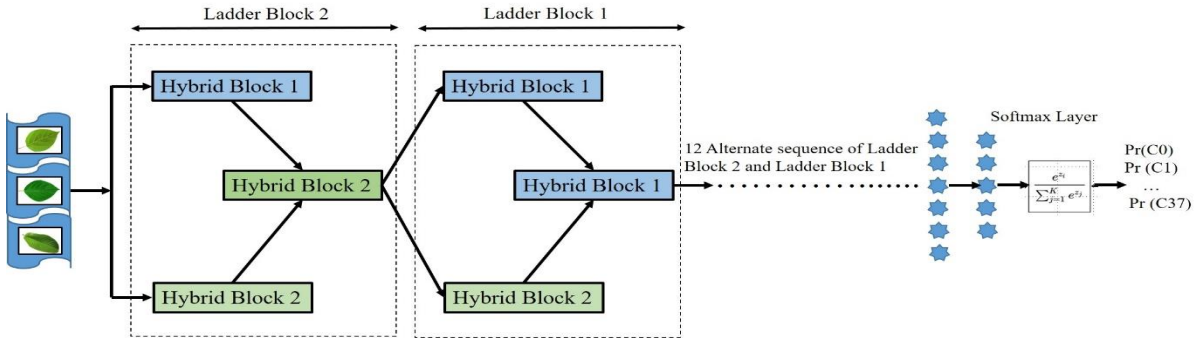

Figure 11- Proposed Classification Framework Consisting of Hybrid Blocks 1 and 2.

Algorithm 2: Pseudocode of proposed leaf classification approach

#Input: Set of leaf images Output:
#Output: Type of leaf
Comment 1: # Load and preprocess the leaf images
1. leaf_images = load_images(image_paths); leaf_images = preprocess_images(leaf_images)
Comment 2: # Initialize the CNN model
2. model = initialize_cnn_model()
***Comment 3*:** # Pass the input images through the initial layers/blocks
3. conv_1 = conv2d(*leaf_images*, *kernel_size*=3, *filters*=64, *padding*='same', *activation*='relu')
4. bn_1 = batch_normalization(conv_1)
5. max_pool_1 = max_pooling2d(*bn_1*, *pool_size*=2, *strides*=2)
6. initial_features = max_pool_1
Comment 4: # Define the sequence of hybrid block modules
7. ***for*** module_idx in range(14):
8. ***if*** module_idx % 3 == 0:
Comment 5: :# Two consecutive Hybrid Block 2 modules
9. features = hybrid_block_2(features); features = hybrid_block_1(features)
Comment 6: # Followed by a Hybrid Block 1 module
10. features = hybrid_block_1(*features*)
else:
Comment 6: # Single Hybrid Block 2 module
11. features = hybrid_block_2(*features*)
Comment 7: # Followed by a Hybrid Block 1 module
12. features = hybrid_block_1(*features*)
Comment 8: # Pass the final features through the SoftMax layer
13. flatten = flatten_layer(*features*)
14. dense = fully_connected_layer(*flatten*, *MB*=128, *activation*='relu')
15. dropout = dropout_layer(*dense*, *rate*=0.5)
16. logits = fully_connected_layer(*dropout*, *MB*=2, *activation*='softmax')
Comment 9: # Compute the predictions (Diseased or Healthy)
17. predictions = *argmax*(logits, axis=-1)
18. ***return*** predictions
Comment 10: # Define the Hybrid Block 1 function
Function 1: def hybrid_block_1(input_tensor):
19. conv_1 = conv2d(input_tensor, kernel_size=3, filters=64, padding='same', activation='relu')
20. bn_1 = batch_normalization(conv_1); act_1 = activation_layer(bn_1, activation='relu')
21. depth_conv_1 = depthwise_conv2d(*act_1*, *kernel_size*=3, *depth_multiplier*=1, padding='same', activation='relu')
22. squeeze_1 = squeeze_block(*depth_conv_1*); excite_1 = excitation_block(*squeeze_1*)
23. filter_1 = conv2d(*excite_1*, *kernel_size*=3, *filters*=64, *padding*='same')
24. bn_2 = batch_normalization(filter_1); act_2 = activation_layer(*bn_2*, *activation*='relu')
25. output_tensor = act_2
26. ***return*** output_tensor
Comment 11: # Define the Hybrid Block 2 function
Function 2: def hybrid_block_2(*input_tensor*):
27. conv_1 = conv2d(*input_tensor*, *kernel_size*=3, *filters*=128, *padding*='same', *activation*='relu')
28. bn_1 = batch_normalization(conv_1); act_1 = activation_layer(bn_1, activation='relu')
29. depth_conv_1 = depthwise_conv2d(*act_1*, *kernel_size*=3, *depth_multiplier*=1, *padding*='same', *activation*='relu')
30. squeeze_1 = squeeze_block(*depth_conv_1*)
31. filter_1 = conv2d(*squeeze_1*, *kernel_size*=3, *filters*=64, *padding*='same')
32. excite_1 = excitation_block(filter_1); downsample_1 = max_pooling2d(*excite_1*, *pool_size*=2, *strides*=2)
33. gap_1 = global_average_pooling2d(*downsample_1*); bn_2 = batch_normalization(gap_1)
34. concat_1 = concatenate(*bn_2*, *input_tensor*, *axis*=-1)
35. output_tensor = concat_1
36. ***return*** output_tensor

4. Experimental Setup and Results

This section presents the experimental analysis and demonstrates the effectiveness of the proposed solution. All experiments, including feature extraction, were conducted using Python on a PC with Windows 10, Intel i5-3.6 GHz CPU, and 8 GB of RAM. We evaluated the performance of our algorithm against state-of-the-art methods based on five criteria: (1) Average Classification Accuracy (ACA), (2) Precision, (3) Recall, (4) F-score, and (5) Time/Space complexity. ACA reflects the model's ability to classify various leaf types across multiple classes correctly. Precision measures the reliability of the model's positive predictions, defined as the ratio of True Positives (TP) to total positive predictions. It can be calculated using Equation 6.

$$Precision = \frac{TP}{TP+FP} \tag{6}$$

True Positive (TP) and False Positive (FP) refer to how many cases the model correctly classifies as positive and the number of occurrences the model misclassifies as positive when they are negative.

Recall or sensitivity is an evaluation metric that depicts the system's ability to classify positive instances correctly. It refers to the ratio of the correct positive predictions made by the model to the total number of positive cases in the dataset. Mathematically, recall is calculated as:

$$Recall = \frac{TP}{TP+FN} \tag{7}$$

F-score or F1 score is the harmonic mean of precision and recall. It is one of the most efficient and widely used evaluation metrics among other evaluation metrics. These measures of precision and recall balance each other out in some cases. The F-measure is applied significantly when the number of positive examples far outweighs the number of negative examples in the dataset. Mathematically, the F-score is calculated as:

$$F = \frac{2*Precison*Recall}{Precison+Recall} \tag{8}$$

In machine learning, time complexity refers to how much a model scales with computational resources in performing tasks such as prediction or other operations. Generally, this is assessed regarding the computational cost incurred during training and the predictive cost incurred while inferring. Our work utilized a five-fold cross-validation methodology that split the respective datasets into training, validation, and testing sets for evaluation. The model was trained on the training set and fine-tuned using hyperparameters on the validation set. The trained model was tested against those performances for proper classification accuracy and other measures. The performance results on both datasets are summarized in the following subsections.

4.1. Hyperparameter Tuning Using Bayesian Optimization

Bayesian optimization is used to tune the hyper-parameters of the proposed deep learning model (Victoria et al. 2021). A Gaussian process was used as the surrogate model to estimate the performance of different hyperparameter configurations. In the Expected Improvement (EI) acquisition function, exploration and exploitation of new and known promising regions are balanced. The primary objective was to achieve maximum accuracy, and other performance metrics such as validation loss, precision, recall, and F1-score were also monitored during training. This ensured that the model performed well in accuracy and showed robustness and generalization when used with other performance indicators. The list of optimal hyperparameters is given in Table 1.

Table 1- Detail of hyperparameter search space and their optimal values during training

Hyperparameter	*Search Space*	*Optimal Value*
Learning rate (α)	0.0001 – 0.01	0.001
Batch Size	16 – 128	64
Dropout Rate	0.1 – 0.5	0.3
Number of Layers	2 – 10	6
Number of Neurons	64 – 512	256
Weight Decay	0.00001 – 0.001	0.0001

4.2. Experiment 1: Results on plant village dataset

The performance of the proposed model is validated on the Plant Village Dataset using a five-fold cross-validation technique. The multiclass classification results, demonstrating the model's effectiveness across various plant disease categories, are presented in Table 2. The classification results on the Plant Village dataset point out excellent performance in most categories, which can then be generalized into three accuracy levels: above 99%, between 90% and 99%, and below 90%. Classes with accuracy Above 99% classify high performance by almost perfect differentiation. For instance, Cherry (Powdery Mildew) and

Cherry (healthy) attain 100% precision, recall, and an F-score value of 1.00. Grape (Leaf Blight) and Peach (healthy) were no exceptions in accomplishing the 100% accuracy line that guarantees no false negatives or false positives would be counted. The Orange class reached an Accuracy of 99.16% with a precision of 1.00, recall of 0.99, and F-score of 0.99; more evidence that the model indeed makes good predictions regarding this disease.

Classes with accuracy Between 90% and 99% dominate the results. Here, the model performs very well for the entire range of plant conditions. Apple (healthy) had an accuracy of 98.24%, with 0.98 precision, 0.99 recall, and an F-score of 0.99. This means that the model classifies healthy apples as being robust. Corn Common Rust achieved 96.54% accuracy at precisions and recalls of 0.98 and 0.97, respectively. The F-score for the model is 0.97, meaning it is very reliable for this condition. Grape, Black Rot results came back with 93.18% accuracy, 0.92 precision, 0.97 recall, and 0.95 F-score, showing somewhat lower performance but still quite good. The accuracies are not as high as those of the top-performing classes. Classes with accuracy below 90% represent a small portion of the dataset where the model faces challenges. For instance, Apple (Black Rot) showed an accuracy of 90.00%, with 0.92 precision, 0.90 recall, and a 0.91 F-score, indicating that while the model performs respectably, overlapping features with other classes might lead to slight misclassifications. Similarly, Tomato (healthy) had an accuracy of 88.42%, with 0.75 precision, 1.00 recall, and a 0.98 F-score, suggesting that the model struggles slightly with precision but compensates with strong recall. These lower accuracy classes point to areas where additional tuning or training data might be needed to improve model performance.

Table 2- Different performance measures for the PlantVillage dataset

Class	*Precision*	*Recall*	*F-Score*	*Support*	*Accuracy*
Apple___Apple_scab	0.97	0.92	0.95	126	96.20
Apple___Black_rot	0.92	0.90	0.91	108	97.40
Apple___Cedar_apple_rust	0.98	0.95	0.96	55	97.23
Apple___healthy	0.98	0.99	0.99	392	98.24
Blueberry___healthy	0.98	0.98	0.98	300	98.02
Cherry_(including_sour)___Powdery_mildew	1.00	1.00	1.00	100	100
Cherry_(including_sour)___healthy	0.99	1.00	0.99	264	99.66
Corn_(maize)___Cercospora_leaf_spot Gray_leaf_spot	0.80	0.84	0.82	184	84.34
Corn_(maize)__Common_rust	0.98	0.97	0.97	292	96.54
Corn_(maize)___Northern_Leaf_Blight	0.93	0.96	0.95	318	93.41
Corn_(maize)___healthy	0.98	0.99	0.98	341	97.66
Grape___Black_rot	0.92	0.97	0.95	234	93.18
Grape___Esca_(Black_Measles)	0.98	1.00	0.99	138	98.44
Grape___Leaf_blight_(Isariopsis_Leaf_Spot)	1.00	1.00	1.00	215	100
Grape___healthy	0.99	1.00	0.99	85	99.16
Orange___Haunglongbing_(Citrus_greening)	1.00	0.99	0.99	1102	99.16
Peach___Bacterial_spot	0.90	1.00	0.95	462	92.14
Peach___healthy	1.00	1.00	1.00	72,	100
Pepper,_bell___Bacterial_spot	0.99	1.00	0.99	147	99.14
Pepper,_bell___healthy	0.95	0.95	0.95	388,	98.23
Potato___Early_blight	0.94	0.98	0.96	200	95.54
Potato___Late_blight	0.94	0.98	0.96	207	93.14
Potato___healthy	0.98	1.00	0.99	192	96.66
Raspberry___healthy	0.97	0.99	0.98	78	93.34
Soybean___healthy	1.00	1.00	1.00	508	100
Squash___Powdery_mildew	0.99	0.99	0.99	330	98.74
Strawberry___Leaf_scorch	0.90	0.99	0.95	110	92.14
Strawberry___healthy	0.96	0.94	0.95	234	89.13
Tomato___Bacterial_spot	0.97	0.96	0.92	425	91.33
Tomato___Early_blight	0.90	0.94	0.95	98	95.33
Tomato___Late_blight	0.95	0.96	0.97	192	90.47
Tomato___Leaf_Mold	0.97	0.98	0.97	154	91.66
Tomato___Septoria_leaf_spot	0.97	0.98	0.93	190	92.34
Tomato___Spider_mites Two-spotted_spider_mite	0.94	0.93	0.98	318	98.21
Tomato___Target_Spot	0.99	0.97	0.94	869	93.54
Tomato___Tomato_Yellow_Leaf_Curl_Virus	0.94	0.93	0.99	854	91.12
Tomato___Tomato_mosaic_virus	0.99	0.99	0.86	373	91.24
Tomato___healthy	0.75	1.00	0.98	93	88.42

The accuracy vs. epochs graph shown in Figure 12 represents the performance of the proposed approach during training and validation in 35 epochs, showing critical behaviors in the model's learning process. In the early epochs, both training and validation accuracies sharply rise, which is expected since, at that point, the model is just starting its training and sensing patterns from the data. Rapid increases in training accuracy suggest that a model fits quite rapidly with the training data. Validation accuracy also learns much faster than the training set, suggesting generalization to unseen data by the model. After epoch 5, the

validation accuracy starts to drop steeply while the training accuracy continues to climb increasingly smoothly. That is a sign of overfitting, where the model begins to memorize specific patterns unique to the training data, reducing its ability to generalize to new data. The validation accuracy does see this drop, but the oscillations indicate instability in the model's generalization capability at this stage. As the training progresses, both curves stabilize, especially after epoch 15. The training accuracy tracks into a plateau around a high value, suggesting that the model had nearly maximized its performance on the training set. Validated accuracy stabilizes, too, but suffers more variability from the training curve of the model, indicating that although the model's generalization ability is enhanced, it remains sensitive to the fluctuations within the validation data set. It seems more of a converging model but sometimes overfits or displays extreme sensitivity precisely to specific validation samples on later epochs.

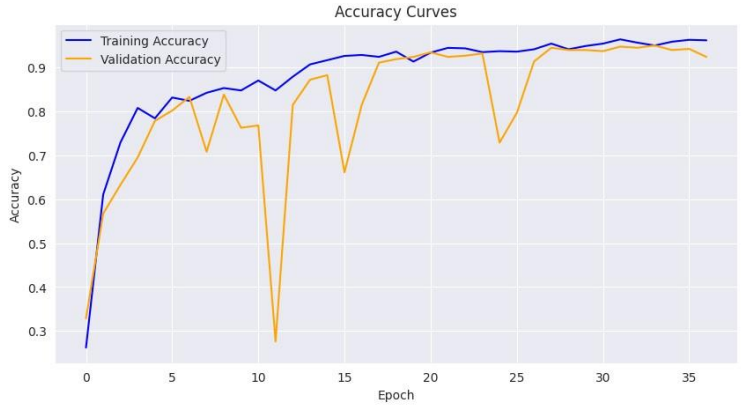

Figure 12- The Accuracy vs Epoch curve for training and testing of the proposed approach

The training and validation loss for 35 epochs are shown in **Figure 13**. The primary movement in the early epochs in the training data is the drastic drop in the training and validation loss curves, showing that the model learned well and substantially reduced its errors. While the training loss decreases as the training progresses, it indicates better generalization by the model on the training data. Instead, the validation loss often fluctuates and displays instability in generalization. It peaks at a significant validation loss around epoch 10, indicating overfitting. That means the training set error is correctly lowered at this epoch but fails to generalize when attracted to the unseen validation data. Later, after epoch 15, the training loss drops to almost zero, marking an indicator of convergence towards the model's training data. The validation loss also keeps reducing in value gradually, though with occasional small spikes. These spikes, particularly around epochs 20 and 25, suggest that even though the model performs well, it is still sensitive to specific validation batches.

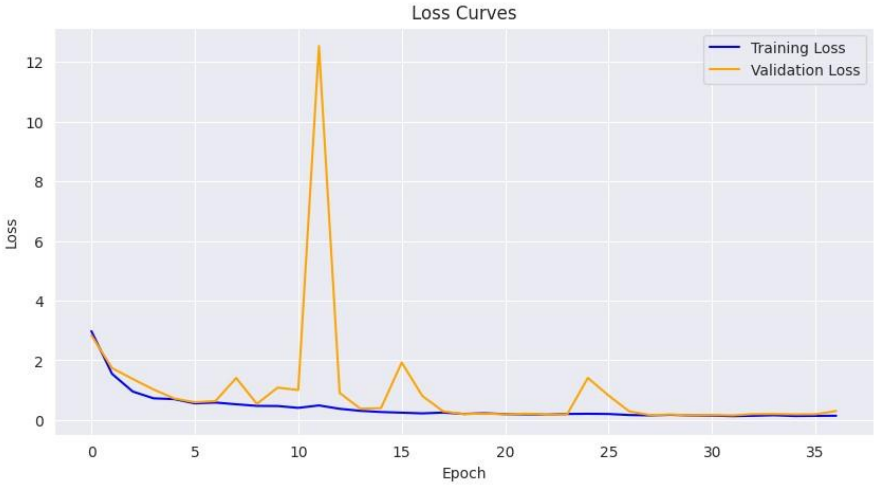

Figure 13- The Loss vs Epoch curve for training and testing of the proposed approach

The Receiver Operating Characteristics (ROC) curve for the proposed classification is shown in Figure 14. Each line in the plot is the ROC curve for a given class and is plotted against the false positive rate versus the true positive rate for a range of classification thresholds. The curves indicate how well the classifier can distinguish between classes. In this curve, almost all individual class curves reach the top-left corner nearly perfectly, except for fewer than five classes, while most classes have AUC values close to 1.00. There are three classes with AUC values below 1.00: Class 37, with an AUC of 0.98, and Class 36 and Class 35, each with an AUC of 0.99. All of them give perfect classification performance; however, their AUC values indicate some degradation in distinguishing a positive instance from a negative one compared to other classes that scored ideally and had an AUC of 1.00. In other words, the model has a perfect discrimination ability for those classes.

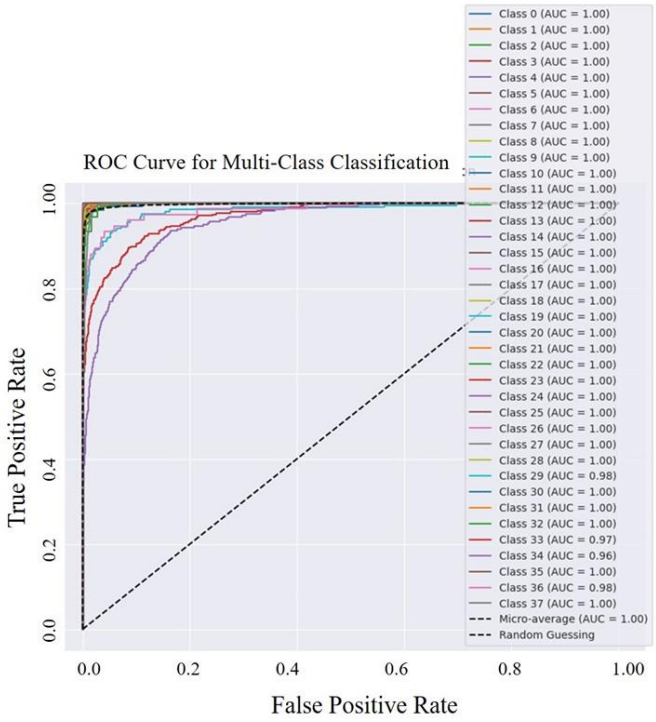

Figure 14- ROC curve for Multiclass Leaf Classification Model

4.3. Experiment 2: Results on rose leaf disease dataset

Similar to the PlantVillage dataset, the Rose leaf disease dataset is also a multiclass dataset having three classes: (1) Healthy_Leaf_Rose, (2) Rose_Rust, and (3) Rose_swafly_Rose_slug. The classification results for all three classes are shown in Table 3. For Healthy_Leaf_Rose, the model has a value of 0.99 precision, which means 99% of all the predicted instances for this class are correct. However, the recall of this class is a little low, with just 5% being missed. As a result, the class F1-score is 0.97, balancing strength in precision and slightly lower recall from showing a very high classification accuracy for this class. For Healthy_Leaf_Rose, 995 samples in the dataset give this model an accuracy of 95.38%, high though a bit less strong than the performance observed for the other two classes.

For Rose_Rust (Class 1), the model achieves a precision of 0.98, indicating that almost all predicted instances for this class are correct. The recall is also strong at 0.97, meaning that 97% of the true Rose_Rust instances are correctly identified. The F1-score, at 0.98, indicates excellent overall performance for this class, with a strong balance between precision and recall. Out of 991 samples in the dataset, the model achieves an accuracy of 97.47%, slightly better than Healthy_Leaf_Rose. This model performs very well for Rose_swafly_Rose_slug with Class 2, having recall at 0.98, or almost all true class instances are correctly detected. Precision is slightly lower than others at 0.94, showing more false positives for this class. F1-score is still very good at 0.96, showing a good balance between precision and recall. For this model, with 996 samples, class-specific accuracy shows the maximum at 98.61%, indicating that it is a strong classifier for detecting this class. The model's average accuracy for the classes is 97.15%. The model's effectiveness in classifying each category is high, though its performance for all classes is excellent. Despite a minor reduction in precision, it is best with its highest accuracy in the case of Rose_swafly_Rose_slug (Class 2). This means the model is pretty good at distinguishing between classes and is only sometimes confused, primarily in the case of Rose_swafly_Rose_slug and other categories.

Table 3- Different performance measures for the Rose Leaf dataset

Class	*Precision*	*Recall*	*F1-Score*	*Support*	*Accuracy*
Healthy_Leaf_Rose (0)	0.99	0.95	0.97	995	95.38%
Rose_Rust (1)	0.98	0.97	0.98	991	97.47%
Rose_swafly_Rose_slug (2)	0.94	0.98	0.96	996	98.61%
Average Accuracy	-	-	-	2982	97.15%

The confusion matrix shown in Figure 15 demonstrates how the model performs on the three classes. In class 0, it classified 947 correctly and mislabeled 48 instances as class 1, showing a moderate level of confusion between these two classes. The confusion was minimal since there were no misclassifications from class 0 to class 1, indicating a clear distinction between the two categories. For class 1, 962 cases were correctly classified, with only ten misclassifications as class 0 and nineteen misclassifications as class 2. It shows that although the model is excellent, there is interference between class 1 and the remaining

classes but with the slightest interference with class 2. The model accurately classified 976 instances and misclassified 20 of class 2 as class 1. For class 2, the model correctly classified 976 cases, with 20 misclassifications as class 1. However, no instances of class 2 were misclassified as class 0, indicating a strong ability to distinguish class 2 from class 0.

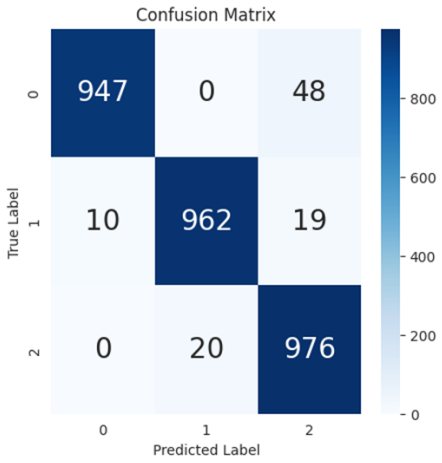

Figure 15- Confusion matrix for the Rose Leaf dataset

The graph shown in Figure 16 indicates the performance of the proposed model in training the Roseleaf dataset over 100 epochs and compares it with the testing accuracy. During training, the model steadily increases in both metrics and reaches a plateau after about 80 epochs. The testing accuracy remains stable at about 97.15%, implying the model's generalization capability is high. Here, a similar trajectory was seen between the training and testing curves, with negligible divergence between them. This indicates that the model did not suffer from an overfitting problem as the gap between training and testing accuracy continued to narrow throughout the process. In terms of convergence, the model achieves smooth progression, with significant improvements in accuracy observed during the first 40 to 50 epochs. After reaching around 60 epochs, the learning rate appears to slow, stabilizing accuracy between 95% and 97%. This trend indicates diminishing returns from further training. The final test accuracy of 97.15% shows that the model performs exceptionally well in its classification performance, demonstrating good robustness and reliability on the Roseleaf dataset. The near identity of the training and testing accuracy also indicates that the model generalizes well to unseen data without glaring signs of overfitting, as the two accuracies converge closely towards the last epochs.

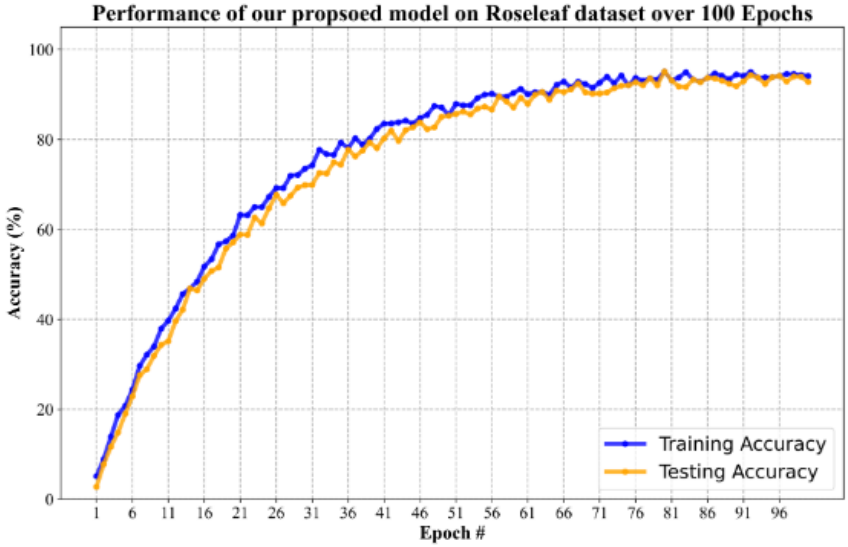

Figure 16- The Accuracy vs Epoch curve for training and testing of the proposed approach

Figure 17 represents the training and validation loss for a range of epochs in the training of our model. The blue curve shows the training loss, and the orange curve refers to the validation loss. During the early epochs in the learning process, the training loss and validation loss are relatively high, and the model hasn't yet entirely fitted the data well. Gradually, as the number of epochs increases, the training loss decreases continuously, showing the model is learning and minimizing errors in the training data. However, the validation loss has a higher variance. Between epochs 1 and 4, the validation loss drops steeply, indicating that the model first generalizes well to the unseen data. After that point, the validation loss peaks around epoch 6, rising sharply before dropping again. Such fluctuations demonstrate the likelihood of overfitting: the model is doing very well in training but

fails with the validation set. From approximately epoch ten onwards, the validation loss increases again- the increase could indicate divergence in training loss. It might be due to overfitting because the model performs worse on unseen data (validation set) but keeps improving on training data. The upward drift in both curves at epochs later than 12 indicates the requirement of early stopping or even some other regularization technique that would prevent overfitting to the training data.

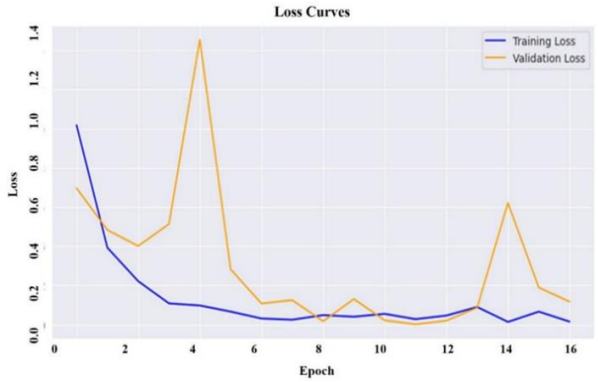

Figure 17- The Loss vs Epoch curve for training and testing of the proposed approach

The ROC for the proposed multiclass classification model is shown in Figure 18. Class 0's AUC value reaches 0.999; thus, the classifier almost perfectly differentiates instances of this particular class from others. Class 1 stands out with an AUC of 1.000, signifying flawless classification performance, meaning the model can perfectly distinguish Class 1 instances. Similarly, Class 2 has an AUC of 0.999, reflecting near-perfect classification. Also, the micro-average AUC of 0.999 aggregates performance across classes, which is another facet that proves the model can predict with high accuracy for many classes. The curves are tightly concentrated in the top-left corner, demonstrating high TPR with very low FPR, meaning the model achieves a strong balance between sensitivity and specificity.

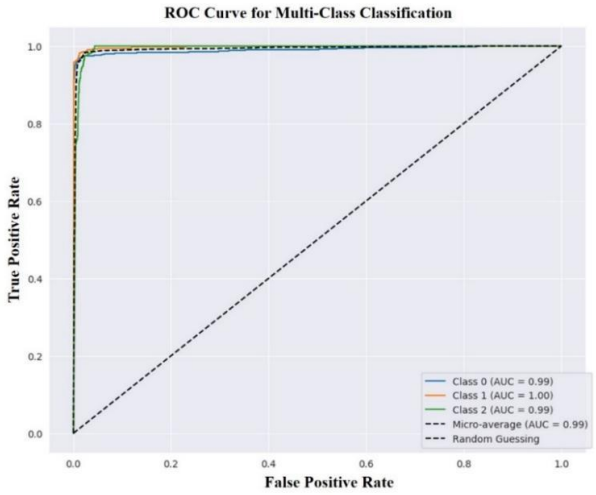

Figure 18- ROC curve for Multiclass Leaf Classification Model

4.4. Results Comparison with State-of-the-Art Methods

Its performance was compared against five baseline models: (1) the VGG16 Net, (2) Inception Net, (3) RESNET-50, (4) Conventional Inception-Visual Geometry Group Network (CIVGGN), and (5) EfficientNetV2. All the above networks were pre-trained on the Imagenet data set and have widespread medical imaging and leaf disease detection applications. The comparison on the PlantVillage dataset focused on computational efficiency and key metrics like accuracy, precision, recall, and F1-score. Our suggested approach outperforms VGG16 Net (93.5%), Inception Net (94.2%), RESNET-50 (95.1%), conventional Inception-Visual Geometry Group Network (CIVGGN) (95.64%), and EffecientNetV2 (95.18%) with a classification accuracy of 96.4% (Table 4). In Figure 22, we compare the relative performance with our approach. The results show a relative improvement of 3.1% over VGG16 Net, 2.2% over Inception Net, 1.3% over RESNET-50, 0.8% over CIVGGN, and 1.23% over EfficientNetV2.

Here, the VGG16 Net model demonstrates a poor performance mainly due to its extensive number of parameters, which process computationally very slowly and multiply memory consumption considerably. It makes it inefficient at training and

inference periods and less desirable for high-performance applications, requiring faster speed and information processing. The Inception Net architecture, though known for its parallel convolutional layers and efficient handling of features, may not perform as well in capturing complex hierarchical features compared to newer models. While it offers better accuracy than VGG16, its ability to scale for highly intricate tasks is somewhat limited. The third baseline model, RESNET-50, is known to have robust architectures. Using residual connections mitigates the vanishing gradient problem; however, it is intense and computationally expensive. Though increased depth add more accuracy to the model, its overhead on its efficiency has been a problem since real-time applications require quick response times. The CIVGGN model, which combines elements from both Inception and VGG architectures, introduces a level of complexity that doesn't always translate to superior performance. The hybrid nature of the model can result in suboptimal handling of specific tasks, particularly when compared to models designed explicitly for efficient feature extraction and classification. Although compound scaling optimizes parameters, depth, and resolution for EfficientNetV2, sometimes the trade-off between complexity and performance may be slightly required.

To validate the superiority of our proposed approach, we performed a *p*-value analysis to compare its classification accuracy with that of widely used models. The accuracy of classification in our proposed method is significantly more significant compared to VGG16Net (93.5%) with a *p*-value of 0.002, Inception Net (94.2%) with $p = 0.008$, and RESNET (95.1%) with $p = 0.015$. Even with the latest models in the EfficientNetV2 (95.18%) and Conventional Inception-VGG (95.64%), improvements boast statistical significance with *p*-values of 0.012 and 0.021, respectively. Since all the *p*-values are less than the threshold of 0.05, results confirm that the improvement inaccuracies are not by chance alone, indicating our proposed approach's robustness. This implies our method provides not only greater accuracy but also statistically significant gains over the models already existing.

The proposed approach shows the best execution time performance, with an execution time of 45 MB, much faster than all other models. EfficientNetV2 indicates a relatively lower execution time of 53 MB, thus making it more efficient than conventional models. VGG16Net and Inception Net slightly increase in some time MB, for instance, 50 and 55 MB, respectively. On the other hand, RESNET and Conventional Inception-Visual Geometry Group Network have an execution time of 75 and 83 MB, respectively, which is way higher than the proposed approach, indicating that it requires more computational power and less time-efficient as compared to this newly recommended approach. Regarding memory consumption, it also reflects that the proposed approach is the most efficient due to the utilization of 150 MB, reflecting the lowest memory consumption among all the other models. EfficientNetV2 has 167 MB, balancing accuracy and memory efficiency well. Inception Net and VGG16Net require moderate memory consumption of 170 and 180 MB, respectively. On the other hand, RESNET and Conventional Inception-Visual Geometry Group Network consume the largest MB in memory, which are 190 and 240 MB, respectively, translating to a more significant computer resource requirement and larger space complexity.

Table 4- Performance measures for different baseline methods on the PlantVillage dataset

Classification Framework	*Classification Accuracy*	*Execution Time*	*Memory Consumption (In MB)*
VGG16Net (Simonyan & Zisserman 2014)	93.5%	50	180
Inception Net (Szegedy et al. 2016)	94.2%	55	170
RESNET (He et al. 2016)	95.1%	75	190
Conventional Inception-Visual Geometry Group Network (Pal & Kumar 2023)	95.64%	83	240
EffecientNetV2 (Devi et al. 2023)	95.18%	53	167
Proposed Approach	96.40%	45	150

The results achieved on the Rose Leaf dataset show significant improvement in the ability to classify images and computational efficiency compared to the baseline models (Table 5). The VGG16Net model achieved an accuracy of 93.5% but executes in 48 milliseconds, and its memory consumption is around 121 MB. Although VGG16Net seems relatively accurate, it has many hyperparameters, making it slow for real-time applications as it is computationally expensive. The Inception Net outperformed VGG16Net with an accuracy of 94.2% and reduced running time to 19 milliseconds and memory consumption to 107 MB. This result proves that Inception Net, due to its usage of parallel convolutional layers, made this more efficient by enhancing speed and lower memory usage. However, it attains lower precision compared to more sophisticated models. Here, the testing accuracy is 95.1%, with a memory consumption of 141 MB and an execution time of 33 milliseconds. Its deeper architecture with residual connections enhanced feature extraction but consume more resources and be slower than faster models. The Conventional Inception-Visual Geometry Group Network can achieve a higher accuracy at 96.33% but at the cost of execution time (83 milliseconds) and memory usage (203 MB). Hybrid design combines features from both the Inception and the VGG architectures, making for a heavier load computationally. Therefore, the application needed to be fast and work on fewer resources simultaneously, such as edge and other terminal devices. The EfficientNetV2 balances accuracy with computation efficiency; with both parameters, classification performance is 95.24%, and execution time is 63 milliseconds while using up to 151 MB of memory. This architecture looks good at providing a good performance, but model scaling is still lacking compared with other, even more efficient models. The proposed approach outperforms the other models with the highest classification accuracy of 97.15%, lowest execution time of 13 milliseconds, and moderate memory consumption of 117 MB. This framework manages the complexities of the Rose Leaf dataset well while maintaining a high level of accuracy with fast

processing and optimized usage of resources. Therefore, the supremacy of the proposed model in classification performance and computational efficiency results in its suitability for applications like real-time plant disease detection tasks.

The proposed approach attained 97.15% classification accuracy with a *p*-value of 0.001, statistically significantly better than VGG16Net of 93.5%, Inception Net of 94.2% with $p = 0.004$, and RESNET with $p = 0.012$. Comparing the proposed approach with even more recent models in the literature like EfficientNetV2, which attained 95.24%, and Conventional Inception-VGG, which gained 96.33%, the improvements are still statistically significant with *p*-values of 0.009 and 0.017, respectively. These *p*-values -- all <0.05 -- confirm that the increase in classification accuracy brought by our proposed method cannot be attributed to chance and that, thus, it's robust and performs far better across different models.

Table 5- Performance measures for different baseline methods on the Rose Leaf dataset

Classification Framework	Classification Accuracy	Execution Time	Memory Consumption
VGG16Net (Simonyan & Zisserman 2014)	93.5%	48	121
Inception Net (Szegedy et al. 2016)	94.2%	19	107
RESNET (He et al. 2016)	95.1%	33	141
Conventional Inception-Visual Geometry Group Network (Pal & Kumar 2023)	96.33%	83	203
EffecientNetV2 (Devi et al. 2023)	95.24%	63	151
Proposed Approach	97.15%	13	117

4.5. Research Limitations

Although the proposed leaf classification network performed well on two public datasets, several limitations must be addressed. A list of a few research limitations are discussed below:

1) The alternating hybrid blocks (EfficientNet and Squeeze-and-Excitation networks) complicate the model's design. This complexity can make it harder to fine-tune and balance accuracy with the time taken to process the data.
2) Although SE blocks enhance quality feature extraction, they introduce more calculations. The result is an increase in the training and prediction time by the model, primarily when large databases are run with a low level of computing hardware.
3) The customized BM3D filtering technique removes image noise but takes more processing time than the other methods. It becomes a problem when large images are considered because this method might slow down the entire system's performance.
4) The model is validated only on two datasets used in the study, so it may not perform as well when applied to different datasets without significant modifications. It could limit its flexibility for other types of image classification problems.
5) Adding EfficientNet along with SE blocks adds up the model's memory requirement. It makes it less useful for memory-constrained devices such as cell phones or embedded systems, where excessive memory usage is impossible.

5. Conclusion and Future Scope

In this article, we proposed a new hybrid classification framework that uses the Efficient Neural Network with Squeeze and Excitation Network for leaf classification. Our architecture uses a self-attention mechanism focused on the input scans' most relevant regions of interest. We designed a dense CNN architecture with two hybrid blocks comprising SEN and EfficientNetB0 modules. Such hybrid modules were alternatively utilized in our architectures of CNNs over the 14 modules to achieve better performance. The proposed classification model achieved significant margins of 96.40% on the PlantVillage dataset and 97.15% on the Rose Leaf Disease dataset over VGG16, Inception V3, RESNET-50, Conventional Inception-Visual Geometry Group Network, and EfficientNetV2. The proposed model depicted better accuracy, recall, F-score, memory usage, and execution time in all the compared states. The primary limitation of the proposed CNN model is its "black box" nature due to the complex interconnections among layers and blocks. To address this, techniques such as saliency maps, Grad-CAM, Layer-wise Relevance Propagation (LRP), SHAP, and LIME can be explored to improve interpretability. These methods can help visualize feature importance and enhance transparency.

Furthermore, researchers should attempt to generalize the model by testing it on diverse datasets, including medical imaging and satellite image analysis. Incorporating novel interconnections like Highway Networks, Interleaved Connections, and Residual Dense Connections may improve the model's performance. Various search space optimization methods can also be a practical approach to enhance the overall performance of the proposed model (Tiwari et al. 2021). A few novel interconnections, such as Highway Networks (Srivastava et al. 2015), Interleaved Connections (Li et al. 2020), and Residual Dense Connections (Zhang et al. 2018) can also be used among different layers to enhance the performance of the proposed model.

Credit Authorship Contribution Statement

Declaration of Competing Interest

The authors declare that they have no known competing financial interests or personal relationships that could have appeared to influence the work reported in this paper.

Data Availability

Many data, models, and codes in this work are open source. However, the final outputs are not available to the public, but can be sent to interested researchers.

Funding Declaration

No sponsor or funder supported this study.

Reference

Agarwal G, Belhumeur P, Feiner S, Jacobs D, Kress W J, Ramamoorthi R & White S (2006). First steps toward an electronic field guide for plants. *Taxon* 55(3): 597-610 https://doi.org/10.2307/25065637

Ahmad I, Hamid M, Yousaf S, Shah S T & Ahmad M O (2020). Optimizing pretrained convolutional neural networks for tomato leaf disease detection. *Complexity* 2020(1): 8812019 https://doi.org/10.1155/2020/8812019

Akilan T, Wu Q J, Safaei A & Jiang W (2017). A late fusion approach for harnessing multi-CNN model high-level features. *In 2017 IEEE International Conference on Systems, Man, and Cybernetics (SMC)* 566-571. https://doi.org/10.1109/smc.2017.8122666

Ashwinkumar S, Rajagopal S, Manimaran V & Jegajothi B (2022). Automated plant leaf disease detection and classification using optimal MobileNet based convolutional neural networks, *Materials Today: Proceedings* 51(1): 480-487, https://doi.org/10.1016/j.matpr.2021.05.584

Bi C, Wang J, Duan Y, Fu B, Kang J R & Shi Y (2022). MobileNet based apple leaf diseases identification. *Mobile Networks and Applications*, 1-9. https://doi.org/10.1007/s11036-020-01640-1

Bock C H, Barbedo J G, Del Ponte E M, Bohnenkamp D & Mahlein A K (2020). From visual estimates to fully automated sensor-based measurements of plant disease severity: status and challenges for improving accuracy. *Phytopathology Research*, 2, 1-30. https://doi.org/10.1186/s42483-020-00049-8

Chai Ali, C A, Li BaoJu L B, Shi YanXia S Y, Cen ZheXin C Z, Huang HaiYang H H & Liu Jun L J (2010). Recognition of tomato foliage disease based on computer vision technology. *Acta Horticulturae Sinica*, 37(9), 1423-1430

Chen G H, Yang L & Xie S L (2006). Gradient-based structural similarity for image quality assessment. *In 2006 international conference on image processing* 2929-2932. IEEE. http://doi.org/10.1109/ICIP.2006.313132

Chen Q & Wu D (2010). Image denoising by bounded block matching and 3D filtering. *Signal Processing* 90(9): 2778-2783. https://doi.org/10.1016/j.sigpro.2010.03.016

Devi R S, Kumar V R & Sivakumar P (2023). EfficientNetV2 Model for Plant Disease Classification and Pest Recognition. *Computer Systems Science & Engineering* 45(2). https://doi.org/10.32604/csse.2023.032231

Ferentinos K P (2018). Deep learning models for plant disease detection and diagnosis. *Computers and electronics in agriculture*, 145, 311-318. https://doi.org/10.1016/j.compag.2018.01.009

Ghazi M M, Yanikoglu B & Aptoula E (2017). Plant identification using deep neural networks via optimization of transfer learning parameters. *Neurocomputing* 235: 228-235. https://doi.org/10.1016/j.neucom.2017.01.018

Guan Z X, Tang J, Yang B J, Zhou Y F, Fan D Y & Yao Q (2010). Study on recognition method of rice disease based on image. *Chinese Journal of Rice Science* 24(5): 497

He K, Zhang X, Ren S & Sun J (2016). Deep residual learning for image recognition. *In Proceedings of the IEEE conference on computer vision and pattern recognition* 770-778. https://doi.org/10.1109/cvpr.2016.90

Hu J, Shen L & Sun G (2018). Squeeze-and-excitation networks. *In Proceedings of the IEEE conference on computer vision and pattern recognition* (pp. 7132-7141). https://doi.org/10.1109/cvpr.2018.00745

Hu J, Shen L & Sun G (2018). Squeeze-and-excitation networks. In Proceedings of the IEEE conference on computer vision and pattern recognition 7132-7141. https://doi.org/10.1109/cvpr.2018.00745

Hughes D & Salathé M (2015). An open access repository of images on plant health to enable the development of mobile disease diagnostics. arXiv preprint arXiv:1511.08060

Kamilaris A & Prenafeta-Boldú F X (2018). Deep learning in agriculture: A survey. *Computers and electronics in agriculture, 147, 70-90*. https://doi.org/10.1016/j.compag.2018.02.016

Kawasaki Y, Uga H, Kagiwada S & Iyatomi H (2015). Basic study of automated diagnosis of viral plant diseases using convolutional neural networks. *In Advances in Visual Computing: 11th International Symposium, ISVC 2015*, Las Vegas, NV, USA, December 14-16, 2015, Proceedings, Part II 11 (pp. 638-645). Springer International Publishing. https://doi.org/10.1007/978-3-319-27863-6_59

Koonce B (2021). Convolutional neural networks with swift for tensorflow: Image recognition and dataset categorization 109-123). New York, NY, USA: Apress.

Li F, Cong R, Bai H & He Y (2020). Deep interleaved network for image super-resolution with asymmetric co-attention. arXiv preprint arXiv:2004.11814.

Li L, Zhang S & Wang B (2021). Plant disease detection and classification by deep learning—a review. *IEEE Access*, 9, 56683-56698. https://doi.org/10.1109/access.2021.3069646

Liu N & Kan J M (2016). Improved deep belief networks and multi-feature fusion for leaf identification. *Neurocomputing*, 216, 460-467. https://doi.org/10.1016/j.neucom.2016.08.005

Ma J, Du K, Zheng F, Zhang L, Gong Z & Sun Z (2018). A recognition method for cucumber diseases using leaf symptom images based on deep convolutional neural network. *Computers and electronics in agriculture*, 154, 18-24. https://doi.org/10.1016/j.compag.2018.08.048

Mohanty S P, Hughes D P & Salathé M (2016). Using deep learning for image-based plant disease detection. Frontiers in plant science, 7, 1419. https://doi.org/10.3389/fpls.2016.01419

Pal A & Kumar V (2023). AgriDet: Plant Leaf Disease severity classification using agriculture detection framework. *Engineering Applications of Artificial Intelligence* 119: 105754. https://doi.org/10.1016/j.engappai.2022.105754

Reyes A K, Caicedo J C & Camargo J E (2015). Fine-tuning Deep Convolutional Networks for Plant Recognition. CLEF (Working Notes) 1391: 467-475

Ronneberger O, Fischer P & Brox T (2015). U-Net: Convolutional networks for biomedical image segmentation. *In Medical image computing and computer-assisted intervention–MICCAI 2015: 18th international conference*, Munich, Germany, October 5-9, 2015, proceedings, part III 18 (pp. 234-241). Springer International Publishing. https://doi.org/10.1007/978-3-662-54345-0_3

Sai Reddy B & Neeraja S (2022). Plant leaf disease classification and damage detection system using deep learning models. *Multimedia tools and applications* 81(17): 24021-24040. https://doi.org/10.1007/s11042-022-12147-0

Sazzad S, Rajbongshi A, Shakil R, Akter B & Kaiser M S (2022). RoseNet: Rose leave dataset for the development of an automation system to recognize the diseases of rose. Data in Brief, 44, 108497. https://doi.org/10.1016/j.dib.2022.108497

Simonyan K & Zisserman A (2014). Very deep convolutional networks for large-scale image recognition. arXiv preprint arXiv:1409.1556.

Srivastava R K, Greff K & Schmidhuber J (2015). Highway networks. arXiv preprint arXiv:1505.00387.

Strange R N & Scott P R (2005). Plant disease: a threat to global food security. *Annual Review of Phytopathology*. 43: 83-116

Sun Y, Liu Y, Wang G & Zhang H (2017). Deep learning for plant identification in natural environment. *Computational intelligence and neuroscience*, 2017. https://doi.org/10.1155/2017/7361042

Szegedy C, Vanhoucke V, Ioffe S, Shlens J & Wojna Z (2016). Rethinking the inception architecture for computer vision. *In Proceedings of the IEEE conference on computer vision and pattern recognition*. 2818-2826. https://doi.org/10.1109/cvpr.2016.308

Tan M & Le Q (2019). Efficientnet: Rethinking model scaling for convolutional neural networks. In International conference on machine learning 6105-6114. PMLR.

Theckedath D & Sedamkar R R (2020). Detecting affect states using VGG16, ResNet50 and SE-ResNet50 networks. SN Computer Science 1(2): 79. https://doi.org/10.1007/s42979-020-0114-9

Tiwari A (2023). A hybrid feature selection method using an improved binary butterfly optimization algorithm and adaptive β–hill climbing. *IEEE Access* 11: 93511-93537. https://doi.org/10.1109/access.2023.3274469

Tiwari A & Chaturvedi A (2021). A novel channel selection method for BCI classification using dynamic channel relevance. *IEEE Access*, 9: 126698-126716. https://doi.org/10.1109/access.2021.3110882

Tiwari A & Chaturvedi, A. (2022). A hybrid feature selection approach based on information theory and dynamic butterfly optimization algorithm for data classification. *Expert Systems with Applications*, 196, 116621. https://doi.org/10.1016/j.eswa.2022.116621

Tiwari A & Chaturvedi A (2023). Automatic EEG channel selection for multiclass brain-computer interface classification using multiobjective improved firefly algorithm. Multimedia Tools and Applications, 82(4), 5405-5433. https://doi.org/10.1007/s11042-022-12795-2

Tiwari V, Joshi R C & Dutta M K (2021). Dense convolutional neural networks based multiclass plant disease detection and classification using leaf images. *Ecological Informatics* 63: 101289. https://doi.org/10.1016/j.ecoinf.2021.101289

Victoria A H & Maragatham G (2021). Automatic tuning of hyperparameters using Bayesian optimization. Evolving Systems, 12(1), 217-223. https://doi.org/10.1007/s12530-020-09345-2

Weiss K, Khoshgoftaar T M & Wang D (2016). A survey of transfer learning. *Journal of Big data* 3: 1-40

Wong T T, & Yang N Y (2017). Dependency analysis of accuracy estimates in k-fold cross validation. *IEEE Transactions on Knowledge and Data Engineering* 29(11): 2417-2427. https://doi.org/10.1109/tkde.2017.2740926

Yanikoglu B, Aptoula E & Tirkaz C. (2014). Automatic plant identification from photographs. Machine vision and applications 25: 1369-1383. https://doi.org/10.1007/s00138-014-0612-7

Zhang Y, Tian Y, Kong Y, Zhong B & Fu Y (2018). Residual dense network for image super-resolution. In Proceedings of the IEEE conference on computer vision and pattern recognition (pp. 2472-2481).

Zhao H, Jia J & Koltun V (2020). Exploring self-attention for image recognition. *In Proceedings of the IEEE/CVF conference on computer vision and pattern recognition* 10076-10085. https://doi.org/10.1109/cvpr42600.2020.01009

Zhao Z Q, Zheng P, Xu S T & Wu X (2019). Object detection with deep Learning: A review. *IEEE transactions on neural networks and learning systems* 30(11): 3212-3232. https://doi.org/10.1109/tnnls.2018.2876865

Journal of Agricultural Sciences
(Tarim Bilimleri Dergisi)

J Agr Sci-Tarim Bili
e-ISSN: 2148-9297
jas.ankara.edu.tr

JAS

The Effect of Good Agricultural Practices on Yield Characteristics of Black Cumin Genotypes

Çiğdem Bozdemir[a]*, Serkan Uranbey[b]

[a]*Central Research Institute for Field Crops, Ankara, TÜRKİYE*

[b]*Department of Field Crops, Faculty of Agriculture, University of Ankara, TÜRKİYE*

ARTICLE INFO

Research Article

Corresponding Author: Çiğdem Bozdemir, E-mail: cbozdemir72@hotmail.com, cigdem.bozdemir@tarimorman.gov.tr

Received: 24 April 2024 / Revised: 14 November 2024 / Accepted: 27 November 2024 / Online: 25 March 2025

Cite this article

Bozdemir Ç, Uranbey S (2025). The Effect of Good Agricultural Practices on Yield Characteristics of Black Cumin Genotypes. *Journal of Agricultural Sciences (Tarim Bilimleri Dergisi)*, 31(2):413-426. DOI: 10.15832/ankutbd.1473047

ABSTRACT

Black cumin (*Nigella sativa* L.) is an annually flowering medicinal plant from the Ranunculaceae family. The objective of this study was to reveal the yield characteristics of a substantial number of black cumin (*Nigella sativa* L.) genotypes under good agricultural practises without fertilization or spraying. The study was carried out in Ankara/Haymana reflecting semi-arid agricultural area of Central Anatolia in 2019 and 2020. Different black cumin genotypes collected and obtained from different agroecological regions such as Egypt, India, Pakistan, Syria, Ethiopia, Türkiye (Konya, Afyonkarahisar, Denizli, Burdur, Ankara, Diyarbakır, Bursa, Kırıkkale provinces) and a commercial cultivar (Çameli) were used and compared. The genotypes gave very different responses in terms of seed yield and yield components. The average data of the two years varied between 17.3-36.14 cm for plant height, 1.59-2.52 for branches/plant, 1.50-2.62 for pods/plant, 29.87-54.64 for seeds/capsule, 2.08-3.08 g for thousand-seed weight, 11.80-31.48 cm for first pod height and 259.6-501.0 kg/ha for seed yield. The yield was affected by climatic changes to a great extent between 259.6 kg/ha and 501.0 kg/ha in terms of seed yield. As a result of the study, these prominent genotypes were considered promising for future variety breeding and other studies.

Keywords: Black cumin, Seed yield, Genotype, Cultivar, Good agriculture practices (GAP)

1. Introduction

Nigella is a plant genus belonging to the Ranunculaceae family and includes a total of 20 species (Seçmen et al. 2000). Although 12 of such species are spread in Türkiye, black cumin seeds (*Nigella sativa* L.) is a globally well-known and widely used for flavoring and medicinal purposes. The recent increase in the cultivation and production of black cumin in the worldwide is a result of its growing popularity as a health supplement, with its seeds and oil offering a range of benefits to human health. Due to valuable phenolic compounds and antioxidant capacity, the fixed oil and secondary metabolites contained in the seed are widely used in medicine and traditional medicine today (Lutterodt et al. 2010). The composition of the seed includes 30-45% fixed oil, 0.01-0.5% essential oil, 20-30% protein, alkaloids and saponins (Kılıç 2016; Kamçı 2019). The unsaturated fatty acids present in black cumin seeds are predominantly linoleic, oleic, and palmitoleic acids, collectively accounting for approximately 79-82% of the total fatty acid composition (Asil & Konuşkan 2021; Orhan & Eroğlu 2024). Linoleic acid represents the most abundant of these acids. The essential oil of the plant was found to contain primarily thymoquinone (TQ), dithymoquinone (DTQ), thymohydroquinone (THQ), and thymol (THY) (Ghosheh et al. 1999). While black cumin seeds are used as flavouring in some foods such as pastry, cheese, pickles, and bakery products, their fixed oil and essential oil have an important role in the areas of health, food technology, cosmetics, and perfumery. As evidenced by pharmacological studies, thymoquinone, a prominent component of the essential oil, exhibits a multitude of effects, including anti-tumour, anti-bacterial, anti-oxidant, antihistamine, antidiabetic, antihypertensive, anti-inflammatory, and antimicrobial activities, as well as antifungal activity. Additionally, there is substantial evidence to suggest that thymoquinone can bolster immune system function (Rahim et al. 2022).

Nigella sativa L. is annual species originated from arid and semi-arid zones (D'Antuno et al. 2002). Dry farming conditions cause low seed yield and quality losses of black cumin in the world. It is widely grown in Thrace, Northern Anatolia, Central Western Anatolia, Lakes Region and Mediterranean regions of Türkiye. It is sown as winter in temperate regions and as summer in regions with harsh climates of Türkiye. Optimal conditions for sowing are an ambient temperature of 5 °C to 8 °C and 60% soil moisture (Rahman et al. 2020).

Due to increasing demand, there have been significant increases in black cumin production and export in Türkiye between 2012 and 2023. From 2012 to 2023, its cultivation area, production, and exports increased in general (2012; 2 299 decare, 161 tonnes, 2023: 53 358 decare, 5 386 tonnes), with the highest cultivation area (108 029 decare) and yield (10 089 tonnes) being realized in 2022 and the highest export revenue in 2021 (1 020.876 tonnes, 3 189 836 US dollars). In 2017, the year with the highest imports, 5 500.803 tons of black seed worth 5 558 042US dollars were purchased (Anonymous 2021).

However, because of black cumin production is still inadequate in Türkiye, it is necessary to expand cultivation area and to increase seed yield. New black cumin varieties with superior yield/quality characteristics, suitable for mechanization and compatible with the different agroecological conditions of Türkiye, should be also immediately bred.

Environment (edaphic factors: chemical properties of the soil such as structure, water availability and air content, nutrient uptake, soil reaction (pH); orographic factors: elevation (height above sea level), direction as well as slope exposure of the cultivation area; biotic factors: microorganisms, fungi and bacteria in the soil), climatic factors (temperature, light, water, CO_2, wind, precipitation), and agronomic practices (planting time/depth/frequency, fertilization, spraying) affect the yield and quality characteristics of black cumin. The cultivation of medicinal plants and spices within the scope of good agricultural practices is an important factor that increases the chances of competition in foreign markets and export value. The market value of medicinal and aromatic plant species and pharmaceuticals grown naturally and organically is significantly higher. While the interests of the country are protected by offering safe products to foreign markets, citizens are ensured to consume healthy, quality, and reliable products domestically. It ensures a decrease in the production costs of producers and an increase in their earnings. In addition, it serves to take necessary measures for a sustainable world thanks to its environmentally sensitive agricultural production method that protects natural resources. In this regard, the World Health Organization (WHO) has prepared Good Agricultural and Collection Practices (GACP) (2003) specifically for medicinal plants in line with the requests of member countries. Good agricultural practices (IOSTA2013) are also regulated separately for spices. In these studies, detailed explanations are given on the techniques and precautions necessary for the proper cultivation, collection, and processing of quality products. To ensure the quality of products, production must be carried out in strict compliance with GAP (Good Agricultural Practice) and GMP (Good Manufacturing Practice) rules. The effective and correct use of the plant in different industrial branches will only be possible through the development of quality, efficient, and standardized black cumin varieties and the cultivation of the plant following organic and good agricultural practices.

The plant's high adaptability has enabled its cultivation in diverse climatic zones across the country. Based on data from official records, it was cultivated in 5 provinces in 2012 but increased to 34 provinces in 2022. The black cumin plant, which occupies a significant position in the country's historical narrative, represents a crucial source of revenue from herbal exports. The foreign exchange inflow clearly demonstrates that our country's black cumin plant is of superior quality and commands a higher price in the foreign market than competing plants from other countries. However, since it is a black cumin variety developed by 2024, it is primarily cultivated by local populations. Therefore, it is very important to determine the important yield characteristics of local and introduced black cumin genotypes of different regions of Türkiye where the plant is grown most intensively in terms of sustainable agriculture with good agricultural practices.

The aim of this study is to determine the effect of good agricultural practices on the yield characteristics of 31 advanced black cumin genotypes of different origins under ecological conditions of Ankara province, the use of the genotypes with superior characteristics as a source in later variety breeding studies and raising awareness among farmers about the positive effects of good agricultural practices on the producer, the consumer, and human-environment-animal health.

2. Material and Methods

2.1. Plant material

30 genotypes of black cumin with different agronomic and morphological characteristics were obtained from domestic local populations (Ankara, Burdur, Bursa, Denizli, Konya, Eskişehir, Afyonkarahisar, Diyarbakır, Kırıkkale provinces), from international gene banks of different countries (Syria, Egypt, India, Pakistan, Ethiopia). Moreover, 'Çameli' black cumin seed variety registered by the Transitional Zone Agricultural Research Institute in 2014 were also genotype (Table 1).

2.2. The experimental area and its characteristics

This research was carried out in 2019 and 2020 in the trial fields of the Field Crops Central Research Institute (FCRI) Research and Application Farm/Ankara/Türkiye. The research area is located at an altitude of 1055 m above sea level and 39°36'55.8"N latitude and 32°40'34.1"E longitude points. The experimental plots were 5 m long, 30 cm between rows and 5 rows per plot. The seed rate was calculated as 15 kg per hectare. A distance of 250 cm was left between blocks (replications) and 50 cm between plots. The experiment was conducted in 2019 in an area that was left fallow after wheat harvest in the previous year and in 2020 in an area where Tef *(Eragrostis tef* [Zucc.] Trotter) was planted the year before. At the onset of autumn rains, the soil was plowed with a moldboard plow at a depth of 15-18 cm for stubble-plowing, and sweep and harrow was used before planting in early spring (in March). The sowing process was carried out on March 12-13, 2019, and March 4-5, 2020, by hand sowing in the

rows opened with the marker. While irrigation was carried out once in May 2019, irrigation was not carried out in 2020 due to heavy rainfall. As regards the weed population, the weeds within the plots were removed by hand once before the isolation covers were laid and once after the covers were removed, and the weeds between the replications were removed twice with the help of a rotavator.

Table 1- Genotypes of black cumin used in the study

GN	*Origin*	*GN*	*Origin*
1	Denizli[1]	17	Seed Exchange[4]
2	Denizli[1]	18	Seed Exchange [4]
3	Burdur[1]	19	Seed Exchange [4]
4	Burdur[1]	20	Seed Exchange [4]
5	Ethiopia[2]	21	India[2]
6	Syria[2]	22	Bursa/ Keles/Yatıbaşı Köyü[1]
7	Egypt[2]	23	Gazi Osmanpaşa Üniv. Faculty of Agriculture
8	Syria[2]	24	Afyonkarahisar[1]
9	Denizli[3]	25	USDA- Pakistan
10	Burdur/Yeşilova-Merkez Kayadibi[3]	26	USDA- Egypt
11	Burdur/ Kemer-Elmacık-Olukderesi[3]	27	Burdur[1]
12	Konya/ Akören/Kayasu[3]	28	Kırıkkale/Halitli Köyü[1]
13	Konya/Meram/Evliyatekke[3]	29	Ankara[1]
14	Konya/ Akören/Kayasu[3]	30	Ankara[1]
15	Diyarbakır[1]	31	Çameli (cultivar)
16	Syria[2]		

GN: Genotype Numbers; [1] Local black cumin genotypes obtained from different producers cultivating *Nigella sativa* L*;* [2] Black cumin genotypes obtained from abroad through company Naturoil; [3] Local black cumin genotypes obtained through provincial agriculture and forestry directorates; [4] Black cumin genotypes obtained from companies Bağda (GN:17), Bahartat (GN: 18), Destan (GN: 19) and Lokman (GN: 20)

2.3. *Soil and climate characteristics of the experimental area*

An isolation study was carried out on June 12-13, 2019, and June 1-3, 2020, against the danger of foreign pollination of the black cumin plant, and the trial was preserved with gauze until the end of flowering. Within the scope of good agricultural practices, no commercial fertilizer was applied, and chemical treatment was not carried out against diseases and pests. The plants were harvested by hand between August 2-10, 2019, and between July 23-August 5, 2020. Plant height, first pod height, number of branches per plant, and number of pods per plant were calculated for 10 plants randomly selected from each plot by excluding 1 row from the edges and 0.5 m from the plot ends; the number of seeds per pod was calculated for randomly selected 20 plants; and seed yield per decare was calculated based on the plot yield.

According to the results of the analysis of the soil samples taken from 0-20 cm depth of the trial site before planting; the soil of the trial year 2019 showed a clayey (C) texture, while the trial year 2020 showed a clayey-loamy (CL) texture. Soil pH was 7.95-7.73 in 2019 and 2020, respectively, and was classified as slightly alkaline. The lime content was 30.5% and 30.0%, which are considered to be very calcareous, while the salt content (0.60 and 0.64 dS/m) was considered to be non-saline. In both trial years (in order of years); available organic matter (1.55-1.97%), phosphorus (P: 4.50-4.50 kg/da), manganese (Mn: 2.99-3.03 ppm) and zinc (Zn: 0.28-0.30 ppm) contents were at low levels, copper (Cu: 1.29-1.33 ppm) was at an adequate level, iron (Fe: 3.43-3.38 ppm) was at moderate level, magnesium (Mg: 921-905 ppm) and calcium (Ca: 7118-7420 ppm) were at a good level, and potassium (K: 207-306 kg/da) amount was at a level considered high.

The region has a typical continental climate, and the average temperatures (14.4 ºC -15.0 ºC) during the 6-month vegetation period from the beginning of March to the end of August in 2019 and 2020 were 1 ºC lower in 2019, and 0.4 ºC lower in 2020, than the long-term meteorological observation averages (LTA) (Table 2). A comparison of the LTA with the 2019-2020 period revealed notable discrepancies in the monthly minimum and maximum temperatures, whereas the monthly average temperatures exhibited a greater degree of similarity.

Accordingly, the monthly average temperature was highest in August (20.7 ºC) in 2019, July (23.1 ºC) in 2020 and August (22.5) for LTA. In addition, August (27.6 ºC) in 2019, July (30.6 ºC) in 2020 and July (39.6 ºC) in 2020 were the months with the highest average maximum temperature; March was recorded as the month with the lowest average minimum temperature in 2019-2020 and for LTA (-1.0 °C, -0.1 °C and -13.6 ºC, respectively).

Table 2- Meteorological data of long years and growing season of 2019 and 2020 at Ankara

Climatic Factors	*Years*	*Month*							
		March	*April*	*May*	*June*	*July*	*August*	*Average*	*Total*
Minimum Temperature (°C)	2019	-1.0	2.4	8.6	13.6	12.5	14.0	8.3	-
	2020	-0.1	2.3	6.4	10.8	15.1	14.8	8.2	-
	LY	-13.6	-5.1	-0.1	4.7	2.8	5.9	-0.9	-
Maximum Temperature (°C)	2019	11.2	14.0	21.9	25.7	26.8	27.6	21.2	-
	2020	12.2	14.3	20.2	24.2	30.6	30.5	22.0	-
	LY	24.5	28.0	31.7	34.9	39.6	38.4	32.9	-
Average Temperature (°C)	2019	4.6	7.8	15.0	18.7	19.2	20.7	14.4	-
	2020	5.6	8.2	13.2	17.2	23.1	22.7	15.0	-
	LY	5.1	9.7	14.4	18.6	22.1	22.5	15.4	-
Relative Humidity (%)	2019	58.5	61.3	55.2	59.6	50.2	47.1	55.3	-
	2020	60.6	54.7	56.2	53.8	42.3	37.5	50.9	-
	LY	72.0	64.3	63.1	59.3	46.4	45.6	58.5	-
Precipitation (mm)	2019	20.6	23.4	3.8	15.0	31.8	9.2	-	103.8
	2020	14.8	26.0	42.8	27.4	0.6	0.0	-	111.6
	LY	42.1	24.3	47.8	38.9	10.1	8.7	-	171.9
Soil Temperature 5 cm (°C)	2019	10.6	14.6	23.7	27.3	28.8	28.9	22.3	-
	2020	11.0	15.7	22.0	24.0	33.8	34.4	23.5	-
	LY	5.9	10.9	16.6	21.3	25.1	25.8	17.6	-
Soil Temperature 10 cm (°C)	2019	8.7	12.1	19.3	23.9	25.1	25.4	19.1	-
	2020	9.0	13.0	18.6	20.9	27.7	28.0	19.5	-
	LY	6.0	10.8	16.2	20.6	24.5	25.1	17.2	-

Data were obtained from Turkish State Meteorological Service, Ankara

Total precipitation levels in 2019 and 2020 were 103.8 mm and 111.6 mm, respectively. Total precipitation levels during the experiment, was lower than the long-term average. The distribution of precipitation over the vegetation period was irregular in both trial years. The relative humidity in 2019 was 3.2% lower than the long-term average and the relative humidity in 2020 was 7.6% lower than the long-term average. In 2019, there was heavy rainfall and hail on June 12, flood damage from excessive rainfall on June 21-22, and heavy rainfall on July 15-19; in 2020, it was very cold between March 13-20 and there was heavy snowfall on March 18-19. In addition, rainfall was above climate norm and continuous throughout June.

2.4. Experimental design and statistical analysis

The study was designed according to the Randomized Complete Block Experimental Design with 3 replications for two years. All data were subjected to analysis of variance (ANOVA) using the MSTAT-C computer based Statistical software packages (Anonymous 1990). The significant differences between the group means were separated using The Duncan's Multiple Comparison test (Yurtsever 1984).

3. Results and Discussion

3.1. Plant height (cm)

According to the results of the combined analysis in terms of plant height, there were significant differences between years and genotypes at 1% level, while the differences in terms of year x genotype interactions were statistically insignificant. The difference between genotypes for both years was found to be significant at 1% level, and the difference between replications was found to be statistically insignificant in 2019 and significant at 5% level in 2020.

Plant height of the genotypes varied between 14.90-28.71 cm in 2019 and 19.15-43.57 cm in 2020, while this value was between 17.03-36.14 cm in the combined analysis (Table 3). In both years and as a result of the combined analysis, genotype number 1 (2019: 28.71 cm, 2020: 43.57 cm, combined: 36.14 cm) was the tallest, and genotype number 11 (2019: 14.90 cm, 2020: 19.15 cm, combined: 17.03 cm) was the least tall genotype.

The differences in the results of the research can be explained by the differences in the climate and soil conditions of the ecology where the studies were carried out, the genetic structure of the genotypes used, and the cultural practices. In 2019, very low precipitation and irregular temperature during the first growth period caused the plant to be stressed and shorten the vegetative development, and quickly transition to the generative period, which resulted in a plant height shorter than the one in 2020 (average plant height in 2019: 20.21 cm, and in 2020: 30.39 cm). The fact that the trial was carried out with good agricultural practices and that no fertilizers were used may be considered as the reason for the lower results of the study compared to some previous studies. Especially NPK fertilizers demonstrated a more pronounced and substantial influence on black cumin height

compared to other fertilizers and it was found that an average of 6-8 kg nitrogen and 4 kg phosphorus provided optimal growth (Shah 2004; Özgüven & Şekeroğlu 2007; Tunçtürk et al. 2012; Yimam et al. 2015; Sağlık 2020).

Sowing time is another trait that affects yield and yield components. In general, it has been observed that winter sowing in regions with favourable climates has a positive effect on plant height since it is exposed to more water regime and the growing period covers a longer period (Tonçer & Kızıl 2004; Özel et al. 2009; Tektaş 2015; Kılıç & Arabacı 2016; Keser 2019; Saraç 2019). Narrow row spacing is another cultural practice that has a positive effect on plant height. Because the plant's height increases as it will compete with others to benefit from the light. Accordingly, early sowing increased plant height, while plant height decreased with delayed sowing. It is seen that plant height is an important criterion in the selection of productive lines and in minimizing yield loss, especially in machine harvesting.

3.2.First pod height (cm)

According to the combined analysis results, the differences between years and genotypes and the year x genotype interactions were found to be significant at 1% level. According to the results of the analysis of variance of the first pod height data, performed separately for 2019 and 2020, a significant difference between genotypes was detected at 1% level in both years, while the difference between replications was insignificant in 2019 but significant at 5% level in 2020.

The first pod height of the genotypes varied between 9.02-22.03 cm (year average: 14.42 cm) in 2019 and 14.35-40.93 cm (year average: 26.85 cm) in 2020, while this value was between 11.80-31.48 cm in the combined analysis. As a result of the analysis made for both years and the combined analysis, genotype number 1 (2019: 22.03 cm, 2020: 40.93 cm, combined: 31.48 cm) was the black cumin genotype with the highest first pod height, while the genotype with the lowest first pod height was found to be genotype number 17 (2019: 9.02 cm) in 2019 and genotype number 11 (2020: 14.35 cm, combined: 11.80 cm) both in 2020 and as a result of the combined analysis (Table 3).

As a result of the research, our findings regarding the first pod height values obtained from black cumin genotypes (9.02-40.93 cm) were close to and shorter than the values reported by Şahin (2013) (16.9-41.6 cm), and similar to and longer than the results of Keser (2019) (15.00-29.56 cm), Kızılyıldırım (2019) (19.76-29.40 cm) and Bozdemir et al. (2022) (11.6-26.6 cm).

While the genotypes with the highest first pod height were the same genotypes in both trial years, the difference in the genotypes with the lowest first pod height is explained by the statistically significant year x genotype interactions in the averages of the locations. In other words, the height of the first pod has varied over the years. In addition, as is the case in plant height, also the height of the first pod depends on the genotype structure of the black cumin plant and may vary according to cultural practices (plant density, irrigation, fertilization, sowing time, winter and summer planting) and ecological conditions. In general, it was determined that genotypes with higher plant height also had higher first pod height, which was in a positive relationship. Therefore, the genotypes with the tallest and shortest plant height were also the genotypes with the highest and lowest first pod height.

The height of the first pod is a highly desirable criterion for mechanization in black cumin crops. The fact that the plant is suitable for machine harvesting is very important in terms of reducing labor costs and saving time. Erskine et al. (1988) reported that the height of the first pod should be at least 12 cm for machine harvesting in lentil plants, which have similar phenotypic characteristics. Accordingly, it is seen that all genotypes included in our trial can be harvested with a combined harvester according to the results of the 2020 trial and combined analyses (considering that the actual performance of the plant could not be observed due to climatic negativities experienced in 2019).

Table 3- Average yield values from different black cumin genotypes in Ankara conditions and the resultant groups

Genotypes	*Plant height (cm)*			*First pod height (cm)*			*Thousand-seed weight (g)*		
	2019	*2020*	*2019-2020*	*2019*	*2020*	*2019-2020*	*2019*	*2020*	*2019-2020*
1	28.71 a	43.57 a	36.14 a	22.03 a	40.93 a	31.48 a	2.84 af	2.22 jm	2.53 fı
2	25.67 ab	31.23 bj	28.45 bg	21.20 ab	29.00 bı	25.10 df	2.93 ad	2.60 cg	2.77 ag
3	23.57 ae	39.60 ad	31.58 ac	18.70 ac	34.87 ae	26.78 ad	2.84 af	2.52 eh	2.68 cg
4	21.17 bı	39.03 ad	30.10 ae	16.31 be	35.93 ad	26.12 ae	2.50 ch	2.58 dg	2.54 fı
5	18.33 ej	32.29 aı	25.31 cj	13.17 dj	29.03 bı	21.10 ek	2.88 ae	2.60 cg	2.74 bg
6	20.20 bj	34.37 ag	27.28 bh	15.13 ch	28.94 bı	22.03 cı	3.06 ac	2.59 cg	2.83 af
7	16.08 hj	23.00 gk	19.54 ıl	11.97 ej	18.46 jm	15.21 ln	3.04 ac	2.77 ad	2.90 ae
8	16.47 gj	22.67 gk	19.57 ıl	9.88 hj	16.43 km	13.15 mn	3.06 ac	2.68 be	2.87 ae
9	24.26 ad	42.78 ab	33.52 ab	17.80 ad	37.97 ac	27.88 ab	2.67 ag	2.28 ıl	2.48 gj
10	23.40 ae	37.80 ae	30.60 ad	17.70 ad	31.47 bg	24.58 bg	1.89 h	2.27 ıl	2.08 k
11	14.90 j	19.15 k	17.03 l	9.25 j	14.35 m	11.80 n	3.25 a	2.90 ab	3.08 a
12	21.17 bı	23.43 gk	22.30 fl	15.10 cı	23.47 fm	19.28 gl	2.29 eh	2.07 ln	2.18 jk
13	22.67 bf	25.50 fk	24.08 dk	17.40 ad	25.63 ek	21.52 cj	2.18 gh	2.07 ln	2.13 k
14	21.00 bı	25.99 fk	23.49 el	15.20 ch	22.18 gm	18.69 hm	2.20 gh	2.03 mn	2.11 k
15	19.40 cf	25.13 fk	22.27 gl	13.83 cj	19.70 ım	16.77 ın	2.63 bg	2.52 eh	2.58 eh
16	16.81 fj	25.00 fk	20.90 hl	10.40 fj	21.55 hm	15.97 kn	2.53 bg	2.54 dh	2.54 fı
17	16.10 hj	28.00 dk	22.05 gl	9.02 j	23.80 fl	16.41 jn	2.98 ad	2.67 cf	2.83 af
18	14.94 j	22.43 hk	18.69 jl	9.25 j	17.67 jm	13.46 mn	3.13 ab	2.69 be	2.91 ad
19	15.03 j	19.83 jk	17.43 kl	9.68 ıj	16.43 km	13.06 n	3.10 ac	2.98 a	3.04 ab
20	15.63 ıj	21.73 ık	18.68 jl	9.10 j	17.35 jm	13.23 mn	2.57 bg	2.71 be	2.64 cg
21	24.53 ac	33.58 ah	29.06 be	18.10 ad	28.73 cı	23.41 bh	2.25 fh	1.95 n	2.10 k
22	19.43 cj	41.19 ac	30.31 ad	13.37 cj	38.20 ab	25.78 bf	2.72 ag	2.58 dg	2.65 cg
23	23.73 ae	38.81 ae	31.27 ac	18.20 ad	35.68 ad	26.94 ac	2.42 dh	1.93 n	2.18 jk
24	21.60 bh	33.07 aı	27.33 bh	15.33 cg	32.33 af	23.83 bh	2.21 gh	2.14 kn	2.18 jk
25	18.40 dj	30.27 ck	24.33 dj	13.43 cj	29.20 bh	21.31 dk	2.93 ad	2.42 gl	2.68 cg
26	19.23 cj	39.43 ad	29.33 be	14.70 cı	35.81 ad	25.26 bf	2.73 ag	2.18 km	2.46 gj
27	21.67 bh	36.40 af	29.03 bf	16.03 be	35.69 ad	25.86 bf	2.21 gh	2.23 ım	2.22 ık
28	22.00 bg	28.93 dk	25.47 cı	15.43 cf	25.41 fl	20.42 fl	2.52 bg	2.08 ln	2.30 hk
29	20.63 bj	30.20 ck	25.41 cj	14.77 cı	26.60 dj	20.68 el	2.77 ag	2.45 fı	2.61 dh
30	18.41 dj	20.49 jk	19.45 ıl	10.00 gj	16.03 lm	13.01 n	3.10 ac	2.82 ac	2.96 ac
31	21.23 bı	27.07 ek	24.15 dk	15.44 cf	23.55 fm	19.50 gl	2.84 af	2.33 hk	2.58 dh
Mean	20.21	30.39	25.30	14.42	26.85	20.63	2.69	2.43	2.56
LSD (0.05)	5.86**	11.78**	6.74**	5.43**	9.43**	5.54**	0.61**	0.23**	0.33**
CV (%)	17.77	23.74	23.32	23.04	21.51	23.51	13.91	5.72	11.36

**: indicate statistical differences at P≤0.01, means within a column having different letters are significantly different by Duncan's Multiple Comparison Test

3.3. Thousand-seed weight (g)

According to the combined analysis results, the differences between years and genotypes were found to be significant at 1% level, while no statistically significant difference was found between year x genotype interactions. According to the results of the analysis of variance performed separately for the years 2019 and 2020 with the thousand-seed weight data, the difference between genotypes was found to be significant at 1% level for both years, while the difference between replications was found to be insignificant in 2019 and significant at 1% level in 2020.

When Table 3 was examined, it was seen that different groups were formed among the genotypes according to the results of the 2019 and 2020 trials and combined analysis. The thousand-seed weight of the genotypes varied between 1.89-3.25 g (year average: 2.69 g) in 2019 and 1.93-2.98 g (year average: 2.43 g) in 2020, while this value was between 2.08-3.08 g in the combined analysis. The genotype with the highest thousand-seed weight was number 11 (3.25 g) in 2019, number 19 (2.98 g) in 2020, and number 11 (3.08 g) in the combined analysis. The black cumin genotype with the lowest thousand-seed weight was genotype 10 (2019: 1.89 g, combined: 2.08 g) in 2019 and in the combined analysis, and genotype number 23 (1.93 g) in 2020.

In previous studies, it was observed that fertilization had a significant effect on black cumin and that especially with soil-available phosphorus, higher amounts of dry matter and thus higher thousand-seed weight were obtained in plants (Tunçtürk et al. 2011). The results of various studies indicate that the application of NPK (Nataraja et al. 2003; Shah 2004) and, on occasion, vermicompost (Sağlık 2020) has a beneficial impact on thousand-grain weight. Although the research was carried out within the scope of good agricultural practices and the soil in which the genotypes were grown had insufficient organic matter and phosphorus content, it is seen that the majority of the genotypes included in the trial had higher thousand-seed weights than the trial material included in many research results.

The findings of various studies indicate that seed time (Mahmood et al. 2012; Bayhan 2019) and sowing frequency (Ahmed & Haque 1986; Geren et al. 1997; Abdolrahimi et al. 2012) have a significant impact on the number of branches, capsules, and

weeds per plant and per unit area, which in turn affects thousand-grain weight. Despite the plant being sown at the optimal time for Ankara (summer) and at a frequency that permitted its growth, the variability in climate had a considerable impact on the thousand-grain weight, as evidenced in this study.

All these research results demonstrate that thousand-seed weight is one of the most important yield and quality factors and it varies depending on the plant's genetic structure, cultivation techniques (irrigation and irrigation method, amount and type of fertilization, planting density and time, number of seed sown, sowing frequency), climatic factors and soil properties.

3.4. Number of branches per plant (branch/plant)

According to the combined analysis results, while the differences between years were found to be significant at 1% level, no statistically significant difference was found between year x genotype interactions and genotypes. According to the results of the analysis of variance performed separately for the years 2019 and 2020 using the data on the number of branches; while no statistically significant difference was found in terms of any source of variation in 2019, a statistically significant difference was found only between the replications at the 1% level in 2020.

The number of branches of the genotypes varied between 1.77-3.13 branch/plant in 2019 (year average: 2.12 branch/plant) and between 1.37-2.25 branch/plant in 2020 (year average: 1.76 branch/plant), while this value was between 1.59-2.52 branch/plant in the combined analysis. The most branched genotype was genotype number 1 (2019: 3.13 branch/plant, combined: 2.52 branch/plant) in 2019 and in the combined analysis, and genotype number 22 (2.25 branch/plant) in 2020; while the least branched genotype was genotype number 29 (1.77 branch/plant) in 2019 and genotype number 19 (2020: 1.37 branch/plant, combined: 1.59 branch/plant) in 2020 and in the combined analysis (Table 4).

Table 4- Average yield values from different black cumin genotypes in Ankara conditions and the resultant groups

Genotypes	*Number of branches per plant (branch/plant)*			*Number of pods per plant (pods/plant)*		
	2019	**2020**	**2019-2020**	**2019**	**2020**	**2019-2020**
1	3.13 a	1.90 ad	2.52 a	3.26 a	1.98 bd	2.62 a
2	2.40 ad	1.70 ad	2.05 ad	2.23 be	1.73 be	1.98 ce
3	2.00 cd	1.90 ad	1.95 bd	2.14 be	1.77 be	1.95 ce
4	2.37 ad	1.99 ad	2.18 ac	2.07 be	2.08 bd	2.08 bd
5	2.03 cd	2.00 ad	2.01 ad	2.33 bd	1.97 bd	2.15 ad
6	1.97 cd	2.03 ac	2.00 ad	2.07 be	2.20 b	2.13 ad
7	2.08 bd	1.50 cd	1.79 bd	1.86 ce	1.63 be	1.75 ce
8	2.13 bd	1.82 ad	1.98 bd	1.78 de	1.87 be	1.82 ce
9	2.13 bd	2.20 ab	2.17 ac	2.06 be	3.00 a	2.53 ab
10	1.81 d	1.78 ad	1.79 bd	2.07 be	2.17 bc	2.12 ad
11	1.90 cd	1.55 cd	1.73 cd	2.00 be	1.45 de	1.73 ce
12	1.83 cd	1.69 ad	1.76 cd	2.04 be	1.73 be	1.88 ce
13	2.32 bd	1.67 ad	1.99 ad	1.94 ce	1.60 be	1.77 ce
14	2.32 bd	1.61 ad	1.96 bd	2.08 be	1.53 be	1.81 ce
15	2.60 ac	1.53 cd	2.07 ad	2.83 ab	1.65 be	2.24 ac
16	2.15 bd	1.93 ad	2.04 ad	1.82 ce	1.94 be	1.88 ce
17	1.89 cd	1.83 ad	1.86 bd	1.93 ce	2.03 bd	1.98 ce
18	1.80 d	1.73 ad	1.77 bd	1.74 de	1.71 be	1.72 ce
19	1.81 d	1.37 d	1.59 d	1.73 de	1.67 be	1.70 de
20	1.87 cd	1.60 bd	1.73 cd	1.75 de	1.72 be	1.73 ce
21	2.17 bd	1.57 bd	1.87 bd	2.00 ce	1.73 be	1.87 ce
22	2.10 bd	2.25 a	2.18 ac	1.87 ce	2.19 b	2.03 be
23	2.54 ad	2.03 ac	2.28 ab	2.37 bd	2.08 bd	2.22 ac
24	1.90 cd	1.70 ad	1.80 bd	1.94 ce	1.70 be	1.82 ce
25	2.16 bd	1.70 ad	1.93 bd	1.84 ce	1.73 be	1.79 ce
26	2.10 bd	1.80 ad	1.95 bd	1.86 ce	2.03 bd	1.95 ce
27	1.93 cd	1.67 ad	1.80 bd	1.83 ce	1.82 be	1.82 ce
28	1.87 cd	1.40 cd	1.64 d	1.77 de	1.28 e	1.52 e
29	1.77 d	1.69 ad	1.73 cd	1.50 e	1.51 ce	1.50 e
30	2.82 ab	1.60 bd	2.21 ac	2.59 ac	1.69 be	2.14 ad
31	1.79 d	1.86 ad	1.83 bd	1.97 ce	2.00 bd	1.98 ce
Mean	2.12	1.76	1.94	2.04	1.84	1.94
LSD (0.05)	0.78	0.65	0.52	0.80	0.68*	0.53*
CV (%)	22.54	22.56	23.57	24.01	22.68	23.73

*: indicate statistical differences at P≤0.05, means within a column having different letters are significantly different by Duncan's Multiple Comparison Test

Seed yield is directly affected by the number of branches, number of pods, number of seeds in pods, and thousand-seed weight. Branching in black cumin is desirable up to a certain point. In this study, when different black cumin populations were compared, the differences between them were due to environmental and climatic factors (as years and replications were significant, while genotypes were insignificant) and the ability of the material to adapt to these factors, rather than their genotypic characteristics.

According to Tavas et al. (2014), branching in black cumin is a yield component determined by genotype rather than ecological conditions, but according to Yılmaz (2008), it is a trait depending on genotype and environment. Plant density (the number of seeds sown per unit area, inter-row spacing) and sowing time (winter or summer planting), agronomic treatments such as the application of different fertilizer types in varying doses, irrigation, climate (humidity-precipitation), and light exposure are among the important factors that affect branching.

In the relevant studies, it was determined that sparse sowing generally encourages branching in plants (Ceylan 1979), and in general, the number of branches decreases as the number of seeds increases (Tektaş 2015). It has been reported that the number of branches and thus seed yield values increase significantly with a certain level of increase in different intra-row spacing applications (plant density) (Das et al. 1992; El Deen & Ahmed 1997).

It has been established by many studies that the number of branches is higher in winter planting than in summer planting because winter planting is exposed to more soil moisture and precipitation and removes nutrients from the soil for a longer period. In many studies on winter planting, it has been reported that there are significant differences among black cumin populations in terms of branch number (Tonçer & Kızıl 2004; Mahmood et al. 2012; Tektaş 2015; Kılıç & Arabacı 2016; Bayhan 2019; Kamçı 2019; Kızılyıldırım 2019; Özdemirel & Kaçar 2021; Saraç 2019).

In the fertilizer trials, it was observed that the application of nitrogen fertilizer had a positive effect on the number of plant branches, increasing nitrogen doses up to a certain level increased the number of plant branches, and at higher nitrogen doses, the average number of plant branches decreased slightly. It has been reported by some researchers that nitrogen and phosphorus applications had positive effects on the development and yield of black cumin plants and that increasing nitrogen and phosphorus doses increased the number of plant branches (El Deen & Ahmed 1997; Tunçtürk et al. 2012; Shah 2004; Özgüven & Şekeroğlu 2007; Sultana et al. 2019). The highest number of branches in extreme fertilizer trials was obtained from chicken manure application by Sağlık (2020).

The black cumin genotypes in the study differed from the previous studies in terms of the number of branches. This may be attributed to the differences in the genotypes used in the studies and the fact that they were genotypes with less branching capacity, the adverse conditions experienced in the climate in the years when the studies were carried out, and the difficulties experienced in the adaptation of the genotypes to these conditions, the application of cultivation techniques (not using fertilizer due to good agricultural practices, high weed density) and soil properties.

3.5. Number of pods per plant (pods/plant)

According to the results of the combined analysis, there were significant differences between years at 1% level and between genotypes at 5% level, while no statistically significant difference was found between year x genotype interactions. According to the results of the analysis of variance performed separately for the years 2019 and 2020 using the data on pod number; while no statistically significant difference was found in terms of any source of variation in 2019, a statistically significant difference was found between genotypes and replications at the 5% level in 2020.

The number of genotype pods varied between 1.50-3.26 pods/plant in 2019 (year average: 2.04 pods/plant) and between 1.28-3.00 pods/plant in 2020 (year average: 1.84 pods/plant), while this value was between 1.50-2.62 pods/plant in the combined analysis. The genotype with the highest number of pods was genotype number 1 (2019: 3.26 pods/plant, combined: 2.62 pods/plant) in 2019 and in the combined analysis, and genotype number 9 (3.00 pods/plant) in 2020; while the genotype with the lowest number of pods was genotype number 29 (1.50 pods/plant) in 2019 and in the combined analysis, and genotype number 28 (1.28 pods/plant) in 2020 (Table 4).

Pod number is one of the important yield factors related to branching in black cumin plants. Since the plant has a branched structure and each branch ends with a pod; the increase in the number of branches means a higher number of pods. Therefore, according to the results of the combined variance analysis, it is expected that the genotype with the maximum number of branches is the genotype with the maximum number of pods. Some agronomic and cultural practices have been very effective in the number of pods. It was observed that fertilizer applications of N, P and K (Geren et al. 1997, Mohamed et al. 2000; Nataraja et al. 2003; Özgüven & Şekeroğlu 2007; Shah 2007; Tunçtürk et al. 2012; Ali et al. 2015; Tulukçu 2011; Yimam et al. 2015; Muhammad et al. 2017; Sağlam 2018; Kızılyıldırım 2019), kinetin and gibberellic acid (Shah 2004), biofertilizer application (Sen et al. 2018) and chicken manure application (Sağlık 2020) significantly increased the number of pods. In studies conducted with plant density, it has been proved by various studies (Ahmed & Haque 1986; Das et al. 1992; El Deen & Ahmed 1997; Geren et al. 1997; Tonçer & Kızıl 2004; Özel et al. 2009; Abdolrahimi et al. 2012; Baydar 2013) that the increase in branching and thus

the number of pods increases the yield in plants sowed with certain inter-row spacing. Sowing time was also effective in the increase in the number of pods, and it was determined that in general, winter planting (Tonçer and Kızıl 2004; Özel et al. 2009; Mahmood et al. 2012; Tektaş 2015; Bayhan 2019; Kızılyıldırım 2019; Saraç 2019) produced more pods.

The herb growth of the plants was limited because the study was carried out in an arid/semi-arid region and the course of the climate was unfavorable and irregular. Genetic differences among genotypes, their different responses to environmental and climatic factors, agronomic practices (fertilizer-free cultivation), and soil structure had a significant effect on the number of pods. Therefore, the values obtained were generally lower than some values reported in the literature.

3.6. Number of seeds per pod (seeds/pod)

According to the combined analysis results, significant differences were found between genotypes at 1% level, while no statistically significant difference was found between year x genotype interactions and years. According to the results of the analysis of variance performed separately for the years 2019 and 2020 using the data on the number of seeds per pod; while there was no statistically significant difference between the replications in 2019, a statistically significant difference was found at 1% level between the replications and at 5% level between genotypes in 2020.

The number of seeds per genotype pod was 25.71-56.74 seeds/pod in 2019 (year average: 41.33 seeds/pod) and 31.57-57.03 seeds/pod in 2020 (year average: 41.68 seeds/pod), while this value was between 29.87-54.64 seeds/pod in the combined analysis. The genotype with the highest number of seeds per pod was genotype number 1 in 2019 (56.74 seeds/pod), and genotype number 9 in 2020, and in the combined analysis (2020: 57.03 seeds/pod, combined: 54.64 seeds/pod), while the genotype with the lowest number of seeds per pod was the black cumin genotype number 30 (2019: 25.71 seeds/pod, combined: 29.87 seeds/pod) in 2019 and number 11 (31.57 seeds/pod) in 2020 (Table 5).

According to Ahmed and Haque (1986) and Arslan (1994), the factors to be taken into consideration in terms of yield in black cumin plants are the number of branches obtained from unit area, the number of pods, thousand-seed weight and the number of seed per pod. When the findings of the study were compared with the previous studies, it was observed that the number of seeds per pod may vary due to the genetic differences of black cumin populations as well as the cultivation in different regions (different soil structures and climate) and under different conditions and cultivation technique practices. In addition, the size of the seeds in the pod affects the number of seeds in the pod, while the size of the pods affects the number of seeds in the pod.

Although black cumin plant can tolerate water deficit (Ghamarnia et al. 2010), it has been observed that adequate irrigation, especially when rainfall is insufficient until the flowering period, has a rather positive effect on the number of seeds per pod as well as on many yield criteria of the plant (Safaei et al. 2014; Arslan 2015).

In general, winter sowing has a higher number of seeds per pod than summer sowing, the reason for which is considered to be the removal of the nutrients as well as the moisture needed from the soil for a longer period. In general, it was determined that as the vegetation period shortened, the number and weight of seeds per plant decreased. Indeed, D'Antuono et al. (2002) reported that the vegetation period was effective on the number of seeds per plant in black cumin depending on sowing time. It has been observed that many fertilizer trials had positive effects on the number of seeds per pod besides increasing the number of pods per plant. Researchers found that the application of N-P and K (Geren et al. 1997; Nataraja et al. 2003; Mollafilabi et al. 2010; Ali et al. 2015; Yimam et al. 2015), organic fertilizers (Ghiyasi et al. 2017), chicken manure (Sağlık 2020) bio-fertilizer (Sen et al. 2018) and kinetin and gibberellic acid (Shah, 2004) at different levels had positive effects on the number of seeds per pod in different ecologies.

Many researchers have reported based on their studies that plant density, one of the agronomic practices, directly affects black cumin yield, number of branches, number of pods, thousand-seed weight, and number of seeds per pod (Ahmed & Haque 1986; Das et al. 1992; Geren et al. 1997; Mollafilabi et al. 2010).

In the study, a positive relationship was found between the number of seeds per pod and thousand-seed weight, and the genotypes with minimum and maximum values were similar genotypes.

3.7. Seed yield (kg/ha)

According to the results of the combined analysis, significant differences were found at 1% level between genotypes and year x genotype interactions, while no statistically significant difference was found between years. According to the results of the analysis of variance performed for the years 2019 and 2020 using seed yield data; the differences between genotypes for both years were found to be statistically significant at the 1% level, and the differences between the replications for 2020 were found to be statistically significant at the 5% level.

When Table 5 was examined, it was seen that different groups were formed among the genotypes according to the results of 2019 (year average: 378.9 kg/ha), 2020 (year average: 367.8 kg/ha), and combined analysis. The highest seed yield was obtained

from genotype number 4 with 624.4 kg/ha-501.0 kg/ha in 2019 and in the combined analysis, respectively, and from genotype number 7 with 507.9 kg/ha in 2020. The lowest seed yield was given by genotype number 30 (188.2 kg/ha) in 2019, genotype number 11 (238.9 kg/ha) in 2020, and genotype number 21 (259.6 kg/ha) in the combined analysis (Table 5).

Since the seed is the part used in the black cumin plant, the most important target in terms of yield is seed yield. According to the results of many studies, seed yield is directly related to the number of branches, number of pods, number of seeds per pod, and thousand-seed weight. In the studies carried out in different ecologies, including the above-mentioned, various studies conducted with different black cumin populations, the differences in seed yield are due to the differences in ecological conditions (precipitation, temperature, etc.) as well as genotypes and agricultural practices (soil preparation, irrigation, fertilization, weeding, spraying, plant density, seed quantity, harvest time, etc.).

Ceylan (1987) reported that the most suitable pre-plant for black cumin seed is hoe crops, that it should be sown after these crops, that the soil should be prepared very well just before sowing as in other small-seeded plants and that sowing as early as possible in spring for summer planting is the first step to be taken in terms of yield. In general, in places where the climate is suitable, winter planting makes the yield three times more productive than summer planting (Bayhan 2019). The general principle here is that the plant is exposed to more water and nutrients in the soil and that it can avoid water stress and develop adequately. Failure to meet the water needs of the plant on time, in sufficient quantity and frequency, with the most appropriate method during dry times can have a great impact on yield. Studies have shown that the best yield results are obtained when 100% of the water requirement of the plant is met by a drip irrigation system every two days (El-Mekawy 2012; Ghamarnia & Jalili 2013; Nadeem et al. 2013). Weed species, density, timing and number of times weeds are controlled, and harvest time are other factors affecting yield (Nadeem et al. 2013; Amirnia & Rezaei-Chiyaneh 2016).

Another factor that is as effective as water in plant growth and therefore yield and quality is micro-macro plant nutrients and their ratios in the soil. According to Dinç et al. (1988), in the climate zone in which our country is located, the clay, lime, and pH of the soils are high, and the organic matter content of the soils is low. These chemical properties of the soil structure limit the benefits of phosphorus to plants (Mengel & Kirkby 1987; Rodriguez et al. 2000). In particular, phosphorus deficiency leads to a significant decrease in dry weight and leaf area of plants and thus adversely affects plant growth and photosynthesis (Colomb et al. 2000; Rodriguez et al. 2000). Nitrogen, one of the macronutrients, is also an important contributing factor to plant growth, development and yield (Shah 2004). For this reason, in cases where plant nutrients are insufficient, external supplementation, that is, fertilization is an extremely important, positive parameter in terms of yield.

In different studies conducted in and outside the country on *Nigella sativa* L. plant, it was reported that plant density, sowing frequency, inter-row and intra-row spacing, and seed amount (Tonçer & Kızıl 2004; Özel et al. 2009; Abdolrahimi et al. 2012; Tektaş 2015; Kılıç & Arabacı 2016; Saraç 2019); sowing time and winter-summer planting (Tektaş 2015; Mahmood et al. 2012; Haq et al. 2015; Sultana et al. 2019; Bayhan 2019; Kamçı 2019; Keser 2019; Gülhan & Taner 2020); irrigation program, time, frequency, method and growing under dry/water conditions (Ghamarnia et al. 2010; Al-Kayssi et al. 2011; El-Mekawy 2012; Ghamarnia & Jalili 2013; Nadeem et al. 2013; Safaei et al. 2014; Amirnia & Rezaei-Chiyaneh 2016; Şenyiğit & Arslan 2018; Yiğitbaşı 2019); different chemical treatments such as N-P-K and kinetin and gibberellic acid (Mohamed et al. 2000; Nataraja et al. 2003; Shah 2004; Özgüven & Şekeroğlu 2007; Mollafilabi et al. 2010; Rana et al. 2012; Tunçtürk et al. 2011-2012; Rasool et al. 2014; Ali et al. 2015; Tulukçu 2011; Yimam et al. 2015; Ghiyasi et al. 2017; Horvat et al. 2017; Muhammad et al. 2017; Sağlam 2018; Sultana et al. 2019; Sağlık 2020) had positive and significant effects on yield.

Rather than the genetic structure of the materials included in the experiment, their response to the adverse climatic factors experienced in the years of the study, insufficient organic matter and macronutrients in the soil, and the lack of fertilization and spraying within the framework of good agricultural practices caused the yield results to be lower than some of the previous research results.

Table 5- Average yield values from different black cumin genotypes in Ankara conditions and the resultant groups

Genotypes	*Number of seeds per pod (seeds/pod)*			*Seed yield (kg/ha)*		
	2019	**2020**	**2019-2020**	**2019**	**2020**	**2019-2020**
1	56.74 a	52.01 ab	54.37 ab	573.4 ac	369.0 ag	471.2 ac
2	45.67 af	39.11 bf	42.39 ch	516.1 ad	283.3 eg	399.7 aı
3	43.78 bg	45.13 af	44.46 bg	442.5 cf	289.4 eg	365.9 ck
4	43.07 bg	46.98 ae	45.02 ag	624.4 a	377.7 ag	501.0 a
5	36.80 eı	49.19 ac	42.99 ch	272.0 gk	435.2 ad	353.6 dk
6	43.23 bg	48.44 ad	45.84 ae	366.9 dj	414.1 af	390.5 bı
7	34.21 fı	36.25 cf	35.23 fı	423.9 cg	507.9 a	465.9 ac
8	37.35 dı	40.82 bf	39.09 eı	453.1 be	392.6 af	422.8 ag
9	52.25 ac	57.03 a	54.64 a	493.1 ad	376.0 ag	434.5 af
10	48.61 ae	49.92 ac	49.26 ad	421.9 cg	380.2 af	401.1 ah
11	38.44 dı	31.57 f	35.00 gı	440.5 cf	238.9 g	339.7 dk
12	45.10 ag	39.53 bf	42.32 dh	461.1 ae	305.4 dg	383.2 bj
13	47.59 ae	34.80 df	41.19 dh	399.0 dh	280.4 eg	339.7 dk
14	42.88 bg	37.97 cf	40.43 dh	371.9 dı	275.5 fg	323.7 gk
15	40.00 ch	32.13 f	36.06 eı	517.3 ad	363.4 bg	440.4 ae
16	39.90 ch	36.70 cf	38.30 eı	229.2 ık	500.8 ab	365.0 ck
17	32.63 gı	40.11 bf	36.37 eı	456.5 be	496.3 ac	476.4 ab
18	36.90 dı	39.60 bf	38.25 eı	300.4 ek	373.2 ag	336.8 dk
19	29.00 hı	39.38 bf	34.19 hı	239.8 hk	373.1 ag	306.5 hk
20	32.72 gı	40.94 bf	36.83 eı	203.3 jk	438.0 ad	320.6 gk
21	49.80 ad	41.46 bf	45.63 ae	205.7 jk	313.4 dg	259.6 k
22	41.97 cg	47.16 ae	44.56 ag	611.9 ab	278.4 fg	445.2 ad
23	55.02 ab	50.04 ac	52.53 ac	319.6 ek	419.8 ae	369.7 bj
24	41.72 ch	40.04 bf	40.88 dh	372.9 dı	360.7 bg	366.8 ck
25	39.27 dh	37.94 cf	38.61 eı	305.6 ek	485.1 ac	395.4 aı
26	44.11 ag	36.35 cf	40.23 dh	388.9 dı	279.6 eg	334.2 ek
27	40.95 ch	44.20 af	42.58 ch	265.0 gk	382.2 af	323.6 gk
28	41.85 ch	33.77 ef	37.81 eı	270.6 gk	311.0 dg	290.8 ık
29	33.08 fı	39.48 bf	36.28 eı	285.6 fk	369.1 ag	327.4 fk
30	25.71 ı	34.02 ef	29.87 ı	188.2 k	373.7 ag	281.0 jk
31	40.81 ch	49.92 ac	45.37 af	324.6 ek	358.7 cg	341.7 dk
Mean	41.33	41.68	41.50	378.9	367.8	373.3
LSD (0.05)	12.92**	14.02*	10.17**	164.5**	140.7**	109.5**
CV (%)	19.14	20.59	21.45	26.59	23.42	25.68

*, **: indicate statistical differences at P≤ 0.05, P≤ 0.01 respectively; means within a column having different letters are significantly different by Duncan's Multiple Comparison Test

4. Conclusions

This study investigated the effect of good agricultural practices method on yield characteristics of black cumin genotypes of different origins at the advanced yield stage. Increasing black cumin production in our country can only be achieved by increasing its areas of cultivation. The development of varieties with superior characteristics and high yield potential in foreign pollinated plants, such as black cumin, increases the yield in terms of seed per unit area. It is important to grow the plant with good agricultural practices widely accepted in the world or by using the organic farming method, in order to prevent toxicity to human health and natural habitat and at the same time to support the producer economically. As in all cultured plants, yield and other yield-related characteristics in black cumin cultivation vary depending on climatic factors, soil properties, and cultivation techniques, apart from the genetic characteristics of the plant. Therefore, this study also aimed to provide information to black cumin producers and consumers on the effects of reliable and human-nature-friendly good agricultural practices and black cumin cultivation on yield and other yield criteria. The present study also elucidated morphological, and genetic characteristics of 31 genotypes and to determine the best one.

In conclusion, it is known that the genetic base of the *Nigella* genus in the world is limited and shows very low genetic variation. The narrow genetic base makes breeding studies of black cumin difficult. However, a high level of variation was found among black cumin genotypes in terms of yield and yield parameters. Environment conditions markedly influence the expression of most phenotypic traits. It was also determined in our study that variations in climate and the physical and chemical properties of the experimental soil were highly influential on the results. The genotypes 4 (501.0 kg/ha), 17 (476.4 kg/ha), 1(471.2 kg/ha), and 7 (465.9 kg/ha), stand out in terms of seed yield. Our results suggest that these genotypes can be shown as promising genotypes that can be cultivated in Ankara and similar ecological and can be used in breeding studies. Moreover, it is very important to repeat the study under different climatic and soil conditions in order to eliminate the negative results of the experiment arising from climatic variability and thus to determine the actual performance of the black cumin genotypes. Diversification of studies to determine organic fertilization and other agricultural factors suitable for organic and good

agricultural practices in black cumin cultivation, and the development of efficient and high-quality varieties will contribute greatly to the socio-economic development of the regions where the plant is grown and to the national economy.

It will be also useful for the construction of a black cumin germplasm collection for providing for breeding programs. The present characterization strategies will help to black cumin breeding programmes for breeding of F1 hybrids with desired traits.

References

Abdolrahimi B, Mehdikhani P & Hasanzadeh G T (2012). The effect of harvest index, yield and yield components of three varieties of black seed (*Nigella sativa* L.) in different planting densities. *International Journal of Agriscience* 2(1): 93-101

Ahmed N U & Haque K R (1986). Effect of row spacing and time of sowing on the yield of black cumin (*Nigella sativa* L.). *Bangladesh Journal of Agriculture* 11(1): 21-24, Bangladesh

Al-Kayssi A W, Shibab R M & Mustafa S H (2011). Impact of soil water stress on Nigellone oil content of black cumin seeds grown in calcareous-gypsifereous soils. Agricultural Water Management 100(2011): 46-57

Ali M M K, Hasan M A & İslam M R (2015). Influence of fertilizer levels on the growth and yield of black cumin (*Nigella sativa* L.), The Agriculturists 13(2): 97-104

Amirnia R & Rezaei-Chiyaneh E (2016). Effect of different levels of irrigation and harvesting time on seed yield and essential oil production of black cumin (*Nigella sativa* L.). III. Medicinal and Aromatic Plants Symposium, Antalya. Book of Full Text Proceedings 125-128 (In Turkish)

Anonymous (1990). MSTAT-C, MSTAT users guide: A microcomputer program for the desing, management, and analysis of agronomic research experiments. Michigan State University, East Lansing, Chapter 3.1.1. 1990, pp. 3.3-3.7

Anonymous (2021). Turkish Statistical Institute (TurkStat). Website: www.tuik.gov.tr. Access Date 27.03.2024

Arslan N (1994). Effect of sowing time and plant density on black cumin (*Nigella sativa*) yield. *Journal of Ankara University*, Central Research Institute of Field Crops Volume: 3, Issue: (1-2):73-80 (In Turkish)

Arslan N, Javani M & Taher M (2015). Good agricultural practices in cultivation of medicinal plants. Turkey Seed Growers Association (TÜRKTOB) 4 (16): 32-38 (In Turkish)

Asil H & Bozdoğan Konuşkan D (2021). Investigation of fatty acid compositions of obtained from different oilseeds by cold pressed method. Mustafa Kemal University Journal of Agricultural Sciences 26(3): 670-678

Baydar H (2013). Science and Technology of Medicinal and Aromatic Plants. Süleyman Demirel University Press House, Isparta, Turkey. ISBN 978- 975-7929-79-6, 339 (In Turkish)

Bayhan A (2019). The effect of different sowing times to some important agriculturel and quality characters of black cumin (*Nigella sativa*) in Samsun conditions. (MSc. Thesis). On Dokuz Mayıs University, Institute of Natural and Applied Sciences, Department of Field Crops, Samsun, Turkey

Bozdemir Ç, Bahtiyarca Bağdat R, Subaşı İ, Akçi N & Çinkaya N. (2022). Determination of yield and quality characteristics of various genotypes of black cumin (*Nigella Sativa* L.) cultivated through without fertilizers. *International Journal of Life Sciences and Biotechnology* 5(3): 386-406

Ceylan A (1979). Medicinal Plants I. General Section. Ege Univ. Faculty of Agriculture. Publication No: 312, İzmir, Turkey (In Turkish).

Ceylan A (1987). Medicinal Plants (Essential Oil Containers). Ege University Faculty of Agriculture Publications No: 481, pp. 173-174 İzmir, Turkey (In Turkish)

Colomb B, Kiniry R J & Debaeke P (2000). Effect of soil phosphorus on leaf development and senescence dynamics of field-grown maize. *Argon J*. 2: 428- 435

D'Antuono İ, Filippo Moretti A & Lovato Antonio F S (2002). Seed yield, yield components, oil content and essential oil content and composition of *Nigella sativa* and *Nigella damascena*. Industrial Crops and Products 15(1): 59-69

Das A, Sadhu M K, Som M G & Bose T K (1992). Effect of spacing on growth and yield of black cumin (*Nigella Sativa* L.). India Cocoa, *Arecanut and Spices Journal* 16(1): 17-18

Dinç U, Şenol, S, Sayın M, Kapur S & Güzel N (1988). Soils of South Eastern Anatolia Region (GAT) I. Harran Plain, TÜBİTAK, Agriculture Forestry Research Group, Guided Research Project Final Result Report, TAOG, 534, Adana, Turkey (In Turkish)

El Deen E & Ahmed T (1997). Influence of plant distance and some phosphorus fertilization sources on black cumin (*Nigella sativa* L.) plants. *Assian Journal of Agricultural Sciences* 28(2): 39-56

El-Mekawy M A M (2012). Growth and yield of *Nigella sativa* L. plant influenced by sowing date and irrigation treatments plant production. Faculty of Environmental Agriculture Science, El-Arish, Suez Canal University, *Egypt American-Eurasian Journal of Agriculture and Environmental Sciences* 12(4): 499-505

Erskine W, Nassib A M & Telaye A (1988). Breeding For Morphological Traits. World Crops: Cool Season Food Legumes. Editor: R.J. Summerfield. Kluwer Academic Publishers 117 pp The Netherlands

Geren H, Bayram E & Ceylan A (1997). Effect of Different Sowing Times and Phosphorus Fertiliser Application on Yield and Quality of Black Cumin (*Nigella sativa* L.). 2nd Field Crops Congress of Turkey, 22-25 September, pp. 376-380, Samsun, Turkey

Ghamarnia H, Khosravy H & Sepehri S (2010). Yield and water use efficiency of (*Nigella sativa* L.) under different irrigation treatments in a semi arid region in the West of Iran. *Journal of Medicinal Plants Research* 4(16): 1612-1616

Ghamarnia H & Jalili Z (2013). Water stress effects on different black cumin (*Nigella sativa* L.) components in a semi-arid region. *International Journal of Agronomy and Plant Production* 4(4): 753-762, 2051-1914 Victor Quest Publications

Ghiyasi M, Amirni R & Fazelimanesh M (2017). Improving yield and quality of black cumin (*Nigella sativa* L.) organic fertiliser extract foliar application approach, Oxidation Communications 40, No 3: 1254-1264

Ghosheh O A, Houdi A A and Crooks P A (1999). High performance liquid chromatographic analysis of the pharmacologically active quinones and related compounds in the oil of the black seed (*Nigella sativa* L.). *Journal of Pharmaceutical and Biomedical Analysis* 19(5): 757-62

Gülhan M F & Taner S (2020). Determination of yield, chemical content and antioxidant capacity of black cumin (*Nigella sativa* L.) at different planting times in Aksaray ecological condition. *Ejons International Journal On Mathematics, Engineering and Natural Sciences* 15: 475-488 (In Turkish)

Haq M Z, Hossain M M, Haque M M, Das M R & Huda M S (2015). Blossoming characteristics in black cumin genotypes in relation seed yield influenced by sowing time American. *Journal of Plant Sciences* 6: 1167-1183

Horvat D, Vukobratovic M, Karalic K & Zidovec V (2017). Influence of sowing period and fertilization on yield and quality of seeds of *Nigella damascena* and *Nigella sativa*, Acta Sci. Pol. Agricultura 16(1): 35-43

Kamçı G (2019). Determination of the effect of sowing time and irrigation on yield and quality characteristics in black cumin (*Nigella sativa* l.). (MSc. Thesis). Dicle University, Institute of Natural and Applied Sciences, Department of Field Crops, Diyarbakir, Turkey

Keser E (2019). Determination of agricultural and quality examinations of winter and summer black cumin (*Nigella* sp.) genotypes in Kahramanmaras ecological conditions. (MSc. Thesis). Sütçü İmam University, Institute of Natural and Applied Sciences, Department of Field Crops, Kahramanmaraş, Turkey

Kılıç C & Arabacı O (2016). The effect of different sowing times and seed rate on the yield and quality of black cumin (*Nigella sativa* L.). *Journal of Adnan Menderes University Agricultural Faculty* 13(2): 49-56 (In Turkish)

Kızılyıldırım H (2019). The effect of different nitrogen dosage applications on the yield and quality of black cumin (*Nigella sativa*) in Kahramanmaras ecological conditions. (MSc. Thesis). Sütçü İmam University, Institute of Natural and Applied Sciences, Department of Field Crops, Kahramanmaraş, Turkey

Lutterodt H, Luther M, Slavin M, Yin J J, Parry J, Gao J M & Yu L L (2010). Fatty acid profile, thymoquinone content, oxidative stability, and antioxidant properties of cold-pressed black cumin seed oils. LWT-Food Sci. Technol. 43(9): 1409–1413. https://doi.org/10.1016/j.lwt.2010.04.009.

Mahmood T, Idress M, Muhammed N, Aslam M, Akram H M, Sattar A & Ghaffar A (2012). Effect of sowing dates and method of sowing on the yield of black cumin (*Nigella sativa* L.). In National seminar on role of agronomy in national food security. Conference paper. Pakistan society of agronomy str (pp. 76-79)

Mengel K & Kirkby E A (1987). Principles of Plant Nutrition (4. ed.), Int. Potash. Inst., Bern, Switzerland, 655 pp

Mohamed S A, Medani R A & Khafaga E R (2000). Effect of nitrogen and phosphorus applications with or without micronutrients on black cumin (*Nigella sativa* L.) plants. Annals of Agricultural Science (Cairo) 3: Special, pp. 1323-1338

Mollafilabi A, Moodi H, Rashed M H & Kafi M (2010). Effect of plant density and nitrogen on yield and yield components of black cumin (*Nigella sativa* L.). Acta Horticulturae 853: 115-126

Muhammad A G, Ahmad R M & Muhammad K E (2017). Response of growth, yield and oil content of two black seed species to nitrogen fertilizer in sulaimani district euphrates. *Journal of Agriculture Science* 9(4): 18-52

Nadeem M A, Tanveer A, Naqqash T, Jhala A J & Mubeen K (2013). Determining Critical Weed Competititon Periods for Black Seed. *The Journal of Animal & Plant Sciences* 23(1): 216-221

Nataraja A, Farooqi A A, Sreeramu B S & Srinivasappa K N (2003). Influence of nitrogen, phosphorus and potassium on growth and yield of black cumin (*Nigella sativa* L.) *Journal of Spices and Aromatic Crops* 12(1): 51-54

Özdemir Orhan N & Eroğlu Z (2024). Evaluation of the potential use of black cumin oil oleogel as a fat alternative in cracker production. *Black Sea Journal of Engineering and Science* 7(2): 342-350

Özdemirel F & Kaçar O (2021). Determination of agricultural characteristics and fixed oil ratios of different originated black cumin (*Nigella sativa* L.) genotypes grown in Bursa ecological conditions. *Journal of Agricultural Faculty of Bursa Uludağ University* 35(1): 13-31 (In Turkish)

Özgüven M & Şekeroğlu N (2007). Agricultural practies for high yield and quality of black cumin (*Nigella sativa* L.) cultivated in Turkey, Acta Hotriculturae 756: 329-337

Özel A, Demirel U, Güler İ & Erden K (2009). Effect of different row spacing and seeding rates on black cumin (*Nigella sativa* L.) yields and some agricultural characters. *Harran University Journal of Faculty of Agriculture* 13(1):17-25 (In Turkish)

Rahim M A, Shoukat A, Khalid W, Ejaz A, Itrat N & Majeed I (2022) A narrative review on various oil extraction methods, encapsulation processes, fatty acid profiles, oxidative stability, and medicinal properties of black seed (*Nigella sativa*). Foods 11(18): 2826

Rahman A, Akbar D, Bhattarai S, Trotter T, Thomson M & Timilsina S (2020). Market Analysis of Kalonji. CQ University Australia, Cooperative Research Centre for Developing Northern Australia (CRCNA)

Rana S, Singh P P, Naruka İ S & Rathore S S (2012). Effect of nitrogen and phosphoruson growth, yield and quality of black cumin (*Nigella sativa* L.). *International Journal of Seed Spices* 2(2): 5-8

Rasool A A & Muhmad Rashid A G (2014). Effect of nitrogen fertilization and gibberellic asit spray on seed yield and oil content of black seed (*Nigella sativa* L.). J. of Zankoy Sulaimani- Part A, Special Issue Vol.16

Rodriguez D, Andrade F H & Goudrian J (2000). Does assimilate supply limit leaf expansion in wheat grown in the field under low phosphorus availability. Field Crops Research 67: 227-238

Safaei Z, Azizi M, Maryam Y, Aroiee H & Davarynejad G (2014). The effect of different irrigation intervals and anti-transpiration compounds on yield and yield components of black cumin (*N. sativa* L.). *International journal of Advanced Biological and Biomedical Research* 4(2): 326-335

Sağlam T (2018). Effect of nitrogen and potassium application on yield and quality of black cumin (*Nigella sativa* L.). (MSc. Thesis). Osmangazi University, Institute of Natural and Applied Sciences, Department of Field Crops, Eskişehir, Turkey

Sağlık A (2020). The effect of different organic fertilizer applications on yield and quality in black cumin (*Nigella sativa* l.) plant growed in Çukurova conditions. (MSc. Thesis). Çukurova University, Institute of Natural and Applied Sciences, Department of Field Crops, Adana, Turkey

Saraç S (2019). Effect of row spacing with sowing rate at winter sowing time on yield and some quality components of black cumin (*Nigella sativa* L.). (MSc. Thesis). Namık Kemal University, Institute of Natural and Applied Sciences, Department of Field Crops, Tekirdağ, Turkey

Seçmen Ö, Gemici Y, Görk, G, Bekat L & Leblebici E (2000). Systematics of Seed Plants. Ege University, Faculty of Science Books Series No: 116, İzmir, Turkey (In Turkish)

Sen A, Choudhuri P, Chatterjee R & Jana J C (2018). İnfluence of inorganic nutrient, organic nutrient and bio-fertilizer on growth, yield and quality of cumin black (*Nigella sativa* L.) in eastern Himalayan region of West Bengal, Journal of Pharmacognosy and Phytochemistry 7(2): 2571-2575

Shah S H (2004). Morphophysiological response of black cumin (*Nigella sativa* L.) to nitrogen, gibberellic asit and kinetin application. Ph.D Thesis. Aligarh Muslim University, Aligarh, India

Shah S H (2007). Influence of combined application of nitrogen and kinetin on nutrient uptake and productivity of black cumin (*Nigella sativa* L.). *Asian Journal of Plant Sciences* 6(2): 403-406

Sultana S, Mondal A, Das S, Rudra B C, Alam B & Roy S (2019). Effect of nitrogen and phosphorous fertilizer application on growth and yield of black cumin cultivation in Malda District (WB). *Int. J. Curr.Microbiol.App.Sci.* 8(04): 2813-2817

Şahin B (2013). Some medical plants grown in different times of sowing yield and quality of determination of properties. (MSc. Thesis). Selçuk University, Institute of Natural and Applied Sciences, Department of Field Crops, Konya, Turkey

Şenyiğit U & Arslan M (2018). Effects of irrigation programs formed by different approaches on the yield and water consumption of black cumin (*Nigella sativa* L.) under transition zone in the West Anatolia Conditions. *Journal of Agricultural Sciences* pp. 22-32

Tavas N, Katar N & Aytaç Z (2014). Yield, yield components and oil composition of black cumin (*Nigella sativa* L.) grown in Eskisehir ecological conditions. Proceedings of the II. Medicinal and Aromatic Plants Symposium, 23-25 September 2014, Yalova pp. 623-629

Tektaş E (2015). Effect of seed numbers on yield and some plant characters of black cumin (*Nigella sativa* L.) under the Harran plain conditions. (MSc. Thesis). Harran University, Institute of Natural and Applied Sciences, Department of Field Crops, Şanlıurfa, Turkey.

Tonçer Ö & Kızıl S (2004). Effect of seed rate on agronomic and technologic characters of *Nigella sativa* L. *International Journal of Agriculture & Biology* 6(3): 529-532

Tulukçu E (2011). The effects of varying nitrojen doses on yield and some yield components of black cumin (*Nigella sativa* L.). Cyprus, First Mediterranean Symposium on Medicinal and Aromatic Plants Magosa, 15 pp

Tunçtürk M, Tunçtürk R & Yıldırım B (2011). The effects of varying phosphorus doses on yield and some yield components of black cumin (*Nigella sativa* L.). Advances in Environmental Biology 5(2): 371-374

Tunçtürk R, Tunçtürk M & Çiftçi V (2012). The effects of varying nitrojen doses on yield and some yield components of black cumin (*Nigella sativa* L.), Advances in Environmental Biology 6(2): 855-858

Yılmaz G (2008). New approaches in cultivation of medicinal aromatic plants. Medicinal and Aromatic Plants. Postgraduate course notes (Unpublished). Gazi Osman University Faculty of Agriculture, Institute of Science and Technology, Department of Field Crops, Tokat, Turkey (In Turkish)

Yiğitbaşı H H (2019). The investigation on yield and some quality characteristics of black cumin (*Nigella spp*.) species. (MSc. Thesis). Selçuk University, Institute of Natural and Applied Sciences, Department of Field Crops, Konya, Turkey

Yimam E, Nebiyu A, İbrahim A M & Getachew M (2015). Effect of nitrogen and phosphorus fertilizers on growth, yield and yield components of black cumin (*Nigella sativa*) at Konta district, South West Ethiopia. *Journal of Agronomy* 14(3): 112-120

Yurtsever N (1984). Experimental Statistics Methods. Soil and Fertiliser Research Institute Publications, General Publication No: 121, Technical Publication No: 56, Ankara, Turkey

Journal of Agricultural Sciences
(Tarim Bilimleri Dergisi)

J Agr Sci-Tarim Bili
e-ISSN: 2148-9297
jas.ankara.edu.tr

JAS

Hybrid GIS-MCDM Based Modeling Approach for Determination of Land Suitability of Wheat Cultivation in Konya Closed Basin, Türkiye

Aydan Yaman[a*], Mert Mutlu[b]

[a]*Department of Geomatics Engineering, Aksaray University, 68100 Aksaray, TÜRKIYE*
[b]*Department of Mining Engineering, Aksaray University, 68100 Aksaray, TÜRKIYE*

ARTICLE INFO
Research Article
Corresponding Author: Aydan Yaman, E-mail: aydanyaman@aksaray.edu.tr
Received: 16 September 2024 / Revised: 01 November 2024 / Accepted: 27 November 2024 / Online: 25 March 2025

Cite this article
Yaman A, Mutlu M (2025). Hybrid GIS-MCDM Based Modeling Approach for Determination of Land Suitability of Wheat Cultivation in Konya Closed Basin, Türkiye. *Journal of Agricultural Sciences (Tarim Bilimleri Dergisi),* 31(2):427-446. DOI: 10.15832/ankutbd.1550882

ABSTRACT
In countries with high population growth and migration potential, such as Türkiye, agricultural lands are gradually decreasing due to the increase in food demand and the misusage policies and urbanization applied to the lands. Land suitability activities carried out within the scope of agricultural sustainability in order to increase agricultural production and soil productivity are important. This study focuses on identifying the agricultural lands suitable for wheat cultivation by evaluating the Konya closed basin in the Central Anatolia Region of Türkiye by using a hierarchy developed with the integration of the AHP method, which is one of the GIS and MCDM techniques. Within this framework, 15 criteria were delineated under 4 main headings as meteorological criteria, topographic criteria, soil criteria, infrastructure and economic criteria and their weight values for their sub-criteria were calculated. The most effective criteria were determined as the average temperature of October (0.1379), followed by the average annual temperature (0.1300) and the land use capability (0.1191). Finally, the land suitability map was created for wheat cultivation. According to the suitability map, 0.39% (15 815 km^2) of the study area is found to be very highly suitable for wheat cultivation, 61.24% (2 494 461 km^2) is found to be highly suitable in terms of suitability. The districts of Kadinhani, Sarayonu, Altinekin, Cihanbeyli, Kulu, Karapinar and Emirgazi, which are located in the north of the study area, have been determined as very suitable regions for wheat cultivation. This study aims to contribute to the existing literature by identifying precise and suitable areas by combining GIS and AHP in the wheat cultivation site selection process. In the study, a new research perspective is presented by taking into account the uncertainty in the site selection process and the concept of sustainability in four different dimensions: meteorological, topographical, soil, and infrastructure and economic, thus aiming to guide decision-makers for future studies. According the current literature, that no comprehensive study has yet been conducted that covers such a large basin for the wheat plant, which is the raw material of humanity's basic nutritional needs. In addition, the average annual pressure criterion that is not examined in the literature was discussed in the study and its importance for wheat plant development was also examined. Consequently, the outcome of this study delineates that the methods and criteria used in this study may be guiding for site selection for wheat cultivation in future studies covering such wide areas.

Keywords: Land suitability assessment, Geographic Information Systems (GIS), Analytic Hierarchy Process (AHP), Multi-criteria decision making (MCDM)

1. Introduction

Negative effects on environmental impacts of ever-increasing population pressure, increasing food demand, and misusage policies on land have been increasing. For this reason, it is necessary to switch to a sustainable agricultural policy with good agricultural planning in order to increase agricultural production and soil productivity (Bilgilioglu 2021; Zhang et al. 2015). Land use plans should be developed first in order to ensure that the land can be used in the most efficient way. The prerequisite is the assessment of land suitability, which will determine the best use of the land (Kılıc et al. 2022). Assessment of land suitability (LS) is the first step in designing sustainable land use and management systems to reduce the impact of adverse environmental conditions on fertile lands on agriculture (Ostovari et al. 2019). Performing this analysis is one of the most useful applications of the Geographical Information System (GIS) in the preparation of land usage maps, planning and management of land resources (Maddahi et al. 2017). LS analysis is one of the most important stages of land use planning for the cultivation of a particular crop according to local conditions (FAO 1993; Tashayo et al. 2020). The selection of the most appropriate algorithm for the assessment of LS is important for both current and future land use planning (Zhang et al. 2015). Product-oriented land assessment studies have additional importance especially for countries with high population growth and migration potential such as Türkiye (Dedeoglu & Dengiz 2019). It is necessary to determine to what extent the ecological requirements of the product can be met within the ecological structure of that region in order to use the land in the most appropriate way (FAO 1976). LS analyses are widely used in these evaluations (FAO 1985; Bilgilioglu 2021).

Based on the GIS environment, LS analysis is a process that aims to determine the most appropriate development locations by considering environmental and agricultural sustainability (Ostovari et al. 2019). In determining the importance of the criteria used in this process and in calculating the weights of the factors, GIS tools should be integrated with other methods in order to improve the results of LS analysis. In this case, MCDM methods are strong approaches to assess LS (Bagheri et al. 2013; Aburas et al. 2017).

Modeling the suitability of agricultural lands for certain products on a regional scale plays an important role in designing the best sustainable management systems (Tashayo et al. 2020). The aim of the study is to investigate the LS assessment for the production of wheat, which is the raw material for bread, the staple food of people, throughout Konya Province, which is the first center of wheat production in Türkiye.

Wheat has been the most basic nutritional source for humans throughout history. It is known that wheat was first domesticated in southeast Türkiye. Although it is known that there are many wheat species today, wheat is generally divided into three groups. These are defined as pasta, bread, and biscuit wheat (Aydin 2022). Since wheat is the raw material of many staple foods, it has always been of special importance in agricultural products and its consumption has been increasing in recent years. Accordingly, it is also extremely important to increase the production of wheat. In addition, since the production amounts of the countries differ depending on the climatic conditions, the fact that some countries need much more wheat than they can produce in some years increases the wheat trade. European Union (EU) countries ranked first with a share of 20.3% of total wheat production in the world, followed by China (17.4%), India (13.5%), Russia (9.7%) and the USA (6.8%) in 2019. Türkiye ranks 10th by meeting 2.5% of the world wheat production (Tarhan & Dellal 2021).

Although wheat is a plant with a strong adaptive ability, it is a grain suitable for growing in a cool climate that does not like too much heat and humidity. While 8-10 °C is suitable for germination period, 10-15 °C and partly cloudy and underlit weather are suitable (RTMAF 2015).

It is expressed as MCDM process including different qualitative and quantitative information and at the same time evaluating more than one criterion for a specific purpose. This process helps decision makers determine the most logical choice in evaluating many parameters and analyzing the relationship between these parameters. Because not all criteria handled have equal importance and the contribution of each criterion to suitability is at different levels (Prakash 2003; Kılıc et al. 2022). GIS and MCDM integration allow the preparation of a comprehensive spatial database to be used by multi-criteria methodologies in land assessment and suitability analysis and is also an excellent spatial analysis tool that enables users to evaluate different criteria on the basis of multiple and contradictory goals (Karaca et al. 2021; Orhan 2021; Kılıc et al. 2022; Sarğın et al. 2024).

MCDM methods offer structured approaches to informed decision-making in situations where multiple criteria are present. Each method possesses distinctive strengths and is better suited to different types of problems. Consequently, it is crucial to select the method that aligns with the specific decision context. In order to maintain the use of land for a long time without deterioration, it is necessary to consider not only the natural capacity of the land, but also its socio-economic and environmental conditions. Therefore, it is extremely difficult to assign relative weights to the different criteria involved in decision making regarding land use. Therefore, a technique for estimating weights needs to be adopted. This is possible with the MCDM techniques, such as AHP method (Saaty 1977; Chuong 2011). The AHP method is an important technique used to determine LS today and is classified under the multi-criterion decision analysis approach. It is also an effective technique that helps planners and decision makers analyze all data before making a decision on future land use alterations (Bagheri et al. 2013; Aburas et al. 2017). The AHP method involves multiple choices based on the importance and weight of the relevant criteria relative to each other within a hierarchical system (Saaty 1980). It is a useful method in cases where it is difficult to reveal the exact relationship and result between a vast number of criteria. In addition to the classical methods like AHP, Fuzzy Analytic Hierarchy Process (F-AHP), Fuzzy Ideal Solution Similarity Ranking Performance Technique (F-TOPSIS), Fuzzy VIKOR (F-VIKOR), Fuzzy PROMETHEE (F-PROMETHEE) methods are also alternatives of the same methods that are solved with the support of fuzzy logic (Mutlu & Sari, 2017; Mutlu & Sari 2022). To affords decision-makers greater freedom to express their opinions in a realistic manner, the linguistic terms employed in FMCDM (Fuzzy MCDM) techniques a converted to numerical values by using fuzzy sets can be applied by integrating different innovative combinations of FMCDM techniques interval-valued Pythagorean fuzzy sets (PFS)s and interval type-2 fuzzy sets (IT2FS)s (Mutlu et al. 2024). However, since the process steps in these methods are complex and the decision-making process is difficult and time-consuming for decision makers, it is seen that the AHP method is often preferred in the literature, as in this study.

A plethora of studies in the literature have employed the MCDM method to evaluate the suitability of specific areas. To illustrate, rice cultivation in the Amol Region of Iran (Maddahi et al. 2017), wheat cultivation (WC) in the Tozanlı region (Kılıc et al. 2022), Antalya, citrus fruit in Türkiye (Tercan & Dereli 2020), corn cultivation in Iran (Tashayo et al. 2020), for paddy fields in Tanzania (Al-Hanbali et al. 2021), Ethiopia sorghum crop (Tadesse & Negese 2020), olive cultivation in Mersin, Türkiye (Bilgilioglu 2021), saffron (*Crocus sativus L.*) cultivation in Khost Province of Afghanistan, (Wali et al. 2016) corn production in Ondonesia (Habibie et al. 2021), coffee in Peru (Lopez et al. 2020), Mersin, Türkiye for citrus (Orhan 2021), many LS studies for example tobacco in China (Zhang et al. 2015; Bilgilioglu 2021), wheat-barley cultivation in Tusba district of Van (Sargın & Karaca 2023), Sogulca Basin for wheat (Dedeoglu & Dengiz 2019) are studies conducted with the integration of AHP method

and GIS technique. Dedeoglu & Dengiz (2019), evaluated mostly soil-related physical and chemical criteria in their study. In this study, meteorological, topographical, soil, infrastructure and economic criteria were evaluated. There are many studies in the literature within the scope of LS assessment. However, there has not been a comprehensive study conducted on a provincial basis for the wheat plant, which is the raw material for the basic nutritional needs of humanity. It was aimed to fill this gap in the literature with current study.

Türkiye is a very suitable country for WC both geographically and climatologically. Konya ranks first among the provinces that grow wheat the most. This study aimed to determine the most suitable regions for WC with the AHP-GIS method throughout Konya province. If the soil is used in accordance with the correct policy within the scope of the LS assessment studies to be carried out, the natural resources will be used in the most beneficial way without deterioration and will be transferred to future generations in the most efficient way.

Combination of AHP-GIS, it was aimed to obtain the agricultural lands suitable for WC by evaluating the whole of Konya province in the Central Anatolia Region in Türkiye within the scope of the study. In this context, the current farmers in Konya province and the relevant literature were taken into consideration, and 15 criteria and their sub-criteria were determined under four main headings. The weight values of these criteria were calculated in order to obtain suitable areas for WC.

1.1. Study area

Konya basin is the largest province of Türkiye in terms of surface area and consists of 31 districts. Its surface area is 39 000 km^2 and it is located in a plain in the Central Anatolia Region of Turkey, between the coordinates 4050000–4350000 N and 345000 630000 E (WGS-84, Universal Transverse Mercator UTM-m, 36 Regions) (Figure 1). Continental climate is seen in Konya. The summers are dry and hot, the winters are cold and snowy. The temperature difference between night and day is between 16-22 degrees in summer. This difference decreases to 9-12 °C due to humidity in spring and winter. Another feature of the Konya climate is that summers start very late and winters end very late. Summer drought, which is a characteristic of steppe climate, makes it possible to grow the best quality wheat in Türkiye. The Province of Konya meets 11% of the wheat need of Türkiye. The economy of Konya province depends on agriculture especially wheat agriculture. The main agricultural products are wheat, sugar beet, sunflower, potato, onion, and poppy.

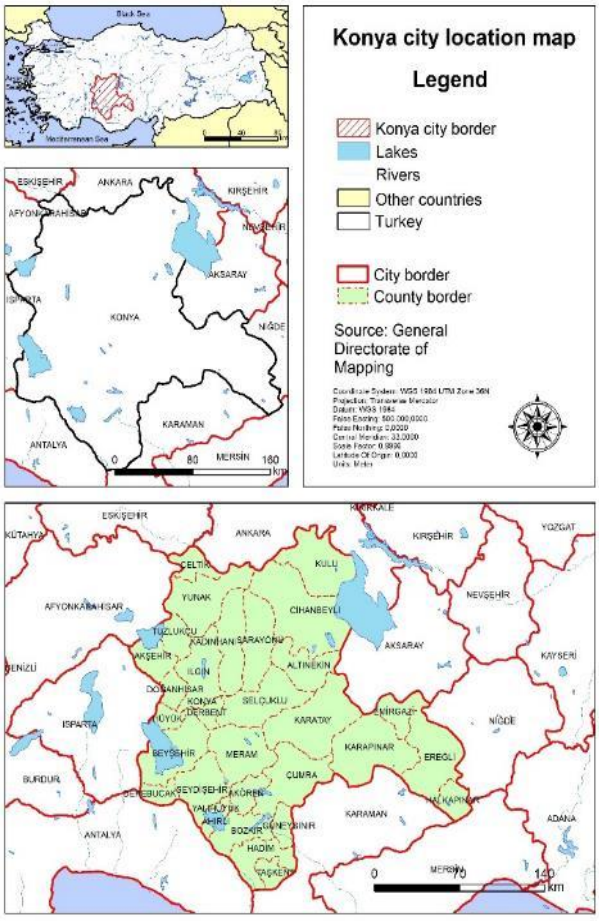

Figure 1- Study area

2. Material and Methods

In this study, the aim is to determine potential WC areas based on Konya province wide. First of all, the factors that are thought to affect the growing conditions of the wheat plant were determined, and then an exclusion analysis was made in order to except the not suitable regions for WC. The weights for each criterion in the hierarchy were computed by using the AHP technique. In the final stage of this study, a LS map was created for wheat growing throughout Konya province. Climatic conditions, topographic conditions, soil, and economic conditions suitable for WC were determined in consultation with 20 farmers and 5 agricultural engineers in Konya province, and at the same time, previous literature studies and current practices were benefitted from.

The 15 criteria, which were divided into four main headings and further subdivided into sub-criteria, were evaluated within the scope of the hierarchy created in the study (Figure 2). The first of these criteria are meteorological criteria such as average annual temperature, average temperature of October, average annual relative humidity, average annual pressure, average annual precipitation criteria. Elevation, slope, and aspect criteria were evaluated among the topographic factors, which are the second main criteria in the hierarchy. Thirdly, land capability and soil depth criteria including soil conditions were evaluated. Finally, the criteria of proximity to lakes, proximity to rivers, proximity to roads and proximity to settlements, which are infrastructure and economic factors, were evaluated. Then, the level of importance for each evaluation criterion and sub-criteria were defined. General evaluation criteria are given in Table 1. All evaluation and exclusion criteria were resampled to 30 m spatial resolution in the WGS-84 Universal Transverse Mercator (UTM) region 36 coordinate system and included in the AHP hierarchy for LS analysis.

2.1. Exclusion and evaluation criteria

Among the excluded factors, protected areas, areas where meteorological parameters are not suitable for WC, economically and topographic unsuitable areas for WC were excluded, and the rest of the study area was classified as 50.32% (2049.82 km^2) suitable areas for WC. Heights with an average temperature below 5 °C and above 2600 m, VI, VII and VIII class lands according to the LS map and places below 30 m distance according to the road proximity map were selected as inappropriate areas (Figure 2). To define the suitable areas for WC throughout Konya province, 4 main criteria as meteorological criteria, topographic criteria, soil criteria, and infrastructure and economic criteria were received for consideration (Figure 2) (Table 1).

Table 1- Data types and sources of evaluation criteria

Criteria	*Unit*	*Data type*	*Scale/resolution*	*Data source*
Average annual temperature	°C	Raster	30 arc second	Turkish State Meteorological Service
Average temperature of October	°C			
Average annual humidity	(%)	Point	Observation data obtained from meteorological stations	
Average annual pressure	(hPa)			
Average annual precipitation	(mm)			
Elevation	(m)	Raster	30m	SRTM
Slope	(%)			
Aspect	Categorical			
Land use capability	Categorical	Polygon	1/100000	RTMAF
Soil depth	(m)			
Proximity to roads	(km)	Polyline	1/100000	Environmental plan obtained from MEU (2021)
Proximity to settlement	(km)	Polygon		
Proximity to rivers	(km)	Polyline		
Proximity to lakes	(km)	Polygon		
Groundwater depth	(m)	Raster		DSI Konya Regional Directorate

*: RTMAF Republic of Türkiye Ministry of Agriculture and Forestry; **: MEU Türkiye Ministry of Environment and Urbanization

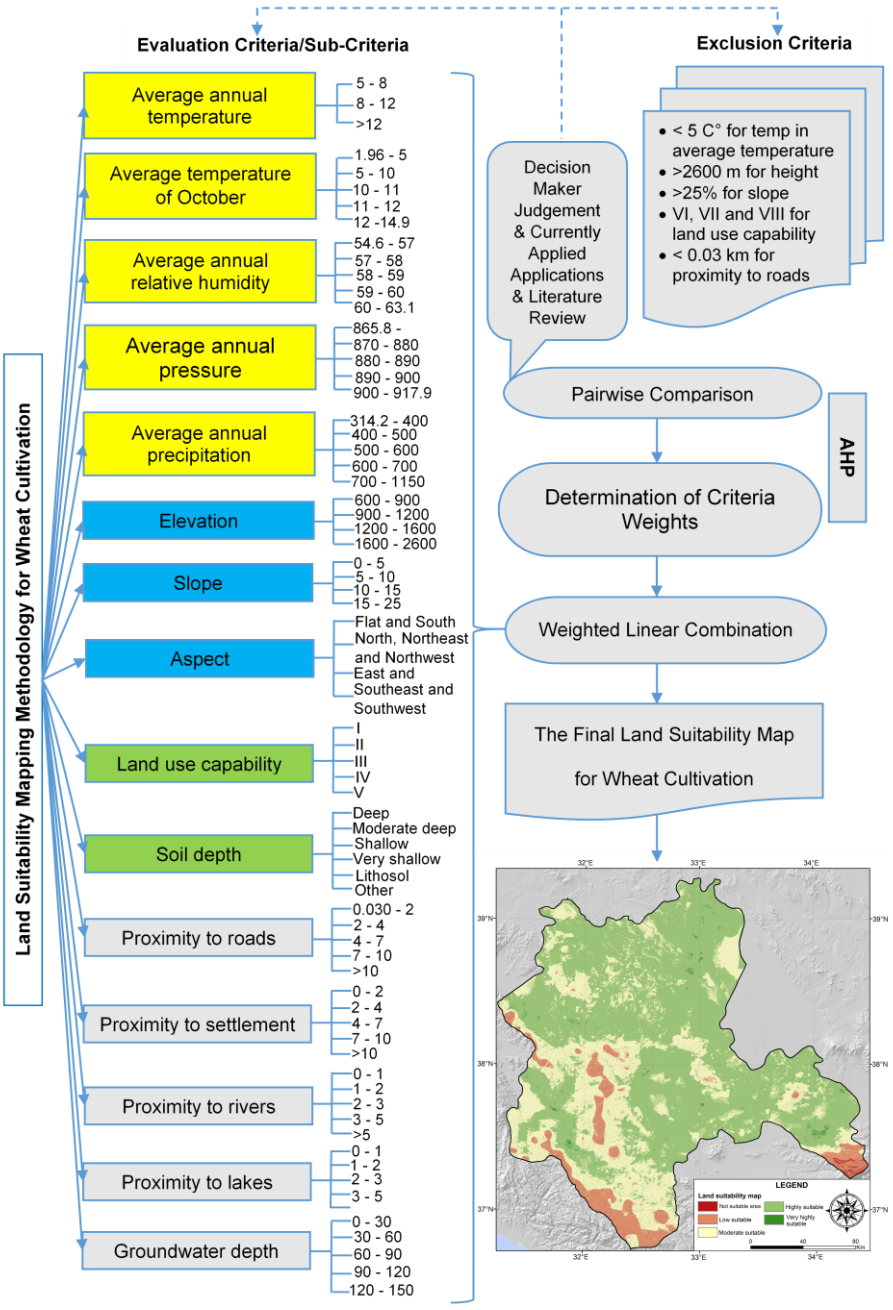

Figure 2- The flowchart of the GIS-MCDM-based LS mapping hierarchy

2.2.1. Meteorological criteria

Average temperature of October, average annual precipitation, average annual relative humidity, average annual pressure, average annual temperature, criteria are important for the meteorological criteria for WC. The average annual pressure criterion that is not examined in the literature was discussed in the study and its importance for wheat plant development was also examined. The meteorological data used in this study were provided from the Regional Directorate of Meteorology. For each of these stations, data collected from the date the stations started collecting data (January 2000 for the Konya Airport station, January 2004 for the Konya regional station, January 2016 for the Konya Meram/Urban Forest station) to December 2023 were used. The locations of meteorological stations are shown in Figure 3. Meteorological data were evaluated using the inverse distance weighted (IDW) interpolation method and necessary maps were created. IDW approach has been regarded as one of the deterministic spatial interpolation techniques (Lu & Wong 2008; Tercan & Dereli 2020). The principle of the IDW is that the unknown value of estimated point is calculated by computing the value as a distance weighted average of sampled points in a defined neighbourhood (Rahmouni et al. 2017), where a higher degree of influence assigned to nearby points and consequently more far points presents less effect (Gouareh et al. 2021). In this study, IDW was chosen as the interpolation method, as in many studies in the literature (Hossain & Das 2010; Ayehu & Besufekad 2015; Roy & Saha 2018; Mokarram & Miesoleimani 2018; Souidi et al. 2020; Tercan & Dereli 2020; Bilgilioglu 2021; Orhan 2021; Ozsahin & Ozdes 2022; Pathan et al. 2022; Salifu et al. 2022; Sarkar et al. 2023; Ozegin et al. 2024).

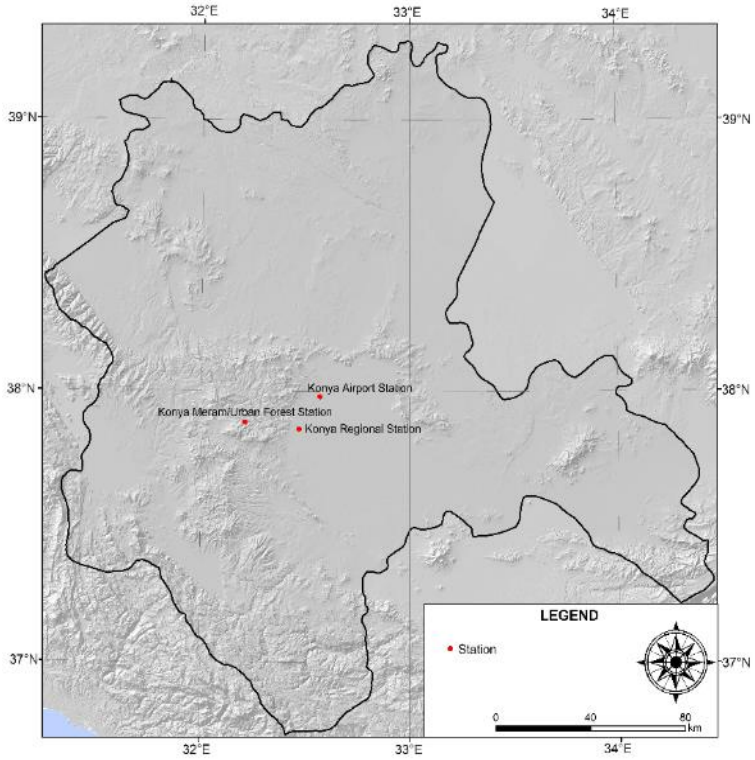

Figure 3- The location of meteorological stations

When the literature review is made for classified in accordance with the literature.

2.2.2. Average annual temperature

Temperature is an important criterion for climate conditions for WC. Wheat needs the appropriate temperature to complete its development period after being planted as a seed. The appropriate temperature for the growth and development of the wheat plant is the temperature range between 10-15 °C (Porter & Gawith 1999; Wang et al. 2023). Wheat is a plant that is sensitive to extreme temperatures during critical developmental periods. These extreme temperatures cause freezing of leaves and roots, winter deaths, internodes and cause the flowers to be damaged by frost and high temperatures also damage them. It has been observed that an increase in temperature leads to a decrease in grain weight of wheat plants due to heat stress (Asseng et al. 2011). The wheat plant does not like high temperatures in the early stages of its development, such as germination. During these periods if the temperature is 5-10 °C it continues to develop normally. Therefore, in the average annual temperature map, regions of 5 °C and below were excluded and the residual areas were classified into 3 groups (Figure 4a).

2.2.3. Average temperature of october

One of the most important elements to determine the planting time in wheat farming is the soil temperature in the seed bed. When the soil temperature is 8-10 °C if the planting process is performed, the root development is fast, and the root crown is deep. This convenient planting process increases resistance of wheat to cold and drought. Early planting process and late planting process are ill-favored as they will cause damage to the plant due to severe colds in the winter period. The study results indicate that wheat sown on both 20th and 30th October produced longer spikes and a higher number of grains (Baloch et al. 2012; Komer et al. 2014). For this reason, the most appropriate WC time in Konya Province and Central Anatolia Region is October in order to maintain the normal development of wheat. Meteorological data were also obtained from the regional directorate and the average temperature map for October was divided into 5 classes (Figure 4b)

2.2.4. Average annual relative humidity

Moisture comes second among the climatic conditions in WC. Moisture is the most important determinant of yield in dry farming areas where wheat farming is widespread. Relative humidity has a direct impact on the water relations of plants and indirectly affects leaf growth, photosynthesis, pollination, disease occurrence, and ultimately economic yield. If the relative humidity is above 60% in the early stages of wheat development, wheat continues to develop normally (Sandhu & Dhaliwal 2016). Wheat requires relatively high humidity before earing. In the study, an annual average relative humidity map was produced and divided into five classes (Figure 4c).

2.2.5. Average annual pressure

Pressure values are among the least noticeable of the climate criteria. Although changes in air pressure occurring hourly and daily are felt less by people, especially those occurring in a short time play a very important role in the development and change of weather events (Ircan 2020). Upon examination of the studies in the literature, it was determined that low pressure was effective in the germination and growth of wheat plant and that this plant also could grow in standard atmosphere (Massimino & Andre 1999; Rodríguez-Puebla et al. 2007; Guo et al. 2008). The pressure map created was divided into 5 classes (Figure 4d).

2.2.6. Average annual precipitation

Water is the leading element among the essential elements for plants to continue their vital activities. The water required for the plants is met by agricultural irrigation and precipitation. The water source in the cropland is precipitation. For the development period of wheat plant, annual precipitation of 350-1150 mm is sufficient for a quality and abundant product (Marijanović et al. 2010; RTMAF 2015; Jolánkai et al. 2018; Dogan & Kan 2019). The annual average precipitation map was divided into 5 classes (Figure 4e).

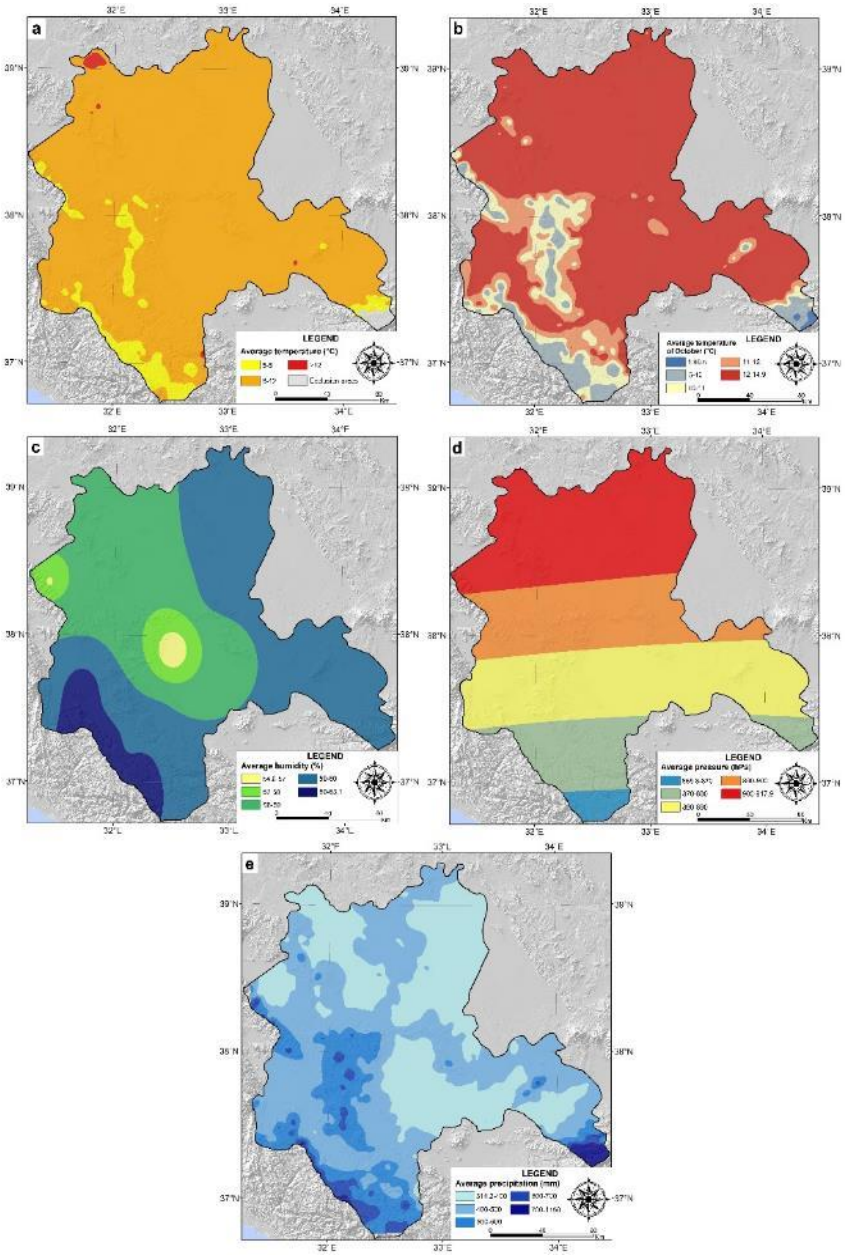

Figure 4- Meteorological criteria (a) average annual temperature; (b) average temperature of October; (c) average annual relative humidity; (d) average annual pressure; (e) average annual precipitation

2.2.2. Topographical criteria

Elevation

Altitude is a crucial factor in agricultural production and diversity. The elevation increases as we move from the coast to inland regions. This variation in altitude also affects the duration of winter and summer months, making the former longer and the latter shorter and cooler (Kapluhan 2013). Due to the changing climatic conditions with altitude, the same plant species may exhibit physiological and morphological differences (Ozkan & Kantarci 2008). Therefore, one plant of the same species matures faster than the other due to differences in their vegetation period. The duration of vegetation directly affects the harvest time and profitability of crop production (Everest et al. 2021).

Wheat is the leading cereal among the cereals in terms of being able to grow in high altitude regions. The most suitable elevation for wheat is between 2000-2600 m (Fekadu & Negese 2020; Kılıc et al. 2022). The elevation map was disunited into 4 classes according to the literature and the areas above the 3000 meters' elevation were selected as the exclusion area (Figure 5a). SRTM data were used as elevation data source.

Slope

The degree of slope negatively affects irrigation and machine use, and as this value increases, the risk of erosion increases accordingly. At the same time, this situation leads to the loss of organic matter and nutrients in the soil. For these reasons, slope is considered a limiting factor in the approach to land evaluation for wheat. (FAO 1977; Sauer et al. 2010; Begum et al. 2013; Dedeoglu & Dengiz 2019).

Wheat prefer slopes less than 8% forthe highest productivity (Sys et al. 1991; Fekadu & Negese 2020). It has been specified that slope levels below 25% are suitable for WC, taking into account the expert opinions in Konya province and at the same time, in order for the machines used to work efficiently (Bilgilioglu 2021). In this context, areas with a slope of more than 25% are taken as exclusion areas (Figure 5b). The slope data which presented in Figure 4b are generated from SRTM elevation data.

Aspect

Plants need sunlight at regular intervals to achieve proper vegetative growth. Since plants need sunlight in periods such as root and shoot development, flowering, fertilization, total yield, and quality are also directly affected by sun exposure (Begum et al. 2013; Dedeoglu & Dengiz 2019). Although the duration of the need for sunlight varies according to the type of plant, most cultigens show optimum growth in the south and west directions that receive sunlight for a significant part of the day (Akıncı et al. 2013). For this reason, direction of cropyard is one of the important factors affecting plant development in receiving sufficient amount of sunlight and it has been considered as a criterion in LS assessment for wheat in the study (Dedeoglu & Dengiz 2019). SRTM data were used to state the view in the study region (Figure 5c).

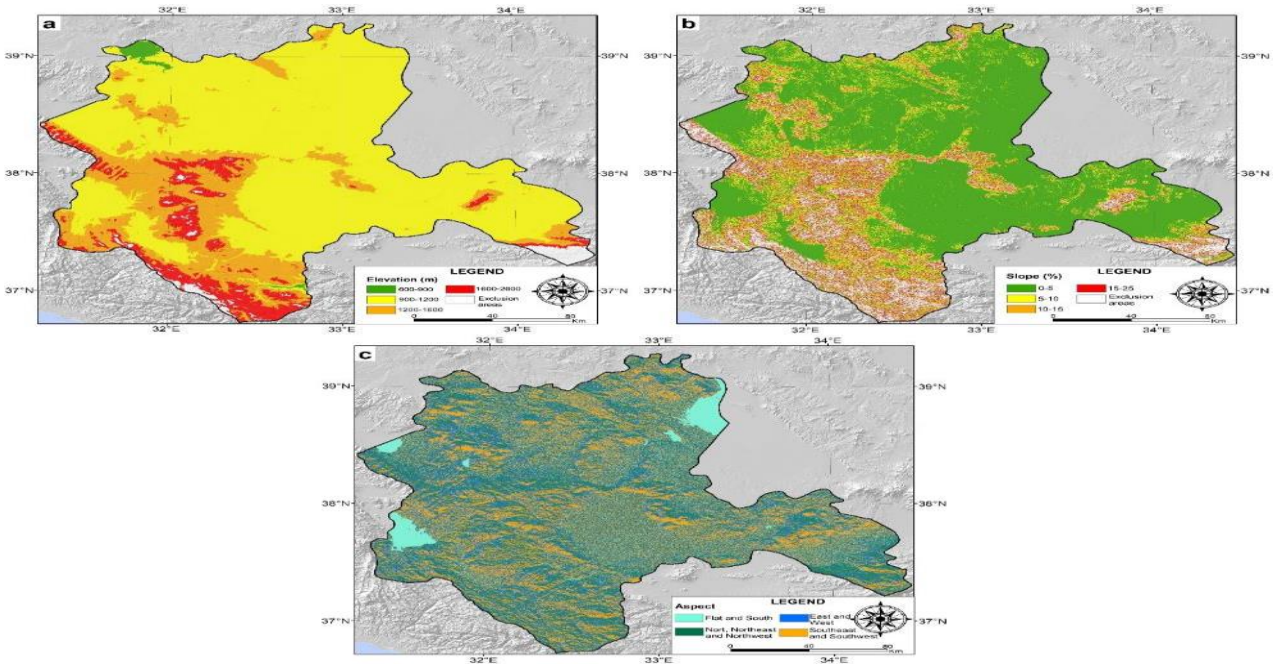

Figure 5- Topographic criteria (a) elevation; (b) slope; (c) aspect

2.2.3. Soil criteria

Land use capability

In determining the land use capability, land characteristics affecting soil and land usage such as drainage, land slope, geological and geomorphological location, soil structure, vegetation, stoniness, texture, erosion, groundwater, and salinity were taken into consideration (Cengiz & Akbulak 2009; Akıncı et al. 2013; Pramanik 2016; Orhan 2021). The study region is divided into 5 classes according to land use capability. First class areas have been selected as areas where there is no risk of erosion and where agricultural activities can be conducted in the most efficient and economical way. Areas with land use capability suitable for WC are divided into 5 classes, and areas that are not suitable for agricultural activities are excluded based on expert opinions. Land usage capability data of the study region were retrieved from the Republic of Türkiye Ministry of Agriculture and Forestry (Figure 6a).

Soil depth

Soil depth is a crucial factor in the hydrological dynamics of soils and plant growth (Rhoton & Lindbo 1997; Hirzel & Matus 2013; Kılıc et al. 2022) and a significant criterion for soil classification. Although wheat plants can grow in different soil species under suitable climatic conditions, they usually grow efficiently in places with the best soil depth that will provide effective root development (Dedeoglu & Dengiz 2019). In order for the wheat to be planted properly and grow efficiently, it is sufficient to plough the soil at a depth of 15-20 cm during the planting process. For this reason, the depth areas in the soil map of the study area are divided into 6 classes (very shallow <15 cm, shallow 15-20 cm, medium deep 20-50 cm, deep >50 cm) (Orhan 2021; Kılıc et al. 2022). In the classification, areas with unsuitable lithosol soil without vegetation have also been evaluated. Soil depth data for the study region were retrieved from the Republic of Türkiye Ministry of Agriculture and Forestry (Figure 6b).

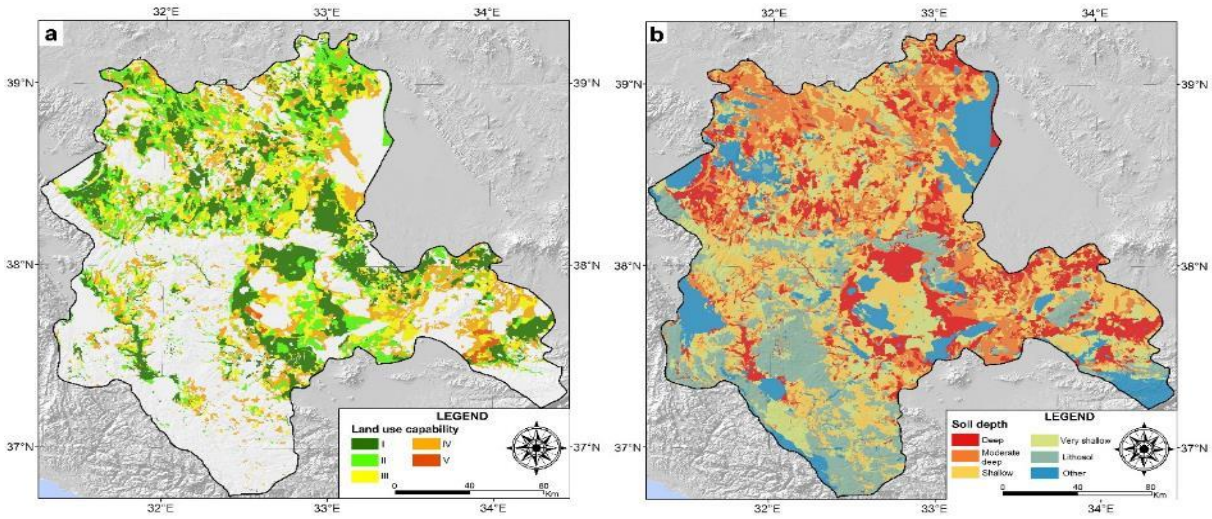

Figure 6- Soil criteria (a) land use capability; (b) soil depth

2.2.4. Infrastructure and economic criteria

Proximity to roads (km)

It is expected that the potential areas suitable for WC will be close to the roads in order to reduce the related agricultural costs such as transportation, production and maintenance. Furthermore, the short distance between fields and roads facilitates access for more convenient transport during crop production and harvesting (Morelli 2011; Habibie et al. 2021). When the infrastructure and economic criteria are evaluated, the criterion of proximity to roads is important. In addition, a certain amount of buffer zone should be created in order to minimize the impact of road expansion studies and unfavorable environmental impacts (Tercan & Dereli 2020; Orhan 2021; Bilgilioglu 2021). A 30 m buffer zone was created and removed from the study area for this purpose. The map showing the proximity of the areas divided into 5 classes to the roads is shown in Figure 7a.

Proximity to settlement (km)

It is an important criterion that the areas suitable for wheat production should be as close as possible to the settlement areas in order to carry out the transportation operations at the lowest cost possible after the wheat is harvested from the cropyard (Bilgilioglu 2021; Orhan 2021). In addition, the map showing the proximity of suitable regions for WC to the settlements is divided into 5 classes and presented in Figure 7b.

Proximity to rivers, irrigation ponds and lakes (km)

An annual precipitation of 350-1150 mm is sufficient for the development of the wheat plant. However, the criterion of proximity to rivers and lakes is important in order to meet the water needs easily for times when precipitation is insufficient (Massawe et al. 2019; Bilgilioglu 2021; Orhan 2021). Figure 7c shows the proximity to rivers; Figure 7d shows the proximity maps to lakes.

Groundwater depth (m)

The measurements of static water levels in observation wells indicate that the groundwater level in Konya closed basin has decreased by up to 46.88 meters from the ground surface. This suggests a serious and ongoing decline, with some areas of the basin already reaching critical levels (Worqlul et al. 2017; Orhan & Makineci 2023; DSI Konya Regional Directorate 2024). Therefore, it is recommended to promote dry agriculture in the Konya closed basin, which is self-contained and not reliant on external sources. It is advisable to cultivate crops that require less water, such as wheat. This study considers this criterion to be significant and has included it in the analysis. The locations of groundwater boreholes throughout the Konya closed basin are shown in Figure 8 (DSI Konya Regional Directorate 2024).

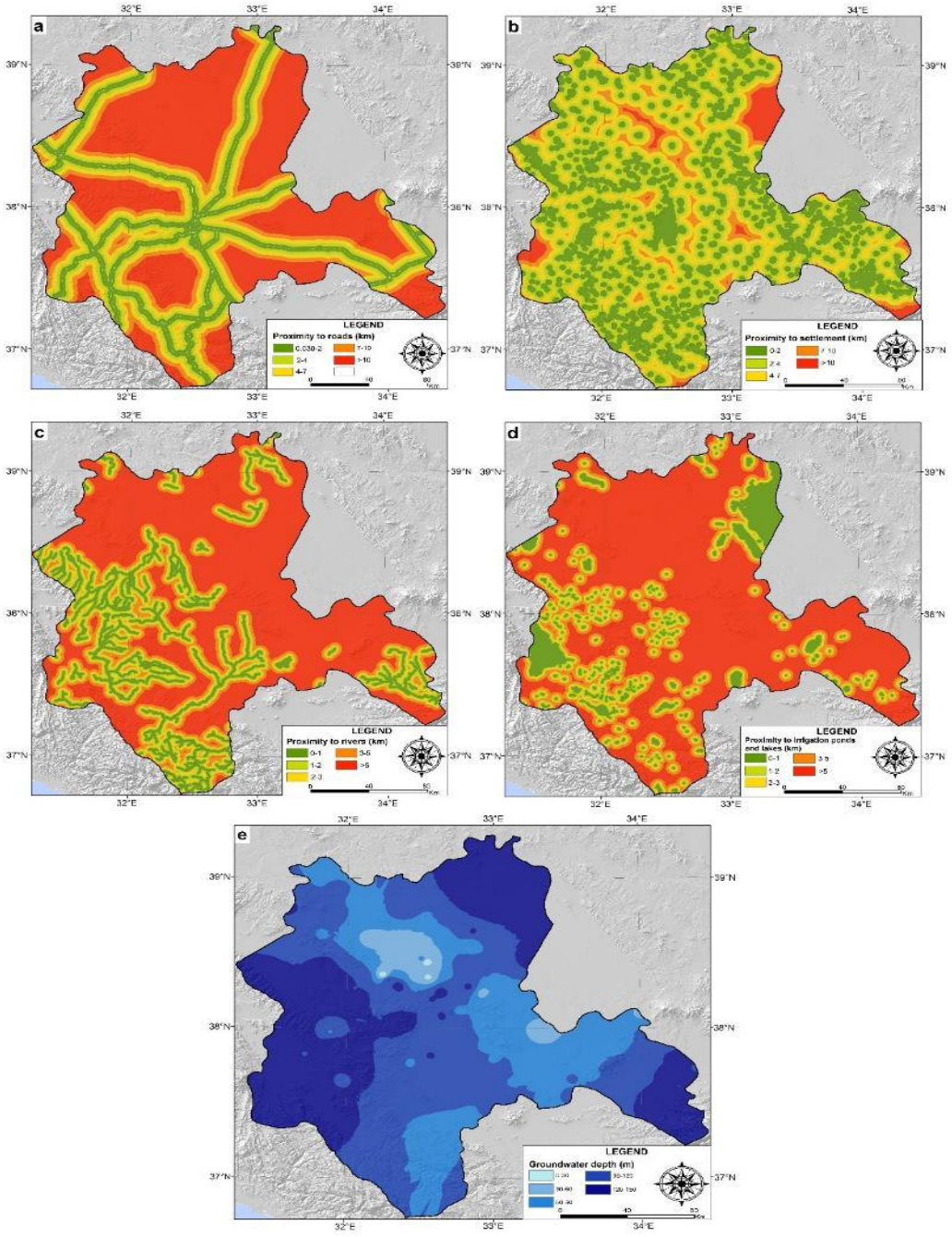

Figure 7- Infrastructural and economic criteria (a) proximity to roads; (b) proximity to settlements; (c) proximity to rivers; (d) proximity to rivers, irrigation ponds and lakes; (e) groundwater depth

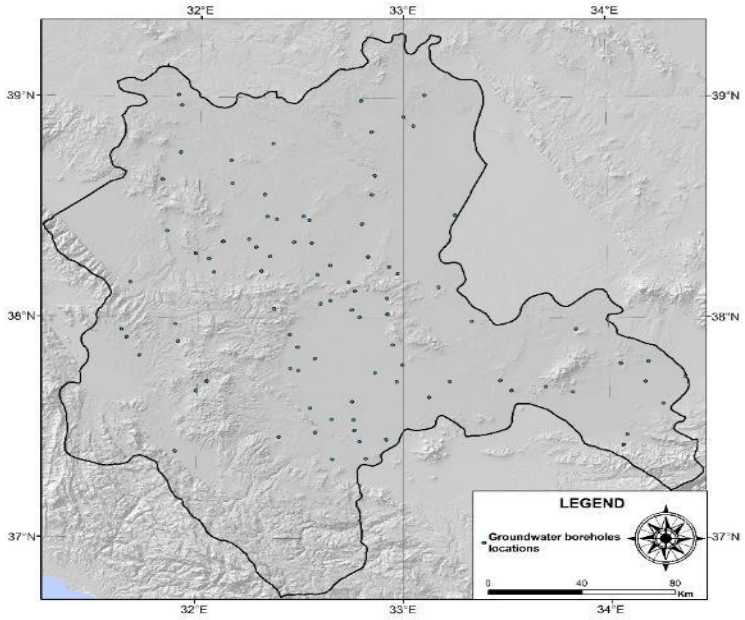

Figure 8- The locations of groundwater boreholes throughout the Konya closed basin

2.3. Analytic hierarchy process (AHP)

MCDM provides the choice of the best decision to achieve final goal with multiple criteria. The selection of a limited number of alternatives is usually expressed as mathematical models that are scaled, complex and formed by the use of a large number of criteria for the purpose of sorting, classifying, weighting or selection (Yoon & Hwang 1995). These methods stand out due to their use in terms of providing the decision maker with the opportunity to choose in a short time and easily. In MCDM, many different techniques can be used to rank alternatives according to more than one criterion (Mutlu & Sari 2017). In this study, a GIS-based MCDM model was enhanced to determine the suitability of land for WC by employing the AHP method, which is one of the MCDM techniques.

The AHP method is the most well-known an MCDM technique for dealing with MCDM problems that was first proposed by T. L. Saaty in 1970s firstly, and finalized in 1980. The AHP method is based on the determination of the problem and the creation of a top-down hierarchy, the creation of comparative decision making, the creation of a preference matrix in general, and the synthesis of multiple criteria and priorities (Saaty 1977; Saaty 1980). In complex MCDM problems, this method that evaluates qualitative and quantitative variables together, taking into account the priorities of decision makers. The most powerful aspect of the AHP method is that it breaks the problem down into meaningful sub-parts. Thus, it helps decision makers choose the most appropriate one when there are more than one goal or criterion (Karaca et al. 2023).

The information about all equations and steps involved in the AHP method can be found in various papers (Saaty 1980; Kursunoglu & Onder 2015; Kasap & Subasi 2017; Bilgilioglu 2021; Mutlu & Sari 2022); therefore, it is not explained in detail here. If the computed Consistency Ratio (CR) value ≤ 0.10 which is calculated for matrices in the AHP hierarchy, comparisons can be accepted for the algorithm done by researchers (Wind & Saaty 1980; Saaty 1990; Saaty et al. 2003; Mutlu & Sari 2022).

The weights of all criteria were computed using the MS Excel program. The next stage after the completion of the weight calculations for the criteria is the production of the LS map. The method generally used at this step is the weighted linear combination (WLC) method (Malczewski 1999; Bilgilioglu 2021; Bilgilioglu et al. 2022).

The WLC technique is the most prevalent in multi-criteria evaluation analysis, wherein the suitability of a given option is determined by the relative importance of the criteria. This technique is also referred to as the "scoring method." In this approach, the analyst or decision-maker directly quantifies the weights in accordance with the relative importance of each criterion under consideration. Subsequently, the relative weight assigned to this attribute is multiplied to yield a final value for each alternative. Once the final value has been determined for each option, it can be concluded that the alternatives with higher values will be the optimal choice for the desired purpose (Malczewski 2004). In this method, total weights should be equal to 1. The output will be a number between 0 and 1 (Malczewski 1999; Shenavr & Hosseini 2014; Ghosh & Das 2019). The weighted linear combination method provides a means of evaluating different criteria concurrently, in addition to offering a straightforward, comprehensible, and adaptable approach. Moreover, this method can be applied by leveraging the overlapping capabilities of GIS and the system. This functionality enables the integration of the layers comprising the criteria map, thereby facilitating the generation of a composite map layer (Dai et al. 2001; Zhang et al. 2013; Myagmartseren et al. 2017). The evaluation is made with the values calculated using the following formula (Equation (1)) (Malczewski 1999).

$$WCSI_i = \sum_{j=1}^{n} W_j \times x_{ij} \quad (1)$$

$WCSI_i$ in the formula refers to the wheat cultivation land suitability index, n criteria number, W_j the weight of $j$criteria, and x_{ij}expression refers to the sub-criteria weight corresponding to i cell of the j criterion.

Finally, by using ArcGIS software, the site suitability map was derived to select the most suitable place for WC by evaluating the calculated weights for all criteria in the hierarchy in five different classes (very high suitable, high suitable, medium suitable, low suitable areas, and areas not suitable) for WC according to the calculated weighted climatic suitability index ($WCSI$) values and integrated into the GIS Model Builder.

3. Results and Discussion

A GIS-based MCDM hierarchy was developed under 15 criteria, determined under 4 main headings and their sub-criteria. This hierarchy was used to produce 15 weighted raster maps, which were then combined with the WLC technique to create a LS map for the latest WC within the scope of this study. The pairwise comparison matrices were constructed as a result of interviews with experts on the subject within the scope of the hierarchy. The weights of the aforementioned criteria and sub-criteria, which are believed to be effective in location selection, were calculated in the Microsoft Excel program using the AHP method (Table 2 and 3).

It was determined that all of the CR values calculated for the pairwise comparison matrices of the criteria in the hierarchy designed for the purpose of the study were below 0.10, and that all of the comparisons made were consistent. The pairwise comparison matrix created for the main criteria and the calculated weight values are shown in Table 2 (Figure 9). Similarly, separate matrices were created for the sub-criteria of each main criterion. The complete set of CR values and criterion weights calculated for the pairwise comparison matrices of the main criteria and sub-criteria is presented in detail in Table 2 and Table 3.

When the main criteria were examined, it was seen that the weights of the meteorological criteria for WC come to the fore (Figure 9). When the weights computed for the main criteria in the hierarchy were evaluated, it was determined that the most effective main criterion was the average temperature of October (0.1379), followed by the average annual temperature (0.1300) and land use capability (0.1191). The average annual precipitation (0.1063) can be said to be the 4th most important criterion. As a result of the weight calculations made for the sub-criteria, when the average annual temperature for WC is 8-12 °C (0.7380), south-facing regions (0.4688) with an altitude of 900-1200 m (0.5894) with a slope of 0-5% (0.6402) and regions within 1 kilometer of rivers and lakes (0.4432; 0.4338) were determined as the most suitable conditions for WC (Table 3). When the appropriate time and suitable regions for WC are selected, sustainability will be ensured in WC for Konya province.

Table 2- The pairwise comparisons matrix and calculated weights of the main criteria

Pairwise comparison	*A*	*B*	*C*	*D*	*E*	*F*	*G*	*H*	*I*	*J*	*K*	*L*	*M*	*N*	*O*	*Weights*	
Average annual temperature (A)	1	2	3	5	1	2	3	3	1	2	3	2	4	4	4	0.1300	
Average temperature of October (B)	1/2	1	3	3	1/2	3	4	3	3	4	3	3	3	3	5	0.1379	
Average annual relative humidity (C)	1/3	1/3	1	1	1/4	1/2	1/2	1/3	1/4	1/2	1/3	1/2	1/2	1/2	1/5	0.0238	
Average annual pressure (D)	1/5	1/3	1	1	1/4	1/4	1/3	1/2	1/3	1/2	1/3	1/3	1/2	1/2	1/6	0.0217	
Average annual precipitation (E)	1	2	4	4	1	1	2	3	1/2	2	3	2	3	2	2	0.1063	
Elevation (F)	1/2	1/3	2	4	1	1	1	1/2	1/2	2	1/2	1/2	1/2	1/2	1	0.0487	
Slope (G)	1/3	1/4	2	3	1/2	1	1	1/2	1/3	1/2	1/2	1/2	1/2	1	1/3	0.0358	
Aspect (H)	1/3	1/3	3	2	1/3	2	2	1	1/3	2	1/2	1/2	1	1/2	1/2	0.0462	λ_{max}= 16.1509
Land use capability (I)	1	1/3	4	3	2	2	3	3	1	4	4	2	3	2	3	0.1191	CI = 0.0822
Soil depth (J)	1/2	1/4	2	2	1/2	1/2	2	1/2	1/4	1	2	1/2	2	1/2	1/2	0.0442	CR = 0.0517 ≤ 0.1
Proximity to roads (K)	1/3	1/3	3	3	1/3	2	2	2	1/4	1/2	1	1/3	2	2	1	0.0554	
Proximity to settlement (L)	1/2	1/3	2	3	1/2	2	2	2	1/2	2	3	1	2	2	1	0.0708	
Proximity to rivers (M)	1/4	1/3	2	2	1/3	2	2	1	1/3	1/2	1/2	1/2	1	1/2	1/3	0.0393	
Proximity to lakes (N)	1/4	1/3	2	2	1/2	2	1	2	1/2	2	1/2	1/2	2	1	1	0.0521	
Ground water depth (O)	1/4	1/5	5	6	1/2	1	3	2	1/3	2	1	1	3	1	1	0.0687	

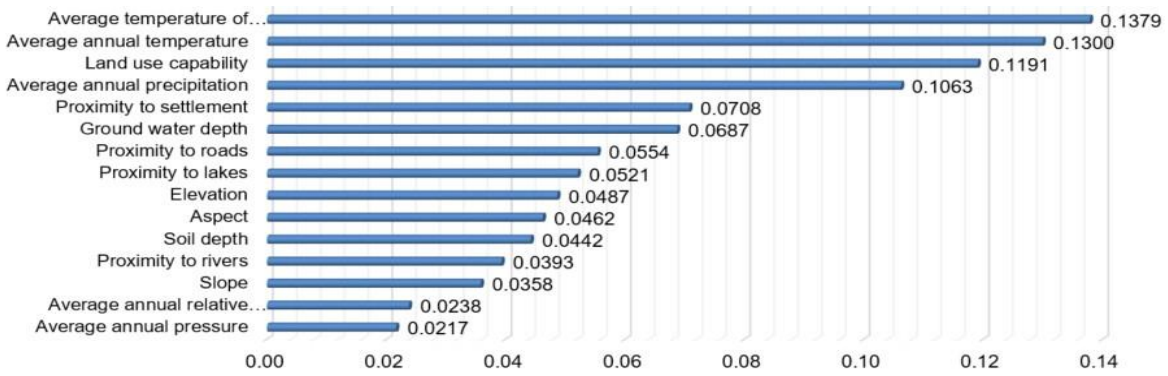

Figure 9- The final AHP weights of the main criteria

Table 3- The AHP model weights of the sub-criteria and the CR values for pair-wise comparison matrix

Criteria	*Sub-criteria*	*AHP weights*	*CR values*
Average annual temperature (°C)	5 - 8	0.1676	0.0122 < 0.10
	8 - 12	0.7380	
	> 12	0.0944	
Average temperature of October (°C)	1.96 - 5	0.0489	0.0254 < 0.10
	5 - 10	0.0629	
	10 - 11	0.2361	
	11 - 12	0.2928	
	12 - 14.9	0.3593	
Average annual humidity (%)	54.6 - 57	0.0665	0.0650 < 0.10
	57 - 58	0.1036	
	58 - 59	0.2272	
	59 - 60	0.2626	
	60 - 63.1	0.3401	
Average annual pressure (hPa)	865.8 - 870	0.1078	0.0436 < 0.10
	870 - 880	0.1433	
	880 - 890	0.1867	
	890 - 900	0.2422	
	900 - 917.9	0.3200	
Average annual precipitation (mm)	314.2 - 400	0.3803	0.0210 < 0.10
	400 - 500	0.3427	
	500 - 600	0.1572	
	600 - 700	0.0734	
	700 - 1150	0.0464	
Elevation (m)	600 - 900	0.0479	0.0754 < 0.10
	900 - 1200	0.5894	
	1200 - 1600	0.2172	
	1600 - 2600	0.1455	
Slope (%)	0 - 5	0.6402	0.0419 < 0.10
	5 - 10	0.1074	
	10 - 15	0.1798	
	15 - 25	0.0726	
Aspect	Flat and South	0.0630	0.0293 < 0.10
	North, Northeast and Northwest	0.1493	
	East and West	0.3189	
	Southeast and Southwest	0.4688	
Land use capability	I	0.2147	0.0439 < 0.10
	II	0.1939	
	III	0.2323	
	IV	0.3049	
	V	0.0542	
Soil depth	Deep	0.1150	0.0926 < 0.10
	Moderate deep	0.1987	
	Shallow	0.1447	
	Very Shallow	0.2824	
	Lithosol	0.1775	
	Other	0.0817	

Table 3 (continued)- The AHP model weights of the sub-criteria and the CR values for pair-wise comparison matrix

Criteria	*Sub-criteria*	*AHP weights*	*CR values*
Proximity to roads (km)	0.030 - 2	0.4162	0.0153 < 0.10
	2 - 4	0.2618	
	4 - 7	0.1610	
	7 – 10	0.0986	
	> 10	0.0624	
Proximity to settlement (km)	0 - 2	0.4204	0.0159 < 0.10
	2 - 4	0.2448	
	4 - 7	0.1641	
	7 - 10	0.1078	
	> 10	0.0629	
Proximity to rivers (km)	0 - 1	0.4338	0.0485 < 0.10
	1 - 2	0.2347	
	2 - 3	0.1743	
	3 - 5	0.0965	
	> 5	0.0607	
Proximity to lakes (km)	0 - 1	0.4432	0.0283 < 0.10
	1 - 2	0.2399	
	2 - 3	0.1585	
	3 - 5	0.0971	
	> 5	0.0613	
Groundwater depth (m)	0-30	0.4233	0.0193 < 0.10
	30-60	0.2954	
	60-90	0.1616	
	90-120	0.0767	
	120-150	0.0430	

According to Figure 10, 49.68% (2 023 615 km^2) of the area is not suitable for WC.

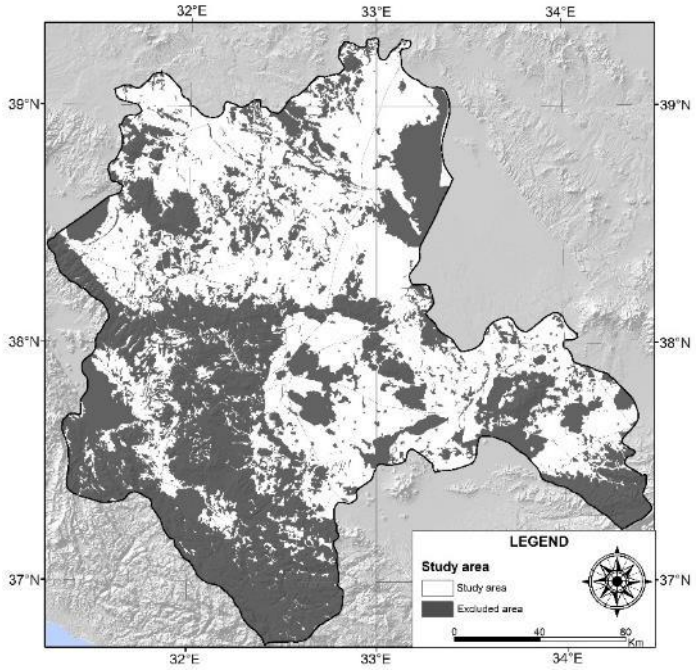

Figure 10- Excluded and study areas

The calculated weights of all the criteria in the hierarchy were taken into account and integrated into the GIS Model Builder in ArcGIS 10.0 software and combined with weighted linear combination overlay analysis and the final LS map was produced for WC shown in Figure 11. The derived LS map was divided into 5 classes as very highly suitable, highly suitable, moderate suitable and low suitable areas and areas not suitable for agricultural activities within the scope of the study. When the LS classification on the basis of Konya province is evaluated, the study region is categorized as very highly suitable 0.39% (15 815 km^2), highly suitable 61.24% (2 494 461 km^2), moderate suitable 31.01% (1 263 350 km^2), low suitable 7.14% (290 717 km^2) for WC. Besides, it was concluded that 0.22% (9 094 km^2) the study region is not suitable for WC (Table 4). According to the

LS map, very highly and highly suitable areas for WC in Konya province are determined as Kadinhani, Sarayonu, Altinekin, Cihanbeyli, Kulu, Karapinar and Emirgazi districts (Figure 11).

Table 4- Suitability classification of wheat cultivation

Land Suitability for wheat cultivation	*Area (km^2)*	*Ratio of area (%)*
Very highly suitable	15 815	0.39
Highly suitable	2 494 461	61.24
Moderate suitable	1 263 350	31.01
Low suitable	290 717	7.14
Not suitable area	9 094	0.22
Total area	4 073 436	100.00

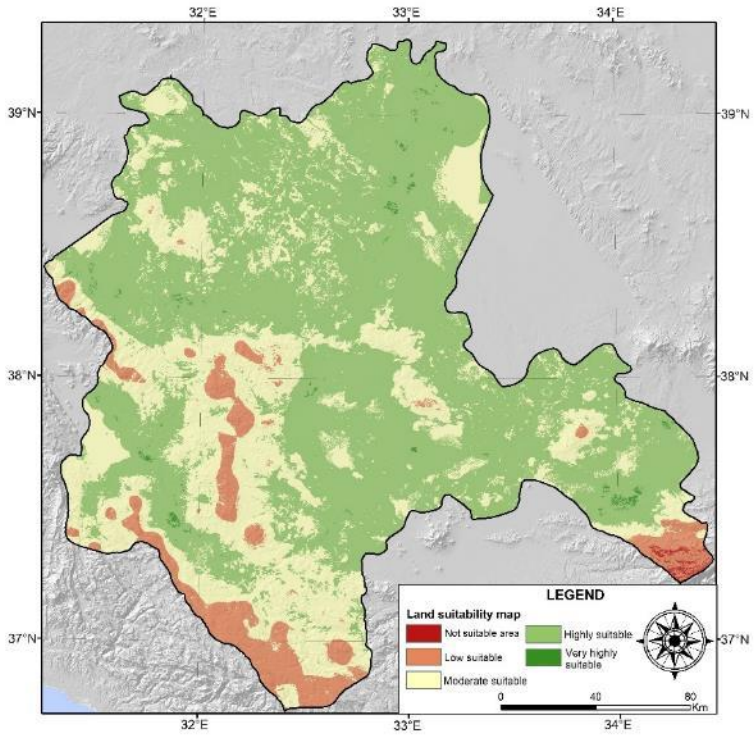

Figure 11- The final land suitability map for wheat cultivation

When the studies in the literature are examined, it is seen that the land suitability map is evaluated as 2-class (Fekadu & Negese 2020; Günal et al. 2022), 3-class (Akıncı et al. 2013; Ayehu & Besufekad 2015; Chivasaa et al. 2019; Pilevar et al. 2020; Tercan & Dereli 2020; Salifu et al. 2022), 4-class (Mendas & Delali 2012; Roy & Saha 2018; Dedeoğlu & Dengiz 2019; Souidi et al. 2020; Tuğaç 2021; Kılıc et al. 2022; Sarkar et al. 2022; Sarğın & Karaca 2023; Makar et al. 2024; Almayyahi & Al-Atab 2024) and 5-class (Pramanik 2016; Otgonbayar et al. 2017; Mandal et al. 2020; Bilgilioğlu 2021; Sarkar et al. 2023; Rangzan et al. 2024). In this study, the land suitability map was evaluated in accordance with the existing literature and divided into five classes in order to provide a more detailed analysis.

When the LS map (Figure 11) and the land productivity map (Figure 12) for the whole Konya closed basin are analyzed, it is seen that the areas with dry farming in the land productivity map overlap with the areas that are very suitable, suitable and moderately suitable for WC in the suitability map. Since Konya closed basin is a basin that is not dependent on external resources, it is important to encourage dry agriculture in this region. For this reason, it is recommended to grow crops that require less water such as wheat in areas suitable for WC according to the LS map.

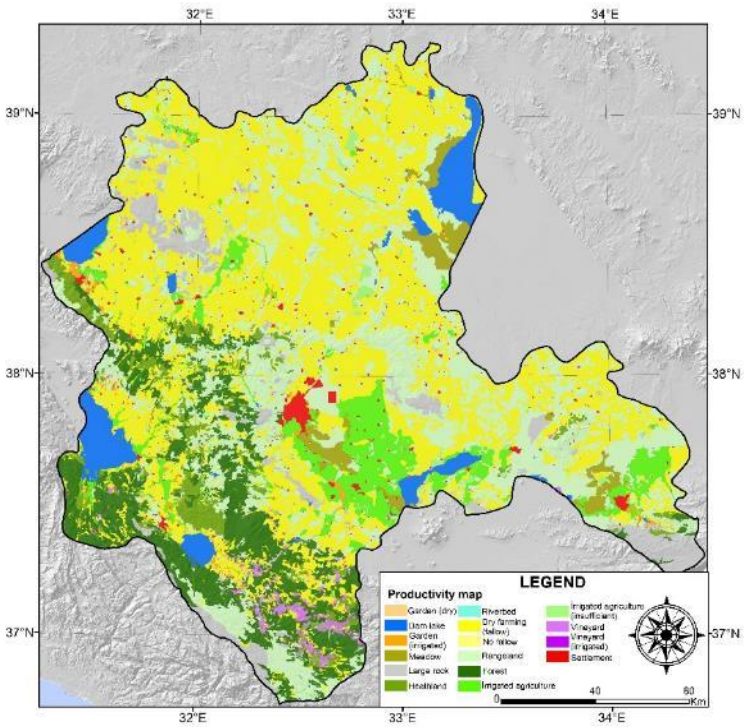

Figure 12- The land productivity map

When the studies on land suitability for wheat cultivation in the literature are examined, it is seen that (Makar et al. 2024) aimed to evaluate the land suitability of wheat in a selected area in El-Beheira Governorate of Egypt. The study employed an evaluation of five principal criteria. It was observed that the temperature criterion was the most significant factor. Sarğın & Karaca (2023) conducted a land suitability assessment in the Van province located in the Eastern Anatolia region and used 13 criteria in this context. It was observed that meteorological criteria were not used in the study, and the slope came to the fore among the criteria used, followed by the organic matter content. Kılıc et al. (2022), conducted a land suitability assessment in the Tozanlı region (located in the upper part of Yeşilırmak basin) in their study. In this context, nine criteria were evaluated, and it was determined that soil depth and elevation were the most pertinent. Dedeoglu & Dengiz (2019), in their study, they considered the Soğulca basin of Ankara province (central Anatolia regional of Turkey), used 10 criteria, and stated that soil depth is an important parameter for wheat production. In a study conducted by Pilevar et al. (2020), a land suitability assessment was carried out for wheat and corn production in the semi-arid regions of eastern Iran. The evaluation was based on 11 sub-criteria, grouped under three main headings. The results demonstrated that the soil texture criterion emerged as the most significant factor. Mendas & Delali (2012) selected the Mleta region in Algeria for wheat production in their study. The study examined ten criteria, and it was found that the drainage and soil criteria were salient. In their study, Fekadu & Negese (2020) conducted a suitability analysis for wheat and barley production on a basin basis in the Lay-Gayint region. A total of 15 criteria were employed in the studies, with pH and soil texture criteria emerging as the most prominent, followed by rain and slope criteria. It is stated that the most important criteria are climatic, topographic and soil parameters in their study. In their study, Rangzan et al. (2024) concentrate on the identification of the most appropriate regions for wheat cultivation in the northwestern part of Khuzestan Province in southwestern Iran. In the study, meteorological, topographic and soil criteria were evaluated, and precipitation and average temperature were identified as the most significant factors among these criteria.

A review of the literature revealed that, in studies conducted for wheat, the selected study areas were predominantly basins, districts, or specific regions. In this study, the entire province of Konya, which is the largest province in Turkey in terms of surface area, was evaluated as the study area. In addition, when the criteria discussed were evaluated, it was seen that 4-15 criteria were evaluated in the studies, soil criteria came to the forefront among them, and in the studies where soil criteria were not used, precipitation and average temperature criteria, which are very important for wheat plant development, came to the fore. In this study, the average temperature criterion came to the fore and it was observed that it was compatible with other studies. In addition, in this study, the average annual pressure criterion was discussed and its importance for the development of wheat plants was investigated. The fact that the soil criterion was not considered in this study is among the limitations of the study and this criterion will be taken into consideration in future studies.

4. Conclusions

The consumption of wheat, which always has a special importance in agricultural products, has been increasing in recent years. At the same time, due to poor land usage policies, the areas suitable for wheat production are gradually decreasing. Considering

the rapidly changing environmental impacts, Effective and good agricultural planning is needed to increase agricultural production efficiency. Wheat production has both economic and strategic importance in Türkiye. The share of WC area in the total cultivation area in Türkiye is 49.7% and Konya closed basin is in the first place with 9.1%.

In this study, areas suitable for WC throughout Konya province were determined by using a hierarchy developed with the integration of the AHP method, which is one of the GIS and MCDM techniques. For this purpose, 15 criteria and their sub-criteria were determined under 4 main headings, weight calculations were made, and a LS map was created with the WLC technique according to expert opinions and literature studies on the subject. The LS map derived is divided into 5 classes as very high suitable 0.39%, high suitable 61.24%, medium suitable 31.01%, low suitable 7.14% and areas not suitable for agricultural activities 0.22%. The AHP method used in this study is appropriate, easy to understand and flexible about possible future planning. This process saves time for decision makers and quick results can be obtained for different goals.

Although sustainable agriculture is very important for countries like Türkiye with high population growth and migration potential, demand for wheat, which has strategic importance for Türkiye and is the raw material for staple foods such as bread, flour, and pasta, has been increasing. Therefore, it is important to cultivate and produce according to the suitability of the land. It is thought that the criteria used in this study will be taken into consideration in WC in the Konya closed basin in the future.

Declarations

Data availability Not applicable.
Code availability Not applicable.
Funding No funding support has been received from any institution for this study.
Conflict of interest The authors declare that there is no conflict of interest.

References

Aburas M M, Abdullah S H O, Ramli M F & Asha'ari Z H (2017). Land suitability analysis of urban growth in Seremban Malaysia, using GIS based Analytical Hierarchy Process. Procedia Engineering 198: 1128-1136. https://doi.org/10.1016/j.proeng.2017.07.155

Akıncı H Ozalp A Y & Turgut B (2013). Agricultural land use suitability analysis using GIS and AHP technique. Computers and Electronics in Agriculture 97: 71-82. https://doi.org/10.1016/j.compag.2013.07.006

Al-Hanbali A, Shibuta K, Alsaaideh B, Tawara Y (2021). Analysis of the land suitability for paddy fields in Tanzania using a GIS-based analytical hierarchy process. Geo-spatial Information Science 25(2): 212-228. https://doi.org/10.1080/10095020.2021.2004079

Almayyahi M S & Al-Atab S M (2024). Evaluating land suitability for wheat cultivation criteria analysis fuzzy-AHP and geospatial techniques in northern Basrah Governorate. *Basrah Journal of Agricultural Sciences* 37(1): 212-223. https://doi.org/10.37077/25200860.2024.37.1.16

Asseng S, Foster I & Turner N C (2011). The impact of temperature variability on wheat yields. Global change biology 17(2): 997-1012. https://doi.org/10.1111/j.1365-2486.2010.02262.xAyehu G T & Besufekad S A (2015). Land suitability analysis for rice production: A GIS based multi-criteria decision approach. *American Journal of Geographic Information System* 4(3): 95-104. https://doi.org/10.5923/j.ajgis.20150403.02Bagheri M, Sulaiman W N A & Vaghefi N (2013). Application of geographic information system technique and analytical hierarchy process model for land-use suitability analysis on coastal area. *Journal of Coastal Conservation* 17(1):1-10. https://doi.org/10.1007/s11852-012-0213-4

Baloch M S, Nadim M A., Zubair, Muhammad., Awan, I.U., Khan, E.A., Ali, SAJID., 2012. Evaluation of wheat under normal and late sowing conditions. Pak. J. Bot, 44(5): 1727-1732

Begum F, Bajracharya R M, Sitaula B K & Sharma S (2013). Seasonal dynamics, slope, aspect and land use effects on soil mesofauna density in the mid-hills of Nepal. Farida. *International Journal of Biodiversity Science*, Ecosystem Services & Management 9(4): 290-297. https://doi.org/10.1080/21513732.2013.788565

Bilgilioglu S S (2021). Land suitability assessment for olive cultivation using GIS and multi-criteria decision-making in Mersin city, Turkey. *Arabian Journal of Geosciences* 14: 2434. https://doi.org/10.1007/s12517-021-08768-8

Bilgilioglu S S, Gezgin C, Orhan O & Karakus P (2022). A GIS-based multi-criteria decision-making method for the selection of potential municipal solid waste disposal sites in Mersin, Turkey. Environmental Science and Pollution Research 29: 5313–5329. https://doi.org/10.1007/s11356-021-15859-2

Cengiz T & Akbulak C (2009). Application of analytical hierarchy process and geographic information systems in land-use suitability evaluation: a case study of Dümrek village (Çanakkale, Turkey) . *International Journal of Sustainable Development & World Ecology* 16(4): 286–294. https://doi.org/10.1080/13504500903106634

Chivasaa W, Mutanga O & Biradarc C (2019). Mapping land suitability for maize (Zea mays L.) production using GIS and AHP technique in Zimbabwe. *South African Journal of Geomatics* 8(2): 265-281. http://dx.doi.org/10.4314/sajg.v8i2.11

Chuong H V (2011). Land suitability analysis and evaluation for productıon of fruıt trees usıng GIS technology A case study at Thua Thien Hue. *Hue University Journal of Science: Agriculture and Rural Development* 67(4): 13-22. https://doi.org/10.26459/jard.v67i4.3105

Dai F C, Lee CF & Zhang X H (2001). GIS-based geo-environmental evaluation for urban land-use planning: a case study. Engineering Geology 61(4): 257–271. https://doi.org/10.1016/S0013-7952(01)00028-X

Dedeoglu M & Dengiz O (2019). Generating of land suitability index for wheat with hybrid system approach using AHP and GIS. Computers and Electronics in Agriculture167: 105062. https://doi.org/10.1016/j.compag.2019.105062

Dogan H G & Kan A (2019). The effect of precipitation and temperature on wheat yield in Turkey: a panel FMOLS and panel VECM approach. Environment. Development and Sustainability 21(1): 447-460. https://doi.org/10.1007/s10668-018-0298-5

Everest T, Sungur A & Ozcan H (2021). Determination of agricultural land suitability with a multiple-criteria decision-making method in Northwestern Turkey. *International Journal of Environmental Science and Technology* 18: 1073-1088. https://doi.org/10.1007/s13762-020-02869-9

FAO (1976). A framework for land evaluation. FAO, Soils Bulletin 32, Rome
FAO (1977). A framework for land evaluation. International Institute for Land Reclamation and Improvement 22, 87
FAO (1985). Guidelines: land evaluation for irrigated agriculture. FAO Soils Bulletin, 55
Fekadu E & Negese A (2020). GIS assisted suitability analysis for wheat and barley crops through AHP approach at Yikalo sub-watershed, Ethiopia. Cogent Food & Agriculture 6(1): 1-21. https://doi.org/10.1080/23311932.2020.1743623
Ghosh S & Das A (2019). Urban expansion induced vulnerability assessment of east kolkata wetland using fuzzy MCDM method. Remote Sensing Applications: Society and Environment 13: 191–203. https://doi.org/10.1016/j.rsase.2018.10.014
Gouareh A, Settou B & Settou N (2021). A new geographical information system approach based on best worst method and analytic hierarchy process for site suitability and technical potential evaluation for large-scale CSP on-grid plant: An application for Algeria territory. Energy Conversion and Management 235: 113963. https://doi.org/10.1016/j.enconman.2021.113963
Guo S, Tang Y, Gao F, Ai W & Qin L (2008). Effects of low pressure and hypoxia on growth and development of wheat. Acta Astronautica, 63 (7-10): 1081-1085. https://doi.org/10.1016/j.actaastro.2008.02.006
Günal H, Kılıç O M, Ersayın K & Acir N (2022). Land suitability assessment for wheat production using analytical hierarchy process in a semi-arid region of Central Anatolia. Geocarto International 37(27): 16418-16436. https://doi.org/10.1080/10106049.2022.2108911
Habibie M I, Noguchi R, Shusuke M & Ahamed T (2021). Land suitability analysis for maize production in Indonesia using satellite remote sensing and GIS-based multicriteria decision support system. *GeoJournal* 86(2): 777–807. https://doi.org/10.1007/s10708-019-10091-5
Hirzel J & Matus I (2013). Effect of soil depth and increasing fertilization rate on yield and its components of two durum wheat varieties. *Chilean Journal of Agricultural Research* 73(1): 55–59. https://doi.org/10.4067/S0718-58392013000100008
Hossain M S & Das N G (2010). GIS-based multi-criteria evaluation to land suitability modelling for giant prawn (Macrobrachium rosenbergii) farming in Companigonj Upazila of Noakhali, Bangladesh. Computers and electronics in agriculture 70(1): 172-186. https://doi:10.1016/j.compag.2009.10.003
Ircan M R (2020). Climate characteristics and drought analysis of Sanliurfa, MSc thesis, Cankiri Karatekin University Institute of Social Sciences, Cankiri (in Turkish).
Jolánkai M, Kassai M K, Tarnawa Á, Pósa B & Birkás M (2018). Impact of precipitation and temperature on the grain and protein yield of wheat (Triticum aestivum L.) varieties. Időjárás= *Quarterly Journal of the Hungarian Meteorological Service* 122(1): 31-40. https://doi.org/10.28974/idojaras.2018.1.3
Kapluhan E (2013). Drought and drought in Turkey effect of agriculture. Marmara Geographical Review (27): 487-510
Karaca S, Dengiz O, Turan, I D, Ozkan B¸ Dedeoglu M, Gülser F, Sargin B, Demirkaya S & Ay, A (2021). An assessment of pasture soils quality based on multi-indicator weighting approaches in semi-arid ecosystem. Ecological Indicators 121: 107001. https://doi. org/10.1016/j.ecolind.2020.107001
Karaca S, Sargin B, Alaboz P & Dengiz O (2023). Determination of soil quality characteristics with multi-criteria decision-making analysis-GIS in apple orchards in Van-Edremit district. *Journal of Agriculture and Nature* 26(2): 393-408. https://doi.org/10.18016/ksutarimdoga.vi.1074149
Kasap Y & Subasi E (2017). Risk assessment of occupational groups working in open pit mining: analytic hierarchy process. *Journal of Sustainable Mining* 16(2): 38-46. https://doi.org/10.1016/j.jsm.2017.07.001
Kılıc O M, Ersayin K, Gunal H, Khalofah A & Alsubeie M S (2022). Combination of fuzzy-AHP and GIS techniques in land suitability assessment for wheat (Triticumaestivum) cultivation. *Saudi Journal of Biological Sciences* 29(4): 2634-2644. https://doi.org/10.1016/j.sjbs.2021.12.050
Komer P, Abraham A & Snášel V. (Eds.) (2014). Proceedings of the fifth international conference on innovations in bio-inspired computing and applications IBICA 2014 (Vol. 303). Springer
Kursunoglu N & Onder M (2015). Selection of an appropriate fan for an underground coal mine using the analytic hierarchy process. Tunnelling and Underground Space Technology 48: 101–109. https://doi.org/10.1016/j.tust.2015.02.005
Lopez R S, Fernandez, D G, Lopez J O S, Briceno N B R, Oliva M, Murga R E T, Trigoso D I, Castillo E B & Gurbillon M A B (2020). Land Suitability for Coffee (Coffeaarabica) Growing in Amazonas, Peru: Integrated Use of AHP, GIS and RS. *ISPRS International Journal of Geo-Information* 9(11): 1-21. https://doi.org/10.3390/ijgi9110673
Lu G Y & Wong D W (2008). An adaptive inverse-distance weighting spatial interpolation technique. Computers & Geosciences 34(9): 1044–1055. https://doi.org/10.1016/j.cageo.2007.07.010
Maddahi Z, Jalalian A, Kheirkhah, Zarkesh, M M & Honarjo N (2017). Land suitability analysis for rice cultivation using a Gis-based fuzzy multi-criteria decision making approach: Central part of Amol district, Iran. Soil and Water Research 12(1): 29-38. https://doi.org/10.17221/1/2016-SWR
Makar R S, Shahin S A & Abd El-Hady M (2024). Development of a parametric-based Analytical Hierarchy Process (AHP) utilizing Geographic Information Systems (GIS) for wheat land suitability evaluation. *Journal of Applied and Natural Science* 16(1): 390-399. https://doi.org/10.31018/jans.v16i1.5405
Malczewski J (1999). GIS and Multicriteria Decision Analysis. John Wiley and Sons, New York
Malczewski J (2004). GIS-based land-use suitability analysis: a critical overview. Progress in Planning 62(1): 3–65. https://doi.org/10.1016/j.progress.2003.09.002
Mandal V P, Rehman S, Ahmed R, Masroor MD, Kumar P & Sajjad H (2020). Land suitability assessment for optimal cropping sequences in Katihar district of Bihar, India using GIS and AHP. Spatial Information Research 28: 589-599. https://doi.org/10.1007/s41324-020-00315-z
Marijanović M, Markulj A, Tkalec M, Jozić A & Kovačević V (2010). Impact of precipitation and temperature on wheat (Triticum aestivum L.) yields in eastern Croatia. Acta Agriculturae Serbica 15(30): 117-123
Massawe B H J, Kaaya A K, Winowiecki L & Slater B K (2019). Multi-criteria land evaluation for rice production using GIS and analytic hierarchy process in Kilombero Valley, Tanzania. *Tanzania Journal of Agricultural Sciences* 18(2): 88-98.
Massimino D & Andre M (1999). Growth of wheat under one tenth of the atmospheric pressure. Advances in Space Research 24(3): 293-296. https://doi.org/10.1016/S0273-1177(99)00316-6
Mendas A & Delali A (2012). Integration of MultiCriteria Decision Analysis in GIS to develop land suitability for agriculture: Application to durum wheat cultivation in the region of Mleta in Algeria. Computers and Electronics in Agriculture 83: 117-126. https://doi:10.1016/j.compag.2012.02.003

Mokarram M & Mirsoleimani A (2018). Using Fuzzy-AHP and order weight average (OWA) methods for land suitability determination for citrus cultivation in ArcGIS (Case study: Fars province, Iran). Physica A: Statistical Mechanics and its Applications 508: 506-518. https://doi.org/10.1016/j.physa.2018.05.062

Morelli F (2011). Importance of road proximity for the nest site selection of the Red-backed shrike (Lanius collurio) in an agricultural environment in central Italy. *Journal of Mediterranean Ecology* 11: 21–29

Mutlu M & Sari M (2017). Multı-crıterıa decision-making methods and use of in mining industry. Scientific Mining Journal 56(4): 181–196. https://doi.org/10.30797/madencilik.391953

Mutlu M & Sari M (2022). Risk-based classification of underground coal mine basins in Turkey using the analytic hierarchy process (AHP). *Arabian Journal of Geosciences* 15(8): 752. https://doi.org/10.1007/s12517-022-10005-9

Mutlu M & Cetin N C, Onder S (2024) A novel risk assessment approach for open-cast coal mines using hybrid MCDM models with interval type-2 fuzzy sets: A Case study in Türkiye. Systems 12(8): 267. https://doi.org/10.3390/systems12080267

Myagmartseren P, Buyandelger M & Brandt S A (2017). Implications of a spatial multicriteria decision analysis for urban development in Ulaanbaatar, Mongolia. Mathematical Problems in Engineering 1: 2819795. https://doi.org/10.1155/2017/281979

Orhan O (2021) Land suitability determination for citrus cultivation using a GIS based multi-criteria analysis in Mersin, Turkey. Computers and Electronics in Agriculture 190: 106433. https://doi.org/10.1016/j.compag.2021.106433

Orhan O & Makineci H B (2023). Agricultural land suitability analysis. in encyclopedia of smart agriculture technologies (pp. 1-9). Cham: Springer International Publishing. https://doi.org/10.1007/978-3-030-89123-7_270-1

Ostovari Y, Honarbakhsh A, Sangoony H, Zolfaghari F, Maleki K & Ingram B (2019). GIS and multi-criteria decision-making analysis assessment of land suitability for rapeseed farming in calcareous soils of semi-arid regions. Ecological Indicators 103: 479-487. https://doi.org/10.1016/j.ecolind.2019.04.051

Otgonbayar M, Atzberger C, Chambers J, Amarsaikhan D, Böck S & Tsogtbayar J (2017). Land suitability evaluation for agricultural cropland in Mongolia using the spatial MCDM method and AHP based GIS. *Journal of Geoscience and Environment Protection* 5(9): 238-263. https://doi.org/10.4236/gep.2017.59017

Ozegin K O, Ilugbo S O & Akande O N (2024). Leveraging geospatial technology and AHP for groundwater potential zonation in parts of South and North-Central Nigeria. Sustainable Water Resources Management 10(4): 146. https://doi.org/10.1007/s40899-024-01124-0

Ozsahin E & Ozdes M (2022). Agricultural land suitability assessment for agricultural productivity based on GIS modeling and multi-criteria decision analysis: the case of Tekirdağ province. Environmental Monitoring and Assessment 194(1): 41. https://doi.org/10.1007/s10661-021-09663-1

Pathan A I, Agnihotri P G & Patel D (2022). Integrated approach of AHP and TOPSIS (MCDM) techniques with GIS for dam site suitability mapping: a case study of Navsari City, Gujarat, India. Environmental Earth Sciences 81(18): 443. https://doi.org/10.1007/s12665-022-10568-6

Pilevar A R, Matinfar H R, Sohrabi A & Sarmadian F (2020). Integrated fuzzy, AHP and GIS techniques for land suitability assessment in semi-arid regions for wheat and maize farming. Ecological Indicators 110: 105887. https://doi.org/10.1016/j.ecolind.2019.105887

Prakash T N (2003). Land suitability analysis for agricultural crops: a fuzzy multicriteria decision making approach. Enchede, The Netherlands: ITC

Pramanik M K (2016). Site suitability analysis for agricultural land use of Darjeeling district using AHP and GIS techniques. Modeling Earth Systems and Environment 2: 1-22. https://doi.org/10.1007/s40808-016-0116-8

Porter J R & Gawith M (1999). Temperatures and the growth and development of wheat: a review. *European Journal of Agronomy* 10(1): 23-36

Rahmouni S, Negrou B, Settou N, Dominguez J & Gouareh A (2017). Prospects of hydrogen production potential from renewable resources in Algeria. *International Journal of Hydrogen Energy* 42(2): 1383-1395. https://doi.org/10.1016/j. ijhydene.2016.07.214

Rangzan K, Kabolizadeh M, Zaheri Abdehvand Z, Karimi D, Jafarnejadi A, Mokarram M (2024). Optimized Land Suitability Mapping for Wheat Cultivation by Integrating Fuzzy Hierarchical Analysis and Satellite Images. *Journal of the Indian Society of Remote Sensing* 52(5): 1135-1151. https://doi.org/10.1007/s12524-024-01863-9

Rhoton F E & Lindbo D L (1997). A soil depth approach to soil quality assessment. Journal of Soil and Water Conservation, 52 (1)

Rodríguez-Puebla C, Ayuso S M, Frias M D & Garcia-Casado L A (2007). Effects of climate variation on winter cereal production in Spain. Climate Research 34 (3): 223-232

Roy J & Saha S (2018). Assessment of land suitability for the paddy cultivation using analytical hierarchical process (AHP): A study on Hinglo river basin, Eastern India. *Modeling Earth Systems and Environment* 4: 601-618. https://doi.org/10.1007/s40808-018-0467-4.

Saaty T L (1977). A scaling method for priorities in hierarchical structures. *J. Math. Psychol.* 15 (3): 234-281. https://doi.org/10.1016/0022-2496(77)90033-5.

Saaty T L (1980). The Analytic Hierarchy Process. McGraw Hill, New York, USA

Saaty T L (1990). How to make a decision: The analytic hierarchy process. *Eur. J. Oper. Res.* 48(1): 9-26. https://doi.org/10.1016/0377-2217(90)90057-I

Saaty T L, Vargas L G & Dellman K (2003). The allocation of intangible resources: the analytic hierarchy process and linear programming. Socio-Eco Plan Sci. 37: 169-189. https://doi.org/10.1016/S0038-0121(02)00039-3

Salifu E, Agyare W A & Abdul-ganiyu S (2022). Evaluation of land suitability for crop production in Northern Ghana using GIS and AHP based techniques. *International Journal of Environment and Geoinformatics* 9(4): 46-56. https://doi. 10.30897/ijegeo.1022275

Sandhu S K & Dhaliwal L K (2016). Crop geometry effects on relative humidity variation within wheat crop

Sarğın B & Karaca S (2023). Land suitability assessment for wheat-barley cultivation in a semi-arid region of eastern Anatolia in Turkey. PeerJ, 11, e16396. https://doi.org/10.7717/peerj.16396

Sarğın B, Alaboz P, Karaca S & Dengiz O (2024). Pythagorean fuzzy SWARA weighting technique for soil quality modeling of cultivated land in semi-arid terrestrial ecosystems. Computers and Electronics in Agriculture, 227, 109466. https://doi.org/10.1016/j.compag.2024.109466

Sarkar B, Das P, Islam N, Basak A, Debnath M & Roy R (2022). Land suitability analysis for paddy crop using GIS-based fuzzy- ahp(F-AHP) method in koch bihar district, west bengal. Geocarto International 37(25): 8952-8978. https://doi.org/10.1080/10106049.2021.2007299

Sarkar D, Saha S & Mondal P (2023). Modelling agricultural land suitability for vegetable crops farming using RS and GIS in conjunction with bivariate techniques in the Uttar Dinajpur district of Eastern India. Green Technologies and Sustainability, 1(2): 100022. https://doi.org/10.1016/j.grets.2023.100022

Sathiyamurthi S, Saravanan S, Sankriti R, Aluru M, Sivaranjani S & Srivel R (2024). Integrated GIS and AHP techniques for land suitability assessment of cotton crop in Perambalur District, South India. *International Journal of System Assurance Engineering and Management* 15(1): 267-278. https://doi.org/10.1007/s13198-022-01705-2

Sauer T, Havlik P, Schneider U A, Schmid E, Kindermann G & Obersteiner M (2010). Agriculture and resource availability in a changing world: The role of irrigation. Water Resources Research 46(6): 1-12. https://doi.org/10.1029/2009WR007729

Sengupta S, Mohinuddin S, Arif M, Sengupta B & Zhang W (2022). Assessment of agricultural land suitability using GIS and fuzzy analytical hierarchy process approach in ranchi district, India. Geocarto International 37(26): 13337-13368. https://doi.org/10.1080/10106049.2022.2076925

Shenavr B & Hosseini S M (2014). Comparison of multi-criteria evaluation (AHP and WLC approaches) for land capability assessment of urban development in GIS. *International Journal of Geomatics and Geosciences* 4(3): 435-446

Souidi H, Ouadif L, Bahi L, Edderkaoui R, Jaouda I, Bahi Y & Belhaj S (2020). Research of suitability area of agriculture in coastal CHAOUIA by integration the AHP, IDW, and MCDA to GIS. In E3S web of conferences (Vol. 150, p. 03009). EDP Sciences. https://doi.org/10.1051/e3sconf/202015003009

Sys C, Van Ranst E & Debaveye I J (1991). Landevaluation. part II: methods in land evaluation. General administration for development cooperation,247. Agricultural publication-No. 7

Tadesse M & Negese A (2020). Land suitability evaluation for sorghum crop by using GIS and AHP techniques in agamsa sub-watershed. Ethiopia, Cogent Food Agric. 6(1): 1-18. https://doi.org/10.1080/23311932.2020.1743624

Tarhan S & Dellal İ (2021). The effect of soil products office purchasing policies on wheat production practices of producers: the case of Ankara province Gölbaşı district, Agriculture Engineering, 373:19-28. https://doi.org/10.33724/zm.891801

Tashayo B, Honarbakhsh A, Akbari M & Eftekhari M (2020). Land suitability assessment for maize farming using a GIS-AHP method for a semi- arid region, Iran. J Saudi Soc Agric Sci 19(5): 332-338. https://doi.org/10.1016/j.jssas.2020.03.003

Tercan E & Dereli M A (2020). Development of a land suitability model for citrus cultivation using GIS and multi-criteria assessment techniques in Antalya province of Turkey. Ecol. Indic., 117, 106549

Tuğaç M G (2021). GIS-based land suitability classification for wheat cultivation using fuzzy set model. *International Journal of Agriculture Environment and Food Sciences* 5(4): 524-536. https://doi.org/10.31015/jaefs.2021.4.12

RTMAF (2015). Republic of Turkey Ministry of Agriculture and Forestry. Ankara provincial directorate, Turkey https://ankara.tarimorman.gov.tr/Belgeler/liftet/bugdayyetistiriciligi.pdf (accessed 10 Feb 2022)

Wali E, Datta A, Shrestha R P & Shrestha S (2016). Development of a land suitability model for saffron (Crocus sativus L.) cultivation in Khost Province of Afghanistan using GIS and AHP techniques, Archives of Agronomy and Soil Science 62(7): 921-934. https://doi.org/10.1080/03650340.2015.1101519

Wang Y C, Lu Y H, Chiang L C & Hsu C C (2023). Assessing crop suitability of rice, wheat, and maize on agricultural lands in Taiwan. Natural Resources Research 32(2): 813-834. https://doi.org/10. 1007/s11053-023-10162-y

Wind Y & Saaty T L (1980). Marketing applications of the analytic hierarchy process. Management Science 26(7): 641-658. https://doi.org/10.1287/mnsc.26.7.641

Worqlul A W, Jeong J, Dile Y T, Osorio J, Schmitter P, Gerik T, Srinivasan R & Clark N (2017). Assessing potential land suitable for surface irrigation using groundwater in Ethiopia. Applied Geography 85:1–13. https://doi.org/10.1016/j.apgeog.2017.05.010

Yoon K P & Hwang C L (1995). Multiple Attribute Decision Making: An Introduction 104. Sage publications, London

Zhang X, Fang C, Wang Z & Ma H (2013). Urban construction land suitability evaluation based on improved multi-criteria evaluation based on GIS (MCE-GIS): Case of New Hefei City Chinese Geographical Science 6: 740–753. https://doi.org/10.1007/s11769-013-0609-6

Zhang J, Su Y, Wu J & Liang H (2015). GIS based land suitability assessment for tobacco production using AHP and fuzzy set in Shandong province of China. Computers Electronics in Agriculture 114: 202–211. https://doi.org/10.1016/j.compag.2015.04.004

Journal of Agricultural Sciences
(Tarim Bilimleri Dergisi)

J Agr Sci-Tarim Bili
e-ISSN: 2148-9297
jas.ankara.edu.tr

JAS

Evaporation and precipitation prediction for future time frames via combined machine learning-climate change models: Quri Gol Wetland Case

Mohammad Reza Abdollahpour Azad[a], Mohammad Reza Jalali[a], Mohammad Taghi Sattari[b,c*], Reza Mastouri[a]

[a]*Department of Civil Engineering, Arak Branch, Islamic Azad University, Arak, IRAN*

[b]*Department of Water Engineering, Faculty of Agriculture, University of Tabriz, Tabriz, IRAN*

[c]*Department of Agricultural Engineering, Faculty of Agriculture, Ankara University, Ankara, 06110, TURKEY*

ARTICLE INFO

Research Article

Corresponding Author: Mohammad Taghi Sattari, E-mail: mtsattar@gmail.com

Received: 03 July 2024 / Revised: 26 November 2024 / Accepted: 05 December 2024 / Online: 25 March 2025

Cite this article

Azad M R A, Jalali M R, Sattari M T, Mastouri R (2025). Evaporation and precipitation prediction for future time frames via combined machine learning-climate change models: Quri Gol Wetland Case . *Journal of Agricultural Sciences (Tarim Bilimleri Dergisi),* 31(2):447-469. DOI: 10.15832/ankutbd.1509731

ABSTRACT

Evaporation is a critical component in the management of water resources. Due to the complex interactions between various meteorological variables involved in evaporation calculations, numerous nonlinear models have been developed. The applicability and performance of these models vary depending on the specific climatic conditions of each region. This study evaluates the impacts of climate change on evaporation and precipitation patterns in the Quri Gol Wetland, located in East Azerbaijan, Iran, using machine learning models and climate change projections. Evaporation values for the present period (1991-2020) were estimated using six machine learning models: Random Forest (RF), Gradient Boosted Tree (GBT), Generalized Linear Model (GLM), Support Vector Machine (SVM), Gaussian Process Regression (GPR), and deep learning (DL). Future projections (2021-2050, 2051-2080, 2081-2100) were based on the LARS-WG and SDSM models under three climate scenarios (RCP 2.6, RCP 4.5, and RCP 8.5). The performance of the machine learning models was assessed using statistical metrics including R^2, Scatter Index (SI), Mean Absolute Error (MAE), Willmott's Index (WI), and Kling-Gupta Efficiency (KGE). The RF and DL models provided the most accurate predictions, with RF achieving an R^2 of 0.821 and an MAE of 0.902, while DL reached an R^2 of 0.822 and an MAE of 0.915 in the validation phase. Results from climate change projections indicated a significant increase in evaporation over the next century, with cumulative evaporation rising by up to 50.01% under the RCP 8.5 scenario by 2081-2100. In contrast, the projected increase in precipitation was much smaller, reaching a maximum of 16% in the same period. This imbalance between evaporation and precipitation highlights the potential for increasing water stress in the Quri Gol Wetland. The findings emphasize the need for adaptive water management strategies to mitigate the effects of increased evaporation and maintain ecological stability in the region.

Keywords: Climate change, Meteorological variables, Evaporation, Machine learning, Statistical indices

1. Introduction

Climate change is a critical challenge facing our planet in the 21st century, necessitating effective evaluation and prediction of its impacts, particularly on water resources. The adverse effects of climate change on water availability not only threaten ecosystems but also have significant environmental, economic, and social consequences. Each year, vast quantities of freshwater are stored in reservoirs; however, evaporation contributes to water quality degradation by increasing salinity levels. To address these challenges, understanding and accurately estimating surface water evaporation is crucial for sustainable water management in a changing climate.

Various methods have been developed for estimating surface water evaporation, typically classified into four main categories: (1) Pan evaporation measurement, (2) water balance, (3) energy balance, and (4) mass transfer (Gianniou & Antonopoulos 2007). Among these, the pan evaporation method is often preferred due to its simplicity, cost-effectiveness, and relatively high accuracy compared to more complex energy balance methods (Hamel 2009; Anderson 2004). This preference underscores the importance of reliable evaporation estimation techniques, particularly in light of the escalating impacts of climate change on hydrological cycles.

As noted, evaporation prediction is critical due to the increasing challenges posed by climate change and water resource depletion. Early research, such as Terzi (2010), employed genetic programming to model daily evaporation from Lake Egirdir, Turkey, showing its potential as a replacement for traditional methods. Kim et al. (2012) applied generalized regression neural networks (GRNN), support vector machines (SVM), and multilayer perceptron (MLP) to predict pan evaporation in arid and temperate zones, with artificial neural network (ANN) models outperforming empirical and multiple linear regression (MLR)

methods. Similarly, Guven & Kisi (2013) compared the Stephens-Stewart (SS) model, ANN, adaptive neuro-fuzzy inference system (ANFIS), fuzzy genetic (FG), and linear genetic programming (LGP) for estimating pan evaporation. They found LGP to be the most accurate model using meteorological data from Turkey. Goyal et al. (2014) extended the use of machine learning by comparing ANFIS, fuzzy logic, ANN, and least squares support vector regression (LS-SVR) for daily pan evaporation in India's subtropical climate, with LS-SVR and fuzzy logic providing more accurate predictions. Kisi (2015) employed M5 Model Trees (M5Tree), multivariate adaptive regression splines (MARS), and LSSVM at Turkish stations, with MARS proving superior. Similarly, Keshtegar et al. (2016) modeled pan evaporation using meteorological inputs in Iran, with their proposed models outperforming M5Tree and ANFIS. Wang et al. (2017a) applied six heuristic computing techniques across various climates in China, finding MLP superior to other models in most cases. Lu et al. (2018) also demonstrated the effectiveness of gradient boosted decision trees (GBDT) for daily pan evaporation in China's Poyang Lake Basin, with GBDT outperforming RF and M5Tree models.

Further advancements in machine learning and hybrid techniques are evident in Ghorbani et al. (2018), who integrated MLP with the firefly algorithm (MLP-FFA) for daily pan evaporation, showing it outperformed single models. Zounemat-Kermani et al. (2019) explored optimization algorithms, such as genetic algorithm (GA), particle swarm optimization (PSO), and others based on ANFIS, finding GA and PSO most effective. Shiri (2019) assessed ANN and ANFIS for pan evaporation in the U.S., recommending supplementary information for areas lacking local climatological data. Kisi & Heddam (2019) compared M5Tree, MARS, and MLP, with MARS proving to be the most accurate. Majhi et al. (2020) demonstrated that deep neural networks (DNN) provided superior accuracy in estimating daily pan evaporation in India, while Ghaemi et al. (2019) coupled M5Tree and MARS with the maximum overlap discrete wavelet transform (MODWT) to improve prediction performance in Turkey. Wang et al. (2020) introduced a hybrid technique combining kernel-based nonlinear Arps decline (KNEA) and the salp swarm algorithm (SSA) for evaporation prediction in China's arid regions, showing SSA-KNEA's high potential compared to MARS and M5Tree. Seifi & Soroush (2020) employed whale optimization algorithm (WOA), grey wolf optimization (GWO), and GA in combination with ANNs to predict daily pan evaporation across Iranian stations, finding hybrid models superior to single methods in most locations. Shaker Sureh et al. (2024) used data-driven models and atmospheric circulation indices to improve meteorological drought prediction in the Lake Urmia basin, finding that the M5 Tree model provided the most accurate results.

Climate change significantly influences hydrological processes, as evidenced by various studies utilizing climate models to evaluate its effects. Zarghami et al. (2011) investigated the impact of climate change on runoff in East Azerbaijan province using General Circulation Models (GCM) alongside statistical data from six meteorological stations. By applying the LARS-WG method and simulating flow through artificial neural networks, they demonstrated a substantial projected reduction in flow across three basins in the region. Similarly, Helfer et al. (2012) examined temperature and evaporation trends in Australia, revealing that rising temperatures during spring and summer correspondingly increase annual average air temperature and evaporation rates. Goyal & Ojha (2014) utilized GCMs to assess the effects of climate change on temperature extremes and evaporation in the Rajasthan River Basin, India. Their analysis of historical data from 1948 to 2000 and projections for 2001 to 2100 indicated that the modified M5 decision tree model exhibited the highest accuracy in predicting both minimum and maximum temperature.

In the context of Lake Urmia, Azizi et al. (2017) evaluated the role of climate change in reducing water levels, highlighting the combined effects of increased agricultural water demands, which contributed to a 46% reduction in total inflow, alongside a 16% impact from climatic variables. Ahmadaali et al. (2018) further explored the consequences of climate change on sustainable agricultural development in the Lake Urmia region by employing the WEAP21 model to assess five water management scenarios. Their findings indicated that the scenario integrating improved crop patterns and enhanced irrigation efficiency yielded the most favorable environmental indicators for agricultural sustainability. These studies underscore the critical need for robust climate models to inform water resource management strategies amid the ongoing challenges posed by climate change.

In light of the ongoing global climate crisis, this study aims to address the significant challenge of accurately predicting evaporation rates in sensitive ecological zones, specifically the Quri Gol Wetland in Iran. The primary goal is to assess the impacts of climate change on evaporation by employing GCM and various diffusion scenarios (A2, B1, A1B). Furthermore, the research investigates the efficiency of statistical downscaling methods (SDSM and LARS-WG) for microscale evaporation simulation, a crucial step in understanding localized climate impacts. In addition, this study develops advanced data mining methods such as Gaussian process regression and support vector machine, comparing their performance against other robust machine learning models like random forest, gradient boosted tree, generalized linear model, and deep learning methods. The evaluation of these models through multiple performance metrics represents a comprehensive effort to improve the accuracy and reliability of evaporation forecasts.

The novelty of this study stems from the integration of advanced machine learning techniques with GCM projections to predict future evaporation under varying climate scenarios. Unlike previous studies that predominantly relied on empirical models or singular machine learning approaches, this research leverages a hybrid methodology that integrates GCM output with the best-performing machine learning model, offering a novel approach for regional climate adaptation strategies. This dual-method comparison contributes to filling a gap in the existing literature where the combination of statistical downscaling and cutting-edge data mining techniques has not been thoroughly explored. By focusing on the Quri Gol Wetland, the study not only provides valuable insights for local environmental and water management but also offers a model that can be adapted to other

regions globally. This research advances the science of hydrology by offering a scalable framework that can enhance climate resilience planning, especially in regions vulnerable to evaporation changes driven by climate variability.

2. Methods and Material

2.1 Study area

Quri Gol Wetland is located in the East Azerbaijan province of Iran, approximately 40 kilometers southeast of the provincial capital, Tabriz. Situated at an altitude of 1890 meters above sea level, the wetland covers an area of about 200 hectares. Geographically, it lies between 37°55′N latitude and 46°42′E longitude. This wetland is surrounded by the Sahand Mountain range, which significantly influences its climate and hydrology.

Quri Gol Wetland is located in a semi-arid to arid climate zone, characterized by cold winters and warm, dry summers. The region experiences significant temperature variations due to its altitude and geographic location. Annual precipitation is relatively low, averaging around 300-400 mm, with the bulk of rainfall occurring in the spring and autumn months. Winter precipitation is primarily in the form of snow, contributing to the wetland's water supply as it melts in the warmer months. The wetland is primarily fed by seasonal rainfall, snowmelt, and a few small streams originating from the surrounding mountains. Evaporation rates are high during the summer, significantly influencing the water balance of the wetland, especially under the pressures of climate change.

Quri Gol is a freshwater, endorheic (closed basin) wetland, meaning it does not drain into any sea or ocean. Its hydrology is heavily dependent on the balance between precipitation, runoff, and evaporation. The wetland's water level fluctuates seasonally, with higher levels in spring and early summer due to snowmelt and precipitation, followed by a reduction during the hot, dry summer months due to increased evaporation. One of the key environmental challenges facing Quri Gol Wetland is water loss through evaporation. Due to its relatively shallow depth and open surface area, the wetland is highly susceptible to evaporative water loss, which is exacerbated by rising temperatures and changing precipitation patterns associated with climate change.

Quri Gol Wetland's unique hydrological and climatic conditions, coupled with its ecological significance and vulnerability to climate change, make it a crucial area for studying evaporation and water resource management. Understanding the impacts of climate variability on this wetland will contribute valuable insights for managing similar ecosystems facing the pressures of changing environmental conditions. In this study, the meteorological data of maximum and minimum temperature, solar radiation, precipitation, and evaporation on a daily scale from Tabriz weather station were used over a 30-year period (1991-2020) to provide a comprehensive understanding of the evaporation dynamics in the wetland. Figure 1 illustrates the study area, highlighting the geographical context of this research.

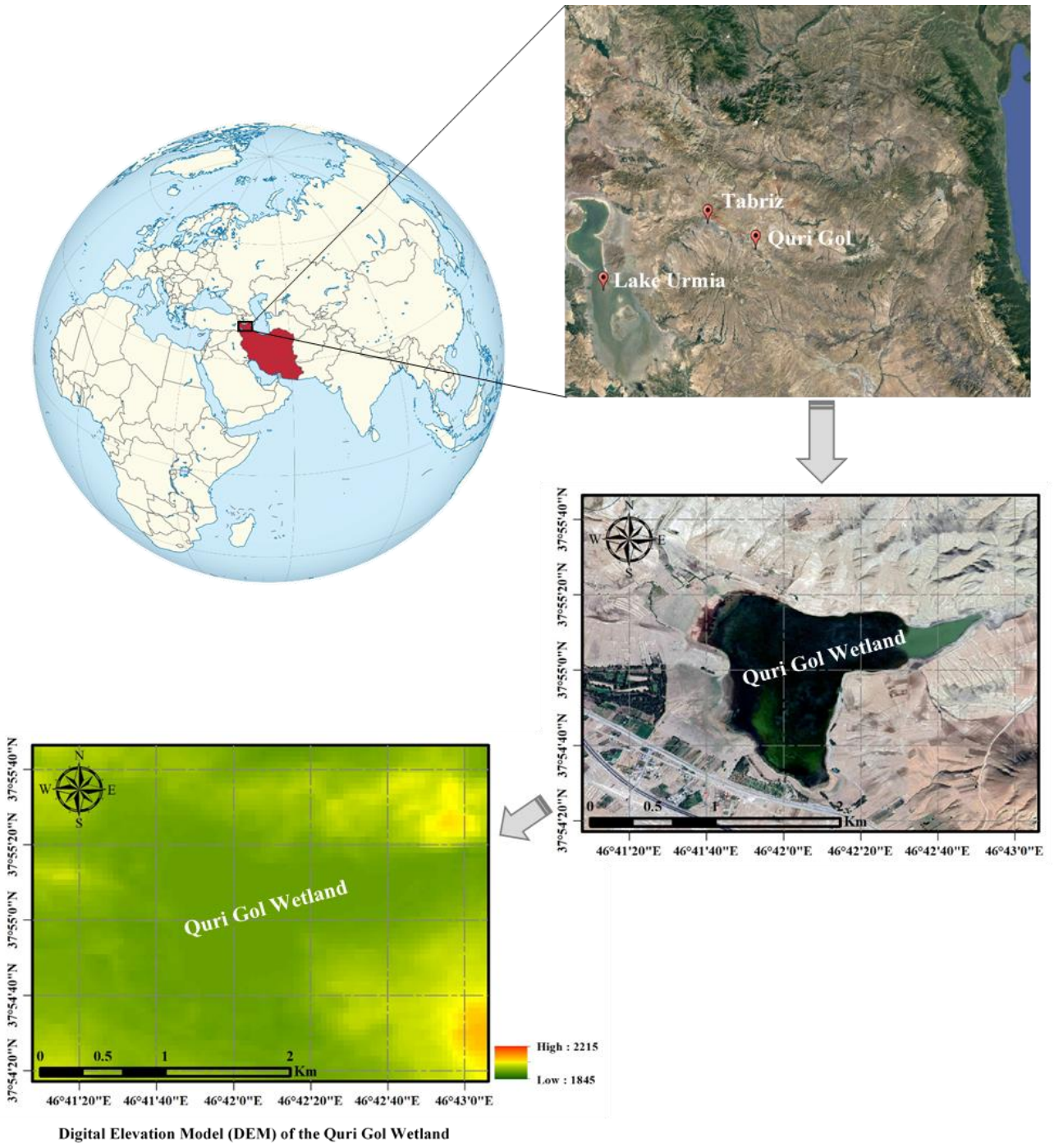

Figure1- Geographical context of the study area, (Sourced from ASTER GDEM)

In this study, the input parameters for evaporation modeling were selected based on their correlation with evaporation rates, ensuring that the most relevant meteorological variables were chosen to optimize model accuracy. The combinations of input parameters are structured to progressively increase complexity, starting with the most basic meteorological data and expanding to include additional variables that influence evaporation. The first combination (I) uses maximum (Tmax) and minimum (Tmin) temperatures as inputs, which are essential for evaporation as temperature directly influences energy availability for the evaporation process. In the second combination (II), solar radiation (Radi.) is added to account for the additional energy input from the sun, a critical factor driving the evaporation rate. The third and most comprehensive combination (III) includes Tmax, Tmin, solar radiation, and precipitation (Prec.), which introduces the role of water availability and atmospheric moisture. The combination of these parameters was determined by evaluating their correlation coefficients with evaporation, ensuring that the selected variables have the highest predictive power for the evaporation process. This approach allows for a systematic exploration of how adding more meteorological data impacts the accuracy of the model, providing a thorough understanding of the most significant contributors to evaporation in the study area. The specific combinations of input variables are detailed in Table 1.

Table1- Input combinations for evaporation modeling using machine learning methods

Combination number	*Input*	*Output*
I	T_{max}, T_{min}	Evap.
II	T_{max}, T_{min}, Radi.	Evap.
III	T_{max}, T_{min}, Radi., Prec.	Evap.

To strengthen the study's robustness, LARS-WG (Long Ashton Research Station Weather Generator) and SDSM (Statistical DownScaling Model) models were implemented to estimate future meteorological data. The LARS-WG model generates synthetic weather data that retain the essential statistical characteristics of historical climatic observations on a daily scale. The SDSM model downscales large-scale atmospheric data to local meteorological variables, thereby increasing the spatial resolution of future climate projections. To ensure the models' accuracy, a rigorous validation process was conducted, comparing the generated data to historical records using performance metrics. This validation demonstrated the models' reliability in capturing key climatic trends. Additionally, an uncertainty analysis was performed to account for potential discrepancies arising from model assumptions, parameter choices, and the inherent variability in climate scenarios. By thoroughly discussing the implementation, accuracy, and uncertainties of the LARS-WG and SDSM models, the robustness of the results is underscored. The predictive meteorological data obtained from these models were subsequently utilized as inputs for the best-performing machine learning model, enabling precise calculations of future evaporation rates under various climate change scenarios. This comprehensive approach bolsters the credibility and reliability of our findings.

2.2 Methods

2.2.1 Random forest (RF)

RF is a technique that utilizes an ensemble of tree-based algorithms to generate repeated forecasts for individual instances. Single decision trees often suffer from overfitting and limited generalizability. Minor changes in training data can significantly alter the structure of a decision tree (Quinlan, 1993). In contrast, RF is adept at learning complex patterns and accounting for the nonlinear relationships between explanatory and dependent variables. Additionally, RF's ability to handle non-normally distributed data allows it to incorporate and integrate diverse data types in the analysis.

The process of combining multiple decision trees is known as ensemble learning. An ensemble consists of several base learners, which are individual models typically generated from training data using base learning algorithms, such as decision trees, neural networks, or other methods. The generalizability of an ensemble model generally surpasses that of its individual base learners. Ensemble methods are particularly valued for their capacity to enhance the performance of weaker models (Schapire 1990).

RF, an advanced method derived from decision tree algorithms, combines the predictions of multiple individual models by employing predefined rules. The fundamental principle of ensemble learning techniques is based on the hypothesis that they are more accurate than single-model training algorithms. This increased accuracy arises from the idea that a collection of predictive models outperforms any single model. Furthermore, ensembles amplify the strengths of individual models while simultaneously mitigating their weaknesses (Kostantis & Pintelas 2004).

2.2.2 Gradient boosted tree (GBT)

The GBT procedure is one of the best learning algorithms and performs categorization with excellent exactitude for many datasets. In this method, the trees are trained one after the other. Each individual tree is mainly instructed with records that were misclassified by the foregoing tree (Malohlava & Candel 2018). This causes the model to concentrate more on intricate cases and less on problems that are straightforward to forecast. Consequently, this approach yields superior outcomes compared to numerous methods, including the linear regression technique and the bagging approach (Breiman 2001). The basic idea of this method was proposed by Breiman (1999) as a method that can interpret the optimization algorithm on a suitable cost function.

2.2.3 Support vector machine (SVM)

Support vector machine is among the directed learning techniques applicable for both categorization and regression tasks. This approach is grounded in the statistical learning framework proposed by Vapnik (1995). SVM is a technique for binary categorization in any given feature space, making it an appropriate technique for forecasting issues (Vapnik 1998). The SVM fundamentally operates as a binary classifier that distinguishes classes with a linear separator. In this technique, the examples nearest to the decision margin are termed support vectors. These vectors define the formula of the decision margin Traditional intelligent modeling techniques, like artificial neural networks, typically aim to reduce the absolute size of the error or the cumulative sum of the squared errors of the training data, whereas SVM models employ the concept of minimal structural error. Using the concept of internal product multiplication, Vapnik demonstrated that the input vector x could first be transferred by a nonlinear conversion to a space with a large dimension, in which space performed the internal product and proved that if a kernel were symmetric, the condition of the theorem could be reviewed. Applying this kernel in a low-dimensional input space can

greatly reduce the product. If the input vector xi is mapped to the specific space by the nonlinear function Φ(x), the decision function will look like Eq (1):

$$f(w.x)=w.\Phi(x)+b \quad (1)$$

Where; w and b are the function parameter vectors. The problem of nonlinear regression can be like the problem of optimization as Eq. (2)

$$\min 1/2 \sum_{ij}^{1} [\![(\partial_i - [\![\partial_i]\!]^*)([\![\partial_j - [\![\partial_j]\!]^*)\times\langle\Phi(x_i).\Phi(x_j)\rangle$$

$$+\varepsilon\sum_{(i=1)}^{1} [\![(\partial_i - [\![\partial_i]\!]^*)]\!] -\sum_{(i=1)}^{1} [\![y_i (\partial_i = [\![\partial_i]\!]^*)]\!] \quad (2)$$

Express with the following limitations (Hamel 2009):

$$\sum_{ij}^{1} [\![(\partial_i - [\![\partial_i]\!]^*)=0]\!]$$
$$0\leq\partial_i\leq C, \quad i=1,2,\ldots l$$
$$0\leq [\![\partial_i]\!]^*\leq C, \quad i=1,2,\ldots l \quad (3)$$

Where; ε is the error tolerances, ∂i and ∂i* are the LaGrange coefficients, C is the cost constant, and <Φ(xi).Φ(xj)> is the internal multiplication of the Φ(xi) and Φ(xj) functions.

2.2.4 Gaussian process regression (GPR)

Gaussian processes represent intricate machine learning algorithms employed for predictive modeling (Williams & Rasmussen 1996) and classification (Williams & Barber 1998). The Gaussian process comprises a collection of random variables, any finite number of which adhere to Gaussian distributions. The Gaussian process is entirely defined by its mean function m(x) and its covariance function k(x, x'). It naturally extends the Gaussian distribution, wherein the mean and covariance are represented by a vector and a matrix, respectively (refer to Eq 4).

$$f\sim GP(m,k) \quad (4)$$

Regression models utilizing Gaussian processes operate on the premise that observations are mutually informative. Gaussian processes specify priors directly within the function space, thereby extending Gaussian distribution principles, where the mean and covariance are represented as vectors and matrices, respectively. Unlike Gaussian distributions which apply to vectors, Gaussian processes apply to functions. Consequently, models based on Gaussian processes inherently comprehend functional and data interdependencies, obviating the need for a separate validation process for generalization. This inherent understanding facilitates the testing of GPR models.

2.2.5 Deep learning (DL)

Deep Belief Networks (DBNs) are recognized as some of the most powerful algorithms in the field of DL. These networks are constructed by combining multiple nonlinear transformations designed to provide a richer and more useful representation of existing data (Bengio 2009). As the number of layers in a neural network increases, the complexity of the optimization problem also escalates (Keyvanrad & Homayounpour 2015). To address this challenge, one of the training methods used for these networks involves unsupervised pre-training algorithms. In this approach, each layer is trained individually at first, followed by a precise and integrated fine-tuning of the entire network (Bengio 2009). In addition to structural differences, Deep Belief Networks and MLPs differ significantly in their training methodologies. For instance, employing backpropagation in training Deep Belief Networks can result in the vanishing gradient problem (Hinton & Osindero 2006).

In Deep Belief Networks, the training process begins with a Restricted Boltzmann Machine (RBM). Once trained, the hidden layer of the RBM becomes the input for the next RBM. This sequential training continues, with each layer being trained based on the output of the previous layer (Glorot & Bengio 2010).

2.2.6 Generalized linear model (GLM)

GLMs are analytical tools for different types of data, and their mathematical relationships were developed by Nelder & Baker (1972). The theory of this model was developed by McCullagh (1984) and applied to hydrology and meteorology by Chandler & Wheater (2002). GLMs include a wide range of statistical models such as linear regression for normally distributed responses, logistic models for binary data, linear models for counting data, and many other useful statistical models through their general method. GLMs can be used when observations of the normal distribution do not exist and when other regression model methods

are not appropriate. This model's effectiveness is satisfactory when compared to conventional modeling techniques (Pregibon & Hastie 2017). These models have been developed with the aim of reducing limiting assumptions in linear regression and can consider dependent variables from any probabilistic distribution of the exponential family (such as binomial distribution, gamma distribution, Poisson distribution, or normal distribution). In GLMs, instead of a response variable, a transformation of the response variable is modeled using a link function.

2.2.7 Statistical down scaling model (SDSM)

The statistical downscaling model employs a dual-step conditional resampling approach for downscaling purposes (Wilby et al. 2007). Initially, this technique downscales predictor variables like temperature and precipitation through integrated regression and stochastic weather generation methods, followed by replication at the station's site (Tatsumi et al. 2013). In fact, SDSM is a combination of the generative method of statistical meteorology and transformed functions. This model was first prepared by Wilby et al. (2002) under the title of version 2.1 in England. This approach relies on employing a mix of regression techniques and the creation of artificial weather data to achieve downscaling. In this model, the local climate is expressed by the macro-scale climate of the region in the form R = F(X), where R represents the small-scaled local climate variable, X is an array of large-scale climatic factors, and F is a subordinate of determination conditional on X, which is obtained based on training and validation of historical data. This model is one of the most widely used downscaling statistical tools that has many applications in meteorological, hydrological, geographical, and environmental studies (Wilby & Harris 2006). Because in this method, large-scale daily circulation templates, such as atmospheric humidity variables, are used on a station scale, it is used when quick and low-cost estimation of climate changes is needed, and in the case of random weather generators and methods of transformed functions, the results can be obtained. This program performs statistical downscaling in five separate steps (Wilby et al. 2002): 1) Screening predictor variables, 2) Model calibration, 3) Feedback of producing observational data artificially, 4) Production of climate change scenarios, and 5) Troubleshooting test and statistical analysis. Figure 2 illustrates the SDSM model's method for downscaling and creating climate scenarios.

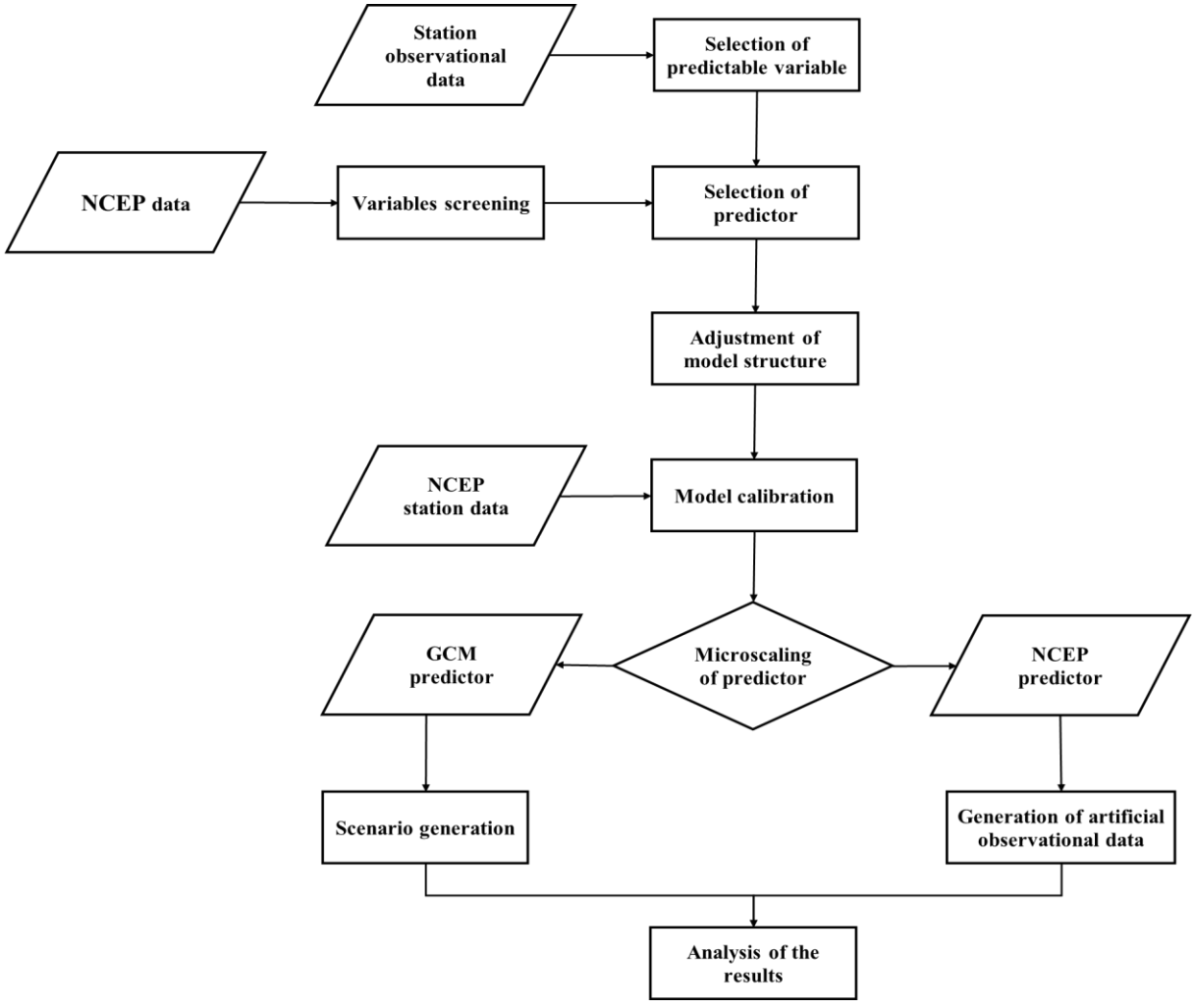

Figure 2- Process of downscaling and climate scenario generation by the SDSM model

2.2.8 Long ashton research station weather generator (LARS-WG)

The Long Ashton Research Station Weather Generator model stands out as a renowned tool for producing stochastic weather data, offering greater utility through iterative computations, minimal data requirements, and straightforward, effective operation (Hay et al. 2000; Dibike & Coulibaly 2005; Kilsby et al. 2007). This model was first presented by Roscoe et al. (1991) and then amended and advanced by Semnoff et al. (1998) at the Langston Research Center. The main reason for producing this model was to surmount the weaknesses of the Markov chain. The 6th version of this model (LARS-WG6) was updated and published in 2018 to microscale the data of the fifth report (CIMP5). Currently, this model is used for two purposes: producing future daily data artificially and generating data for a time frame or stations without statistics.

To generate synthetic data, the model compares long-term daily data (at least 30 years) related to the station (temperature, precipitation, sunshine hours) as inputs. If these two categories of data match, the model is able to produce future time series. For the second function, i.e., generating data for stations without information, the model uses the data of the closest station to the unknown station, checks these data and their statistical characteristics, and due to the same climatic characteristics of these two stations' proximity to each other, uses the data of the known station and their statistical characteristics to generate data for the unknown station. Despite its simpler simulation process and data requirements, this microscaling model possesses a strong predictive capacity for climate change (Semenov & Stratonovitch 2010).

This model's inputs include daily average low and high temperatures, mean precipitation, and hours of sunlight per day. The process of predicting future data is done by this model in four stages:

1. Basic data analysis: Analyzing the statistical characteristics of observational data for the purpose of establishing the statistical characteristics of the data.

2. Initial data generation: Artificially generating data by the model in the base period and determining the statistical attributes of the generated artificial data.

3. Statistical comparison: Matching and comparing the analytical characteristics of observational data and synthetic data.

4. Production of daily data in the future: Using the statistical characteristics of basic data, greenhouse gas emission scenarios, and the output of GCM in the production of daily time series projected into the future with identical statistical characteristics of the basic data.

2.3 Error evaluation indicators

To evaluate the performance of various models, several statistical indicators were employed: the coefficient of determination (R^2), mean absolute error (MAE) to assess the consistency between observed and modeled data, the scatter index (SI) to compare measured values with computed values, Willmott's index (WI) to evaluate the agreement between observed and estimated data, and the Kling-Gupta efficiency (KGE), which provides a comprehensive measure of model performance by accounting for correlation, bias, and variability. The equations for these indicators are presented in Equations (5) to (10).

$$R^2=1-(\sum_{i=1}^{N}〖(O_i-P_i)^2〗)/(\sum_{i=1}^{N}〖(O_i-\bar{O})^2〗) \quad (5)$$

$$MAE=(\sum_{i=1}^{N}(|O_i-P_i|))/N \quad (6)$$

$$SI=\sqrt{((\sum_{i=1}^{N}〖(O_i-P_i)^2〗)/n)}/\bar{O} \quad (7)$$

$$WI=1-[(\sum_{i=1}^{N}〖(O_i-P_i)^2〗)/(\sum_{i=1}^{N}(|P_i-\bar{O}|+|O_i-\bar{O}|)^2)] \quad (8)$$

$$KGE=1-\sqrt{((r-1)^2+(\alpha-1)^2+(\beta-1)^2} \quad (9)$$

In equations (5) to (9), Oi and Pi represent the observed and predicted (calculated) values, respectively, while $\bar{O}$ denotes the average of the observed values, and N is the total number of observations. For equation (9), which corresponds to the KGE, r is the linear correlation coefficient between the observed and simulated data, measuring the strength of their relationship. α represents the ratio of the standard deviation of the simulated data (σsim) to the standard deviation of the observed data (σobs), indicating variability. Additionally, β denotes the ratio of the mean of the simulated data to the mean of the observed data, representing the bias between the two datasets.

The machine learning models employed in this study were developed using RapidMiner Studio 9.10 software, which provides a robust platform for data analysis and predictive modeling.

Figure 3 shows a schematic structure of methods adopted in this study.

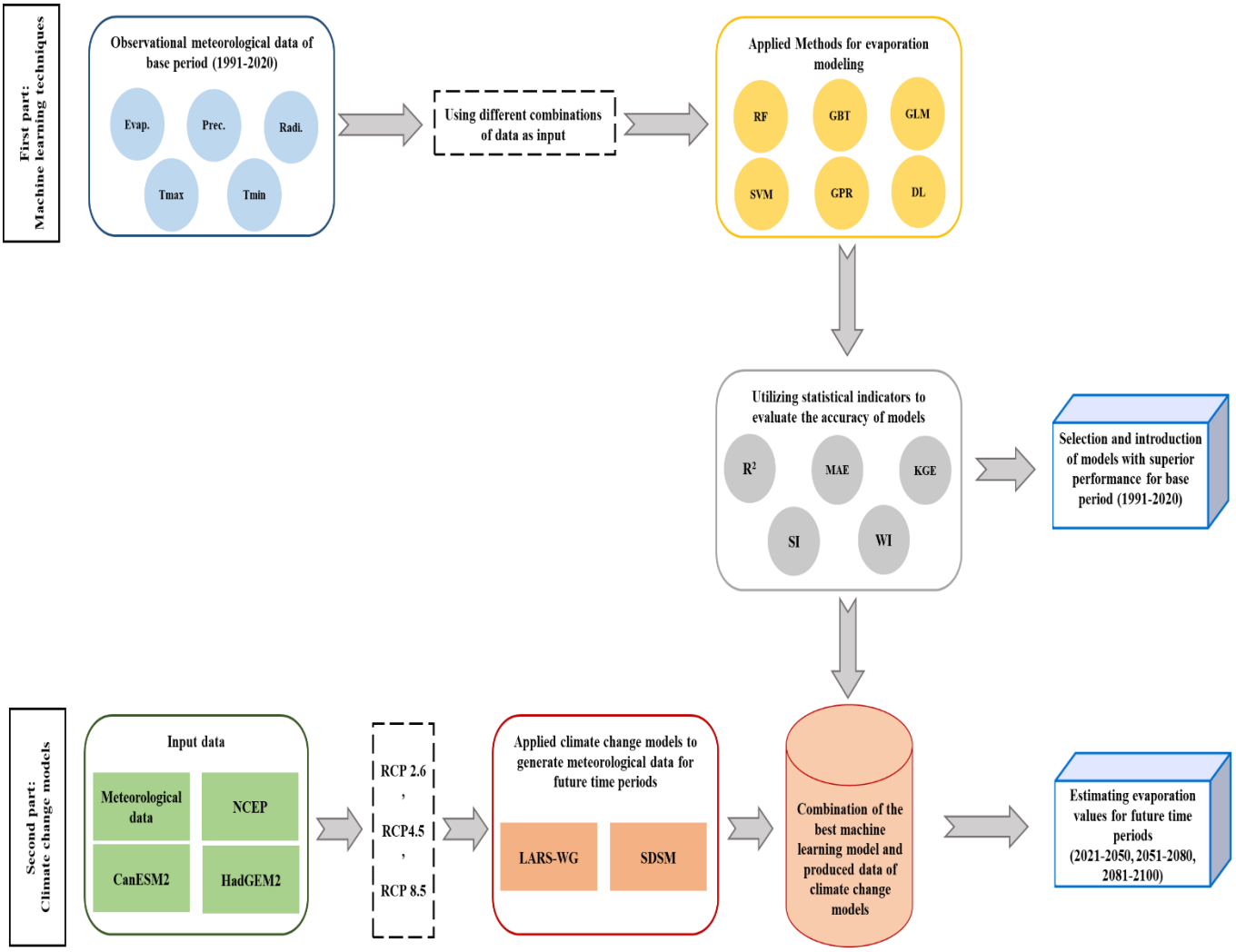

Figure 3- Schematic structure of methods adopted in this study

3. Results

In this study, daily evaporation values for the Quri Gol Wetland were estimated using six machine learning models: RF, GBT, SVM, GPR, GLM, and DL over a 30-year period (1991-2020). The input data included minimum and maximum temperatures, precipitation, and solar radiation, which were combined into three different scenarios. A 70-30% data split was applied, with 70% of the data used for model calibration and 30% for validation. In addition, climate change models were employed to predict future meteorological parameters under three Representative Concentration Pathway scenarios (RCP 2.6, RCP 4.5, and RCP 8.5) for future periods (2021-2050, 2051-2080, and 2081-2100). The estimated meteorological values from these climate change models were then used as inputs to the best-performing machine learning model to predict evaporation for future periods, and the results were compared to the observed evaporation values of the base period.

In this section, the results first evaluate the performance of the machine learning models for the base period, followed by an assessment of the combined machine learning-climate change models.

3.1 Performance of machine learning models

Table 2 presents the statistical parameters, including the coefficient of determination, mean absolute error, scatter index, Willmott's index, and Kling-Gupta efficiency for the machine learning models during the calibration phase.

Table 2- Statistical parameters (R^2, SI, MAE, WI and KGE) values of studied machine learning models in calibration section

Method	*Scenario*	*R^2*	*SI*	*MAE*	*WI*	*KGE*
RF	I	0.811	0.425	0.879	0.946	0.152
	II	0.829	0.405	0.838	0.951	0.143
	III	**0.839**	**0.394**	**0.822**	**0.954**	**0.139**
GBT	I	0.808	0.540	1.391	0.874	0.448
	II	0.833	0.523	1.349	0.883	0.441
	III	0.839	0.519	1.339	0.885	0.439
GLM	I	0.720	0.517	1.221	0.915	0.215
	II	0.729	0.508	1.192	0.919	0.208
	III	0.730	0.507	1.191	0.919	0.207
SVM	I	0.755	0.485	1.005	0.930	0.175
	II	0.759	0.481	0.996	0.931	0.171
	III	0.761	0.479	0.993	0.932	0.170
GPR	I	0.751	0.489	1.019	0.929	0.174
	II	0.736	0.507	1.053	0.924	0.175
	III	0.755	0.489	1.040	0.928	0.176
DL	I	0.771	0.466	0.979	0.934	0.180
	II	0.776	0.462	0.988	0.934	0.186
	III	**0.779**	**0.459**	**0.964**	**0.938**	**0.161**

Table 2 shows the performance of the machine learning models during the calibration phase across three different scenarios. For all methods, the results demonstrate relatively strong performance across the statistical metrics, with RF and GBT generally showing higher R^2 values, indicating better model fit during the calibration phase. Particularly, the RF method achieves the highest R^2 values across all three scenarios, reaching a maximum of 0.839, which suggests a strong correlation between predicted and actual evaporation rates. Additionally, the DL model exhibits competitive performance, with R^2 values ranging from 0.771 to 0.779, showing its ability to capture complex patterns in the data. Moreover, WI values for all methods are consistently above 0.90, indicating high agreement between observed and predicted values. However, models such as the GLM and SVM show slightly lower performance, with higher SI and MAE values. Despite this, the KGE values indicate that all models, while varied in their predictive abilities, perform reasonably well, with RF and GBT models being the most effective overall during calibration. Table 3 presents the statistical parameters (R^2, SI, MAE, WI, and KGE) for the machine learning models in the validation phase, providing an assessment of the models' performance on unseen data. This phase of the analysis is crucial as it reflects the models' ability to generalize beyond the training data, ensuring they are reliable for real-world applications such as evaporation prediction.

Table 3- Statistical parameters (R^2, SI, MAE, WI and KGE) values of studied machine learning models in validation section

Method	*Scenario*	*R^2*	*SI*	*MAE*	*WI*	*KGE*
RF	I	0.809	0.426	0.924	0.943	0.196
	II	0.820	0.417	0.902	0.946	0.200
	III	**0.821**	**0.414**	**0.902**	**0.946**	**0.196**
GBT	I	0.802	0.558	1.489	0.861	0.478
	II	0.810	0.554	1.478	0.863	0.478
	III	0.814	0.550	1.471	0.865	0.475
GLM	I	0.764	0.473	1.190	0.927	0.226
	II	0.775	0.467	1.159	0.928	0.237
	III	0.774	0.467	1.160	0.928	0.237
SVM	I	0.799	0.436	0.956	0.943	0.170
	II	0.807	0.428	0.933	0.945	0.180
	III	0.809	0.426	0.932	0.945	0.179
GPR	I	0.770	0.471	1.029	0.931	0.213
	II	0.746	0.500	1.090	0.922	0.231
	III	0.766	0.477	1.044	0.927	0.233
DL	I	0.816	0.420	0.932	0.944	0.206
	II	0.813	0.433	0.972	0.938	0.239
	III	**0.822**	**0.411**	**0.915**	**0.947**	**0.193**

According to Table 3, in the validation phase, RF and DL emerge as the best-performing models across all statistical parameters. Both models maintain high R^2 values, with RF showing values between 0.809 and 0.821, and DL performing similarly well with R^2 values ranging from 0.813 to 0.822. This indicates that both models exhibit a strong correlation between predicted and observed values, confirming their ability to accurately predict evaporation rates. Additionally, the low SI values for both models, ranging from 0.411 to 0.426, demonstrate minimal error spread, which further supports their precision. These low SI values indicate a tight clustering of predicted data around the observed values, highlighting the high predictive capability of these models in evaporation forecasting.

The MAE values, which measure the average magnitude of the errors between predicted and observed values, also favor RF and DL models. DL models consistently record low MAE values between 0.915 and 0.972, while RF models show slightly lower error margins, ranging from 0.902 to 0.924. These results suggest that DL and RF are particularly adept at minimizing the deviation between predicted and observed evaporation values, making them highly reliable for accurate predictions. Furthermore, the WI values for these models are exceptionally high, with RF scoring between 0.943 and 0.946 and DL between 0.938 and 0.947. The near-perfect WI values indicate strong agreement between the predicted and observed values, reinforcing the reliability of these models.

A significant feature of the analysis is the KGE, which combines aspects of correlation, variability, and bias to offer a comprehensive assessment of model performance. RF and DL again demonstrate balanced performance, with KGE values ranging from 0.193 to 0.239, indicating that these models not only predict evaporation accurately but also capture the overall variability and distribution of the data.

On the other hand, models like GBT and GLM show moderate performance. While the R^2 values for GBT (0.802-0.814) and GLM (0.764-0.775) indicate reasonable correlation, they fall short of the performance seen in RF and DL. This limitation is further reflected in their SI values, where GBT shows higher error spreads (0.550-0.558), signalling reduced precision. Also, the MAE values for GBT (1.471-1.489) are significantly higher than those for RF and DL, indicating that GBT struggles to minimize errors as effectively. Similarly, GLM's MAE values (1.159-1.190) show a lower degree of accuracy compared to the top models. Despite these weaknesses, GLM maintains relatively high WI values (0.927-0.928), indicating that while it may struggle with error minimization, it still demonstrates reasonable agreement between predicted and observed values.

SVM and GPR models occupy an intermediate position in terms of performance. Both models perform reasonably well, with R^2 values close to 0.8, which suggests they can adequately capture the relationship between the inputs and evaporation. SVM models perform particularly well in terms of error minimization, with low MAE values (0.932-0.956) and SI values comparable to those of RF and DL. However, both SVM and GPR models exhibit slightly lower KGE values, indicating potential challenges in balancing bias and variability.

With a general review of the results, RF and DL emerge as the most reliable models for predicting evaporation, demonstrating superior performance across all metrics. The best RF model, particularly in Scenario III, displayed a high R^2 (0.821), low SI (0.414), and a minimal MAE (0.902). Similarly, the DL model, especially in Scenario III, achieved the highest R^2 (0.822), a low SI (0.411), and the lowest MAE (0.915). Both models offer accurate, consistent, and reliable predictions, with low error margins and strong agreement between predicted and observed values. The slightly weaker performance of GBT and GLM suggests that these models may not be as suited for tasks requiring high precision in evaporation prediction, though they still offer a reasonable degree of accuracy. SVM and GPR, while not as robust as RF or DL, offer solid performance but may require further refinement to handle variability and bias more effectively. Overall, the validation results highlight the capability of machine learning models to accurately predict complex hydrological processes like evaporation, with RF and DL proving to be the most effective approaches for this task.

The comparison of calibration and validation results reveals the consistency and reliability of the machine learning models across different phases of evaluation. During the calibration phase, all models demonstrated satisfactory performance, with RF and DL models emerging as the most effective, achieving higher values for metrics such as R^2, WI, and KGE, alongside lower MAE and SI. This strong performance was maintained in the validation phase, where RF and DL models continued to exhibit superior predictive accuracy, though there was a slight decrease in performance compared to the calibration phase, which is common in model testing on unseen data. The consistent performance across both phases indicates that these models can generalize well beyond the training data, offering reliable predictions even under new conditions. Other models, such as GBT and GLM, showed moderate performance, particularly in validation, where a slight increase in MAE and SI was observed, signaling that they may be more prone to overfitting. Overall, as stated above, the results indicate that RF and DL are the most robust and adaptable models for predicting evaporation. Figure 4 provides a comparative visual representation of the simulated and observed evaporation values for the superior scenarios across all six machine learning models. The primary aim of this figure is to evaluate how effectively each model captures the temporal dynamics of evaporation rates over the study period.

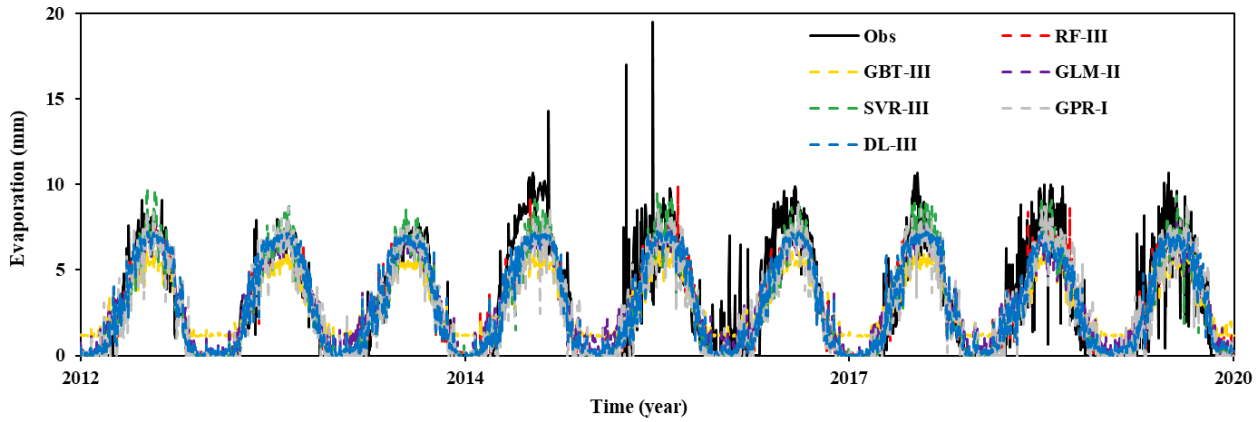

Figure 4- Variation diagrams of simulated and observed evaporation values for the superior scenarios in all six methods

As illustrated in Figure 4, the alignment between the observed and simulated values demonstrates the ability of each model to track real-world variations in evaporation. Both RF and DL show strong agreement with the observed data, reflecting minimal deviations and closely following the seasonal fluctuations of evaporation. This is particularly significant, as it indicates that these models can accurately capture the complex nonlinear interactions between meteorological variables that influence evaporation. The consistent performance of RF and DL, with their ability to maintain accuracy across different time scales and scenarios, underscores their robustness and reliability in modeling evaporation processes. In contrast, models like GLM and SVM exhibit more noticeable discrepancies between observed and simulated values. This suggests that these methods may struggle with capturing the full complexity of evaporation patterns, particularly during peak evaporation periods or abrupt changes in climatic conditions. The larger deviations observed with these models could be attributed to their relatively linear nature (in the case of GLM) or their sensitivity to specific parameter choices (in the case of SVM), which may limit their flexibility in modeling evaporation dynamics. Furthermore, the overall trend illustrated in Figure 4 highlights the seasonal and annual fluctuations in evaporation, with most models effectively capturing the general trend. However, the precision and fit to the data vary depending on the model, with RF and DL demonstrating superior performance in both accuracy and consistency. This visual comparison not only reinforces the quantitative findings from the calibration and validation phases but also provides a clear indication of the predictive strength of RF and DL, especially in handling seasonal variations and sudden shifts in evaporation rates. The figure thus serves as a critical tool for assessing model accuracy in simulating evaporation, offering valuable insights into the strengths and limitations of each approach. The strong performance of RF and DL is particularly noteworthy, as these models demonstrate the capacity to adapt to the inherent variability of evaporation, making them well-suited for hydrological applications in climate-sensitive regions. Figure 5 presents the distribution diagrams comparing the simulated and observed evaporation values for the superior scenarios using the six machine learning models. This figure provides a more detailed statistical view by focusing on how well the models replicate the distributional characteristics of the observed data, particularly in terms of variability, spread, and the prediction of extreme values.

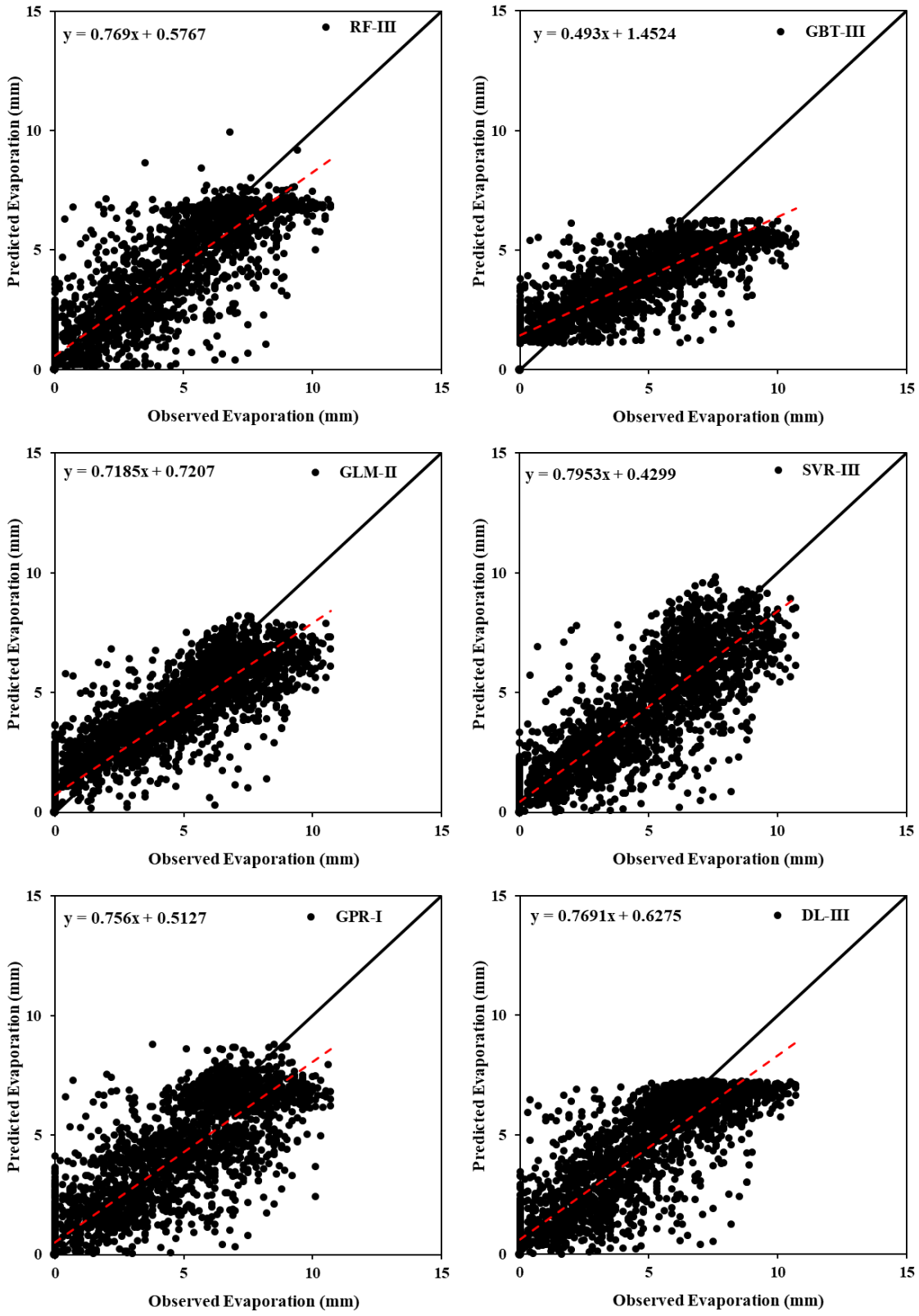

Figure 5- Distribution diagrams of simulated and observed evaporation values for the superior scenarios in all six methods

The distribution plots allow for a deeper examination of the models' ability to capture not just the mean values but also the full range of evaporation rates. As shown in Figure 5, RF and DL once again show a strong alignment with the observed distributions, demonstrating their capability to not only model average evaporation levels but also to accurately reflect the variability and extremes within the dataset. This indicates that both models have a high degree of generalizability and are able to predict not only typical evaporation rates but also more extreme values, which are often critical for understanding hydrological changes under climate stress. The closeness of the simulated distributions to the observed ones for RF and DL suggests that these models effectively handle the inherent variability in evaporation data, including the tail ends of the distribution where extreme

evaporation values may occur. This ability to model variability is crucial in climate change projections, as shifts in extreme values can have significant implications for water resource management. RF and DL's proficiency in capturing both central tendencies and extreme values enhances their applicability for real-world hydrological forecasting and management. Other models, such as GLM and GBT, display greater deviations from the observed distribution shapes. This suggests that while these models may perform adequately for predicting mean evaporation values, they are less adept at capturing the full range of data, particularly at the higher and lower ends of the distribution. The larger spread observed in the GBT model's predictions, for instance, indicates that it may struggle with outlier predictions, making it less reliable in scenarios where accurate modeling of extremes is necessary. Similarly, GLM's inability to capture nonlinear relationships may contribute to its reduced accuracy in reflecting the variability of evaporation values.

By visually comparing the range and distribution of evaporation rates, Figure 5 provides essential insights into the models' ability to handle variability, which is a critical aspect of hydrological forecasting. The clear superiority of RF and DL in these distribution diagrams corroborates earlier quantitative results, reaffirming their role as the most effective models for evaporation prediction in this study. The results also highlight the need for caution when using models such as GLM and GBT in applications where the prediction of extreme or highly variable values is essential. This distribution-based evaluation adds another layer of depth to the overall analysis, providing further evidence that RF and DL models are not only effective in general prediction accuracy but also in handling the distributional complexities of evaporation data, making them suitable for diverse hydrological applications under climate change scenarios.

3.2. Future projections of evaporation and precipitation

Table 4 provides a detailed projection of evaporation values for future periods (2021-2050, 2051-2080, and 2081-2100) using two climate change models, LARS-WG and SDSM, under three different Representative Concentration Pathways (RCP 2.6, RCP 4.5, and RCP 8.5). These models provide critical insight into how climate change is expected to affect evaporation rates in the study area.

Based on the data presented in Table 4, in the period from 2021 to 2050, the LARS-WG model shows a considerable increase in average evaporation values across all scenarios compared to the base period (1991-2020). For example, under the RCP 2.6 scenario, evaporation is projected to increase by 30.40%, while under RCP 8.5, this rise reaches 31.30%. The cumulative evaporation values reflect this trend, showing a significant increase, with the largest being 10565.5 mm under RCP 8.5. On the other hand, the SDSM model also predicts an increase in evaporation, though to a lesser extent than LARS-WG. The SDSM model shows a rise of 5.08% to 11.11% in evaporation across the RCP scenarios, with the RCP 8.5 scenario showing the highest cumulative evaporation increase of 3749.65 mm. Although both models project rising evaporation levels, the LARS-WG model consistently predicts a more substantial increase than the SDSM model. The next period, 2051-2080, follows the same trend, but the rate of increase in evaporation becomes more pronounced. The LARS-WG model shows that cumulative evaporation increases between 33.97% (RCP 2.6) and 41.79% (RCP 8.5). In this period, the average evaporation values rise steadily as well, with a noticeable increase in cumulative evaporation for all scenarios, particularly in the RCP 8.5 scenario, where it reaches 14109.2 mm. Similarly, the SDSM model continues to project an increase in evaporation, though still at a lower magnitude than LARS-WG. In this period, the SDSM model estimates an increase of between 11.08% and 21.49% in average evaporation across the three scenarios, with cumulative values reaching up to 7253.03 mm increase under RCP 8.5. By the final period (2081-2100), the evaporation values predicted by both models have increased significantly compared to the base period, with LARS-WG projecting an even more substantial rise in evaporation. Cumulative evaporation values increase by 32.63% (RCP 2.6) to 50.01% (RCP 8.5), reflecting the growing impact of climate change. Under RCP 8.5, evaporation levels reach 33870.8 mm, demonstrating the severity of expected changes. Meanwhile, the SDSM model also shows continued increases, with cumulative evaporation values rising by 15.95% (RCP 2.6) to 30.14% (RCP 8.5). While the increase in evaporation projected by SDSM remains lower than that of LARS-WG, the rise is still substantial, signaling potential challenges for water management in the region. Overall, both models predict a significant rise in evaporation over the next century, though LARS-WG consistently projects higher rates, especially under the more extreme climate scenarios (RCP 8.5). This projection of substantial evaporation increases highlights the potential for intensified water stress and the need for adaptive strategies in water management.

Table 4- Statistical values of evaporation for future time periods using LARS-WG and SDSM models

Method	*Period*	*Scenario*	*Xmax*	*Xmin*	*Xmean*	***SX***	***SP - SO***
Observations	1991-2020	---	11.500	0.000	3.083	33758.2	---
	2001-2020	---	11.500	0.000	3.093	22579.4	---
LARS-WG	2021-2050	RCP 2.6	8.002	0.114	4.020	44020.2	+10262
		RCP 4.5	7.940	0.114	4.002	43816.5	+10058.3
		RCP 8.5	7.932	0.114	4.048	44323.7	+10565.5
	2051-2080	RCP 2.6	8.000	0.114	4.130	45226.1	+11467.9
		RCP 4.5	8.488	0.114	4.207	46068.3	+12310.1
		RCP 8.5	8.002	0.114	4.371	47867.4	+14109.2
	2081-2100	RCP 2.6	7.907	0.114	4.102	29948.0	+7368.62
		RCP 4.5	8.492	0.114	4.307	31440.6	+8861.21
		RCP 8.5	8.002	0.114	4.640	33870.8	+11291.4
SDSM	2021-2050	RCP 2.6	9.532	0.130	3.240	35474.3	+1716.06
		RCP 4.5	9.250	0.130	3.233	35406.8	+1648.57
		RCP 8.5	9.118	0.130	3.425	37507.9	+3749.65
	2051-2080	RCP 2.6	8.696	0.130	3.424	37498.1	+3739.89
		RCP 4.5	8.758	0.130	3.568	39072.3	+5314.14
		RCP 8.5	9.469	0.130	3.745	41011.2	+7253.03
	2081-2100	RCP 2.6	9.935	0.130	3.586	26180.9	+3601.53
		RCP 4.5	8.842	0.130	4.025	29384.1	+6804.74
		RCP 8.5	8.958	0.130	3.914	28569.0	+5989.61

Table 5 provides a projection of precipitation values for the same future periods (2021-2050, 2051-2080, and 2081-2100) using the LARS-WG and SDSM models under RCP 2.6, RCP 4.5, and RCP 8.5 scenarios.

As detailed in Table 5, unlike the substantial increases in evaporation presented in Table 4, the increase in precipitation is much smaller and varies across the models and scenarios. During the period from 2021 to 2050, the LARS-WG model shows relatively minor changes in cumulative precipitation. Under RCP 2.6, the cumulative precipitation slightly decreases by 106.78 mm, while in the more severe RCP 8.5 scenario, it increases by 530.52 mm, reflecting an increase of about 7%. This is far less than the concurrent rise in evaporation. The SDSM model similarly projects only modest changes in precipitation during this period, with cumulative precipitation increases ranging from 34.12 mm (RCP 2.6) to 321.72 mm (RCP 8.5). Although these projections indicate a slight increase in rainfall, the gap between rising evaporation and precipitation is stark, suggesting potential challenges for water resources in the future. For the 2051-2080 period, the LARS-WG model shows a further increase in precipitation under RCP 2.6 and RCP 8.5, but again, the changes remain modest in comparison to evaporation. Cumulative precipitation increases range from 510.12 mm (RCP 2.6) to 634.72 mm (RCP 8.5), representing an increase of approximately 8%. Similarly, the SDSM model shows a slight increase in cumulative precipitation, with a maximum increase of 330.52 mm under RCP 2.6. These results indicate that while precipitation will rise, the increase is not proportional to the expected rise in evaporation, leading to potential water deficits in the region. By the 2081-2100 period, the discrepancy between evaporation and precipitation becomes more pronounced. The LARS-WG model predicts cumulative precipitation increases of 156.21 mm (RCP 2.6) to 775.61 mm (RCP 8.5), representing a maximum increase of 16% under RCP 8.5. However, this increase is far lower than the corresponding rise in evaporation, which reaches 50.01% under the same scenario. The SDSM model also shows only slight increases in precipitation, with the highest cumulative increase being 234.51 mm under RCP 2.6. In the more severe RCP 8.5 scenario, the model even predicts a slight decrease in cumulative precipitation (-217.59 mm), further highlighting the growing gap between precipitation and evaporation.

Table 5- Statistical values of precipitation for future time periods using LARS-WG and SDSM models

Method	Period	scenario	Xmax	Xmin	Xmean	SX	SP – SO
Observations	1991-2020	---	46.4	0	0.668	7316.68	---
	2001-2020	---	46.4	0	0.662	4833.89	---
LARS-WG	2021-2050	RCP 2.6	46.8	0	0.658	7209.90	-106.78
		RCP 4.5	33	0	0.685	7501.00	+184.32
		RCP 8.5	37	0	0.717	7847.20	+530.52
	2051-2080	RCP 2.6	41.2	0	0.715	7826.80	+510.12
		RCP 4.5	41.2	0	0.654	7161.60	-155.08
		RCP 8.5	38.1	0	0.726	7951.40	+634.72
	2081-2100	RCP 2.6	37.2	0	0.684	4990.10	+156.21
		RCP 4.5	40.2	0	0.701	5117.80	+283.91
		RCP 8.5	42.3	0	0.768	5609.50	+775.61
SDSM	2021-2050	RCP 2.6	38.1	0	0.671	7350.80	+34.12
		RCP 4.5	39.9	0	0.676	7402.80	+86.12
		RCP 8.5	33.5	0	0.698	7638.40	+321.72
	2051-2080	RCP 2.6	38.9	0	0.698	7647.20	+330.52
		RCP 4.5	43.1	0	0.674	7377.20	+60.52
		RCP 8.5	34.6	0	0.686	7516.90	+200.22
	2081-2100	RCP 2.6	38.1	0	0.694	5068.40	+234.51
		RCP 4.5	36.2	0	0.688	5019.60	+185.71
		RCP 8.5	32.3	0	0.632	4616.30	-217.59

The data in Table 5 indicate that while precipitation is expected to increase slightly under most scenarios, these increases are far outweighed by the substantial rise in evaporation. This imbalance between rising evaporation and relatively stable or slightly increasing precipitation suggests that the region may face growing water stress in the future, as the rate of water loss due to evaporation will likely exceed the rate of water replenishment through precipitation. This situation underscores the potential for dehydration in the study area and highlights the need for proactive water management strategies to mitigate the effects of climate change. Additionally, these findings indicate that further research is required to fully understand the complex interactions between evaporation and precipitation in the region and to develop comprehensive plans for managing water resources under future climate conditions.

Figure 6 illustrates the time distribution of observed and calculated evaporation values over the future periods using the LARS-WG and SDSM models, providing a critical comparative analysis between historical data (1991-2020) and model predictions for the future periods of 2021-2050, 2051-2080, and 2081-2100 under various climate scenarios (RCP 2.6, RCP 4.5, and RCP 8.5). The primary aim of this figure is to track how evaporation is expected to change over time in response to climate change, as projected by both models.

Figure 6. Time distribution diagram of observed and calculated evaporation values for future time periods using LARS-WG and SDSM models

Figure 6 highlights a clear upward trend in evaporation rates, with both models consistently showing an increase in evaporation for future time frames, particularly under the RCP 8.5 scenario, which represents a more extreme climate change projection. The calculated evaporation values for both LARS-WG and SDSM align closely with historical observations for the initial period, indicating that both models are well-calibrated for the region. As the future periods progress, however, the models begin to diverge slightly, with the LARS-WG model projecting somewhat higher evaporation values compared to the SDSM model. This discrepancy may be attributed to differences in how each model handles various climatic factors such as temperature, solar radiation, and humidity. The LARS-WG model shows a steeper increase in evaporation, particularly in the second half of the century (2051-2100), which suggests that this model may be more sensitive to extreme climate change scenarios. This is important for understanding long-term shifts in water balance, as rising evaporation could exacerbate water shortages in the region. On the other hand, the SDSM model exhibits a more moderate increase in evaporation values, potentially reflecting a more conservative response to climate variables. Overall, the time distribution diagrams in Figure 6 underscore the robustness of both models in predicting long-term shifts in evaporation patterns. These results highlight the urgent need for adaptive water resource management strategies to mitigate the impacts of rising evaporation in the Quri Gol Wetland region, as projected by both models.

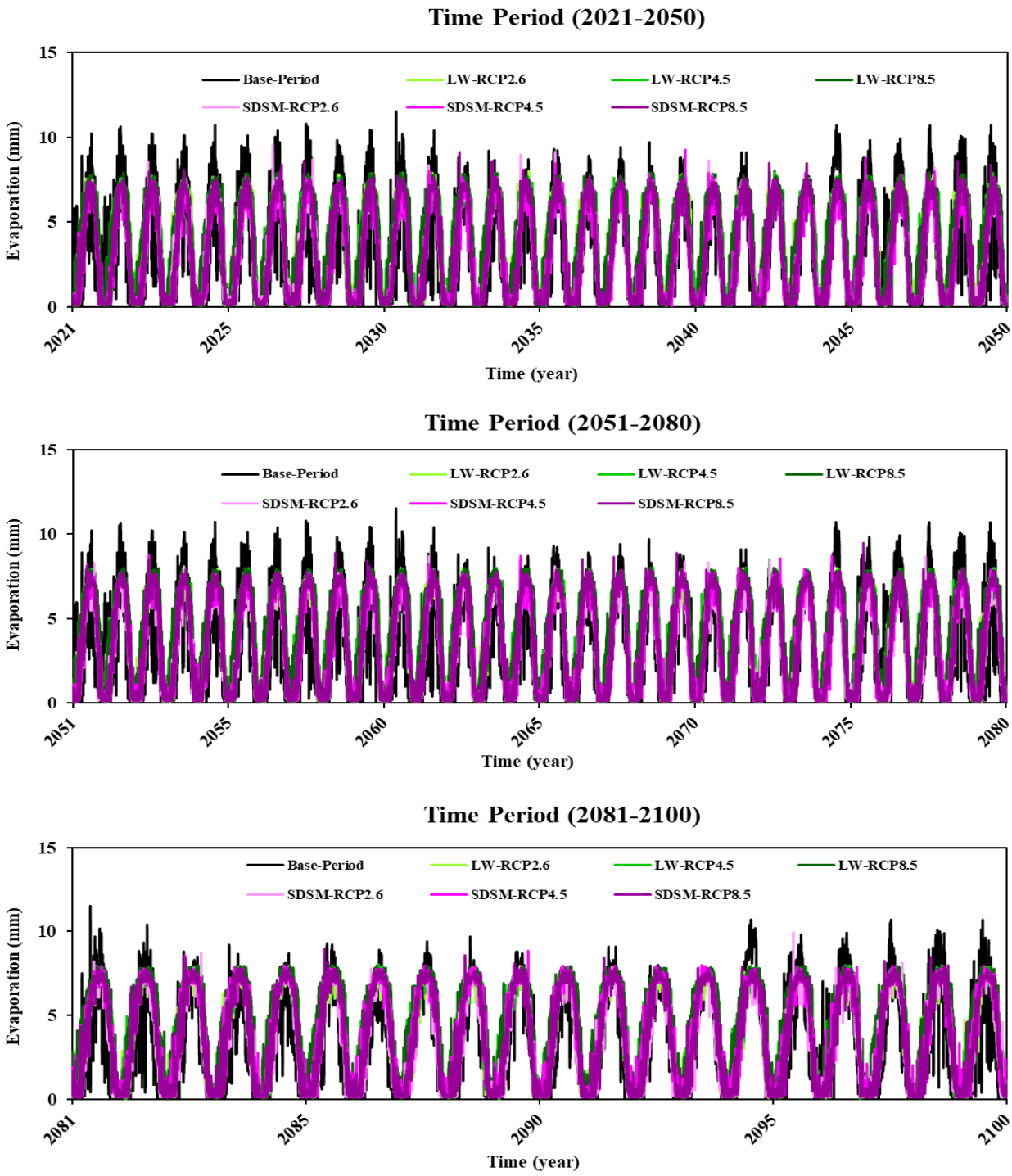

Figure 6- Time distribution diagram of observed and calculated evaporation values for future time

Figures 7 and 8 provide comparative visual analyses of future climate projections using both the LARS-WG and SDSM models. Figure 7 presents violin plots, combining the advantages of box plots and density plots, to offer a statistical comparison of observed and calculated evaporation values. These plots comprehensively visualize the distribution, density, and variability of evaporation data across different time periods and climate scenarios. Figure 8, on the other hand, uses barplots to compare observed and calculated precipitation values, providing a visual representation of precipitation predictions under varying RCP scenarios. Together, these figures highlight the differences in projected evaporation and precipitation trends, providing a clear depiction of their statistical characteristics.

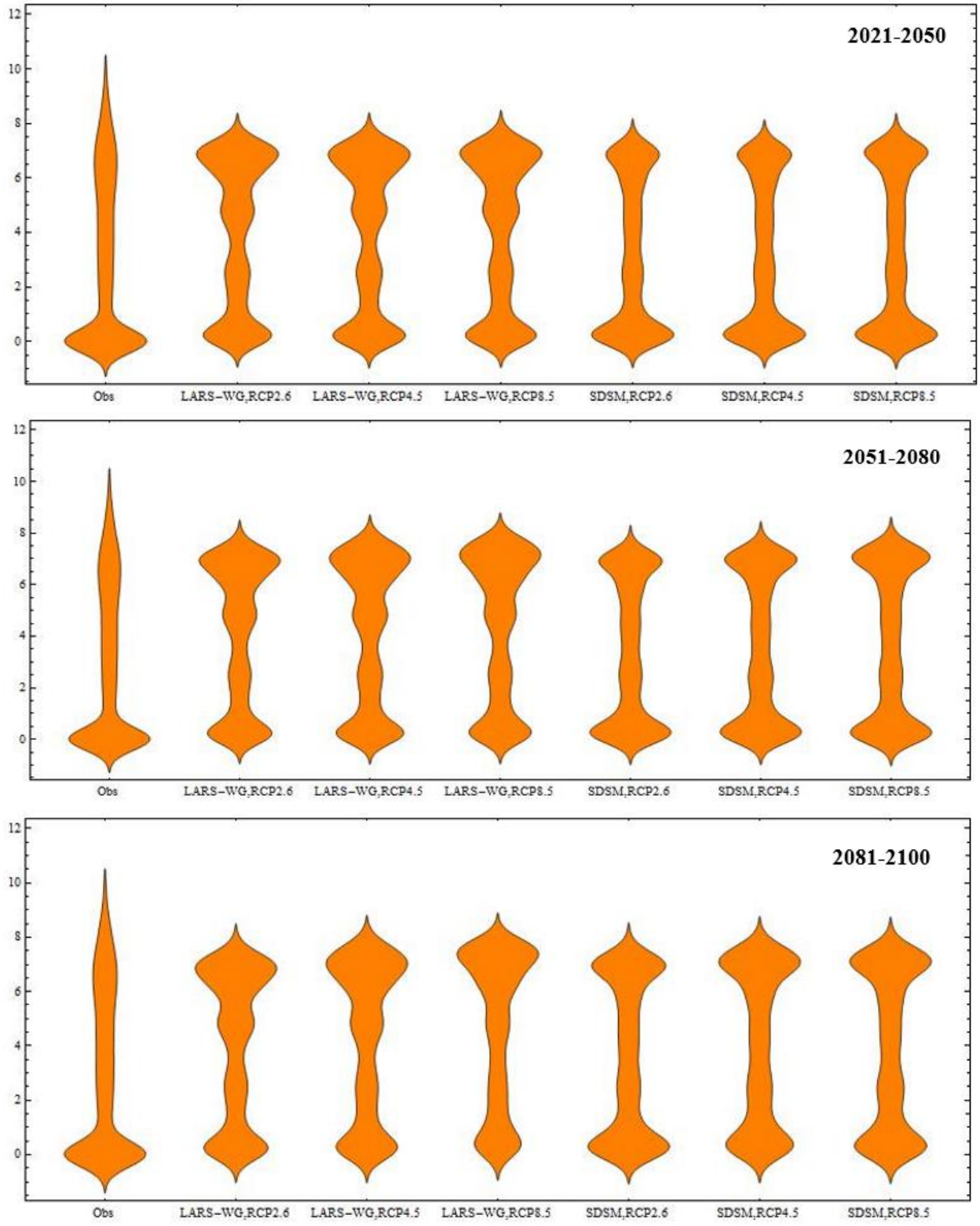

Figure 7- Violin plots of observed and calculated evaporation values for future time periods using LARS-WG and SDSM models

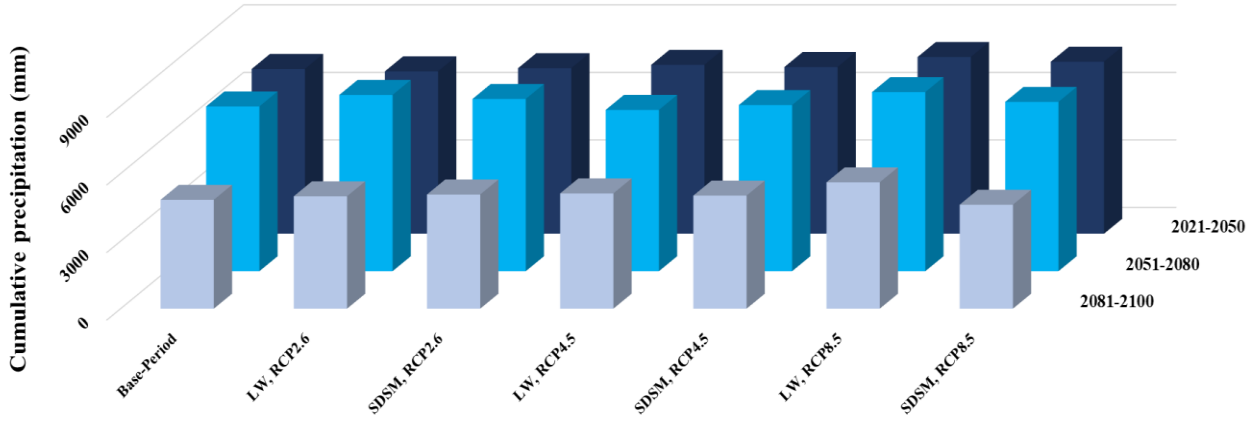

Figure 8- Barplots of observed and calculated precipitation values for future time periods using LARS-WG and SDSM models

According to Figure 7, the width of the violin plots represents the density of data points at various levels of evaporation, with wider sections indicating a higher concentration of values. The observed evaporation values, representing the historical period, display a relatively compact distribution, indicating lower variability in evaporation during the historical period. In contrast, the future predictions show broader distributions, particularly under the more severe climate scenarios (RCP 4.5 and RCP 8.5), indicating greater variability and uncertainty in future evaporation rates. The violin plots reveal that LARS-WG tends to predict slightly higher variability in evaporation values compared to SDSM, especially in the upper quartiles. This suggests that LARS-WG is more sensitive to extreme events and may be better at capturing the tails of the distribution, where extreme evaporation values occur. The SDSM model, while still showing an increase in variability compared to historical data, exhibits a narrower range of predicted values, implying that it projects more conservative changes in evaporation. These plots are critical in understanding the uncertainty associated with future projections, as the broader distribution of values in both models reflects the increased variability in climate-driven evaporation. The higher density of extreme evaporation values in LARS-WG, particularly under RCP 8.5, emphasizes the potential for more frequent and intense evaporation events, which could have significant implications for water availability in the region. The violin plots in Figure 7 serve as a visual confirmation of the increased risk of hydrological extremes due to climate change, reinforcing the need for proactive water management policies to address potential water shortages in the Quri Gol Wetland.

As revealed in Figure 8, the observed data, representing the historical period (1991-2020), show a relatively stable range of precipitation values. This suggests that historical precipitation levels have been relatively consistent, which provides a baseline for comparing future projections. Both models predict an increase in variability for future precipitation values, but the magnitude of the change is far less pronounced compared to the increases in evaporation depicted in Figures 6 and 7. The LARS-WG model predicts a slightly higher median precipitation value compared to SDSM, particularly under the more severe climate scenarios (RCP 4.5 and RCP 8.5). This could indicate that LARS-WG is more optimistic about potential increases in precipitation. However, the overall range of projected precipitation values remains relatively limited, and the barplots for both models indicate that extreme precipitation events are expected to be less prominent compared to extreme evaporation trends. The SDSM model demonstrates a more consistent range, with a smaller spread of predicted values, suggesting a relatively stable projection for future precipitation levels under various scenarios. Despite the slight increases in precipitation shown in both models, the changes are marginal when compared to the substantial increases in evaporation. This imbalance between rising evaporation and relatively stable precipitation levels suggests that the Quri Gol Wetland region could experience increased water deficits in the future. The barplots in Figure 8 reinforce the notion that precipitation alone will not be sufficient to counterbalance the expected rise in evaporation, emphasizing the need for integrated water resource management strategies that account for both increasing evaporation rates and limited precipitation changes.

4. Discussion

This study provides a comprehensive evaluation of how climate change may impact evaporation and precipitation dynamics in the Quri Gol Wetland, employing a combination of machine learning models and climate change projections. The integration of these approaches offers valuable insights into the region's hydrological future, highlighting trends, challenges, and opportunities for sustainable water resource management.

The analysis highlights the effectiveness of machine learning models in capturing the intricate relationships between meteorological variables and evaporation. Advanced techniques, particularly RF and DL, excelled in predicting evaporation patterns. Their ability to model complex nonlinear relationships demonstrates their suitability for hydrological applications. These models reliably reflected observed trends while maintaining accuracy across varying climatic conditions, indicating their

robustness for long-term forecasting. In contrast, other methods like GLM and GBT showed moderate performance. While useful for capturing general trends, these models appeared less adept at handling the variability and extremes that characterize evaporation processes. This underscores the importance of selecting methods tailored to the study's objectives, especially when accurate representation of complex patterns is critical. The comparative analysis of the present study with similar studies is given in Table 6.

Table 6- Comparative analysis of the present study with similar research

Study	*Models Used*	*Location*	*Key Variables*	*Performance Metrics*	*Key Findings*
Present Study	RF, GBT, GLM, SVM, GPR, DL	Quri Gol Wetland (Iran)	maximum and minimum temperature, solar radiation, and precipitation	RF(III) (R^2=0.821, SI= 0.414, and MAE= 0.902) and DL(III) (R^2=0.822, SI= 0.411, and MAE= 0.915) had the highest accuracy	RF and DL models performed better than other models
Tezel & Buyukyildi 2016	MLP, radial basis function network (RBFN), and SVR	Beysehir (Turkey)	temperature, relative humidity, wind speed, and precipitation	the best performance was obtained using MLP (SCG 4,2,2,1) with R^2=0.905.	The comparison of all obtained model performances indicated that all ANN models were more successful than SVR
Wang et al. 2017b	FG, least square support vector regression (LSSVR), MARS, M5Tree and MLR	Dongting Lake Basin (China)	air temperature, surface temperature, wind speed, relative humidity, and sunshine hours	LSSVR and FG models perform better than the MARS, M5Tree and MLR models with respect to statistical indices (MAE, RMSE, and R^2).	the FG, LSSVR and MARS models outperform the M5Tree model, and surface temperature, sunshine hours and air temperature were most important influencing variables
Rezaei-Balf et al. 2019	SVM, model tree (MT), ensemble empirical mode decomposition (EEMD) coupled with support vector machine (EEMD-SVM) and EEMD model tree (EEMD-MT)	Siirt and Diyarbakir stations (Turkey)	wind speed, temperature, relative humidity, and solar radiation	The EEMD-MT model had more accurate performance for both Siirt (NSE=0.89, WI=0.97, and LMI=0.70) and Diyarbakir (NSE=0.92, WI=0.98, and LMI=0.80) stations	It was concluded that the proposed pre-processing technique is very promising for complex time series forecasting
Malik et al. 2022	DL and Gradient Boosting Machine (GBM)	Kiashahr (Iran) and Ranichauri (India)	Monthly maximum temperature and monthly pan evaporation	The best DL models in Kiashahr and Ranichauri stations recorded MAE values of 0.5691 & 0.3693 mm/month, respectively	The DL model was more accurate in both Kiashahr and Ranichauri stations
Bilali et al. 2023	Extra Tree, XGBoost, SVR, and DNN	Bouregreg watershed (Morocco)	air temperature, Relative Humidity, atmospheric pressure, wind speed, and solar radiation	the developed models were accurate in reproducing the daily pan evaporation with NSE ranging from 0.76 to 0.83	the air temperature, solar radiation, followed by relative humidity were the most important climate variables for evaporation estimation in the study area.
Wang et al. 2023	physical model PenPan, MARS, RF, and MLR	China	atmospheric pressure, relative humidity, sunshine hours, air temperature, and wind speed	The RF model had the highest R^2 (0.95± 0.029/ 0.98 ± 0.019) and lowest RMSD (0.62 ± 0.17 mm day^{-1}/9.06 ± 3.45 mm $month^{-1}$) values	It was concluded that the MARS and RF estimates were better than PenPan, and the results of MLR were the worst.

Table 6 offers a detailed comparison between the results of the present study and similar research conducted in various regions, focusing on the use of different machine learning models for predicting evaporation. The table highlights the models employed, key input variables (such as temperature, solar radiation, and precipitation), performance metrics, and key findings. In this study, as highlighted previously, RF and DL models emerged as the most accurate for predicting evaporation in the Quri Gol Wetland (Iran), with the best performance metrics, demonstrating their effectiveness in capturing evaporation patterns. When compared with other studies, models like RF and DL consistently performed better than traditional statistical methods such as MLR and even other machine learning methods like SVM and GBM. The superior accuracy of RF and DL, particularly in handling nonlinear relationships and complex climatic interactions, is evident across different regions and datasets. This comparative analysis underscores the robustness of these models in hydrological applications and highlights their adaptability to various climatic conditions. Table 6 effectively demonstrates that machine learning models, especially RF and DL, provide

reliable and accurate predictions for evaporation, reaffirming their utility in water resource management under diverse climatic conditions.

Climate change projections indicate that evaporation in the Quri Gol Wetland will increase substantially in the coming decades, with the magnitude of the change intensifying under more extreme climate scenarios. This upward trend aligns with rising temperatures and enhanced solar radiation driven by global warming. These changes suggest an urgent need for strategies to address the anticipated water losses from the wetland. In contrast, projected changes in precipitation are comparatively modest. While there are slight increases in precipitation under certain scenarios, these do not compensate for the significant rise in evaporation. This imbalance highlights the potential for water stress in the wetland, which could adversely affect its ecological health and the agricultural activities dependent on it. Such findings underscore the vulnerability of water systems in arid and semi-arid regions under changing climatic conditions.

The study's findings emphasize the need for proactive water resource management strategies to address the anticipated challenges posed by climate change. Adaptation measures should focus on reducing water loss and ensuring sustainable usage. These may include optimizing irrigation systems, enhancing water storage infrastructure, and implementing conservation practices to preserve wetland ecosystems. The application of machine learning models provides a reliable tool for forecasting and monitoring hydrological variables, enabling more informed decision-making. The flexibility and precision of RF and DL models, in particular, make them valuable for real-time applications, offering opportunities to anticipate and mitigate the impacts of climatic variability. Furthermore, incorporating climate change projections into management policies can help stakeholders better prepare for the long-term impacts on water availability.

While the study offers robust insights, several limitations should be acknowledged. The projections depend heavily on the quality of input data and assumptions within the climate change scenarios used. Non-climatic factors, such as human interventions and land use changes, were not accounted for, potentially limiting the scope of the findings. Additionally, the study primarily focused on meteorological variables, omitting other important factors like groundwater interactions and soil moisture dynamics. Future research should aim to address these gaps by integrating additional variables and exploring the interplay between climatic and non-climatic factors. A more holistic approach would provide a deeper understanding of the hydrological processes affecting the wetland. Expanding the analysis to include seasonal and annual variations could also yield more nuanced insights, particularly in capturing short-term dynamics alongside long-term trends.

5. Conclusions

This study evaluated the future impacts of climate change on evaporation and precipitation in the Quri Gol Wetland by integrating machine learning models with climate change projections. Evaporation values for the present period (1991-2020) were estimated using machine learning models (RF, GBT, GLM, SVM, GPR, and DL), and future predictions were made by combining machine learning methods with climate models (LARS-WG and SDSM) under three different RCP scenarios (2.6, 4.5, and 8.5). This comprehensive approach assessed potential hydrological changes in the wetland for the future periods of 2021-2050, 2051-2080, and 2081-2100.

Machine learning models performance:

RF and DL emerged as the most accurate models for predicting evaporation during the calibration and validation phases.

In the validation phase, the best RF model achieved an R^2 of 0.821, an SI of 0.414, and an MAE of 0.902, while the best DL model recorded an R^2 of 0.822, an SI of 0.411, and an MAE of 0.915.

These results indicate the robustness of RF and DL in capturing complex nonlinear relationships between meteorological variables and evaporation.

Future evaporation and precipitation trends:

Evaporation rates are expected to increase significantly across all future periods, with the highest rise projected under the RCP 8.5 scenario.

The LARS-WG model forecasted a maximum increase of 50.01% in evaporation by 2081-2100, while the SDSM model projected a smaller rise of up to 30.14%.

Precipitation increases were comparatively smaller, with a maximum of 16% projected by the LARS-WG model under the RCP 8.5 scenario during the same period.

Implications for hydrological balance:

The imbalance between rapidly increasing evaporation and relatively stable precipitation levels highlights potential water scarcity challenges for the Quri Gol Wetland.

These findings underscore the wetland's vulnerability to climate change and its implications for ecological and agricultural sustainability.

The findings of this study underline the critical need for adaptive strategies to address the challenges posed by climate change on the Quri Gol Wetland. As evaporation rates are projected to rise significantly, outpacing smaller increases in precipitation, effective water resource management becomes imperative to sustain the ecological and agricultural viability of the region. Future research should expand the scope of analysis by considering a broader range of climate scenarios and incorporating additional variables such as land use changes, socio-economic factors, and groundwater interactions. These additions would provide a more holistic understanding of the hydrological impacts of climate change and improve the predictive accuracy of the models. Moreover, it is essential to investigate the implications of these hydrological changes on groundwater recharge and ecosystem health, as these factors are vital for maintaining the wetland's long-term stability. Integrating these variables into future studies will offer deeper insights into the complex interactions between climate, hydrology, and human activity. Such research can guide the development of sustainable resource management practices, ensuring that the Quri Gol Wetland and similar regions can effectively adapt to the pressures of a changing climate.

References

Ahmadaali J, Barani G A, Qaderi K, Hessari B (2018). Analysis of the effects of water management strategies and climate change on the environmental and agricultural sustainability of Urmia Lake basin, Iran. Water 10: 160

Azizi G, Nazif S, Abbasi F (2017). An assessment of the influence of climate change on Urmia Lake water level reduction. Journal of Interdisciplinary Studies in the Humanities 9(4): 1-21

Bilali A E, Abdeslam T, Ayoub N, Lamane H, Ezzaouini M A, Elbeltagi A (2023). An interpretable machine learning approach based on DNN, SVR, Extra Tree, and XGBoost models for predicting daily pan evaporation. J. Environ. Manage. 327: 116890

Bengio Y (2009). Learning Deep Architectures for Artificial Intelligence. Found. Trends Mach. Learn. 2(1): 1-127

Breiman L (1999). Using adaptive bagging to debias regressions. Technical Report 547, Statistics Department, University of California.

Breiman L (2001). Random forests. Mach. Learn. 45(1): 5-32

Chandler R E & Wheater H S (2002). Analysis of rainfall variability using generalized linear models: a case study from the west of Ireland. Water Resour. Res. 38(10): 1-10

Dibike Y B & Coulibaly P (2005). Hydrologic impact of climate change in the Saguenay Watershed: Comparison of Ownscaling Methods and Hydrologic Models. *J. Hydrol.* 307: 145-163

Ghaemi A, Rezaie-Balf M, Adamowski J, Kisi O, Quilty J (2019). On the applicability of maximum overlap discrete wavelet transform integrated with MARS and M5 model tree for monthly pan evaporation prediction. Agric. For. Meteorol. 278:107647. https://doi.org/10.1016/j.agrformet.2019.107647.

Ghorbani M A, Deo R C, Karimi V, Yaseen Z M, Terzi O (2018). Implementation of a hybrid MLP-FFA model for water level prediction of Lake Egirdir, Turkey. Stoch. Env. Res. Risk Assess. 32(6): 1683-1697. https://doi.org/10.1007/s00477-017-1474-0.

Glorot X & Bengio Y (2010). Understanding the difficulty of training deep feedforward neural networks. Proceedings of Machine Learning Research 9:249-256

Goyal M K, Bharti B, Quilty J, Adamowski J & Pandey A (2014). Modeling of daily pan evaporation in sub tropical climates using ANN, LS-SVR, Fuzzy Logic, and ANFIS. Expert Syst. Appl. 41(11): 5267-5276

Goyal M K & Ojha C S P (2014). Evaluation of rule and decision tree induction algorithms for generating climate change scenarios for temperature and pan evaporation on a lake basin. *J. Hydrol. Eng.* 19:828-835

Guven A & Kisi O (2013). Monthly pan evaporation modeling using linear genetic programming. *J. Hydrol.* 503:178-185

Hamel L (2009). Knowledge Discovery with Support Vector Machines. John Wiley, Hoboken, New Jersey.

Hay L E, Wilby R L & Leavesley G H (2000). A comparison of delta change and downscaled GCM scenarios for three mountainous basins in the United States. J. Am. Water Resour. Assoc. 36: 387-397

Helfer F, Lemckert C H & Zhang H (2012). Impacts of climate change on temperature and evaporation from a large reservoir in Australia. *J. Hydrol.* 1-38

Hinton G E, Osindero Y W S (2006). A fast learning algorithm for deep belief nets. Neural Comput. 18(7): 1527-1554

Keshtegar B, Piri J & Kisi O (2016) A nonlinear mathematical modeling of daily pan evaporation based on conjugate gradient method. Comput. Electron. Agric. 127:120-130

Keyvanrad MA, Homayounpour MM (2015) Deep belief network training improvement using elite samples minimizing free energy. Int. J. Pattern Recognit. Artif. 29(5): 155-166

Kilsby C G, Jones P D, Burton A, Ford A C, Fowler H J, Harpham C, James P, Smith A & Wilby R L (2007). A daily weather generator for use in climate change studies. Environ. Model. Softw. 22: 1705-1719

Kim S, Shiri J, Kisi O (2012). Pan evaporation modeling using neural computing approach for different climatic zones. Water Resour. Manage. 26(11):3231-3249.

Kisi O (2015). Pan evaporation modeling using least square support vector machine, multivariate adaptive regression splines and M5 model tree. J. Hydrol. 528: 312-320

Kisi O & Heddam S (2019). Evaporation modelling by heuristic regression approaches using only temperature data. *Hydrol. Sci. J.* 64(6):653-672

Kotsiantis S & Pintelas P (2004). Combining bagging and boosting. *Int. J. Comput. Intell. Syst.* 1(4):324-333

Lu X, Ju Y, Wu L, Fan J, Zhang F & Li Z (2018). Daily pan evaporation modeling from local and cross-station data using three tree-based machine learning models. *J. Hydrol.* 566: 668-684

Majhi B, Naidu D, Mishra A P & Satapathy S C (2020). Improved prediction of daily pan evaporation using Deep-LSTM model. Neural Comput. Appl. pp. 1-16

Malik A, Saggi M K, Rehman S, Sajjad H, Inyurt S, Bhatia A S, Farooque A A, Oudah A Y & Yaseen Z M (2022). Deep learning versus gradient boosting machine for pan evaporation prediction, Eng. Appl. Comput. Fluid Mech. 16(1): 570-587

Malohlava M & Candel A (2018). Gradient boosting machine with H2O. http://docs.h2o.ai/h2o/latest-stable/h2o-docs/data-science/gbm.html .Accessed 24 FEBRUARY 2020.

McCullagh P (1984). Generalized linear models. *Eur. J. Oper. Res.* 16(3): 285-292

Nelder J A & Baker R J (1972). Generalized Linear Models. Wiley Online Library, New Jersey.

Pregibon D& Hastie T J (2017). Generalized linear models. In: Statistical Models in S. Routledge.

Quinlan J R (1993). C4.5 programs for machine learning. Morgan Kaurmann, San Mateo, CA.

Rezaie-Balf M, Kisi O & Chua L H C (2019). Application of ensemble empirical mode decomposition based on machine learning methodologies in forecasting monthly pan evaporation. Hydrol. res. 50(2): 498-516

Schapire R (1990). The strength of weak learnability. *Journal of Machine learning* 5: 197-227

Seifi A & Soroush F (2020). Pan evaporation estimation and derivation of explicit optimized equations by novel hybrid meta-heuristic ANN based methods in different climates of Iran. Comput. Electron. Agric. 173: 105418

Semenov M A & Stratonovitch P (2010). Use of multi-model ensembles from global climate models for assessment of climate change impacts. Clim. Res. 41:1-14

Shiri J (2019). Evaluation of a neuro-fuzzy technique in estimating pan evaporation values in low-altitude locations. Meteorol. Appl. 26(2):204-212

Shaker Sureh F, Sattari M T, Rostamzadeh H & Kahya E (2024). Meteorological Drought Assessment and Prediction in Association with Combination of Atmospheric Circulations and Meteorological Parameters via Rule Based Models. *J Agr Sci-Tarim Bili.* 30(1):61-78. doi:10.15832/ankutbd.1067486

Tatsumi K, Oizumi T & Yamashiki Y (2013). Introduction of daily minimum and maximum temperature change signals in the Shikoku region using the statistical downscaling method by GCMs. Hydrol. Res. Lett. 7(3): 48-53

Terzi O (2010). Modeling of daily pan evaporation of lake Egirdir using data-driven techniques. International symposium on innovations in Intelligent systems and Applications. Istanbul. Turkey. pp. 320-324

Tezel G & Buyukyildiz M (2016). Monthly evaporation forecasting using artificial neural networks and support vector machines. Theor. Appl. Climatol. 124: 69-80

Vapnik V (1995). The Nature of Statistical Learning Theory. Springer, New York.

Vapnik V (1998). Statistical Learning Theory. Wiley, New York.

Wang L, Kisi O, Zounemat-Kermani M & Li H (2017a). Pan evaporation modeling using six different heuristic computing methods in different climates of China. *J. Hydrol.* 544: 407-427

Wang L, Niu Z, Kisi O, Li C & Yu D (2017b). Pan evaporation modeling using four different heuristic approaches. Comput. Electron. Agric. 140: 203-213

Wang H, Yan H, Zeng W, Lei G, Ao C & Zha Y (2020). A novel nonlinear Arps decline model with salp swarm algorithm for predicting pan evaporation in the arid and semi-arid regions of China. *J. Hydrol.* 582: 124545

Wang H, Sun F, Liu F, Wang T, Liu W & Feng Y (2023). Reconstruction of the pan evaporation based on meteorological factors with machine learning method over China. Agric. Water Manag. 287:108416.

Wilby R L, Dawson C W & Barrow E M (2002). SDSM a decision support tool for the assessment of regional climate change impacts. Environ. Model. Softw. 17:147-159

Wilby RL, Harris I (2006). A frame work for assessing uncertainties in climate change impacts: low flow scenarios for the River Thames, UK. Water Resour. Res. https://doi.org/10.1029/2005wr004065

Wilby R L, Tomlinson O J, Dawson C W (2007). Multi-site simulation of precipitation by condition resampling. *J. Clim. Res.* 23: 183-194

Williams C K I, Barber D (1998). Bayesian classification with gaussian processes. IEEE Trans. Pattern Anal. Mach. Intell. 20(12): 1342-1351

Williams C K I, Rasmussen C E (1996). Gaussian processes for regression. In: Advances in Neural Information Processing Systems. MIT Press, pp. 514–520

Zarghami M, Abdi A, Babaeian I, Hassanzadeh Y İ & Kanani R (2011). Impacts of climate change on runoffs in East Azerbaijan, Iran. Glob Planet Change 78: 137-146

Zounemat-Kermani M, Kisi O, Piri J & Mahdavi-Meymand A (2019). Assessment of artificial intelligence–based models and metaheuristic algorithms in modeling evaporation. *J. Hydrol. Eng.* 24(10): 04019033. https://doi.org/10.1061/(ASCE)HE. 1943-5584.0001835.

Journal of Agricultural Sciences
(Tarim Bilimleri Dergisi)

J Agr Sci-Tarim Bili
e-ISSN: 2148-9297
jas.ankara.edu.tr

JAS

Biomonitoring of Non-Native Species Through eDNA Metabarcoding Method and Risk Screening for Ballast Water in Northwest Türkiye

Yusuf Koray Küçük[a,b], Akasya Topçu[b], Esra Mine Ünal[c,d], Emre Keskin[b,c,d,g], Ali Serhan Tarkan[e,f], İlknur Meriç Turgut[b*]

[a] *Department of State Information Coordination Center, General Directorate of Security Affairs, Presidency of the Republic of Türkiye, Ankara, TÜRKIYE*
[b] *Department of Fisheries and Aquaculture Engineering, Faculty of Agriculture, Ankara University, Ankara, TÜRKIYE*
[c] *Ankara University Agricultural Faculty Department of Fisheries and Aquaculture Evolutionary Genetics Laboratory (eGL), Ankara, TÜRKIYE*
[d] *AgriGenomics Hub Animal and Plant Genomics Research Innovation Centre, Ankara, TÜRKIYE*
[e] *Department of Ecology and Vertebrate Zoology, Faculty of Biology and Environmental Protection, University of Lodz, Lodz, POLAND*
[f] *Department of Basic Sciences, Faculty of Fisheries, Muğla Sıtkı Koçman University, Menteşe, Muğla, TÜRKIYE*
[g] *Ankara University Aquaculture Research and Application Center (ASAUM), Ankara, TÜRKIYE*

ARTICLE INFO
Research Article
Corresponding Author: İlknur Meriç Turgut, E-mail: meric@agri.ankara.edu.tr
Received: 19 August 2024 / Revised: 05 November 2024 / Accepted: 05 December 2024 / Online: 25 March 2025

Cite this article
Küçük Y K, Topçu A, Ünal E M, Keskin E, Tarkan A S, Turgut İ M (2025). Biomonitoring of Non-Native Species Through eDNA Metabarcoding Method and Risk Screening for Ballast Water in Northwest Türkiye. *Journal of Agricultural Sciences (Tarim Bilimleri Dergisi),* 31(2):470-495. DOI: 10.15832/ankutbd.1535703

ABSTRACT
The exponential development of maritime transport has made ballast water a primary vector for the spread of invasive organisms across the aquatic realm. This research aims to present a comprehensive overview of methodological and bioinformatic considerations for eDNA metabarcoding applied to ballast water from ships in İzmit Gulf, northwest Türkiye, with an emphasis on non-native species. The data related to DNA sequences for *COI*, *18Sv8*, *18Sv4*, *16S*, and *12S* presented a broad diverse taxonomic group for both microbial and macroscopic species, even for rare ones, with numbers of 93, 191, 241, 19, and 44, respectively. Additionally, the research unveiled the presence of highly invasive species such as *Rhopilema nomadica* and identified their invasiveness risk for İzmit Gulf, primarily due to elevated water temperatures in relation to climate change. The outlined results indicate that metabarcoding offers a potential tool for early detection of non-indigenous species and implementing management plans in view of current global warming interactions.

Keywords: İzmit Gulf, Monitoring, Biodiversity, Quantitative metabarcoding, Risk identification

1. Introduction

The remarkable evolution of ships in terms of technology, engineering, and social classification over the last century has significantly contributed to the advancement of maritime transport. As ships modernized, maritime trade experienced a surge, becoming a driving force for globalization (Ojaveer et al. 2018; Rey 2019). However, this rapid evolution, particularly the extensive displacement of ballast water has led to increased dominance of non-native species in the biodiversity of aquatic ecosystems. Recognizing that ballast water and sediment, representing 30-35% of the ship's carrying capacity, are a significant vector for both the transportation and spread of benthic and planktonic organisms, toxic dinoflagellates, and fish eggs, larvae and itselves, with some of these presumed to be non-native species (Verling et al. 2005; Gibb et al. 2013; Bradie 2016), there is a need to address the socio-economic, environmental, and human welfare impacts (Williams 2013).

In accordance with "The Control and Management of Ships' Ballast Water and Sediment Convention (BWMC)" framework in 2004 introduced by International Maritime Organization (IMO), the BWMC guidelines should be a main axis in port-based research for identifying areas and detecting target species. The identification of highly risky invasive species relies on comparing environmental identity and species composition in target ports as outlined by IMO guidelines from 2004. This "species-specific risk assessment" approach, which focuses on the biogeographic region in question when adopted in 2007 and upated in 2017, would be the most suitable method. To enhance this aspect, specific protocols tailored to exemptions could be developed by the Black Sea Commission operating under the Bucharest Convention and this would contribute to ensure the protection from potential threats posed by invasive species. The application of ballast water purification processes necessitates the use of advanced treatment technologies, particularly through mechanical and physico-chemical methods. In accordance with IMO standards, ballast water treatment systems are engineered to fulfill either the D-1 standard, which dictates the specific location for ballast water discharge, or the D-2 standard, which establishes permissible limits on viable organisms present in discharged

water. To ensure regulatory compliance, these onboard systems are equipped with monitoring tools that verify treatment efficacy and data logging mechanisms designed to meet IMO reporting requirements. In recent years, there has been a notable shift towards employing accurate and effective methods for determining the invasive potential of non-native species. Molecular metabarcoding methods, in particular, are increasingly outpacing morphological-based taxonomy (Shaw et al. 2017; Jeunen et al. 2019). These methods prove advantageous in monitoring and evaluating biodiversity effectively (Ghabooli et al. 2016; Blackman et al. 2017) via allowing numerous samples to be scanned in a short time period (Pochon et al. 2013; Zhan et al. 2013; Deiner et al. 2017) and exhibit heightened sensitivity for detecting rare, elusive, and cryptic species (Wee et al. 2023), particularly noteworthy within certain taxa (Fonseca et al. 2023). Moreover, the depending on the taxonomic knowledge abundance, species identification varies among groups due to the differences in primer selection and the completeness of the reference database (Pascher et al. 2022).

The acceleration of metabarcode-based studies, such as eDNA metabarcoding, enables comprehensive monitoring of marine biodiversity (Lacoursière-Roussel et al. 2018; Giroux et al. 2022). This approach is particularly useful for assessing ballast water and port areas for invasive species (Comtet et al. 2015; Xiong et al. 2016), detecting subtle population changes (Wright et al. 2019) and conducting ecological status assessments (Aylagas et al. 2018; Antich et al. 2021). Moreover, it allows for the simultaneous characterization of the spatio-temporal distribution of multiple taxa (Oka et al. 2021; Polanco-Fernández et al. 2021; Wee et al. 2023). The rapid response of applied molecular methods highlights their economic benefits in affirming the impact of port and shipping activities.

The accuracy and efficiency of the eDNA metabarcoding method depend significantly on the choice of primers used for PCR amplification (Alberdi et al. 2018; Gold et al. 2021). The selection of primers has a substantial impact on the taxonomic coverage and resolution of the metabarcoding studies, given that different primers target distinct genomic areas. Recognizing this, employing multiple primers (Ammon et al. 2018; Grey et al. 2018) can scan the employing of multiple primers (Ammon et al. 2018; Grey et al. 2018) has an ability to scan a diversified amount of species present in ballast water, reliably and capture a comprehensive spectrum. Employing several primers not only overcomes the constraints posed by primer biases (Alberdi et al. 2018; Chambert et al. 2018; Doi et al. 2019; Gold et al. 2021) but also provides a deeper understanding of the varied assemblages of microbes, algae, and aquatic organisms in ballast water. Using multiple sets of primers targeting various marker genes or regions (Borrell et al. 2017), researchers can enhance sensitivity in spotting rare species and gain a more thorough comprehension of the ecological dynamics and potential risks associated with the transoceanic convection of ballast water. So, it is essential to carefully choose and use a variety of primers for eDNA metabarcoding studies in ballast water to ensure the accuracy and comprehensiveness of the results. This approach ultimately contributes to informing management and mitigation strategies aimed at reducing the spread of invasive species through ballast water exchange. While a wide variety of metabarcoding primers have been developed for fish, revealing significant differences in taxonomic richness and discriminant power within species (Zhang et al. 2020), a comprehensive and comparative evaluation for aquatic species based on amplification or taxonomic classification is not yet available in the literature.

In order to document spatio-temporal changes in biodiversity, especially within İzmit Gulf, as a large-scale marine habitat, pose challenges and substantial costs (Gold et al. 2021; Pascher et al. 2022), a pooled eDNA metabarcoding approach was chosen considering the challenging nature of marine habitats and this method proves advantageous, making it time-consuming and costly to undertake individual assessments. This sample pooling strategy enabled the improvement of sensitivity, statistical power, and efficiency of the methodology while working with numerous samples moreover, this has a contribution like identifying low-abundance species, which are important signs of impending invasions, by integrating various samples into a single pool. Like restructuring the lab processes, minimizing batch impacts and preserving constant quality control throughout the evaluation were the other benefits of this type of sampling. A current study (He et al. 2023) also indicated that, working with greater water volume ensues an incline of eDNA-based species richness. This approach provides light on the ecological effects of ballast water exchange and the efficacy of current biosecurity measures in avoiding the introduction of invasive species; also offers an integrative/alternative one in comparison to traditional surveys (Stat et al. 2019; He et al. 2023).

To prevent against ecological disruptions (Elton 1942) and safeguard natural ecosystems and native species, it is imperative to proactively implement strategies and allocate resources (Tarkan et al. 2022). One effective approach involves the identification of suitable habitats for non-native species and an assessment of their potential threats. Screening techniques for assessing risks, such as Aquatic Species Invasiveness Screening Kit-AS-ISK (Copp et al. 2016), offer a valuable tool for appraising the potential risks posed by non-native species within a specific region (Tarkan et al. 2017). This, in turn, empowers us to prioritize and implement appropriate preventative measures.

This study centers on the critical environmental challenges posed by the extensive port facilities and marine transport in the northwest region of Türkiye, specifically the İzmit Gulf. Utilizing eDNA metabarcoding, our goal is to identify non-native species and gauge their invasive potential through an innovative risk screening tool. Thus wise, the importance of predicting the invasiveness of identified species and formulating effective management strategies for the area could be enabled.

2. Material and Methods

2.1. Study area

The study site encompasses the Marmara Sea, specifically within the Kocaeli province, focusing on Dilovası (11 port facilities), Yarımca (6 port facilities), and Hereke (3 port facilities) (Figure 1). This selection was made based on the high-density impact of voyages in Türkiye, making it a region of significant interest for the study.

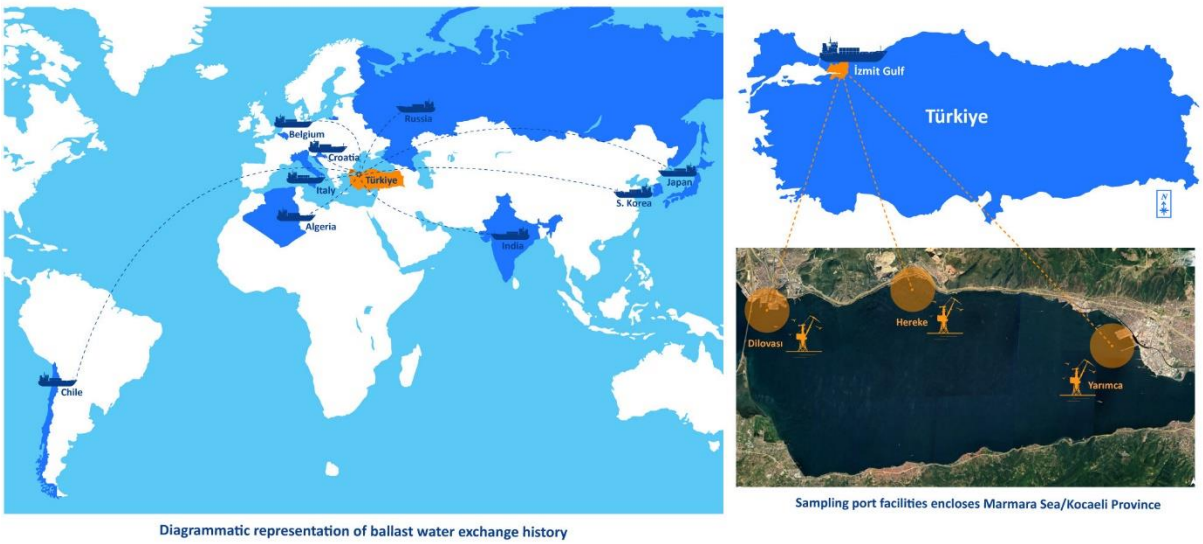

Figure 1- The documented last ballast water exchanges for ships and the selected sites (Dilovası, Yarımca, Hereke) showing port facilities in the Marmara Sea as a diagrammatic representation

2.2. Procedures of ballast water sampling

A total of 20 sampling ships was included in the investigation, from which ballast water samples were taken from 3 port facilities in İzmit Gulf. The sampling technique was carried out in triplicate over two separate seasons, specifically February and May. The Ministry of Transportation and Infrastructure utilized the Marine Traffic Programme to evaluate the present position and appropriateness of the ships for sampling. The ballast water exchange history of the vessels was investigated, and the most recent exchanges were recorded in the territorial seas of Russia, Italy, Croatia, Belgium, India, Algeria, South Korea, Japan, and Chile (Figure 1), as documented in both the Ballast Record Book and Port of Call List.

The sample collection was conducted in triplicate utilizing two particular methods, namely manhole and overflowing. Each replication consisted of 2 L of sample. The on-site filtration process involved passing each 2 L sample through Sterivex filters consisting of polyethersulfone (PES) membrane with a pore size of 0.22 µm. These filters are renowned for their ability to facilitate high flow rates and minimize protein adsorption. Subsequently, these filters were transferred to the laboratory while maintaining a controlled temperature environment.

Stringent methods were established throughout the trial to reduce contamination during sample collection, transport, and laboratory processing. Negative field controls, comprising deionized water samples subjected to the same treatment as the environmental samples, were incorporated at each site during collection to identify any possible contamination from the field. The gathered samples were conveyed under regulated, sterile settings to prevent any extraneous DNA contamination. In the laboratory, negative transport controls and equipment controls were utilized, wherein deionized water was filtered and processed concurrently with environmental samples to detect contamination introduced during DNA extraction or PCR. Moreover, laboratory technicians employed rigorous aseptic protocols, utilizing sterile gloves, pipette tips, and designated workspaces for each phase of the research. PCR configurations incorporated negative controls to guarantee the absence of contamination during amplification. These procedures jointly preserved the integrity of the eDNA samples and reduced the likelihood of false-positive results stemming from contamination.

Upon reaching the laboratory, the filtered samples from each set of three (6 L) were combined into a single composite sample. For every sampling instance, three sets of three 2 L samples were combined to form a total volume of 18 L. The purpose of this

was to enhance sensitivity, save costs and time, raise statistical power, and provide quality control in the composition of eDNA. Aggregating samples prior to filtration aids in the identification of species with low abundance and facilitates the efficiency of extensive monitoring initiatives (e.g., Deiner et al. 2017; Aylagas et al., 2018). Pooling enhances the identification of low-abundance species, but it can also lead to the omission of data regarding the diversity of individual samples.

Three types of controls were used during the entire water sampling and transport process according to Goldberg et al. (2013). These were negative field controls, negative transport controls and negative equipment controls, containing deionized water samples. All controls were treated the same as the site ones.

2.3. eDNA metabarcoding

Once the water samples were combined into a single batch measuring 18 L, the pooled sample underwent filtration using 36 Sterivex filters with a pore size of 0.22 μm. To ensure long-term preservation, the Sterivex filters were treated with Longmire solution. In addition, we collected three types of quality-control samples: a field control sample, a transit control sample, and a test control sample, using the approach outlined by Goldberg et al. (2013). The aforementioned samples were obtained from vessels that engage in the practice of exchanging ballast in the seas of Russia, Italy, Croatia, Belgium, Algeria, India, South Korea, Japan, and Chile.

The DNeasy® Blood and Tissue Kit (QIAGEN, Stockach, Germany) was used to isolate samples from Sterivex capsule filters, following the method described by Spens et al. (2017). The DNA isolates were assessed for quality and quantity using gel electrophoresis and the Qubit™ 3.0 Fluorometer, respectively. Firstly, the buffer solution and filter isolates from the same filter sample were merged after combining three isolates from each sample.

PCR analyses were performed using specific primer pairs recommended for each group of organisms. The primer pairs used were MiFish_U_F&R for fish (Bradley et al. 2016), mlCOIintF&jgHCO2198 for invertebrates (Leray et al. 2013), Vert-16S-eDNAF1&R for vertebrates (Miya et al. 2015), and V4F&R and V8F&R for microorganisms and eukaryotes (Vences et al. 2016). The DNA library was created using the two-step PCR technique described by Miya et al. (2015) and following the guidelines of Bourlat et al. (2016) for the Illumina TruSeq Nano DNA Library Preparation Protocol. The quality and quantity of the PCR products were assessed using the Qubit™ 3.0 Fluorometer and Bioanalyzer 2100 equipment, while the primer was employed to verify that the amplified product had the intended size. The Illumina MiSeq platform was employed for paired-end sequencing with 2 × 250 bp base pairs following library preparation.

The DNA library was generated using a two-step PCR approach, commonly referred to as the dual-indexing method, following the protocol described by Miya et al. (2015), with some changes to incorporate the Illumina TruSeq Nano DNA Library Preparation Kit. This approach guarantees the precise amplification and indexing of specific DNA sequences for sequencing.

Initial Polymerase Chain Reaction (PCR) for the purpose of generating amplicons:

- Distinct primer pairs were employed for different groups of organisms: MiFish_U_F&R for fish (Miya et al. 2015), mlCOIintF&jgHCO2198 for invertebrates (Leray et al. 2013), Vert-16S-eDNAF1&R for vertebrates (Miya et al. 2015), and V4F&R and V8F&R for microbes and eukaryotes (Vences et al. 2016).

- The PCR reactions were conducted in a 25 μL solution, consisting of 12.5 μL of 2X KAPA HiFi HotStart ReadyMix (KAPA Biosystems, Wilmington, MA, USA), 0.2 μM of each primer, and 5 μL of DNA template.

- The thermocycling protocol consisted of an initial denaturation step at 95 °C for 3 minutes, followed by 35 cycles of 98 °C for 20 seconds, 55 °C for 15 seconds, and 72 °C for 30 seconds. The process concluded with a final extension step at 72 °C for 5 minutes.

- PCR amplification for the second time with indexing:

- The amplicons obtained from the initial PCR were utilized as templates in the subsequent PCR to incorporate Illumina Nextera XT dual indices and sequencing adapters.

- The PCR reactions were conducted in a 50 μL solution, consisting of 25 μL of 2X KAPA HiFi HotStart ReadyMix, 5 μL of each Nextera XT Index Primer, and 5 μL of the first PCR result.

- The thermocycling protocol consisted of an initial denaturation step at 95 °C for 3 minutes, followed by 8 cycles of denaturation at 98 °C for 20 seconds, annealing at 55 °C for 15 seconds, and extension at 72 °C for 30 seconds. The final extension step was performed at 72 °C for 5 minutes.
- Quantification and quality control of library samples:

- The PCR products that were marked with an index were cleansed using AMPure XP beads (Beckman Coulter, Brea, CA, USA) and measured using the Qubit™ 3.0 Fluorometer.

- The Bioanalyzer 2100 (Agilent Technologies, Santa Clara, CA, USA) was used to evaluate the size distribution and quality of the libraries.

- Sequencing:

- The libraries were combined in equal concentrations and subjected to sequencing on an Illumina MiSeq platform using the MiSeq Reagent Kit v3 (600-cycle) for paired-end sequencing (2 × 300 bp).

2.4. Bioinformatic analysis

The OBITOOLS software package (Boyer et al. 2016) was employed for the bioinformatics workflow. The MiSeq device's fastq sequences' quality as well as the key statistics regarding these sequences were examined using the FastQC program (Andrews 2010). Illumina pairedend code, which considers coupling quality (phred score 30), was used to align and merge forward and backward reads pertaining to the same sample. Following the merging of the forward and reverse sequences, samples with different tags were demultiplexed within the same fastq file using the ngsfilter and obisplit commands. Sequence data was then prepared for processing separately and filtered based on count (10) and sequence length (minimum of 100 bp). Depending on the maximum read count in the negative controls, which was 9, we determined the cut-off number for the read count. As a result, we set the read number cut-off for each sample at less than 10. The relevant literature such as Yamamoto et al. (2017) and Gehri et al. (2021) also frequently uses this strategy. Raw data were examined for species exclusions linked to insertions and deletions that were not found in our study prior to filtering. More broad filters were used and tested down to 100 base pairs. To make taxonomic designations, all sequences were uploaded to NCBI GenBank as a batch megablast file, during which 98% of species level identifications based on similarity were omitted from the dataset.

2.5. Risk screening

The Aquatic Species Invasiveness Screening Kit (AS-ISK) decision-support tool was applied to assess the invasiveness risk of *Rhopilema nomadica* in the İzmit Gulf, referred to as the Risk Assessment (RA) area, based on detectable species identified through eDNA metabarcoding. The AS-ISK adheres completely to the "minimum standards" (Roy et al. 2018) for evaluating non-native species as outlined in the European Commission Regulation on the prevention and management of invasive non-native species. It has proven successful in accurately screening potentially invasive non-indigenous aquatic organisms in various RA areas globally (Vilizzi et al. 2021).

DNA metabarcoding data gathered in this investigation directly influenced the utilization of AS-ISK. *Rhopilema nomadica* was identified by conducting a thorough examination of DNA sequences obtained from samples of ballast water and it was the only non-native species that had the essential biological and ecological data required to address the 55 inquiries of the AS-ISK screening questionnaire.

The AS-ISK screening protocol consists of 55 questions (Copp et al. 2016). The initial 49 questions focus on the Basic Risk Assessment (BRA), examining species' biogeographical and biological aspects. The remaining six questions pertain to the Climate Change Assessment (CCA), requiring the assessor to evaluate how future climate conditions might influence the risks associated with the species' introduction, establishment, dispersal, and impact. Valid screening necessitates providing a response, a level of confidence in the response, and a justification for each question. Upon completing the screening, the species was assigned a BRA score and a BRA+CCA (composite) score, ranging from -20 to 70 and -32 to 82, respectively. Scores below 1 indicated a low risk of invasiveness, while higher scores classified the species as posing either a medium or high risk. The distinction between medium and high-risk levels was determined by a predetermined "threshold" value, which in this study was based on the calibrated BRA score of 6.5 for non-native jellyfishes in the Mediterranean Sea (Killi et al. 2020). The confidence levels associated with each question-related response in the AS-ISK were ranked as follows: 1= low, 2= medium, 3= high, and 4= very high. These confidence rankings aligned with those recommended by the Intergovernmental Programme on Climate Change (IPCC 2005). The overall confidence levels (CL_{Total}), as well as CL_{BRA} and CL_{CCA}, were calculated based on the allocated confidence level for each response across all 55 questions.

3. Results

3.1. eDNA metabarcoding

The data presented were generated from operational taxonomic unit groups (OTUs) consisted of 5 different primers as *12S*, *16S*, COI, *18Sv4* and *18Sv8* and the number of OTUs assigned to species using each primer sets were presented in Figure 2 and Figure 3. The first 20 readings were dominated by terrestrial species, mainly humans and cattle (Figure 2). Apart from these, arthropods,

microalgae, protists, ciliate parasites, rotifers, algae, annelids and bacteria were also present. As for fish species, only one species, *Chelon labrosus*, was identified among the top 20 species (Figure 2 and 3).

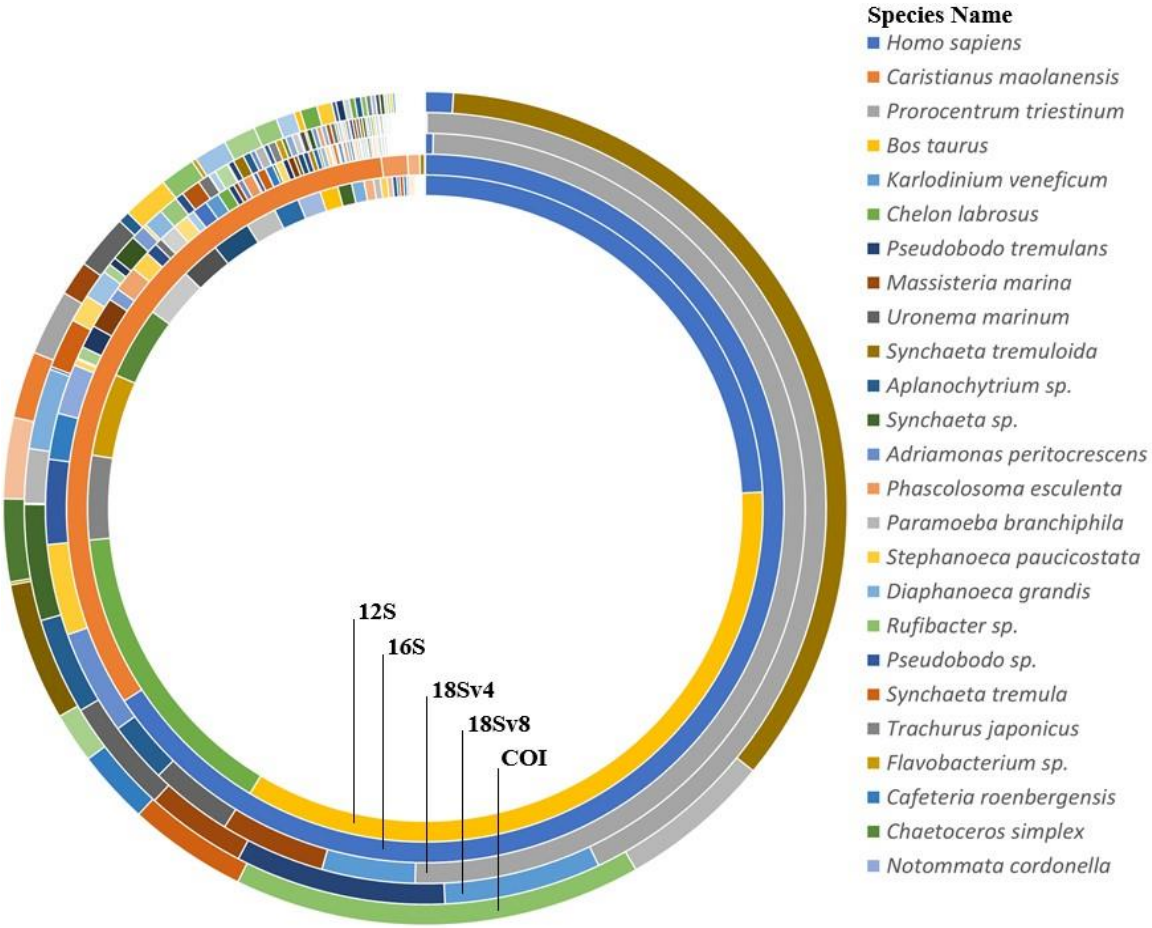

Figure 2- Results of OTUs assigned to species using all the primer sets in this study are presented. The complete list of samples is available in Supplementary Material 1. Circles belong to *12S*, *16S*, *18Sv4*, *18Sv8*, and *COI* from the inside out, respectively."

In the realm of biodiversity, the analysis revealed the identification of 93 species with *COI*, 191 species with *18Sv8*, 241 species with *18Sv4*, 19 species with *16S*, and 44 species with *12S* primers. Results from the *12S* primers indicated that 86% of the data pertained to the targeted group (fish/vertebrates), with 14% identified as those with fewer than 10 reads and species exhibiting less than 98% matching, flagged as suspicious reads. The *16S* primers demonstrated that only 11% of the results belonged to the target group (vertebrates), while the remaining 89% belonged to groups that were incorrectly marked regard to number of reads and percentage of matches. For other primers targeting specific groups, the matching success was calculated as 15% for *COI* targeting invertebrates, 23% for *18Sv4* primers targeting eukaryotic microorganisms, and 27% for *18Sv8*.

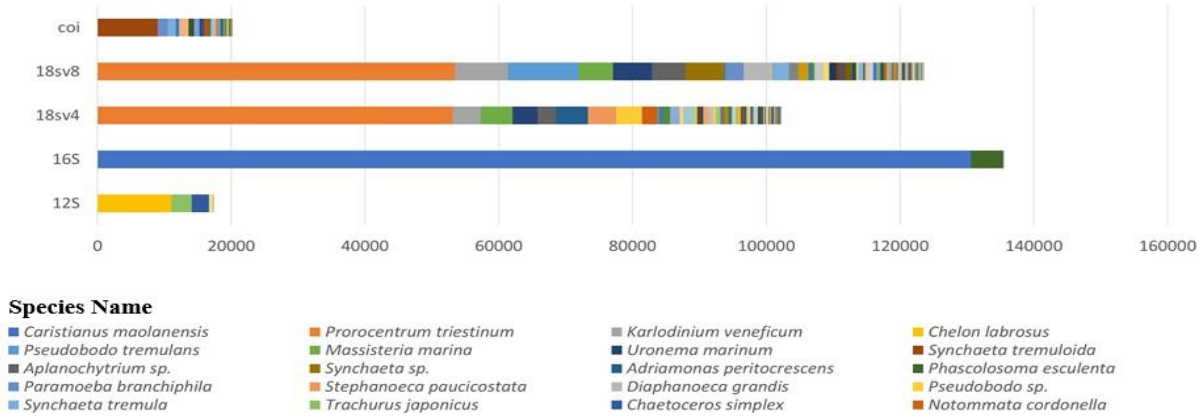

Figure 3- Results of OTUs assigned to species (only the first 20 species with the highest number of reads are presented) for each primer set separately. The complete list of samples is available in Supplementary Material 1.

This work showed us that non-indigenous species as *Nostoc* sp., *Prorocentrum micans*, *R. nomadica*, *Alexandrium minutum* and *Prorocentrum mexicanum*, even *Penaeus vannamei*, most cultured crustacean, could be detected (Supplementary Material 1), but the reads of these species were found suspicious. A pathogenic parasite and an amoeba known as *Uronema marinum* and *Paramoeba branchipila*, also were seen according to OTUs, respectively (Figure 3).

The identification of *Rhopilema nomadica*, as well as other non-native species including *Nostoc sp.*, *Prorocentrum micans*, *Alexandrium minutum*, and *Prorocentrum mexicanum*, demonstrated the efficacy of the multi-primer method.

3.2. Risk screening

According to the calibrated threshold values, BRA scores for *Rhopilema nomadica* indicated a high-risk category for the İzmit Gulf, with a score of 22.5 (Table 1). Considering the potential impact of climate change, it increased to 26.5, signifying an even higher risk for the species to become invasive in this RA area under predicted climate change conditions. Several factors and traits contributed to the increase in the BRA score, with most being biological and ecological features, followed by biogeographical and historical attributes. The history of invasiveness elsewhere is by far the most important factor increasing the overall score in biological and ecological attributes, whereas undesirable threats, reproduction, and dispersal mechanisms where the most score-increasing factors. However, factors like domestication/cultivation in biological and ecological attributes and limited resource exploitation and lack of tolerance attributes by the species in the RA in biological and ecological features lowered the overall score. The mean CL associated with responses to the BRA, CCA and BRA+CCA questions were as follows: CL_{BRA} = 2.41±0.08, CL_{CCA} = 2 and CL_{TOTAL} = 2.36±0.07. These values indicate medium-to-high confidence in all cases (Supplementary material 2).

Table 1- Scoring output from the AS-ISK for nomad jellyfish *Rhopilema nomadica* in the İzmit Gulf

Section/category	***Score***
Biogeography/Historical	13.5
Domestication/Cultivation	0.0
Climate, distribution and introduction risk	3.0
Invasive elsewhere	10.5
Biology/Ecology	9.0
Undesirable (or persistence) traits	5.0
Resource exploitation	0.0
Reproduction	2.0
Dispersal mechanisms	2.0
Tolerance attributes	0.0

4. Discussion

Here, in the present study, according to the recent occurrence of extensive marine mucilage, mainly in İzmit Gulf, has highlighted the deficiencies in wastewater treatment facilities for anthropogenic waste and the lack of effective monitoring of existing facilities. Given the high pollution pressure on this region, introducing of invasive species could have a detrimental impact on the Gulf biodiversity, and the prepotent monitoring could not be carried out in this context due to the limited number of inspections conducted by port state control officers under the BWMC. Our observations for this study, also, stress out mandatory regulation set by the IMO, in compliance with the Ballast Water Performance Standard which many companies have facilitated through ballast water treatment until September 2024.

To identify potentially invasive species, we used various sets of primers targeting distinct genomic areas to amplify and analyze eDNA from a wide range of taxa in order to thoroughly examine the biodiversity and possible dangers associated with ballast water exchange. We were able to overcome the possible biases and restrictions brought with single primer techniques by using different primer sets, leading to a more thorough and precise evaluation of the microbiological and macroscopic diversity found in ballast water. Our results using this multi-primer approach shed light on the complexity and variability of species compositions in ballast water, facilitating a deeper comprehension of the ecological implications and assisting in the development of efficient biosecurity measures to mitigate the introduction and spread of invasive species through ballast water discharge.

The eDNA metabarcoding data for this study provides valuable insights into the species biodiversity (Bautista et al. 2023) within complex environmental samples, particularly ballast waters (Antich et al. 2021; Dugal et al. 2023). This method allows for both species- and taxon-specific identification by aligning genetic sequences (barcodes) with reference sequences in a database, applying universal primers (Pascher et al. 2022). The application of various primers, including *COI*, *18Sv8*, *18Sv4*, *16S*, and *12S*, revealed a wide range of species diversity in ballast water samples. The study showcased the adaptability and utility of eDNA metabarcoding, capturing diverse taxonomic groups and providing a comprehensive understanding of microbial and macroscopic organisms transported through ballast water, with 93, 191, 241, 19, and 44 species identified using each respective primer set as reported by Dugal et al. (2023).

The importance of primer selection in eDNA metabarcoding cannot be overstated, as highlighted in recent studies by van Driessche et al. (2023) and Bautista et al. (2023). These studies emphasize the significant impact of primer choice on the precision and reliability of results. Variations in species detection among different primer sets, such as the superior matching success of *COI* primers targeting invertebrates compared to *18Sv4* and *18Sv8* primers, underscore the critical nature of selecting primers tailored to the taxonomic groups of interest (Keskin & Atar 2013). Additionally, the analysis of *12S* primers yielded results flagged as questionable reads, highlighting the need for cautious interpretation and consideration of primer biases. This raises the possibility of false positives, although Zhang et al. (2020) presented conflicting results and suggested a richer taxonomic composition with the use of *12S* primers over *16S* primers based on sequence references.

The discrepancies in species detection across various primer sets highlight the necessity for meticulous primer selection to improve the precision and taxonomic breadth of eDNA metabarcoding research. Contamination by human DNA is a recognized issue in environmental DNA research, and *Homo sapiens* DNA was identified in our samples. This phenomenon can be ascribed to multiple factors, such as human activities proximate to the sampling locations, airborne pollutants during sample acquisition, or laboratory manipulation. To mitigate these risks, we instituted stringent contamination control measures, including the application of negative field, transport, and equipment controls treated identically to the actual samples, and the enforcement of rigorous laboratory practices such as the utilization of sterile equipment and designated workspaces. Notwithstanding these efforts, the ubiquitous presence of human DNA renders total eradication of contamination challenging. Nonetheless, its existence functions as a crucial procedural safeguard, confirming that contamination control methods were implemented and successful. The identification of human DNA is unlikely to influence our main goal of evaluating the biodiversity of non-native and invasive species, given the studies are concentrated on recognizing species of ecological significance. This study highlights the necessity of continuous efforts to improve contamination control and augment the dependability of eDNA metabarcoding in biodiversity research.

The occurrence of *Homo sapiens* (human) DNA in ballast water eDNA metabarcoding studies poses a technical challenge, primarily due to contamination factors (Rishan et al. 2023; Wee et al. 2023). Contamination can arise from human activities near sampling sites, introducing human genetic material during sample collection and handling (Furlan and Gleeson, 2016; Valdivia-Carrillo et al. 2021). Laboratory procedures, including DNA extraction, PCR amplification, and sequencing, may also introduce human DNA from researchers or surfaces, leading to potential contamination (Goldberg et al. 2016, Huerlimannet al. 2020, Valdivia-Carrillo et al. 2021). Sequencing errors and the use of overlapping taxonomic primers can contribute to false-positive results. Additionally, human DNA from home sewage systems may be present in ballast water discharged from treated wastewater. The persistence of eDNA further complicates the assessment, potentially indicating the presence of species outside their natural habitats (Giroux et al. 2022). To mitigate this issue, researchers should use primers designed to minimize human DNA amplification, implement rigorous quality control measures such as negative controls and blank samples, and maintain sterile analytical procedures to manage potential sources of contamination (Carraro et al. 2020; McClenaghan et al. 2020; Rishan et al. 2023).

Several factors contribute to the presence of non-target species in the current eDNA metabarcoding process. Firstly, the choice of primers significantly influences the specificity of amplification. If the selected primers share partial similarity with off-target species, they may unintentionally amplify undesired sequences. Another reason is primer bias, a characteristic of various primer sets that can lead to unequal amplification of DNA from different taxa, potentially overrepresenting some species and underrepresenting others. Additionally, environmental samples may undergo DNA degradation, which can vary among organisms (Sanchez et al. 2022). This degradation results in shorter fragments that might only partially match the primer sequences, leading to the amplification of degraded DNA from unintended species (Thomsen et al. 2012; Sassoubre et al. 2016). Another significant concern is contamination from various sources, including laboratory chemicals, tools, and human handling. These impurities may contain DNA from non-target species, leading to the inadvertent amplification of off-target species during PCR. Cross-reactivity is another issue, where certain primer sets mistakenly amplify DNA from organisms or species that share genetic sequences. Additionally, during amplification, PCR artifacts such as chimeras, in which non-target DNA sequences mix with target sequences, can occur, potentially resulting in false-positive detections.

Researchers should carefully construct and assess primer sets for specificity and coverage to reduce the amplification of non-target organisms. Their potential can be found using in silico techniques, which can include screening against reference databases and testing on known DNA samples. While minimizing biases, a multi-primer technique mixing various primer sets might enhance the detection of various taxonomic groups. Incorporating negative controls and blank samples into laboratory protocols aids in monitoring and spotting potential contamination. The reliability and accuracy of eDNA metabarcoding analyses can be improved by using strict quality control procedures as optimizing calibration and validation at every single stage of procedures (Rishan et al. 2023) and careful result interpretation to separate real detections from false positives. By solving these problems, eDNA metabarcoding might produce more precise and instructive information on species biodiversity from environmental samples like ballast waters and as well as, some data proposed that the contribution to eDNA method with taxonomic based species identification could be adopted (Jeunen et al. 2019; Rey 2019) for the elimination of environmental factors leads to DNA degradation in eDNA researches.

The results of this work emphasize the need for eDNA metabarcoding studies to use a multi-primer method, as each primer set has advantages and disadvantages in terms of taxonomic coverage and specificity. Achieving a more comprehensive assessment of biodiversity in ballast waters involves carefully selecting a combination of primers targeting various marker genes (Xiong et al. 2022; Bautista et al. 2023). This method ensures a broader taxonomic representation, enhancing the ability to detect rare species—vital indicators of potential invasive species incursions (Freeland 2017; Pawluczyk et al. 2015; Lacoursière-Roussel et al. 2018).

Considering the invasive potential amongst the species for this work, *Uronema marinum*, a pathogen, can pose a risk to fish population already limited this highly polluted area, İzmit Gulf with systemic tissue damagement and high mortality (Li et al. 2018; Huang et al. 2021) coherent with the very first findings of Türe (2021). Nonetheless, among the species within the assessment scope, only *R. nomadica* stands out as it is known for forming blooms along the Eastern Mediterranean coasts of Türkiye. In these regions, it can account for up to 60% of the total catch in trawls, purse seines, and gillnets (Turan et al. 2011). This species has established populations causing substantial swarms in the Levantine Basin of the Mediterranean Sea (Galil et al. 1990; Kıdeys & Gücü 1995). It is suggested that *R. nomadica* entered the RA area via currents and ship ballast waters, using the Suez Canal as a conduit (Killi et al. 2020). Occurrences of *R. nomadica* blooms have been documented across various mediterranean coastal regions in Türkiye, often leading to net clogging in fishing activities (Öztürk & İşinibilir 2010; Turan et al. 2011). Furthermore, its traumatogenic effects have resulted in instances of hospitalization (Gülşahin 2017). Given its preference for warmer waters, the positive climate change score (+4) suggests that *R. nomadica* could potentially benefit from global warming conditions. While increasing temperatures might impact multiple species similarly, the potential for this species to expand beyond its native range to more northerly territories could be augmented due to elevated water temperatures (Walther et al. 2002). While our study predominantly confirms ballast water transportation for this species, it is worth noting that global warming might also facilitate its establishment in new regions.

In addition to *R. nomadica*, other invasive species detected in the current study could also experience shifts in distribution and ecological impact as a result of climate change. For instance, *U. marinum*, already posing a risk in the heavily polluted İzmit Gulf, could see its pathogenic effects exacerbated under warmer water conditions, as elevated temperatures may increase host susceptibility and accelerate pathogen life cycles (Li et al. 2018). Climate-induced stress on native fish populations could make them more vulnerable to pathogens like *U. marinum*, potentially causing more significant ecosystem imbalances and impacting local fisheries. Furthermore, rising water temperatures, combined with changing salinity and oxygen levels, could alter habitat suitability for multiple detected species, potentially facilitating their spread beyond current ranges (Walther et al. 2002). Such shifts could increase competitive pressures on native species, disrupt trophic relationships, and lead to unexpected ecological impacts (Hellmann et al. 2008). For example, invasive species adapted to warmer, low-oxygen environments may outcompete native species as climate change alters baseline ecosystem conditions, promoting their establishment and success (Rahel & Olden 2008).

4.1. Linking metabarcoding data to the AS-ISK screening protocol

The combination of eDNA metabarcoding with the AS-ISK screening process showcases the practical implementation of molecular approaches in ecological risk assessment. The extensive data obtained through metabarcoding offered a strong foundation for evaluating the invasive capacity of identified species, as is the case for *R. nomadica* in the present study. By employing numerous primers, a wide range of taxonomic groups were included, hence improving the identification of infrequent and hard-to-find species that could otherwise go unnoticed.

This paper contributes to the expanding body of research on the application of eDNA metabarcoding for the surveillance of invasive species in ballast water. Prior research has shown that metabarcoding is useful for identifying non-native species and assessing their spread (Comtet et al. 2015; Xiong et al. 2016). This study provides a comprehensive method for monitoring the risks of invasive species in maritime ecosystems by integrating metabarcoding data with current risk assessment frameworks, such as AS-ISK.

Combining samples prior to filtering has been demonstrated to enhance the identification of species that are present in low quantities and simplify extensive monitoring initiatives. The pooling technique employed in this work was selected to augment the sensitivity and efficiency of species detection, particularly in a vast and intricate sample environment like ballast water. Pooling samples has benefits, including enhanced statistical power and the capacity to identify rare species by amalgamating DNA from several sources; nevertheless, it also presents certain constraints. A major concern is the possible loss of information on the geographical and temporal diversity of species distributions, as aggregation obscures differences that may occur across individual samples. This may impact the capacity to precisely evaluate species abundance and diversity, resulting in the over- or underestimating of certain taxa. The statistical efficacy of the pooling method is contingent upon the sample size and the quantity of water treated, which subsequently affect the detection probability of uncommon or low-abundance species. While pooling is useful for comprehensive biodiversity assessments, it entails error margins due to the unequal distribution and shedding rates of eDNA among species. Future research could enhance its findings by employing a hybrid approach that integrates pooled and individual sampling to attain a more thorough picture of species diversity. This approach offers advantages such as heightened sensitivity, cost-effectiveness, and time efficiency (Deiner et al. 2017; Aylagas et al. 2018). This method improves the capacity

to obtain a complete and detailed overview of the variety of life forms present in the studied environment. However, it is important to carefully assess any possible drawbacks, such as the potential reduction in the variability of individual samples.

5. Conclusions

DNA-based tools emerge as a promising alternative to traditional taxonomic surveys, particularly marine habitats facing pollution from ballast water discharge to enhance a prepotent ecological monitoring. In this regard, eDNA metabarcoding proves to be a crucial tool offering extensive taxonomic coverage, even for cryptic, rare and elusive species, with the simultaneous benefits of high identification sensitivity, cost-efficiency, and rapid scanning of entire ecosystems. Metabarcoding can play a pivotal role in supporting management initiatives aimed at reducing the risk of established species and focusing efforts on preventing introductions and spreading. Therefore, a rigorous tracking of invasive species is imperative for long-term and sustainable biomonitoring of aquatic environments. The data from this study also underscores the importance of using a variety of primers to mitigate biases and enhance the precision of species identification. Utilizing novel eDNA metabarcoding with species-selective primers, this combined approach of risk identification and eDNA metabarcoding contributes to a better understanding of early detection, management strategies, and policymaking concerning invasive species, especially for the conservation of marine and freshwater systems.

References

Alberdi A, Aizpurua O, Gilbert M T P & Bohmann K (2018). Scrutinizing key steps for reliable metabarcoding of environmental samples. *Methods in Ecology and Evolution* 9: 134–147. https://doi.org/doi:10.1111/2041-210X.12849.

Ammon U V, Wood S A, Laroche O, Zaiko A, Tait L, Lavery S, Inglis G J & Pochon X (2018). Combining morpho-taxonomy and metabarcoding enhances the detection of non-indigenous marine pests in biofouling communities. *Scientific Reports*, 8(1): 1-11. https://doi.org/10.1038/s41598-018-34541-1.

Andrews S (2010). FastQC: A quality control tool for high throughput sequence data. http://www.bioinformatics.babraham.ac.uk/projects/fastqc/.

Antich A, Palacín C, Cebrian E, Golo R, Wangensteen O S & Turon X. (2021). Marine biomonitoring with eDNA: Can metabarcoding of water samples cut it as a tool for surveying benthic communities? *Molecular Ecology*, 30: 3175–3188. https://doi.org/10.1111/mec.15641.

Aylagas E, Borja Á, Muxika I & Rodríguez-Ezpeleta N (2018). Adapting metabarcoding-based benthic biomonitoring into routine marine ecological status assessment networks. *Ecological Indicators*, 95: 194–202. https://doi.org/10.1016/j.ecolind.2018.07.044.

Bautista J A, Manubag J J, Sumaya N H, Martinez J G & Tabugo S R (2023). Environmental DNA (eDNA) metabarcoding and fish visual census reveals the first record of *Doboatherina magnidentata* in the Philippines. *Biodiversitas*, 24(5): 3063-3072. https://doi.org/10.13057/biodiv/d240562.

Blackman R C, Constable D, Hahn C, Sheard A M, Durkota J, Hänfling B & Lawson Handley L (2017). Detection of a new non-native freshwater species by DNA metabarcoding of environmental samples-first record of *Gammarus fossarum* in the UK. *Aquatic Invasions*, 2(2): 177-189. https://doi.org/10.3391/ai.2017.12.2.06.

Bradie J (2016). METEOR Voyage M116/2: Report on performance of ballast water collection and analysis devices. Prepared for BSH (German Federal Maritime and Hydrographic Agency): 130 pages.

Bradley I M, Pinto A J & Guest J S (2016). Design and evaluation of Illumina MiSeq-compatible, 18S rRNA gene-specific primers for improved characterization of mixed phototrophic communities. *Applied and Environmental Microbiology*, 82(19): 5878-5891. https://doi.org/10.1128/AEM.01630-16.

Borrell Y J, Miralles L, Do Huu H, Mohammed-Geba K & Garcia-Vazquez E (2017). DNA in a bottle—rapid metabarcoding survey for early alerts of invasive species in ports. *PloS One*, 12(9): 1-17. https://doi.org/10.1371/journal.pone.0183347.

Bourlat S J, Haenel Q, Finnman J & Leray M (2016). Preparation of amplicon libraries for metabarcoding of marine eukaryotes using Illumina MiSeq: the dual-PCR method. *Methods in molecular biology*, 1452: 197-207. https://doi.org/10.1007/978-1-4939-3774-5_13.

Boyer F, Mercier C, Bonin A, Le Bras Y, Taberlet P, Coissac E (2016). Obitools: a unix-inspired software package for DNA metabarcoding. *Molecular Ecology Resources*, 16(1): 176–182. https://doi.org/10.1111/1755-0998.12428.

Carraro L, Mächler E, Wüthrich R & Altermatt F (2020). Environmental DNA allows upscaling spatial patterns of biodiversity in freshwater ecosystems. *Nature Communications*, 11(1): 1–12. https://doi.org/10.1038/s41467-020-17337-8.

Chambert T, Pilliod D S, Goldberg C S, Doi H & Takahara T (2018). An analytical framework for estimating aquatic species density from environmental DNA. *Ecology and Evolution*; 8: 3468–3477.https://doi.org/10.1002/ece3.3764.

Comtet T, Sandionigi A, Viard F & Casiraghi M (2015). DNA (meta) barcoding of biological invasions: a powerful tool to elucidate invasion processes and help managing aliens. *Biological invasions*, 17(3): 905-922. https://doi.org/10.1007/s10530-015-0854-y.

Copp G H, Vilizzi L, Tidbury H, Stebbing P D, Tarkan A S, Moissec L & Goulletquer P (2016). Development of a generic decision-support tool for identifying potentially invasive aquatic taxa: AS-ISK. *Management of biological invasions*, 7(4): 343–350. https://doi.org/10.3391/mbi.2016.7.4.04.

Deiner K, Bik H M, Mächler E, Seymour M, Lacoursière-Roussel A, Altermatt F, Creer S, Bista I, Lodge D M, de Vere N, Pfrender M E & Bernatchez L (2017). Environmental DNA metabarcoding: Transforming how we survey animal and plant communities. *Molecular ecology*, 26: 5872-5895. https://doi.org/10.1111/mec.14350.

Doi H, Fukaya K, Oka S, Sato K, Kondoh M & Miya M (2019). Evaluation of detection probabilities at the waterfiltering and initial PCR steps in environmental DNA metabarcoding using a multispecies site occupancy model. *Scientific Reports*, 9: 3581. https://doi.org/10.1038/s41598-019-40233-1.

Dugal L, Thomas L, Meenakshisundaram A,·Simpson T, Lines R, Colquhoun J, Jarman S & Meekan M (2023). Distinct coral reef habitat communities characterized by environmental DNA metabarcoding. *Coral Reefs*, 42: 17-30. https://doi.org/10.1007/s00338-022-02301-3.

Elton C S (1942). Voles, mice and lemmings: problems in populations dynamics. Clarendon press, Oxford.

Fonseca V G, Davison P I, Creach V, Stone D, Bass D & Tidbury H J (2023). The Application of eDNA for Monitoring Aquatic Non-Indigenous Species: Practical and Policy Considerations. *Diversity*, 15: 631. https://doi.org/10.3390/d15050631.

Freeland J R (2017). The importance of molecular markers and primer design when characterizing biodiversity from environmental DNA. *Genome*, 60: 358–374. https://doi.org/10.1139/gen-2016-0100.

Furlan E M & Gleeson D (2016). Improving reliability in environmental DNA detection surveys through enhanced quality control. *Marine and Freshwater Research*, 68(2), 388–395. https://doi.org/10.1071/MF15349.

Galil B S, Spanier E & Ferguson W W (1990). The Scyphomedusae of theMediterranean coast of Israel, including two lessepsian migrants new to theMediterranean. *Zoologische Mededelingen*, Leiden 64: 95-105.

Gehri R R, Larson W A, Gruenthal K, Sard N M & Shi Y (2021). eDNA metabarcoding outperforms traditional fisheries sampling and reveals fine-scale heterogeneity in a temperate freshwater lake. *Environmental DNA*, 3(5): 912–929. https://doi.org/10.1002/edn3.197.

Ghabooli S, Zhan A, Paolucci E, Hernandez M R, Briski E. Cristescu M E & MacIsaac H J (2016). Population attenuation in zooplankton communities during transoceanic transfer in balast water. *Ecology and Evolution*, 6: 6170–6177. https://doi.org/10.1002/ece3.2349.

Gibb C, Pratt N & Sessa R (2013). The Youth Guide to Biodiversity. http://www.fao.org/3/i3157e/i3157e02.pdf. Access: 07.11.2023.

Giroux M S, Reichman J R, Langknecht T, Burgess R M & Ho K T (2022). Environmental RNA as a Tool for Marine Community Biodiversity Assessments. *Scientific Reports*, 12: 17782. https://doi.org/10.1038/s41598-022-22198-w.

Gold Z, Sprague J, Kushner D J, Zerecero Marin E & Barber P H (2021). eDNA metabarcoding as a biomonitoring tool for marine protected areas. *PloS one*, 16(2): e0238557. https://doi.org/10.1371/journal.pone.0238557.

Goldberg C S, Sepulveda A, Ray A, Baumgardt J & Waits L P (2013). Environmental DNA as a new method for early detection of New Zealand mudsnails (*Potamopyrgus antipodarum*). *Freshwater Science*, 32(3): 792-800. https://doi.org/10.1899/13-046.1.

Goldberg C S, Turner C R, Deiner K, Klymus K E, Thomsen P F, Murphy M A, Spear S F, McKee A, Oyler–McCance S J & Cornman R S (2016). Critical considerations for the application of environmental DNA methods to detect aquatic species. *Methods in Ecology and Evolution*, 7(11): 1299–1307. https://doi.org/10.1111/2041-210X.12595.

Grey E K, Bernatchez L, Cassey P, Deiner K, Deveney M, Howland K L, Lacoursière-Roussel A, Leong S C Y, Li Y, Olds B, Pfrender M E, Prowse T A A, Renshaw M A & Lodge D M (2018). Effects of sampling effort on biodiversity patterns estimated from environmental DNA metabarcoding surveys. *Scientific Reports*, 8(1): 1-10. https://doi.org/10.1038/s41598-018-27048-2.

Gülşahin N (2017). A Freshwater Jellyfish in Pond Ula, Muğla: *Craspedacusta sowerbii* Lankester, 1880. *Journal of Aquaculture Engineering and Fisheries Research*, 3(2): 82-86.

He X, Jeffery N W, Stanley R R E, Hamilton L C, Rubidge E M & Abbott C L (2023). eDNA metabarcoding enriches traditional trawl survey data for monitoring biodiversity in the marine environment. *ICES Journal of Marine Science*, 80: 1529–1538. https://doi.org/10.1093/icesjms/fsad083.

Hellmann J J, Byers J E, Bierwagen B G & Dukes J S (2008). Five potential consequences of climate change for invasive species. *Conservation Biology*, 22(3): 534-543. https://doi.org/10.1111/j.1523-1739.2008.00951.x

Huerlimann R, Cooper M, Edmunds R, Villacorta–Rath C, Le Port A, Robson H, Strugnell J, Burrows D & Jerry D (2020). Enhancing tropical conservation and ecology research with aquatic environmental DNA methods: an introduction for non-environmental DNA specialists. *Animal Conservation*, 23(6): 632–645. https://doi.org/10.1111/acv.12583.

IMO (2004). International Convention for the Control and Management of Ships' Ballast Water and Sediments.

IMO 2023. Access: 07.11.2023. https://wwwcdn.imo.org/localresources/en/About/Conventions/StatusOfConventions/StatusOfTreatiesByCountry%20(2).pdf

IPCC (2005). Carbon Dioxide Capture and Storage. Metz B, Davidson O, de Coninck H, Loos M & Meyer L (Eds.) Cambridge University Press, UK. pp 431.

Jeunen G J, Knapp M, Spencer H G, Taylor H R, Lamare M D, Stat M, Bunce M & Gemmell N J (2019). Species-level biodiversity assessment using marine environmental DNA metabarcoding requires protocol optimization and standardization. *Ecology and Evolution*, 9(3): 1323-1335. https://doi.org/10.1002/ece3.4843.

Keskin E & Atar H H (2013). DNA Barcoding: Molecular Identification Using Mitochondrial COI Gene. *Türk Bilimsel Derlemeler Dergisi*, 6(2): 01-08.

Kıdeys A E & Gücü A C (1995). *Rhopilema nomadica*: A Lessepsian scyphomedusan new to the Mediterranean coast of Turkey. *Israel Journal of Zoology*, 41: 615–617. https://doi.org/10.1080/00212210.1995.10688827.

Killi N, Tarkan A S, Kozic S, Copp G H, Davison P I & Vilizzi L (2020). Risk screening of the potential invasiveness of non-native jellyfishes in the Mediterranean Sea. *Marine Pollution Bulletin*, 150: 110728. https://doi.org/10.1016/j.marpolbul.2019.110728.

Lacoursière-Roussel A, Howland K, Normandeau E, Grey E K, Archambault P, Deiner K, Lodge D M, Hernandez C, Leduc N & Bernatchez L (2018). eDNA metabarcoding as a new surveillance approach for coastal Arctic biodiversity. *Ecology and Evolution*, 8(16): 7763-7777. https://doi.org/10.1002/ece3.4213.

Li R, Gao Y, Hou Y, Ye S, Wang L, Sun J & Li Q (2018). Mitochondrial genome sequencing and analysis of scuticociliates (*Uronema marinum*) isolated from Takifugu rubripes. *Mitochondrial DNA Part B*, 3(2): 736-737. https://doi.org/10.1080/23802359.2018.1483757.

McClenaghan B, Fahner N, Cote D, Chawarski J, McCarthy A, Rajabi H, Singer G & Hajibabaei M (2020). Harnessing the power of eDNA metabarcoding for the detection of deep–sea fishes. *PLoS One*, 15(11): e0236540. https://doi.org/10.1371/journal.pone.0236540.

Miya M, Sato Y, Fukunaga T, Sado T, Poulsen J Y, Sato K, Minamoto T, Yamamoto S, Yamanaka H, Araki H, Kondoh M & Iwasaki W (2015). MiFish, a set of universal PCR primers for metabarcoding environmental DNA from fishes: detection of more than 230 subtropical marine species. *Royal Society Open Science*, 2(7): 150088. https://doi.org/10.1098/rsos.150088.

Oka S I, Doi H, Miyamoto K, Hanahara N, Sado T & Miya M (2021). Environmental DNA metabarcoding for biodiversity monitoring of a highly diverse tropical fish community in a coral reef lagoon: Estimation of species richness and detection of habitat segregation. *Environmental DNA*, 3: 55–69. https://doi.org/10.1002/edn3.132.

Ojaveer H, Galil B S, Carlton J T, Alleway H, Goulletquer P, Lehtiniemi M, Marchini A, Miller W, Occhipinti-Ambrogi A, Peharda M, Ruiz G M, Williams S L & Zaiko A (2018). Historical baselines in marine bioinvasions: Implications for policy and management. *PLoS One*, 13: e0202383. https://doi.org/10.1371/journal.pone.0202383.

Öztürk B & İşinibilir M (2010). An alien jellyfish Rhopilema nomadica and its impacts to the Eastern Mediterranean part of Turkey. *J. Black Sea/Mediterranean Environment*, 16(2): 149-156.

Pascher K, Švara V & Jungmeier M (2022). Environmental DNA-Based Methods in Biodiversity Monitoring of Protected Areas: Application Range, Limitations, and Needs. *Diversity*, 14: 463. https://doi.org/10.3390/d14060463.

Pawluczyk M, Weiss J, Links M G, Aranguren M E, Wilkinson M D & Egea-Cortines M (2015). Quantitative evaluation of bias in PCR amplification and next-generation sequencing derived from metabarcoding samples. *Analytical and Bioanalytical Chemistry*, 407: 1841–1848. https://doi.org/10.1007/s00216-014-8435-y.

Pochon X, Bott N J, Smith K F & Wood S A (2013). Evaluating detection limits of next- generation sequencing for the surveillance and monitoring of international marine pests. *PLoS One*, 8: e73935. https://doi.org/10.1371/journal.pone.0073935.

Polanco Fernández A, Marques V, Fopp F, Juhel J B, Borrero-Pérez G H, Cheutin M C, Dejean T, Corredor J D G, Acosta-Chaparro A, Hocdé R, Eme D, Maire E, Spescha M, Valentini A, Manel S, Mouillot D, Albouy C & Pellissier L (2021). Comparing environmental DNA metabarcoding and underwater visual census to monitor tropical reef fishes. *Environmental DNA*, 3 (4): 142–156. https://doi.org/10.1002/edn3.140.

Rahel F J & Olden J D (2008). Assessing the effects of climate change on aquatic invasive species. *Conservation Biology*, 22(3): 521-533. https://doi.org/10.1111/j.1523-1739.2008.00950.x

Rey A (2019). From port to ballast water: application of ADN metabarcoding of shipborne biodiversity. *Thesis*, 207 p. http://hdl.handle.net/10651/52628.

Rishan S T, Kline R J & Rahman S (2023). Applications of environmental DNA (eDNA) to detect subterranean and aquatic invasive species: A critical review on the challenges and limitations of eDNA metabarcoding. *Environmental Advances*, 12: 100370. https://doi.org/10.1016/j.envadv.2023.100370.

Roy H E, Rabitsch W, Scalera R, Stewart A, Gallardo B, Genovesi P, Essl F, Adriaens T, Bacher S, Booy O, Branquart E, Brunel S, Copp G H, Dean H, D'hondt B, Josefsson M, Kenis M, Kettunen M, Linnamagi M, Lucy F, Martinou A, Moore N, Nentwig W, Perg A J, Peyton J, Roques A, Schindler S, Schönrogge K, Solarz W, Stebbing P D, Trichkova T, Vanderhoeven S, van Valkenburg J & Zenetos A (2018). Developing a framework of minimum standards for the risk assessment of alien species. *Journal of Applied Ecology*, 55 (2): 526–538. https://doi.org/10.1111/1365-2664.13025.

Sanchez L, Boulanger E, Arnal V, Boissery P, Dalongeville A, Dejeand T, Deterf J, Guellatia N, Holonf F, Juhela J B, Lenfantg P, Leprieura F, Valentinid A, Manela S & Mouillota D (2022). Ecological indicators based on quantitative eDNA metabarcoding: the case of marine reserves. *Ecological Indicators*, 140: 108966. https://doi.org/10.1016/j.ecolind.2022.108966.

Sassoubre L M, Yamahara K M, Gardner L D, Block B A & Boehm A B (2016). Quantification of Environmental DNA (eDNA) Shedding and Decay Rates for Three Marine Fish. *Environmental Science & Technology*, 50: 10456–10464. https://doi.org/10.1021/acs.est.6b03114.

Shaw J L A, Weyrich L & Cooper A (2017). Using environmental (e)DNA sequencing for aquatic biodiversity surveys: a beginner's guide. *Marine and Freshwater Research*, 68(1): 20–33. https://doi.org/10.1071/MF15361.

Spens J, Evans A R, Halfmaerten D, Knudsen S W, Sengupta M E, Mak S S T, Sigsgaard E E & Hellström M (2017). Comparison of capture and storage methods for aqueous macrobial eDNA using an optimized extraction protocol: advantage of enclosed filter. *Methods in Ecology and Evolution*, 8: 635–645. https://doi.org/10.1111/2041- 210X.12683.

Stat M, John J, Di Battista J D, Newman S J, Bunce M & Harvey E S (2019). Combined use of eDNA metabarcoding and video surveillance for the assessment of fish biodiversity. *Conservation Biology*, 33:196–205. https://doi.org/10.1111/cobi.13183.

Tarkan A S, Vilizzi L, Top N, Ekmekçi G, Stebbing P D & Copp G H (2017). Identification of potentially invasive freshwater fishes, including translocated species, in Turkey using the Aquatic Species Invasiveness Screening Kit (AS-ISK). *International Review of Hydrobiology*, 102: 47-56. https://doi.org/10.1002/iroh.201601877

Tarkan A S, Emiroğlu Ö, Aksu S, Başkurt S, Aksu I, Vilizzi L & Yoğurtçuoğlu B (2022). Coupling molecular and risk analysis to investigate the origin, distribution and potential impact of non-native species: an application to ruffe *Gymnocephalus cernua* in Turkey. *The European Zoological Journal*, 89(1): 109-121. https://doi.org/10.1080/24750263.2021.2022222.

Thomsen P F, Kielgast J, Iversen L L, Møller P R, Rasmussen M & Willerslev E (2012). Detection of a Diverse Marine Fish Fauna Using Environmental DNA from Seawater Samples. *PLoS ONE*, 7: e41732. https://doi.org/10.1371/journal.pone.0041732.

Turan C, Gürlek M, Özbalcılar B, Yağlıoğlu D, Ergüden D, Öztürk B & Güngör M (2011). Jellyfish bycatch data by puse seine, trawl and net fisheries during March–April 2011 in the Mediterranean coasts of Turkey. In First National Workshop on Jellyfish and Other Gelatinous Species in Turkish Marine Waters, Bodrum, 20–21 May 2011. Turkish Marine Research Foundation, (In: Turan, C., Öztürk, B. eds.) (Istanbul, Turkey).

Türe M (2021). Molecular identification of *Uronema marinum* (Protozoa, Ciliophora, Scuticociliatia) in cultured turbot (*Psetta maxima*) larvae. *Veterinary Research Forum*, 12(1): 121-124. https://doi.org/10.30466/vrf.2020.110220.2614.

Valdivia–Carrillo T, Rocha–Olivares A, Reyes–Bonilla H, Domínguez–Contreras J F & Munguia–Vega A (2021). Integrating eDNA metabarcoding and simultaneous underwater visual surveys to describe complex fish communities in a marine biodiversity hotspot. *Molecular Ecology Resources*, 21(5): 1558–1574. https://doi.org/10.1111/1755-0998.13375.

Van Driessche C, Everts T, Neyrinck S & Brys R (2023). Experimental assessment of downstream environmental DNA patterns under variable fish biomass and river discharge rates. *Environmental DNA*, 5(1): 102-116. https://doi.org/10.1002/edn3.361.

Vences M, Lyra M, Bina Perl R G, Bletz M C, Stanković D, Lopes C, Jarek M, Bhuju S, Geffers R, Haddad C & Steinfartz S (2016). Freshwater vertebrate metabarcoding on Illumina platforms using double-indexed primers of the mitochondrial 16S rRNA gene. *Conservation Genetics Resources*, 8(3): 2–6. https://doi.org/10.1007/s12686-016-0550-y.

Verling E, Ruiz G M, Smith L D, Galil B, Miller A W & Murphy K R (2005). Supply-side invasion ecology: characterizing propagule pressure in coastal ecosystems. *Proceedings of the Royal Society B: Biological Sciences*, 272(1569): 1249–1257. https://doi.org/10.1098/rspb.2005.3090.

Vilizzi L, Copp, G H, Hill J E, Adamovich B, Aislabie L, Akin D, Al-Faisal A J, Almeida D, Azmai M N A, Bakiu R, Bellati A, Bernier R, Bies J M, Bilge G, Branco P, Bui T D, Canning-Clode J, Cardoso Ramos H A, Castellanos-Galindo G A, Castro N, Chaichana R, Chainho P, Chan J, Cunico A M, Curd A, Dangchana P, Dashinov D, Davison P I, de Camargo M P, Dodd J A, Durland Donahou A L, Edsman L, Ekmekçi F G, Elphinstone-Davis J, Erős T, Evangelista C, Fenwick G, Ferincz Á, Ferreira T, Feunteun E, Filiz H, Forneck S C, Gajduchenko H S, Gama Monteiro J, Gestoso I, Giannetto D, Gilles A S Jr, Gizzi F, Glamuzina B, Glamuzina L, Goldsmit J, Gollasch S, Goulletquer P, Grabowska J, Harmer R, Haubrock P J, He D, Hean J W, Herczeg G, Howland KL, İlhan A, Interesova E, Jakubčinová K, Jelmert A, Johnsen S I, Kakareko T, Kanongdate K, Killi N, Kim J E, Kırankaya Ş G, Kňazovická D, Kopecký O, Kostov V, Koutsikos N, Kozic S, Kuljanishvili T, Kumar B, Kumar L, Kurita Y, Kurtul I, Lazzaro L, Lee L, Lehtiniemi M, Leonardi G, Leuven R.S E W, Li S, Lipinskaya T, Liu F, Lloyd L, Lorenzoni M, Luna S A, Lyons T J, Magellan K, Malmstrøm M, Marchini A, Marr S M, Masson G, Masson L, McKenzie, C H, Memedemin D, Mendoza R, Minchin D, Miossec L, Moghaddas S D, Moshobane M C, Mumladze L, Naddafi R, Najafi-Majd E, Năstase A, Năvodaru I, Neal J W, Nienhuis S, Nimtim M, Nolan E T, Occhipinti-Ambrogi A, Ojaveer H, Olenin S, Olsson

K, Onikura N, O'Shaughnessy K, Paganelli D, Parretti P, Patoka J, Pavia R T B Jr, Pellitteri-Rosa D, Pelletier-Rousseau M, Peralta E M, Perdikaris C, Pietraszewski D, Piria M, Pitois S, Pompei L, Poulet N, Preda C, Puntila-Dodd R, Qashqaei A T, Radočaj T, Rahmani H, Raj S, Reeves D, Ristovska M, Rizevsky V, Robertson D R, Robertson P, Ruykys L, Saba A O, Santos J M, Sarı H M, Segurado P, Semenchenko V, Senanan W, Simard N, Simonović P, Skóra M E, Slovák Švolíková K, Smeti E, Šmídová T, Špelić I, Srėbalienė G, Stasolla G, Stebbing P, Števove B, Suresh V R, Szajbert B, Ta K A T, Tarkan A S, Tempesti J, Therriault T W, Tidbury H J, Top-Karakuş N, Tricarico E, Troca D F A, Tsiamis K, Tuckett Q M, Tutman P, Uyan U, Uzunova E, Vardakas L, Velle G, Verreycken H, Vintsek L, Wei H, Weiperth A, Weyl O L F, Winter E R, Włodarczyk R, Wood L E, Yang R, Yapıcı S, Yeo S S B, Yoğurtçuoğlu B, Yunnie A LE, Zhu Y, Zięba G, Žitňanová K & Clarke S (2021). A global-scale screening of non-native aquatic organisms to identify potentially invasive species under current and future climate conditions. *Science of the Total Environment*, 788: 147868. https://doi.org/10.1016/j.scitotenv.2021.147868.

Walther G R, Post E, Convey P, Menzel A, Parmesan C, Beebee T J, Fromentin J M Hoegh-Guldberg O & Bairlein F (2002). Ecological responses to recent climate change. *Nature*, 416: 389-395. https://doi.org/10.1038/416389a.

Wee A K S, Salmo III S G, Sivakumar K, Then AY-H, Basyuni M, Fall J, Habib K A, Isowa Y, Leopardas V, Peer N, Artigas-Ramirez M D, Ranawana K, Sivaipram I, Suleiman M & Kajita T (2023). Prospects and challenges of environmental DNA (eDNA) metabarcoding in mangrove restoration in Southeast Asia. *Frontiers in Marine Science*, 10: 1033258. https://doi.org/10.10.3389/fmars.2023.1033258.

Williams S L, Davidson I C, Pasari J R, Ashton G V, Carlton J T, Crafton R E, Fontana R E, Xiong W, Li H & Zhan A (2016). Early detection of invasive species in marine ecosystems using high-throughput sequencing: technical challenges and possible solutions. *Marine Biology*, 163(6): 139. https://doi.org/10.1007/s00227-016-2911-1.

Wright D A, Mitchelmore C L, Place A, Williams E & Orano-Dawson C (2019). Genomic and Microscopic Analysis of Ballast Water in the Great Lakes Region. *Applied Sciences*, 9: 2441. https://doi.org/10.3390/app9122441.

Xiong F, Shu L, Zeng H, Gan X, He S & Peng Z (2022). Methodology for fish biodiversity monitoring with environmental DNA metabarcoding: The primers, databases and bioinformatic pipelines. *Water Biology and Security*, 1(1): 100007. https://doi.org/10.1016/j.watbs.2022.100007.

Yamamoto S, Masuda R, Sato Y, Sado T, Araki H, Kondoh M, Minamoto M & Miya M (2017). Environmental DNA metabarcoding reveals local fish communities in a species-rich coastal sea. *Scientific Reports*, 7: 40368. https://doi.org/10.1038/srep40368.

Zhan A, Hulák M, Sylvester F, Huang X, AdeGulfo A A, Abbott C L, Adamowicz S J, Heath D D, Cristescu M E & MacIsaac H J (2013). High sensitivity of 454 pyrosequencing for detection of rare species in aquatic communities. *Methods in Ecology and Evolution*, 4: 558–565. https://doi.org/10.1111/2041-210X.12037.

Zhang S, Zhao J & Yao M (2020). A comprehensive and comparative evaluation of primers for metabarcoding eDNA from fish. *Methods in Ecology and Evolution*, 11(12): 1609-1625. https://doi.org/10.1111/2041-210X.13485.

Appendix 1- List of *12S, 16S, 18Sv4, 18Sv8* and *COI* primer results and related figures

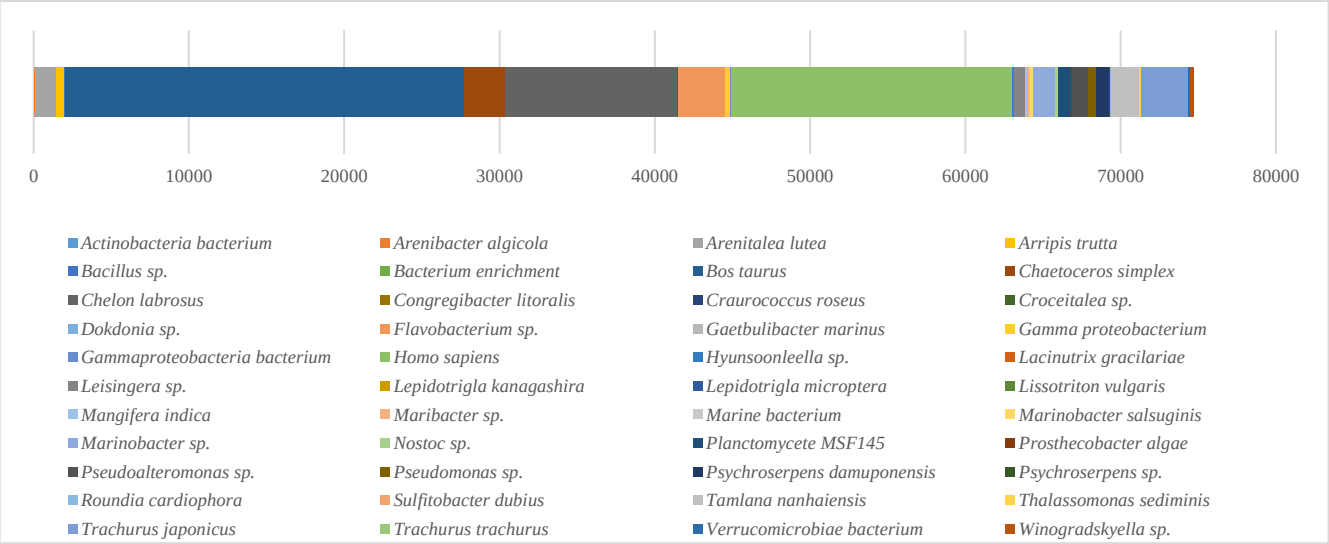

Figure S1. *12S* (Fish/Vertebrate) *Red indicates those either with less than 10 read counts and/or less than 97% identification rate

Table S1. *12S* (Fish/Vertebrate) Primer Results

Species	Read Count	Classification
Actinobacteria bacterium	49	Bacterium
Arenibacter algicola	29	Bacterium
Arenitalea lutea	1399	Flavo Bacterium
*Arripis trutta**	500	Fish
Bacillus sp.	28	Bacterium
Bacterium enrichment	15	Bacterium
Bos taurus	25751	Cow
Chaetoceros simplex	2598	Diatom
Chelon labrosus	11054	Fish
Congregibacter litoralis	19	Bacterium
Craurococcus roseus	14	Bacterium
Croceitalea sp.	51	Bacterium
Dokdonia sp.	23	Flavo Bacterium
Flavobacterium sp.	2985	Flavo Bacterium
Gaetbulibacter marinus	17	Bacterium
Gamma proteobacterium	336	Bacterium
Gammaproteobacteria bacterium	93	Bacterium
Homo sapiens	18092	Human
Hyunsoonleella sp.	14	Flavo Bacterium
Lacinutrix gracilariae	115	Bacterium
Leisingera sp.	647	Bacterium
Lepidotrigla kanagashira	2	Fish
Lepidotrigla microptera	67	Fish
Lissotriton vulgaris	1	Newt
Mangifera indica	135	Plant
Maribacter sp.	95	Flavo Bacterium
Marine bacterium	47	Bacterium
Marinobacter salsuginis	194	Bacterium
Marinobacter sp.	1385	Bacterium
Nostoc sp.	241	Cyanobacteria
Planctomycete MSF145	827	Bacterium
Prosthecobacter algae	14	Bacterium
Pseudoalteromonas sp.	1102	Bacterium
Pseudomonas sp.	446	Bacterium
Psychroserpens damuponensis	903	Bacterium
Psychroserpens sp.	74	Flavo Bacterium
Roundia cardiophora	23	Diatom
Sulfitobacter dubius	14	Bacterium
Tamlana nanhaiensis	1794	Bacterium
Thalassomonas sediminis	158	Bacterium
Trachurus japonicus	3045	Fish
Trachurus trachurus	3	Fish
Verrucomicrobiae bacterium	65	Bacterium
Winogradskyella sp.	239	Flavo Bacterium

Appendix 1-(continued)

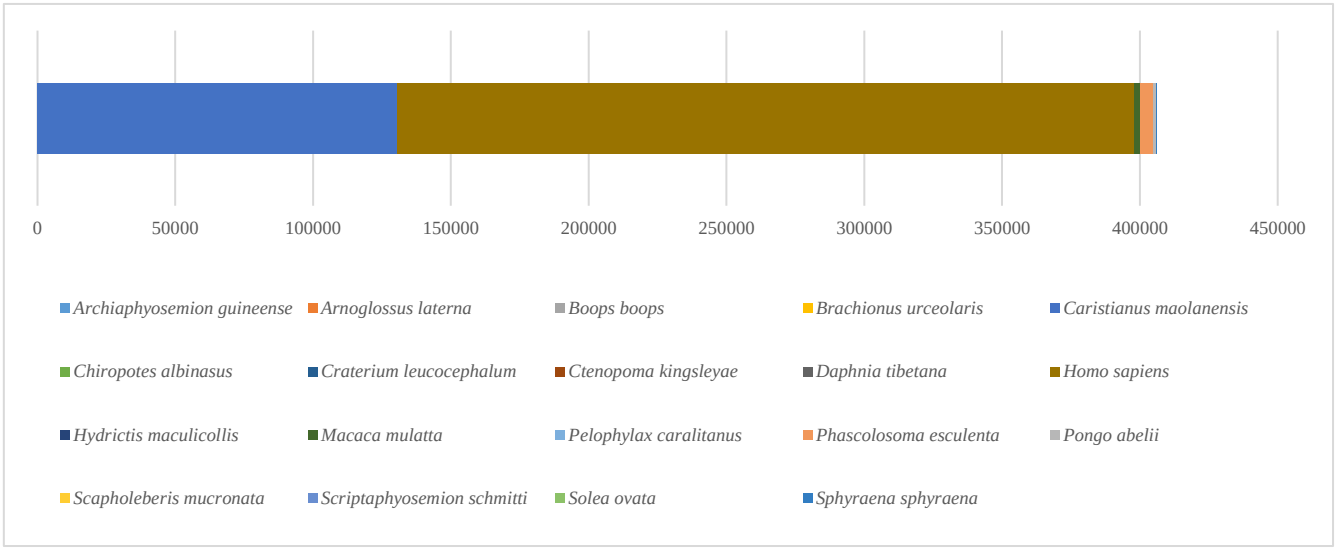

Figure S2. ***16S*** **(Vertebrate) privot** *Red indicates those either with less than 10 read counts and/or less than 97% identification rate

Table S2. ***12S*** **(Fish/Vertebrate) Primer Results**

Species	**Read Count**	**Classification**
*Archiaphyosemion guineense**	3	Fish
Arnoglossus laterna	1	Fish
Boops boops	1	Fish
Brachionus urceolaris	2	Rotifer
Caristianus maolanensis	130608	Insect
Chiropotes albinasus	4	Monkey
Craterium leucocephalum	7	Fungi
Ctenopoma kingsleyae	1	Fish
Daphnia tibetana	1	Crustacean
Homo sapiens	267354	Human
Hydrictis maculicollis	55	Sea otter
Macaca mulatta	2233	Macacus rhesus
Pelophylax caralitanus	1	Frog
Phascolosoma esculenta	4793	Seaworm
Pongo abelii	882	Sumatran orangutan
Scapholeberis mucronata	11	Crustacean
Scriptaphyosemion schmitti	1	Fish
Solea ovata	1	Fish
Sphyraena sphyraena	1	Fish

Appendix 1-(continued)

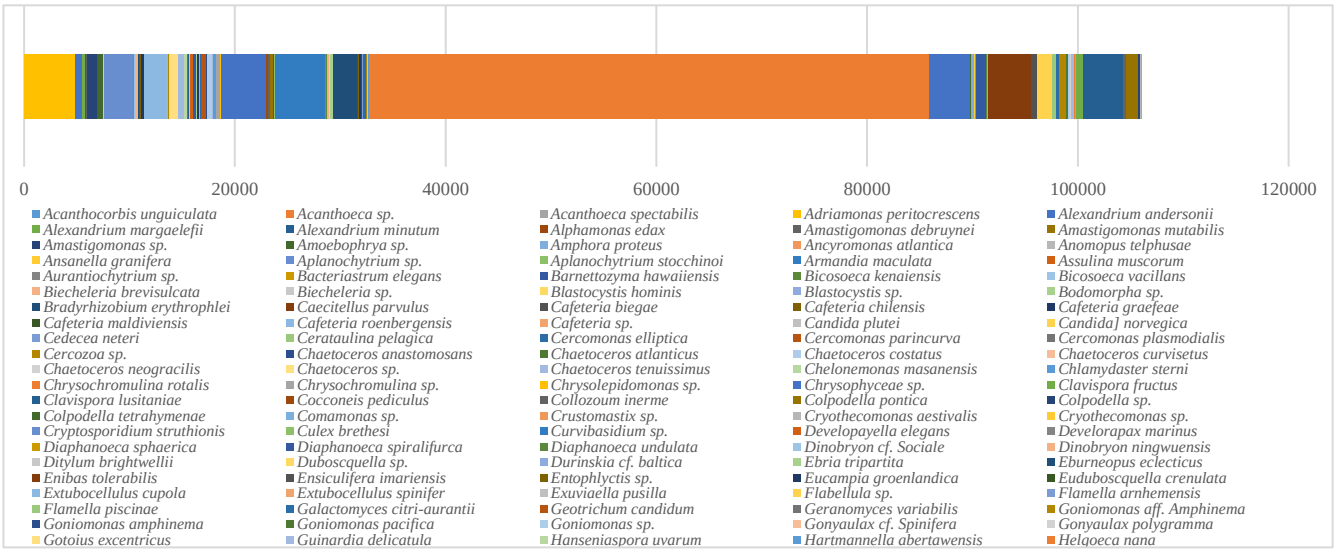

Figure S3. ***18Sv4*** **Eukaryote (Plankton/Algae/Diatom) privot** *Red indicates those either with less than 10 read counts and/or less than 97% identification rate

Table S3. ***18Sv4*** **Eukaryote (Plankton/Algae/Diatom) Primer Results**

Species	Read Count	Classification
*Acanthocorbis unguiculata**	1	Choanocyte
Acanthoeca sp.	4	Choanocyte
Acanthoeca spectabilis	52	Choanocyte
Adriamonas peritocrescens	4793	Flagellate
Alexandrium andersonii	641	Dinoflagellate
Alexandrium margaelefii	328	Dinoflagellate
Alexandrium minutum	49	Dinoflagellate
Alphamonas edax	4	Flagellat
Amastigomonas debruynei	105	Invertebrate
Amastigomonas mutabilis	15	Invertebrate
Amastigomonas sp.	916	Invertebrate
Amoebophrya sp.	588	Dinoflagellate
Amphora proteus	1	Diatome
Ancyromonas atlantica	16	Protist
Anomopus telphusae	10	Rotifer
Ansanella granifera	85	Dinoflagellate
Aplanochytrium sp.	2778	Parasite
Aplanochytrium stocchinoi	3	Parasite
Armandia maculata	1	Sea worm
Assulina muscorum	1	Algae
Aurantiochytrium sp.	64	Protist
Bacteriastrum elegans	3	Diatom
Barnettozyma hawaiiensis	3	Yeast
Bicosoeca kenaiensis	1	Flagellate
Bicosoeca vacillans	80	Flagellate
Biecheleria brevisulcata	264	Dinoflagellate
Biecheleria sp.	15	Dinoflagellate
Blastocystis hominis	3	Algae
Blastocystis sp.	1	Algae
Bodomorpha sp.	58	Algae
Bradyrhizobium erythrophlei	4	Bacterium
Caecitellus parvulus	84	Flagellate
Cafeteria biegae	25	Nanoflagellate
Cafeteria chilensis	103	Nanoflagellate
Cafeteria graefeae	336	Nanoflagellate
Cafeteria maldiviensis	3	Nanoflagellate
Cafeteria roenbergensis	2108	Flagellate
Cafeteria sp.	11	Nanoflagellate
Candida plutei	10	Yeast
Candida norvegica	3	Fungi

Cedecea neteri	2	Bacterium
Cerataulina pelagica	93	Diatome
Cercomonas elliptica	1	Algae
Cercomonas parincurva	4	Algae
Cercomonas plasmodialis	2	Algae
Cercozoa sp.	112	Algae
Chaetoceros anastomosans	1	Diatome
Chaetoceros atlanticus	2	Diatome
Chaetoceros costatus	9	Diatome
Chaetoceros curvisetus	20	Diatome
Chaetoceros neogracilis	11	Diatome
Chaetoceros sp.	806	Diatome
Chaetoceros tenuissimus	551	Diatome
Chelonemonas masanensis	286	Eukaryote (whip)
Chlamydaster sterni	6	Eukaryote
Chrysochromulina rotalis	14	Kelp
Chrysochromulina sp.	23	Kelp
Chrysolepidomonas sp.	27	Algae
Chrysophyceae sp.	17	Algae
Clavispora fructus	2	Yeast
Clavispora lusitaniae	79	Yeast
Cocconeis pediculus	4	Diatome
Collozoum inerme	3	Algae
Colpodella pontica	2	Flagellate (carnivore)
Colpodella sp.	3	Flagellate (carnivore)
Colpodella tetrahymenae	6	Flagellate (carnivore)
Comamonas sp.	44	Bacterium
Crustomastix sp.	4	Algae
Cryothecomonas aestivalis	3	Algae
Cryothecomonas sp.	61	Algae
Cryptosporidium struthionis	1	Parasite
Culex brethesi	6	Mosquito
Curvibasidium sp.	37	Fungi
Developayella elegans	246	Flagellate
Develorapax marinus	1	Algae
Diaphanoeca sphaerica	47	Choanocyte
Diaphanoeca spiralifurca	225	Choanocyte
Diaphanoeca undulata	31	Choanocyte
Dinobryon sociale	2	Algae
Dinobryon ningwuensis	5	Algae
Ditylum brightwellii	1	Diatome
Duboscquella sp.	5	Parasite
Durinskia baltica	6	Dinoflagellate
Ebria tripartita	35	Algae
Eburneopus eclecticus	1	Arthropod
Enibas tolerabilis	9	Choanocyte
Ensiculifera imariensis	14	Dinoflagellate
Entophlyctis sp.	12	Fungi
Eucampia groenlandica	183	Diatome
Eduboscquella crenulata	6	Dinoflagellate
Extubocellulus cupola	28	Diatome
Extubocellulus spinifer	7	Diatome
Exuviaella pusilla	45	Dinoflagellate
Flabellula sp.	6	Amoeba
Flamella arnhemensis	2	Amoeba
Flamella piscinae	4	Amoeba
Galactomyces citri-aurantii	32	Yeast
Geotrichum candidum	547	Yeast
Geranomyces variabilis	15	Fungi
Goniomonas amphinema	15	Nanoflagellate
Goniomonas pacifica	1	Nanoflagellate
Goniomonas sp.	548	Nanoflagellate
Gonyaulax cf. Spinifera	1	Dinoflagellate
Gonyaulax polygramma	15	Dinoflagellate
Gotoius excentricus	3	Dinoflagellate
Guinardia delicatula	4	Diatome
Hanseniaspora uvarum	7	Yeast
Hartmannella abertawensis	246	Amoeba
Helgoeca nana	84	Eukaryote (whip)

Homo sapiens	357	Human
Incisomonas marina	144	Flagellate
Karlodinium veneficum	4204	Dinoflagellate
Katablepharis japonica	13	Algae
Kazachstania africana	24	Fungi
Kluyveromyces marxianus	179	Yeast
Kluyveromyces sp.	215	Yeast
Labyrinthulochytrium haliotidis	220	Fungi
Lepidoglyphus destructor	5	Mite
Leptocylindrus convexus	80	Diatome
Leptocylindrus danicus	1	Diatome
Lingulamoeba sp.	8	Amoeba
Lithodesmioides polymorpha	6	Diatome
Malacoceros fuliginosus	2	Worm (annelid)
Malassezia globosa	2	Fungi
Mantamonas plastica	135	Flagellate
Massisteria marina	4737	Algae
Massisteria sp.	22	Algae
Massisteria voersi	30	Algae
Metromonas simplex	31	Amoeba
Microcaecilia unicolor	1	Amphibian
Micrometopion nutans	83	Amphibian
Minorisa minuta	69	Plankton
Monorhizochytrium globosum	170	Algae
Monosiga brevicollis	1	Eukaryote (whip)
Navicula trivialis	12	Diatome
Neocercomonas sp.	2	Algae
Nolandella sp.	363	Amoeba
Notommata cordonella	2289	Rotifer
Ovulinata parva	20	Algae
Parabirojimia similis	19	Algae
Paraphysomonas butcheri	153	Algae
Paraphysomonas mikadiforma	113	Algae
Paraphysomonas sp.	105	Algae
Parvicardium exiguum	5	Bivalvia
Paulinella micropora	1	Algae
Pectinaria koreni	61	Trumpet worm
Perideraion elongatum	2	Diatome
Philodina sp.	14	Rotifer
Pichia fermentans	71	Yeast
Pichia kudriavzevii	217	Yeast
Picomonas judraskeda	42	Plankton
Pierrecomperia catenuloides	22	Diatome
Pirsonia guinardiae	58	Parasite
Plagiopyliella pacifica	27	Ciliate
Planomonas brevis	2	Flagellate
Planomonas elongata	62	Flagellate
Planomonas micra	17	Flagellate
Platyophrya bromelicola	10	Algae
Polarella glacialis	2	Dinoflagellate
Polykrikos kofoidii	1	Dinoflagellate
Polyoeca dichotoma	1	Eukaryote (whip)
Prorocentrum mexicanum	62	Dinoflagellate
Prorocentrum triestinum	53124	Dinoflagellate
Protaspis sp.	11	Algae
Protostelium nocturnum	19	Amoeba
Pseudobodo sp.	3859	Zooflagellate
Pseudochilodonopsis mutabilis	6	Algae
Pseudochlorella pringsheimii	8	Algae (green)
Pseudocohnilembus persalinus	5	Algae
Pseudophyllomitus vesiculosus	26	Flagellate
Pseudostaurosira madagascariensis	15	Diatome
Pyramimonas sp.	1	Algae (green)
Pyxinia crystalligera	15	Algae
Reckertia gemma	354	Algae
Rhizophlyctis rosea	1	Fungi
Rhoicosphenia abbreviata	9	Diatome
Rhopilema nomadica	71	Jelly fish
Roubikia sp.	1	Insect

Saccamoeba sp.	4	Bacterium
Salpingoeca macrocollata	5	Eukaryote (whip)
Salpingoeca urceolata	13	Eukaryote (whip)
Savillea micropora	5	Eukaryote (whip)
Schizochytrium minutum	11	Algae
Scrippsiella sp.	1054	Dinoflagellate
Sicyoidochytrium sp.	5	Protist
Sourniaea diacantha	4	Dinoflagellate
Spizellomyces pseudodichotomus	14	Fungi
Spondylosium pulchellum	1	Plant
Spumella sp.	31	Algae
Stellarchytrium dubum	47	Algae
Stephanoeca diplocostata	1	Eukaryote (whip)
Stephanoeca norrisii	1	Eukaryote (whip)
Stephanoeca paucicostata	2489	Eukaryote (whip)
Stephanoeca paucicostata	1678	Eukaryote (whip)
Stephanopyxis turris	479	Eukaryote (whip)
Strombidium sp.	5	Ciliate (planktonic)
Symbiodinium sp.	5	Dinoflagellate
Syncystis mirabilis	1	Parasite
Syracosphaera pulchra	6	Algae
Teleaulax amphioxeia	2	Algae
Teleaulax gracilis	11	Algae
Telonema subtilis	1402	Protist
Tetraselmis cordiformis	17	Algae (green)
Tetraselmis rubens	409	Algae (green)
Tetraselmis sp.	233	Algae (green)
Thalassiosira gessneri	6	Diatome
Thalassiosira gravida	1	Diatome
Thalassiosira profunda	690	Diatome
Thalassiosira sp.	22	Diatome
Thaumatomastigidae sp.	187	Algae
Thaumatomastix sp.	108	Algae
Thecamoeba sp.	53	Amoeba
Thraustochytriidae sp.	87	Algae (brown)
Thraustochytrium multirudimentale	38	Protist
Thraustochytrium sp.	271	Fungi
Tokophrya quadripartita	1	Fungi
Trachyrhizium urniformis	11	Amoeba
Triparma pacifica	131	Algae
Tunicothrix wilberti	1	Algae
Ulkenia aff. visurgensis	3	Fungi
Umbraulva japonica	1	Algae (green)
Uncinata gigantea	729	Ciliate
Uronema marinum	3753	Parasite
Vannella samoroda	1	Amoeba
Ventrifissura artocarpoidea	283	Algae
Ventrifissura sp.	1155	Algae
Vexillifera abyssalis	176	Amoeba
Vexillifera bacillipedes	1	Amoeba
Vexillifera sp.	50	Amoeba
Wangodinium sinense	1	Dinoflagellate
Wolffia angusta	19	Plant
Yarrowia deformans	1	Yeast
Yarrowia lipolytica	75	Fungi
Yarrowia sp.	1	Yeast

Appendix 1-(continued)

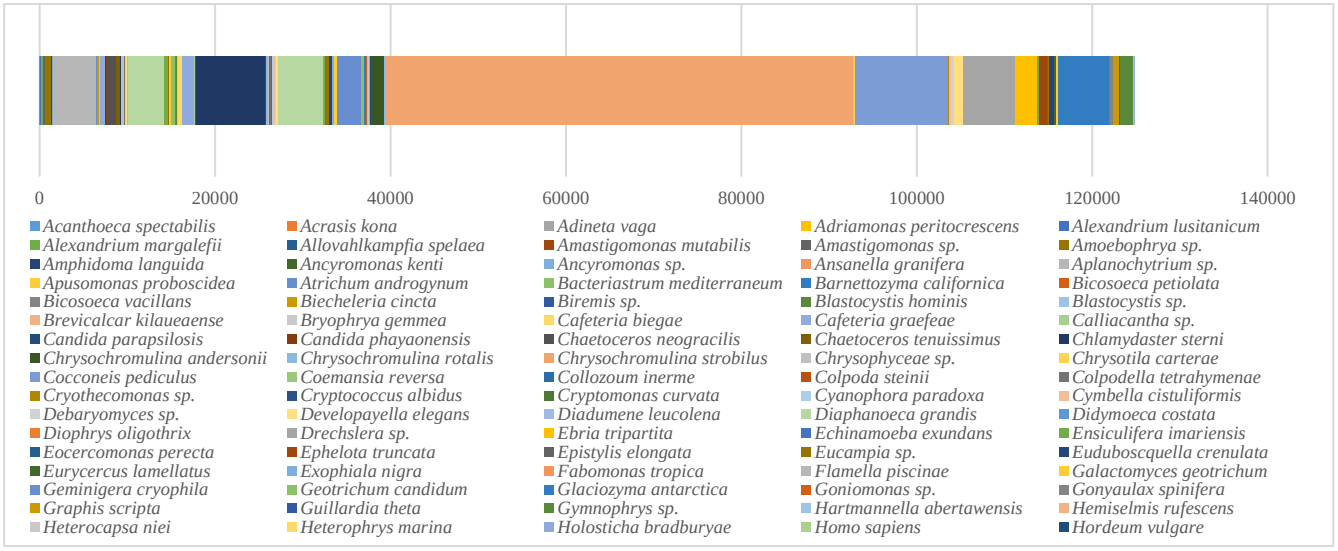

Figure S4. ***18Sv8*** **Eukaryote (Plankton/Algae/Diatom) privot** *Red indicates those either with less than 10 read counts and/or less than 97% identification rate

Table S4. ***18Sv8*** **Eukaryote (Plankton/Algae/Diatom) Primer Results**

Species	**Read Count**	**Classification**
Acanthoeca spectabili	44	Protozoa
*Acrasis kona**	2	Protozoa
Adineta vaga	4	Rotifer
Adriamonas peritocrescens	48	Flagellate
Alexandrium lusitanicum	57	Dinoflagellate
Alexandrium margalefii	242	Dinoflagellate
Allovahlkampfia spelaea	10	Amoeba
Amastigomonas mutabilis	26	Protozoa
Amastigomonas sp.	163	Apusozoa
Amoebophrya sp.	736	Dinoflagellate
Amphidoma languida	71	Dinoflagellate
Ancyromonas kenti	6	Protozoa
Ancyromonas sp.	64	Eukaryote
Ansanella granifera	99	Dinoflagellate
Aplanochytrium sp.	4923	Eukaryote
Apusomonas proboscidea	4	Flagellate
Atrichum androgynum	48	Plant
Bacteriastrum mediterraneum	6	Bacteria
Barnettozyma californica	42	Fungi
Bicosoeca petiolata	2	Bicosoecida
Bicosoeca vacillans	34	Bicosoecida
Biecheleria cincta	188	Dinoflagellate
Biremis sp.	2	Diatome
Blastocystis hominis	6	Parasite
Blastocystis sp.	18	Parasite
Brevicalcar kilaueaense	26	Fungi
Bryophrya gemmea	4	Plant
Cafeteria biegae	30	Eukaryote
Cafeteria graefeae	596	Eukaryote
Calliacantha sp.	16	Eukaryote
Candida parapsilosis	6	Fungi
Candida phayaonensis	242	Fungi
Chaetoceros neogracilis	980	Diatome
Chaetoceros tenuissimus	429	Diatome
Chlamydaster sterni	88	Algae
Chrysochromulina andersonii	42	Seaweed
Chrysochromulina rotalis	11	Seaweed
Chrysochromulina strobilus	22	Seaweed
Chrysophyceae sp.	315	Algae

Chrysotila carterae	8	Algae
Cocconeis pediculus	16	Algae
Coemansia reversa	2	Arthropod
Collozoum inerme	4	Eukaryote
Colpoda steinii	18	Eukaryote
Colpodella tetrahymenae	6	Eukaryote
Cryothecomonas sp.	22	Kelp
Cryptococcus albidus	18	Yeast
Cryptomonas curvata	36	Flagellate
Cyanophora paradoxa	24	Flagellate
Cymbella cistuliformis	2	Diatome
Debaryomyces sp.	17	Yeast
Developayella elegans	244	Plankton
Diadumene leucolena	24	Anemone
Diaphanoeca grandis	4120	Eukaryote (whip)
Didymoeca costata	12	Eukaryote (whip)
Diophrys oligothrix	8	Kelp
Drechslera sp.	12	Fungi
Ebria tripartita	28	Algae
Echinamoeba exundans	2	Eukaryote
Ensiculifera imariensis	388	Dinoflagellate
Eocercomonas perecta	12	Kelp
Ephelota truncata	2	Protozoa
Epistylis elongata	2	Kelp
Eucampia sp.	69	Diatome
Eudubosquella crenulata	18	Dinoflagellate
Eurycercus lamellatus	4	Arthropod
Exophiala nigra	2	Fungi
Fabomonas tropica	10	Eukaryote
Flamella piscinae	6	Amoeba
Galactomyces geotrichum	237	Yeast
Geminigera cryophila	4	Algae
Geotrichum candidum	470	Fungi
Glaciozyma antarctica	4	Yeast
Goniomonas sp.	50	Algae
Gonyaulax spinifera	2	Dinoflagellate
Graphis scripta	6	Fungi
Guillardia theta	2	Algae
Gymnophrys sp.	86	Eukaryote
Hartmannella abertawensis	68	Eukaryote
Hemiselmis rufescens	2	Algae
Heterocapsa niei	66	Dinoflagellate
Heterophrys marina	462	Eukaryote
Holosticha bradburyae	1374	Ciliate
Homo sapiens	89	Human
Hordeum vulgare	4	Plant
Hyphochytrium catenoides	12	Eukaryote
Ichthyophonus irregularis	114	Parasite
Ipomoea trifida	42	Plant
Karlodinium veneficum	7908	Dinoflagellate
Katablepharis japonica	16	Algae
Kluyveromyces marxianus	241	Yeast
Korotnevella pelagolacustris	2	Protozoa
Labyrinthuloides minuta	103	Kelp
Laetisaria fuciformis	23	Fungi
Leptocylindrus convexus	18	Diatome
Leptocylindrus danicus	2	Diatome
Leptomyxa reticulata	22	Amoeba
Leptosphaeria biglobosa	50	Fungi
Leucosporidium sp.	165	Fungi
Leucosporidium yakuticum	25	Fungi
Lingulamoeba leei	32	Amoeba
Malassezia globosa	29	Fungi
Mallomonas akrokomos	232	Algae
Mallomonas tonsurata	82	Algae
Mamiella gilva	136	Plankton
Mantamonas plastica	214	Flagellate
Marchantia quadrata	2	Plant
Massisteria marina	5093	Kelp

Massisteria sp.	104	Kelp
Massisteria voersi	32	Kelp
Melosira varians	2	Diatome
Micromonas pusilla	4	Algae
Monosiga brevicollis	8	Eukaryote (whip)
Myrothecium sp.	158	Fungi
Nausithoe rubra	8	Jelly fish
Neohodgsonia mirabilis	2	Plant
Neoparamoeba branchiphila	33	Parasite
Neoparamoeba sp.	394	Parasite
Nolandella sp.	344	Amoeba
Nurscia albofasciata	10	Arthropod
Nusuttodinium poecilochroum	264	Dinoflagellate
Ovulinata parva	16	Kelp
Paraflabellula hoguae	4	Amoeba
Paramoeba aestuarina	276	Kelp
Paramoeba branchiphila	2773	Amoeba
Paramoeba perurans	324	Parasite
Paraphysomonas imperforata	178	Algae
Parauronema virginianum	160	Protozoa
Paulinella chromatophora	4	Amoeba
Pectinaria koreni	46	Sea worm
Penaeus duorarum	4	Shrimp
Pentapharsodinium sp.	11	Dinoflagellate
Peridinium sociale	2	Dinoflagellate
Phoma herbarum	70	Fungi
Pichia fermentans	114	Yeast
Pichia sp.	32	Fungi
Picomonas judraskeda	40	Plankton
Pinus taeda	2	Plant (pine tree)
Pirsonia guinardiae	99	Flagellate
Plagiopyliella pacifica	8	Kelp
Planomonas brevis	54	Flagellate
Planomonas elongata	12	Flagellate
Platyamoeba contorta	2	Amoeba
Prorocentrum mexicanum	1484	Dinoflagellate
Prorocentrum micans	10	Dinoflagellate
Prorocentrum triestinum	53452	Dinoflagellate
Pseliodinium pirum	26	Dinoflagellate
Pseudobodo sp.	139	Algae
Pseudobodo tremulans	10618	Algae
Pseudo-nitzschia delicatissima	41	Diatome
Pseudoparamoeba pagei	2	Amoeba
Pyramimonas tetrarhynchus	10	Algae (green)
Rhizoclosmatium sp.	6	Fungi
Rhodotorula mucilaginosa	29	Fungi
Rhogostoma schuessleri	2	Kelp
Rhopilema nomadica	41	Jelly fish
Salpingoeca urceolata	22	Choanocyte
Savillea micropora	148	Choanocyte
Scrippsiella sp.	405	Dinoflagellate
Scrippsiella trochoidea	1004	Dinoflagellate
Slooffia sp.	10	Fungi
Soletellina diphos	2	Bivalvia
Strombidium sp.	2	Ciliate
Strombidium stylifer	2	Ciliate
Synchaeta sp.	5918	Rotifer
Synchaeta tremula	2560	Rotifer
Syncystis mirabilis	2	Parasite
Synura sp.	162	Algae
Taphrina vestergrenii	2	Fungi
Tetraselmis marina	976	Algae (green)
Thalassiosira minima	14	Algae
Thaumatomastix sp.	110	Kelp
Thaumatomonas seravini	546	Kelp
Thraustochytrium sp.	304	Algae (brown)
Tintinnidium mucicola	2	Kelp
Toxorhynchites amboinensis	6	Mosquito
Trichia sordida	6	Protozoa

Trichodina meretricis	232	Kelp
Tripos tenuis	2	Dinoflagellate
Ulkenia profunda	2	Fungi (Marine)
Uronema marinum	5849	Parasite
Vacuolaria virescens	20	Algae (green)
Vannella calycinucleolus	340	Amoeba
Vannella samoroda	702	Amoeba
Vannella sp.	158	Amoeba
Ventrifissura artocarpoidea	1402	Kelp
Vexillifera abyssalis	98	Amoeba
Vexillifera armata	64	Amoeba
Vexillifera sp.	21	Amoeba
Yarrowia deformans	4	Fungi
Yarrowia lipolytica	28	Fungi

Appendix 1-(continued)

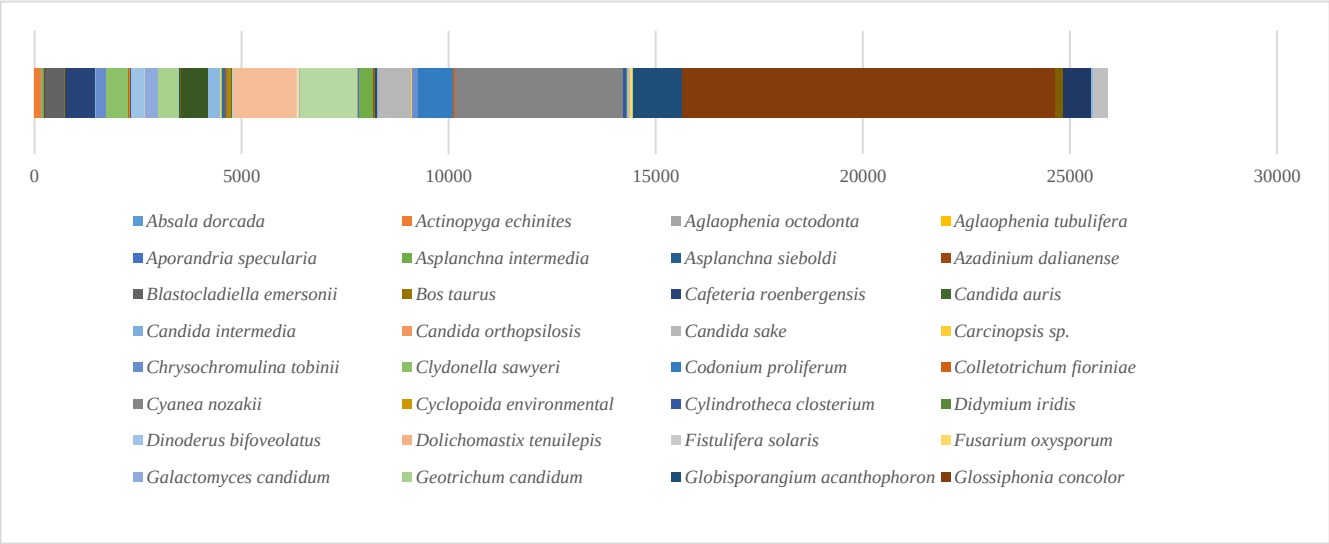

Figure S5. *COI* (Invertebrate) privot *Red indicates those either with less than 10 read counts and/or less than 97% identification rate

Table S5. *COI* (Invertebrate) Primer Results

Species	Read Count	Classification
*Absala dorcada**	1	Heterocera
Actinopyga echinites	169	Tripang
Aglaophenia octodonta	11	Hydrozoa
Aglaophenia tubulifera	1	Hydrozoa
Aporandria specularia	5	Heterocera
Asplanchna intermedia	60	Rotifer
Asplanchna sieboldi	2	Rotifer
Azadinium dalianense	26	Dinoflagellate
Blastocladiella emersonii	460	Fungi
Bos taurus	1	Cow
Cafeteria roenbergensis	739	Flagellate
Candida auris	1	Yeast
Candida intermedia	9	Yeast
Candida orthopsilosis	1	Yeast
Candida sake	1	Yeast
Carcinopsis sp.	3	Insect
Chrysochromulina tobinii	234	Kelp
Clydonella sawyeri	547	Ameoba
Codonium proliferum	1	Hydrozoa
Colletotrichum fioriniae	3	Fungi
Cyanea nozakii	1	Jellyfish
Cyclopoida environmental	44	Copepod
Cylindrotheca closterium	7	Diatome
Didymium iridis	9	Mold
Dinoderus bifoveolatus	321	Insect
Dolichomastix tenuilepis	2	Algae (green)

Fistulifera solaris	10	Diatome
Fusarium oxysporum	1	Fungi
Galactomyces candidum	327	Yeast
Geotrichum candidum	507	Yeast
Globisporangium acanthophoron	13	Fungi
Glossiphonia concolor	4	Worm
Gonium pectorale	4	Algae (green)
Gorilla beringei	13	Gorilla
Haliplus fasciatus	4	Insect
Heterocapsa circularisquama	660	Dinoflagellat
Homo sapiens	277	Human
Hordeum vulgare	9	Barley
Hypochilus bonneti	10	Spider
Lichtheimia ramosa	8	Fungi
Lizzia blondina	10	Hydrozoa
Lytocarpia myriophyllum	1	Hydrozoa
Malassezia globosa	73	Fungi
Maribacter sp.	41	Bacterium
Minutocellus polymorphus	14	Diatom
Neoparamoeba sp.	115	Ameba
Nitzschia frustulum	1	Diatom
Nitzschia palea	5	Diatom
Pan troglodytes	29	Chimpanzee
Paramoeba branchiphila	1515	Parasite
Paramoeba perurans	44	Ameoba
Paravannella minima	42	Ameoba
Penaeus vannamei	5	Shrimp
Penilia avirostris	1392	Crustacean
Phaeocystis pouchetii	11	Algae
Phoma sp.	1	Fungi
Phytophthora boehmeriae	6	Fungi
Phytophthora cajani	15	Fungi
Phytophthora moyootj	16	Fungi
Pichia kudriavzevii	349	Yeast
Plecotus auritus	2	Bat
Plecotus ognevi	2	Bat
Pneumocystis jirovecii	4	Fungi
Pongo abelii	28	Sumatra orangutan
Prorocentrum micans	54	Dinoflagellate
Pseudoceratina purpurea	2	Sponge
Pseudogymnoascus pannorum	9	Fungi
Pseudopedobacter saltans	7	Bacterium
Pyropia haitanensis	813	Algae (red)
Pythium biforme	5	Fungi
Pythium emineosum	150	Fungi
Rhagoletis zephyria	11	Fruit Mosquito
Rhodotorula mucilaginosa	831	Fungi
Rhopilema nomadica	62	Jellyfish
Rufibacter sp.	4055	Bacterium
Saccharomyces cerevisiae	1	Fungi
Scapholeberis mucronata	60	Crustacean
Schizophyllum commune	26	Fungi
Scrippsiella precaria	41	Dinoflagellate
Selenops sp.	30	Arthropod
Shiraia bambusicola	1	Fungi
Squamamoeba japonica	51	Ameoba
Symbiodinium sp.	1	Microalgae
Synchaeta oblonga	15	Rotifer
Synchaeta tremula	1181	Rotifer
Synchaeta tremuloida	9012	Rotifer
Taphrina wiesneri	10	Plant pathogen
Thecamonas trahens	185	Bacterium
Tremella fuciformis	673	Fungi
Trichoderma hamatum	1	Fungi
Tristramella simonis	49	Fish
Vanderwaltozyma polyspora	8	Fungi
Vexillifera sp.	350	Ameoba

Appendix 2- *Rhopilema nomadica* AS-ISK analysis

AS-ISK v2

Taxon and Assessor details	
Category	Invertebrates (marine)
Taxon name	*Rhopilema nomadica*
Common name	Nomad jellyfish
Assessor	Ali Serhan Tarkan
Risk screening context	
Reason and socio-economic benefits	
Risk assessment area	Izmit Gulf
Taxonomy	
Native range	
Introduced range	
URL	

			Response	Justification (references and/or other information)	Confidence
A. Biogeography/Historical					
1. Domestication/Cultivation					
1	1,01	Has the taxon been the subject of domestication (or cultivation) for at least 20 generations?	No	No report is available for domestication or cultivation of this species	Medium
2	1,02	Is the taxon harvested in the wild and likely to be sold or used in its live form?	No	No report found on this	Medium
3	1,03	Does the taxon have invasive races, varieties, sub-taxa or congeners?	Yes	Yu, H., Li, C., Li, R., Xing, R., Liu, S., Li, P., 2007. Factors influencing hemolytic activity of venom from the jellyfish Rhopilema esculentum Kishinouye. Food and Chemical Toxicology, 45(7), 1173-1178.	High
2. Climate, distribution and introduction risk					
4	2,01	How similar are the climatic conditions of the Risk Assessment (RA) area and the taxon's native range?	Medium	According to Köppen-Geiger classification scheme	Medium
5	2,02	What is the quality of the climate matching data?	Medium	According to Köppen-Geiger classification scheme	Medium
6	2,03	Is the taxon already present outside of captivity in the RA area?	No	There is no report or documentation that the species present outside of captivity in the RA area	Medium
7	2,04	How many potential vectors could the taxon use to enter in the RA area?	>1	There is a report that it was detected in ballast water of the ships (Koray, 2022) and it could transported by natural ways (currents) from Mediterranean Sea. Koray, K. 2022. Gemi Balast Suları ile Taşınan Yabancı Türlerin eDNA Metabarkodlama Yöntemiyle Tespiti ve Risk Analizleri: İzmit Körfezi. Institute of Science. Ankara Universtiy	Medium
8	2,05	Is the taxon currently found in close proximity to, and likely to enter into, the RA area in the near future (e.g. unintentional and intentional introductions)?	Yes	This species have been recorded (established) (Gulsahin & Tarkan 2011) from neighbouring sea basin (Aegean Sea) so given no pyhisical barries between seas and high ship traffic it is likely to enter into RA. Gülşahin, N., Tarkan, A. N., 2011. The first confirmed record of the alien jellyfish Rhopilema nomadica Galil, 1990 from the southern Aegean coast of Turkey. Aquatic Invasions, 6 (Suppl 1), S95-S97.	High
3. Invasive elsewhere					
9	3,01	Has the taxon become naturalised (established viable populations) outside its native range?	Yes	Cinar, ME, Bilecenoğlu, M, Yokeş M.B, Ozturk B, Taşkin E, Bakir K, et al.(2021). Current status (as of end of 2020) of marine alien species in Turkey. PLoSONE16(5): e0251086.	Very high
10	3,02	In the taxon's introduced range, are there known adverse impacts to wild stocks or commercial taxa?	Yes	Galil, B. S., 1993. Lessepsian migration: new findings on the foremost anthropogenic change in the Levant basin fauna. Ist. Sci. Ambientali Mar., Santa Margherita Ligure (Italy), 307-318.	High
11	3,03	In the taxon's introduced range, are there known adverse impacts to aquaculture?	No	No evidence	Medium
12	3,04	In the taxon's introduced range, are there known adverse impacts to ecosystem services?	Yes	Turan, C., Gürlek, M., Özbalcılar, B., Yağlıoğlu, D., Ergüden, D. et al., 2011. Jellyfish bycatch data by puse seine, trawl and net fisheries during March-April 2011 in the Mediterranean coasts of Turkey, p.1- First National Workshop on Jellyfish and Other Gelatinous Species in Turkish Marine Waters,Bodrum, 20–21 May 2011. Turkish Marine Research Foundation,(In: Turan, C., Öztürk, B. eds.) Istanbul, Turkey.	High
13	3,05	In the taxon's introduced range, are there known adverse socio-economic impacts?	Yes	ÖZTÜRK, B. & ISINIBILIR, M., 2010. An alien jellyfish Rhopilema nomadica and its impacts to the Eastern Mediterranean part of Turkey. Journal of the Black Sea/Mediterranean Environment, 16 (2): 149-156.	High

Appendix 2-(continued)

B. Biology/Ecology					
4. Undesirable (or persistence) traits					
14	4,01	Is it likely that the taxon will be poisonous or pose other risks to human health?	Yes	Gusmani, L., Avian, M., Galil, B., Patriarca, P., Rottini, G., 1997. Biologically active polypeptides in the venom of the jellyfish Rhopilema nomadica. Toxicon, 35(5), 637-648.	High
15	4,02	Is it likely that the taxon will smother one or more native taxa (that are not threatened or protected)?	No	No report/evidence	Medium
16	4,03	Are there any threatened or protected taxa that the non-native taxon would parasitise in the RA area?	No	No evidence	Medium
17	4,04	Is the taxon adaptable in terms of climatic and other environmental conditions, thus enhancing its potential persistence if it has invaded or could invade the RA area?	Yes	N. Killi, A.S. Tarkan, S. Kozic, G.H. Copp, P.I. Davison, L. Vilizzi Risk screening of the potential invasiveness of non native jellyfishes in the Mediterranean Sea Mar. Pollut. Bull., 150 (2020) 110728,	High
18	4,05	Is the taxon likely to disrupt food-web structure/function in aquatic ecosystems if it has invaded or is likely to invade the RA area?	No	The species has not been found to occur and establish in RA area so it is higly unlikely that it could disrupt the ecosystem as such	Medium
19	4,06	Is the taxon likely to exert adverse impacts on ecosystem services in the RA area?	Yes	It is likely that it affects fishing activities by clogging the nets and disrupts gears	Medium
20	4,07	Is it likely that the taxon will host, and/or act as a vector for, recognised pests and infectious agents that are endemic in the RA area?	No	No evidence	Medium
21	4,08	Is it likely that the taxon will host, and/or act as a vector for, recognised pests and infectious agents that are absent from (novel to) the RA area?	No	No evidence	Medium
22	4,09	Is it likely that the taxon will achieve a body size that will make it more likely to be released from captivity?	Not applicable	This species is not kept at captivity	Medium
23	4,10	Is the taxon capable of sustaining itself in a range of water velocity conditions (e.g. versatile in habitat use)?	Yes	ÖZTÜRK, B. & ISINIBILIR, M., 2010. An alien jellyfish Rhopilema nomadica and its impacts to the Eastern Mediterranean part of Turkey. Journal of the Black Sea/Mediterranean Environment, 16 (2): 149-156.	High
24	4,11	Is it likely that the taxon's mode of existence (e.g. excretion of by-products) or behaviours (e.g. feeding) will reduce habitat quality for native taxa?	No	No evidence	Medium
25	4,12	Is the taxon likely to maintain a viable population even when present in low densities (or persisting in adverse conditions by way of a dormant form)?	Yes	N. Killi, A.S. Tarkan, S. Kozic, G.H. Copp, P.I. Davison, L. Vilizzi Risk screening of the potential invasiveness of non native jellyfishes in the Mediterranean Sea Mar. Pollut. Bull., 150 (2020) 110728,	High
5. Resource exploitation					
26	5,01	Is the taxon likely to consume threatened or protected native taxa in the RA area?	No	No evidence	Medium
27	5,02	Is the taxon likely to sequester food resources (including nutrients) to the detriment of native taxa in the RA area?	No	No evidence	Medium
6. Reproduction					
28	6,01	Is the taxon likely to exhibit parental care and/or to reduce age-at-maturity in response to environmental conditions?	No	The species does not have such features	Medium
29	6,02	Is the taxon likely to produce viable gametes or propagules (in the RA area)?	No	No report for maturation nor reproduction is avalable in RA area	Medium
30	6,03	Is the taxon likely to hybridise naturally with native taxa?	Not applicable	This species has no such reproduction system allowing hybridization	High
31	6,04	Is the taxon likely to be hermaphroditic or to display asexual reproduction?	Yes	N. Killi, A.S. Tarkan, S. Kozic, G.H. Copp, P.I. Davison, L. Vilizzi Risk screening of the potential invasiveness of non native jellyfishes in the Mediterranean Sea Mar. Pollut. Bull., 150 (2020) 110728,	High
32	6,05	Is the taxon dependent on the presence of another taxon (or specific habitat features) to complete its life cycle?	No	No evidence	Medium
33	6,06	Is the taxon known (or likely) to produce a large number of propagules or offspring within a short time span (e.g. < 1 year)?	Yes	N. Killi, A.S. Tarkan, S. Kozic, G.H. Copp, P.I. Davison, L. Vilizzi Risk screening of the potential invasiveness of non native jellyfishes in the Mediterranean Sea Mar. Pollut. Bull., 150 (2020) 110728,	High
34	6,07	How many time units (days, months, years) does the taxon require to reach the age-at-first-reproduction?	6	months - N. Killi, A.S. Tarkan, S. Kozic, G.H. Copp, P.I. Davison, L. Vilizzi Risk screening of the potential invasiveness of non native jellyfishes in the Mediterranean Sea Mar. Pollut. Bull., 150 (2020) 110728,	High

Appendix 2-(continued)

7. Dispersal mechanisms					
35	7,01	How many potential internal vectors/pathways could the taxon use to disperse within the RA area (with suitable habitats nearby)?	One	ballast waters: Koray, K. (2022). Gemi Balast Suları ile Taşınan Yabancı Türlerin eDNA Metabarkodlama Yöntemiyle Tespiti ve Risk Analizleri: İzmit Körfezi. Institute of Science. Ankara Universtiy	Medium
36	7,02	Will any of these vectors/pathways bring the taxon in close proximity to one or more protected areas (e.g. MCZ, MPA, SSSI)?	No	No relevant information is available	Medium
37	7,03	Does the taxon have a means of actively attaching itself to hard substrata (e.g. ship hulls, pilings, buoys) such that it enhances the likelihood of dispersal?	Yes	N. Killi, A.S. Tarkan, S. Kozic, G.H. Copp, P.I. Davison, L. Vilizzi Risk screening of the potential invasiveness of non native jellyfishes in the Mediterranean Sea Mar. Pollut. Bull., 150 (2020) 110728,	High
38	7,04	Is natural dispersal of the taxon likely to occur as eggs (for animals) or as propagules (for plants: seeds, spores) in the RA area?	Yes	N. Killi, A.S. Tarkan, S. Kozic, G.H. Copp, P.I. Davison, L. Vilizzi Risk screening of the potential invasiveness of non native jellyfishes in the Mediterranean Sea Mar. Pollut. Bull., 150 (2020) 110728,	High
39	7,05	Is natural dispersal of the taxon likely to occur as larvae/juveniles (for animals) or as fragments/seedlings (for plants) in the RA area?	Yes	N. Killi, A.S. Tarkan, S. Kozic, G.H. Copp, P.I. Davison, L. Vilizzi Risk screening of the potential invasiveness of non native jellyfishes in the Mediterranean Sea Mar. Pollut. Bull., 150 (2020) 110728,	High
40	7,06	Are older life stages of the taxon likely to migrate in the RA area for reproduction?	No	No evidence	Medium
41	7,07	Are propagules or eggs of the taxon likely to be dispersed in the RA area by other animals?	No	N. Killi, A.S. Tarkan, S. Kozic, G.H. Copp, P.I. Davison, L. Vilizzi Risk screening of the potential invasiveness of non native jellyfishes in the Mediterranean Sea Mar. Pollut. Bull., 150 (2020) 110728,	Medium
42	7,08	Is dispersal of the taxon along any of the vectors/pathways mentioned in the previous seven questions (35–41; i.e. either unintentional or intentional) likely to be rapid?	Yes	N. Killi, A.S. Tarkan, S. Kozic, G.H. Copp, P.I. Davison, L. Vilizzi Risk screening of the potential invasiveness of non native jellyfishes in the Mediterranean Sea Mar. Pollut. Bull., 150 (2020) 110728,	High
43	7,09	Is dispersal of the taxon density dependent?	No	No evidence	Medium
8. Tolerance attributes					
44	8,01	Is the taxon able to withstand being out of water for extended periods (e.g. minimum of one or more hours) at some stage of its life cycle?	No	No evidence	Medium
45	8,02	Is the taxon tolerant of a wide range of water quality conditions relevant to that taxon? [In the Justification field, indicate the relevant water quality variable(s) being considered.]	No	No evidence	Medium
46	8,03	Can the taxon be controlled or eradicated in the wild with chemical, biological, or other agents/means?	No	No report in regard	Medium
47	8,04	Is the taxon likely to tolerate or benefit from environmental/human disturbance?	Yes	Purcell, J. E., Uye, S. I., Lo, W. T., 2007. Anthropogenic causes of jellyfish blooms and their direct consequences for humans: a review. Marine Ecology Progress Series, 350, 153-174.	High
48	8,05	Is the taxon able to tolerate salinity levels that are higher or lower than those found in its usual environment?	No	No evidence	Medium
49	8,06	Are there effective natural enemies (predators) of the taxon present in the RA area?	Yes	N. Killi, A.S. Tarkan, S. Kozic, G.H. Copp, P.I. Davison, L. Vilizzi Risk screening of the potential invasiveness of non native jellyfishes in the Mediterranean Sea Mar. Pollut. Bull., 150 (2020) 110728,	Medium
C. Climate change					
9. Climate change					
50	9,01	Under the predicted future climatic conditions, are the risks of entry into the RA area posed by the taxon likely to increase, decrease or not change?	Increase	Based on climate change projections (mainly on global warming) and the species warm-water character	Medium
51	9,02	Under the predicted future climatic conditions, are the risks of establishment posed by the taxon likely to increase, decrease or not change?	No change	As there is no report on establishment of the species in RA area - that's not likely	Medium
52	9,03	Under the predicted future climatic conditions, are the risks of dispersal within the RA area posed by the taxon likely to increase, decrease or not change?	Increase	Based on climate change projections (mainly on global warming) and the species warm-water character	Medium
53	9,04	Under the predicted future climatic conditions, what is the likely magnitude of future potential impacts on biodiversity and/or ecological integrity/status?	No change	As there is no report on establishment of the species in RA area - that's not likely	Medium
54	9,05	Under the predicted future climatic conditions, what is the likely magnitude of future potential impacts on ecosystem structure and/or function?	No change	As there is no report on establishment of the species in RA area - that's not likely	Medium
55	9,06	Under the predicted future climatic conditions, what is the likely magnitude of future potential impacts on ecosystem services/socio-economic factors?	No change	As there is no report on establishment of the species in RA area - that's not likely	Medium

Appendix 2-(continued)

Statistics	
Scores	
BRA	**22,5**
BRA Outcome	**-**
BRA+CCA	**26,5**
BRA+CCA Outcome	**-**
Score partition	
A. Biogeography/Historical	**13,5**
1. Domestication/Cultivation	*0,0*
2. Climate, distribution and introduction risk	*3,0*
3. Invasive elsewhere	*10,5*
B. Biology/Ecology	**9,0**
4. Undesirable (or persistence) traits	*5,0*
5. Resource exploitation	*0,0*
6. Reproduction	*2,0*
7. Dispersal mechanisms	*2,0*
8. Tolerance attributes	*0,0*
C. Climate change	**4,0**
9. Climate change	*4,0*
Answered Questions	
Total	***55***
A. Biogeography/Historical	**13**
1. Domestication/Cultivation	*3*
2. Climate, distribution and introduction risk	*5*
3. Invasive elsewhere	*5*
B. Biology/Ecology	**36**
4. Undesirable (or persistence) traits	*12*
5. Resource exploitation	*2*
6. Reproduction	*7*
7. Dispersal mechanisms	*9*
8. Tolerance attributes	*6*
C. Climate change	**6**
9. Climate change	*6*
Sectors affected	
Commercial	**9**
Environmental	**4**
Species or population nuisance traits	**18**

Thresholds	
BRA	**-**
BRA+CCA	**-**
Confidence	
BRA+CCA	**0,59**
BRA	**0,60**
CCA	**0,50**

Journal of Agricultural Sciences
(Tarim Bilimleri Dergisi)

J Agr Sci-Tarim Bili
e-ISSN: 2148-9297
jas.ankara.edu.tr

JAS

A Comparative Study on Yayık Butter Produced with Commercial and Endemic Yogurt Starter Culture Strains

Marwa Haddar[*a], Ebru Şenel Özkan[b], Elif Ayse Anli[b]

[a] *Department of Dairy Technology, Graduate School of Natural and Applied Sciences, Ankara University, TÜRKİYE*
[b] *Department of Dairy Technology, Faculty of Agriculture, Ankara University, TÜRKİYE*

ARTICLE INFO
Research Article
Corresponding Author: Marwa Haddar, E-mail: haddar.marwa3@gmail.com
Received: 12 August 2024 / Revised: 17 November 2024 / Accepted: 13 December 2024 / Online: 25 March 2025

Cite this article
Haddar M, Şenel Özkan E, Anli E A (2025). A Comparative Study on Yayık Butter Produced with Commercial and Endemic Yogurt Starter Culture Strains. *Journal of Agricultural Sciences (Tarim Bilimleri Dergisi),* 31(2):496-515. DOI: 10.15832/ankutbd.1532397

ABSTRACT
Starter cultures are involved in biochemical reactions during fermentation resulting in the diversity of foods. They are also used for aroma/flavor, texture, nutritional quality enhancement, and shelf-life extension. This study aimed to evaluate the effects of using four different starter culture combinations of which two were isolated starter cultures of *Streptococcus thermophilus* (St) and *Lactobacillus delbrueckii* subsp. *bulgaricus* (Lb) and two were commercial cultures of the same bacteria in Yayık butter characteristics. For this purpose, four different yogurt samples were prepared and then churned to obtain four different Yayık butter samples. Physico-chemical analysis, free fatty acids, volatile compounds, and sensory analysis were performed on the 1st, 30th, and 60th days of storage. No significant differences were observed in moisture, fat, titratable acidity, acid degree, and peroxide value between the samples (P>0.05). However, endemic isolated combined cultures showed better performance in terms of free fatty acid formation and sensorial attributes. The serum pH differed significantly among the samples with higher values in isolated cultures (P<0.05). Storage time was significantly effective on the titratable acidity (°SH) of all Yayık butter samples (P<0.01). The peroxide values were lower than the threshold value of 2.0 meq O_2/kg fat. Acid degree varied between 1.70-1.75 mg KOH/g during the storage period. Endemic isolated cultures exhibited the highest free fatty acid accumulation. In the Yayık butter samples, a total of 31 volatile compounds were quantified. The highest number was detected in the butter samples produced with isolated strains (27St/27Lb and 27St/ALb). Yayık butter samples produced with 27St/27Lb contained 16, while with 27St/ALb had 7 compounds identified. Butyric acid and hexanoic acid were the most abundant carboxylic acids while ketones were the predominant volatile compound detected in all Yayık butter samples. This study highlights the importance of preserving traditional culture strains and offers another perspective on using them in dairy industry.

Keywords: Yayık butter, Isolated strains, Lipolysis, Oxidative stability, Volatile compounds, Sensory analysis

1. Introduction

Butter is one of the essential products of the dairy industry known for its sensory attributes and nutritional value (Anonymous 2005; Üçüncü 2005). The production of butter remains significant in the Turkish dairy market, with over 70,000 tonnes being produced (TÜİK 2023). Among the butter types, Yayık butter is a traditional dairy product originating from yogurt and differs from cream butter in terms of raw material. Yayık butter is made from a concentrated form of the milk fat found in yogurt. The yogurt is produced 12-48 hours before churning and serves as the raw material of Yayık butter. This unique process contributes to specific flavor-aroma characteristics that set Yayık butter apart from butter made from cream (Atamer et al. 2004; Atamer et al. 2005). Yayık butter is primarily produced in the northwestern regions of Türkiye, including the Black Sea, and Southern and central Anatolia (Atamer et al. 2006). The production of this butter is typically carried out on a family scale and sold in local markets (Şenel et al. 2010). Yayık butter combines the health benefits and unique organoleptic properties of yogurt with the long shelf-life advantage provided by fermentation.

In recent years, consumer demand for fermented dairy products has grown significantly due to their health-enhancing capacity. Lactic acid bacteria (LAB) are used as starter cultures in the production of dairy products such as yogurt, cheese, and butter. They play a crucial role in enhancing some characteristics such as flavor, texture, and nutritional value (Kleerebezem & Hugenholtz 2003; van Hylckama & Hugenholtz 2007). LAB can synthesize acetic acid, acetaldehyde, ethanol, diacetyl, and alcohol that contribute to the flavor and texture of fermented products. This is primarily due to lactic acid metabolism, which is the main component in fermentation processes (van Hylckama & Hugenholtz 2007; Caplice & Fitzgerald 1999). LAB have been employed in food development for their therapeutic properties and preservative effects since ancient times (Chittora et al. 2022). They serve multiple roles, such as acting as starter cultures in food fermentation, adjunct cultures that enhance taste, texture and nutritional quality, and as bio-protective agents against spoilage and pathogenic bacteria. Additionally, they contribute to texture improvement through the production of exopolysaccharides and play various roles in medicine and agriculture (Maiouet et al.

2024). Traditional production practices applied in fermented dairy products supply diversity in the culture environment and affect the organoleptic properties of these products. These variations ultimately influence the shelf life of the final product, as they are impacted by variations in pH, the environment, the fermenting population, fermentation conditions, etc. (Aleksanyan et al. 2024).

In yogurt fermentation, LAB such as *Streptococcus thermophilus (*St) and *Lactobacillus delbrueckii* subsp. *bulgaricus* (Lb) are used in a 1:1 combination ratio and are responsible for the aroma/flavor of yogurt and Yayık butter (Sağdıç et al. 2004). The back-slopping fermentation used in traditional yogurt making involves transferring a small amount of previously fermented yogurt into the fresh, heat-treated milk. In commercial applications, commercial starter cultures are used in yogurt production (Wirawati et al. 2019). The back-slopping enhances both microbiological diversity and the sensory attributes of yogurt. While using commercial cultures can lead to standardization in processing, it may result in some loss of the characteristic quality criteria of yogurt (Uzunsoy et al. 2021).

Numerous studies have been conducted on Yayık butter; covering various aspects such as its general composition, and microbiological properties. In one of the previous researches on Yayık butter; Hayaloglu and Konar (2001) focused on Yayık butter samples sold in local markets. Alwazeer et al. (2024) examined the impact of using hydrogen, nitrogen, and synthetic antioxidants (BHT) on some characteristics of Yayık butter samples. While some studies investigated the use of commercial starter culture in production (Sağdıç et al. 2004; Gundogdu et al. 2020), some others examined the potential production technologies of Yayık butter at the laboratory scale (Atamer et al. 2005; Şenel 2006; Atamer et al. 2007; Öztekin Öztürk 2010; Şenel et al. 2010). In a study conducted by Sağdıç et al. (2002), the researchers isolated and identified LAB from Yayık butter samples collected from different locations of Türkiye. They also determined the physico-chemical and sensory properties of cream butter samples produced using these isolated LAB strains. As reported by Şenel & Atamer (2015), starter cultures used in yogurt making are key factors influencing the Yayık butter quality. However, a review of the literature reveals that there have been no studies investigating the use of traditionally produced yogurt-originated isolated endemic strains of LAB in Yayık butter production.

The conducted study is a comparative analysis focusing on the investigation of quality attributes of Yayık butter samples produced using two different isolated strain combinations and two commercial yogurt starter cultures. The samples were analyzed according to their chemical and sensorial properties, volatile compounds, and storage stability during a 60-day storage period. The study aims to investigate the use of isolated strains of yogurt bacteria obtained from local yogurt samples in Turkish regions for the production of Yayık butter. Moreover, it compares the attributes of Yayık butter samples produced by commercial culture used. Given the diversity of local dairy products in our region; it is important to reveal the effects of isolated strains on product characteristics, for both potential culture preservation and industrial applications. The results obtained from this study could serve as a base for further research in this area and for exploring the use of LAB in the dairy industry.

2. Material and Methods

2.1. Material

The raw cow's milk was obtained from the Dairy Plant of Ankara University Faculty of Agriculture (Ankara, Türkiye) and the raw cow's milk cream used for standardizing the fat content of milk up to 7%, was obtained from Atatürk Orman Ciftligi Dairy Plant (Ankara, Türkiye). Details about the samples and the design of the study are given in Table 1. The isolated strains used in the study were *Streptococcus thermophilus* (27St) and *Lactobacillus delbrueckii* subsp. *bulgaricus* (27Lb), which belonged to the culture collection of Dairy Technology Department of Ankara University Faculty of Agriculture (Uzunsoy et al. 2018). While the other isolated *Lactobacillus delbrueckii* subsp. *bulgaricus* (ALb) strain was obtained from the starter culture collection of the Food Engineering Department of İnönü University (Malatya, Türkiye). The other two starter cultures used in the study were commercial starter cultures. The culture CH-1 (Chr. Hansen Bøge Allé 10-12 DK-2970 Hørsholm, Denmark) and Lyofast Y 080 F (Sacco, Italy) were obtained from the Dairy Plant of Ankara University Faculty of Agriculture, Ankara, Türkiye, and Milkaş Gıda San., and Tic. LLC. Company (İstanbul, Türkiye), respectively.

Table 1- Design of Yayık butter production

Sample Code		***Starter culture***	
Yayık Butter	***Yogurt***	***Isolated strains***	***Commercial cultures***
A	YA	27St / 27Lb	-
B	YB	27St / ALb	-
C	YC	-	CH1
D	YD	-	Y080

Sample codes denote; A: Yayık butter produced by yogurt (YA) inoculated by isolated strains of 27St/27Lb culture combination; B: Yayık butter produced by yogurt (YB) inoculated by isolated strains of 27St/ALb culture combination; C: Yayık butter produced by yogurt (YC) inoculated by commercial culture of CH1; D: Yayık butter produced by yogurt (YD) inoculated by commercial culture of Y080; Isolated strains: 27St: denotes the isolated strain of *Streptococcus thermophilus,* 27Lb: denotes the isolated strain of *Lactobacillus delbrueckii* subsp. *bulgaricus,* ALb: denotes the isolated strain of *Lactobacillus delbrueckii* subsp. *bulgaricus,* Commercial cultures: CH1: denotes the commercial starter culture of CH-1, Y080: denotes the commercial starter culture of Lyofast Y080 F

2.2. Culture preparation and yogurt making

Each isolated strain (20 µL) was initially pre-activated in 5 mL of MRS broth (Merck, Darmstadt, Germany) for *Lactobacillus delbrueckii* subsp. *bulgaricus* and in 5 mL of M17 Broth (Merck, Darmstadt, Germany) for *Streptococcus thermophilus*. Incubation was followed at 37 °C for 72h under anaerobic conditions and at 37 °C for 24h under aerobic conditions for *Lactobacillus delbrueckii* subsp. *bulgaricus* and *Streptococcus thermophilus*, respectively.

From each pre-activated culture (approximately 7 log CFU/ mL each), 0.5 mL was transferred to 50 mL of sterile reconstituted milk (12% w/v) for preparing combined yogurt starter cultures in 1:1 ratio and incubated at 43 °C until complete gelation. After that serial transfer was done from 50 mL bulk culture to the required 500 mL culture for yogurt making and again incubated at similar conditions. The commercial starter cultures were also activated in 500 mL of sterile reconstituted milk (12% w/v) at 43 °C until gelation. The active cultures were stored at 4 °C overnight before yogurt production.

The design of the study is given in Table 1 and starter culture activation, yogurt preparation, and Yayık butter production stages are given in Figure 1 as a flow diagram. In the production of Yayık Butter, the first step was the activation of both the isolated strains and the commercial strains used in yogurt making. For yogurt preparation which served as the raw material of Yayık butter (Table 1), the milk was initially divided into four equal parts and inoculated by four different yogurt starter cultures prepared in the first step and in the production of yogurt samples (YA, YB, YC, YD) and the Yayık butter samples (A, B, C, D) the flow diagram (Figure 1) was followed.

2.3. Yayık butter production

In the production of Yayık butter, the yogurt samples (YA, YB, YC, YD) prepared the day before churning were kept refrigerated overnight at 4±1 °C. For each Yayık butter sample (A, B, C, D) 15 kg of yogurt was prepared. The study was conducted in triplicate. Yayık butter production was followed according to the method proposed by Atamer et al. (2007) and given in Figure 1. Finally, Yayık butter samples were packaged in sterile polystyrene containers and stored at 4±1 °C for 60 days. Some stages of Yayık butter production were represented by photographs in Figure 2. In the study, yogurt samples were analyzed on the 1st day of production, while Yayık butter samples were analyzed in the 1st, 30th, and 60th days of storage.

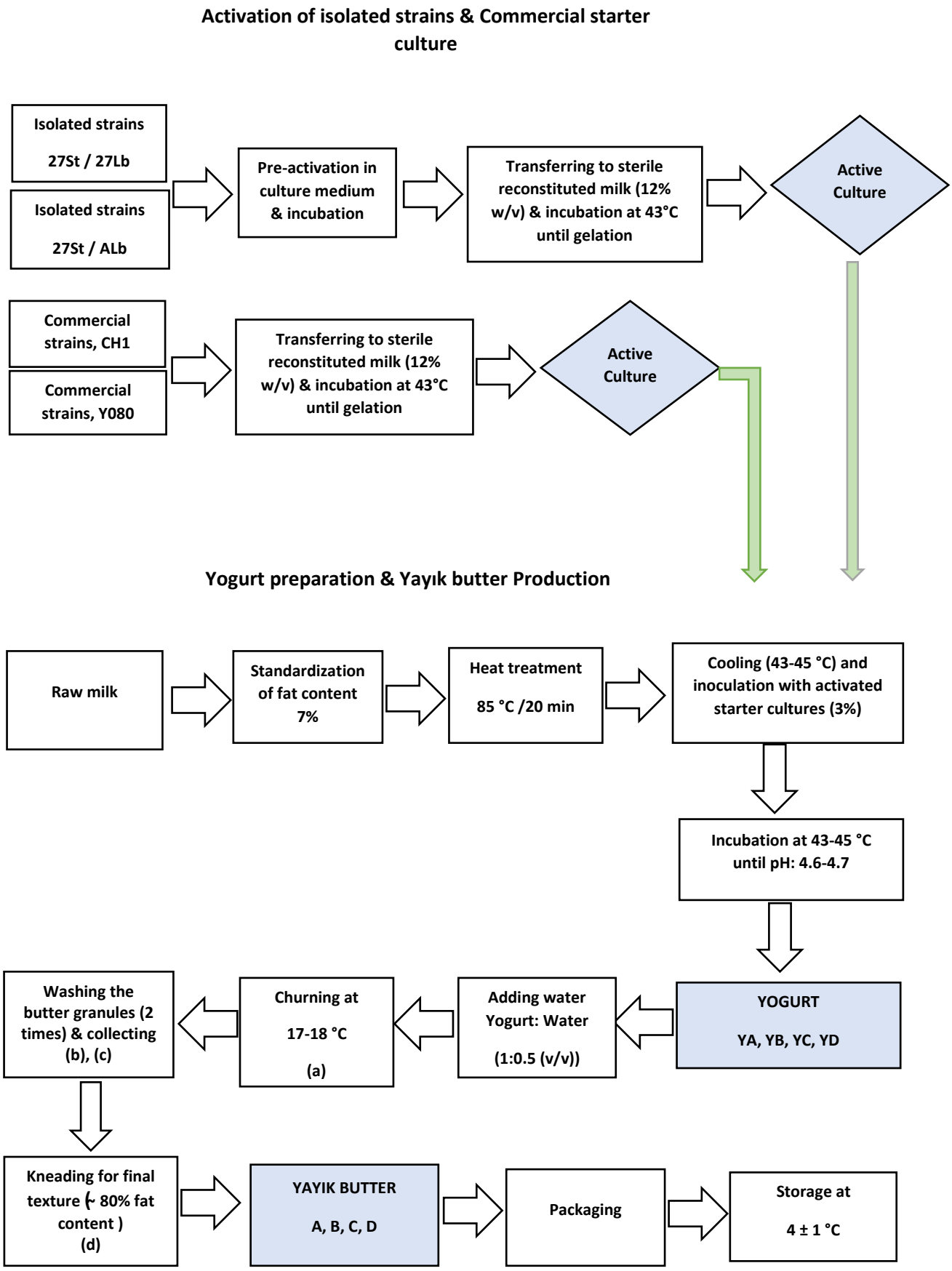

Figure 1- Flowchart of Culture Activation, Yogurt Preparation, and Yayık Butter Production Processes

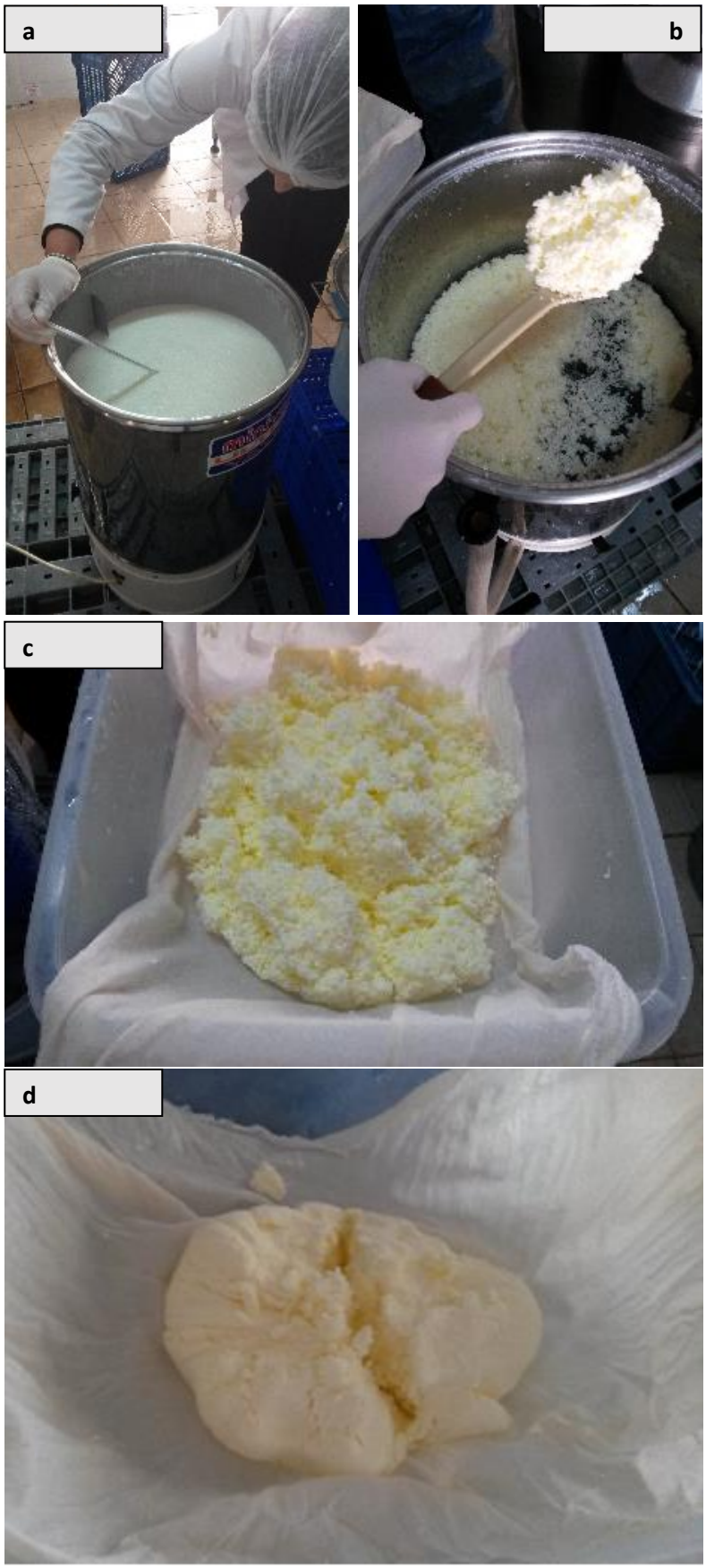

Figure 2- Yayık butter production stages by photographs
(a: Temperature control in the churning stage, b: collecting the butter granules after the washing stage, c: collected butter granules prior to kneading, d: kneading stage for reaching the final texture of butter)

2.4. Determination of chemical characteristics of yogurt and Yayık butter samples

The fat contents of both yogurt samples and Yayık butter samples were determined by the Gerber method and the dry matter contents (%) of yogurt samples and Yayık butter samples were determined using the gravimetric method (AOAC 1997). The pH values of yogurt samples and the serum pH values of Yayık butter were measured by a digital pH meter (Mettler Toledo Seven2Go S2; Schwerzenbach, Switzerland). The titratable acidity values of yogurt and Yayık butter samples were determined by titration (AOAC 1997) and calculated as Soxhlet-Henkel (˚SH). The dry matter content of the butter samples was determined by the gravimetric method (AOAC 1997), the water content of the samples was calculated by subtracting from 100.

2.5. The oxidative stability and lipolysis of Yayık butter samples

The oxidative stability and degree of lipolysis of Yayık butter samples were determined by the methods peroxide value (meq O_2/kg fat) and acid degree (mg KOH/g fat) of Downey (1975), respectively. The peroxide values of the samples were calculated by Eq. 1 and the acid degree values of the samples were calculated by Eq.2. For the analysis, fat extraction from Yayık butter samples was followed according to the methods given in AOAC (2000).

$$Peroxide\ value\ (meq\ O_2/kg\ fat) = (\mu gFe/gfat \times 55.85) = F/(m \times 55.85) \quad \text{(Eq.1)}$$

F: Amount of μg Fe corresponding to the measured absorbance value
m: Fat analyzed in grams

$$Acid\ degree\left(\frac{mgKOH}{gfat}\right) = \frac{(Amount\ 0.1N\ KOH\ \ x\ Normality\ of\ KOH\ x\ 56.1)}{Sample\ amount\ (g)} \quad \text{(Eq. 2)}$$

2.6. Determination of free fatty acids (FFAs) by Gas Chromatography

The free fatty acid content of yogurt samples and Yayık butter samples was determined by the method of Deeth, Fitz-Gerald, and Snow (1983), and details related to the process were given by Şenel et al. (2011a and 2011b). The FFA content of yogurt samples was determined on the 1st day and for Yayık butter samples on the 1st, 30th and 60th days of storage. The sample preparation involved weighing 2.5 g of yogurt and 1.5 g of butter, followed by adding 2.5 g of Na_2SO4 for each sample. The 5 mL of internal standard (C_7) and 300 µL of H_2SO_4 were then poured, and the mixture was thoroughly vortexed for 1 minute. The 5 mL of hexane was added, and the samples were rested for 1 hour prior to extracting the liquid phase from Biorad column with deactivated alumina. Each sample was eluted twice per column. The columns were then washed twice with 5 mL of hexane/diethyl ether (1:1) and dried with 5 psi of air. The FFAs held by dried alumina were transferred to test tubes and then 2 mL of 6% formic acid in ether was added. After centrifuging at 2000g for 10 minutes, the clear portion was transferred to vials using a Pasteur pipette and samples were stored at -18 °C until performing analysis. Analysis was done by GC instrument (Agilent 6890 series, Agilent Tech. Inc., CA, USA) by the operation conditions as; Flame Ionization Detector (FID) (Agilent Tech. Inc., CA, USA) with an operating temperature of 260 °C, a polyethylene glycol capillary column with dimensions of 30 m x 320 µm (inner diameter) and a 0. 25 µm film thickness (HP-FFAP Agilent Tech. Inc., Model 19091F-433). Injection conditions were as split injection with a 1:10 split ratio, with an injection volume of 5 µL at 250 °C, flow rates for the gases were as H_2: Air: N_2 = 33:370:30 ml min^{-1}. The oven temperature program was set as; starting at 120 °C for 0 minutes, increasing to 200 °C at a rate of 10 ºC min^{-1} and holding at 200 °C for 2 minutes, increasing to 205 °C at a rate of 10 ºC min^{-1} and holding for 2 minutes, then increasing to 210 °C at a rate of 10 °C min^{-1} and holding for 2 minutes, then increasing to 215 °C at a rate of 10 °C min^{-1} and holding for 3 minutes, and finally increasing to 230 °C at a rate of 10 min^{-1} and holding for 3 minutes. In the analysis standard mix solutions were also prepared in a 6% (v/v) formic acid in ether solution and 5 µL of these solutions was injected into the GC system with the same conditions as samples injection. The chromatographic-grade fatty acid standards used in the mixed solutions were supplied by Agilent (Agilent Tech. Inc., CA, USA). The calculation of the detected FFA content of the samples was done automatically by the instrument software (HP Chenstation, USA) by selecting the internal standard calculation mode (ISTD).

2.7. Determination of volatile compounds of yogurt samples and Yayık butter samples

Volatile compounds of yogurt samples were analyzed on the 1st day of production and Yayık butter samples were analyzed on storage days of 1st, 30th and 60th by the method of Whetstine et al. (2003) using Gas Chromatography/Mass (GC/MS) instrument (Agilent 7890A GC-5975 MSD, Agilent Technologies, CA, USA). Volatile compounds of the samples were extracted by solid-phase microextraction (SPME) method. The samples were weighed in 40 mL amber vials (10 grams) and mixed with 1 g NaCl and 10µL of internal standard (2- methyl-3- heptanon and 2-methyl pentanoic acid in 81mg/kg methanol). Samples were stored at -18 °C until injection to the GC/MS instrument. Before injection samples in vials were heated and stirred at 40 °C for 30 min by Reacti Term system (Pierce Reacti-Therm I #18821) and then kept at that condition with fiber (50/30 µm Divinylbenzene/Carboxen/Polydimethylsiloxane (DVB/CAR/PDMS) for absorption of volatile compounds for 30 minutes. The fiber was then injected into the capillary column of the GC/MS device. The operation conditions for GC/MS were as follows; the volatile compounds were separated using the DB Wax column; the initial temperature of the oven was 40 °C, kept for 5 minutes, then raised to 100 °C at a rate of 10 °C per minute and then increased to 200 °C at a rate of 20 °C per minutes and held

for 10 minutes. The total run time was 47 minutes. Later, the detected volatile compounds were identified in the mass spectrometer and NIST/Flavournet libraries were scanned.

In the evaluation, the peak area of volatile compounds was compared with the peak area of the internal standard Equation 3.

$$Relative\ amount\ of\ volatile\ compound\ \left(\frac{\mu g}{kg}\right) = \left[\frac{Peak\ area\ of\ volatile\ compound}{Peak\ area\ of\ internal\ standard}\right] x\ correction\ factor \quad \text{(Eq. 3)}$$

2.*8. Sensory analysis*

Sensory analysis of the Yayık butter samples was carried out by ten panelists of Dairy Technology Department Staff, experienced in sensory evaluation of dairy products, on the 1st, 30th, and 60th days of storage. Samples were coded with randomized three-digit codes and served to the panelists in plastic containers with lids, a cup of water, and a cracker for cleansing the palate. In the conducted scoring test, the panelists were asked to evaluate the samples according to taste, odor, appearance, texture, and overall acceptability by using a 9-point hedonic scale (9=like immensely, 8=like very much, 7= like moderately, 6=like slightly, 5=neither like or dislike, 4=dislike slightly, 3=dislike moderately, 2=dislike very much, 1=dislike extremely).

2.9. Statistical analysis

All the data was statistically evaluated by Minitab statistical software (version 16.0, Minitab Inc., State College, PA, USA). The significance of the difference between the means of yogurt and Yayık butter samples was determined by using Duncan's Multiple Comparison Test at significance levels of $P<0.05$ and / or $P<0.01$. The study was designed in factorial order by considering storage time as a factor with 3 levels (1st, 30th, and 60th day) and the use of four different yogurt starter culture combinations (27St/27Lb, 27St/Alb, CH1, and Y0.80) as another factor.

3. Results and Discussion

3.1. *The chemical characteristics of yogurt samples*

Some chemical characteristics of yogurt samples used as the raw material of Yayık butter samples are given in Table 2.

Table 2 - Chemical characteristics of yogurt samples

Parameter	***Yogurt samples***			
	YA	***YB***	***YC***	***YD***
Dry matter (%)	14.13 ± 0.42	13.73 ± 0.72	14.25 ± 0.15	13.86 ± 0.63
Fat (%)	6.10 ± 0.58	5.67 ± 0.40	6.23 ± 0.09	6.07 ± 0.50
Titratable acidity (°SH)	36.87 ^{ab}± 0.01	26.24 ^{b} ± 0.36	47.30 ^{a}± 1.05	41.61 ^{a} ± 0.35

Data given were the $\bar{X} \pm S_X$ of the parameters analyzed in all yogurt samples of three replicates **(n=3)** Yogurt samples: YA: Yogurt inoculated by isolated strains of 27St/27Lb culture combination; YB: Yogurt inoculated by isolated strains of 27St/ALb culture combination; YC: Yogurt inoculated by commercial culture of CH1; YD: Yogurt inoculated by commercial culture of Y080. *Within a row, the difference between group averages is statistically significant ($P<0.05$). Differences between means that share the same letter are not statistically significant.

According to Table 2, no significant difference was observed among the yogurt samples (YA, YB, YC, YD) in terms of dry matter (%) and fat (%) content due to standardization of fat content applied to the raw milk prior to yogurt-making ($P>0.05$). As it was observed in the samples (Table 2), the increase in dry matter (%) is expected to be parallel with the increase in fat (%) content. However, there was a significant difference ($P<0.05$) in the titratable acidity of yogurt samples (Table 2) possibly associated with the use of different starter cultures with different acidification capacities in yogurt making. Among the yogurt samples, YB was significantly different from YC and YD inoculated with commercial starter cultures ($P<0.05$). The yogurt YC got the highest titratable acidity value followed by YD, YA, and YB samples in order.

3.2. The physico-chemical properties of Yayık butter samples

Table 3 illustrated the changes in the physico-chemical properties of Yayık butter samples during the storage period. The effect of using different starter culture combinations and storage time on the parameters analyzed were discussed according to the statistically significance issue in the following parts.

Table 3 – Chemical, oxidative stability and lipolysis characteristics of Yayık butter samples during storage*

	Yayık butter samples											
	A			*B*			*C*			*D*		
Parameter	*Day 1*	*Day 30*	*Day 60*	*Day 1*	*Day 30*	*Day 60*	*Day 1*	*Day 30*	*Day 60*	*Day 1*	*Day 30*	*Day 60*
Moisture (%)	15.91 ± 0.41	15.30 ± 0.60	16.00 ± 0,37	16.82 ± 0.66	16.27 ± 0.46	15.94 ± 0.50	17.78 ± 0.80	16.03 ± 0.35	17.70 ± 0.91	16.54 ± 0.37	16.35 ± 0.19	16.91 ± 0.29
Fat (%)	80.92 ± 0.36	80.92 ± 0.80	80.83 ± 0.60	81.83 ± 0.88	80.08 ± 0.08	80.50 ± 0.29	79.75 ± 0.38	79.83 ± 0.88	80.00 ± 1.32	80.17 ± 0.44	80.25 ± 0.25	81.25 ± 0.00
Serum pH	4.62 ± 0.21	4.39 ± 0.35	4.47 ± 0.22	4.96± 0.05	4.80 ± 0.18	4.85 ± 0.13	4.23 ± 0.02	4.09 ± 0.13	4.12 ± 0.03	4.15 ± 0.08	4.03 ± 0.17	4.21 ± 0.07
Titratable acidity (°SH)	3.43 ± 0.16	3.97 ± 0.39	3.67 ± 0.33	3.83± 0.18	3.97 ± 0.08	3.77 ± 0.18	3.96 ± 0.87	4.32 ± 0.92	3.91 ± 0.77	3.63 ± 0.76	4.25 ± 0.18	4.13 ± 0.44
Acid degree (mg KOH/g fat)	1.74 ± 0.12	1.63 ± 0,08	1.75 ± 0.12	1.70± 0.08	1.78 ± 0,20	1.75 ± 0.15	1.68 ± 0.10	1.72 ± 0,13	1.81 ± 0.15	1.71 ± 0.12	1.60 ± 0,10	1.79 ± 0.13
Peroxide value (meq O_2/kg fat)	0.12 ± 0.07	0.23 ± 0.05	0.31 ± 0.06	0.23 ± 0.05	0.27 ± 0.02	0.25 ± 0.13	0.21 ± 0.01	0.28 ± 0.05	0.31 ± 0.03	0.22 ± 0.04	0.28 ± 0.02	0.24 ± 0.03

*: Values are the $\bar{X} \pm S_{\bar{X}}$ on storage days of 1st, 30th and 60th (n=3) with no significant difference (P>0.05). Yayık butter samples: A: Yayık butter produced by yogurt (YA) inoculated by isolated strains of 27St/27Lb culture combination; B: Yayık butter produced by yogurt (YB) inoculated by isolated strains of 27St/ALb culture combination; C: Yayık butter produced by yogurt (YC) inoculated by commercial culture of CH1; D: Yayık butter produced by yogurt (YD) inoculated by commercial culture of Y080

The data in Table 4, were given as means ± SE of values of Yayık butter samples from the 1st day to the 60th day of storage.

Table 4 - Chemical properties of Yayık butter samples during the storage period*

Parameter	*Yayık butter samples*			
	A	***B***	***C***	***D***
Moisture (%)	15.74 ± 0.26	16.34 ± 0.30	17.16 ± 0.46	16.60 ± 0.17
Fat (%)	80.89 ± 0.59	80.81 ± 0.38	79.86 ± 0.47	80.56 ± 0.23
Serum pH	4.49^{ab*} ± 0.14	4.83^{a*} ± 0.08	4.15^{b*} ± 0.04	4.13^{b*} ± 0.06
Titratable acidity (˚SH)	3.69 ± 0.17	3.86 ± 0.08	4.06 ± 0.43	4.00 ± 0.30
Acid degree (mg KOH/g fat)	1.71 ± 0.06	1.75 ± 0.08	1.74 ± 0.06	1.70 ± 0.06
Peroxide value (meq O_2/kg fat)	0.24 ± 0.03	0.25 ± 0.04	0.27 ± 0.02	0.25 ± 0.02

*: Values are the $\bar{X} \pm S_{\bar{X}}$ from 1st day to 60th day of storage (n=9). * Denotes the significance level of difference P<0.05. A: Yayık butter produced by yogurt (YA) inoculated by isolated strains of 27St/27Lb culture combination; B: Yayık butter produced by yogurt (YB) inoculated by isolated strains of 27St/ALb culture combination; C: Yayık butter produced by yogurt (YC) inoculated by commercial culture of CH1; D: Yayık butter produced by yogurt (YD) inoculated by commercial culture of Y080

The moisture content of butter samples should be lower than 16% for a successful shelf life (Anonymous 2005) and kneading is a crucial step in butter processing that influences the final moisture content. However, since the Yayık butter samples were hand-kneaded during production, minor fluctuations occurred in experimental Yayık butter samples (Table 3), but these fluctuations were not found statistically significant on storage days (P>0.05) for the samples and among the mean values of the samples during on the 1st, 30th and 60th days of storage (P>0.05) (Table 4). In terms of fat content (%), all Yayık butter samples were consistent with the legal limits of 80% fat content at least, given for legal regulations of cream butter (Anonymous 2005).

Among the parameters tested for Yayık butter samples, means ± SE of serum pH was a unique item found statistically significant among the samples during 60-day storage (P<0.05) and ranged between the values of 4.13-4.83 (Table 4). The use of different starter culture combinations (Table 1) with different acidification potential in yogurt productions (YA, YB, YC, YD) and in Yayık butter samples (A, B, C, D) was responsible for these differences, and among the used cultures, commercial cultures exhibited higher activity. The serum pH of sample B got the highest mean values (4.83 ± 0.08) during the storage period and was significantly different than C and D (P<0.05). In literature, researchers have obtained varying results regarding serum pH (Sağdiç et al. 2002; Şenel et al. 2011b; Gundogdu et al. 2020). However, the Yayık butter samples were not statistically different than each other during 60-day storage in terms of titratable acidity (means ± SE) (P>0.05) (Table 4). According to Table 2, titratable acidity values of yogurt samples (YA, YB, YC, YD) indicated that YA and YB had less acidic character than YC and

YD. This is likely because the commercial cultures used in YC and YD had superior acidification capacity compared to the isolated strains used in YA and YB. Similar results were observed for the serum pH of samples C and D with lower pH and higher titratable acidity values than samples A and B (Table 4). Means of titratable acidity values of all Yayık butter samples were statistically different between day 1 and day 30 ($P<0.01$) (Table 5). These values were found to be consistent with earlier studies conducted by numerous researchers (Atamer et al. 2006; Şenel 2006; Şenel et al. 2011b).

Table 5 – Change in titratable acidity values of all Yayık butter samples on storage days*

	Storage days		
	1	***30***	***60***
Titratable acidity (°SH) [a]	$3.71 \pm 0.26^{b**}$	$4.13 \pm 0.26^{a**}$	$3.87 \pm 0.12^{ab**}$

*: Values are the $\bar{X} \pm S_{\bar{X}}$ of all Yayık butter samples on storage days of 1st, 30th and 60th (n=12), ** Denotes the significance level of difference $P<0.01$

According to the results given in Table 5, the highest titratable acidity values were observed on day 30 and values decreased on day 60 ($P<0.01$). A significant portion of lactose is converted to lactic acid by yogurt bacteria during yogurt production (Özer 2010) and after churning, some of the microorganisms involved in the fermentation and a small amount of residual lactose pass into the Yayık butter, resulting in a limited formation of lactic acid. Therefore, the small change in the values and a decrease on day 60 could be due to the existence of limited residual lactose in Yayık butter samples. Additionally, the increase in titratable acidity might be associated with the inhibition activity of mold/yeast on lactic acid bacteria (Kılıç 2010). In this study, although no sensorial defect related to mold/yeast was perceived on the 30th day of storage an increase in titratable acidity was detected in all samples (Table 3).

The mean values for the acid degree for Yayık butter samples during the storage period ranged from 1.70-1.75 mg KOH/g fat (Table 4). The acid degree value indicates the extent of the lipolysis which is the reaction of hydrolyzation of triglycerides to free fatty acids (FFAs) by lipase. The lipolysis of butter is one of the determinants of the shelf life of butter since some aroma/flavor defects (rancid flavor) can occur related to the extent of this reaction (Atamer et al. 2006). The storage and processing conditions and the quality of the cream are among the factors contributing to this reaction (Fardet et al. 2019). It was concluded that the rancid taste and aroma can occur when the acid degree value in cream butter exceeds 1.36 mg KOH/g fat and 1.53 mg KOH/g fat by Atamer (1983) and Ergin (1978), respectively. The panelists detected aroma/flavor defects when the acid degree values reached 1.08 mg KOH/g fat (Şenel et al. 2010). The threshold values mentioned here are about two times higher than those stated by Downey (1975). According to Table 4, acid degree values were higher than those reported by Sagdic et al. (2002) and Sagdic et al. (2004) but only a mild rancid flavor was perceived by the panelists in C samples on the 60th day of storage. The presence of $C_{(4:0)}$ and $C_{(6:0)}$ mainly among the short-chain fatty acids was associated with butter rancidity (Walstra et al. 1999). The possible reason for the perceived milk rancid flavor in sample C could be explained as the highest amount of $C_{(4:0)}$ and $C_{(6:0)}$ fatty acids during the storage period was detected in sample C (41.88 ppm) and followed by samples B (40.64 ppm), A (40.52 ppm) and D (39.96 ppm), respectively (Table 7).

According to Table 4, all Yayık butter samples were of good quality in terms of peroxide values ranging from 0.24-0.27 meq O_2/kg fat. The peroxide value is the indicator of oxidative degradation of butter, limiting the shelf-life of high-fat dairy products due to sensorial defects. The oxidation reaction primarily occurs in the presence of unsaturated fatty acids and oxygen (Şenel & Atamer 2015). The carbonyl compounds formed due to oxidation cause oxidized flavor in the products and are especially detected when the limits of peroxide value reach 2.0 meq O_2/kg fat (Downey 1975). The sensory threshold level for peroxide value in butter was reported as 6.3 meq O2/kg fat (Pearson 1974). However, Atamer & Sezgin (1984) and Atamer et al. (2006) expressed no correlation between the peroxide value and the aroma/flavor of butter. Peroxides do not effect the flavor directly since they decompose to carbonyl compounds that are responsible for the oxidized flavor defects in the products. Higher peroxide values occur in high-fat products indicating weaker oxidative stability. However, factors such as the oxygen concentration, the existence of metals (Cu^{+2}, Fe^{+3}), the presence of antioxidant substances and the water activity etc. affect this reaction and makes the interpretation of the results more challenging (Şenel & Atamer 2015).

3.3. Free fatty acids (FFAs) composition

3.3.1. Free fatty acids (FFAs) composition of yogurt

The FFA composition of yogurt samples is given in Table 6. The highest amount of short-chain saturated FFAs was observed in YB yogurt followed by YC, YD, and YA, in order. The concentration of medium and long-chain FFAs in all yogurt samples were close to each other and the highest amount was observed in YC (511.50 ppm) followed by YB (488.30 ppm), YD (414.40 ppm), and YA (411.28 ppm). The YC and YA samples were rich in unsaturated FFAs with values of 210.54 ppm and 210.13 ppm, respectively (Table 6). The FFA formation occurs during fermentation by lactic acid bacteria and the extent of this reaction depends on the strain (Mantzourani et al. 2022). The proto-cooperation reaction occurs between two yogurt bacteria *Streptococcus thermophilus* and *Lactobacillus delbrueckii* subsp. *bulgaricus* was found responsible for milk acidification, aromatic compounds, FFA formation, and organoleptic characteristics of yogurt and Yayık butter (Guler & Park, 2010). Based on the total amount of FFAs, it can be concluded that among the isolated strains, the combination of 27St/ALb used in YB yogurt

and among the commercial cultures CH1 used in YC yogurt favored FFAs formation mostly. The FFA content of yogurt samples is closely linked with its organoleptic characteristics and health effects in humans depending on their saturation degree, their chain length (short, medium, and long), and storage period (Gu et al. 2021; Mantzourani et al. 2022). Mantzourani et al. (2022) reported that higher amounts of FFA result in flavor defects in the products mainly associated with the increase in short-chain FFAs (Ozcan et al. 2016). Among short-chain FFAs, the butyric acid, known as the principal flavor component of butter, was observed in the highest amount in YB and followed by YC, YD, and YA, in order. Dairy products rich in short and medium-chain FFAs are associated with many health benefits. Short-chain FFAs are easily digested due to their lower melting point than the human body and are used as an energy source. Additionally, they are known with their antiviral and antimicrobial activities, especially butyric acid which has cancer-inhibiting activity (Ozcan et al. 2016).

Table 6 - The FFA composition of yogurt samples on the 1st day of storage (n=3)

	Yogurt samples ($\bar{X} \pm S_{\bar{X}}$)			
FFA (ppm)	***YA***	***YB***	***YC***	***YD***
Butyric ($C_{4:0}$)	6.01 ± 0.49	13.53 ± 5.10	11.7 ± 2.57	10.63±2.98
Caproic ($C_{6:0}$)	6.44 ± 0.44	12.36 ± 3.60	11.64 ±3.94	12.27±4.45
Caprylic ($C_{8:0}$)	4.68^{b*} ± 0.12	9.51^{a*} ±1.82	7.61^{a*}±2.40	7.25^{a*}±2.40
Capric ($C_{10:0}$)	8.55^{b*}±2.82	17.72^{a*}±6.59	20.44^{a*}±7.92	16.25^{a*}±5.91
∑($C_{4:0}$- $C_{10:0}$)	**25.86**	**53.12**	**51.39**	**46.40**
Lauric ($C_{12:0}$)	12.43^{b**} ±5.25	28.0^{a**}±12.30	34.50^{a**}±14.50	25.80^{ab**}±11.20
Myristic ($C_{14:0}$)	41.38±9.74	64.00±34.90	77.5±42.70	59.70±33.30
Palmitic ($C_{16:0}$)	211.97±1.80	277.80±97.50	274.00±146.00	221.00±121.00
Stearic ($C_{18:0}$)	145.50±26.40	118.50±51.90	125.50±62.70	107.90±57.70
∑($C_{12:0}$- $C_{18:0}$)	**411.28**	**488.30**	**511.50**	**414.40**
Oleic ($C_{18:1}$)	191.70±37.00	145.20±68.90	166.70±86.60	132.20±72.40
Linoleic ($C_{18:2}$)	18.43^{c**}±2.04	35.73^{b**}±1.41	43.84^{a**}±1.05	39.21^{ab**}±0.54
∑($C_{18:1}$- $C_{18:2}$)	**210.13**	**180.93**	**210.54**	**171.41**
Total FFA	**647.04**	**722.35**	**773.43**	**632.21**

Values are the $\bar{X} \pm S_{\bar{X}}$ of all Yogurt samples used in Yayık butter production on the 1st day of storage prior to Yayık butter production (n=3), Yogurt samples: * P <0.05 /** P<0.01 / $^{a-c}$: Different letters in the same row indicate significant differences among groups. YA: Yogurt inoculated by isolated strains of 27St/27Lb culture combination; YB: Yogurt inoculated by isolated strains of 27St/ALb culture combination; YC: Yogurt inoculated by commercial culture of CH1; YD: Yogurt inoculated by commercial culture of Y080.

The linoleic acid ($C_{18:2}$) content of YA differed significantly from YB, YC, and YD within the unsaturated fatty acids (P<0.05). Among saturated fatty acids, palmitic acid was found to be the most abundant in all samples with no significant difference (P>0.05) (Table 6). The lauric acid ($C_{12:0}$) content of YA yogurt was significantly different than YB and YC (P<0.05). The level of caprylic acid ($C_{8:0}$) was found to be the lowest among all fatty acids present in the yogurt samples and was significantly different in YA yogurt than in other yogurt samples (P<0.05). The most predominant FFAs in all yogurt samples were observed in the medium-long chain (palmitic acid ($C_{16:0}$), stearic acid ($C_{18:0}$), and in unsaturated FFAs as oleic acid ($C_{18:1}$) (Table 6). Similarly, as found by Şenel et al. (2011a) palmitic acid ($C_{16:0}$), oleic acid ($C_{18:1}$) and capric acid ($C_{10:0}$) were predominant in goat's milk yogurt samples.

3.3.2. Free fatty acids (FFAs) composition of Yayık butter samples

The distribution of free fatty acids (FFAs) in Yayık butter samples is shown in Figure 3, and the changes in free fatty acids (FFAs) content that occurred in the storage period of Yayık butter samples are given in Table 7. The highest free fatty acid accumulation was observed in Yayık butter samples A and B with isolated strains of *Streptococcus thermophilus* and *Lactobacillus delbrueckii* subsp. *bulgaricus* and followed by C and D samples (Table 1). From the results, it is concluded that the selected strains used in A and B were thought to have higher lipolytic activity compared to the commercial starter cultures of the same bacteria (Figure 3).

Free fatty acid fraction (FFA) is generated through a lipolysis reaction catalyzed by the lipase enzyme (Collins et al. 2003). From Figure 3, the high-molecular-weight saturated fatty acids ($C_{12:0}$-$C_{18:0}$) were found to be predominant acids in all samples. These groups accounted for about 73% of the total free fatty acids. Similar results were reported in another study on Yayık butter (Şenel 2006). The extent of lipolysis, which results in higher levels of FFAs, limits the shelf life of dairy products due to undesirable changes in aroma/flavor characteristics during storage (Deeth et al. 1983). In dairy products, the rancid flavor is formed at high levels of FFAs (exceeding 1.5 mmol/L) (Deeth & Fitz-Gerald 2006).

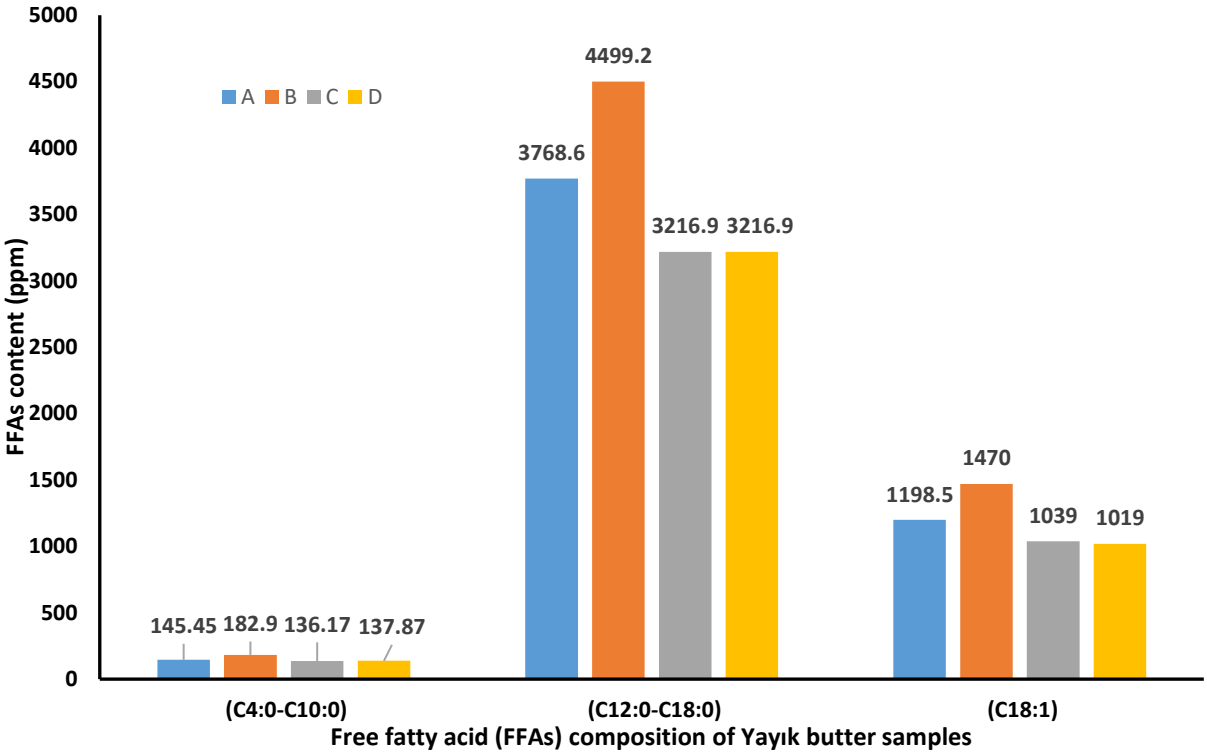

Figure 3- Means of the total amount of free fatty acids (FFAs) of Yayık butter samples during the storage period depending on the molecular weight (n=9)

Free fatty acids (FFAs): ($C_{4:0}$-$C_{10:0}$): Low-molecular-weight saturated fatty acids; ($C_{12:0}$-$C_{18:0}$): High-molecular weight saturated fatty acids; ($C_{18:1}$-$C_{18:2}$): Unsaturated fatty acids: Yayık butter samples; A: Yayık butter produced by yogurt (YA) inoculated by isolated strains of 27St/27Lb culture combination; B: Yayık butter produced by yogurt (YB) inoculated by isolated strains of 27St/ALb culture combination; C: Yayık butter produced by yogurt (YC) inoculated by commercial culture of CH1; D: Yayık butter produced by yogurt (YD) inoculated by commercial culture of Y080

In Yayık butter samples, nine different free fatty acids (FFAs) were extracted and identified (Table 7). Butyric acid (C_4), is a low-molecular-weight saturated, water-soluble bioactive element found in milk fat. It is responsible for the characteristic aroma and flavor of butter (Tamime & Robinson 1999), also known to reduce the risk of infectious intestine disease and lower the level of blood cholesterol (Deeth & Fitz-Gerald 2006; Van Immerseel et al. 2010). However, the level of butyric acid was found to be significantly lower in butter samples than in yogurt samples (Table 6) possibly due to the removal of a large proportion of water-soluble butyric acid during churning and washing the granules. According to the studies, the total amount of butyric acid in butter can vary between 3.12 – 8.83 ppm. Similar results have been obtained by Sağdıç et al. (2004) and Öztekin (2010). However, in a study conducted by Şenel (2006), the concentration of butyric acid was found to be higher than in our study, varying from 23.80 ppm on the first day of storage to 15.85 ppm at the end of the storage.

During the storage period, FFAs showed irregular changes in Yayık butter samples except for the amount of caproic acid ($C_{6:0}$) in sample C, in which a very slight decrease was observed. Similar to Sağdıç et al. (2004), our study also found that the most predominant FFAs in Yayık butter samples were palmitic acid ($C_{16:0}$), oleic acid ($C_{18:1}$), stearic acid ($C_{18:0}$) and myristic acid (C14:0). Furthermore, neither of the two unsaturated fatty acids linoleic acid ($C_{18:2}$) and linolenic acid ($C_{18:3}$) were detected in Yayık butter samples.

Table 7 - Changes in free fatty acid (FFAs) composition of Yayık butter samples during storage period*

FFAs (ppm)	*Storage Day*	*Yayık butter samples ($\bar{X} \pm S_{\bar{X}}$)*			
		A	***B***	***C***	***D***
Butyric ($C_{4:0}$)	1	3.12 ± 0.05	3.35 ± 1.14	4.44 ± 0.47	4.74 ± 0.21
	30	4.25 ± 1.74	6.83 ± 2.33	4.32 ± 0.92	3.38 ± 0.34
	60	5.47 ± 0.10	6.22 ± 0.10	5.23 ± 0.90	4.71 ± 0.10
Caproic (C6:0)	1	8.13 ± 0.91	10.62 ± 3.69	9.76 ± 3.59	9.42 ± 3.55
	30	8.20 ± 1.47	12.70 ± 2.83	9.51 ± 0.74	9.96 ± 0.65
	60	11.35 ± 1.56	9.92 ± 0.54	8.62 ± 2.54	7.75 ± 3.32
Caprylic ($C_{8:0}$)	1	21.17 ± 2.22	31.90 ± 13.20	23.80 ± 10.6	25.40 ± 10.90
	30	20.43 ± 0.05	36.80 ± 10.5	27.15 ± 2.20	29.05 ± 2.27
	60	29.77 ± 4.97	26.27 ± 2.61	21.61 ± 8.63	21.49 ± 9.22
Capric ($C_{10:0}$)	1	105.3 ± 10.09	134.2 ± 49.6	91.50 ± 45.00	95.80 ± 47.30
	30	91.39 ± 2.62	156.8 ± 37.00	111.8 ± 6.61	117.44 ± 4.02
	60	127.8 ± 13.90	113.14 ± 5.69	90.70 ± 32.30	84.00 ± 35.20
Lauric ($C_{12:0}$)	1	209.80 ± 19.80	264.90 ± 90.70	168.10 ± 82.80	176.40 ± 87.70
	30	190.10 ± 10.70	304.00 ± 69.60	218.70 ± 14.10	228.43 ± 7.16
	60	256.40 ± 14.20	224.16 ± 2.98	173.00 ± 60.30	161.30 ± 66.50
Myristic ($C_{14:0}$)	1	597.80 ± 70.30	774.00 ± 258.00	484.00 ± 239.00	503.00 ± 251.00
	30	550.70 ± 46.50	891.00 ± 193.00	633.90 ± 45.20	651.70 ± 27.60
	60	754.00 ± 30.00	653.41 ± 9.39	503.00 ± 178.00	463.00 ± 193.00
Palmitic ($C_{16:0}$)	1	2060 ± 209	2638 ± 895	1631 ± 804	1713.00 ± 851
	30	1943 ± 225	3060 ± 659	2147 ± 167	2229.40 ± 85.90
	60	2510 ± 113	1869 ± 324	1708 ± 585	1563.00 ± 644
Stearic ($C_{18:0}$)	1	707.20 ± 77.90	933.00 ± 349.00	594.00 ± 289.00	617.00 ± 304.00
	30	675.10 ± 72.20	1134.00 ± 246.00	759.80 ± 43.70	795.60 ± 22.50
	60	851.40 ± 41.70	752.90 ± 21.40	631.00 ± 219.00	549.00 ± 229.00
Oleic ($C_{18:1}$)	1	1161. 00 ± 106.00	1501.00 ± 563.00	919.00 ± 444.00	939.00 ± 464.00
	30	1065.00 ± 105.00	1711.00 ± 430.00	1206.20 ± 80.60	1259.70 ± 10.30
	60	1369.50 ± 65.30	1199.00 ± 36.20	993.00 ± 337.00	859.00 ± 352.00

*: Values are the $\bar{X} \pm S_{\bar{X}}$ of all Yayık butter samples on storage days of 1st, 30th, and 60th (n=9), Yayık butter samples; A: Yayık butter produced by yogurt (YA) inoculated by isolated strains of 27St/27Lb culture combination; B: Yayık butter produced by yogurt (YB) inoculated by isolated strains of 27St/ALb culture combination; C: Yayık butter produced by yogurt (YC) inoculated by commercial culture of CH1; D: Yayık butter produced by yogurt (YD) inoculated by commercial culture of Y080

3.4. The volatile compound distribution of the samples

3.4.1. Volatile compounds of yogurt samples

The volatile compounds of yogurt samples (YA, YB, YC, YD) are presented in Table 8. In total, twelve volatile compounds were identified, including four acids, six ketones, one aldehyde, and one ester (Table 8). Acetaldehyde is one of the most important carbonyl compounds produced by fermentation, contributing to the typical yogurt aroma (Rascón-Díaz et al. 2012) and giving fresh and green flavor (Tian et al. 2020). The concentration of acetaldehyde in yogurt ranges from 2 to 41 mg/L, influenced by the difference in the LAB strains and processes during fermentation (Li et al. 2024). However, a study reported that the yogurt develops its ideal flavor only if the concentration of acetaldehyde is greater than 8 mg/L (Chen et al. 2017). In yogurts inoculated with isolated-strains A and B yogurt samples, the acetaldehyde was not detected and only C and D yogurts got acetaldehyde in amounts of 8.31 mg/kg and 8.80 mg/kg, respectively. This concentration is adequate for a good flavor. In accordance with our findings, a study conducted by Şenel et al. (2011a) reported that the level of acetaldehyde in fresh yogurt was 9.11 mg/kg. This level remained stable for up to 45 days of storage. The starter culture effect on acetaldehyde formation is concluded by Gundogdu et al. (2020). Li et al. (2024) associated the production of the key flavor component in yogurt with the use of *Streptococcus. thermophilus* and *Lactobacillus delbrueckii* subsp. *bulgaricus* as dominant starter cultures. However, yogurt fermented solely with *Lactobacillus casei* lacks the characteristic flavor compounds of yogurt.

As a result, our findings can be related to the higher metabolic activity of the commercial yogurt starter bacteria. Some researchers reported the loss of acetaldehyde in yogurt during the storage period. It was reported that acetaldehyde is converted to acetic acid and ethanol depending on pH and water activity (Gundogdu et al. 2020).

Table 8- The volatile compounds of yogurt samples on the 1st day of storage (ppm) (n=3)

	Yogurt samples			
Volatile compounds (mg/kg)	***YA***	***YB***	***YC***	***YD***
2,3-Butanedione	6.00	103.5	31.24	nd
2,3-Pentanedione	429.18	nd	nd	nd
2-Butanone	4.30	nd	nd	nd
2-Butanone, 3-hydroxy	17.73	26.21	28.88	17.94
2-Nananone	nd	nd	3.73	nd
2-Pentanone, 3-hydroxy	81.93	nd	nd	nd
2-Undecanone	nd	nd	nd	10.46
Acetaldehyde	nd	nd	8.31	8.80
Acetic acid	120.70	5.10	17.47	30.60
Butyric acid	54.36	68.61	54.03	48.74
Hexanoic acid	66.07	69.45	48.82	47.94
Octanoic acid	220.02	nd	nd	nd

Values are the means of all Yogurt samples used in Yayık butter production on the 1st day of storage prior to Yayık butter production (n=3), Yogurt samples: YA: Yogurt inoculated by isolated strains of 27St/27Lb culture combination; YB: Yogurt inoculated by isolated strains of 27St/ALb culture combination; YC: Yogurt inoculated by commercial culture of CH1; YD: Yogurt inoculated by commercial culture of Y080. nd: non-detected.

The acetic acid content of YA was quite higher than the other yogurt samples possibly due to this conversion reaction of acetaldehyde to acetic acid. The following compounds - 2-Butanone 3-hydroxy (acetoin), acetic acid, butyric acid, and hexanoic acid - were identified as common volatile compounds in all yogurt samples. A study reported that the starter culture had no effect on 2-butanone content, but storage time was found to have a significant impact (Gundogdu et al. 2020). 2,3-Butanedione (diacetyl) was identified in all yogurt samples except for YD. This common carbonyl compound is typically found in yogurt and butter, and its concentration depends on the specific combination of cultures used. In other words, it depends on the strains involved. Diacetyl is a volatile compound naturally produced by LAB and is responsible for the typical butter aroma in fermented dairy products, such as cheeses, butter, and yogurts (Papagianni 2012). Many microorganisms are able to produce diacetyl, such as Streptococcus, Leuconostoc, former-Lactobacillus, and other microbial genera, in quantities ranging from 0,4 to 8.2 g/L (Chen et al. 2017). In our study, the starter culture combination used in YB had a higher capacity to produce 2,3-Butanedione (diacetyl).

3.4.2. Volatile compounds of Yayık butter samples

The distribution of a total of thirty-one volatile compound detected in Yayık butter samples was summarized in Table 9. These compounds were classified into 9-acids (the most common includes acetic acid, benzene acetic acid, butyric acid, hexanoic acid-2-methyl, pentanoic acid-2-methyl, 4-hydroxymandelic acid, and peracetic acid), 4 alcohols (heptanol, hexanol, hexane, octadecane, methane, heptane, dodecane), 8-ketones (2-heptanone, methyl-ethyl-ketone, 2-butanone, 2-butanone hydroxyl, 2-nonanone, 2-octanone, 2-pentanone, 2-butanedione), 3 aldehydes (acetaldehyde, isobutyraldehyde, and hexanal), as well as seven unknown compounds. However, only seven volatile compounds were found to be common in all the Yayık butter samples (Figure 4).

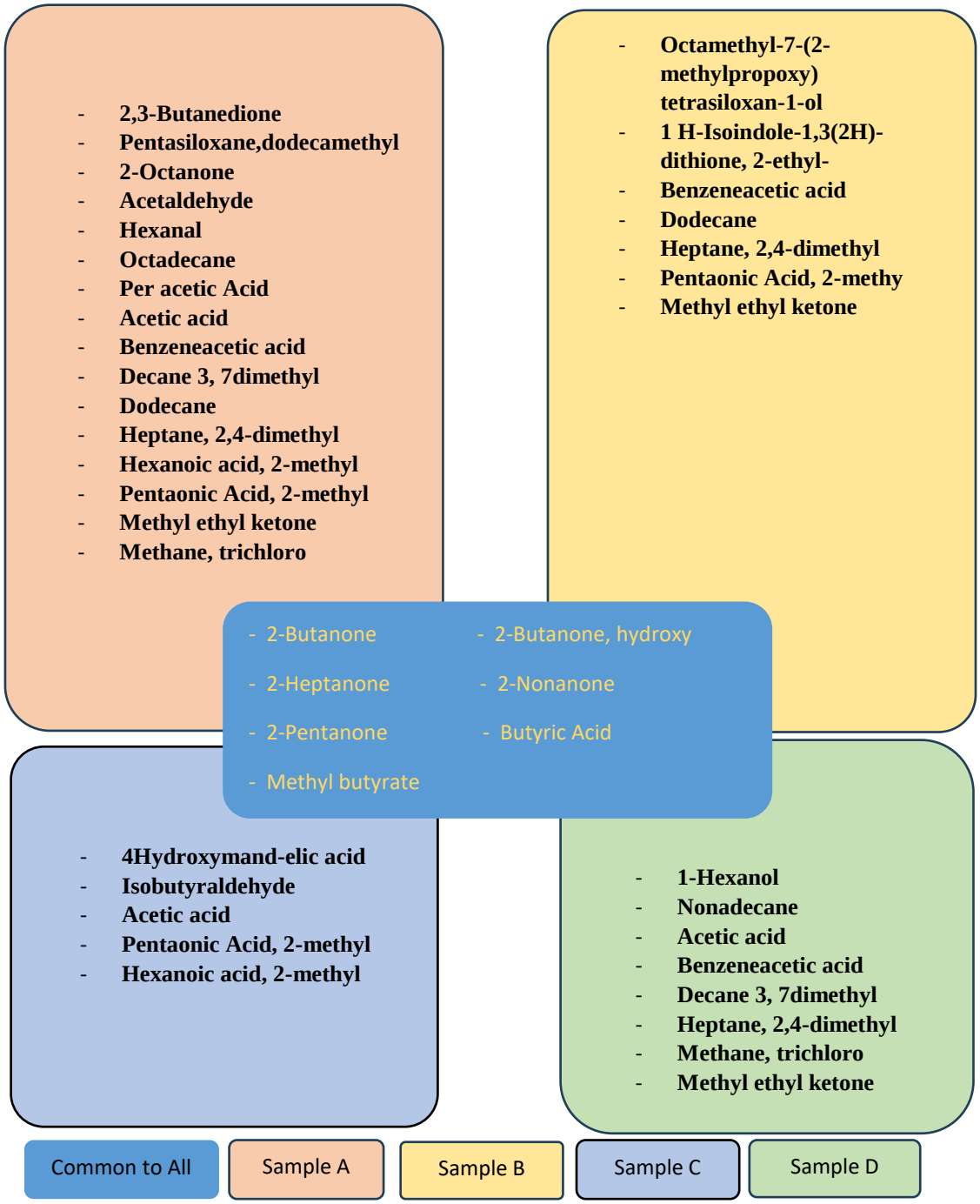

Figure 4 - Distribution of volatile compounds in Yayık butter samples

The aroma of the butter can vary based on different factors such as the breed of animal, their diet, the season, the raw material used (such as milk, yogurt, and cream), the production method, and the storage conditions. The characteristic aroma of butter is produced during storage, as a result of various biochemical reactions that occur due to microbial, enzymatic, and chemical transformation of milk components such as lipolysis, proteolysis, glycolysis, and pyruvate metabolism (Vanbergue et al. 2017).

Table 9- The volatile compounds of Yayık butter samples (n=3)

Volatile compounds (mg/kg)	*Storage Day*	*Yayık butter samples*			
		A	***B***	***C***	***D***
Hexanol	1	nd	nd	nd	nd
	30	nd	nd	nd	21.08
	60	nd	nd	nd	nd
1H-Isoindole-1,3(2H) dithione,2 ethyl-	1	nd	nd	nd	nd
	30	nd	20.65	nd	nd
	60	nd	nd	nd	nd
2,3-Butanedione	1	nd	nd	nd	nd
	30	14.18	nd	nd	21.08
	60	nd	nd	nd	nd
2-Butanone	1	43.36	78.15	81.25	118.34
	30	31.71	107.95	349.41	206.44
	60	76.73	nd	197.52	56.30
2-Butanone, hydroxy	1	7.68	4.12	27.76	25.64
	30	15.98	78.36	62.74	58.92
	60	40.63	nd	40.26	nd
2-Heptanone	1	64.38	27.36	39.05	32.25
	30	79.37	65.75	131.99	96.27
	60	nd	42.19	121.21	74.56
2-nonanone	1	nd	nd	nd	nd
	30	nd	nd	nd	42.33
	60	368.55	35.25	56.39	nd
2-Octanone	1	nd	nd	nd	nd
	30	nd	nd	nd	nd
	60	26.56	nd	nd	nd
2-Pentanone	1	nd	nd	nd	nd
	30	nd	nd	nd	43.57
	60	483.39	125.19	60.35	32.05
4-Hydroxymandelic acid, ethyl ester,di-TMS	1	nd	nd	nd	nd
	30	nd	nd	85.58	nd
	60	nd	nd	nd	nd
Acetaldehyde	1	3.11	nd	nd	nd
	30	nd	nd	nd	nd
	60	nd	nd	nd	nd
Acetic acid	1	49.58	nd	nd	nd
	30	49.57	nd	nd	75.49
	60	nd	nd	21.91	nd
Benzeneacetic acid	1	nd	nd	nd	nd
	30	nd	nd	nd	95.18
	60	27.20	458.87	nd	nd
Butyric acid	1	66.76	10.85	nd	47.44
	30	66.76	nd	33.50	34.71
	60	53.87	57.75	27.0	40.81
Carbon disulfide	1	nd	nd	43.23	nd
	30	nd	nd	nd	nd
	60	nd	nd	16.70	nd
Decane,3,7-dimethyl-	1	43.55	nd	nd	nd
	30	nd	nd	nd	19.49
	60	102.32	nd	nd	nd
Dodecane	1	102.38	nd	nd	nd
	30	nd	12.71	nd	nd
	60	38.18	nd	nd	nd
Heptane,2,4dimethyl-	1	74.9	nd	nd	nd
	30	nd	104.53	nd	23.20
	60	109.16	16.85	nd	19.17
Hexanal	1	nd	nd	nd	nd
	30	nd	nd	nd	nd
	60	28.11	nd	nd	nd
Hexane	1	nd	nd	nd	nd
	30	142.90	177.47	nd	nd
	60	70.03	nd	nd	68.10
Hexanoic acid	1	62.32	nd	29.78	nd
	30	57.49	nd	37.57	36.31
	60	nd	10.46	27.07	26.88

Table 9(Continue)- The volatile compounds of Yayık butter samples (n=3)

Volatile compounds (mg/kg)	*Storage Day*	*Yayık butter samples*			
		A	***B***	***C***	***D***
Hexanoic acid, 2 methyl-	1	16.55	nd	nd	nd
	30	nd	nd	nd	nd
	60	nd	nd	32.47	nd
Isobutyraldehyde	1	nd	nd	nd	nd
	30	nd	nd	nd	nd
	60	nd	nd	30.97	nd
Methane, trichloro-	1	nd	nd	nd	32.47
	30	11.73	nd	nd	nd
	60	nd	nd	nd	nd
Methyl butyrate	1	66.20	44.31	75.26	65.64
	30	46.84	nd	nd	100.45
	60	nd	nd	nd	nd
Methyl ethyl ketone	1	nd	19.47	nd	nd
	30	nd	nd	nd	80.43
	60	50.74	nd	nd	31.25
Nonadecane	1	nd	nd	nd	nd
	30	nd	nd	nd	65.27
	60	nd	nd	nd	nd
Octadecane	1	nd	nd	nd	nd
	30	nd	nd	nd	nd
	60	27.97	nd	nd	nd
Pentanoic acid, 2methyl-	1	27.92	21.45	35.36	nd
	30	nd	nd	nd	nd
	60	13.36	nd	6.80	nd
Pentasiloxane, dodecamethyl-	1	29.62	nd	nd	nd
	30	nd	nd	nd	nd
	60	nd	nd	nd	nd
Per acetic acid	1	27.95	nd	nd	nd
	30	nd	nd	nd	nd
	60	nd	nd	nd	nd

Yayık butter samples; A: Yayık butter produced by yogurt (YA) inoculated by isolated strains of 27St/27Lb culture combination; B: Yayık butter produced by yogurt (YB) inoculated by isolated strains of 27St/ALb culture combination; C: Yayık butter produced by yogurt (YC) inoculated by commercial culture of CH1; D: Yayık butter produced by yogurt (YD) inoculated by commercial culture of Y080. nd: non-detected

Among all the thirty-one volatile compound, ketones were the predominant chemical groups present in all samples during the storage period. Specifically, 2-butanone and 2-heptanone were the most abundant ketones detected in all butter samples nearly observed in all storage periods except for B on the 60th day for 2-Butanone and except for A on the 60th day for 2-Heptanone (Table 9). Ketones are also identified in fresh cream butter (Lee 2020) and cheeses (Qian & Reineccius 2002). Sample C was the richest Yayık butter in 2-Butanone and 2-Heptanone (349.41 mg/kg and 131.99 mg/kg on the 30th day of storage, respectively). Similar to our findings, Gundogdu et al. (2020) identified 11 ketones in butter samples, with the most abundant ones being 2-pentaone, 2-heptanone, acetoin, and 2-nonanone. The 2-heptanone is formed as the result of beta-oxidation of saturated fatty acids during thermal processing (Peterson & Reineccius 2003). Lactones are mainly responsible of the butter's creamy, fruity, or otherwise pleasant odors while sulfur-containing compounds contribute to its "corn-like" and "garlic" odor and dodecanoic acid gives it a "soapy" odor (Mallia 2008). Butyric acid and hexanoic acid were the most abundant carboxylic acids released from triglycerides and found in all Yayık butter samples. Hexanoic acid has been reported as a critical odorant in different cheese types, mainly cheddar cheese (Christensen & Reineccius 1995) and Grana Padano (Moio & ADDEO 1998). The highest concentration of butyric acid was detected in sample A and followed by sample D on all storage days (Table 9). Contrary to these results, Şenel et al. (2011b) found that only butyric acid was detected in trace amounts in all Yayık butter samples. Acetic acid produced by lactic starter cultures was detected in Yayık butter samples A, C, and D during storage (Figure 4, Table 9). The importance of acetic acid to the flavor of dairy products was established by Lozano et al. (2007) for butter, Delgado et al. (2010) for cheese, Bendall (2001) for milk, and Pan et al. (2014) for fermented milk. In Yayık butter samples pentanoic acid 2-methyl, benzene-acetic acid, hexanoic acid, 2-methyl, and peracetic acid were detected in lower amounts (Table 9). Hexanoic acid is associated with the pungent odor of blue cheese. In contrast, acetic acid, which is a result of lactose, lactate and citrate metabolism, has a pungent, vinegary acidic odor in dairy products (Dan et al. 2018).

In this study, only three aldehydes were detected in Yayık butter samples. Two of these aldehydes were found in sample A on the 1st day, and 60th days. Iso-butyraldehyde was only detected in sample C on the 60th day of storage (Table 9). Aldehydes

are frequently detected in dairy products and tend to convert into acids or alcohols such as methyl-butanal and hexanal during production (Afzal et al. 2012).

3.5. Sensory properties of Yayık butter samples

The sensory evaluation results of Yayık butter samples on storage days are presented in Figure 5. According to the results, the use of different starter culture combinations and storage periods as well as the interaction between different culture combinations and storage periods, did not have a statistically significant effect on all sensory attributes analyzed (P>0.05).

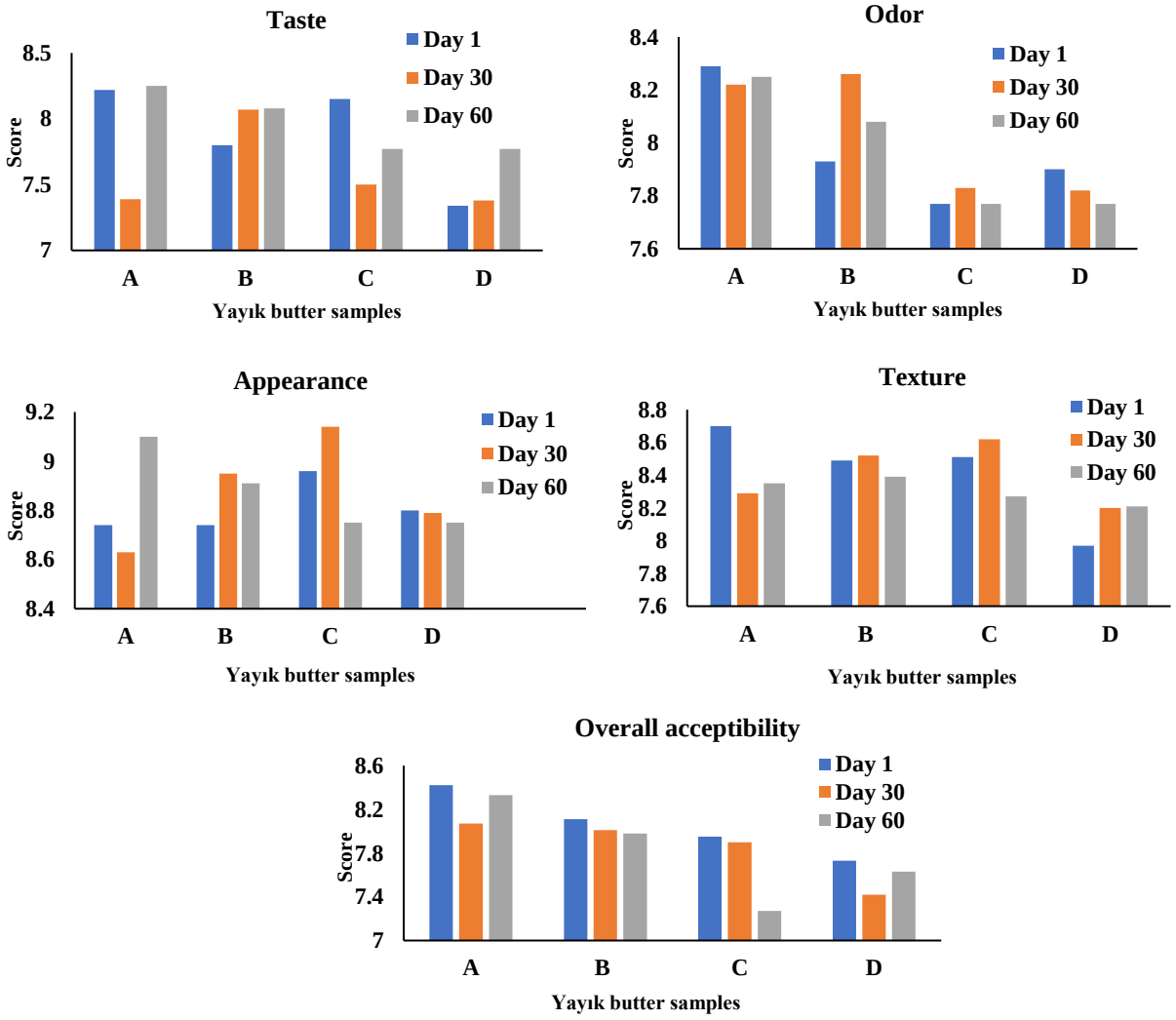

Figure 5 – Sensory properties of Yayık butter samples on storage days

Yayık butter samples; A: Yayık butter produced by yogurt (YA) inoculated by isolated strains of 27St/27Lb culture combination; B: Yayık butter produced by yogurt (YB) inoculated by isolated strains of 27St/ALb culture combination; C: Yayık butter produced by yogurt (YC) inoculated by commercial culture of CH1; D: Yayık butter produced by yogurt (YD) inoculated by commercial culture of Y080

The figure 5 reflects the mean values of each sensory attribute of Yayık butter samples during the storage period. In terms of taste, A got the highest score on the 1st and 60th days of storage followed by C on the 1st day and B on the 30th and 60th days. Sample D got the lowest scores all over the storage period. Yayık butter samples produced by isolated starter culture combinations showed superior odor properties as sample A got the highest score on the 1st and 60th days and sample B on the 30th day of storage. The samples produced by the commercial cultures (C and D) exhibited weaker odor characteristics. Regarding the appearance, Yayık butter samples (C and D) with commercial cultures, exhibited more uniform changes during storage, however, sample D got the lowest scores. Nearly all the Yayık butter samples were evaluated with high scores (> 8.00) in texture and samples A, B, and C were almost similar, but sample D got the lowest score in texture. Sample A was evaluated with the highest scores in all storage days followed by sample B in terms of overall acceptability attribute. Commercial culture used Yayık butter samples (C and D) were least accepted by the panelists during the storage period (Figure 5). In cream butter and Yayık butter samples, free fatty acid content, peroxide value, and acid degree value play a crucial role in sensory attributes (Şenel et al. 2016). According to the sensory evaluation, no distinct sensory defect was reported by the panelists except sample C in

which only a slight rancid flavor was pronounced by the panelists on day 60. From Table 4, the moisture content of sample C was the highest among the samples which might lead to amplification in enzymatic and microbial activity causing the breakdown of fats into free fatty acids and the release of short-chain fatty acids (Deeth & Fitz-Gerald 1976). Additionally, the yogurt (YC) used in the production of C butter had the highest total amount of FFAs content (773.43 ppm) (Table 6). As previously reported by Mantzourani et al. (2022), the high amount of FFA can cause flavor defects in dairy products. Based on these results, it can be concluded that culture combinations prepared by isolated strains gave satisfactory results sensorially when compared with commercial cultures.

4. Conclusions

This study was conducted to observe the effect of using two different isolated strain combinations of yogurt bacteria and two commercial yogurt starter cultures in Yayık butter production, to identify the potential effects on its quality attributes during a storage period of 60 days. The acidification potential of commercial cultures used was superior to the isolated strains combined. Both culture types used in Yayık butter samples exhibited similar FFA formation potential with a slight variation in FFA concentration. The highest free fatty acid accumulation was observed in endemic isolated combined cultures. One of the isolated combined cultures had the highest butyric acid content. Butyric acid and hexanoic acid were the most abundant carboxylic acids while ketones were the predominant volatile compound detected in Yayık butter samples. Culture combinations prepared by isolated strains gave satisfactory sensory results when compared with commercial cultures. The use of different starter culture combinations creates various FFA profiles influencing the nutritional properties, biological value, and aroma potential of the final product. This could contribute to both physico-chemical and organoleptic richness in industrial applications. The results of this study could serve as preliminary data for the possible use of traditional sources of starter cultures in scientific and industrial areas. It also emphasizes the importance of preserving traditional dairy products that reflect the cultural heritage.

References

Afzal M I, Delaunay S, Paris C, Borges F, Revol-Junelles A M & Cailliez-Grimal C (2012). Identification of metabolic pathways involved in the biosynthesis of flavor compound 3-methylbutanal from leucine catabolism by Carnobacterium maltaromaticum LMA 28. *International Journal of Food Microbiology* 157(3): 332-339

Alwazeer D, Bulut M, Ceylan M M, Çelebi Y, Kavrut E, Çetintaş Y, Hayaloğlu A A (2024). Hydrogen incorporation into butter improves its microbial and chemical stability, biogenic amine safety, quality attributes, and shelf-life. *LWT* 206: 116550

Anonymous (2005). Tereyağı, Diger Süt Yagı Esaslı Sürülebilir Ürünler ve Sadeyağ Tebliği.Yayın No: 2005/91. 25784 sayı ve 12.04.2005 tarihli Resmi Gazete.

AOAC (1997) Official methods of analysis, 16th ed. Association of Official Analytical Chemists, Washington, DC

AOAC (2000). Official methods of analysis of AOAC international (17th ed.). Gaitherburg, MD, USA:AOAC International.

Atamer M (1983). Ankara'da Tereyağına İşlenen Kremaların Özellikleri ve Bunlardan Elde Edilen Tereyağlarının Niteliklerinin Saptanması. Ankara Üniversitesi Ziraat Fakültesi Tarım Ürünleri Teknolojisi Süt Teknolojisi Ana BilimDalı. *Fen Bilimleri Enstitüsü, Ankara*

Atamer M & Sezgin E (1984). Tereyağlarında Lipolitik ve oksidatif bozulmaların saptanmasında yararlanılan asit ve peroksid değerleri ile aroma arasındaki ilişki. *Gıda 9*(6).

Atamer M, Şenel E & Öztekin F Ş (2004). A Traditional Product: Yayık Tereyağ Conventional Way of Manufacturing and Its Some Properties. International Dairy Symposium. *Recent Developments in Dairy Science and Technology* pp. 149-152

Atamer M, Şenel E & Öztekin F Ş (2005). Yoğurttan Üretilen Tereyağlarının (YayıkTereyağı) Bazı Niteliklerinin Belirlenmesi. *TUBITAK, TOGTAG-3035 nolu proje*.

Atamer M, Şenel E & Öztekin F Ş (2006). Yayık Tereyağlarında Asit, Peroksit, Tirozin Değerleri ile Titrasyon Asitligine İliskin Sınır Değerlerinin Saptanması. Ankara Üniversitesi Bilimsel Arastırma Projesi Kesin Raporu. Proje No:07–110–03–HPD, Ankara.

Atamer M, Şenel E & Öztekin F Ş (2007). A comparative study on some properties of butter produced from yoghurt and cream, Food Industry Milk and Dairy Products. *Journal of Chemist and Technologists Association Belgrad* (1-2): 18

Bendall J G (2001). Aroma compounds of fresh milk from New Zealand cows fed different diets. *Journal of Agricultural and Food Chemistry* 49(10): 4825-4832

Caplice E & Fitzgerald G F (1999). Food fermentations: role of microorganisms in food production and preservation. *International Journal of Food Microbiology* 50(1-2): 131-149

Chen C, Zhao S, Hao G, Yu H, Tian H & Zhao G (2017). Role of lactic acid bacteria on the yogurt flavour: A review. *International Journal of Food Properties* 20(1): 316-330

Christensen K R & Reineccius G A (1995). Aroma extract dilution analysis of aged Cheddar cheese. *Journal of Food Science* 60(2): 218-220

Chittora D, Meena B R, Jain T & Sharma K (2022). Biopreservation: Bacteriocins and Lactic Acid Bacteria. *Journal of Postharvest Technology* 10(2): 1-15

Collins Y F, McSweeney P L & Wilkinson M G (2003). Lipolysis and free fatty acid catabolism in cheese: a review of current knowledge. *International Dairy Journal* 13(11): 841-866

Dan T, Jin R, Ren W, Li T, Chen H & Sun T (2018). Characteristics of milk fermented by Streptococcus thermophilus MGA45-4 and the profiles of associated volatile compounds during fermentation and storage. *Molecules* 23(4): 878

Deeth H C & Fitz-Gerald C H (1976). Lipolysis in dairy products: a review. *Australian Journal of Dairy Technology* 31: 53-64

Deeth H C, Fitz-Gerald CH & Snow A J (1983). A gas chromatographic method for the quantitative determination of free fatty acids in milk and milk products. *New Zealand Journal of Dairy Science and Technology* 18: 13-20

Deeth H C & Fitz-Gerald C H (2006). Lipolytic enzymes and hydrolytic rancidity. In *Advanced Dairy Chemistry*, Volume 2 Lipids (pp. 481-556). Boston, MA: Springer US

Delgado F J, González-Crespo J, Cava R, García-Parra J & Ramírez R (2010). Characterisation by SPME–GC–MS of the volatile profile of a Spanish soft cheese PDO Torta del Casar during ripening. *Food Chemistry* 118(1): 182-189

Downey W K (1975). Butter Quality. Published by An Foras Taluntais 19 Sadyamount Avenue Dublin 4, Dairy Research & Review Series No. 7, 142 pp

Ergin G (1978). Tereyağının dayanıklılığına Muhafaza Sıcaklığı, Krema Asitliği ve pastörizasyonu ve Tuzlamanın Etkileri Üzerine Bir Araştırma. *Fen Bilimleri Enstitüsü, Gıda Mühendisliği Anabilim Dalı, Erzurum*

Fardet A, Dupont D, Rioux L E & Turgeon S L (2019). Influence of Food Structure On Dairy Protein, Lipid and Calcium Bioavailability: A Narrative Review Of Evidence. *Critical Reviews in Food Science and Nutrition* 59(13): 1987-2010

Gu Y, Li X, Chen H, Guan K, Qi X, Yang L & Ma Y (2021). Evaluation of FAAs and FFAs in yogurts fermented with different starter cultures during storage. *Journal of Food Composition and Analysis* 96: 103666

Gundogdu E, Cakmakci S & Hayaloglu A A (2020). Effects of starter culture and storage on volatile profiles and sensory characteristics of yogurt or cream butter. *Mljekarstvo* 70(3): 184-200

Guler Z & Park Y W (2010). Evaluation of correlations between chemical compositions and sensory properties in Turkish Set-type yogurts. *Journal of Dairy Science*

Hayaloglu A A & Konar A (2001). A comparative study on physicochemical and sensorial properties of butter made from yogurt and cream. Milchwissenschaft - Milk Science International 56(12)

Kılıç S (2010). Maya ve küfler, Süt Mikrobiyolojisi. Sidas Medya Ltd. Şti, Izmir, Türkiye pp. 485-554

Kleerebezem M & Hugenholtz J (2003). Metabolic pathway engineering in lactic acid bacteria. *Current Opinion in Biotechnology* 14(2): 232-237

Lee J H (2020). Changes in flavor compounds and quality parameters of goat cream butter during extended refrigerated storage. *International Journal of Food Properties* 23(1): 306-318

Li D, Cui Y, Wu X, Li J, Min F, Zhao T & Zhang J (2024). Graduate Student Literature Review: Network of flavor compounds formation and influence factors in yogurt. *Journal of Dairy Science*

Lozano P R, Miracle E R, Krause A J, Drake M & Cadwallader K R (2007). Effect of cold storage and packaging material on the major aroma components of sweet cream butter. *J. of Agricultural and Food Chemistry* 55(19): 7840-7846.

Maiouet I, Mahi K E, Abouloifa H & Rhallabi N (2024). Technological characterization of lactic acid bacteria isolated from raw milk. *Interactions* 245(1): 218

Mallia S (2008). *Oxidative stability and aroma of UFA/CLA (unsaturated fatty acids/conjugated linoleic acid) enriched butter* (Doctoral dissertation, ETH Zurich)

Mantzourani C, Batsika C S, Kokotou M G & Kokotos G (2022). Free fatty acid profiling of Greek yogurt by liquid chromatography-high resolution mass spectrometry (LC-HRMS) analysis. *Food Research International* 160: 111751

Moio L & ADDEO F (1998). Grana Padano cheese aroma. *Journal of Dairy Research* 65(2): 317-333

Ozcan T, Akpinar-Bayizit A, Yilmaz-Ersan L, Cetin K & Delikanli B (2016). Evaluation of fatty acid profile of Trabzon butter. *International Journal of Chemical Engineering and Applications* 7(3): 190-194

Özer B (2010). Strategies for yogurt manufacturing. *Development and manufacture of yogurt and other functional dairy products* pp. 47-96

Öztekin Öztürk F Ş (2010). Yoğurdun sulandırma oranı ve granüllerin yıkama sayısının yayık tereyağının nitelikleri üzerine etkisi

Pan D D, Wu Z, Peng T, Zeng X Q & Li H (2014). Volatile organic compounds profile during milk fermentation by Lactobacillus pentosus and correlations between volatiles flavor and carbohydrate metabolism. *Journal of dairy science* 97(2): 624-631

Papagianni M (2012). Metabolic engineering of lactic acid bacteria for the production of industrially important compounds. *Computational and Structural Biotechnology Journal* 3(4), e201210003

Pearson D (1974). The assessment of rancidity of oils on a common cholorfm extract with special reference to TBA values. *J. of the Ass. of Public Analysts* 12: 73-76

Peterson D G & Reineccius G A (2003). Characterization of the volatile compounds that constitute fresh sweet cream butter aroma. *Flavour and Fragrance Journal* 18(3): 215-220

Qian M & Reineccius G (2002). Identification of aroma compounds in Parmigiano-Reggiano cheese by gas chromatography/olfactometry. *Journal of Dairy Science* 85(6): 1362-1369

Rascón-Díaz M P, Tejero J M, Mendoza-Garcia P G, García H S & Salgado-Cervantes M A (2012). Spray drying yogurt incorporating hydrocolloids: Structural analysis, acetaldehyde content, viable bacteria, and rheological properties. *Food and Bioprocess Technology* 5: 560-567

Sağdiç O, Arici M & Simşek O (2002). Selection of starters for a traditional Turkish yayik butter made from yoghurt. *Food Microbiology* 19(4): 303-312

Sağdıç O, Dönmez M & Demirci M (2004). Comparison of characteristics and fatty acid profiles of traditional Turkish yayik butters produced from goats', ewes' or cows' milk. *Food Contro* 15(6): 485-490

Şenel E (2006). Bazı Üretim Parametrelerinin Yogurttan Üretilen Yayık Tereyağının Nitelikleri Üzerine Etkisi. Ankara Üniversitesi Fen Bilimleri Enstitüsü Süt Teknolojisi Anabilim Dalı, Doktora Tezi, 168.

Şenel E, Atamer M & Öztekin Ş (2010). Yayıklama parametrelerinin yayık ayranı ve yayık tereyağının bazı nitelikleri üzerine etkisi. *Gıda* 35(4): 267-274

Şenel E, Atamer M, Gürsoy A & Öztekin F Ş (2011a). Changes in some properties of strained (Süzme) goat's yoghurt during storage. *Small Ruminant Research* 99(2-3): 171-177

Şenel E, Atamer M & Öztekin F Ş (2011b). The oxidative and lipolytic stability of Yayık butter produced from different species of mammals milk (cow, sheep, goat) yoghurt. *Food Chemistry* 127(1): 333-339

Şenel E, Atamer M, Şanlı T, Kocabaş Z & Türkmen N (2016). Geleneksel Yayık Tereyağının Aroma Karakterizasyonu ve Duyusal Özelliklerinin Belirlenmesi. Ankara Üniversitesi Bilimsel Araştırma Projeleri, Proje No: 12B4347004. Ankara

Şenel E & Atamer M (2015). Yayik Butter Profiles from Different Species of Mammals' Milk. In *Processing and Impact on Active Components in Food* (pp. 215-221). Academic Press

Tamime A Y & Robinson R K (1999). Yogurt Science and Technology CRC. Press. Woodhead Publishing Ltd. Cambridge, England.

Tian H, Yu B, Yu H & Chen C (2020). Evaluation of the synergistic olfactory effects of diacetyl, acetaldehyde, and acetoin in a yogurt matrix using odor threshold, aroma intensity, and electronic nose analyses. *Journal of dairy science* 103(9): 7957-7967

TÜİK (2023). Türkiye İstatistik Kurumu. Hayvacılık İstatistikleri. https://biruni.tuik.gov.tr/medas/?kn=79&locale=tr (August 2023).

Uzunsoy I (2018). Determination of suitability of Lactobacillus delbrueckii subsp. bulgaricus and Streptococcus thermophilus strains isolated from traditional J Microbiol Biotech Food Sci / Uzunsoy et al. 2023:13 (1) e9241 8 yogurt samples for industrial yogurt productions and developing starter combinations, Ph.D. thesis. Ankara: Ankara University

Uzunsoy I, Budak S O, Sanli T, Taban B, Aytac A, Yazihan N & Özer B (2021). Assessment of Growth and Technological Performances of Yogurt Bacteria Isolated from Local Turkish Yogurts. *Food Science and Engineering* pp. 52-64

Üçüncü M (2005). *Süt ve mamulleri teknolojisi*. Ege Üniversitesi Mühendislik Fakültesi.

Vanbergue E, Delaby L, Peyraud J L, Colette S, Gallard Y & Hurtaud C (2017). Effects of breed, feeding system, and lactation stage on milk fat characteristics and spontaneous lipolysis in dairy cows.*Journal of Dairy Science* 100(6): 4623-4636

van Hylckama Vlieg J E T & Hugenholtz J (2007). Mining natural diversity of lactic acid bacteria for flavour and health benefits. *International dairy journal* 17(11): 1290-1297

Van Immerseel F, Ducatelle R, De Vos M, Boon N, Van De Wiele T, Verbeke K & Flint H J (2010). Butyric acid-producing anaerobic bacteria as a novel probiotic treatment approach for inflammatory bowel disease. *Journal of medical microbiology* 59(2): 141-143

Walstra P (1999). Dairy technology: Principles of Milk Properties and Processes.

Whetstine M C, Karagul-Yuceer Y O N C A, Avsar Y K & Drake M A (2003). Identification and quantification of character aroma components in fresh Chevre-style goat cheese. *Journal of Food Science-Chicago* 68(8): 2441-2447

Wirawati C U, Sudarwanto M B, Lukman D W, Wientarsih I & Srihanto E A (2019). Diversity of lactic acid bacteria in dadih produced by either back-slopping or spontaneous fermentation from two different regions of West Sumatra, Indonesia. *Veterinary world* 12(6): 823

Journal of Agricultural Sciences
(Tarim Bilimleri Dergisi)

J Agr Sci-Tarim Bili
e-ISSN: 2148-9297
jas.ankara.edu.tr

JAS

Yield Response of Greenhouse Grown Grafted Eggplant to Partial Root Drying and Conventional Deficit Irrigation

Ahmet Tezcan[a], Halil Demir[b], Harun Kaman[a*], Mehmet Can[a]

[a]*Department of Agricultural Structures and Irrigation, Faculty of Agriculture, Akdeniz University, Antalya 07058, TURKEY*

[b]*Department of Horticulture, Faculty of Agriculture, Akdeniz University, Antalya 07058, TURKEY*

ARTICLE INFO

Research Article

Corresponding Author: Harun Karaman, E-mail: hkaman@akdeniz.edu.tr

Received: 03 October 2024 / Revised: 21 November 2024 / Accepted: 13 December 2024 / Online: 25 March 2025

Cite this article

Tezcan A, Demir, Kaman H, Can M (2025). Yield Response of Greenhouse Grown Grafted Eggplant to Partial Root Drying and Conventional Deficit Irrigation. *Journal of Agricultural Sciences (Tarim Bilimleri Dergisi),* 31(2):516-531. DOI: 10.15832/ankutbd.1560489

ABSTRACT

Global climate change negatively affects life, thus complicating the production of vegetables. In addition to this, very little is known about eggplant cultivation under different irrigation strategies. For example, although water use efficiency gives better results in some plant species and varieties without any decrease in yield when the partial root drying (PRD) technique is used, the PRD technique has not been adequately examined in eggplant cultivation. The potential reactions of grafted and ungrafted eggplant plants under different irrigation water levels (100%, 80%, 60% and 40%) with the use of the conventional and deficit irrigation and PRD technique were investigated in this study. The research was conducted in a glass greenhouse during two cultivation seasons in 2019 and 2020. Irrigation was applied equally to both grafted and ungrafted eggplant plants using the drip irrigation method. In the study were examined the growth, quality criteria, yield, yield components, WUE, IWUE, and ky of eggplant to determine the reactions of grafted and ungrafted eggplant plants under different irrigation applications. It was found in the study that the method and amount of irrigation water applied had a significant effect on the grafted and ungrafted eggplant plants. Irrigation water was applied in the first and second season respectively between 148.45 and 365.48 mm, 245.61 and 584.84 mm. The statistical differences were found in the level of importance of yield, evapotranspiration, water-use efficiency, LSD classification of irrigation water-use efficiency values $P<0.01$ and/or $P<0.05$. Regression analysis values between irrigation water and yield of grafted and ungrafted eggplant in both cultivation seasons were found to be at a fairly good level ($0.80<R^2$). In addition, as an important finding, the regression analysis value of grafting in the second season was found to be at the highest level (R^2=91). In general, grafted eggplant plants were found to have had a higher total yield than the ungrafted plants. As the amount of irrigation water applied decreased, the yield also decreased. In the first season, the highest yields were recorded statistically in $FPRD_{100}$, I_{100} and $FPRD_{80}$ (45.26, 44.01 and 39.26 t ha^{-1}, respectively). Similarly, in the second season, the highest yields were obtained in I_{100} and $FPRD_{100}$ (50.97 and 48.96 t ha^{-1}, respectively) followed by $FPRD_{80}$ (48.96 t ha^{-1}). The advantages of the PRD technique over conventional and deficit irrigation have also been revealed. As a result of the research, it could be recommended that the cultivation of grafted eggplant seedlings is more suitable, and irrigation applications could be carried out using the PRD technique.

Keywords: Deficit irrigation, Yield response factor, Irrigation water use efficiency, Water-yield relations, Vegetable

1. Introduction

Precipitation distributions are changing worldwide with climate change, and irrigation is now more needed, including the areas where irrigation was previously unnecessary (Ouma et al. 2024). With the increase in the global population and industrialization, competition for freshwater is increasing gradually, which leads to the need for additional water resources (Ouma et al. 2024). Ensuring food security in a scenario where natural resources such as water are degraded seems to be a major challenge (Singh 2016). In addition, agriculture consumes about 70% of the available freshwater resources worldwide, and it is about 77% in Turkey (Anonymous 2022). The world population is estimated to be 9 billion and food production is expected to increase by 50% by 2050, (Mekonnen & Gerbens-Leenes 2020; Ungureanu et al. 2020). This population is expected to increase the demand for food, clothing and shelter, which are heavily dependent on water resources (Meena et al. 2023). In such a case, the water demand will increase even more and will put severe pressure on the agricultural sector, which uses the most water. Because plant production is one of the sectors most sensitive to and most affected by climate change and variability (Sikka et al. 2018).

Irrigation is compulsory for crop production, especially in arid and semi-arid climates. The reason for this is that the precipitation in the regions is irregular and insufficient. In order for irrigation to be effective, it is necessary to use correct irrigation planning and management. A successful irrigation strategy has three main issues such as (1) method, (2) time, and (3) amount. Correct and appropriate irrigation planning is essential because both excessive and insufficient irrigation damage the crop and lead to economic losses (Bhatnagar & Poonia 2018). In the correct and appropriate irrigation management; the variables

of crop type, evaporation-transpiration, crop growth stage, climate, effective precipitation, soil water, etc. are very effective (Ouma et al. 2024).

Irrigation has some benefits such as reducing plant water stress, increasing yield, and helping to grow more than one crop across the year as the production is not dependent on seasons and precipitation (Zafar et al. 2020). Under conditions where water is required for crop production, growers need to manage the irrigation process very accurately. For example, in cases where water is insufficient, reducing water in each application and/or extending the irrigation interval to reduce the number of irrigations could be a solution. The irrigation mentioned so far is the conventional deficit irrigation strategy that has been applied traditionally. However, for the conventional deficit irrigation strategy to be used effectively, farmers must know in advance the critical-sensitive periods when plants need water (Kirda et al. 2004). On the other hand, another and relatively new type of irrigation applied without the need to know in advance the critical-sensitive periods when plants need water is the partial root drying (PRD) technique (Kirda et al. 2004). The PRD technique increases the efficiency of irrigation water use without reducing efficiency, and this is a very important achievement. This success has been achieved in many studies (Dry et al. 1995; Dry & Loveys 1998; Kang et al. 2000; Kang et al. 2001; Kang et al. 2002; Sonawane & Shrivastava 2022; Kaman et al. 2022; Kaman et al. 2023a; Kaman et al. 2023b; Kaman et al. 2023c). As can be understood from these studies, the PRD technique has been used for many plant species and varieties in the last 10 to 20 years. However, the PRD technique has not yet been examined in the cultivation of grafted and/or ungrafted eggplants.

Cantürk et al. (2023), Darko et al. (2019), Al-Hadidi & Sweity (2022) and Diaz-Perez & Eaton (2015) have highlighted the contribution of deficit irrigation to acceptable yield and quality in eggplant crops and water saving. Bozkurt Çolak (2019) reported that there are very few studies conducted to estimate the optimal amount of water for eggplant plants under deficit irrigation. According to the results of the few available studies in the literature, water use efficiency could be increased under reduced irrigation in eggplant cultivation (Bozkurt Çolak 2019).

Eggplant (*Solanum melongena* L.), which is one of the vegetables from the Solanaceae family, is a vegetable widely and traditionally produced in tropical, subtropical, and Mediterranean countries (Howladar 2018; Mokabel et al. 2022). 59.3 million tons of eggplant are produced worldwide (FAO 2024). In Turkey, eggplant constitutes about 1 million tons of 31.8 million tons of total vegetable production in Turkey in 2023, and has a share of 2.6% of the total production (TUIK 2024).

An important reason why grafted plants perform better than ungrafted plants has been attributed to the root system of grafted plants, which can go deeper by developing roots (Ibrahim et al. 2014; López-Marín et al. 2017). Different researchers have reported that grafting in pumpkin and eggplant plants can increase the WUE value due to an increase in the net CO_2 assimilation rate and/or a decrease in stomatal conductivity and transpiration rate, as reported for grafted eggplant (Khah et al. 2011; Al-Harbi et al. 2018). While the demand for grafted eggplant seedlings is increasing rapidly, research has focused on the effects of rootstock/scion combinations on plant performance in terms of yield and fruit quality (Sabatinoa et al. 2018). In this context, the yield, obvious quality characteristics and chemical composition of fruits obtained from grafted plants should remain equal or improved compared to nongrafted plants (Sabatinoa et al. 2018). According to Gisbert et al. (2011), Moncada et al. (2013), Maršič et al. (2014) and Sabatino et al. (2016), grafting can affect yield and fruit quality in eggplant. On the other hand, research on how greenhouse evaporation and microclimates affect evapotranspiration is needed for greenhouse water management and environmental control (Wang et al. 2024).

This study examined some potential reactions of grafted and ungrafted eggplant plants under the conventional and deficit irrigation and PRD techniques. Within the scope of the research, many observations and measurements were made regarding the growth, quality criteria, yield, yield components, water-use efficiency (WUE), irrigation water-use efficiency (IWUE) and yield-response factor (ky) of eggplant to determine the reactions of grafted and ungrafted eggplant plants under different irrigation applications.

2. Material and Methods

2.1. Climate and soil characteristics of the study site

The experiment was conducted during two spring growing seasons in 2019 (Season 1) and 2020 (Season 2) at the research fields of Akdeniz University, Faculty of Agriculture (30° 38' 30″ - 30° 39′ 45″ East, 36° 53′ 15″ - 36° 54′ 15″ North, 54 m above sea level), Antalya, Turkey. The study was carried out under completely controlled conditions in accordance with the growing season. The greenhouse was designed with a size of 16×60 m, which is widely used in Turkey and is established in a north-south direction.

The Mediterranean climate prevails in the study area Antalya. The average annual temperature is 18.0 °C, the relative humidity 63%, total precipitation is 1063.5 mm and total evaporation is 1886.3 mm (Anonymous 2000).

The soil type of the research area is the Gölbaşı series. The Gölbaşı series, which is developed on massive travertines, is included in the Entisol ordo because they are young soils that do not show much profile development. All the profiles of the soils

of this series, which have an AC horizon and are very young, have a clay-tin texture. They are located in almost flat and almost flat topographies (Sarı et al. 1993). Analysis of spoiled and unspoiled soil samples taken from different parts of the experimental area were analyzed for the physical properties of the soil (Table 1). Based on these values, the greenhouse soil is perfectly suitable as a growing medium for eggplant.

Table 1 - Physical properties of soils in the experimental area

Depth	*BD*	*FC*		*WP*		*TAW*	
(cm)	*(g cm^{-3})*	*(cm^3 cm^{-3})*	*(mm)*	*(cm^3 cm^{-3})*	*(mm)*	*(cm^3 cm^{-3})*	*(mm)*
0-10	1.263	0.348	34.83	0.235	23.46	0.114	11.4
10-20	1.270	0.347	34.67	0.235	23.53	0.111	11.1
20-30	1.404	0.385	38.53	0.260	25.98	0.125	12.5
30-40	1.303	0.356	35.59	0.241	24.08	0.115	11.5
Total (0–40 cm)			143.63		97.06		35.19

BD= Bulk density; FC= Field capacity; WP= Wilting point; TAW= Total available water

2.2. Plant material

The Korsika F1 eggplant variety, whose production is widespread throughout Turkey and around Antalya province, where most greenhouse production takes place, was used as the plant material in the research, and the eggplant plants were grafted on the AGR703 rootstock. AGR703 rootstock is a variety with a strong root structure, high root development at a low rhizosphere temperature and very good rootstock-scion. The effective root depth of the eggplant plant is known to be 30-60 cm. Cultural practices such as fertilization and spraying of eggplant plants were carried out according to standard practices.

2.3. The drip irrigation system, plot sizes and experimental treatments

Irrigation and fertilization were conducted using a drip irrigation system with a 2 L h^{-1} dripper flow rate. Soil preparation (leveling, deep ploughing) was completed before planting. In the area where the research was conducted, soil preparation operations were carried out in a manner like farmer practices in the region. A completely randomized block experimental design, comprising irrigation treatments with three replicates, was used. Replicated sub-plots of each irrigation treatment were 4×2.4 m (9.6 m^2) in size and had 3 rows of 8 plants, with 0.8 m row spacing. The plant spacing in rows was 0.5 m.

The planting dates were 05 February and 07 February in 2019 and 2020, respectively. After the seedlings were planted in the greenhouse, sap water was given until the plants began to take root in the soil. Irrigation and fertilizer applications were carried out with a drip irrigation system with a 2 L h^{-1} dripper flow rate. The irrigation water applied was measured with a flow meter, installed in the water delivery unit of the irrigation system, which was designed for independent control of water delivery to each irrigation treatment. The water delivery unit had both mesh and sand filters for preventing dripper clogging. While irrigation was applied once a week after planting the seedlings, the number of irrigations increased to two per week with the increase in evaporation parallel to the increase in air temperatures. The last harvests were made on 28 June and 27 July, respectively, in 2019 and 2020. The amount of irrigation water was calculated according to the evaporation (ET) measured through the Class-A Evaporation Pan placed in the center of the greenhouse. In addition, the electrical conductivity of the irrigation water used in the study was 0.443 dS m^{-1}.

Various irrigation technologies for conventional deficit-irrigation and fixed-partial root-zone drying (FPRD) treatments were applied together with FULL (Table 2).

2.4. Irrigation water

We had used fixed irrigation interval, seven days until midseason, then two irrigations were applied weekly, at 3- and 4-day intervals. By doing so, irrigation water applied was limited to a maximum quantity of 6 L per plant, which prevented deep percolation (Kirda et al. 2004). Firstly, with the planting of seedlings, water was applied to each plant in equal amounts until rooting. Afterwards, irrigation water was calculated using the evaporation amounts from the evaporation container during the irrigation interval. A Class-A Evaporation Pan located in the center of the greenhouse was used to estimate irrigation water requirement (I, mm) for I_{100} using the Equation (1):

$$I = K \times Ep \quad (1)$$

Where; K is a coefficient comprising plant coverage, wetted area (diameter of 45–50 cm) and pan coefficient; Ep is cumulative evaporation (mm) measured during the allowed irrigation interval. K was allowed to change from 0.30 to 1.27 as the season progressed.

Table 2 - Irrigation treatments

Irrigation treatments	*Description*
	For conventional and deficit irrigation (I)
I_{100}	Irrigation water amount was applied uniformly on the two halves of plant root-zone (CONTROL).
I_{80}	Received 20% less water, compared to I100 irrigation.
I_{60}	Received 40% less water, compared to I100 irrigation.
I_{40}	Received 60% less water, compared to I100 irrigation.
	For fixed-partial root drying irrigation (FPRD)
$FPRD_{100}$	Received 100% water, compared to I100 irrigation; only one half of the plant root zone was relatively irrigated.
$FPRD_{80}$	Received 20% less water, compared to I100 irrigation; only one half of the plant root zone was relatively irrigated.
$FPRD_{60}$	Received 40% less water, compared to I100 irrigation; only one half of the plant root zone was relatively irrigated.
$FPRD_{40}$	Received 60% less water, compared to I100 irrigation; only one half of the plant root zone was relatively irrigated.

2.5. Evapotranspiration (ET), water-use efficiency (WUE), irrigation water-use efficiency (IWUE) and yield response factor (ky)

Plant evapotranspiration (ET, mm) was determined based on the water-budget using the following Equation (2):

$$ET = I \pm \Delta S \tag{2}$$

Where; I is the amount of irrigation water applied (mm); ΔS is the change in soil-water content between the beginning and the end of the season (mm). There was no capillary water inlet in the study, and precipitation had no effect. Thus, capillary water inlet, surface runoff and precipitation were not included in the plant evapotranspiration equation.

The water-use efficiency (WUE, kg m^{-3}) to irrigation regime was determined using the following Equation (3):

$$WUE = \frac{Y}{ET} \tag{3}$$

Where; Y is yield (kg da^{-1}); ET is evapotranspiration (mm).

The irrigation water-use efficiency (IWUE, kg m^{-3}) to irrigation regime was determined using the following Equation (4):

$$IWUE = \frac{Y}{I} \tag{4}$$

Where; Y is the yield (kg da^{-1}); I is the irrigation water applied during the season (mm).

Ky, which is an indicator of the effect of water deficiency on plant yield, was calculated using the following Equation (5) proposed by Doorenbos & Kassam (1979) and Stewart et al. (1977):

$$\left[1 - \frac{Ya}{Ym}\right] = ky \times \left[1 - \frac{ETa}{ETm}\right] \tag{5}$$

Where; Ya is the actual-yield (t ha^{-1}), which corresponds to actual plant evapotranspiration in the environments where the plant is cultivated; Ym is the yield obtained through maximum evapotranspiration in the environments where no water shortage is experienced through the growth season (t ha^{-1}); ky is the yield-response factor, which shows the decrease in the yield due to a unit decrease in evapotranspiration; ETa is the actual evapotranspiration in environments where the plant is cultivated (mm); ETm is the maximum evapotranspiration in environments where the plant is exposed to no water deficit through the growing season of the plant (mm).

2.6. Measurement and observation of fruit quality and other parameters

In addition to those explained above, total yield, mean fruit weight, fruit width, fruit length, biomass, plant height observations and measurements were made. Fruit width and length were measured with a caliper. Biomass and plant height measurements were made by cutting the plants from the soil surface at the end of the season. In addition, plant height measurements were made once a week throughout the growing season. Total soluble solids content (SSC, %), pH, fruit color (L*), fruit color (a*), fruit color (b*) measurements were also made in the fruits. Total SSC amount in the juices obtained from the harvested eggplant fruits with a juicer was determined with a digital refractometer (%). pH values were measured in the juices obtained with a juicer. Colour values were measured with a Minolta CR400 colour chromameter, SSC digital refractometer (Siomas et al. 2002; Madeira et al. 2003).

2.7. Statistical analysis

A completely randomized block experimental design was employed, comprising irrigation treatments with three replicates. The plants from the beginning and end of the rows were excluded from the measurement to prevent the plant edge effect. A one-way analysis of variance (ANOVA) was performed using the SAS package program. The significance of the differences in the means of the different treatments were tested at $P<0.01$ and $P<0.05$ significance levels. The LSD multiple comparison test was used to investigate which of the treatment means differed in cases where the ANOVA results showed a significant difference in the means.

3. Results

3.1. Evaporation from Class-A Pan and amount of irrigation water

As expected, the amount of irrigation water also increased in parallel with the increase in the amount of evaporation for both seasons of study (Figure 1). In the first (2019) season of the study, irrigation water application was applied a total of 35 times in total depending on the evaporation amounts measured in the Class-A evaporation. In the second (2020) season, irrigation water was applied 44 times in total. However, since the process in the second season was longer, the number and amount of irrigations was naturally higher (Figure 1).

3.2. Yield, evapotranspiration, water-use efficiency, irrigation water-use efficiency

The amount of irrigation water was applied between 148.45 and 365.48 mm in the first season, and between 245.61 and 584.84 mm in the second season (Tables 3 and 4). Depending on the amount of irrigation water application, statistical differences (at $P<0.01$ and/or $P<0.05$) were found in the yield values. Similarly, evapotranspiration (ET), water use efficiency, irrigation water use efficiency values were also found to be statistically significant (Tables 3 and 4).

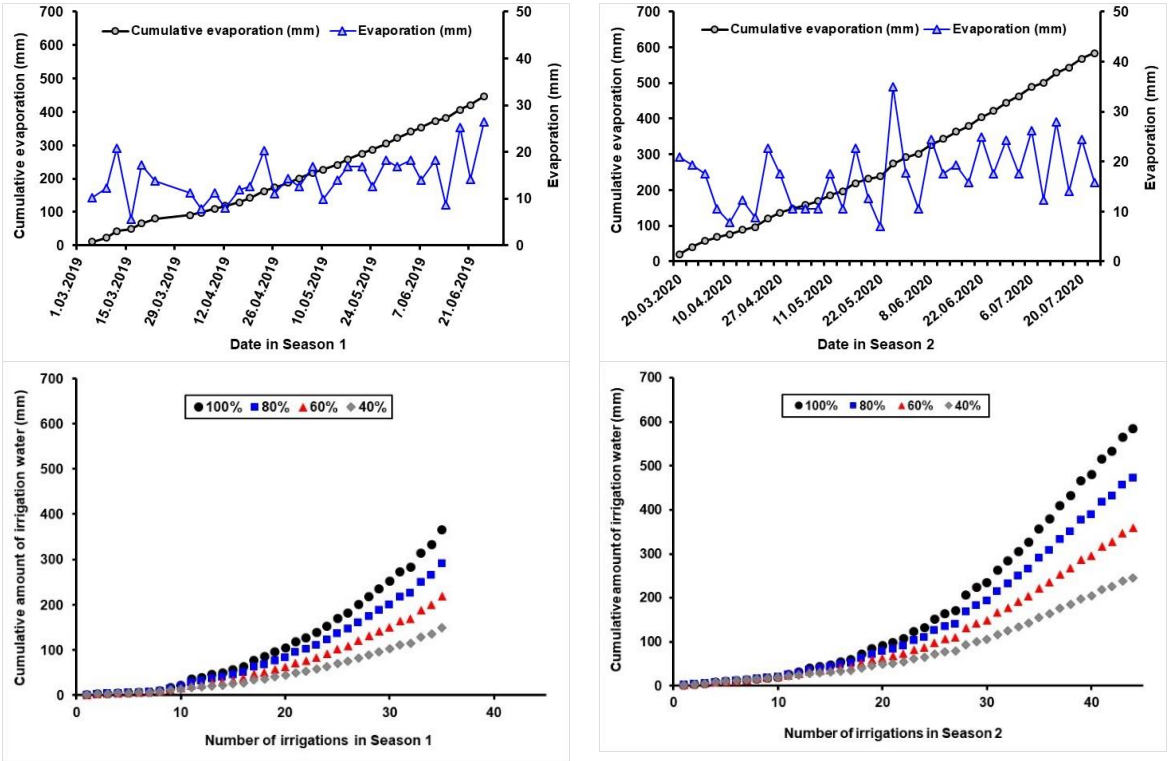

Figure 1 - Evaporation (mm) from Class-A Pan in the greenhouse and cumulative amount of irrigation water (mm) under 100%, 80%, 60% and 40% for ungrafted-grafted eggplant

Table 3 - Irrigation water, yield, ET, WUE, and IWUE in Season 1

Treatments		*I (mm)*	*Yield (t ha^{-1})*	*ET (mm)*	*WUE (kg m^{-3})*	*IWUE (kg m^{-3})*
I_{100}		365.48	44.01 a	390.11 a	11.28	12.04
I_{80}		291.36	31.29 bc	316.57 c	9.91	10.74
I_{60}		219.02	27.72 cd	256.71 d	10.80	12.65
I_{40}		148.45	21.30 d	187.40 f	11.40	14.35
$FPRD_{100}$		365.48	45.26 a	392.98 a	11.52	12.38
$FPRD_{80}$		291.36	39.26 ab	333.43 b	11.78	13.47
$FPRD_{60}$		219.02	30.78 bcd	261.63 d	11.75	14.05
$FPRD_{40}$		148.45	22.93 cd	194.60 e	11.79	15.44
Significance Level of Irrigation (I)		-	**	**	ns	ns
Ungrafted		-	31.30	291.24	10.72	12.41
Grafted		-	34.33	292.13	11.84	13.88
Significance Level of Graft (G)		-	ns	ns	ns	ns
I_{100}	Ungrafted	365.48	40.92	389.01 a	10.52 bd	11.20 cd
	Grafted	365.48	47.10	391.22 a	12.04 ad	12.89 bd
I_{80}	Ungrafted	291.36	27.86	322.76 c	8.63 cd	9.56 d
	Grafted	291.36	34.72	310.38 d	11.19 bd	11.92 bd
I_{60}	Ungrafted	219.02	27.49	260.89 f	10.54 bd	12.55 bd
	Grafted	219.02	27.95	252.54 g	11.07 bd	12.76 bd
I_{40}	Ungrafted	148.45	24.60	184.11 ı	13.36 ab	16.57 ab
	Grafted	148.45	17.99	190.70 hı	9.43 bd	12.12 bd
$FPRD_{100}$	Ungrafted	365.48	45.49	394.91 a	11.52 ad	12.45 bd
	Grafted	365.48	45.03	391.05 a	11.52 ad	12.32 bd
$FPRD_{80}$	Ungrafted	291.36	41.12	329.04 c	12.50 ac	14.11 bd
	Grafted	291.36	37.40	337.82 b	11.07 bd	12.83 bd
$FPRD_{60}$	Ungrafted	219.02	28.10	254.20 fg	11.05 bd	12.83 bd
	Grafted	219.02	33.47	269.06 e	12.44 ac	15.28 bc
$FPRD_{40}$	Ungrafted	148.45	14.83	194.98 h	7.61 d	9.99 d
	Grafted	148.45	31.03	194.23 h	15.97 a	20.90 a
Significance Level of IxG		-	ns	**	*	*

I=Irrigation water (mm); Y=Yield (t ha^{-1}); ET=Evapotranspiration (mm); WUE=Water-use efficiency (kg m^{-3}) and IWUE=Irrigation water-use efficiency (kg m^{-3}); Means with different letters in the same column were significantly different; *: (P<0.05), **: (P<0.01), ns: non-significant

In general, grafted plants had a higher yield than ungrafted plants (Table 4). In other words, the situation was similar in all irrigation treatments and it was revealed that grafting had an increasing effect on yield. The statistical change in yield values is very significant (P<0.01) for the irrigation levels (100%, 80%, 60%, and 40%). The differences between irrigation×grafting (P<0.01) and irrigation×grafting (I×G) correlations were not statistically significant (Tables 3 and 4). However, grafting was also very important (P<0.01) in the second season (Table 4). In the first season, I_{100}, $FPRD_{100}$, and $FPRD_{80}$ treatments had the highest yield value and I_{40} had the lowest yield value (Table 3). In the second season, I_{100} and $FPRD_{100}$ treatments had the highest yield value, and I_{40} and $FPRD_{40}$ had the lowest yield value (Table 4). As the amount of irrigation water increased, the yield values also tended to increase (Tables 3 and 4).

It can be said that grafting, together with irrigation water, also increases yield. Similar results were found for the mass values (Tables 3 and 4). In addition, the differences between the irrigation×grafting (I×G) correlations for mass values were also found to be statistically significant (P<0.01 and P<0.05) (Tables 3 and 4). The differences between the irrigation×grafting (I×G) correlations were found to be statistically significant (P<0.01 and P<0.05). As with irrigation water, the increase in the amount of mass along with the increase in yield values also tended to increase (Tables 3 and 4). Grafting, together with the mass value, could be claimed to have increased yield. The correlation of irrigation×grafting (I×G) in the first season (Table 3) and the change between grafting and irrigation levels (100%, 80%, 60%, and 40%) in the second season (Table 4) were found to be statistically very significant (P<0.01) for WUE. The correlation between irrigation× grafting (I×G) was found to be statistically significant (P<0.01). Similar to the WUE values, the irrigation×grafting (I×G) correlation was found to be important for IWUE in the first season (Table 3) (P<0.05), and grafting was found to be very important in the second season (Table 4) (P<0.01).

Table 4 - Irrigation water, yield, ET, WUE, and IWUE in Season 2

Treatments		*I (mm)*	*Yield (t ha^{-1})*	*ET (mm)*	*WUE (kg m^{-3})*	*IWUE (kg m^{-3})*
I_{100}		584.84	50.97 a	657.70 a	7.75 a	8.71
I_{80}		472.12	32.48 cd	546.08 b	5.96 bcd	6.88
I_{60}		358.73	30.07 d	427.77 d	7.06 abc	8.38
I_{40}		245.61	17.52 e	321.38 f	5.45 cd	7.13
$FPRD_{100}$		584.84	48.96 ab	657.51 a	7.45 ab	8.37
$FPRD_{80}$		472.12	40.88 bc	546.23 b	7.48 ab	8.66
$FPRD_{60}$		358.73	30.57 d	435.84 c	7.00 abc	8.52
$FPRD_{40}$		245.61	15.74 e	332.86 e	4.73 d	6.41
Significance Level of Irrigation (I)		-	**	**	**	ns
Ungrafted		-	29.87 b	491.26	5.88 b	7.02 b
Grafted		-	36.93 a	490.08	7.34 a	8.75 a
Significance Level of Graft (G)		-	**	Ns	**	**
I_{100}	Ungrafted	584.84	46.41	657.50 a	7.06	7.94
	Grafted	584.84	55.52	657.90 a	8.44	9.49
I_{80}	Ungrafted	472.12	25.86	551.49 b	4.69	5.48
	Grafted	472.12	39.09	540.66 b	7.23	8.28
I_{60}	Ungrafted	358.73	21.49	433.74 cd	4.95	5.99
	Grafted	358.73	38.66	421.80 e	9.17	10.78
I_{40}	Ungrafted	245.61	16.23	323.26 g	5.02	6.61
	Grafted	245.61	18.81	319.51 g	5.89	7.66
$FPRD_{100}$	Ungrafted	584.84	47.33	656.57 a	7.21	8.09
	Grafted	584.84	50.58	658.46 a	7.68	8.65
$FPRD_{80}$	Ungrafted	472.12	40.20	549.54 b	7.31	8.51
	Grafted	472.12	41.56	542.92 b	7.66	8.80
$FPRD_{60}$	Ungrafted	358.73	25.69	429.87 de	5.98	7.16
	Grafted	358.73	35.45	441.82 c	8.02	9.88
$FPRD_{40}$	Ungrafted	245.61	15.73	328.12 fg	4.79	6.40
	Grafted	245.61	15.76	337.60 f	4.67	6.42
Significance Level of IxG		-	ns	*	ns	ns

I=Irrigation water (mm); Y=Yield (t ha^{-1}); ET=Evapotranspiration (mm); WUE=Water-use efficiency (kg m^{-3}) and IWUE=Irrigation water-use efficiency (kg m^{-3}); Means with different letters in the same column were significantly different; *: (P<0.05), **: (P<0.01), ns: non-significant.

3.3. Regression analysis between water and yield

Regression analysis values between irrigation water and yield of grafted and ungrafted eggplant in both cultivation seasons were found to be at a fairly good level (R^2>80) (Figure 2). However, as an important finding, the regression analysis value of grafting in the second season was found to be at the highest level with R^2=91 (Figure 2).

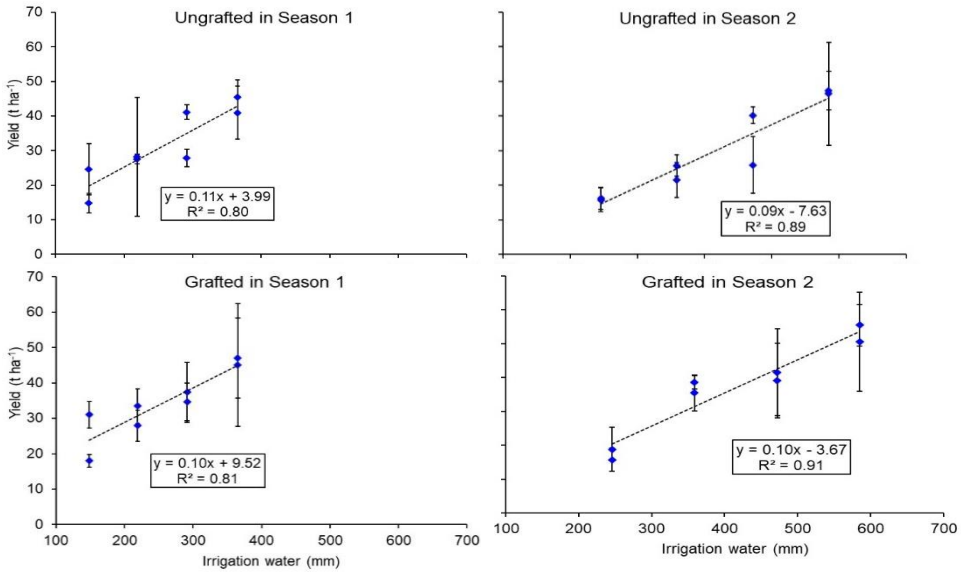

Figure 2 - Correlations between irrigation water and yield on ungrafted-grafted eggplant (The bars show standard deviation)

Similar to the regression analysis results between irrigation water and yield (Figure 2), the regression analysis values between evapotranspiration and yield were calculated at a good level (R^2>80) (Figure 3). As an important result, the regression analysis

value of grafting in the second season occurred at the highest level with R^2=89 (Figure 3). Regression analysis between both irrigation water and yield and evapotranspiration and yield revealed an increasing correlation (Figures 2 and 3). In particular, despite the increase in the amount of irrigation water, there has been no decrease in yield values. This reveals that the amount of irrigation water is applied correctly and under appropriate conditions. In general, the fact that the R^2 values are greater than 0.80 in the regression analysis reveals that irrigation is managed very well and correctly (Figures 2 and 3). It can also be concluded that grafting, together with irrigation management, is very valuable in the eggplant plant.

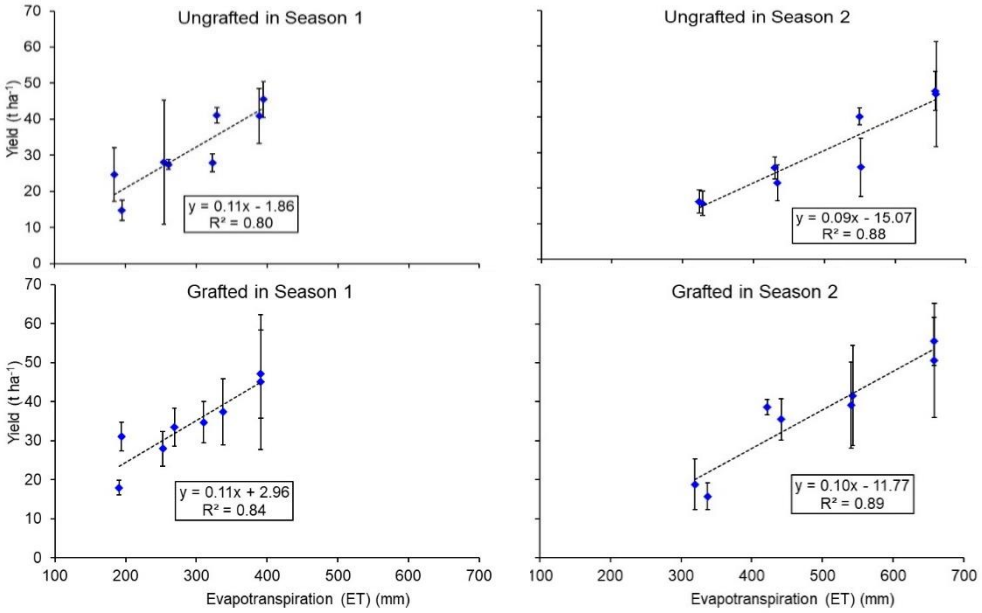

Figure 3 - Correlations between evapotranspiration (ET) and yield on ungrafted-grafted eggplant (The bars show standard deviation)

3.4. Yield response factor

Yield response indicates a decrease in yield in response to a unit decrease in evapotranspiration. Yield response graphs have been prepared as an indicator of the effect of a proportional decrease in plant water consumption on a proportional decrease in ungrafted eggplant yield (Figure 4). In the regression analysis, ky values were found by using seasonal plant water consumption and yield values. In the first season, the ky values changed between 0.68 and 1.87, and in the second season between 0.80 and 2.70 (Figure 4). In response to the proportional decrease in plant water consumption, decreases have also occurred in the yield of ungrafted and grafted eggplants. However, it can be said that the most significant results were obtained in grafted eggplant and FPRD irrigation.

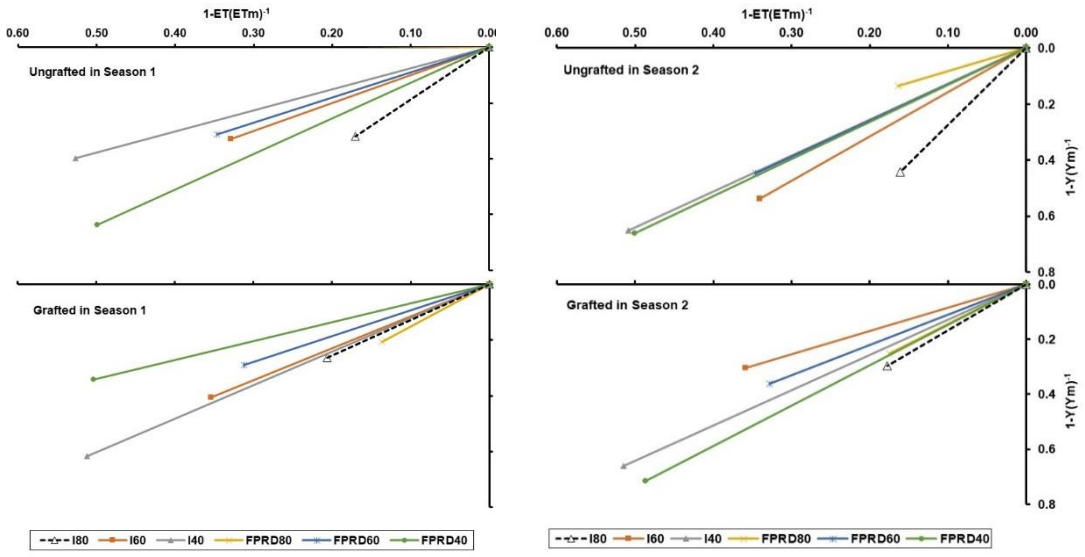

Figure 4 - The yield response factors under 80%, 60% and 40% of irrigation water for ungrafted-grafted eggplant in the study

3.5. Yield components, biomass and plant height

The statistical analysis results of the yield-related parameters such as total yield per plant, average fruit weight, fruit width, and fruit length, as well as dry biomass and plant height values are given in Tables 5 and 6. The biomass and plant height values in the tables were taken on the last day of the research. In addition, plant height changes were also monitored during the season (Figure 5). All parameters regarding the yield were negatively affected by water stress in general.

Table 5 - Total yield, mean fruit weight, fruit width, fruit length, biomass, plant height in Season 1

Treatments		*Total fruit yield (g plant^{-1})*	*Mean fruit weight (g fruit^{-1})*	*Fruit width (mm fruit^{-1})*	*Fruit length (mm fruit^{-1})*	*Biomass (g plant^{-1})*	*Plant height (at the end of the season) (cm plant^{-1})*
I_{100}		1760.44 a	153.10 ab	51.63	15.35 ab	88.69 b	108.25 ab
I_{80}		1251.64 bc	146.72 bc	53.05	14.84 b	66.35 c	94.56 c
I_{60}		1108.68 cd	147.51 bc	52.85	14.56 b	56.80 cd	83.92 ce
I_{40}		851.85 d	135.23 cd	52.30	13.21 c	44.25 e	73.19 e
$FPRD_{100}$		1810.31 a	161.57 a	51.26	15.84 a	115.06 a	111.25 a
$FPRD_{80}$		1570.35 ab	145.74 bc	51.05	14.78 b	90.87 b	96.67 bc
$FPRD_{60}$		1231.30 bd	143.75 bc	52.12	14.67 b	51.92 de	88.58 cd
$FPRD_{40}$		917.08 cd	129.70 d	50.24	13.64 c	48.31 de	76.31 de
Significance Level of Irrigation (I)		**	**	ns	**	**	**
Ungrafted		1252.04	149.90 a	52.95 a	14.48	68.86	87.51 b
Grafted		1373.38	140.93 b	50.68 b	14.74	71.70	95.67 a
Significance Level of Graft (G)		ns	*	**	ns	ns	*
I_{100}	Ungrafted	1636.85	162.84 ab	53.07 ad	15.36 ab	81.73 cd	105.78
	Grafted	1884.02	143.37 bd	50.19 df	15.35 ab	95.65 bc	110.72
I_{80}	Ungrafted	1114.43	147.44 bd	53.88 ac	14.63 ac	71.84 de	91.67
	Grafted	1388.86	146.00 bd	52.22 bf	15.06 ac	60.85 ef	97.44
I_{60}	Ungrafted	1099.52	138.74 ce	52.62 ae	13.98 cf	59.44 ef	82.22
	Grafted	1117.84	156.28 ac	53.09 ad	15.13 ac	54.15 fg	85.61
I_{40}	Ungrafted	984.18	149.64 bd	55.89 a	13.27 df	49.82 fh	69.56
	Grafted	719.52	120.81 e	48.72 f	13.15 ef	38.68 h	76.83
$FPRD_{100}$	Ungrafted	1819.44	170.20 a	51.83 bf	15.84 a	108.26 ab	99.56
	Grafted	1801.18	152.94 ad	50.69 cf	15.83 a	121.85 a	122.94
$FPRD_{80}$	Ungrafted	1644.89	156.30 ac	52.89 ad	15.56 ab	90.85 c	95.11
	Grafted	1495.81	135.18 de	49.22 ef	13.99 cf	90.89 c	98.22
$FPRD_{60}$	Ungrafted	1123.85	152.51 ad	54.67 ab	14.35 be	43.11 gh	87.44
	Grafted	1338.75	134.98 de	49.57 df	14.98 ac	60.72 ef	89.72
$FPRD_{40}$	Ungrafted	593.13	121.56 e	48.74 f	12.83 f	45.79 fh	68.72
	Grafted	1241.04	137.84 ce	51.73 bf	14.45 bd	50.84 fh	83.89
Significance Level of IxG		ns	**	**	*	*	ns

Means with different letters in the same column were significantly different; *: (P<0.05), **: (P<0.01), ns: non-significant

For the irrigation levels in the first season (100%, 80%, 60%, and 40%); the statistical change in the values of total yield per plant, average fruit weight, fruit length, biomass, and plant length were found to be very significant (P<0.01) (Table 5). For grafting, the average fruit weight and plant height were significant (P<0.05), while the fruit width was very significant (P<0.01). In the irrigation×grafting (I×G) correlation, mean fruit weight and fruit width were highly significant (P<0.01), while fruit length and biomass were found to be significant (P<0.05).

In the statistical analysis of irrigation levels in the second season (100%, 80%, 60%, and 40%); total yield per plant, average fruit weight, fruit length, biomass, and plant length were found to be highly significant (P<0.01), while fruit width was found to be significant (P<0.05). For grafting, the total yield per plant and fruit size were highly significant (P<0.01), and plant size was significant (P<0.05). In the irrigation×grafting (I×G) correlation, only the average fruit weight was found to be significant (P<0.05).

In both seasons, the plant height increased gradually at all deficit irrigation levels of ungrafted and grafted eggplants (Figure 5). In the first season, the average height of ungrafted eggplants was 60.32 cm on ungrafted eggplant, the lowest was 20.61 cm, and the highest was 105.78 cm on I100. The average size of grafted eggplant was 64.68 cm, the lowest was 27.28 cm, and the highest was 122.94 cm on $FPRD_{100}$. In the second season, the average was measured at 63.87 cm in grafted eggplant, the lowest was measured as 12.83 cm, and the highest was measured as 114.11 cm in I_{100}. On the grafted eggplant, the average was measured as 69.18 cm, the lowest was measured as 19.33 cm, and the highest was measured as 124.22 cm in the I_{100} treatment.

Table 6 - Total yield, mean fruit weight, fruit width, fruit length, biomass, plant height in Season 2

Treatments		*Total fruit yield (g plant^{-1})*	*Mean fruit weight (g fruit^{-1})*	*Fruit width (mm fruit^{-1})*	*Fruit length (mm fruit^{-1})*	*Biomass (g plant^{-1})*	*Plant height (at the end of the season) (cm plant^{-1})*
I_{100}		2038.67 a	156.31 a	52.01 a	15.58 ab	130.09 a	119.17 a
I_{80}		1299.00 cd	143.85 bc	50.98 ab	14.88 cd	74.52 cd	101.11 bc
I_{60}		1202.88 d	136.35 c	51.79 a	14.42 d	61.75 de	92.83 cd
I_{40}		700.83 e	123.74 d	48.99 b	13.74 e	44.45 f	87.39 d
$FPRD_{100}$		1958.29 ab	154.94 a	52.09 a	15.74 a	109.33 b	114.83 a
$FPRD_{80}$		1635.17 bc	148.25 ab	51.65 a	15.42 ac	81.67 c	107.61 ab
$FPRD_{60}$		1222.92 d	148.13 ab	50.87 ab	15.05 bc	49.03 ef	97.83 bd
$FPRD_{40}$		629.71 e	120.63 d	49.24 b	13.79 e	48.06 ef	86.39 d
Significance Level of Irrigation (I)		**	**	*	**	**	**
Ungrafted		1194.66 b	140.967	51.06	14.62 b	72.19	97.58 b
Grafted		1477.21 a	142.083	50.84	15.03 a	77.54	104.21 a
Significance Level of Graft (G)		**	ns	ns	**	ns	*
I_{100}	Ungrafted	1856.50	151.94 ac	52.18	15.24	131.18	114.11
	Grafted	2220.83	160.68 ab	51.84	15.92	128.99	124.22
I_{80}	Ungrafted	1034.33	144.96 cd	50.78	14.50	78.02	98.56
	Grafted	1563.67	142.73 cd	51.18	15.27	71.02	103.67
I_{60}	Ungrafted	859.42	135.75 de	52.58	14.12	57.07	85.33
	Grafted	1546.33	136.95 de	50.99	14.72	66.44	100.33
I_{40}	Ungrafted	649.17	127.72 ef	48.69	13.69	43.00	85.33
	Grafted	752.50	119.76 fg	49.30	13.78	45.91	89.44
$FPRD_{100}$	Ungrafted	1893.25	146.22 cd	51.50	15.27	98.05	110.89
	Grafted	2023.33	163.67 a	52.68	16.21	120.61	118.78
$FPRD_{80}$	Ungrafted	1607.83	143.68 cd	51.58	15.33	83.51	102.56
	Grafted	1662.50	152.82 ac	51.73	15.51	79.84	112.67
$FPRD_{60}$	Ungrafted	1027.67	150.31 bc	51.28	14.93	43.15	97.67
	Grafted	1418.17	145.94 cd	50.45	15.16	54.92	98.00
$FPRD_{40}$	Ungrafted	629.08	127.15 eg	49.93	13.89	43.56	86.22
	Grafted	630.33	114.11 g	48.55	13.70	52.56	86.56
Significance Level of IxG		ns	*	ns	ns	ns	ns

Means with different letters in the same column were significantly different; *: (P<0.05), **: (P<0.01), ns: non-significant

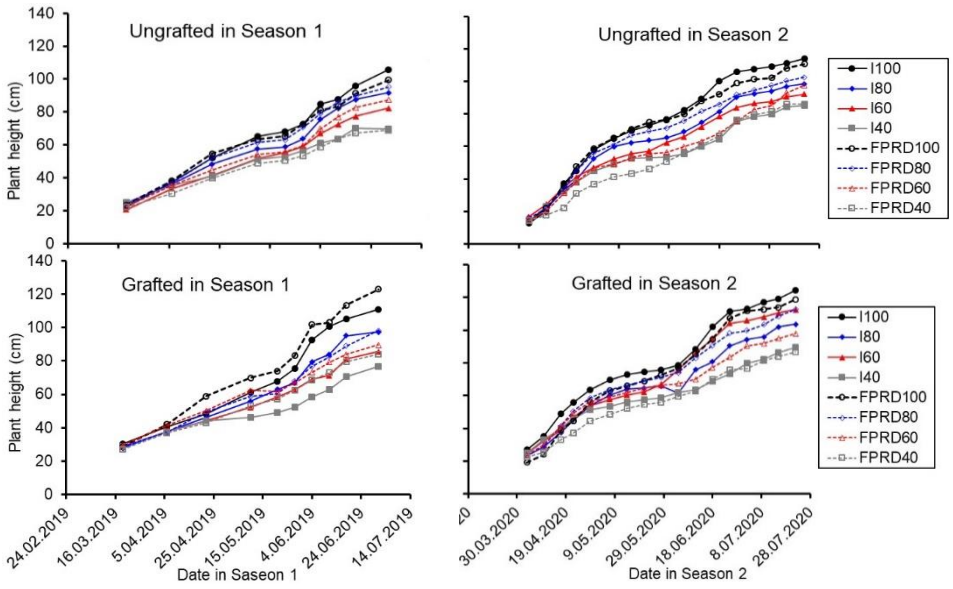

Figure 5 - Variation of plant height with deficit irrigation levels through the growing seasons

3.6. SSC, pH and fruit outer color

The statistical change in irrigation levels in the first season (100%, 80%, 60%, and 40%) and only the pH values for grafting were found to be very significant (P<0.01) (Table 7). In the statistical analysis of the correlation between irrigation levels (100%, 80%, 60%, and 40%) and irrigation×grafting (I×G) in the second season, only pH was highly significant (P<0.01) (Table 8). In the grafting, pH, and fruit color a* were found to be significant (P<0.05).

Table 7 - SSC, pH, fruit color (L*), fruit color (a*), fruit color (b*) in Season 1

Treatments	*SSC*	*pH*	*L**	*a**	*b**
I_{100}	5.38	8.97 cb	36.59	5.20	0.87
I_{80}	5.02	8.81 cb	36.20	4.59	0.77
I_{60}	5.83	8.67 cb	36.76	5.27	0.75
I_{40}	5.72	10.14 a	36.32	4.97	0.75
$FPRD_{100}$	5.43	8.29 c	36.06	5.08	0.80
$FPRD_{80}$	5.05	9.32 b	36.28	5.12	0.81
$FPRD_{60}$	5.47	8.94 cb	36.49	5.70	0.83
$FPRD_{40}$	5.43	8.92 cb	36.65	5.47	0.83
Significance Level of Irrigation (I)	ns	**	ns	ns	ns
Ungrafted	5.45	8.76 b	36.42	5.22	0.79
Grafted	5.37	9.26 a	36.42	5.13	0.81
Significance Level of Graft (G)	ns	**	ns	ns	ns
I_{100} Ungrafted	5.50	9.02	36.42	5.42	0.82
Grafted	5.27	8.92	36.76	4.99	0.92
I_{80} Ungrafted	5.20	8.56	36.06	4.60	0.57
Grafted	4.83	9.06	36.34	4.58	0.98
I_{60} Ungrafted	5.77	8.66	36.82	5.56	0.88
Grafted	5.90	8.68	36.70	4.99	0.62
I_{40} Ungrafted	5.90	9.74	36.79	5.44	0.88
Grafted	5.53	10.54	35.86	4.50	0.61
$FPRD_{100}$ Ungrafted	5.57	7.87	35.70	4.84	0.79
Grafted	5.30	8.71	36.42	5.33	0.81
$FPRD_{80}$ Ungrafted	5.10	9.15	36.30	4.74	0.73
Grafted	5.00	9.48	36.27	5.50	0.89
$FPRD_{60}$ Ungrafted	5.53	8.80	36.77	5.78	0.89
Grafted	5.40	9.09	36.20	5.63	0.77
$FPRD_{40}$ Ungrafted	5.17	8.24	36.46	5.40	0.79
Grafted	5.70	9.60	36.84	5.54	0.86
Significance Level of IxG	ns	Ns	ns	ns	ns

Means with different letters in the same column were significantly different; *: (P<0.05), **: (P<0.01), ns: non-significant

Table 8 - SSC, pH, fruit color (L*), fruit color (a*), fruit color (b*) in Season 2

Treatments	*SSC*	*pH*	*L**	*a**	*b**
I_{100}	5.03	6.20 a	26.76	7.51	0.29
I_{80}	5.40	6.15 ab	26.67	7.26	0.28
I_{60}	5.15	6.20 a	26.57	6.81	0.25
I_{40}	5.70	6.11 b	26.68	6.62	0.22
$FPRD_{100}$	5.03	6.21 a	26.68	6.53	0.24
$FPRD_{80}$	5.38	6.18 a	26.58	6.57	0.21
$FPRD_{60}$	5.13	6.21 a	26.39	6.88	0.16
$FPRD_{40}$	5.00	6.10 b	26.32	6.61	0.17
Significance Level of Irrigation (I)	ns	**	ns	ns	ns
Ungrafted	5.27	6.19 s	26.65	7.05 a	0.23
Grafted	5.19	6.15 b	26.51	6.64 b	0.22
Significance Level of Graft (G)	ns	*	ns	*	ns
I_{100} Ungrafted	5.10	6.19 ad	26.83	7.78	0.30
Grafted	4.97	6.20 ad	26.69	7.23	0.28
I_{80} Ungrafted	5.83	6.11 df	26.92	7.64	0.31
Grafted	4.97	6.19 ad	26.43	6.87	0.24
I_{60} Ungrafted	4.97	6.17 bd	26.65	6.80	0.21
Grafted	5.33	6.23 ac	26.48	6.83	0.29
I_{40} Ungrafted	5.60	6.20 ad	26.88	6.54	0.23
Grafted	5.80	6.02 f	26.48	6.71	0.20
FPR Ungrafted	5.07	6.28 a	26.92	6.67	0.26
D_{100} Grafted	5.00	6.14 ce	26.44	6.39	0.23
FPR Ungrafted	5.30	6.24 ab	26.56	6.74	0.24
D_{80} Grafted	5.47	6.12 de	26.61	6.39	0.17
FPR Ungrafted	5.17	6.23 ac	26.25	7.34	0.15
D_{60} Grafted	5.10	6.18 bd	26.52	6.41	0.16
FPR Ungrafted	5.13	6.07 ef	26.18	6.89	0.18
D_{40} Grafted	4.87	6.13 de	26.45	6.33	0.17
Significance Level of IxG	ns	**	ns	ns	ns

Means with different letters in the same column were significantly different; *: (P<0.05), **: (P<0.01), ns: non-significant

4. Discussion

Soil and irrigation water test results performed at the beginning of the season are presented in Table 1, respectively. The EC (dS m^{-1}) values of the irrigation water at the beginning of the season were found to be suitable for eggplant irrigation as claimed by Machado & Serralheiro (2017). The pH of the irrigation water was also found suitable for the cultivation of eggplant (Okiror et al. 2017).

4.1. Evaporation from Class-A Pan and amount of irrigation water

The amount of irrigation water was recorded between 148.45 and 365.48 mm and between 245.61 and 584.84 mm in the first and second seasons respectively (Tables 3 and 4). Similarly, Ayas (2017) determined the amount of irrigation water required for eggplant cultivation to be between 85 mm and 464 mm, with mass values ranging between 170 mm and 472 mm. During the research, the amount of irrigation water also increased due the increasing evaporation values, the extension of days and plant growth (Figure 1). Similar results have been documented in many studies (e.g. Kirda et al. 2004; Topcu et al. 2007; Cantürk et al. 2023). This reveals that the research and especially the irrigation management have been carried out correctly.

4.2. Yield, evapotranspiration, water-use efficiency, irrigation water-use efficiency

As seen in Tables 3 and 4, it is an important result that the fruit mass values are higher than the irrigation water quantity values throughout the study, because in such a case it may mean that water is not wasted through ways such as surface flow, deep filtration, etc. Therefore, it is an indicator that irrigation has been managed well and that water has been used most effectively.

Depending on irrigation and grafting in the research; the results of ANOVA analysis regarding yield (Y), evapotranspiration (ET) water-use efficiency, and irrigation water-use efficiency values showed a significant change at the $P<0.01$ and/or $P<0.05$ level (Tables 3 and 4). When the grafted and ungrafted eggplant yields in the first season of the study are considered together, depending on the irrigation practices (Table 3), the $FPRD_{100}$ and $FPRD_{80}$ treatments gave similar results. In other words, the highest yield was obtained with less water. Although they had statistically the highest yield compared to the $FPRD_{100}$ and I_{100}, 2.8% more yield was obtained from the $FPRD_{100}$. This reveals the importance of partial-wetting irrigation. A similar result is found in the irrigation treatments producing the highest yield. The results of this research are consistent with previous research in literature. Ertek et al. (2006) found that there was a decrease in eggplant yield when the highest irrigation water was applied in the deficit irrigation study. This means that the amount of water should be optimized to avoid excessive irrigation conditions that may negatively affect crop yield in eggplant cultivation. In this study, the negativity that Ertek et al. (2006) highlighted was not experienced as no excessive irrigation was applied (Figure 1, Tables 3 and 4). In general, grafted plants have produced more yield than ungrafted plants. Grafting was very important for yield values, especially in the second season (Table 4) ($P<0.01$). The increase in yield of grafted eggplants is similar to that reported by Consentino et al. (2022).

Water stress also reduces the ability of plants to perform photosynthesis, which negatively affects their growth and production (Kumar et al. 2019). Semida et al. (2021) also reported that the increase in water stress reduced eggplant yield. This explains that the yield decreases due to an increase in water stress. The results of this research are consistent with the study conducted by Ayas (2017), which found that the yield of eggplant is significantly affected by the irrigation level applied. For example, the studies conducted by Kirda et al. (2004), Topcu et al. (2007), and Kirda et al. (2007) on other vegetables such as tomatoes and peppers, found consistent results with this study. Similarly, cucumbers under deficit irrigation, PRD techniques, and conventional irrigation (Kaman et al. 2022; Kaman et al. 2023a) and also strawberry plants experienced a decrease in yield (Kaman et al. 2023b; Kaman et al. 2023c) due to increased water stress.

In general, these studies also showed a change in yield values as a function of different amounts of irrigation water. The results obtained from this study are similar to the values given in the literature. However, the I_{100}, $FPRD_{100}$ and $FPRD_{80}$ treatments in the first season and the I_{100} and $FPRD_{100}$ treatments in the second season had the highest yield value (Table 3, Table 4). On the other hand, this study did not examine the irrigation levels such as 125% and 150%, and it was found that 80% and 100% irrigation levels gave quite good results. Regression analysis values between the irrigation water and yield of grafted and ungrafted eggplant in both growing seasons were found to be at a fairly good level ($R^2>80$) (Figure 2). However, as an important finding, the regression analysis value of grafting in the second season was found to be at the highest level with $R^2=91$ (Figure 2). The regression analysis between both irrigation water-yield and evapotranspiration-yield revealed an increasing correlation (Figures 2 and 3). In particular, despite the increase in the amount of irrigation water, there was no decrease in yield values. This reveals that the amount of irrigation water was correctly applied under appropriate conditions. In general, the fact that the R^2 values are greater than 0.80 in the regression analysis reveals that irrigation has been managed very well (Figures 2 and 3). It can also be concluded that grafting, together with irrigation management, is very important in eggplant cultivation. Canturk et al. (2023) reported that differences in the amount of water consumption during the cultivation season caused a significant difference in eggplant yield. Many studies have reported that there is a linear relationship between yield and seasonal evapotranspiration (Öktem et al. 2003; Bozkurt Çolak et al. 2018; Karam et al. 2011).

IWUE is an important indicator that shows how efficiently the plant uses the available water to produce a certain yield (Ouma et al. 2024). Similarly, WUE is another important parameter that shows the efficient use of available water. Since plants with water stress fade quicker than the normal conditions, plants under water stress have a higher IWUE (Rodan et al. 2020). In this study, the correlation of irrigation×grafting in the first season for WUE (Table 3) and the irrigation levels with grafting in the second season (Table 4) were found to be statistically very significant ($P<0.01$). In line with these research results, different researchers have reported that the grafting may increase WUE due to a decrease in stoma conductivity and transpiration rate (Khah et al. 2011; Al-Harbi et al. 2018). For IWUE, the irrigation×grafting correlation was found to be important in the first season ($P<0.05$) (Table 3), and grafting was found to be very important in the second season ($P<0.01$) (Table 4). The WUE and IWUE results of this study are generally consistent with the findings of Ouma et al. (2024) Rodan et al. (2020), Darko et al. (2019), Mohawesh (2016) and Wakchaure et al. (2020). In addition, the results of Ayas (2017), Bozkurt Çolak et al. (2017) and Al Ali et al. (2018) regarding IWUE values are similar to those of this research.

4.3. Yield response factor

The yield-response factor is another important parameter indicating a decrease in yield in response to a unit decrease in evapotranspiration. As a result of the regression analysis, the obtained values were found to have changed between 0.68 and 1.87 in the first season and between 0.80 and 2.70 in the second season (Figure 4). A general decrease was experienced in the yield of ungrafted and grafted eggplants in response to the proportional decrease in plant water consumption. However, it could be said that the best results were obtained from the grafted eggplant and the FPRD irrigation.

Canturk et al. (2023) reported that a decrease in evapotranspiration caused a decrease in efficiency. Similarly, Campi et al. (2019) found that deficit irrigation strategies led to a significant reduction in asparagus yield, which was attributed to the development of smaller canopies under water stress conditions. In another study, Abd El-Wahed & Ali (2013) reported that deficit irrigation reduced bean yield to a certain rate. Therefore, previous studies are consistent with the research results of this study.

An important reason why grafted plants perform better than ungrafted plants has been attributed to the deeper and well-developed root system, which can increase the volume of soil that the root system of grafted plants can reach (Ibrahim et al. 2014; López-Marín et al. 2017). Similarly, Consentino et al. (2022) reported that grafted eggplant provided a yield advantage, and this finding is also consistent with that of this study. In line with the results of this research, Sabatino et al. (2018) found that grafted plants consistently produced more fruits per plant than ungrafted ones, and similar findings were found by Sabatino et al. (2016) and Maršič et al. (2014).

4.4. Yield components, biomass and plant height

The results of ANOVA analysis regarding some yield-related parameters showed significant changes at the $P<0.01$ and/or $P<0.05$ level (Tables 5 and 6). It revealed that yield parameters, biomass and plant height were primarily affected by irrigation levels (100%, 80%, 60%, and 40%). A similar result was also observed in the yield, mass, WUE and IWUE values (Tables 3 and 4, Figures 2 and 3). The results of this study were found to be consistent with those of Darko et al. (2019) and Consentino et al. (2022). All parameters were negatively affected by water stress in general. Similar to the results of this research, Ouma et al. (2024) have also reported that deficit irrigation increases eggplant yield. However, the water deficit level mustn't be below 40% for mean fruit weight (g fruit^{-1}).

Gisbert et al. (2011) found that the use of interspecies hybrid rootstock obtained from a fully compatible breed of eggplant with related species could be a valuable approach to improve eggplant production. According to Sabatino et al. (2018) reported that the demand for eggplant grafted seedlings is increasing rapidly, but the yield, obvious quality characteristics and chemical composition of fruits obtained from grafted plants should remain equal or improved compared to ungrafted plants. In addition, Gisbert et al. (2011), Moncada et al. (2013), Maršič et al. (2014) and Sabatino et al. (2016) found that grafting could affect the yield and fruit quality in eggplant. These explanations related to grafting were found to be consistent with the total fruit yield, fruit length, and plant height per plant in Table 6. It is relatively similar to other yield parameters.

Biomass (total leaf+stem) dry weight of the above-ground part of the plant) was generally found to be higher in cultivations where there is no water restriction, and lower in areas where there is water restriction (Tables 5 and 6). Although grafting had no effect, the irrigation×grafting (I×G) correlation with irrigation levels was found to be effective for biomass (Tables 5 and 6). Similar results regarding the biomass were also found in the study conducted by Bozkurt Çolak et al. (2017). In this study, the amount of dry matter was found to increase as the amount of irrigation water applied increased.

In both seasons, the plant size showed a gradual increase in all deficit irrigation levels of ungrafted and grafted eggplant (Figure 5). The plant height was measured as the highest in the grafted eggplant (Tables 5 and 6, and Figure 5) and this is consistent with the findings of Consentino et al. (2022) and Ouma et al. (2024). Grafting had a positive effect on plant height (Tables 5 and 6) and the results are consistent with the results of Miceli et al. (2014).

4.5. SSC, pH and fruit outer color

In the statistical analysis of irrigation levels in both seasons of the study (100%, 80%, 60%, and 40%), grafting and irrigation×grafting (I×G) correlation in the second season, the only change between the pH values was found to be very significant (P<0.01) (Tables 7 and 8). The pH, which measures total acidity or alkalinity, is an important factor in the production of vegetables and fruits as it is related to the fruit quality (Darko et al. 2019). The change between the pH values in the research was found to be similar to that of Ouma et al. (2024).

The change between the SSC values was found to be statistically insignificant and similar results were reported by Miceli et al. (2014), Sabatino et al. (2018) and Consentino et al. (2022).

Color measurements were made as L*, a*, and b* with the Minolta CR400 model color chromometer on eggplant fruits, and the values of C (Chroma) and hº (hue) were calculated using the values of *a and *b (Siomos et al. 2002; Madeira et al. 2003). However, it was seen that grafting in the second season affected only fruit color a* (P<0.05) (Table 8). In other cases, it was found that the color parameters were not significantly affected, and this result is consistent with that of Sabatino et al. (2018).

5. Conclusions

It was found in the study that the method and level of irrigation water applied had a significant effect on ungrafted and grafted eggplant plants. The amount of irrigation water applied in the study was recorded between 148.45 and 365.48 mm, 245.61 and 584.84 mm in the first and second seasons, respectively. Accordingly, statistically significant changes ($p<0.01$ and/or $p<0.05$ significance level) were found in yield, evapotranspiration, water use efficiency, irrigation water use efficiency values. The regression analysis values between irrigation water and yield were determined at a very good level ($0.80<R^2$). In addition, as an important finding, the regression analysis value of grafting was determined at the highest level ($R^2=91$) in the second season. In the first season of the study, the highest yields were statistically determined in FPRD100, I100 and FPRD80 (45.26, 44.01 and 39.26 t ha^{-1}, respectively). Similarly, in the second season, the highest yields were obtained from I100 and FPRD100 with 50.97 and 48.96 t ha^{-1}, respectively, followed by FPRD80 with 48.96 t ha^{-1}.

It has been found when compared in terms of irrigation treatments, that grafted eggplant plants in general had a higher total yield than ungrafted plants. However, as the amount of irrigation water applied decreased, yield has also decreased. Although the different irrigation levels applied to grafted and ungrafted eggplant plants were not statistically significant in the first year, the water use efficiency showed similar reactions in the I_{100}, $FPRD_{100}$, $FPRD_{80}$, and $FPRD_{60}$ treatments in the second year. This reveals the advantages of partial-wetting irrigation compared to conventional irrigation. As a result of the research, the cultivation of grafted eggplant plants is recommended and PRD technique should be used in irrigation.

References

Abd El-Wahed M H & Ali E A (2013). Effect of irrigation systems, amounts of irrigation water and mulching on corn yield, water use efficiency and net profit. Agricultural Water Management 120: 64–71

Al-Hadidi L & Sweity A (2022). Effect of deficit irrigation using treated wastewater on eggplant yields, water productivity, fruit quality and mineral contents. Russian Agricultural Sciences 48(2): 63–73. https://doi.org/10.3103/S1068367422020112

Al Ali M, Gençoğlan C & Gençoğlan S (2018). The effect of irrigation water amount on water-yield relationships of eggplant. Süleyman Demirel Üniversitesi Ziraat Fakültesi Dergisi. 1. Uluslararası Tarımsal Yapılar ve Sulama Kongresi, Special Issue: 385-393

Al-Harbi A R, Al-Omran A M & Alharbi K (2018). Grafting improves cucumber water stress tolerance in Saudi Arabia. *Saudi Journal of Biological Sciences* 25(2): 298–304. https://doi.org/10.1016/j.sjbs.2017.10.025

Anonymous (2000). Long-term climate data for Antalya province. Turkish State Meteorological Service, Antalya.

Anonymous (2022). Ministry of Agriculture and Forestry General Directorate of State Hydraulic Works (DSI). https://cevreselgostergeler.csb.gov.tr/su-kullanimi-i-85738.

Ayas S (2017). The effects of irrigation regimes on the yield and water use of eggplant (Solanum melongena L.). *Soil Water Journal* 6(2): 49-58. https://doi.org/10.21657/topraksu.339835

Bhatnagar V & Poonia R C (2018). Design of prototype model for irrigation based decision support system. *Journal of Informaton and Optmzaton Scences* 39(7): 1607–1612. https://doi.org/ 10.1080/02522667.2018.1507763

Bozkurt Çolak Y, Yazar A & Çolak İ (2017). Effect of different deficit irrigation strategies on subsurface drip irrigated eggplant yields and yield components under Cukurova Condition. Alatarım 16(1): 1-10

Bozkurt Çolak Y, Yazar A, Gönen E & Eroğlu E Ç (2018). Yield and quality response of surface and subsurface drip-irrigated eggplant and comparison of net returns. Agricultural Water Management 206: 165–175. https://doi.org/10.1016/j.agwat.2018.05.010

Bozkurt Çolak Y (2019). Effects of irrigation frequency and level on yield and stomatal resistance of eggplant (Solanum melongena L.) grown in open field irrigated with surface and subsurface drip methods. Applied Ecology and Environmental Research 17(6): 15585–15604. DOI: http://dx.doi.org/10.15666/aeer/1706_1558515604

Cantürk A, Cemek B, Taşan M & Taşan S (2023). Effect of deficit irrigation on yield, water productivity, energy indices and economic productivity in eggplant cultivation. Gesunde Pflanzen 75: 1579-1589. https://doi.org/10.1007/s10343-022-00814-z

Campi P, Mastrorilli M, Stellacci A M, Modugno F & Palumbo A D (2019). Increasing the effective use of water in green aspara gus through deficit irrigation strategies. Agricultural Water Management 217: 119–130

Consentino B B, Rouphael Y, Ntatsi G, De Pasquale C, Iapichino G, D'Anna F, La Bella S & Sabatino L (2022). Agronomic performance and fruit quality in greenhouse grown eggplant are interactively modulated by iodine dosage and grafting. Scientia Horticulturae 295: 110891. https://doi.org/10.1016/j.scienta.2022.110891

Darko R O, Yuan S, Kumi F & Quaye F (2019). Effect of deficit irrigation on yield and quality of eggplant. International Journal of Environment, Agriculture and Biotechnology 4(5): 1325–1333. https://dx.doi.org/10.22161/ijeab.45.5

Diaz-Perez J C & Eaton T E (2015). Eggplant (Solanum melongena L.) plant growth and fruit yield as affected by drip irrigation rate. HortScience 50(11): 1709–1714. https://doi.org/10.21273/HORTSCI.50.11.1709

Doorenbos J & Kassam A H (1979). Yield response to water. FAO Irrigation and Drainage Paper No, 33, Rome, pp 193.

Dry P R & Loveys B R (1998). Factors influencing grapevine vigour and the potential for control with partial rootzone drying. Australian Journal of Grape and Wine Research 4: 140–148. https://doi.org/10.1111/j.1755-0238.1998.tb00143.x

Dry P, Loveys B, Botting D & Düring H (1995). Effects of partial root-zone drying on grapevine vigour, yield, composition of fruit and use of water. In: Proceedings of the ninth Australian Wine Industry Technical Conference pp. 128–131

Ertek A, Şensoy S, Küçükyumuk C & Gedik İ (2006). Determination of plant-pan coefficients for field-grown eggplant (Solanum melongena L.) using class A pan evaporation values. Agricultural Water Management 85(1–2): 58–66. https://doi.org/10.1016/ j.agwat.2006.03.013

FAO (2024). Crops and livestock products. https://www.fao.org/faostat/en/#data/QCL

Gisbert C, Prohens J, Raig´on M D, Stommel J R & Nuez F (2011). Eggplant relatives as sources of variation for developing new rootstocks: effects of grafting on eggplant yield and fruit apparent quality and composition. Scientia Horticulturae 128: 14–22. doi:10.1016/j.scienta.2010.12.007

Howladar S M (2018). Potassium humate improves physio-biochemical attributes, defense systems activities and water-use efficiencies of eggplant under partial root-zone drying. Scientia Horticulturae 240: 179–185. https://doi.org/10.1016/j.scienta.2018.06.020

Ibrahim A, Wahb-Allah M, Abdel-Razzak H & Alsadon A (2014). Growth, yield, quality and water use efficiency of grafted tomato plants grown in greenhouse under dif ferent irrigation levels. *Life Science Journal* 11(2): 118–126. doi:10.7537/marslsj110214.17

Incrocci L, Thompson R B, Fernandez-Fernandez M D, De Pascale S, Pardossi A, Stanghellini C, Rouphael Y & Gallardo M (2020). Irrigation management of European greenhouse vegetable crops. Agricultural Water Management 242: 106393. https://doi.org/10.1016/j.agwat.2020.106393

Kaman H, Özbek Ö & Polat E (2022). Response of greenhouse grown cucumber to partial root zone drying and conventional deficit irrigation. KSU J. Agric Nat. 25(2): 337-347. https://doi.org/10.18016/ ksutarimdoga.vi. 883294

Kaman H, Özbek Ö & Polat E (2023a). Determination of the effect of different irrigation regimes on some quality properties of cucumber. Journal of Tekirdag Agricultural Faculty 20(2): 318-333. DOI: 10.33462/jotaf.1093951

Kaman H, Gübbük H, Tezcan A, Can M & Özbek Ö (2023b). Water-yield relationship of greenhouse-grown strawberry under limited irrigation. Notulae Botanicae Horti Agrobotanici Cluj-Napoca 51(2): 13235. https://doi.org/10.15835/nbha51213235

Kaman H, Gübbük H, Tezcan A, Can M & Özbek Ö (2023c). Yield and quality of strawberry under deficit irrigation and fixed partial root drying regimes. *Pakistan Journal of Agricultural Sciences* 60(4): 555-563. DOI:10.21162/PAKJAS/23.135

Kang S, Hu X, Goodwin I & Jerie P (2002). Soil water distribution, water use, and yield response to partial root zone drying under a shallow groundwater table condition in a pear orchard. Scientia Horticulturae 92(3-4): 277-291. https://doi.org/10.1016/S0304-4238(01)00300-4

Kang S, Liang Z, Pan Y, Shi P & Zhang J (2000). Alternate furrow irrigation for maize production in an arid area. Agricultural Water Management 45(3): 267-274. https://doi.org/10.1016/S0378-3774(00)00072-X

Kang S, Zhang L, Xiaotao H, Li Z & Jerie P (2001). An improved water use efficiency for hot pepper grown under controlled alternate drip irrigation on partial roots. Scientia Horticulturae 89(4): 257–267. https://doi.org/10.1016/S0304-4238(00)00245-4

Karam F, Saliba R, Skaf S, Breidy J, Rouphael Y & Balendonck J (2011). Yield and water use of eggplants (Solanum melongena L.) under full and deficit irrigation regimes. Agricultural Water Management 98(8): 1307-1316. https://doi.org/10.1016/j.agwat.2011.03.012

Khah E M, Katsoulas N, Tchamitchain M & Kittas C (2011). Effect of grafting on eggplant leaf gas exchanges under Mediterranean greenhouse conditions. *International Journal of Plant Production* 5(2): 121–134. https://doi.org/10.22069/ijpp.2012.726

Kirda C, Cetin M, Dasgan Y, Topcu S, Kaman H, Ekici B, Derici M R & Ozguven A I (2004). Yield response of greenhouse grown tomato to partial root drying and conventional deficit irrigation. Agricultural Water Management 69: 191–201. doi:10.1016/j.agwat.2004.04.008

Kirda C, Topcu S, Cetin M, Dasgan H Y, Kaman H, Topaloglu F, Derici M R & Ekici B (2007). Prospects of partial root zone irrigation for increasing irrigation water use efficiency of major crops in the Mediterranean region. Annals of Applied Biology 150: 281-291. doi:10.1111/j.1744-7348.2007.00141.x

Kumar R, Berwal M K & Saroj P L (2019). Morphological, physiological, biochemical and molecular facet of drought stress in horticultural crops. *International Journal of Bio-resource and Stress Management* 10(5): 545-560. DOI: HTTPS://DOI.ORG/10.23910/IJBSM/2019.10.5.2031

López-Marín J, Gálvez A, del Amor F M, Albacete A, Fernández J A, Egea-Gilabert C & Pérez-Alfocea F (2017). Selecting vegetative/generative/dwarfing rootstocks for improving fruit yield and quality in water stressed sweet peppers. Scientia Horticulturae 214: 9–17. https://doi.org/10.1016/j.scienta.2016.11.012

Machado R M A & Serralheiro R P (2017). Soil salinity: effect on vegetable crop growth. management practices to prevent and mitigate soil salinization. Horticulturae 3(2): 30. https://doi.org/10.3390/horticulturae3020030

Madeira A C, Ferreira A, de Varennes A & Vieira M I (2003). SPAD meter versus tristimulus colorimeter to estimate chlorophyll content and leaf color in sweet pepper. Communications in Soil Science and Plant Analysis 34(Nos. 17 &18): 2461-2470. https://doi.org/10.1081/CSS-120024779

Maršič N K, Mikulič-Petkovšek M & Štampar F (2014). Grafting influences phenolic profile and carpometric traits of fruits of greenhouse grown eggplant (Solanum melongena L.). *Journal of Agricultural and Food Chemistry* 62(43): 10504–10514. https://doi.org/10.1021/jf503338m

Meena R P, Karnam V, Sujatha H T, Tripathi S C & Singh G (2024). Practical approaches to enhance water productivity at the farm level in Asia: A review. Irrigation and Drainage 73(2): 770–793. https://doi.org/10.1002/ird.2891

Mekonnen M M & Gerbens-Leenes W (2020). The water footprint of global food production. Water 12: 2696. https://doi.org/10.3390/w12102696

Miceli A, Sabatino L, Moncada A, Vetrano F & D'Anna F (2014). Nursery and field evaluation of eggplant grafted onto unrooted cuttings of Solanum torvum Sw. Scientia Horticulturae 178: 203–210. http://dx.doi.org/10.1016/j.scienta.2014.08.025

Mohawesh O (2016). Utilizing deficit irrigation to enhance growth performance and water-use efficiency of eggplant in arid environments. Journal of Agricultural Science and Technology 18(1): 265–276.

Moncada A, Miceli A, Vetrano F, Mineo V, Planeta D & D'Anna F (2013). Effect of grafting on yield and quality of eggplant (Solanum melongena L.). Scientia Horticulturae 149: 108–114. https://doi.org/10.1016/j.scienta.2012.06.015

Mokabel S, Olama Z, Ali S & El-Dakak R (2022). The role of plant growth promoting rhizosphere microbiome as alternative biofertilizer in boosting solanum melongena l. adaptation to salinity stress. Plants 11(5): 659. https://doi.org/10.3390/plants11050659

Okiror P, Lejju J B, Bahati J, Rugunda G K, Sebuuwufu C I, Mulindwa P & Ocan J J (2017). Suitability of Kabanyolo soils for fruit and vegetable production. *Open Journal of Soil Science* 7(2): 19–33. https://doi.org/10.4236/ojss.2017.72002

Ouma G, Wanyama J, Kabenge I, Jjagwe J, Diana M & Muyonga J (2024). Assessing the effect of deficit drip irrigation regimes on crop performance of eggplant. Scientia Horticulturae 325: 112648. https://doi.org/10.1016/j.scienta.2023.112648

Öktem A, Simsek M & Oktem A G (2003). Deficit irrigation effects on sweet corn (Zea mays saccharata Sturt) with drip irrigation system in a semi-arid region: I. Water-yield relationship. Agricultural Water Management 61(1): 63–74.

Rodan M A, Hassandokht M R, Sadeghzadeh-Ahari D & Mousavi A (2020). Mitigation of drought stress in eggplant by date straw and plastic mulches. *Journal of the Saudi Society of Agricultural Sciences* 19(7): 492–498. https://doi.org/10.1016/j.jssas.2020.09.006

Sabatino L, Iapichino G, Maggio A, D'anna E, Bruno M & D'Anna F (2016). Grafting affects yield and phenolic profile of Solanum melongena L. Landraces. Journal of Integrative Agriculture 15(5): 1017–1024. https://doi.org/10.1016/S2095-3119(15)61323-5

Sabatino L, Iapichino G, D'Anna F, Palazzolo E, Mennella G & Rotino G L (2018). Hybrids and allied species as potential rootstocks for eggplant: Effect of grafting on vigour, yield and overall fruit quality traits. Scientia Horticulturae 228: 81–90. http://dx.doi.org/10.1016/j.scienta.2017.10.020

Sarı M, Aksoy T, Köseoğlu T, Kaplan M, Kılıç Ş & Pilanalı N (1993). Akdeniz Üniversitesi yerleşim alanının detaylı toprak etüdü ve ideal arazi kullanım planlaması. (in Turkish) Akdeniz Üniversitesi Yayınları, Antalya, 145 ss.

Semida W, Abdelkhalik A, Mohamed G, El-Mageed T, El-Mageed S, Rady M & Ali E (2021). Foliar application of zinc oxide nanoparticles promotes drought stress tolerance in eggplant (Solanum melongena L.). Plants 10(2): 421. https://doi.org/ 10.3390/plants10020421

Sikka A K, Islam A & Rao K V (2018). Climate-smart land and water management for sustainable agriculture. Irrigation and Drainage 67(1): 72-81. https://doi.org/10.1002/ird.2162

Singh G (2016). Climate change and food security in India: Challenges and opportunities. Irrigation and Drainage 65): 5–10. https://doi.org/10.1002/ird.2038

Siomos A S, Papadopoulou P P, Niklis N D & Dogras C C (2002). Quality of Romaine and leaf lettuce at harvest and during storage. ISHS Acta Horticulturae 579: II Balkan Symposium on Vegetables and Potatoes, Acta Horticulturae 579: 641-646. DOI:10.17660/ActaHortic.2002.579.113

Sonawane A V & Shrivastava P K (2022). Partial root zone drying method of irrigation: A review. Irrigation and Drainage 71(3): 574–588. https:// doi.org/10.1002/ird.2686

Stewart J I, Cuenca R H, Pruitt W O, Hagan R M & Tosso J (1977). Determination and utilization of water production functions for principal California crops. W-67 CA Contributing Project Report, University of California, Davis, USA.

Topcu S, Kirda C, Dasgan Y, Kaman H, Cetin M, Yazici A & Bacon M A (2007). Yield response and N-fertiliser recovery of tomato grown under deficit irrigation. Europ. J. Agronomy 26: 64–70. doi:10.1016/j.eja.2006.08.004

TUIK (2024). Plant Production Statistics. Turkish Statistical Institute, https://data.tuik.gov.tr/Bulten/Index?p=Bitkisel-Uretim-Istatistikleri-2023-49535.

Ungureanu N, Vl˘aduț V & Voicu G (2020). Water scarcity and wastewater reuse in crop irrigation. Sustainability 12: 9055. https://doi.org/10.3390/su12219055

Wakchaure G C, Minhas P S, Meena K K, Kumar S & Rane J (2020). Effect of plant growth regulators and deficit irrigation on canopy traits, yield, water productivity and fruit quality of eggplant (Solanum melongena L.) grown in the water scarce environment. *Journal of Environmental Management* 262: 110320. https://doi.org/10.1016/j.jenvman.2020.110320

Wang B, Bao R, Yan H, Zheng H, Wu J, Zhang C & Wang G (2024). Study of evapotranspiration and crop coefficients for eggplant in a Venlo-type greenhouse in South China. Irrigation and Drainage 1–13. https://doi.org/10.1002/ird.3025

Zafar U, Arshad M, Masud Cheema M J & Ahmad R (2020). Sensor based drip irrigation to enhance crop yield and water productivity in semi-arid climatic region of Pakistan. *Pakistan Journal of Agricultural Sciences* 57(5): 1293–1301. https://doi.org/10.21162/ PAKJAS/20.83

Journal of Agricultural Sciences
(Tarim Bilimleri Dergisi)

J Agr Sci-Tarim Bili
e-ISSN: 2148-9297
jas.ankara.edu.tr

JAS

Use of Aquatic Plants (*Azolla Caroliniana* and *Lemna Spp*) as a Feed Source in Silkworm Culture

Süleyman Bekcan[a*], Hicran Yavuzcan[a], Hasan Hüseyin Atar[a]

[a]*Ankara University, Faculty of Agriculture, Department of Fisheries Engineering, Ankara, TÜRKIYE*

ARTICLE INFO
Research Article
Corresponding Author: Süleyman Bekcan, E-mail: bekcan@agri.ankara.edu.tr
Received: 15 October 2024 / Revised: 01 October 2024 / Accepted: 18 December 2024 / Online: 25 March 2025

Cite this article
Bekcan S, Yavuzcan H, Atar H H (2025). Use of Aquatic Plants (*Azolla Caroliniana* and *Lemna Spp*) as a Feed Source in Silkworm Culture. *Journal of Agricultural Sciences (Tarim Bilimleri Dergisi),* 31(2):532-537. DOI: 10.15832/ankutbd.1568035

ABSTRACT
This article focuses on the effects of the use of aquatic plants on the growth parameters of silkworm larvae in their artificial feeding. Due to the difficulty of obtaining mulberry leaves, different feeds and substances to be substituted for this food source were tested in various researches. In this study, the silkworm larvae were fed with the diet containing different proportion of azolla (*Azolla caroliniana)* meal and duckweed (*Lemna spp.)* meal found abundant and easily available compared to mulberry leaves in nature. The study aims at defining an appropriate combination of mulberry leaf meal, azolla meal and duckweed meal and the effects of these artificial feeds on the growth rate of silkworm larvae. Consequently, it was determined that 25%, 50%, 75% substitution of azolla meal and duckweed meal up to the 3rd instar (12th day) did not affect the growth and survival rates of silkworm larvae.

Keywords: Azolla meal, Duckweed meal, Mulberry leaves meal, Artificial feeding, Silkworm

1. Introduction

Aquatic plants have many potential benefit areas such as cheap food sources for human and animals and fertilizer due to their high nutritive value and short-term proliferation. The water fern azolla, in symbiosis with blue-green algae is remarkable with its easy cultivation, high productivity and nutrient-rich value (Singh & Subudhi 1978). The growth rate of different azolla species were researched in different environments and doubling time was observed as 3-7 days (Tran & Dao 1973; Talley et al. 1977). Azolla has been reported to contain 25-35% crude protein, 10-15% mineral, amino acids, 14.3% crude fibre (FAO 1989; Kathirvelan et al. 2015; Ara et al. 2015) and also vitamins (vitamin-A, vitamin B12, ß-Karoten), minerals, probiotics and biopolymers (Kamalasanana Pillai et al. 2005; Katayama et al. 2008; Kathirvelan et al. 2015). In addition, it has been shown that azolla in dried and fresh form is used as feed for fish (Gokcinar & Bekcan 2015), pork, chicken, duck, cattle and food source for human (FAO 1989; Indira et al. 2009; Leterme et al. 2010; Gauri-Mahadevappa et al. 2012; Kathirvelan et al. 2015; Rana et al. 2017).

Similar aquatic plant, duckweed includes up to 43% protein, 5% lipid, small amount of fibre and high amount of easily digestible dry matter (Leng et al. 1995; Saha et al. 1999). Duckweed as a natural protein source has a valuable amino acid profile similar to animal protein (Hillman & Culley 1978). It has potential using as a supplementary feed source in feeding of livestock, poultry and fish.

Another herbal product, mulberry leaf is the most important nutritional source in silkworm rearing. In last years, poor environmental conditions and the decrease of mulberry tree cultivation areas have negatively affected rearing of silkworm which is valuable product. These challenges in feeding silkworm lead to do further research on alternative nutrient sources. Due to the difficulty of finding mulberry leaves in the desired period in feeding silkworm, the researches have been recently concentrated on substituting easily available matters such as bovine milk, hen's eggs (Helaly 2018), royal jelly (Nguku et al. 2007) soybean, mushroom (Mahmoud 2013), soybean meal, corn meal (Pallavi et al. 2011) and Spirulina algae powder (Sahay et al. 2011) for mulberry leaves. Feeding materials have determinative effects on not only the developments of silkworm larvae but also the quality and productivity of cocoons in positive way. Besides the quality of cocoons and silk, these improvements reflect on by-products such as silkworm pupae (Ravikumar 1988; Seidavi et al. 2005). Indeed, silkworm pupae is also used as a valuable nutrient source for human (Yang et al. 2010) and animal such as fish (Radha & Geetha 2018) and poultry (Ijaiya & Eko 2009).

The aim of this research was to define an appropriate combination of the artificial feeds used in the trial and to determine their effects on the growth rate of silkworm larvae. For this reason, silkworm larvae were fed with the meals of mulberry leaf, azolla, duckweed and their different combinations. These mentioned aquatic plants are found abundant and easily available compare to mulberry leaf in nature. Thus, it was possible to conduct the research without considering the period of silkworm rearing dependent on mulberry leaves growing season either the plants growing season.

2. Material and Methods

A wooden frame of the size of 2 m x 2m x 0.2 m was covered by a tarpaulin. By preparing a mixture made of 20 kg flower soil, 3 kg cow dung and 40 g super phosphate fertilizer, this slurry was poured on the tarpaulin. Then water was poured into the mixture until total height reached to 20 cm. Azolla was inoculated in the environment. Growing azolla was harvested, dried in the shade and turned into meal. The same processes were also made for obtaining duckweed. The mulberry leaves collected in the season were dried in the shade and turned into meal. All feeds prepared in this way, except vitamins autoclaved at 121 °C for 15 minutes under 15 lbs pressure. The substitution rates of mulberry leaf and azolla meal in the artificial diet were determined to range from 0 to 20, 40, 60, and 80 g, corresponding to 0%, 25%, 50%, 75%, and 100%. The same replacement rates were also applied to mulberry leaf and duckweed meal. Nutrient elements were prepared as paste in the ratio of 1 g of dry matter and 2.6 g of pure water, then stored in glass jars in refrigerator at -18 °C (Tables 1 and 2). The pastes were brought to room temperature before given to the larvae and they renewed every 12 hours. The trial was conducted in a rearing cupboard providing the control of lightening, temperature and humidity. Temperature values were checked three times per day (0.1 sensitivity). Four replicates of 10 larvae per plastic box were established for each treatment. Hatching larvae were randomly selected, transferred into experiment medium and started to feed with artificial diet at the same time, namely 12 hours later (Bhattacharyya et al. 2017). Experiment period was edited as 47 days.

Considering that the larvae could be damaged, weighing was started from the third instar, namely 12th day (0.001 sensitivity). The vapor machine connected to the timer was used for humidity adjustment (Table 3). Light/darkness ratio was set 16hr: 8hr with a timer (Khairmode et al. 2019).

Data obtained were analyzed by analysis of variance (ANOVA) and means were grouped by Duncan's test ($P<0.05$), All percentage and ratio data were transformed to arcsin values prior to analysis (Zar 1984).

Table 1- Composition of the artificial diet ingredients quantities/100 g dry weight (prepared with azolla)

Ingredients	***K***	***A1***	***A2***	***A3***	***A4***
Mulberry leaf meal (g)	80	60	40	20	-
Azolla meal (g)	-	20	40	60	80
Citric Acid (g)	4	4	4	4	4
Ascorbic Acid (g)	2	2	2	2	2
Vitamin Mixture (g)[1]	3	3	3	3	3
Sorbic Acid (mg)	200	200	200	200	200
Propionic Acid (mg)	690	690	690	690	690
Chloramphenicol (mg)	10	10	10	10	10
Agar (g)	7.1	7.1	7.1	7.1	7.1
Sucrose (g)	3.0	3.0	3	3	3

[1]Supradyn: Vitamin A 3333 I.U., vitamin B1 20 mg, vitamin B 25 mg, calcium D-pantothenate 11.6 mg, vitamin B6 10 mg, vitamin B12 5 mcg, vitamin C 150 mg, vitamin D3 500 I.U., vitamin E 10 I.U., D-biotin (vitamin H) 250 mcg, Nicotinamide 50 mg, Folic acid 1 mg; Iron 10 mg, Phosphorus 23.8 mg, Calcium 51.3 mg, Magnesium 21.2 mg, Manganese 0.5 mg, copper 1 mg, Zinc 0.5 mg, Molybdenum 0.1 mg

[2] The pastes were prepared in ratio of 1 g of dry matter and 2.6 g of pure water

Table 2- Composition of the artificial diet ingredients quantities/100 g dry weight (prepared with duckweet)

Ingredients	*K*	*L1*	*L2*	*L3*	*L4*
Mulberry leaf meal (g)	80	60	40	20	-
Duckweet meal (g)	-	20	40	60	80
Citric Acid (g)	4	4	4	4	4
Ascorbic Acid (g)	2	2	2	2	2
Vitamin Mixture (g)[1]	3	3	3	3	3
Sorbic Acid (mg)	200	200	200	200	200
Propionic Acid (mg)	690	690	690	690	690
Chloramphenicol (mg)	10	10	10	10	1
Agar (g)	7.1	7.1	7.1	7.1	7.1
Sucrose (g)	3	3	3	3	3

[1] Supradyn: Vitamin A 3333 I.U., vitamin B1 20 mg, vitamin B 25 mg, calcium D-pantothenate 11.6 mg, vitamin B6 10 mg, vitamin B12 5 mcg, vitamin C 150 mg, vitamin D3 500 I.U., vitamin E 10 I.U., D-biotin (vitamin H) 250 mcg, Nicotinamide 50 mg, Folic acid 1 mg; Iron 10 mg, Phosphorus 23.8 mg, Calcium 51.3 mg, Magnesium 21.2 mg, Manganese 0.5 mg, copper 1 mg, Zinc 0.5 mg, Molybdenum 0.1 mg

[2] The pastes were prepared in ratio of 1 g of dry matter and 2.6 g of pure water

Table 3- The room temperature and humidity during the experimental period

Treatments	*Temperature*	*Humidity*
1st instar	25.06±0.203	82.1±2.98
2nd instar	25.39±0.171	81.4±2.96
3rd instar 12th day	25.56±0.146	79.5±5.40
4th instar 18th day	25.51±0.113	81.36±2.53
5th instar 28th day	25.24±0.094	77.13±2.25
32nd day	25.44±0.108	78.53±1.73
47th day	25.19±0.160	77.00±2.02

3. Results

In the research, hatching larvae were put into feeding medium in 12 hours and feeding process started. All larvae in groups A4 and L4 died before third instar. By considering that the larvae would be sensitive, they were not weighed until third instar (12th day). At the third instar, considering all groups, there was no significant difference in weight gain from each other ($P>0.05$). At the fourth instar, while there was significant difference statistically in weight gain between group K and other groups ($P<0.05$), there was not found significant difference between the groups A1, A2, A3, L1 ($P>0.05$). Nevertheless, all larvae in groups L2 and L3 died. At the fifth instar, on 28th day and 32nd day, while there was a large difference in weight gain between group K and other groups A1, A2 and L1 ($P<0.05$), all larvae in groups A3, L2 and L3 died. Most of the larvae in group K started to cocoon on 34th day (Figure 1).

The groups of A1 and L1 continued to feed until 37th and 43rd day. The mean weights of the individuals in A1 and L1 reached 0.663 g. and 0.378 g. on 43rd day in respectively. Nevertheless, these individuals died after a few days (Table 4).

By the third instar (12th day), it is noteworthy that no deaths occurred across all groups, and the weight gains, particularly in group K (control) and other groups, did not show statistically significant differences (Table 5).

The weights of cocoons and mortality rates of silkworm larvae in control group (K) are demonstrated in (Table 6).

Figure 1- Silkworm larvae and silk moth periods during trial (a. silkworm eggs used in the experiment b. c. d. larvae aged between 12 and 28 days e. larvae on the 32nd day f. g. cocoon weaving stage, h. emergence from the cocoon)

Table 4- Means weight of larvae during the experimental period

	Weight of larvae (mg)					
Treat.	***3rd instar 12th day***	***4th instar 18th day***	***5th instar 28th day***	***32nd day***	***37th day***	***43rd day***
K	17.43±0.836[a]	131.73±7.08[a]	876.37±57.6[a]	1598.4±103[a]	-	-
A1	19.95±0.623[a]	29.63±1.73[b]	116.20±8.97[b]	185.3±15.8[b]	411.87±43.6	662.77±47.6
A2	19.10±0.812[a]	15.71±1.33[b]	45.50±1.50[b]	55.5±3.50[c]	-	-
A3	17.25±0.735[a]	11.56±0.584[b]	-	-	-	-
A4	-	-	-	-	-	-
L1	15.80±0.626[a]	21.14±2.24[b]	60.63±6.75[b]	133.3±23.6[c]	187.33±24.6	378.50±76.2
L2	13.20±0.750[a]	-	-	-	-	-
L3	12.35±0.990[a]	-	-	-	-	-
L4	-	-	-	-	-	-
F	13.45	153.37	71.30	68.87	9.96	10.67
P	0.0001	0.0001	0.0001	0.0001	0.003	0.002

Means with different superscripts (a, b and c) are significantly different (Duncan's multiple range test (P<0.05)). The F and P values were obtained from the analysis of variance (ANOVA)

Table 5- The mortality rates during the experimental period

Treatments	*Mortality %*					
	3rd instar 12th day	*4th instar 18th day*	*5th instar 28th day*	*32nd day*	*37th day*	*43rd day*
K	0.0	0.0	0.0	0.0	-	-
A1	0.0	12.087±3.66	29.888±1.92	29.888±1.92	29.888±1.92	36.002±3.96
A2	0.0	33.055±2.59	77.913±3.66	77.913±3.66	100	-
A3	0.0	47.884±1.67	100	-	-	-
A4	100	-	-	-	-	-
L1	0.0	32.898±3.66	50.832±2.41	56.945±2.59	56.945±2.59	56.945±2.59
L2	0.0	100	-	-	-	-
L3	0.0	100	-	-	-	-
L4	100	-	-	-	-	-
F		23.88	75.93	73.05	70.57	19.60
P		0.0001	0.0001	0.0001	0.0001	0.004

All percentage and ratio data were transformed to arcsin values prior to analysis. In respect of replicates, values 0and 100 were calculated as 1 and 99. The F and P values were obtained from the analysis of variance (ANOVA)

Table 6- The weights of cocoons and mortality rates during the experimental period*

Treatments	*Weight of cocoon (mg)*	*Min*	*Max*	*Mortality %*
K	971.1±17.0	821.0	1084.0	39.17±2.41
A1	-	-	-	100
A2	-	-	-	100
A3	-	-	-	100
A4	-	-	-	100
L1	-	-	-	100
L2	-	-	-	100
L3	-	-	-	100
L4	-	-	-	100

*: Cocoons were weighed on the 47th day

4. Conclusions

In the research, the substitution rates of mulberry leaf and Azolla meal in the artificial diet ranged from 0 to 20, 40, 60, and 80 g, corresponding to 0%, 25%, 50%, 75%, and 100% of the mulberry leaf meal for the four groups (A1, A2, A3, A4). The same substitution rates were also applied to mulberry leaf and duckweed meal for the four groups (L1, L2, L3, L4). Then it was tried to examine the reactions of silkworm larvae to these artificial feeds. All larvae in group A4 fed with 100% azolla meal and group L4 fed with 100% duckweed died before third instar. Up to third instar in all groups except A4 and L4, the fact that the mortality rates are 0% and weight gains are not significantly difference show that there will be a potential of the substitution of aquatic plants for mulberry leaf in early stages of rearing silkworm larvae. After third instar in all groups except control group, the decreases in survival rates and in mean weight gains and after fifth instar not completing the cocooning process point out that even 25% substitution of azolla meal and duckweed meal for mulberry leaf meal is not appropriate. Therefore, it can be suggested doing detailed research on lower substitution than 25%.

On the other hand, feeding with this kind of diets makes it possible to cultivate silkworm larvae all year round independent of the period of harvesting mulberry leaves, provided that appropriate conditions are met. Besides, the durability of substitute materials provides a great advantage compared to mulberry leaf. On the 32nd day, statistically significant difference between groups A1 and L1 means that azolla meal is more advantageous than duckweed meal. However, since the structure of the diets will affect the quality of cocoon and nutritional value of pupae, further researches are necessary. Additionally, it is also suggested further researches to determine the reasons for shortening life span of larvae as the amount of azolla and duckweed meal increases in diet and to detect whether or not completing the cocooning process by feeding larvae only mulberry leaf meal after 12th day.

Acknowledgements

The authors would like to express their gratitude to Kozabirlik Cooperative for assistance for the supply of silkworm eggs.

References

Ara S, Adil S, Banday M T & Khan M A (2015). Feeding Potential of Aquatic Fern-Azolla in Broiler Chicken Ration. *J. Poult. Sci. Technol* 3(1): 15-19. Corpus ID: 55082440.

Bhattacharyya P, Jha S, Ghosh A & Mandal P (2017). Effect of artificial diet components with antioxidant activity on mulberry leaf dependent silkworm rearing system. *Harvest* 2: 31-48

FAO (1989). Azolla and its multiple uses with emphasis on Africa, 52 pp

Gauri-Mahadevappa D, Sanganal-Jagadeesh S, Gopinath C R & Kalibavi C M (2012). Importance of azolla as a sustainable feed for livestock and poultry - A review. *Agricultural Reviews* 33: 93-103. www.arccjournals.com / indianjournals.com. Corpus ID: 82198573.

Gokcinar N C & Bekcan S (2015). The Effects of Partially Replacing Fishmeal with azolla (*Azolla* Sp.) on Growth Parameters of Shabbout Fish (*Tor grypus* H. 1843). *Journal of Applied Biological Sciences* 9(1): 43-46, 2015 ISSN: 1307-1130, E-ISSN: 2146-0108, www.nobel.gen.tr

Helaly W M M Y (2018). Evaluation of two food additives on *Bombyx mori* L. Characters. *Journal of Entomology and Zoology Studied*. 6(2): 3119-3123. E-ISSN: 2320-7078 P-ISSN: 2349-6800.

Hillman W S & Culley D D (1978). The uses of duckweed. American Scientist, 66:442-451. This content downloaded from 193.255.222.254 on Thu, 22 Feb 2024 10:31:15 + 00:00 All use subject to https://about.jstor.org/terms

Ijaiya A T & Eko E O (2009). Effect of replacing dietary fishmeal with silkworm (*Anapheefracta*) caterpillar meal on growth digestibility and economics production of starter broiler chicken. *Pakistan J. Nutr*., 8: 845-849. https://doi.org/10.3923/pjn.2009.845.849

Indira D, Rao K S, Suresh J, Naidu K V & Ravi A (2009). Azolla (*Azolla pinnata*) as feed supplement in buffalo calves on growth performance. *Indian Journal of Animal Nutrition* 26: 345-348. Corpus ID: 85714327

Kamalasanana Pillai P, Premalatha S & Rajamony S (2005). Azolla: a sustainable feed for livestock. Leisa Magazine, 21 (3) September, pp. 26-27. The full article was published in LEISA India, Volume 4 number 1, March 2002. It is available on the website www.leisa.info.

Katayama N, Masamichi Y, Yoshiro K, Chung C L, Watanabe I & Hidenori W (2008). Space Ag. task force-azolla as a component of the space diet during habitation on Mars, *Acta Astronautica*. 63: 1093-1099. doi:10.1016/j.actaastro.2008.01.023

Kathirvelan C, Banupriya S & Purushothaman M R (2015). Azolla- an alternate and sustainable feed for livestock. *Int. J. Sci. Environ. Technol*., 4(4): 1153-1157. ISSN 2278-3687 (O) 2277-663X (P). Published Aug 2, 2015 www.ijset.net

Khairmode P V, Shewale V S, Lawand S T & Tare V S (2019). Photoperiod induced alterations in growth pattern of silkwormScanner. International Conference on Advences in Pure and Applied Sciences ICAPAS. https://www.researchgate.net/publication/333901012.

Leng R A, Stambolie J H & Bell R (1995). Duckweed – a potential high-protein feed resource for domestic animals and fish. Livestock Research for Rural Development 7(1): http://www.lrrd.org/lrrd7/1/3.htm.

Leterme P, Londoño A M, Muñoz J E, Súarez J, Bedoya C A, Souffrant W B & Buldgen A (2010). Nutritional value of aquatic ferns (*Azolla filiculoides Lam.* and *Salvinia molesta* Mitchell) in pigs. *Animal Feed Science and Technology*, 149(1-2): 135-148. doi:10.1016/j.anifeedsci.2008.04.013

Mahmoud M M (2013). Effect of Various Kinds of Dietary Proteins in Semi – Artificial Diets on the Mulberry Silkworm Bombyx mori L. *Egypt. Acad. J. Biolog. Sci*., 6(1): 21-26. ISSN: 1687–8809 DOI:10.21608/eajbsa.2013.13815

Nguku E K, Muli E M & Raina S K (2007). Larvae, cocoon and post-cocoon characteristics of Bombyx mori L. (lepidoptera:bombycidae) fed on mulberry leaves fortified with Kenyan royal jelly. In J. Appl. Sci. Environ. Manage. 11(4): 85-89. JASEM ISSN 1119-8362 Full-text Available Online at www.bioline.org.br/ja.

Pallavi K, Muthuswami M, Bhaskar R N & Naveen V (2011). Role of Food Additives on young age Silkworm (Bombyx mori L.) Rearing. *Int. J. Pure Appl. Sci. Technol.* 7(2): 132-140. ISSN 2229 - 6107 Corpus ID: 18768828

Radha S & Geetha B (2018). Replacement of Fish Meal with Supplementatıon of Silkworm (Bombyx Morı) Pupae Meal On Growth In Common Carp. *Journal of Emerging Technologies and Innovative Research (JETIR*) 5(6): 284-288, www.jetir.org (ISSN-2349-5162)

Rana D, Katoch S, Mane B G, Rani D & Sankhyan V (2017). Biological Evaluation of Azolla in Ration of Commercial Chicken Broiler *Journal of Animal Research* 7(3): 601-607. DOI: 10.5958/2277-940X.2017.00091.2

Ravikumar C (1988). Western ghat as a bivoltine region prospects, challenges and strategies for its development. Indian Silk, 26 (9):39-54

Saha J K, Rahmatullah S M & Mazid M A (1999). Optimization of stocking density of duckweed, *Wolffia arhiza* (Linn.) and *Lemna* sp. *Bangldesh J. Fisheries Res.* 7: 161-168

Sahay A, Satpathy S & Sharan S K (2011). Field trial experiment of artificial diet on tasar silkworm, Antheraea myltta D., Nature Proceedings: hdl:10101/npre. 2011.6701.1: https://core.ac.uk/download/pdf/290525.pdf

Seidavi A R, Bizhannia A R, Sourati R & Mavvajpour M (2005). The nutritional effects of different mulberry varieties on biological characters in silkworm. *Asia Pac J Clin Nutr*.pp 14. Qingdao University*ISSN:* 0964-7058

Singh P K & Subudhi B P R (1978). Utilization of azolla in poultry feed. Indian Farming. 27:37-39

Talley S N, Talley B J & Rains D W (1977). Nitrogen fixation by azolla in rice fields. In Alexander Hollaender, ed. Genetic Engineering for Nitrogen Fixation. Plenum Press, New York and London, pp. 259-281. DOI 10.1007/978-1-4684-0880-5_17

Tran Q T & Dao T T (1973). Azolla a green compost. Vietnamese studies, Agric, Problem 38:119-127

Yang Y, Tang L, Tong L, Liu Y, Liu H & Li X (2010). Initial ground experiments of silkworm cultures living on different feedstock for provision of high quality animal protein for human in space [J]. *Advances in Space Research* 46(6): 707-711. https://doi.org/10.1016/j.asr.2010.04.007.

Zar J H (1984). Biostatistical analysis. Prentice Hall Englewood Cliffs, NJ, 718 pp. ISBN: 978-0-13-100lW6·5

Journal of Agricultural Sciences
(Tarim Bilimleri Dergisi)

J Agr Sci-Tarim Bili
e-ISSN: 2148-9297
jas.ankara.edu.tr

JAS

Comparison of Logistic Regression, Frequency Ratio, Weight of Evidence and Shannon's Entropy Models in Erosion Susceptibility Analysis in Bingöl (Türkiye) with GIS

Orhan İnik[a*], Mustafa Utlu[b]

[a]*Department of Soil Science and Plant Nutrition, Bingöl University, Bingöl, TÜRKIYE*

[b]*Department of Geography Science and Letter Faculty, Mehmet Akif Ersoy University, Burdur, TÜRKIYE*

ARTICLE INFO

Research Article

Corresponding Author: Orhan İnik, E-mail: oinik@bingol.edu.tr

Received: 20 August 2024 / Revised: 21 December 2024 / Accepted: 23 December 2024 / Online: 25 March 2025

Cite this article

İnik O, Utlu M (2025). Comparison of Logistic Regression, Frequency Ratio, Weight of Evidence and Shannon's Entropy Models in Erosion Susceptibility Analysis in Bingöl (Türkiye) with GIS. *Journal of Agricultural Sciences (Tarim Bilimleri Dergisi),* 31(2):538-557. DOI: 10.15832/ankutbd.1535974

ABSTRACT

Soil erosion is one of the most important and critical processes occurring in Türkiye, as in all parts of the world. It is of great importance to understand the processes that occur as soil erosion continues. The aim of this study is to determine the erosion susceptibility occurring in the Çapakçur Stream basin, one of the important erosion areas of Türkiye. In the study, erosion susceptibility analysis was carried out using 4 different methods Shannon Entropy (SE), Logistic Regression (LR), Frequency Ratio (FR) and Weight of Evidence (WoE) that are effectively used today in erosion susceptibility analysis and determination of critical areas in terms of erosion, and 19 conditioning factors based on these methods. Analysis Results Model performances were evaluated using Receiver Operating Characteristic (ROC) and Area under the Curve (AUC) values based on a dataset consisting of 840 training (70%) and 360 testing (30%) points. According to result of the AUC values show that Logistic regression seems to perform well on both training (AUC= 94.7%) and validating datasets (AUC=93.5%). On the other hand, Weight of Evidence training (AUC= 93.5%) and testing datasets (AUC= 91.4%), Frequency Ratio training (AUC= 93.5%) and testing datasets (AUC=92.4%) of the Weight of Evidence result show that AUC and ROC values similar to Logistic Regression result, but slightly lower than Logistic Regression. Additionally, Shannon Entropy shows that it performs lower than other methods on both training (AUC= 55.7%) and testing datasets (AUC= 56.3%). Conducting analyses based on these methods, especially in erosion susceptibility studies, will facilitate both planning and the accuracy of the results obtained.

Keywords: Erosion susceptibility, Logistic regression (LR), Weight of Evidence (WoE), Frequency Ratio (FR), Shannon's Entrophy (SE).

1. Introduction

Soil plays a crucial role in providing essential nutrients for the nourishment of land covers and types (such as forests, grasslands, and agriculture), controlling the emission rates of greenhouse gases, regulating Earth's temperature, retaining and storing water, preventing droughts, floods, and inundations in basins, and serving as a natural purification environment in terms of pollution. However, since the transition of humanity from the Neolithic period (pre-9000 BCE) to settled societies, various civilizations, from ancient times to the present, have exerted significant pressures on natural resources, especially land. Particularly in modern times, the rapid increase in population has led to a surge in demand for and pressure on natural resources, challenging the environment's self-renewal capacity. Factors such as unhealthy industrialization, unplanned urbanization, improper land use, increased pollution, decrease or extinction of species, and climate change, resulting from this population growth, endanger the sustainability of ecosystems due to biodiversity loss. These pressures, combined with natural factors, lead to one of the biggest problems, soil erosion, and cause land degradation by creating an irreversible risk of desertification (Valentin et al. 2005; Dengiz et al. 2014; Zhuang et al. 2015; Saha et al. 2020). Therefore, soil erosion is a major and critical environmental issue that poses a serious and irreversible threat to agricultural productivity and long-term ecosystem stability wherever it occurs globally, impacting the entire world (Chalise et al. 2019; Mohammed et al. 2020; Bag et al. 2022).

One of the most significant environmental problems encountered when soils and lands are not sustainably managed is the risk of desertification. Land degradation and drought, in short desertification, directly or indirectly affect the lives of approximately 1.2 billion people worldwide. The main reasons for this are extreme changes in climate events and the adverse effects of human activities. About 6% of the world's soils are severely desertified, and approximately 29% are at risk of desertification. Desertification has affected all regions of the globe to some extent, with particularly significant impacts felt in South America, Asia, and Africa. Each year, in addition to approximately 6 million hectares of land that become desertified, an

additional 21 million hectares become unusable due to the spread of desertification (UNCCD 2016; Dengiz et al. 2020; İnik 2022; İnik 2023).

Türkiye is among the countries experiencing significant levels of soil erosion mainly due to its topography, climate, soil conditions, and anthropogenic factors, with erosion problems observed in only 13.86% of its land area according to official data (Berberoğlu et al. 2020). Land areas experiencing severe and very severe erosion make up 58.74% of the total landmass. Water erosion, which is the most common type of erosion both in Türkiye and globally, is the primary land degradation problem in our country, affecting 57.15 million hectares of land (Anonymous, 1987; Anonymous, 1998). The susceptibility of Turkish soils to both erosion and desertification is closely related to its geographical location, climate, topography, and soil structure. Soil erosion susceptibility, which we can define as the resistance of soils to erosive forces, varies under changing conditions such as rainfall intensity, slope steepness, changes in soil structure, and hydraulic properties. This situation makes it evident that desertification will have a more pronounced impact in the future under Türkiye conditions (İDEP 2012; Saygın 2013; Karagöz et al. 2015).

In recent years, innovative methods such as Geographic Information Systems (GIS) and machine learning (artificial intelligence algorithms) have been used for the identification of erosion-sensitive areas, resulting in more accurate and successful outcomes (Chakrabortty et al. 2020). Particularly, determining soil erosion susceptibility is of critical importance for implementing measures against erosion. In parallel with these advancements, numerous GIS-based soil erosion models have been developed from the 1990s to the present (Danacıoğlu & Tağıl 2017). In this context, soil erosion susceptibility studies also aim to identify potential areas at risk of soil erosion, particularly within specific sites and river basins. These studies generally focus on areas where erosion is likely to occur, and based on the results of the obtained susceptibility model, potential risk classifications are made. This classification is of great importance for determining measures to be taken for erosion sites within the high-risk category. For example, Bouamrane et al. (2024), examined soil erosion susceptibility maps in the Medjerda basin in North Africa. In this context, they used four different models: Deep Learning Neural Network-AHP (DLNN-AHP), Frequency Ratio-AHP (FR-AHP), Monte Carlo-AHP (MC-AHP), and Fuzzy AHP (F-AHP). They used eight different triggering factors, and the study identified that the distance to the river and rainfall erosivity factor had the greatest impact on soil erosion. Ait Neceur, et al. (2024), examined gully erosion susceptibility mappings in the N'fis River Basin using different machine learning algorithms. A total of 434 inventory data points were used for modeling, with 70% as training data and 30% as test data. The model accuracies were evaluated using the ROC curve. As a result, drainage density, slope, and NDVI were found to be the most influential factors in the field.

Therefore, recent studies on erosion susceptibility have shown a noticeable increase in research where parameter groups and analysis methods are determined by researchers, and independent models are used, alongside ready-made erosion models. Looking at recent studies on erosion susceptibility analysis using GIS technologies in the literature, the majority of them utilize statistical models (Akgün, 2007; Kheir et al. 2008; Conforti et al. 2011; Ogbonna et al. 2011). In this regard, there has been a rapid increase in studies focusing on soil erosion modelling approaches using methods such as frequency ratio (FR), logistic regression (LR), weight of evidence model (WoE), and Shannon entropy (SE), deep learning, machine learning etc.,

This study aims to conduct a soil erosion susceptibility analysis in the Çapakçur Creek basin, which is part of the Murat River Sub-basins and one of the significant soil erosion areas in Türkiye (Avcıoğlu et al. 2022). The purpose is to understand the erosion situation in this basin. For this purpose, four different methods, namely SE, LR, FR, and WoE, were employed to perform susceptibility analyses.

2. Material and Methods

2.1. Description of study site

The Çapakçur Stream basin is located within the borders of Bingöl province, in the Eastern Anatolia Region of Türkiye. It is situated between the latitudes of 38°48' - 38°55' and the longitudes of 40°17' - 40°32', with a basin area of 113.4 km². Generally, it extends in an east-west direction, with a maximum basin length of 21.6 km and a maximum basin width of 9.7 km. The basin has elevations ranging from a minimum of 1044 m to a maximum of 2505 m, with an average elevation of 1735 m, and it is characterized by a highly rugged topography. While the middle and upper parts of the basin have steep relief, only the area towards the city centre of Bingöl represents a relatively flat and plain topography. However, these areas also contain slopes with quite high gradients, and the average slope throughout the basin is 22.5° (Figure 1).

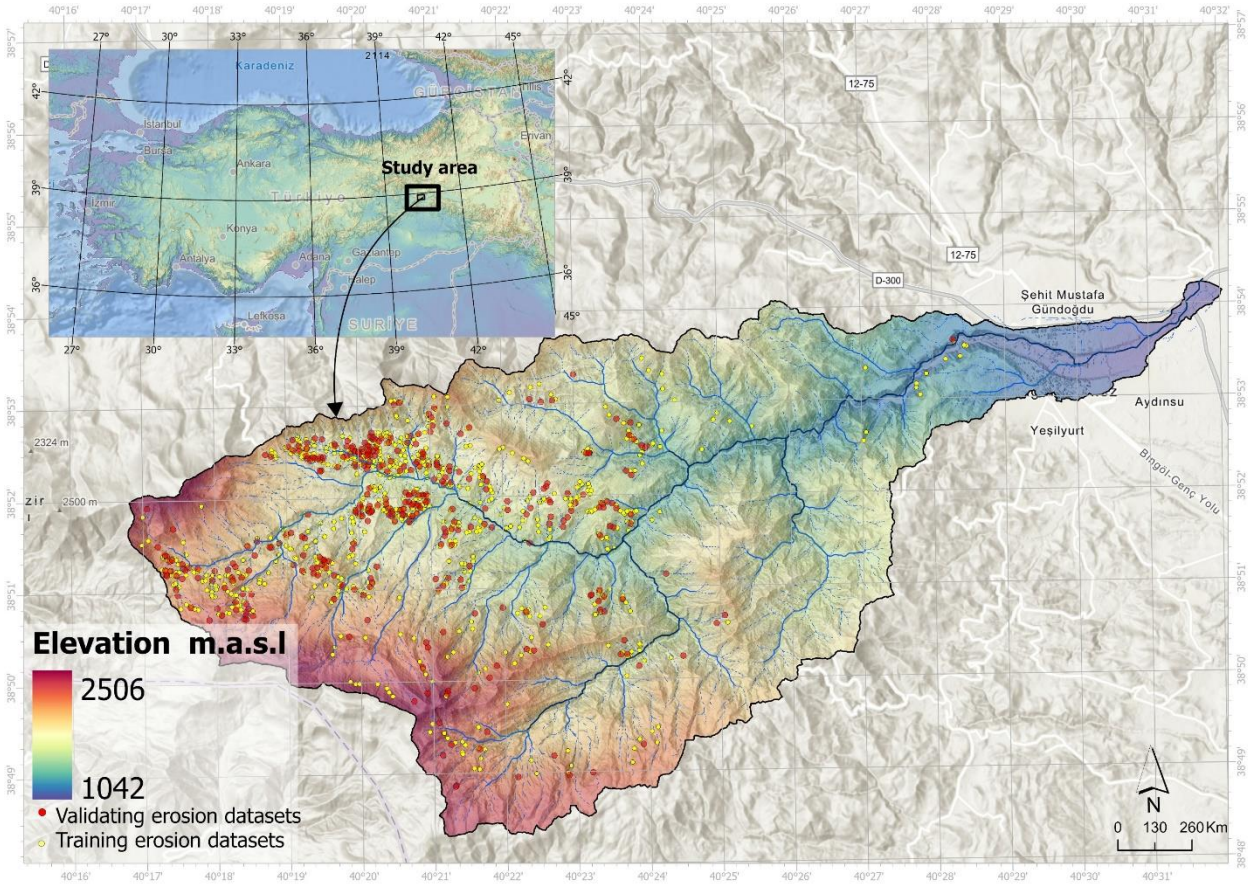

Figure 1- Location of the study area

According to the Koppen-Geiger climate classification, the main climate type is "D", representing a cold and humid temperate climate type (continental climate) in the winter seasons and is the second most common climate type seen in Türkiye (Peel et al. 2007; Öztürk et al. 2017). The sub-climate type is represented as "Dsa". The annual total precipitation in this region is 949 mm, with 117 days of snowfall and a snow cover duration of 76 days (İnik et al. 2022) and the average temperature values fall below 0°C during the winter seasons while exceeding 20 °C during the summer season (Öztürk et al. 2017). Dense erosion observed in the field is strongly controlled not only by climatological characteristics but also by geological and geomorphological features. Therefore, erosion is observed, particularly on steep slopes in the study area (Figure 2). Especially with heavy rainfall, erosion development accelerates in areas where surface runoff occurs, particularly in river valleys with flash floods. According to the general lithological characteristics of the basin, two different basic lithological units are observed in the field. In the lower reaches of the basin, a small portion consists of Quaternary-aged alluviums and volcanic units. One of the intensively observed units consists of sandstone, mudstone, limestone shelf, and sedimentary rocks spreading in areas where erosion events actively occur, while the other unit consists of upper Miocene-Pliocene-aged volcanic rocks, conglomerates, and continental units.

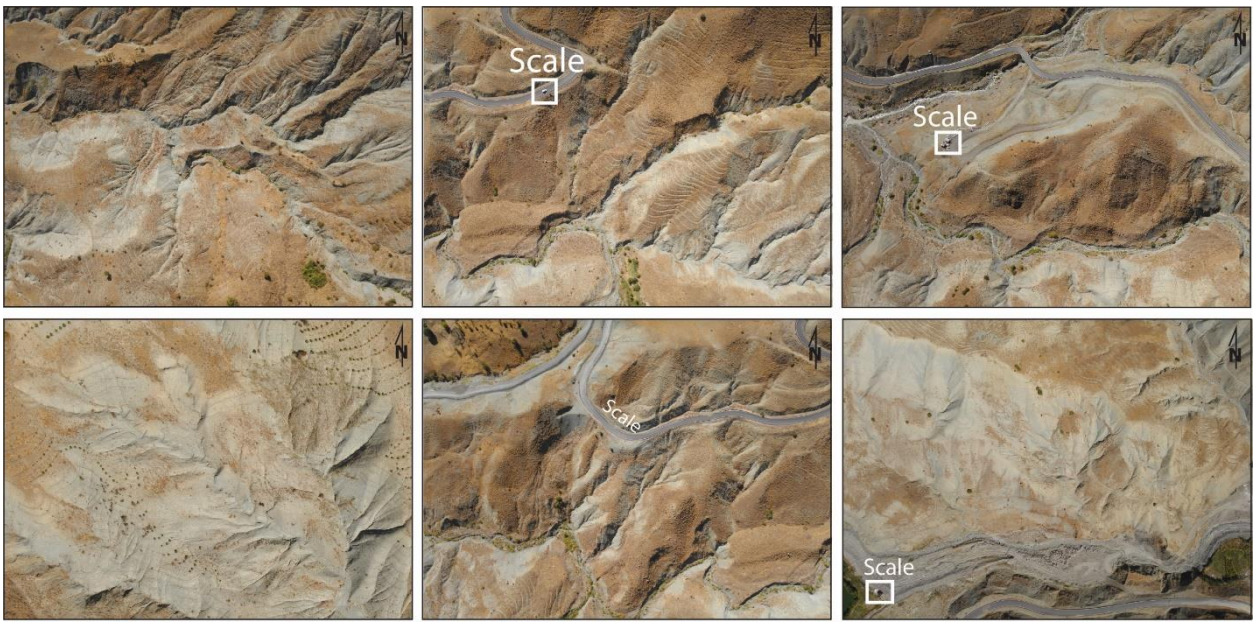

Figure 2- UAV images of the erosion areas in the Çapakçur Stream basin

2.2. Methodology

Geographic information systems and remote sensing technologies were used in this work, and Microsoft Excel and SPSS were used for statistical computations. The general flowchart used in the study is provided in Figure 3. The present study was carried out in the following main steps.

- Firstly, the detection and digitization of erosion areas within the basin boundaries,
- (ii) followed by subsetting the generated inventory data by randomly selecting 70% as training data and 30% as test (validation) data,
- the selection of condition factors and their reclassification and preparation,
- the implementation of LR, FR, WoE, and SE methods,
- the creation of susceptibility models for these methods,
- Testing the performance of erosion susceptibility models using the area under the receiver operating characteristic (AUROC).

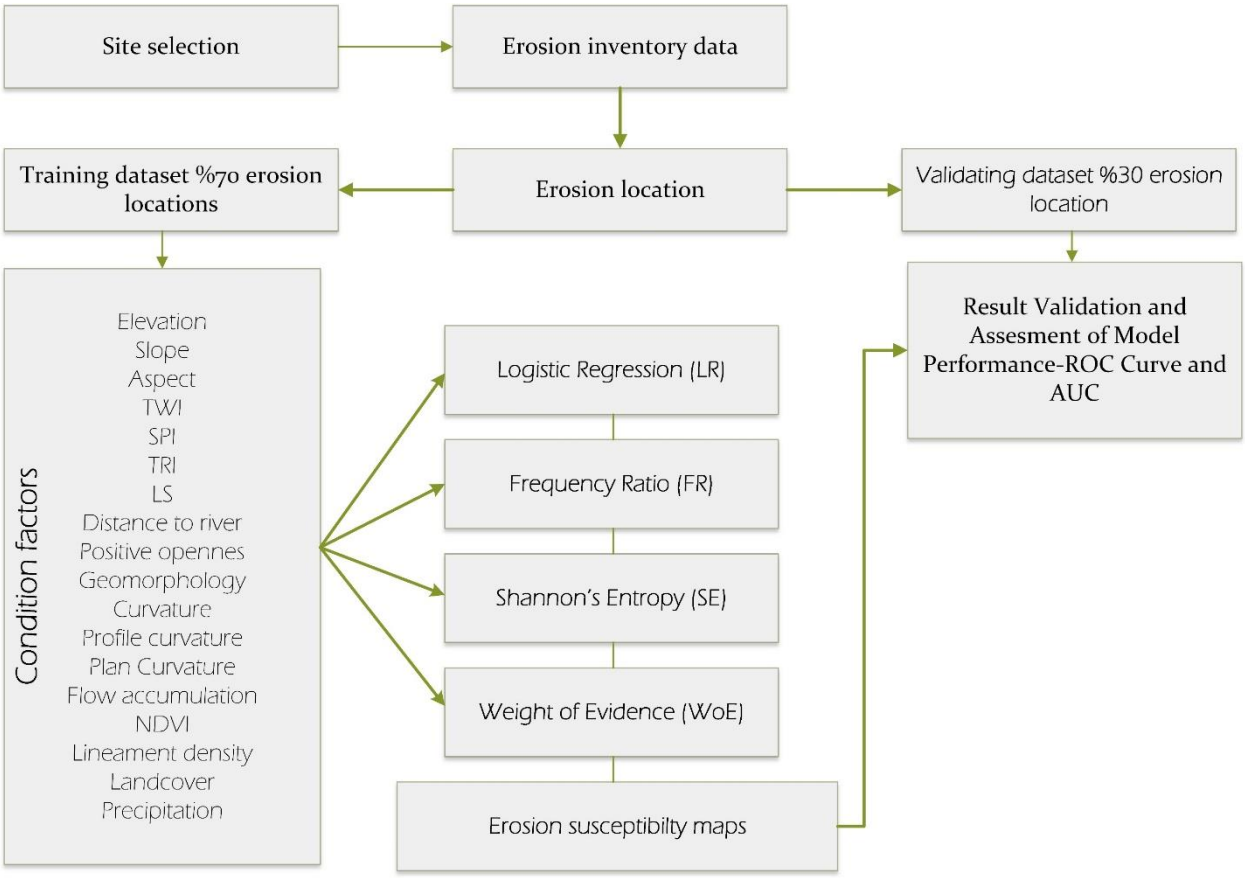

Figure 3- General flowchart of the study

In order to complete this study, 5m resolution DSM data, referred to as "Level-0 DSM5", generated from stereo aerial photographs through automatic matching, have been obtained from the General Directorate of Maps (HGK). From this surface model data, 14 different condition factor datasets have been produced. Additionally, Sentinel-2 satellite imagery with a resolution of 10m has been utilized for NDVI and lineaments analyses, precipitation characteristics from global grid data, and land cover data from global 10m resolution land cover data have been used. In this context, detailed properties of the data used, obtained from different sources and with different resolutions, are presented in Table 1.

Table 1- Details about the data was used in the study

	Data	***Source***	***Type***	***Resolution***	***Product***	***Software***
1	Digital surface model (DSM)	https://www.harita.gov.tr/	Grid	5 m	Slope, Geomorphology, TRI, TWI, LS, Aspect, Curvature (plan, profile), SPI, Positive opennes, Flow acc, Dist to river	ArcGIS Pro SAGA GIS
2	Landcover	https://esa-worldcover.org/en	Grid	10 m	Landcover	ArcGIS Pro
3	Satellite Image	https://scihub.copernicus.eu/Sentinel-2	Grid	10 m	NDVI, Lineaments	ArcGIS Pro
4	Road	https://overpass-turbo.eu/	Vector		Distance to road	ArcGIS Pro
6	Precipitation	Fijk and Hijmans, 2017	Grid	1 km	Precipitation	ArcGIS Pro
7	Geomorphology	https://saga-gis.sourceforge.io/saga_tool_doc/7.3.0/ta_lighting_8.html	Grid	5 m	Geomorphologic unit	SAGA GIS

2.3. Erosion inventory mapping

Susceptibility models are conducted for the purpose of the likelihood of past events recurring in the future. Thus, it is important for making rapid, on-site, and accurate decisions through the identification of potential areas. Therefore, inventory data collected from areas where the erosion have occurred is necessary for susceptibility modelling. Additionally, inventory data plays a critical role in the creation of statistically different susceptibility models and in measuring the performance of the resulting model outcomes. (Choubin et al. 2019). It particularly contributes to the accuracy, reliability, and effectiveness of susceptibility models. This facilitates the comparison of different modelling results for susceptibility models created for study areas. In this study, inventory data were used to determine the influence of each variable on erosion dependent on four different statistical methods for erosion susceptibility modelling (Figure 1). Fieldwork, drone imagery, and Google Earth were utilized to obtain the inventory data. A total of 1200 inventory point data were collected from various points in the study area where erosion occurred. Of these, 70% were used as training data and 30% as test (validating) data (Conforti et al. 2011; Gayen & Saha 2017; Hembram et al. 2019). In the ArcGIS Pro environment, subset features were randomly determined in the study area, resulting in 840 training data points and 360 test data points. The training inventory data were used within the scope of the model creation to learn the relationship between each factor used and the erosion status, while the test data were used to measure the accuracy of the created susceptibility models.

2.4. Erosion conditioning factors

In susceptibility modelling to be conducted in natural disaster research, there are many triggering and controlling factors involved in the occurrence of disasters. Therefore, in the creation of erosion susceptibility models, the most important stage is the selection of these data, as it will significantly impact the quality of the study and the accuracy of the results (Rahmati et al. 2017; Garosi et al. 2018). In erosion susceptibility studies, there are many factors that influence the occurrence, development, and progression of erosion. In this context, the selection of controlling factors has been made taking into account previous studies. However, there is no fixed controlling factor in erosion susceptibility studies (Conoscenti et al. 2013). Therefore, this study has selected 19 factors to improve the identification of erosion susceptibilities with enhanced accuracy and quality, as determined by the researchers (Rahmati et al. 2017; Arabemeri et al. 2020, Lei et al. 2020; Lana et al. 2022). Triggering factors are shaped by climatic, geomorphological, anthropogenic, and geological characteristics. These include elevation, slope, aspect, Normalized Difference Vegetation Index (NDVI), Topographic Wetness Index (TWI), Stream Power Index (SPI), Topographic Ruggedness Index (TRI), slope length (LS), distance to river, distance to road, land cover, lineament density, positive openness, geomorphology, curvature, plan curvature, profile curvature, flow accumulation, and precipitation data (Figure 4). Within the scope of the study, triggering factors were evaluated by classifying them into 5 classes according to the natural breaks method (Jenks, 1967).

Elevation, significantly influences erosion, especially in rill erosion processes. Higher elevations often lead to steeper slopes, which increase surface runoff and erosion potential (Conoscenti et al. 2008, Zhu et al. 2014; Zabihi et al. 2018; Zabihi et al. 2019). Accordingly, the elevation data for the Çapakçur Stream basin ranges from 1042 to 2506 m, with values divided into 5 classes as follows: 1042–1363, 1363–1621, 1621–1680, 1840–2092, and 2092–2506 m (Figure 4).

Slope, plays a key role in determining the extent of surface runoff, which directly affects erosion rates. Steeper slopes increase the potential for soil and sediment transport, making these areas more susceptible to erosion (Dramis and Gentili, 1977; Valentin et al. 2005; Güney, 2018). The slope values range from 0 to 76.1°, classified into 5 categories as follows: 0–15.2, 15.2–30.5, 30.5–45.7, 45.7–60.9, and 60.9–76.1 (Figure 4).

Aspect, one of the most important factors to consider when evaluating erosion susceptibility processes in a specific area or watershed is aspect (Carrara et al. 1991; Maharaj 1993; Guzzetti et al. 1999; Nagarajan et al. 2000; Güney 2018). Aspect is expressed with values ranging from 0 to 360 degrees in a clockwise direction. The aspect of a slope directly or indirectly influences erosion processes as it controls various climatic characteristics and vegetation cover (Dai et al. 2001; Çevik & Topal 2003; Pulice et al. 2009; İnik 2023). Aspect characteristics were evaluated and classified into 9 classes based on intermediate and main directions (Figure 4).

Normalized Difference Vegetation Index (NDVI), is the most commonly used method for analysing information about vegetation using GIS data to measure the amount of vegetation cover in an area. It serves as an indicator of green biomass in the area. NDVI is calculated using Equation 1 (Pettorelli et al. 2005):

$$NDVI = \frac{NIR - RED}{NIR + RED} \quad (1)$$

NIR represents the Near-Infrared band reflectance, RED represents the Red band reflectance. The NDVI values, analyzed in 5 classes, have minimum and maximum values ranging from 0.078 to 0.606. Accordingly, the NDVI values are classified into 5 categories as follows: 0.078–0.125, 0.125–0.203, 0.203–0.294, 0.294–0.405, and 0.405–0.606 (Figure 4).

Topographic wetness index (TWI), is generally defined as the influence of topography on the location and extent of areas where surface water will flow, and it is calculated according to Equation 2.

$$TWI = In\left(\frac{A_s}{Tan\beta}\right) \quad (2)$$

Here, A_s represents the contributing area to the cell, and β represents the slope gradient (Beven & Kirkby 1979). It provides clues about the degree of soil saturation or the movement of water within and on the surface of the soil, depending on the topography. This is because soil moisture content directly affects surface runoff, infiltration of water, ponding and other situations. This demonstrates the impact of TWI on erosion processes and it has been generated as a parameter for use in erosion susceptibility (Conforti et al. 2011; Sharma & Pandey, 2022). Accordingly, the TWI values range from 0.293 to 24.117 and are classified into 5 categories as follows: 0.293–3.188, 3.188–4.963, 4.936–7.392, 7.392–11.036, and 11.036–24.117 (Figure 4).

Stream Power Index (SPI), generated by flowing water or surface runoff on a particular slope directly affects erosion. SPI represents the power index in this context and is one of the key factors controlling erosion processes (Güney, 2018). Additionally, areas where high stream power index values are observed indicate a significant erosion potential, as they have the potential energy to transport sediments, in other words, they indicate locations that could serve as sediment sources (Kakembo et al. 2009). SPI is determined according to Equation 3.

$$SPI = In(As \times tan\beta) \quad (3)$$

Here, A_s represents the contributing area to the cell, and β represents the slope gradient (Nikolova 2022).

Topographic Ruggedness Index (TRI) is used to represent the amount of elevation difference between adjacent cells of a DEM. This scanning function template is used to create a visual representation of TRI with your elevation data. For example, it is assumed that 0-80 m represents a flat terrain surface, 81-116 m represents a nearly flat surface, 117-161m represents a slightly rugged surface, or 959-4367m represents an extremely rugged surface (Różycka et al. 2017; Habib, 2021; Trevisani et al. 2023). The SPI values range from -6.907 to 15.398 and are classified into 5 categories as follows: -6.907 to -3.671, -3.671 to 0.178, 0.178 to 2.189, 2.189 to 5.076, and 5.076 to 15.398 (Figure 4).

The LS factor, is a parameter used to measure soil erosion rates in erosion prediction models such as USLE and RUSLE. It controls surface flow velocity and is considered one of the most important factors for sediment transport (Haan et al. 1994). The technique for calculating the LS factor is provided by Moore and Burch (1986) as follows (Equation 4):

$$LS = \left(\text{Flow accumulation} \times \frac{\text{A}}{22.13}\right)^{0.4} \times sin(\frac{Slope}{0.0896})^{1.3} \quad (4)$$

The LS factor ranges from 0 to 807.97. Accordingly, it is classified into 5 categories as follows: 0–6.377, 6.377–25.348, 25.348–57.033, 57.033–129.90, and 129.90–807.97.

Distance to river, one of the important factors used to assess erosion susceptibility is the distance to the river. This factor is crucial for understanding what is more prone to erosion. Distance to river refers to the distance of an area from the river or streambed. (Arabemeri et al. 2020). Accordingly, the Distance to River ranges from a minimum of 1358 m to a maximum of 18607 m, with 5 classes as follows: 1358–6363, 6363–8663, 8664–10490, 10490–12519, and 12519–18607 (Figure 4).

Distance to road, roads have a negative impact on the sustainability of areas where surface runoff may be suitable for channels. Therefore, determining the distance to the road factor is important in identifying erosion susceptibility maps (Nkonge et al. 2023). In the study, in ArcGIS, the distance from each scanning cell to the road section (meters) was calculated using the Euclidean distance tool. Accordingly, the Distance to road ranges from a minimum of 0.82 m to a maximum of 11601 m, with 5 classes as follows: 0.82, 0.82-2275, 2275-3821, 3822-5960 and 5960-11601 (Figure 4).

Landcover, has a significant impact on geomorphological processes on slopes. Bare areas are generally more susceptible to erosion. The presence of vegetation reduces erosion susceptibility due to its ability to reduce the erosive effect of surface runoff (Anabalagan, 1992; Dai et al. 2001; Çevik & Topal, 2003; Conforti et al. 2011). Therefore, the land use and land cover of the basin have been emphasized as one of the geographical factors affecting erosion susceptibility. Accordingly, there are 7 different land cover types in the study area. These are tree cover, shrubland, bare/scarce vegetation, permanent water bodies, grassland, and cropland (Figure 4).

Lineament density, Surface lines represent weak areas with high permeability and low resistance. The distance to linearity is an important influencing factor for erosion development. This is because it represents a weak surface characterized by heavily fractured rocks in an area. Surface lines also promote soil degradation (Foumelis et al. 2004). The lineament density ranges from

0 to 5046. Accordingly, it is classified into 5 categories as follows: 0–0.396, 0.396–1069, 1069–1781, 1781–2652, and 2652–5046 (Figure 4).

Positive opennes (Po), is important for identifying narrow and deep valleys and determining convex units, especially those affecting erosional processes, within these valleys (Doneus 2013). The Po value ranges from 0.424 to 1687 and is classified into 5 categories as follows: 0.424–1127, 1127–1231, 1231–1315, 1315–1404, and 1404–1687 (Figure 4).

Precipitation, one of the fundamental factors that influences soil erosion, affecting surface runoff and causing increases or decreases in soil erosion and loss, is slope (Zhao et al. 2022)Global grid data was used in generating the rainfall dataset (Fick & Hijmans 2017). The study area has rainfall values ranging from 765 to 1379 mm. Accordingly, the precipitation data, classified into 5 categories, has values ranging from 76–888, 888–1011, 1011–1134, 1134–1256, and 1256–1379 mm (Figure 4).

Geomorphology, in erosion susceptibility mapping, it is important to determine the geomorphons representing the classification of land parcels and category forms. These are generated from a digital elevation model and utilized in the study (Stepinski & Jasiewicz, 2011; Jasiewicz & Stepinski, 2013)**.** According to the geomorphological data, the study area has the following morphological units: flat, summit, ridge, shoulder, spur, slope, hollow, footslope, valley, and depression (Figure 4).

Plan curvature, geomorphological and land morphology definitions, such as plan curvature analysis, are determined. Plan curvature refers to the effect on erosion formation, which is related to whether water moves away or towards during downstream flow. Therefore, the plan curvature layer is an important factor in triggering and developing erosion (Rahmati et al. 2016). The plan curvature values range from -113.78 to 108.39, and the classes are as follows: -113.78 to -10.97, -10.97 to -3.12, -3.12 to 2.971, 2.971 to 10.813, and 10.813 to 108.39 (Figure 4).

Profile curvature, which is believed to control the erosive force of the river, is particularly an important parameter for gully erosion (Conoscenti et al. 2013). The profile curvature values range from -98.501 to 119.071, and the classes are as follows: -98.501 to -12.375, -12.375 to -3.839, -3.839 to 2.136, 2.136 to 11,525, and 11.525 to 119.071 (Figure 4).

Curvature, units with concave landforms (negative curvature) generally affect water accumulation, while points with convex landforms (positive curvature) facilitate easy water flow and increase the likelihood of erosion (Ohlmacher, 2007). Curvature values range from -164.86 to 187.766. The first two classes contain negative values, while the last three classes have positive values (2.46 to 187.766) (Figure 4).

Flow accumulation, affects the direction of water flow and the likelihood of water accumulation It particularly influences the velocity of surface runoff. High flow accumulation results in increased surface runoff, causing soil erosion and carrying more sediment (Zhang et al. 2021). The flow accumulation values range from 0.001 to 6370.808 (Figure 4).

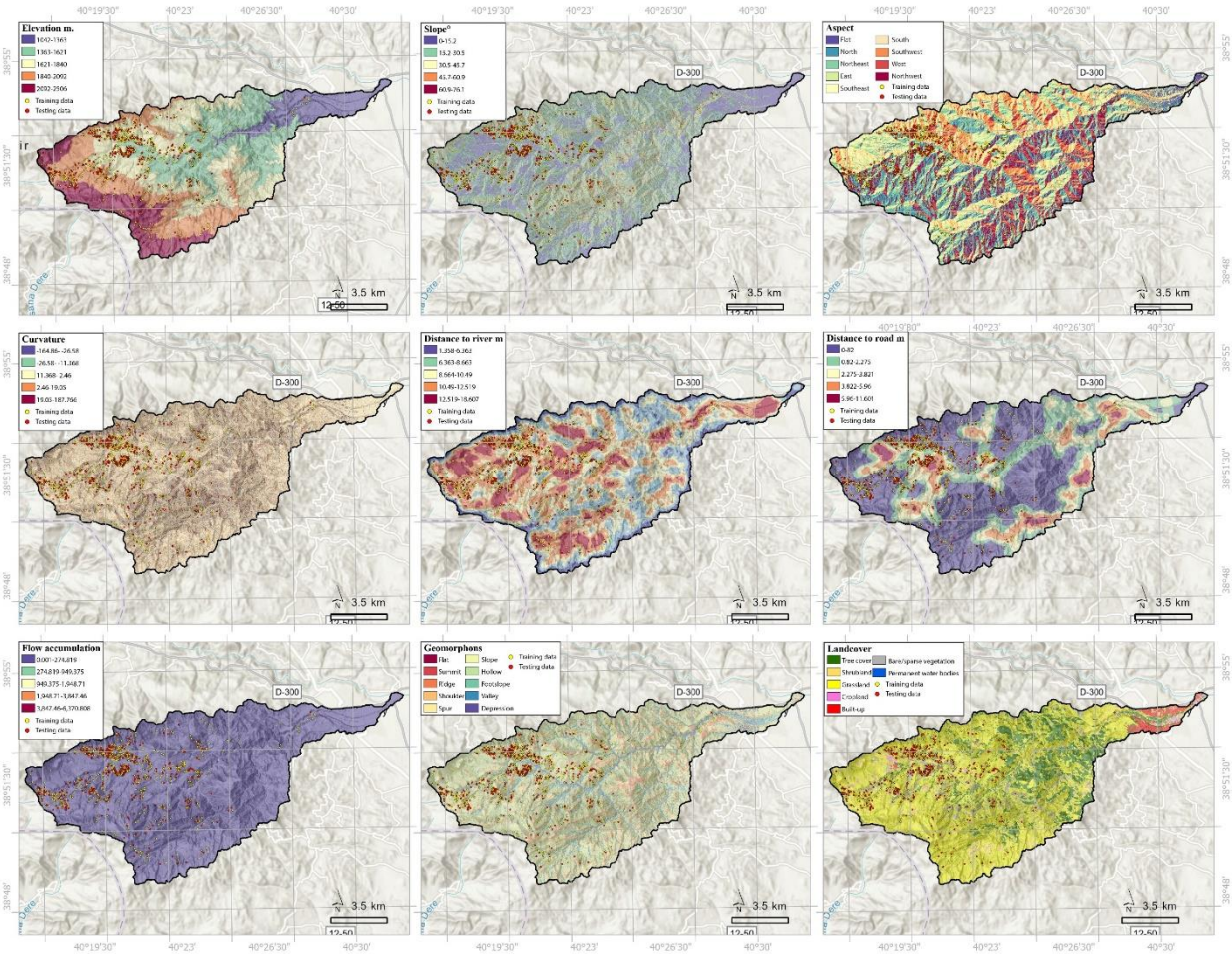

Figure 4- Condition factor of erosion susceptibility analysis

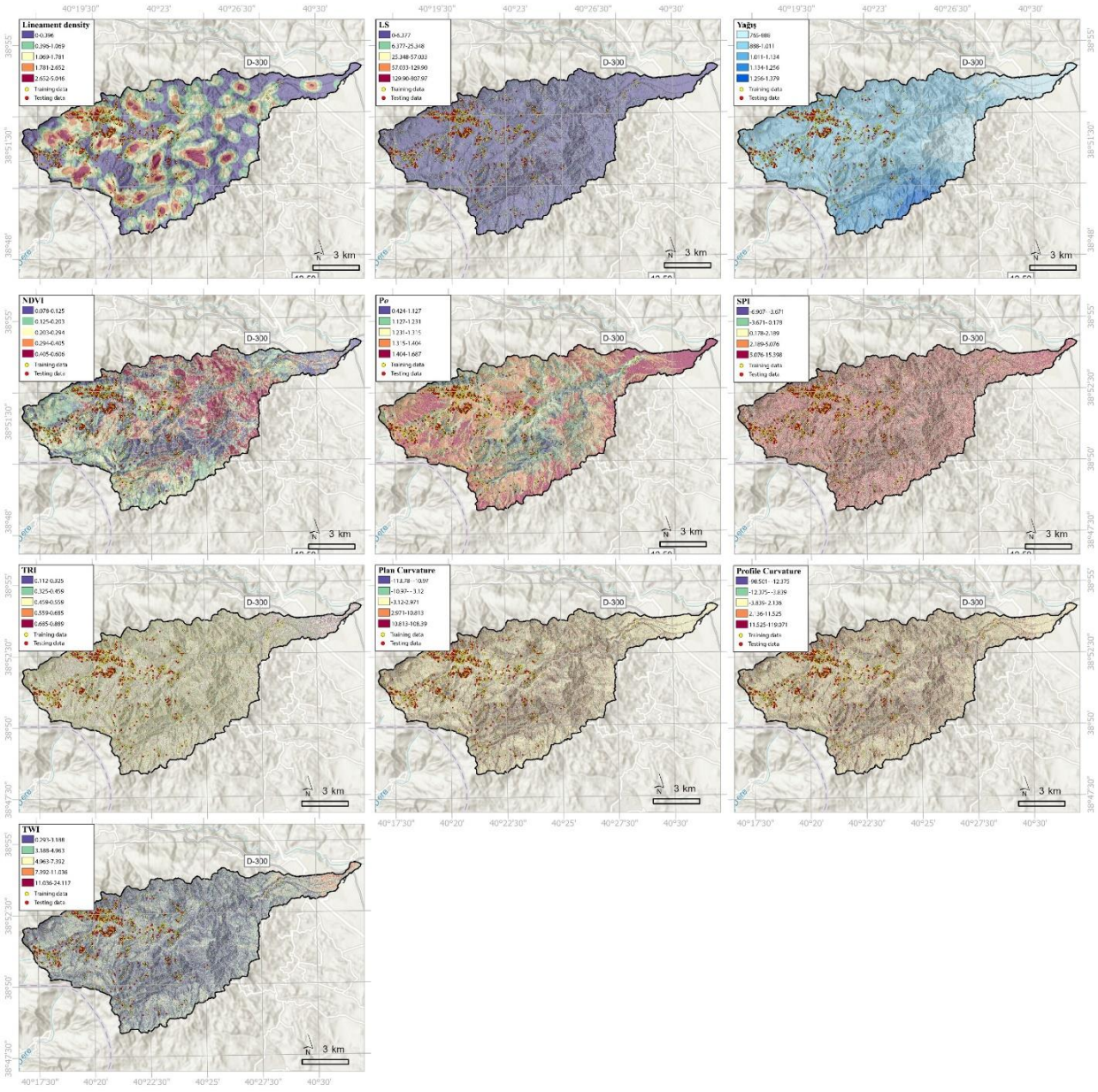

Figure 4- Condition factor of erosion susceptibility analysis (continued)

2.5. Erosion susceptibility mapping

Frequency Ratio (FR)

Frequency ratio (FR) is a commonly used method in erosion susceptibility assessment. FR is defined as the ratio of the probability of an event occurring, using all factors affecting a natural event (such as erosion) that occurred in the past, to the probability of not occurring (Bonham Carter, 1994; Dai and Lee 2002). Parameters used in erosion susceptibility analysis were correlated with erosion surfaces, which are considered evidence of severe erosion in the study area. The frequency ratio allows for the consideration of both the areas where erosion is severe and the extent of the areas covered by the parameters used in the research area. Equation 5 was utilized in the calculation of FO.

$$FO = \frac{X}{Y} \tag{5}$$

In Equation 1, X represents the percentage of erosion surface presence within each subclass of a parameter influencing erosion, while Y represents the percentage of each subclass of a parameter influencing erosion within that parameter. The values for X and Y were calculated based on Equations 6 and 7.

$$X = \frac{A}{B} \times 100 \quad (6)$$

$$Y = \frac{C}{D} \times 100 \quad (7)$$

Weight of Evidence (WoE)

The "Weight of Evidence (WoE)" model is used to calculate the Bayesian probability model more explicitly and which is commonly used in susceptibility modeling for spatial prediction (Akıncı et al. 2017; Kılıçoğlu, 2020). This model is a method within the Bayesian approach where conditional and unconditional probabilities are applied using sufficient data. Through this model, positive weights are assigned to predictions that anticipate erosion occurring in the studied area in the future, while negative weights are assigned to predictions that anticipate no erosion (Akıncı et al. 2017). The WoE model has been mathematically expressed by Van Westen et al. (2003) and Regmi et al. (2010). The determination of weights relies on the following equations.

$$W^{+} = \frac{\frac{A_1}{A_1 + A_2}}{\frac{A_3}{A_3 + A_4}} \quad (8)$$

$$W^{-} = \frac{\frac{A_2}{A_1 + A_2}}{\frac{A_4}{A_3 + A_4}} \quad (9)$$

$$C = W^{+} - W^{-} \quad (10)$$

In these equations; A_1: number of erosion cells in the sub-class, A_2: number of erosion cells outside the sub-class, A_3: number of non-erosion cells in the parameter subclass, A_4: number of non-erosion cells outside the sub-class, W+: Positive weight, W−: Negative weight, C: Represents the weight contrast. Positive weight (W+) is used to indicate the importance of the presence of the factor in terms of erosion formation. If this value is positive (+), the presence of the relevant factor is conducive to erosion formation; if negative (-), it is not conducive. Negative weight (W−) is used to evaluate the importance of the absence of the factor in terms of erosion formation. If this value is positive (+), the absence of the relevant factor is conducive to erosion formation; if negative (-), it is not conducive. C (weight contrast) reflects the spatial relationship of the prediction variable with erosion, indicating the difference between positive and negative weights. A positive value indicates a spatial relationship of the variable with erosion, while a negative value indicates no spatial relationship of the variable with erosion. A weight contrast value equal to zero indicates that the subcategory of the factor causing erosion is not significant (meaningful) for analysis (Van Westen et al. 2003; Neuhauser & Terhorst, 2007; Corsini et al. 2009, Akıncı et al. 2015; Akıncı et al. 2017; Kılıçoğlu, 2020).

Logistic Regression (LR)

There are three common types of multivariate statistical analysis methods widely used in the literature: multiple regression, logistic regression (LR), and discriminant analysis. In multivariate statistical analysis methods, factors that could cause erosion for a known land parcel are relatively examined, and the reasons for the occurrence of events are investigated. The land parcel examined through the analysis methods is based on data obtained by examining whether erosion has occurred or not (Akgün, 2007). The most significant limitation in multivariate statistical analysis studies is the long processing time due to the use of grid cells in the studies. However, the most important advantage of the method is that it is largely an objective method. Logistic regression is one of the most commonly used multivariate analysis methods in producing erosion susceptibility maps. LR analysis is based on a multivariate regression relationship between a dependent variable and multiple independent variables. The logistic regression method is defined by the following Equation (Equation 11):

$$Y = b_0 + b_1 x_1 + b_2 x_2 + \cdots + b_n x_n \quad (11)$$

Shannon's Entropy (SE)

Shannon's entropy method is one of the techniques used in susceptibility analysis. This method is actively utilized in the implementation of susceptibility models for natural disasters such as floods, landslides, and erosion. (Sharma et al. 2012; Hembram et al. 2020; Islam et al. 2022; Utlu, 2023). It is generally based on the concept of entropy, which measures the level of uncertainty or randomness, and abnormality between causality and consequences (Lin 1991; Yufeng & Fengxiang 2009). It determines the maximum and minimum impact levels, or in other words, the entropy level of factors influencing the occurrence of hazards (Yulianto et al. 2020). The ratio of the high and low values of the measure affects the susceptibility level. A high value indicates a high probability situation, while a low value indicates a low probability situation (Al-Hinai & Abdalla 2021). Shannon entropy is computed using the formula as specified below (Equation 12):

$$Pd_{ij} = \frac{FR_{ij}}{\sum_{i=1}^{m_j} FR_{ij}} \quad (12)$$

Pd_{ij}, Represents the probability density, while,FR_{ij} and denotes the frequency rate in the given parameters. After calculating the probability density, the obtained values are used to calculate the entropy (Equation 13-14).

$$Ev_j = \sum_{i=1}^{m_j} Pd_{ij}\, log_2\, Pd_{ij}, j = 1, \dots, n \quad (13)$$

$$Ev_{jmax} = log_{2\, m_j} \quad (14)$$

Ev_j ve Ev_{jmax} Entropy values,m_j represent the number of classes (Equation 15) in calculating the weights of factors used in erosion susceptibility assessment.

$$Ic_j = \left(Evj_{max} - \frac{Ev_j}{Ev_{jmax}}\right), I = (0,1)1j = 1, \dots n \quad (15)$$

The formula is utilized, and in the formulaIc_j: represents the coefficient of the relevant layer (Equation 16),

$$Cw_j = I_j FR \quad (16)$$

Cw_j: It represents the weight value representing the entire relevant layer.

2.6. Model evaluation

In natural disaster studies, the ROC curve and AUC values method is widely used for assessing the model performances of susceptibility models generated to understand flood, landslide, rock fall, and erosion events. ROC and AUC method currently, most of the researchers are actively using this approach (Tehrany et al. 2013; Miao et al. 2023; Utlu, 2023; El Miloudi et al. 2024). Data from the susceptibility model's event inventory is required to measure model performances with accuracy and reliability. As a result, evaluating the results that are produced using the ROC and AUC approaches is simple. Plotting the true positive rate (TPR) and false positive rate (FPR) of binary classification models is carried out for assessing their efficacy using ROC and AUC metrics. Equation 17 displays the y-axis as TPR (True Positive Rate), and Equation 18 shows the x-axis as FPR (False Positive Rate).

$$y\ axis\ TPR = \frac{TP}{TP + FN} \quad (17)$$

$$x\ axis\ FPR = 1 - \frac{FP}{FP + TN} \quad (18)$$

AUC represents the area under the ROC curve and ranges from 0 to 1. Equation 19, (Amiri et al. 2019; Baiddah et al. 2023):

$$AUC = \frac{\sum TP + \sum TN}{P + N} \quad (19)$$

P: the total number of erosion data, N: the total number of data without erosion data (Baiddah et al. 2023).

3. Results

3.1. Multi-collinearity assessment

This evaluation indicates whether there is a linear relationship among multiple independent variables. Especially in susceptibility analyses, the importance of model accuracy and reliability plays a role, and examining and evaluating the correlation between independent variables is crucial (Graham 2003; Rahmati et al. 2017; Roy & Saha 2019; Wang et al. 2021). Thus, variables with high correlation can lead to unstable coefficient estimates and inaccurate predictions, while on the other hand, they can reduce the predictive accuracy of the model. Therefore, the independent variables to be considered should have a VIF (Variance Inflation Factor) value below 10 and a tolerance threshold value above 0.1. Because values that go outside of and beyond these boundaries signify the existence of problems with multicollinearity (Kelava et al. 2008; Arabameri et al. 2020). The VIF values of curvature, plan curvature, and profile curvature among the 19 distinct condition data exhibit strong association among independent variables, suggesting multicollinearity. As a result, 16 factor values were taken into account, and these 3 condition factors were not included in the analysis (Table 2).

Table 2- Multi-collinearity values of conditioning factors

No	*Factors*	*Tolerance*	*VIF*
1	Elevation	0.742	1.347
2	Distance to river	0.315	3.173
3	Distance to road	0.869	1.151
4	TWI	0.226	4.426
5	TRI	0.545	1.837
6	SPI	0.214	4.426
7	Slope	0.161	6.229
8	Geomorphology	0.503	1.989
9	Distance to lineament	0.922	1.085
10	LS	0.442	2.265
11	LU	0.393	2.547
12	NDVI	0.367	2.723
13	Plan curvature	0.020	51.109
14	Profile curvature	0.017	58.948
15	Curvature	0.006	167.909
16	Precipitation	0.279	3.587
17	Positive openness	0.243	4.112
18	Flow accumulation	0.854	1.170
19	Aspect	0.916	1.091

3.1. Erosion susceptibility modelling

Erosion susceptibility analysis has been conducted on the Çapakçur Creek basin using different statistical methods dependent on various algorithms. In this context, FR, LR, WoE, and SE methods were employed, and the results obtained has been classified into 5 classes using the natural breaks classification Jenks algorithm (Jenks, 1967). According to multicollinearity assessment, 16 out of the 19 selected factors were considered. Among the 16 factors used across 4 different methods, those with the highest impact on erosion in the Çapakçur Stream basin are as follows: for the WoE (Weights of Evidence) method, elevation and slope; for the LR (Logistic Regression) method, NDVI, land use, slope, and TWI (Topographic Wetness Index); for the FR (Frequency Ratio) method, NDVI, precipitation, flow accumulation, and elevation; and for the SE (Statistical Evaluation) method, the significant factors are elevation and precipitation data. These classes are very low, low, moderate, high, and very high. The results of the susceptibility model obtained by different methods are presented in Figure 5. According to result of the four methods, the areas with high and very high erosion susceptibility, show quite similar distributions except for the SE method, direct correlation with the geomorphological features of the relief. In the LR, FR, and WoE methods, areas with high and very high susceptibility are found in steep slopes and ridges with narrow and deep valleys, while in the SE method, areas with high susceptibility are observed in river valley bottoms and areas with low slope values close to flat relief. In addition, areas with very low, low, and moderate erosion susceptibility correspond to similar terrain characteristics in the LR, FR, and WoE methods, generally comprising low-lying flat areas and gently sloping terrains. However, in the SE method, these areas appear to be high-slope and steep terrain, contrasting with the high and very high erosion susceptibility areas identified by the three other methods (Figure 5).

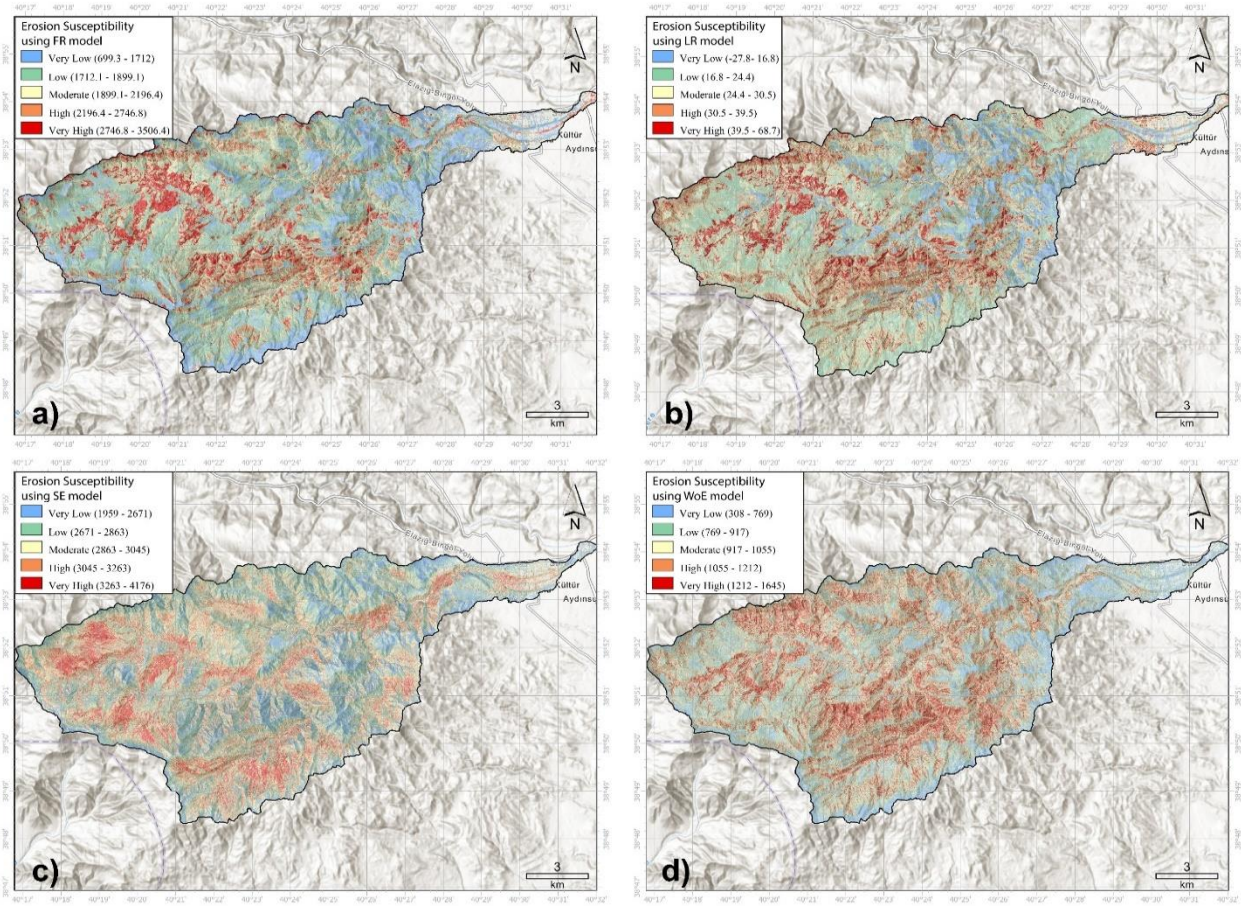

Figure 5- Erosion susceptibility models using different statistical methods a) FR b) LR c) SE d) WoE

Each method shows variations in the distribution of susceptibility classes, which could indicate differences in the susceptibility of the methods or the underlying assumptions they rely on. According to the spatial distributions of each susceptibility classes for different statistical model results are as follows for the LR method: very low class covers 12.2 km² (11%), low class covers 31 km² (27.9%), moderate class covers 37.2 km² (33.5%), high class covers 21.1 km² (19%), and very high class covers 9.5 km² (8.5%) (Figure 6). FR method: very low class covers 20.7 km² (18.7%), low class covers 39.6 km² (37.7%), moderate class covers 25.7 km² (23.1%), high class covers 15 km² (13.5%), and very high class covers 10 km² (9%) (Figure 6). WoE method: very low class covers 14.6 km² (13.1%), low class covers 28.3 km² (25.5%), moderate class covers 30.9 km² (27.8%), high class covers 25.4 km² (22.9%), and very high class covers 11.8 km² (10.7%) (Figure 6). SE method: very low class covers 16.1 km² (14.5%), low class covers 30.2 km² (27.2%), moderate class covers 32.9 km² (29.6%), high class covers 23.6 km² (21.2%), and very high class covers 8.3 km² (7.5%) (Figure 6).

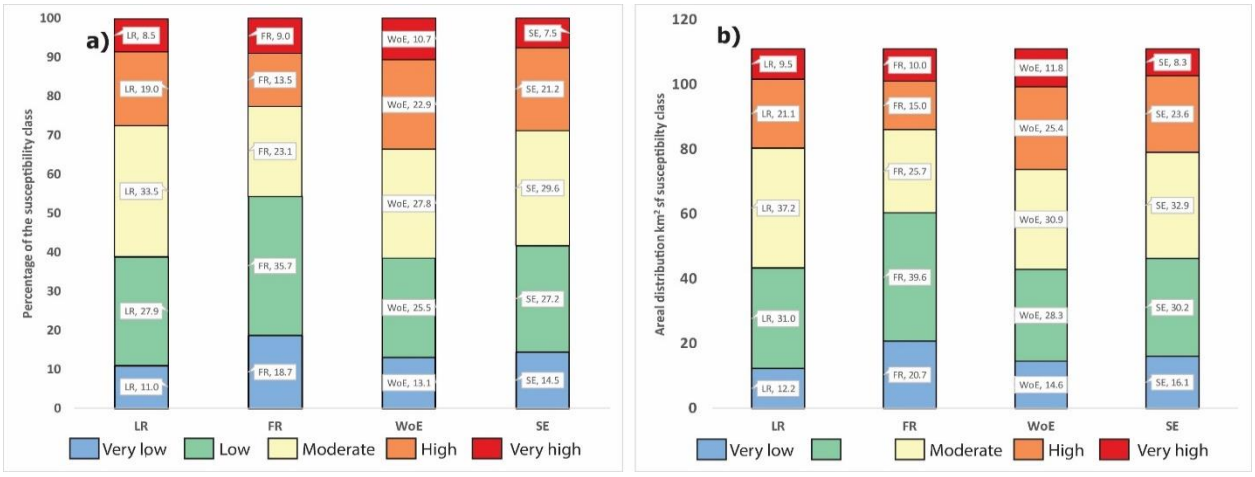

Figure 6- a) The percentage soil erosion susceptibility classes in different models (%), b) The area erosion susceptibility classes in different models (km^2)

3.2. Susceptibility model evaluation and comparison

The performance of the resulting erosion susceptibility models was assessed using the ROC curve and AUC (Du et al. 2017). The AUC value is commonly categorized as follows, and the resulting numbers offer a crucial indication of the model's validity and accuracy. A result falls into one of five categories: poor (0.5–0.6), fair (0.6–0.7), good (0.7–0.8), very good (0.8–0.9), and excellent (0.9–1.0) (Rahmati et al. 2016). As the ROC curve approaches 1, it indicates the presence of a prediction model with perfect accuracy, while moving away from 1 generally signifies a decrease in overall model accuracy (Nkonge et al. 2023). In this study, the performances of susceptibility models created based on different statistical methods were evaluated using both training and test datasets (Figure 7). According to result of the ROC and AUC values, Logistic regression seems to perform well on both training (AUC: 94.7) and validating datasets (AUC: 93.5), with slightly higher performance on the training set compared to the testing set. This indicates that the model might be slightly overfitting the training data, but the drop in performance from training to testing is not substantial and LR result correspond to “excellent” range, demonstrating high predictive accuracy and validity. Weight of Evidence performs consistently on both training (AUC: 93.5) and testing datasets (AUC 91.4), but it shows slightly lower performance compared to Logistic Regression, especially on the validating set. Frequency Ratio performs well, similar to Weight of Evidence and Logistic Regression, but slightly lower than Logistic Regression. It also exhibits consistent performance on both training (AUC: 93.5) and testing datasets (AUC: 92.4) also shows that “excellent” category. These values indicating that it is an effective model for erosion susceptibility prediction. Frequency Ration (FR) shows similar and close results to the WoE method. These values are high for both training and test data. Although it is lower compared to the LR method, it falls within the "excellent" category. In this context, the FR method Training AUC (93.5) and testing AUC (91.4) has yielded good results for the applicability of the soil erosion susceptibility model. Shannon's Entropy shows significantly lower performance compared to the other methods on both training (AUC: 55.7), testing datasets (AUC: 56.3) also indicated that “poor” category. These low values SE is not effectively capturing the patterns needed to predict erosion susceptibility. The AUC values close to 0.5 suggest that this model’s prediction is only slightly better than random guessing, confirming that it is not possible to use for this basin and areas. This suggests that the model built using Shannon's Entropy might not be capturing the underlying patterns effectively. Because, Shannon's Entropy may not be the most appropriate method for modeling erosion susceptibility in your specific study area. The entropy-based model might be too simplistic or fail to capture complex interactions among environmental factors like topography, land use, or soil properties that contribute to erosion. If the data does not exhibit enough "randomness" or variability in relation to erosion patterns, entropy may not be able to generate meaningful insights.

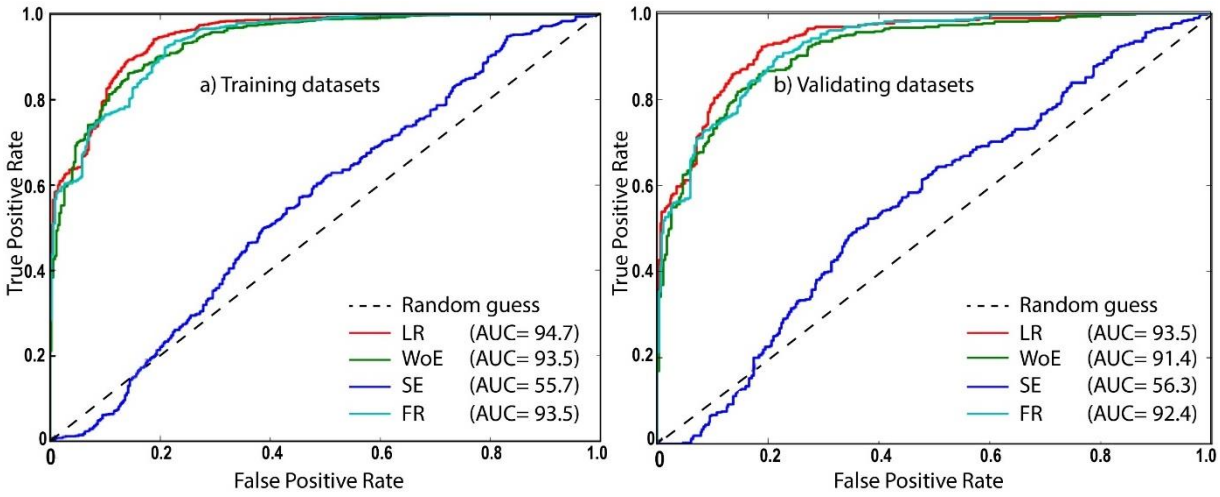

Figure 7- Prediction and success rates of the different susceptibility models based on a) training datasets b) validating datasets

4. Discussion

Due to environmental factors and human activities, the frequency of natural disasters in recent years has increased, and this can lead to loss of life, resources and property (He et al. 2012; Chen et al. 2017). The most common of these is soil erosion. Erosion events have directly and indirectly caused many negative problems, and they are quite diverse. These effects include increased sediment transport, damage to vegetation, soil degradation and the failure of surface water to flow into groundwater. As sediment transport increases and riverbeds fill, inevitable events such as floods and inundations occur. In addition, it results in water pollution and habitat destruction. Soil loss due to erosion restricts the habitat and root system of the vegetation (Sterk, 2003; Podhrazska et al. 2015; Duniway et al. 2019; Saxena, 2021). Therefore, in natural disaster studies, it is very important to take the necessary precautions and make critical planning in case past events recur in the future. Despite efforts to prevent these events, it is important to make inferences about possible future situations or to model them in order to prevent them effectively. Therefore, sensitivity models are developed to take necessary precautions and minimize possible hazards and risks and to reduce erosion and especially desertification risks (Morgan & Nearing, 2016; Batista et al. 2019). However, due to the various

lithological, climatic and geomorphological characteristics of different regions, the suitability of these models varies. Therefore, it is important to test different methods and approaches in a specific area to determine the most suitable model.

In this study, sensitivity modelling was carried out to understand the advanced erosion status in the Çapakçur River basin. According to the literature and multicollinearity analysis, nineteen conditioning factors (elevation, distance to river, distance to road, TWI, TRI, SPI, slope, geomorphology, distance to lineament, LS, LU, NDVI, plan curvature, profile curvature, curvature, positive openness, precipitation, flow accumulation and aspect) (Table 2) and four different methods (LR, FR, WoE and SE) were used to determine the sensitivity and model performances were measured using ROC curves and AUC values to determine the most suitable model (Xu et al. 2012; Demir et al. 2022; Jaafari et al. 2014; Ding et al. 2017; Bhandari et al. 2024).

Logistic Regression shows the highest performance among the methods, both on training and testing datasets, indicating its robustness in capturing the relationship between the predictors and the target variable. LR is a widely used model for classification, especially for binary classification problems (Kleinbaum et al. 2002). Therefore, to obtain a better classifier, WoE and FR models were also included to determine the sensitivity (Chen et al. 2019). Weight of Evidence and Frequency Ratio also perform reasonably well, with consistent performance across training and testing datasets. Shannon's Entropy performs noticeably worse than the other approaches, indicating that it may not be appropriate for this specific purpose or that it may need to be implemented more precisely. In summary, Shannon's Entropy performs noticeably worse than Logistic Regression, which looks to be the best approach for this erosion susceptibility mapping problem. Other methods that perform well include Frequency Ratio and Weight of Evidence. The efficacy of Logistic Regression in mapping erosion susceptibility is highlighted by its good performance in capturing the connection between predictors and the target variable. Furthermore, the trustworthiness of Frequency Ratio and Weight of Evidence as alternative modeling methodologies is highlighted by their constant performance.

5. Conclusions

Many statistical methods are used in earth science studies, especially in performing sensitivity analyses using computer technologies and modern techniques. In addition to these, there are actively preferred and extremely popular methods. These methods include deep learning, machine learning, artificial intelligence and different techniques produced depending on them. Thus, it plays an important role in evaluating the results obtained from many methods used and taking the necessary planning and precautions (Baiddah et al. 2023).

In this study, erosion sensitivity analysis was conducted in the Çapakçur River basin, which is critical in terms of erosion. Logistic regression (LR), frequency ratio (FR), weight of evidence (WoE), and Shannon's entropy methods were used in conducting sensitivity analysis in the study area. Within the scope of sensitivity analysis, 19 methods were utilized, and it was decided to use 16 conditioning factors based on multicollinearity assessment method based on VIF and Tolerance values. These factors include topographic, climatic, anthropogenic, and environmental factors. Based on the results obtained in this study, it has been determined that the most efficient methods are Logistic Regression and Frequency Ratio, as well as the Weight of Evidence method. Dependent on these methods, erosion susceptibility models can be developed in river basins with similar lithological, geomorphological, and climatic characteristics. Consequently, measures and plans can be made to prevent the progression of existing erosion in both large and small-scale basins, based on the results of erosion susceptibility models.

Also, these erosion susceptibility models provide valuable tools for authorities and policymakers to effectively address erosion issues and mitigate associated negative impacts such as sediment transport, soil degradation, and habitat destruction. By identifying areas sensitive to erosion, authorities can prioritize targeted interventions and implement appropriate land management practices to minimize erosion risks. In the future, research could explore both the integration of advanced machine learning techniques and remote sensing data to improve the accuracy and predictive capabilities of erosion susceptibility models using high resolution topographic, climatic datasets. Furthermore, incorporating real-time monitoring data and climate projections can offer insights into evolving erosion patterns and support proactive erosion prevention strategies.

Ethics Statement: There is no study in this study that requires permission from the ethics committee.

Availability of data and materials: Data will be available on request.

Ethics approval: All authors have read, understood, and have complied as applicable with the statement on “Ethical responsibilities of Authors” as found in the Instructions for Authors. Not applicable.

Consent to participate: Not applicable.

Consent for publication: Not applicable.

Competing interests: The authors declare no competing interests.

References

Ait Neceur H, Abdo H G, Igmoullan B, Namous M, Alshehri F & A Albanai J (2024). Implementation of random forest, adaptive boosting, and gradient boosting decision trees algorithms for gully erosion susceptibility mapping using remote sensing and GIS. Environmental Earth Sciences 83(3): 121 https://doi.org/10.1007/s12665-024-11424-5

Akgün A (2007). Ayvalık ve yakın çevresinin erozyon ve heyelan duyarlılığının Coğrafi Bilgi Sistemleri tabanlı incelenmesi. *Doktora Tezi, Dokuz Eylül Üni. Fen Bilimleri Ens*. İzmir.

Akıncı H, Özalp A Y & Kılıçer S T (2015). Assessment of landslide susceptibility in planned areas using geographic information systems and AHP method: Artvin Example. Journal of Natural Hazards and Environment 1(1-2): 40-53 (In Turkish)

Akıncı H, Doğan S & Kılıçoğlu C (2017). Landslide susceptibility mapping of Canik (Samsun) district using bayesian probability and frequency ratio models. *Selcuk University Journal of Engineering Science and Technology* 5(3): 283- 299 https://doi.org/10.15317/scitech.2017.89

Al-Hinai H & Abdalla R (2021). Mapping Coastal Flood Susceptible Areas Using Shannon's Entropy Model: The Case of Muscat Governorate, Oman. *ISPRS Int J Geo-Information* 10: 252. https://doi.org/10.3390/ijgi10040252

Amiri M, Pourghasemi H R, Ghanbarian G A & Afzali S F (2019). Assessment of the importance of gully erosion effective factors using Boruta algorithm and its spatial modeling and mapping using three machine learning algorithms. *Geoderma* 340: 55–69. https://doi.org/10.1016/j.geoderma.2018.12.042

Anabalagan R (1992). Landslide hazard evaluation and zonation mapping in mountainous terrain. Eng Geol 32: 269–277. https://doi.org/10.1016/0013-7952(92)90053-2

Anonymous (1998). Management of Agricultural and Pasture Lands. National Environmental Action Plan. DTP, Ankara. (In Turkish)

Anonymous (1987). Türkiye General Soil Management Planning. Ministry of Agriculture, Forestry and Rural Affairs, General Directorate of Rural Services. Ankara. (In Turkish)

Arabameri A, Chen W, Loche M, Zhao X, Li Y, Lombardo L & Bui DT (2020). Comparison of machine learning models for gully erosion susceptibility mapping. Geoscience Frontiers, 11(5): 1609-1620. https://doi.org/10.1016/j.gsf.2019.11.009

Avcıoğlu A, Görüm T, Akbaş A, Moreno-de las Heras M, Yıldırım C & Yetemen Ö (2022). Regional distribution and characteristics of major badland landscapes in Turkey. Catena, 218, 106562. https://doi.org/10.1016/j.catena.2022.106562

Bag R, Mondal I, Dehbozorgi M, Bank S P, Das D N, Bandyopadhyay J & Nguyen X C (2022). Modelling and mapping of soil erosion susceptibility using machine learning in a tropical hot sub-humid environment. *Journal of Cleaner Production* 364: 132428. https://doi.org/10.1016/j.jclepro.2022.132428

Baiddah A, Krimissa S, Hajji S, Ismaili M, Abdelrahman K & El Bouzekraoui M (2023). Head-cut gully erosion susceptibility mapping in semi-arid region using machine learning methods: insight from the high atlas, Morocco. *Frontiers in Earth Science*, *11*. https://doi.org/10.3389/feart.2023.1184038

Batista P V, Davies J, Silva M L & Quinton J N (2019). On the evaluation of soil erosion models: Are we doing enough?. *Earth-Science Reviews* 197: 102898. https://doi.org/10.1016/j.earscirev.2019.102898

Beven K J & Kirkby M J (1979) A physically based, variable contributing area model ofbasin hydrology/Un modèle à base physique de zone d'appel variable de l'hydrologie du bassin versant. Hydrol Sci J 24(1):43–69. https://doi.org/10.1080/02626667909491834

Bhandari B P, Dhakal S & Tsou C Y (2024). Assessing the Prediction Accuracy of Frequency Ratio, Weight of Evidence, Shannon Entropy, and Information Value Methods for Landslide Susceptibility in the Siwalik Hills of Nepal. *Sustainability*, *16*(5), 2092. https://doi.org/10.3390/su16052092

Bonham Carter G F (1994). Geographic Information Systems for geoscientists, Modeling with GIS. *Pergamon Press*, Oxford.

Bouamrane A, Boutaghane H, Bouamrane A, Dahri N, Abida H, Saber M, Kantoush S A & Sumi T (2024). Soil erosion susceptibility prediction using ensemble hybrid models with multicriteria decision-making analysis: Case study of the Medjerda basin, northern Africa. International Journal of Sediment Research. https://doi.org/10.1016/j.ijsrc.2024.08.003

Carrara A, Cardinali M, Detti R, Guzzetti F, Pasqui V & Reichenbach P (1991). GIS techniques and statistical models in evaluating landslide hazard. Earth Surf Processes and Landforms. 16(5): 427-445. https://doi.org/10.1002/esp.3290160505

Çevik E & Topal T (2003). GIS-based landslide susceptibility mapping for a problematic segment of the natural gas pipeline, Hendek (Turkey). *Environmental Geology* 44 (8): 949-962 https://doi.org/10.1007/s00254-003-0838-6

Chakrabortty R, Pal S C, Sahana M, Mondal A, Dou J, Pham B T & Yunus A P (2020). Soil erosion potential hotspot zone identification using machine learning and statistical approaches in eastern India. Natural hazards. https://doi.org/10.1007/s11069-020-04213-3

Chalise D, Kumar L, Spalevic V & Skataric G (2019). Estimation of sediment yield and maximum outflow using the IntErO model in the sarada river basin of Nepal. Water 11: 952. https://doi.org/10.3390/w11050952.

Chen W, Panahi M & Pourghasemi H R (2017). Performance evaluation of GIS-based new ensemble data mining techniques of adaptive neuro-fuzzy inference system (ANFIS) with genetic algorithm (GA), differential evolution (DE), and particle swarm optimization (PSO) for landslide spatial modelling. *Catena* 157: 310-324

Chen W, Sun Z & Han J (2019). Landslide susceptibility modeling using integrated ensemble weights of evidence with logistic regression and random forest models. Applied sciences 9(1): 171. https://doi.org/10.3390/app9010171

Choubin B, Rahmati O, Tahmasebipour N, Feizizadeh B & Pourghasemi H R (2019). Application of fuzzy analytical network process model for analyzing the gully erosion susceptibility. In *Advances in Natural and Technological Hazards Research* (Vol. 48, pp. 105–125). Springer Netherlands. https://doi.org/10.1007/978-3-319-73383-8_5

Conforti M, Aucelli P P C, Robustelli G & Scarciglia F (2011). Geomorphology and GIS analysis for mapping gully erosion susceptibility in the Turbolo stream catchment (Northern Calabria, Italy). *Natural Hazards* 56(3): 881–898. https://doi.org/10.1007/s11069-010-9598-2

Conoscenti C, Agnesi V, Angileri S, Cappadonia C, Rotigliano E & Märker M (2013). A GIS-based approach for gully erosion susceptibility modelling: a test in Sicily, Italy. *Environ Earth* 70: 1179–1195. https://doi.org/10.1007/s12665-012-2205-y

Conoscenti C, Di Maggio C & Rotigliano E (2008). Soil erosion susceptibility assessment and validation using a geostatistical multivariate approach: a test in Southern Sicily. Natural hazards 46: 287-305. https://doi.org/10.1007/s11069-007-9188-0

Corsini A, Cervi F & Ronchetti F (2009). Weight of evidence and artificial neural networks for potential groundwater spring mapping: an application to the Mt. Modino area (Northern Apennines, Italy). *Geomorphology*, 111(1-2), 79- 87). doi: 10.1016/j.geomorph.2008.03.015

Dai F C & Lee C F (2002). Landslide characteristics and slope instablity modelling using GIS, Lantau Island, Hong Kong. *Geomorphology* 42: 213-228

Dai F C, Lee C F, Li J & Xu Z W (2001). Assessment of landslide susceptibility on the natural terrain of Lantau Island, Hong Kong. *Environmetal Geology* 40(3): 381-391

Danacıoğlu Ş & Tağıl Ş (2017). Assessment of Erosion Risk in Bakırçay Basin Using Rusle Model. *Journal of Balıkesir University Social Sciences Institute* 20(37) (in Turkish)

Demir Y, Meral A & Doğan Demir A (2022). Estimation of Soil Losses in Çapakcur Watershed (Bingol, Turkey) Using RUSLE Method and Comparison of Predicted Soil Losses with Sediment Yield. *Kahramanmaraş Sütçü İmam University Journal of Agriculture and Nature*, 25(Supplement Issue 2) 523–537. https://doi.org/10.18016/ksutarimdoga.vi.1059631 (In Turkish)

Dengiz O, İmamoğlu A, Saygın F, Göl C, Ediş S & Doğan A (2014). Soil erosion risk assessment of Inebolu basin with icona model. *Anatolian Journal of Agricultural Sciences* 29(2): 136-142. doi: 10.7161/anajas.2014.29.2.136-14 (In Turkish)

Dengiz O, Öztaş T, Haliloğlu M & Şahin K (2020). Balancing of Land Degradation. Turkish Agricultural Engineering IX.Technical Congress. 81-104 (In Turkish)

Ding Q, Chen W & Hong H (2017). Application of frequency ratio, weights of evidence and evidential belief function models in landslide susceptibility mapping. Geocarto international, 32(6): 619-639. https://doi.org/10.1080/10106049.2016.1165294

Doneus M (2013). Openness as visualization technique for interpretative mapping of airborne lidar derived digital terrain models. *Remote Sens* 5: 6427–6442. https://doi.org/10.3390/rs5126427

Dramis F & Gentili B (1977). Contributo allo studio delle acclività dei versanti nell'appennino umbro-marchigiano. *Studi Geologici Camerti* 3: 153-164

Du G L, Zhang Y S, Iqbal J, Yang Z H & Yao X (2017). Landslide susceptibility mapping using an integrated model of information value method and logistic regression in the Bailongjiang watershed, Gansu Province, China. *Journal of Mountain Science* 14: 249-268. https://doi.org/10.1007/s11629-016-4126-9

Duniway M C, Pfennigwerth A A, Fick S E, Nauman T W, Belnap J & Barger N N (2019). Wind erosion and dust from US drylands: a review of causes, consequences, and solutions in a changing world. Ecosphere, 10(3), e02650. https://doi.org/10.1002/ecs2.2650

El Miloudi Y, El Kharim Y, Bounab A & El Hamdouni R (2024). Effect of Rockfall Spatial Representation on the Accuracy and Reliability of Susceptibility Models (The Case of the Haouz Dorsale Calcaire, Morocco). *Land*, *13*(2). https://doi.org/10.3390/land13020176

Fick S E & Hijmans R J (2017). WorldClim 2: new 1-km spatial resolution climate surfaces for global land areas. *Int J Climatol* 37:4302–4315. https://doi.org/10.1002/joc.5086

Foumelis M, Lekkas E & Parcharidis I (2004). Landslide susceptibility mapping by GIS-based qualitative weighting procedure in Corinth area. Bulletin of the Geological Society of Greece XXXVI, 904– 912. In: Proceedings of the 10th international congress, Thes- saloniki, April 2004

Garosi Y, Sheklabadi M, Pourghasemi H R, Besalatpour A A, Conoscenti C & Van Oost K (2018). Comparison of differences in resolution and sources of controlling factors for gully erosion susceptibility mapping. *Geoderma* 330: 65–78. https://doi.org/10.1016/j.geoderma.2018.05.027

Gayen A & Saha S (2017). Application of weights-of-evidence (WoE) and evidential belief function (EBF) models for the delineation of soil erosion vulnerable zones: a study on Pathro river basin, Jharkhand, India. *Modeling Earth Systems and Environment*, *3*(3), 1123–1139. https://doi.org/10.1007/s40808-017-0362-4

Graham M H (2003). Confronting Multicollinearity In Ecological Multiple Regression. Ecology 84:2809–2815. https://doi.org/10.1890/02-3114

Güney Y (2018). Use of frequency ratio method in erosion susceptibility analysis: Selendi Stream Basin (Manisa) example. *Journal of Soil Science and Plant Nutrition* 6(2): 73-85. (In Turkish)

Guzzetti F, Carrara A, Cardinali M & Reichenbach P (1999). Landslide hazard evaluation: a review of current techniques and their application in a multi-scale study, Central Italy. Geomorphology 31 (1-4): 181-216. https://doi.org/10.1016/s0169-555x(99)00078-1

Haan C T, Barfield B J & Hayes J C (1994). Design Hydrology and Sedimentology For Small Catchments. Academic Press An Imprint of Elseiver New York 38-101

Habib M (2021). Quantifying topographic ruggedness using principal component analysis. Advances in Civil Engineering, 1-20. https://doi.org/10.1155/2021/3311912

He S, Pan P, Dai L, Wang H & Liu J (2012). Application of kernel-based Fisher discriminant analysis to map landslide susceptibility in the Qinggan River delta, Three Gorges, China. Geomorphology, 171: 30-41. https://doi.org/10.1016/j.geomorph.2012.04.024

Hembram T, Paul G C & Saha S (2019). Spatial prediction of susceptibility to gully erosion in Jainti River basin, Eastern India: a comparison of information value and logistic regression models. *Modeling Earth Systems and Environment* 5(2): 689–708. https://doi.org/10.1007/s40808-018-0560-8

Hembram T K, Paul G C & Saha S (2020). Modelling of gully erosion risk using new ensemble of conditional probability and index of entropy in Jainti River basin of Chotanagpur Plateau Fringe Area, India. Appl Geomatics 12:337–360. https://doi.org/10.1007/s12518-020-00301-y

İDEP (2012). Climate Change National Action Plan 2011-2023, Ministry of Environment and Urbanization, Ankara. (In Turkish)

İnik O (2022). Negative Effects of Land Degradation on Human Life. "Innovative Methods, Theories and Applications in Health Sciences". Iksad Publications.ISBN: 978-625-8213-40-9. Ankara. (In Turkish)

İnik O (2023). Investigation of Land Degradation Balancing Studies in Çapakçur Microcatchment of Bingöl Province. Atatürk University, Institute of Science. (Doctoral Thesis) (In Turkish)

İnik O, İnik Ö, Öztaş T & Yüksel A (2022). Soil Temperature Prediction with Long Short Term Memory (LSTM). Turkish Journal of Agriculture and Natural Sciences , 9(3): 779-785. https://doi.org/10.30910/turkjans.1101753

Islam S, Tahir M & Parveen S (2022) GIS-based flood susceptibility mapping of the lower Bagmati basin in Bihar, using Shannon's entropy model. Model Earth Syst Environ 8:3005–3019. https://doi.org/10.1007/s40808-021-01283-5

Jaafari A, Najafi A, Pourghasemi H R, Rezaeian J & Sattarian A (2014). GIS-based frequency ratio and index of entropy models for landslide susceptibility assessment in the Caspian forest, northern Iran. *International Journal of Environmental Science and Technology* 11: 909-926. https://doi.org/10.1007/s13762-013-0464-0

Jasiewicz J & Stepinski T F (2013). Geomorphology 182: 147-156. ScienceDirect

Jenks G (1967). The Data Model Concept in Statistical Mapping. In *International Yearbook of Cartography* (pp. 7:186-190)

Jenks G F (1967). The data model concept in statistical mapping. International Yearbook of Cartography 7: 186–190

Kakembo V, Xanga W W & Rowntree K (2009). Topographic thresholds in gully development on the hillslopes of communal areas in Ngqushwa Local Municipality, Eastern Cape, South Africa. Geomorphology 110:188–194. https://doi.org/10.1016/j.geomorph.2009.04.006

Karagöz A, Doğan O, Erpul G, Dengiz O, Sönmez B, Tekeli İ, Saygın S D & Madenoğlu S (2015). Evaluation of the Possible Effects of Desertification, Drought and Erosion in Turkey. Proceedings Book of the 8th Turkish Agricultural Engineering Technical Congress-1, 118. (In Turkish)

Kelava A, Moosbrugger H, Dimitruk P & Schermelleh-Engel K (2008). Multicollinearity and Missing Constraints. Methodology 4:51–66. https://doi.org/10.1027/1614-2241.4.2.51

Kheir R B, Abdallah C & Khawlie M (2008). Assessing soil erosion in Mediterranean karst landscapes of Lebanon using remote sensing and GIS. Engineering Geology, 99(3-4): 239-254. https://doi.org/10.1016/j.enggeo.2007.11.012

Kılıçoğlu C (2020). Production of landslide susceptibility map of Vezirköprü district of Samsun province using frequency ratio method and bayesian probability model. Afyon Kocatepe University Journal of Science and Engineering Sciences, 20(1), 138-154 (In Turkish)

Kleinbaum D G, Dietz K, Gail M, Klein M & Klein M (2002). Logistic regression (p. 536). New York: Springer-Verlag.

Lana J C, Castro P D T A & Lana C E (2022). Assessing gully erosion susceptibility and its conditioning factors in southeastern Brazil using machine learning algorithms and bivariate statistical methods: A regional approach. Geomorphology, 402, 108159. https://doi.org/10.1016/j.geomorph.2022.108159

Lei X, Chen W, Avand M, Janizadeh S, Kariminejad N, Shahabi H, Costache R, Shahabi H, Shirzadi A & Mosavi A (2020). GIS-based machine learning algorithms for gully erosion susceptibility mapping in a semi-arid region of Iran. Remote Sensing, 12(15): 2478. https://doi.org/10.3390/rs12152478

Lin J (1991). Divergence measures based on the Shannon entropy. IEEE Trans Inf Theory 37:145–151. https://doi.org/10.1109/18.61115

Maharaj R J (1993). Landslide processes and landslide susceptibility analysis from an Upland Watershed: a case study from St Andrew, Jamaica, West Indies. Engineening Geology 34 (1-2): 53-79. https://doi.org/10.1016/0013-7952(93)90043-c

Miao F, Zhao F, Wu Y, Li L & Török Á (2023). Landslide susceptibility mapping in Three Gorges Reservoir area based on GIS and boosting decision tree model. Stochastic Environmental Research and Risk Assessment, 37(6): 2283-2303. https://doi.org/10.1007/s00477-023-02394-4

Mohammed S, Al-Ebraheem A, Holb I J, Alsafadi K, Dikkeh M, Pham Q B, Linh N T T & Szabo S (2020). Soil management effects on soil water erosion and runoff in Central Syria—a comparative evaluation of general linear model and random forest regression. Water 12, 2529. https://doi.org/10.3390/w12092529.

Moore I & Burch G (1986). Physical Basis of the Length – slope Factor in the Universal Soil Loss Equation. *Soil Science Society of America Journal* 50: 1294-1298

Morgan R P C & Nearing M (2016). Handbook of erosion modelling. John Wiley & Sons.

Nagarajan R, Roy A, Vinod Kumar R, Mukherjee A & Khıre M V (2000). Landslide hazard suspectibility mapping based on terrain and climatic factors for tropical monsoon regions. Bulletin Engineering Geology and the Environment 58(4): 275-287. https://doi.org/10.1007/s100649900032

Neuhauser B & Terhorst B (2007). Landslide susceptibility assessment using "weights-of-evidence" applied to a study area at the Jurassic escarpment (SW-Germany). Geomorphology 86(1-2): 12-24. https://doi.org/10.1016/j.geomorph.2006.08.002

Nikolova V, Mitova M & Dimitrov E (2022). Topographic factor of water erosion–analysis of watershed morphometry and RUSLE LS factor in GIS environment. *Review of the Bulgarian Geological Society* 83(1): 3-14. https://doi.org/10.52215/rev.bgs.2022.83.1.3

Nkonge L K, Gathenya J M, Kiptala J K, Cheruiyot C K & Petroselli A (2023). An Ensemble of Weight of Evidence and Logistic Regression for Gully Erosion Susceptibility Mapping in the Kakia-Esamburmbur Catchment, Kenya. Water (Switzerland), 15(7). https://doi.org/10.3390/w15071292

Nkonge L K, Gathenya J M, Kiptala J K, Cheruiyot C K & Petroselli A (2023). An Ensemble of Weight of Evidence and Logistic Regression for Gully Erosion Susceptibility Mapping in the Kakia-Esamburmbur Catchment, Kenya. *Water (Switzerland)* 15(7): https://doi.org/10.3390/w15071292

Ogbonna J U, Alozie M, Nkemdırım V & Eze M U (2011). GIS analysis for mapping gully erosion impacts on the geo-formation of the Old Imo State, Nigeria. *ABSU Journal of Environment Science and Technology* 1: 48-61

Ohlmacher G C (2007) Plan curvature and landslide probability in regions dominated by earth flows and earth slides. Eng Geol 91:117–134. https://doi.org/10.1016/j.enggeo.2007.01.005

Öztürk D (2017). Investigation of Urban Sprawl with Shannon Entropy and Fractal Analysis: Samsun Example. 16th Turkey Scientific and Technical Congress on Mapping pp. 3-6. (In Turkish)

Öztürk M Z, Çetinkaya G & Aydın S (2017). Climate Types of Turkey According to Köppen-Geiger Climate Classification. *Journal of Geography*, 35: 17–27. https://doi.org/10.26650/jgeog295515

Peel M C, Finlayson B L & McMahon T A (2007). Updated world map of the Köppen-Geiger climate classification. *Hydrology and Earth System Sciences* 11(5): 1633–1644. https://doi.org/10.5194/hess-11-1633-2007

Podhrazska J, Kučera J, Karasek P & Konečná J (2015). Land Degradation by Erosion and Its Economic Consequences for the Region of South Moravia (Czech Republic). Soil & Water Research, 10(2). https://doi.org/10.17221/143/2014-swr

Pulice I, Scarcıglia, F, Leonardi L, Robustelli G, Conforti M, Cuscıno M, Lupiano V & Critelli S (2009). Studio multidisciplinare di forme e processi denudazionali Nell'area di Vrica (Calabria Orientale). Bollettino della Società Geografica Italiana. 87(I–II): 399-414.

Rahmati O, Haghizadeh A, Pourghasemi H R & Noormohamadi F (2016). Gully erosion susceptibility mapping: the role of GIS-based bivariate statistical models and their comparison. *Natural Hazards* 82(2): 1231–1258. https://doi.org/10.1007/s11069-016-2239-7

Rahmati O, Tahmasebipour N, Haghizadeh A, Pourghasemi H R & Feizizadeh B (2017). Evaluation of different machine learning models for predicting and mapping the susceptibility of gully erosion. *Geomorphology* 298: 118–137. https://doi.org/10.1016/j.geomorph.2017.09.006

Regmi N R, Giardino J R & Vitek J D (2010). Modeling susceptibility to landslides using the weight of evidence approach: Western Colorado, USA. Geomorphology, 115(1-2): 172-187. https://doi.org/10.1016/j.geomorph.2009.10.002

Roy J & Saha DS (2019). GIS-based Gully Erosion Susceptibility Evaluation Using Frequency Ratio, Cosine Amplitude and Logistic Regression Ensembled with fuzzy logic in Hinglo River Basin, India. Remote Sens Appl Soc Environ 15:100247. https://doi.org/10.1016/j.rsase.2019.100247

Różycka M, Migoń P & Michniewicz A (2017). Topographic Wetness Index and Terrain Ruggedness Index in geomorphic characterisation of landslide terrains, on examples from the Sudetes, SW Poland. Zeitschrift für geomorphologie, Supplementary issues 61(2): 61-80. https://doi.org/10.1127/zfg_suppl/2016/0328

Saxena S (2021). A study on causes and consequences of soil erosion. Asian Journal of Research in Business Economics and Management, 11(10): 100-105. https://doi.org/10.5958/2249-7307.2021.00036.0

Saygın S D (2013). Climate Change and Global Warming: What Awaits Us? Köy-Koop News, April, 2013 Page: 17. (In Turkish)

Sharma B & Pandey A (2022). Mapping of Erosion Hazard in and around Kharagpur Hills, Bihar using hydrological indices. In MOL2NET'22, Conference on Molecular, Biomed., Comput. & Network Science and Engineering. Basel, Switzerland: MDPI. https://doi.org/10.3390/mol2net-08-12638

Sharma L P, Patel N, Ghose M K & Debnath P (2012). Influence of shannon's entropy on landslide-causing parameters for vulnerability study and zonation-a case study in sikkim, india. *Arab J Geosci* 5: 421–431. https://doi.org/10.1007/s12517-010-0205-3

Stepinski T F & Jasiewicz J (2011). Geomorphometry Papers, Redlands pp. 109-112

Sterk G (2003). Causes, consequences and control of wind erosion in Sahelian Africa: a review. Land Degradation & Development, 14(1): 95-108. https://doi.org/10.1002/ldr.526

Tehrany M S, Pradhan B & Jebur M N (2013). Spatial prediction of flood susceptible areas using rule based decision tree (DT) and a novel ensemble bivariate and multivariate statistical models in GIS. Journal of Hydrology, 504: 69–79. https://doi.org/10.1016/j.jhydrol.2013.09.034

Trevisani S, Teza G & Guth P L (2023). Hacking the topographic ruggedness index. Geomorphology, 439: 108838. https://doi.org/10.1016/j.geomorph.2023.108838

UNCCD (2016). Science-Policy Notes. Balanced Lands-Balancing Land Degradation Scientific Concept Framework. 02 September 2016.).

Utlu M (2023). Flood Susceptibility Analysis of Ezine Stream Basin (Kastamonu-Bozkurt) Using Frequency Ratio and Shannon Entropy Method. *Journal of Geomorphological Research* pp. 160–178. https://doi.org/10.46453/jader.1358845 (In Turkish)

Valentin C, Poesen J & Li Y (2005). Gully erosion: Impacts, factors and control. Catena 63: 132–153. https://doi.org/10.1016/j.catena.2005.06.001

Van Westen C J, Rengers N & Soeters R (2003). Use of geomorphological information in indirect landslide susceptibility assessment, Natural Hazards 30(2003): 399-419. https://doi.org/10.1023/b:nhaz.0000007097.42735.9e

Wang F, Sahana M, Pahlevanzadeh B, Pal S C, Shit P K, Piran M J & Mosavi A (2021). Applying different resampling strategies in machine learning models to predict head-cut gully erosion susceptibility. *Alexandria Engineering Journal* 60(6): 5813-5829. https://doi.org/10.1016/j.aej.2021.04.026

Xu C, Xu X, Lee Y H, Tan X, Yu G & Dai F (2012). The 2010 Yushu earthquake triggered landslide hazard mapping using GIS and weight of evidence modeling. Environmental Earth Sciences 66: 1603-1616. https://doi.org/10.1007/s12665-012-1624-0

Yufeng S & Fengxiang J (2009). Landslide Stability Analysis Based on Generalized Information Entropy. 2009 International Conference on Environmental Science and Information Application Technology. IEEE, pp. 83–85

Yulianto F, Fitriana H L & Sukowati K A D (2020). Integration of remote sensing, GIS, and Shannon's entropy approach to conduct trend analysis of the dynamics change in urban/built-up areas in the Upper Citarum River Basin, West Java, Indonesia. Model Earth Syst Environ 6:383–395. https://doi.org/10.1007/s40808-019-00686-9

Zabihi M, Mirchooli F, Motevalli A, Darvishan A K, Pourghasemi H R, Zakeri M A & Sadighi F (2018). Spatial modelling of gully erosion in Mazandaran Province, northern Iran. Catena, 161: 1-13. https://doi.org/10.1016/j.catena.2017.10.010

Zabihi M, Pourghasemi H R, Motevalli A & Zakeri M A (2019). Gully erosion modeling using GIS-based data mining techniques in Northern Iran: a comparison between boosted regression tree and multivariate adaptive regression spline. *Advances in Natural and Technological Hazards Research*, 1-26. https://doi.org/10.1007/978-3-319-73383-8_1

Zhang Z, Xu W, Li L, Huang J, Deng, L & Wang Q (2021). Effects of temporal conservation measures on water erosion processes of disturbed soil accumulation in construction projects. *Journal of Cleaner Production*, 319, 128612. https://doi.org/10.1016/j.jclepro.2021.128612

Zhao J, Wang Z, Dong Y, Yang Z & Govers G (2022). How soil erosion and runoff are related to land use, topography and annual precipitation: Insights from a meta-analysis of erosion plots in China. Science of The Total Environment, 802, 149665. https://doi.org/10.1016/j.scitotenv.2021.149665

Zhu H, Tang G, Qian K & Liu H (2014). Extraction and analysis of gully head of Loess Plateau in China based on digital elevation model. *Chinese geographical science* 24: 328-338. https://doi.org/10.1007/s11769-014-0663-8

Zhuang Y, Du C, Zhang L, Du Y & Li S (2015). Research trends and hotspots in soil erosion from 1932 to 2013: A literature review. Scientometrics 10: 743–758. doi: 10.1007/s11192-015-1706-3

Journal of Agricultural Sciences
(Tarim Bilimleri Dergisi)

J Agr Sci-Tarim Bili
e-ISSN: 2148-9297
jas.ankara.edu.tr

Diagnosis of Paddy Diseases Using Pre-Trained Architectures and a Proposed Enhanced EfficientNetB3 Model

B Johnson[a*], Thangavel Chandrakumar[a]

[a]*Department of Applied Mathematics and Computational Science, Thiagarajar College of Engineering, Madurai 625015, Tamil Nadu, INDIA*

ARTICLE INFO
Research Article
Corresponding Author: B Johnson, E-mail: johnson.vaigai@gmail.com
Received: 18 September 2024 / Revised: 26 November 2024 / Accepted: 23 December 2024 / Online: 25 March 2025

Cite this article
Johnson B, Chandrakumar T (2025). Diagnosis of Paddy Diseases Using Pre-Trained Architectures and a Proposed Enhanced EfficientNetB3 Model. *Journal of Agricultural Sciences (Tarim Bilimleri Dergisi)*, 31(2):558-576. doi: 10.15832/ankutbd.1552013

ABSTRACT
Rice is an important crop in India and is often affected by pests and diseases, which can lead to a significant drop in production. This research investigates advanced deep learning approaches for accurate paddy disease diagnosis, focusing on comparing several transfer learning models. The study specifically targets diseases such as Tungro, Dead Heart, Hispa, Blast, Downy Mildew, Brown Spot, Bacterial Leaf Blight, Bacterial Panicle Blight, and Bacterial Leaf Streak. The base EfficientNetB3 model attains approximately 95.55 % accuracy during training and 95.12% during evaluation on unseen data. However, it encounters challenges when applied to domain-specific tasks such as diagnosing paddy diseases, frequently experiencing issues such as overfitting and inadequate convergence. To overcome these issues, an Enhanced EfficientNetB3 model was developed, incorporating batch normalization, dropout, and data regularization techniques. The training was conducted using the 'Paddy Doctor' dataset, featuring 10,407 high-resolution images of paddy leaves. It reached an accuracy of 98.92 % during training with a loss rate of 0.1385. For validation, the model reached an accuracy of 98.20 % and a loss rate of 0.1450. On an independent test set, the accuracy 98.50 % obtained with a test loss of 0.1505. With remarkable accuracy and a training time of just 68 minutes, the model demonstrates its significant potential for precise paddy disease diagnosis. Its impressive performance plays a crucial role in advancing disease management and boosting crop yields.

Keywords: Paddy Disease Detection, Transfer Learning, Enhanced EfficientNetB3, Deep Learning in Agriculture, Precision Agriculture, Image Classification

1. Introduction

Rice is a primary food globally; it is very important in ensuring the cultivation of rice with food security. However, paddy crops face numerous diseases that can severely impact both their yield and quality. Understanding and identifying the paddy crop diseases is vital for managing and control the paddy crop. Paddy leaves are susceptible to several significant diseases, such as hispa, blast, tungro, brown spot, downy mildew, dead heart, bacterial leaf streak, bacterial leaf blight, and bacterial panicle blight.

Blast is a highly damaging disease affecting rice, resulting from the fungal pathogen Magnaporthe oryzae. Under optimal conditions for its proliferation, it can cause substantial reductions in crop yield (Rahman et al. 2020; Dubey et al. 2024). Hispa, a pest-related issue, results in leaf damage that can reduce photosynthesis, ultimately affecting crop growth. Dead Heart is a symptom commonly associated with stem borers, which damage the stem and disrupt nutrient flow, leading to dead tillers (Deb et al. 2021). Tungro, a viral disease spread by green leafhoppers, causes stunted growth, reduced tillering, and yellow-orange leaf discoloration, significantly impacting rice yield (Yakkundimath et al. 2022). Brown Spot is another fungal disease that affects Paddy leaves, leading to lesions that can merge and cause extensive damage (Shah et al. 2023). Diseases such as Bacterial Leaf Blight, Downy Mildew, Bacterial Panicle Blight, and Bacterial Leaf Streak are also major concerns for rice cultivation, posing substantial risks to crop yields. These diseases are often characterized by leaf spots, streaks, and blight symptoms that reduce photosynthetic efficiency and weaken plants (Dogra et al. 2023). Timely identification and control of these diseases are essential to maintaining rice yields and safeguarding food security.

Deep learning approaches are now widely utilized for identifying and categorizing paddy diseases due to their effectiveness in analysing and learning from large datasets. Several models, such as Convolutional Neural Networks (CNNs), VGG-16, VGG-19, Inception-v1, ResNet-50, Inception-v3, DenseNet-121, Xception, along with the EfficientNetB2 and EfficientNetB3 architectures, have been explored for various tasks, each exhibiting unique performance levels and contributing to the advancements in the field (Liang et al. 2022; Yakkundimath et al. 2022; Simhadri et al. 2024). These models can examine

paddy leaf images to detect disease symptoms, making them highly effective for prompt diagnosis and management in advanced farming practices.

EfficientNetB3, a newer advancement within deep learning, provides notable enhancements in both accuracy and computational efficiency compared to conventional models. It employs a scaling technique that proportionally adjusts the depth, width, and resolution, resulting in improved performance for image recognition tasks (Li et al. 2022; Verma et al. 2024). To enhance the efficiency, EfficientNetB3's architecture is crafted to obtain high accuracy, making it well-suited for use in environments with restricted computational capacity (Bhujel & Shakya 2022).

This research contributes significantly to the field of paddy disease classification through several advancements:

- The study leverages pre-trained architectures, focusing particularly on the Enhanced EfficientNetB3 model, which effectively balances accuracy with computational efficiency.

- A comprehensive dataset comprising 10,407 images across 10 distinct paddy disease classes is utilized, addressing the limitations in dataset diversity found in prior studies.

- The classification model demonstrates notable performance, achieving an accuracy rate of 98.50% in disease detection, thereby establishing a new benchmark for precision in the field.

Given its advantages, EfficientNetB3 has been adapted to the task of predicting paddy leaf diseases, demonstrating superior accuracy and robustness in disease classification. Studies have shown that this model outperforms other deep learning architectures in terms of both speed and precision, particularly when identifying subtle differences between healthy and diseased paddy leaves (Li et al. 2022; Bhujel & Shakya 2022; Ganesan & Chinnappan 2022). This makes EfficientNetB3 an excellent option for building effective and dependable systems aimed at identifying and managing paddy diseases.

This study investigates leveraging pre-trained architectures and introduces an Enhanced EfficientNetB3 model for identifying paddy diseases. By harnessing the capabilities of EfficientNetB3, this approach seeks to offer a robust and efficient solution for the early identification of diseases, thereby assisting in the management and reduction of crop losses caused by rice diseases.

2. Material and Methods

2.1 Dataset

The dataset used in this research is the widely recognized Paddy Doctor Dataset, which is sourced from (https://www.kaggle.com/competitions/paddy-disease-classification), consisting of 30,000 images (Patil et al. 2023). This dataset includes 10 distinct classes of paddy leaf diseases, such as Dead Heart, Downy Mildew, Bacterial Leaf Streak, Brown Spot, Bacterial Panicle Blight, Tungro, Normal, Hispa, Bacterial Leaf Blight, and Blast. This dataset encompasses a broad spectrum of disease conditions, representing various stages of disease development, ranging from early to later stages. It also covers a variety of environmental conditions in which the images were captured, including differences in lighting, image angles, and the growth conditions of the plants. These factors contribute to the dataset's robustness, making it suitable for building models that are capable of generalizing to real-world agricultural scenarios. For visual illustration, Figure 1 presents sample images of different paddy diseases.

The initial dataset of 30,000 images underwent significant pre-processing steps, which involved cleaning, resizing to a uniform 480 x 640 pixels for enhanced computational efficiency, and removing images that were blurred or noisy. Following these pre-processing steps, the dataset was reduced to a more refined set of 10,407 high-quality images. From this processed dataset, 8,324 images were assigned for training, while 2,083 images were kept for testing purposes (Kumar et al. 2023). Table 1 outlines the specific distribution of images between the training and test sets.

In addition, the dataset is evenly distributed across various disease categories, ensuring that no single disease type dominates. This balanced distribution is vital for preventing model bias and guarantees that the trained model can effectively classify a wide range of paddy diseases. Such diversity and balance improve the model’s generalization capability, making it well-suited to handle varying disease conditions that may be encountered in real-world agricultural settings.

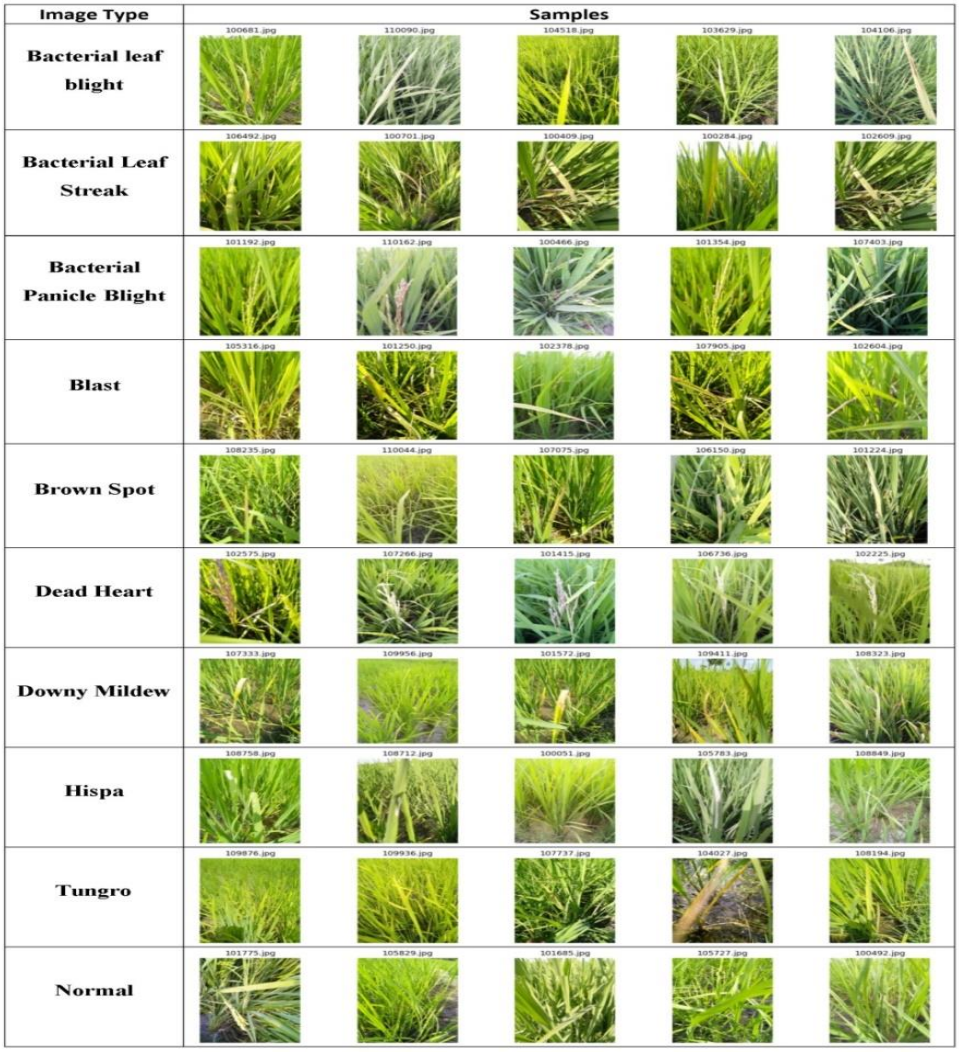

Figure 1- Sample Images of Paddy Diseases

Table 1- Training and Test Dataset Distribution

Disease Category	*Training Images*	*Test Images*
Normal	1411	353
Blast	1390	348
Hispa	1275	319
Dead Heart	1153	289
Tungro	870	218
Brown Spot	772	193
Downy Mildew	496	124
Bacterial Leaf Blight	383	96
Bacterial Leaf Streak	304	76
Bacterial Panicle Blight	270	67
Total	**8324**	**2083**

2.2 Models utilizing convolutional neural networks

The Convolutional Neural Network (CNN) is a widely recognized approach for tasks in natural language processing and image analysis, such as classifying paddy diseases. Its strength lies in its capability to autonomously detect and extract important features using convolutional and pooling layers. This process reduces the complexity of the data while retaining crucial

information. This process allows CNNs to manage complex patterns and enhance computational efficiency (Ozdemir 2024; Malvade et al. 2023; Ganesan et al. 2023)**.** When training CNNs for detecting paddy diseases, the model is exposed to images of healthy and diseased leaves, ultimately providing classifications based on the visual features observed. By leveraging such advanced techniques, farmers can more accurately diagnose and manage diseases affecting their crops, leading to improved agricultural practices and crop yields.

For classifying plant diseases, numerous studies were carried out using Convolutional Neural Networks (CNNs). For instance, Shah et al. (2023) conducted a comparative analysis of CNNs with other models, including Inception V3, VGG16, VGG19, and ResNet50. The authors previously discovered that CNNs achieve strong results in the timely detection of rice plant disorders and effectively distinguish between different leaf conditions. In another study, Liang et al. (2022) introduced an enhanced, lightweight CNN based on VGG16, tailored for paddy disease detection and classification, which achieved notable gains in both accuracy and efficiency. Yakkundimath et al. (2022) also demonstrated the application of CNN models for classifying paddy diseases, showcasing the adaptability of these models to different agricultural contexts. Dogra et al. (2023) also used CNN architecture to diagnose brown spot paddy disease.

Within the scope of this research work, the Enhanced EfficientNetB3 deep learning model was developed to diagnose paddy crop diseases. The effectiveness of this model was assessed by comparing it with several other pretrained deep learning models, including Xception, DenseNet-121, ResNet-50, Inception v1, Inception v3, VGG16, VGG19, as well as EfficientNetB2 and EfficientNetB3. This assessment aimed to gauge its accuracy in detecting and categorizing paddy diseases (Ozdemir et al. 2024).

2.2.1 VGG16

The deep convolutional neural network VGG16 has been effectively employed for image categorization and paddy disease diagnosis. This Oxford Visual Geometry Group model, featuring 16 layers with over half being convolutional, is recognized for its simplicity in architecture and effectiveness in feature extraction due to its use of 3 x 3 extension filters throughout the model. This design allows for the capture of small visual features, making VGG16 particularly suitable for paddy disease detection. Numerous studies have demonstrated VGG16's proficiency in paddy disease discrimination compared to other deep learning models. Notable works include Shah et al. (2023), Sun et al. (2023), Liang et al. (2022), and Gerdan et al. (2023), which highlight the model's efficacy across various agricultural datasets (Liang et al. 2022; Sun et al. 2023; Shah et al. 2023; Gerdan et al. 2023). Figure 2 depicts the VGG16 architecture.

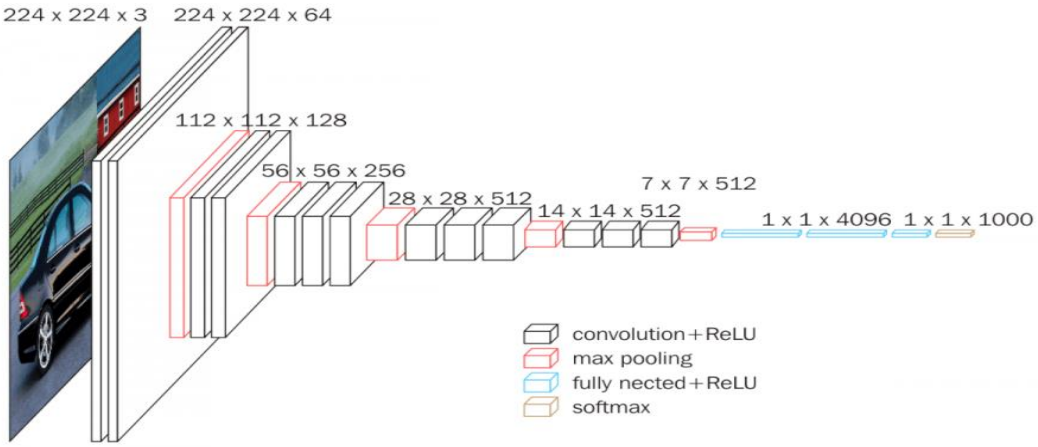

Figure 2- VGG16 architecture

2.2.2 VGG19

VGG19 is an advanced variant of the VGG16 model, incorporating 19 layers for enhanced image classification. This deeper architecture allows VGG19 to capture more intricate features from input images, which is especially advantageous for identifying subtle details in paddy leaf diseases. The model retains the use of small receptive fields with 3×3 filters, which helps preserve the spatial resolution throughout the network. This characteristic is crucial for applications in agriculture, such as precise disease identification in crops (Simonyan & Zisserman 2015). VGG19's effectiveness in paddy disease detection has been demonstrated in various studies applying deep learning techniques to agricultural datasets (Shah et al. 2023; Sun et al. 2023). The architecture of VGG19 is shown in Figure 3.

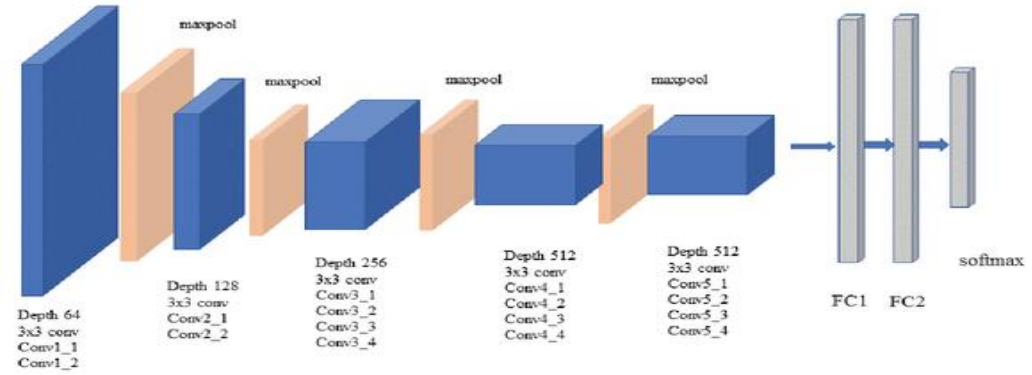

Figure 3- VGG19 architecture

2.2.3 Inception V1

The Inception V1 model is specifically designed to enhance performance in various image recognition and classification challenges. To improve the Inception V1 model's effectiveness with a plant disease image dataset, Particle Swarm Optimization (PSO) techniques are used to adjust and fine-tune the model's hyperparameters. This optimization process helps in achieving better accuracy and efficiency in disease identification (Liang et al. 2022). Using PSO has been demonstrated to markedly enhance the model's performance on unfamiliar datasets, including those related to plant diseases (Rahman et al. 2020). Additionally, deep learning models like Inception V1 have demonstrated their effectiveness in agricultural applications by enhancing disease classification and detection (Sun et al. 2023). Figure 4 shows the Inception V1 architecture.

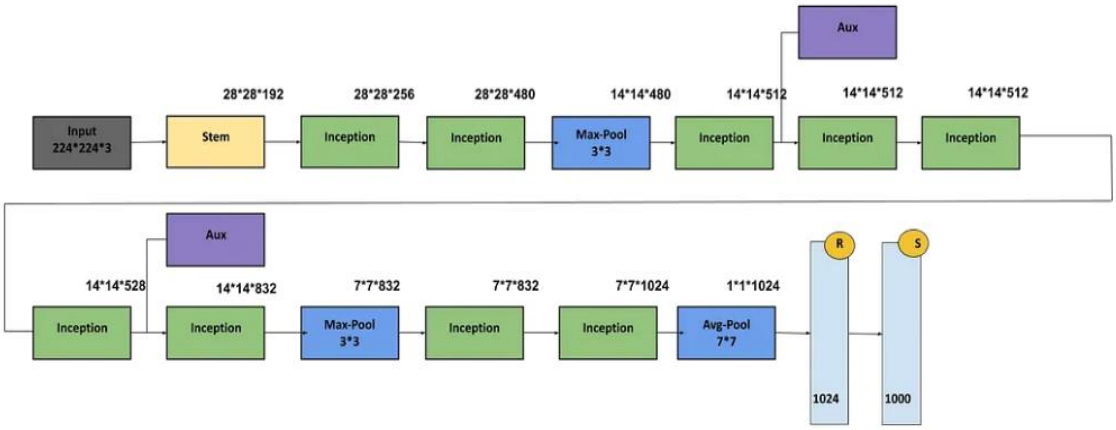

Figure 4- Inception V1 architecture

2.2.4 ResNet-50

The ResNet50 model, where "ResNet" stands for Residual Network, is based on a well-established design that includes fifty layers. This advanced image classification model excels in training with large datasets and achieving leading-edge results. The deep residual learning framework of ResNet50 enhances both feature extraction and classification performance, making it a favoured option for complex image recognition tasks. Research by Shah et al. (2023) and Razavi et al. (2024) has highlighted ResNet50's effectiveness in agricultural and plant disease classification, demonstrating its capability to manage detailed image data efficiently.

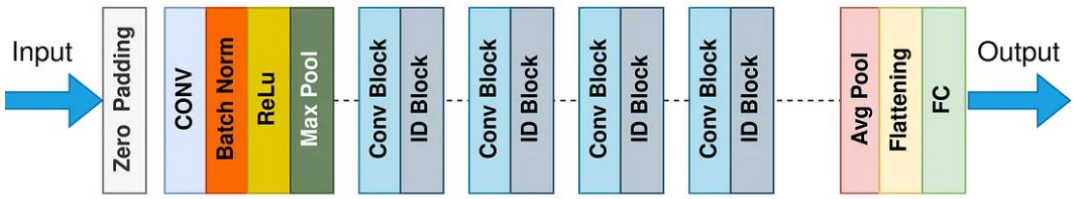

Figure 5- ResNet-50 architecture

2.2.5 Inception V3

The Inception V3 model is a pertained convolutional neural network (CNN) model trained with an extensive image dataset. To enhance its performance on plant disease images, the Particle Swarm Optimization (PSO) techniques are used to adjust and fine-tune the model's hyperparameters. It's a model from Google's Inception CNN series that features several techniques such as label smoothing, factorized 7x7 convolutions, BatchNorm in auxiliary classifiers, and the RMSProp Optimizer. This model is commonly used as a foundational architecture and for transfer learning in disease prediction research. The effectiveness of Inception V3 in plant disease classification is demonstrated by Shah et al. (2023) and Liang et al. (2022), highlighting its value in agricultural research. Figure 6 outlines the architecture of the Inception V3 model.

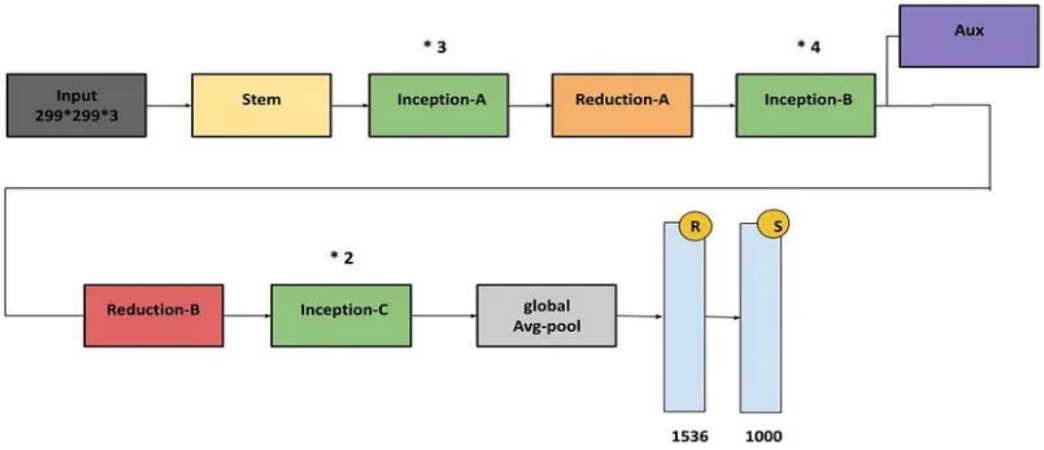

Figure 6- Inception V3 architecture

2.2.6 Densenet-121

The DenseNet121 variant, a notable version of this architecture, includes four dense blocks consisting of 6, 12, 24, and 16 layers in sequence. This architecture's dense connectivity enhances its ability to capture and learn complex features, which proves highly effective for paddy disease detection. The dense connectivity in DenseNet121 supports the extraction and learning of intricate features from paddy leaf images, facilitating the accurate identification of different paddy diseases and improving diagnostic precision. This capability is emphasized by Rahman et al. (2020) and Liu et al. (2022), who showcased how DenseNet models can be highly effective for detecting and classifying paddy diseases. Figure 7 depicts the architecture of DenseNet-121.

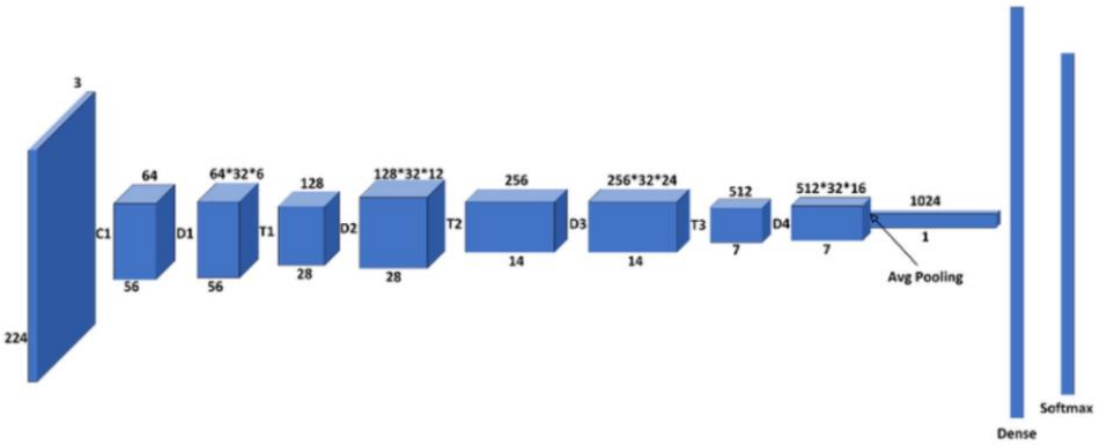

Figure 7- Densenet-121 architecture

2.2.7 Xception

The Xception model is an advanced deep convolutional neural network that utilizes depth wise separable convolutions to enhance the feature extraction process. Building on the Inception model, Xception aims to improve computational efficiency and model performance. Its application in agriculture, especially for detecting paddy diseases, is recognized for efficiently capturing intricate details from images. This capability is enhanced by its depth wise separable convolution layers, which

diminish the number of parameters, thereby minimizing the risk of overfitting—especially beneficial in resource-constrained environments such as smart agriculture systems (Meena et al. 2024). Additionally, the model's effectiveness in various agricultural applications has been documented by Rahman et al. (2020) and Sun et al. (2023), highlighting its robustness and adaptability. Figure 8 illustrates the architecture of Xception.

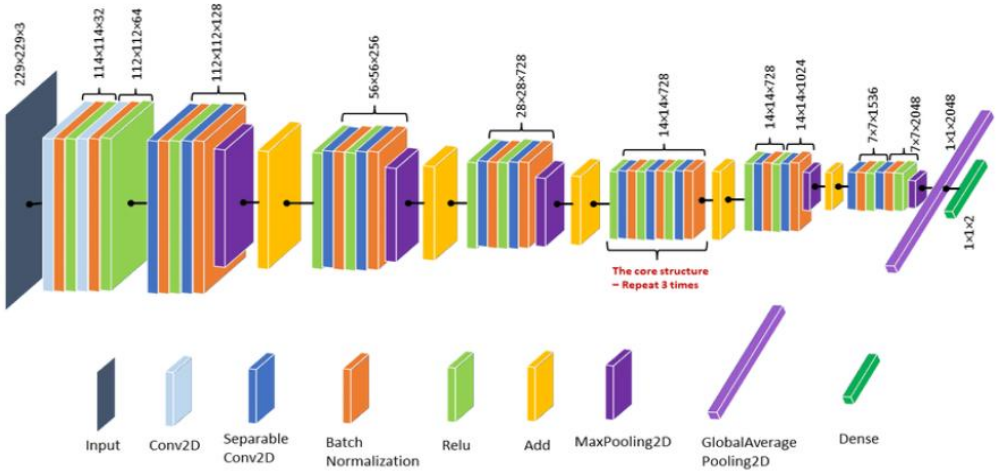

Figure 8- Xception architecture

2.3. Proposed EfficientNetB3 (Enhanced) CNN Model

With reference to (Mingxing and Quoc, 2019) the proposed CNN model EfficientNetB3 was developed. EfficientNetB3 stands out for its capability in feature extraction, attributed to the scaled-up enhancements from the original EfficientNetB0 architecture.

Model Overview

The proposed EfficientNetB3 model is known for its balance between accuracy and efficiency; it requires modifications for specific tasks like diagnosing paddy diseases. The original classification layer was omitted (include top=False), and a Global Average Pooling (GAP) layer was introduced to condense the spatial information from the feature maps into a compact vector. This modification is represented as

$$\bar{x} = \frac{1}{N} \cdot \sum_{i=1}^{N} x_i$$

Where; X_i is the input feature map, and N represents the number of spatial locations.

However, the base EfficientNetB3 model has limitations when applied to domain-specific tasks like paddy disease diagnosis. It typically reaches a training accuracy of about 95.55% and a testing accuracy of approximately 95.12%. Nonetheless, the model often experiences problems with overfitting and may not achieve optimal convergence. When a model adapts too closely to the training data, it leads to overfitting. This makes it worse at handling new data. This issue manifests as a significant discrepancy between the accuracy achieved during training and that observed during testing. Additionally, the model's performance can plateau during training, indicating that it does not fully utilize its learning capacity. Figure 10 illustrate the architecture of base EfficientNetB3 model.

To address these issues, the Enhanced EfficientNetB3 model incorporates several key modifications. Batch Normalization was employed to increase both the stability and efficiency of training by standardizing the inputs at each layer. This method lessens the effects of internal covariate shift, thereby boosting the overall performance of the model. This technique is expressed as

$$\hat{x}^{(k)} = \frac{x^{(k)} - \mu^{(k)}}{\sqrt{\sigma^{2k} + \in}}$$

Where; $x^{(k)}$ is the input to the k^{th} layer, $\mu^{(k)}$ and σ^{2k} denotes the mean and variance of the batch, while $\in$ is a small constant used to ensure numerical stability.

Dense layers with L2 regularization were also added to enhance learning capacity by incorporating more trainable parameters. L2 regularization, given by $\lambda \Sigma_i w_i^2$ in the loss function, penalizes large weights, helping to mitigate overfitting and encourage better generalization.

To further regularize the model, dropout was applied, randomly deactivating a proportion of neurons during training through a Bernoulli (p) process. This method keeps the model from relying too much on certain neurons, which helps avoid over fitting. It was finally finished by adding a Dense Output layer with a Softmax activation function where the Softmax function $\sigma(z)_i = \frac{e^{z_i}}{\Sigma_j e^{z_j}}$ converts raw scores into probabilities, allowing for clear probabilistic interpretation in multi-class classification.

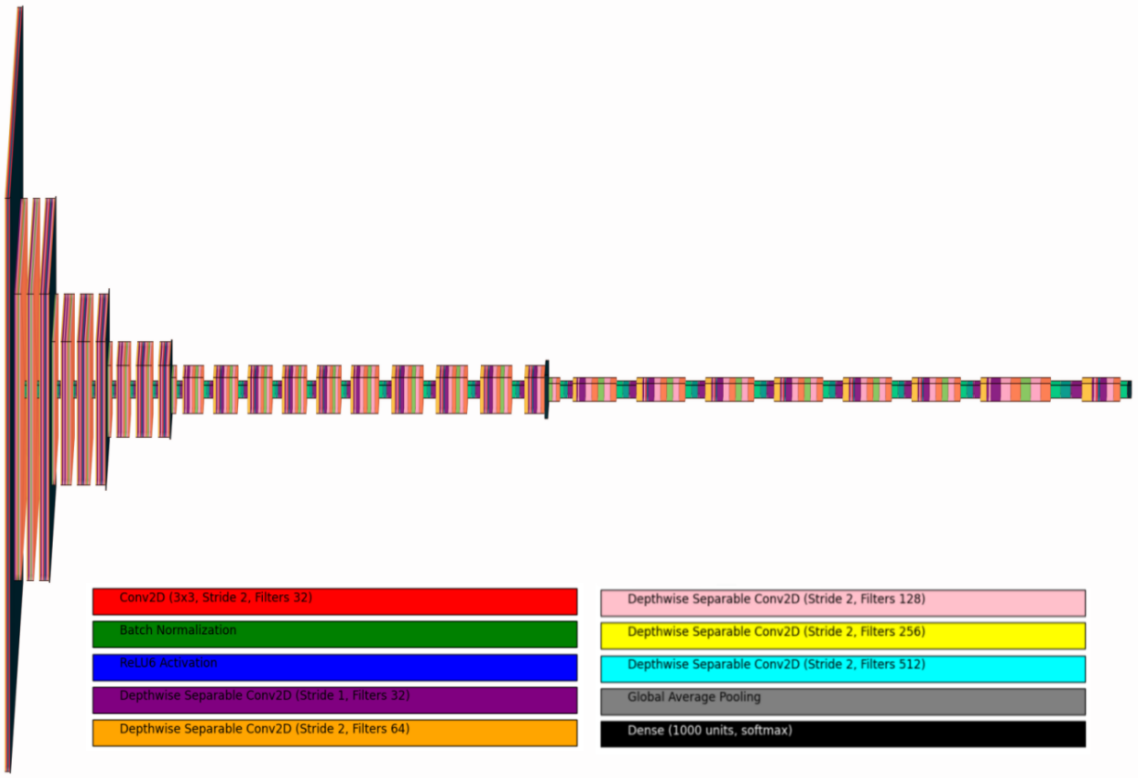

Figure 10- Architecture of Base EfficientNetB3 Model

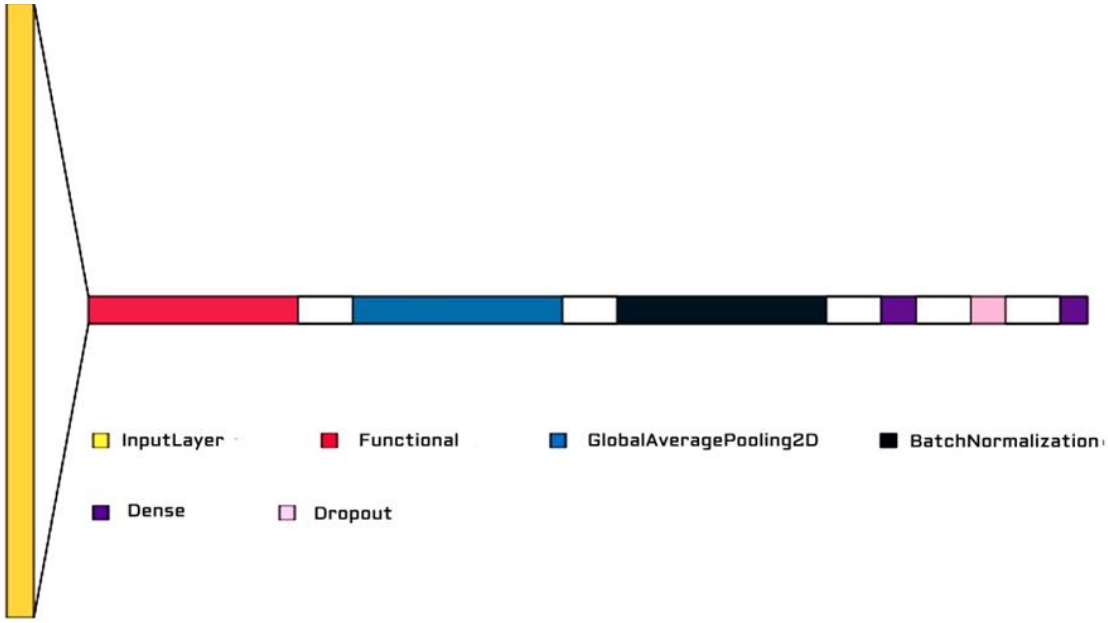

Figure 11- Architecture of the Enhanced EfficientNetB3 Model

Table 2 outlines the parameters of the base EfficientNetB3 model, whereas Table 3 details the updated parameters for the Enhanced EfficientNetB3 model, which aims to enhance both performance and efficiency. Figure 11 illustrates the architecture of the Enhanced EfficientNetB3 model, highlighting key components such as Batch Normalization, Dense layers with L2 regularization, Dropout, and a final Dense layer equipped with a Softmax activation function.

Table 2- EfficientnetB3 Model Architecture

Layer Type	*Input Shape*	*Output Shape*	*Parameters*
Conv2D	(224, 224, 3)	(112, 112, 32)	Kernel size: 3x3, Stride: 2, Filters: 32
Batch Normalization	(112, 112, 32)	(112, 112, 32)	Axis: -1, Momentum: 0.99, Epsilon: 1e-3
Activation (ReLU6)	(112, 112, 32)	(112, 112, 32)	ReLU6 Activation
Depthwise Separable Conv2D	(112, 112, 32)	(112, 112, 32)	Kernel size: 3x3, Stride: 1, Depthwise, Filters: 32
Batch Normalization	(112, 112, 32)	(112, 112, 32)	Axis: -1, Momentum: 0.99, Epsilon: 1e-3
Depthwise Separable Conv2D	(112, 112, 32)	(56, 56, 64)	Kernel size: 3x3, Stride: 2, Depthwise, Filters: 64
Batch Normalization	(56, 56, 64)	(56, 56, 64)	Axis: -1, Momentum: 0.99, Epsilon: 1e-3
Depthwise Separable Conv2D	(56, 56, 64)	(28, 28, 128)	Kernel size: 3x3, Stride: 2, Depthwise, Filters: 128
Batch Normalization	(28, 28, 128)	(28, 28, 128)	Axis: -1, Momentum: 0.99, Epsilon: 1e-3
Depthwise Separable Conv2D	(28, 28, 128)	(14, 14, 256)	Kernel size: 3x3, Stride: 2, Depthwise, Filters: 256
Batch Normalization	(14, 14, 256)	(14, 14, 256)	Axis: -1, Momentum: 0.99, Epsilon: 1e-3
Depthwise Separable Conv2D	(14, 14, 256)	(7, 7, 512)	Kernel size: 3x3, Stride: 2, Depthwise, Filters: 512
Batch Normalization	(7, 7, 512)	(7, 7, 512)	Axis: -1, Momentum: 0.99, Epsilon: 1e-3
Global Average Pooling	(7, 7, 512)	(512)	
Dense (Fully Connected Layer)	(512)	(1000)	Units: 1000, Activation: Softmax

Table 3- Enhanced Part of EfficientNetB3 Model Architecture

Layer Type	*Input Shape*	*Output Shape*	*Parameters*
Batch Normalization	(512)	(512)	Axis: -1, Momentum: 0.9, Epsilon: 0.001
Dense Layer 1	(512)	(256)	Units: 256, Activation: ReLU, Kernel Regularizer: L2(0.016)
Dropout Layer	(256)	(256)	Dropout Rate: 0.5, Seed: 123
Dense Output Layer	(256)	(10)	Units: 10, Activation: Softmax

Furthermore, a custom callback function was utilized to adjust the learning rate dynamically in response to training and validation metrics, thereby enhancing the optimization process. Data generators were employed to handle both the training and validation datasets. Several measures, such as loss, accuracy, confusion matrices, and classification reports, were hired to evaluate the model's effectiveness. The trained model and its weights were preserved for future applications, allowing for potential reuse or additional fine-tuning. These modifications ensure that the Enhanced EfficientNetB3 model effectively overcomes the limitations of the base model, providing improved performance in the task of paddy disease diagnosis. The algorithm for diagnosing paddy diseases using the Enhanced EfficientNetB3 model is detailed below.

Algorithm for diagnosing paddy diseases using the Enhanced EfficientNetB3 model

Input:

Dataset D = (X, Y), where X is the set of images and Y are the corresponding disease labels.

Output:

- Trained Enhanced EfficientNetB3 Model $M_{enhanced}$
- Evaluation Metrics E
- Classification Report R

1 Import libraries:

L ← {TensorFlow, Keras, NumPy, Pandas, Matplotlib};

2 Load and Preprocess Dataset:

(X, Y) ← LoadAndPreprocessDataset(D);

3 Data Splitting:

(X_{train},Y_{train}), (X_{val},Y_{val}), (X_{test},Y_{test}) ← StratifiedSplit(X,Y)

4 Data Augmentation Setup:

DataAugmentation ← ConfigureAugmentation(horizontal_flip=True)

5 Create Data Generators:

TrainingData ← CreateGenerator(DataAugmentation, X_train, Y_train)
ValidationData ← CreateGenerator(None, X_val, Y_val)
TestData ← CreateGenerator(None, X_test, Y_test)

6 Initialize Base Models:

M_base ← EfficientNetB3(include_top=False, weights='imagenet')

7 Add Feature Extraction Layer:

M_base ← M_base + GlobalAveragePooling2D()

8 Enhance Model:

M_enhanced ← M_base
M_enhanced ← M_enhanced + BatchNormalization(axis=-1)
M_enhanced ← M_enhanced + Dense(units, activation='relu')
M_enhanced ← M_enhanced + L2Regularization(strength)
M_enhanced ← M_enhanced + Dropout(rate)
M_enhanced ← M_enhanced + Dense(number_of_classes, activation='softmax')

9 Compile Model:

M_enhanced ← Compile(optimizer, loss_function, evaluation_metrics)

10 Define Training Parameters:

Params ← {batch_size, epochs, learning_rate}

11 Configure Callbacks:

Callbacks ← SetupCallbacks(monitor='val_loss', patience, save_best=True)

12 Train the Model:

M_enhanced ← TrainModel(M_enhanced, TrainingData, ValidationData, Params, Callbacks)

13 Evaluate Model:

E, R ← EvaluateModel(M_enhanced, TestData)

14 Save Trained Model:

SaveModel(M_enhanced, 'model_path.h5')

2.4. Training-Testing data and model evaluation

In this study, the data is divided into three different parts: 80% for training, 10% for validation, and 10% for testing. The choice of these proportions is based on established practices in machine learning to ensure a well-balanced approach. Allocating 80% of the data for training provides a substantial amount of samples for the model to learn from, which is crucial

for developing a robust and effective model (Shah et al. 2023). A segment of the 10% validation set is used to assess the model's effectiveness during training and adjust its hyperparameters. This intermediate evaluation assists in reducing overfitting by providing ongoing feedback (Sun et al. 2023; Kiratiratanapruk et al. 2020). The remaining 10% of the dataset is reserved for testing, offering an unbiased assessment of the model's accuracy with new data. This step ensures that the assessment of its ability to generalize is precise and reflective of real-world conditions (Li et al. 2022; Rahman et al. 2020). Table 4 details the parameters used during the model training phase.

Table 4- Model Training Parameters

Parameter	***Value***
Batch Size	64
Epochs	32
Momentum	0.9
Learning Rate	0.0002
Metric	Categorical Crossentropy
Patience	3
Factor	0.2
Verbose	2
Optimization Method	AdamW
Dropout Rate	0.5
Image Augmentation	Random rotations, flips, brightness adjustments
Regularization	L2 regularization

The parameters in Table 4 were selected to improve model performance and minimize overfitting. A batch size of 64 balances computational efficiency with training stability. Training the model for 32 epochs allows adequate learning without risking overfitting. A momentum of 0.9 speeds up training by incorporating previous gradients, while a learning rate of 0.0002 ensures steady progress. The Categorical Crossentropy metric measures accuracy for multiple classes. The patience of 3 reduces the learning rate if no improvement occurs, using a reduction factor of 0.2 for gradual changes. Verbose level 2 offers detailed training feedback. The AdamW optimizer effectively manages large datasets and prevents overfitting. A dropout rate of 0.5 randomly disables neurons to improve generalization. L2 regularization prevents overly complex models by penalizing high weights. Image augmentation, including rotations, flips, and brightness changes, diversifies training data, enhancing the model's adaptability to different scenarios.

2.4.1 Model evaluation metrics

To evaluate the paddy disease classification model, several metrics are used:

Precision measures the accuracy of positive predictions:

$$\text{Precision} = \frac{\text{TP}}{\text{TP} + \text{FP}}$$

Where; TP denotes true positives and FP denotes false positives.

Recall evaluates the model's ability to identify all relevant positive cases:

$$\text{Recall} = \frac{\text{TP}}{\text{TP+FN}}$$

Where; FN represents false negatives.

F1-Score balances precision and recall:

$$\text{F1-Score} = 2 \text{ x } \frac{\text{Precision x Recall}}{\text{Precision+Recall}}$$

Support refers to the number of actual occurrences of each class, providing context for other metrics.

Training Loss and **Training Accuracy** are calculated to assess performance during training:

$$\text{Training Loss} = -\frac{1}{N} \cdot \sum_{i=1}^{N} y_i \log(\hat{y}_i)$$

And

$$\text{Training Accuracy} = \frac{TP+TN}{TP+TN+FP+FN}$$

Validation Loss and **Validation Accuracy** evaluate performance on the validation set, while **Test Loss** measures effectiveness on the test set.

3. Results

Table 5 presents a comparative evaluation of the Enhanced EfficientNetB3 model alongside several other CNN architectures, emphasizing critical metrics like accuracy and loss during both training and validation phases.

The Enhanced EfficientNetB3 model accomplished an impressive training accuracy of 98.92% and recorded a low training loss of 0.1385. During the validation phase, the system achieved a performance level of 98.20% accuracy and a validation loss of 0.1450. It is also found that a test accuracy of 98.50% with a test loss of 0.1505 for the independent test dataset. These metrics demonstrate the model's robust performance across various evaluation stages, outpacing several other models as shown in Table 5. Figure 12 displays the trends in both training and validation loss and accuracy for the enhanced model.

Table 5- Performance Metrics and Training Time of CNN Models

Model		***Training***		***Validation***		***Test***		***Training Time***
Architectures	**Input Size**	**Loss**	**Accuracy**	**Loss**	**Accuracy**	**Loss**	**Accuracy**	**Minutes**
VGG16	224, 224, 3	0.2239	92.12%	0.2050	91.00%	0.1835	93.88%	120
VGG19	224, 224, 3	0.2105	93.01%	0.1980	92.10%	0.1798	94.12%	130
Inception v1	224, 224, 3	0.1984	93.50%	0.1860	92.75%	0.1759	94.45%	150
ResNet-50	224, 224, 3	0.1893	93.87%	0.1755	93.20%	0.1702	94.80%	160
Inception v3	299, 299, 3	0.1785	94.20%	0.1680	93.50%	0.1651	95.02%	180
DenseNet-121	224, 224, 3	0.1709	94.53%	0.1605	94.00%	0.1604	95.23%	200
Xception	299, 299, 3	0.1627	94.95%	0.1550	94.50%	0.1580	95.40%	210
EfficientNetB2	260, 260, 3	0.1594	95.10%	0.1835	93.90%	0.1928	94.85%	90
EfficientNetB3	300, 300, 3	0.1528	95.55%	0.1752	94.60%	0.1864	95.12%	80
Enhanced EfficientNetB3	224, 224, 3	0.1385	98.92 %	0.1450	98.20%	0.1505	98.50%	68

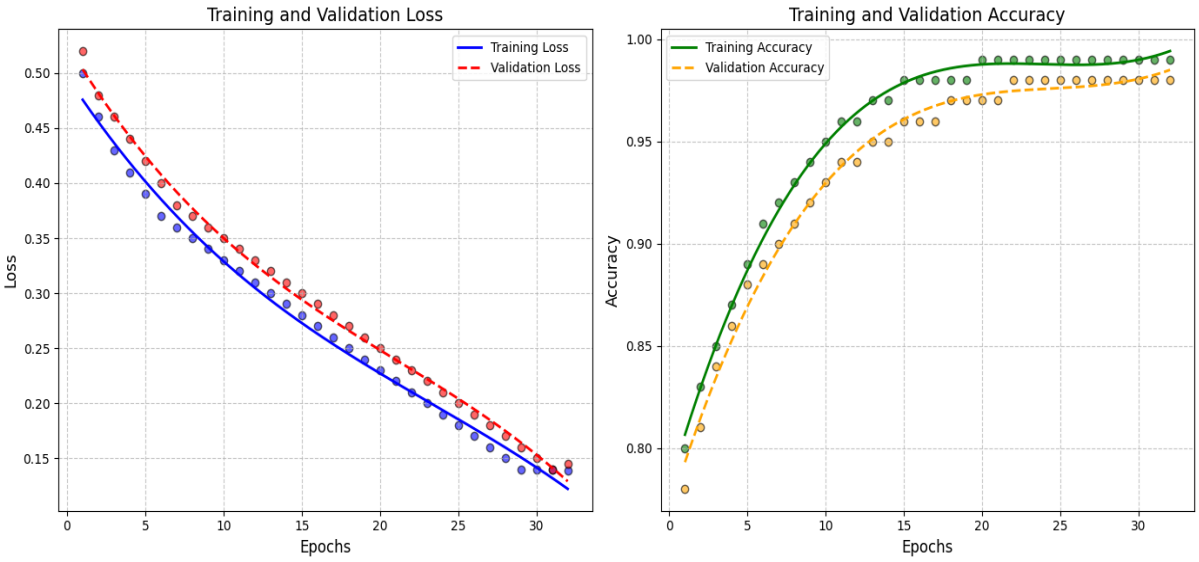

Figure 12- Training and Validation Loss and Accuracy for Enhanced EfficientNetB3

3.1 Confusion matrix

The performance of the Enhanced EfficientNetB3 model was assessed through a confusion matrix, which provided an in-depth evaluation of its ability to classify various paddy diseases. The model achieved remarkable success in accurately identifying both healthy plants and several disease types, such as blast. It showed especially strong performance in recognizing Dead

Heart, where it correctly classified 289 instances, and Blast, with 345 correct predictions. Additionally, the model effectively identified Bacterial Leaf Blight with 94 correct classifications and Bacterial Leaf Streak, correctly identifying all 76 instances. Other diseases, including Brown Spot, Downy Mildew, and Hispa, were also accurately classified with only minor misclassifications. The model performed well in identifying Normal (healthy plants), with 342 correct classifications. The confusion matrix highlights the model's consistent and reliable ability to distinguish between various paddy diseases, reinforcing its potential for practical use in disease diagnosis. The confusion matrix depicted in Figure 13 illustrates the model's proficiency in recognizing different paddy diseases.

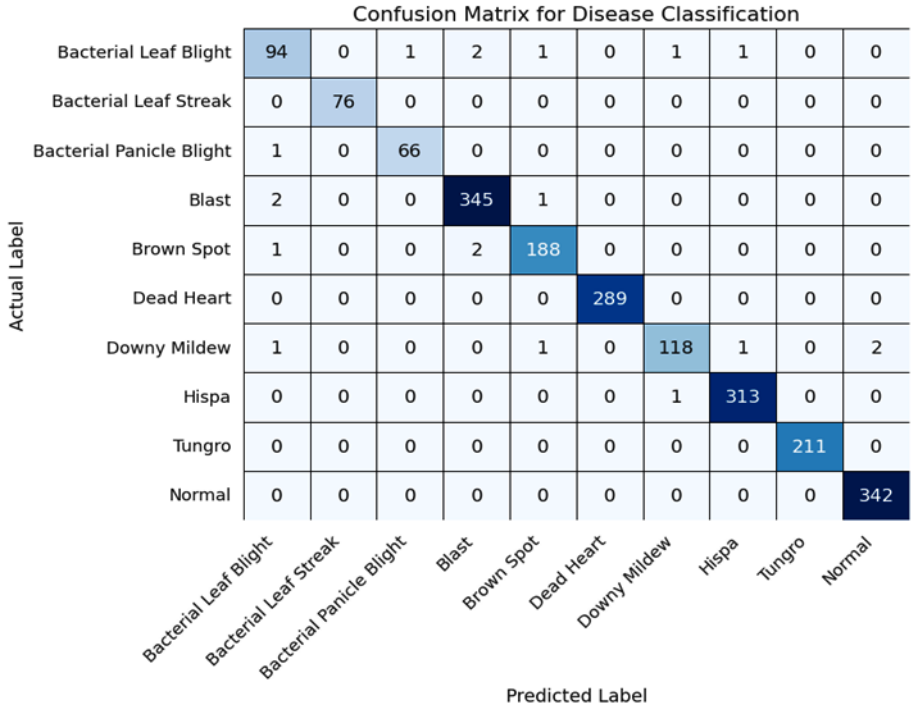

Figure 13- Confusion Matrix for Paddy Disease Classification Model Performance

3.2 Model disease classification

Table 6 displays the Precision, Recall, F1-Score, and Accuracy metrics for the Enhanced EfficientNetB3 model across various paddy disease categories. The model proven exceptional performance, with perfect Precision and Recall of 1.00 for bacterial leaf streak. Additionally, it achieved high accuracy in identifying paddy diseases such as dead heart and blast.

Table 6- Performance Metrics for the Enhanced EfficientNetB3 Model

Disease	***Precision***	***Recall***	***F1-Score***	***Accuracy***
Bacterial Leaf Blight	0.99	0.94	0.96	98.0%
Bacterial Leaf Streak	1.00	1.00	1.00	100%
Bacterial Panicle Blight	0.98	0.98	0.98	98.0%
Blast	0.99	0.98	0.99	98.5%
Brown Spot	0.96	0.98	0.97	97.5%
Dead Heart	1.00	1.00	1.00	99.5%
Downy Mildew	0.95	0.95	0.95	95.0%
Hispa	0.98	0.98	0.98	98.0%
Tungro	0.97	0.99	0.98	98.0%
Normal	0.97	0.99	0.98	98.0%

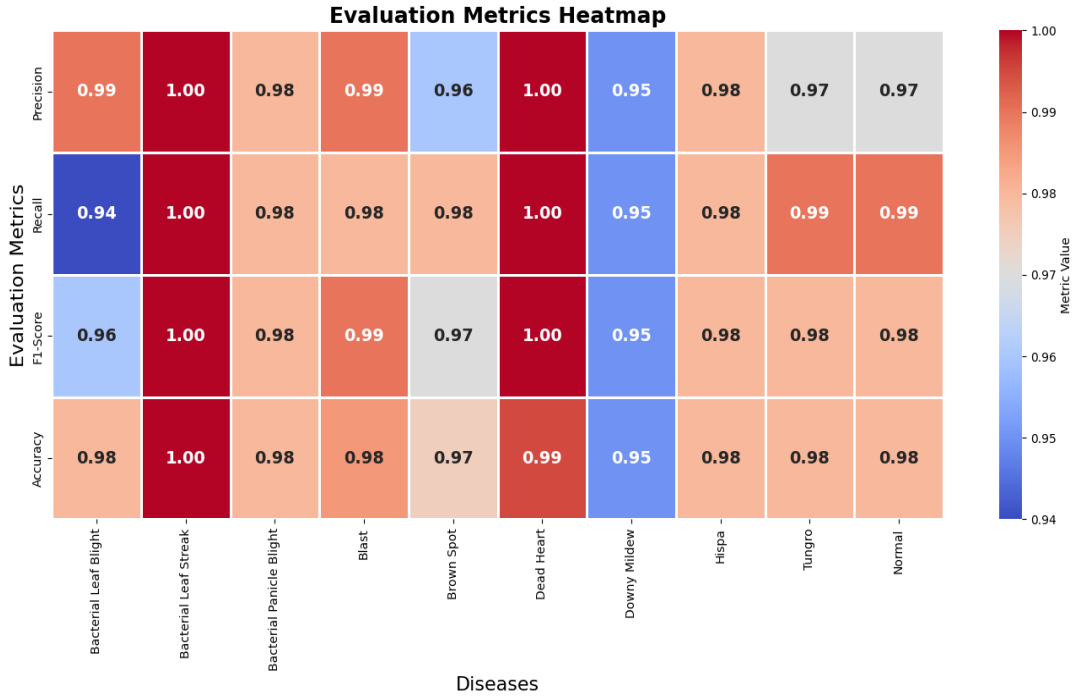

Figure 14- Evaluation Metrics Heatmap

Similar results are observed from the Evaluation Metrics Heatmap in Figure 14 thus ensuring that the model excels most in categorizing paddy diseases. The disease prediction performance of the Enhanced EfficientNetB3 model is compared to other models is shown in Figure 15(a) and 15(b).

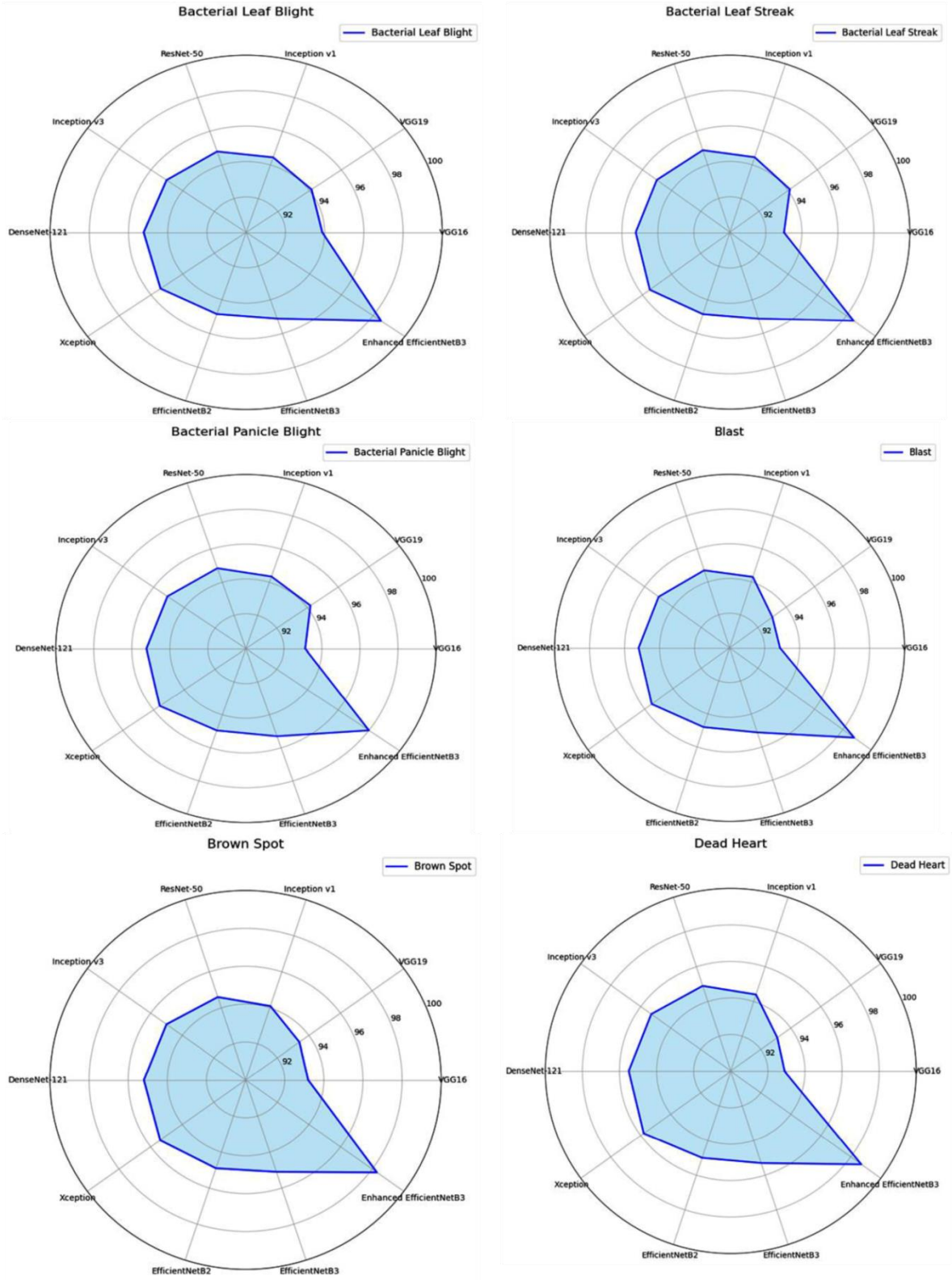

Figure 15 (a)- Predictive Performances of Disease Prediction Models

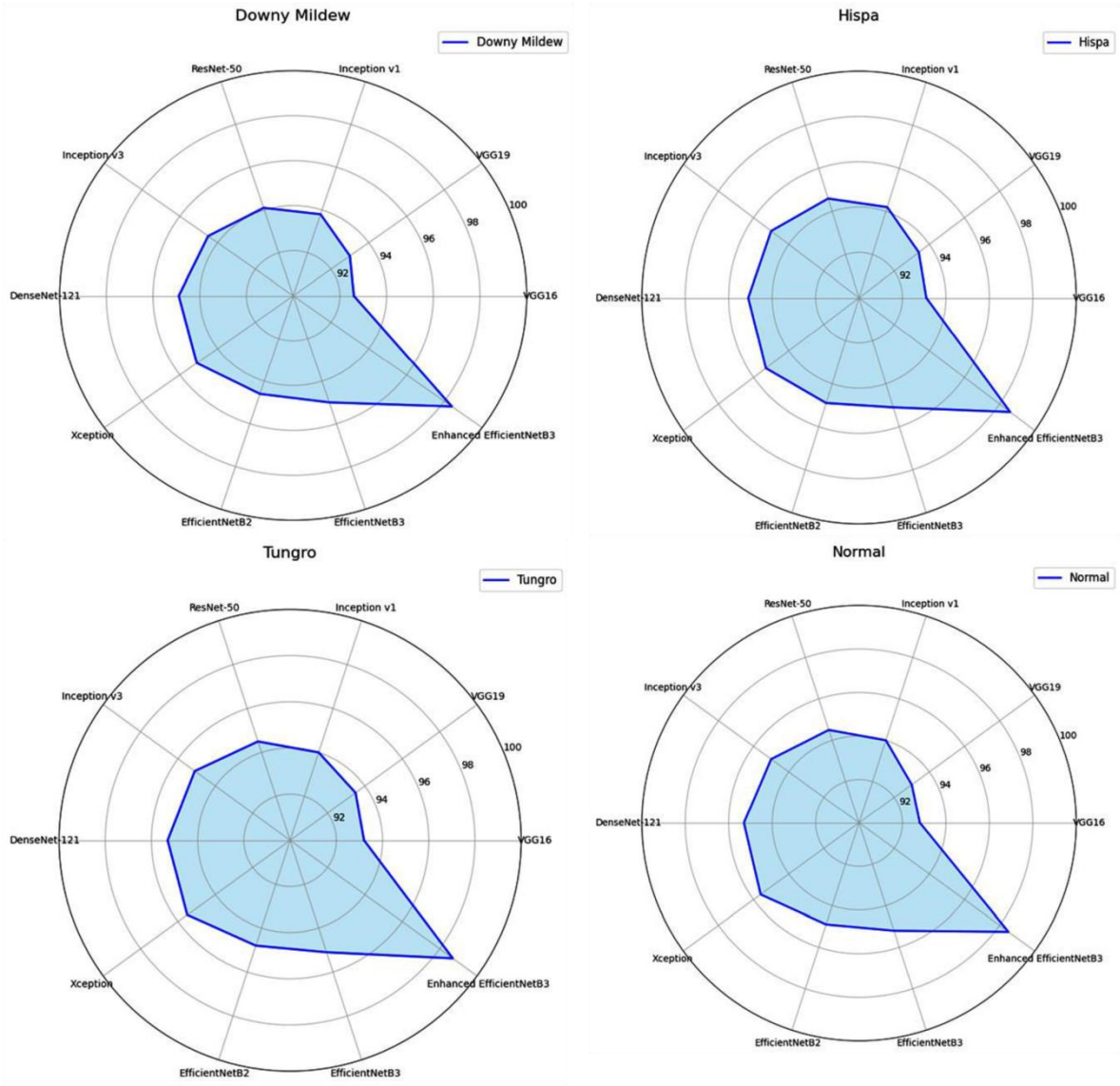

Figure 15 (b)- Predictive Performances of Disease Prediction Models

4. Discussion

The comparative analysis of paddy disease classification models emphasizes the effectiveness of different deep learning architectures for diagnosing paddy diseases. Even simpler models, such as MobileNet, achieve a commendable accuracy of around 90%. In contrast, more advanced models like ResNet50, EfficientNet, and hybrid architectures—such as ResNet-YOLO and DenseNet-UNet—exhibit even higher accuracy, often exceeding 95%. For example, Ganesan & Chinnappan (2022) demonstrated a system that achieved an impressive accuracy of 97.1% using ResNet-YOLO for identifying paddy leaf diseases, showcasing the effectiveness of these advanced architectures in disease detection.

Models incorporating self-attention mechanisms, such as the Self-attention-based ResNet studied by Stephen et al. (2023), achieved an accuracy of 96.7%. This underscores the benefit of self-attention techniques, which enhance model efficiency by focusing on the most critical elements of the dataset. The Enhanced EfficientNetB3 model discussed in this study also aligns with these findings, achieving a test accuracy of 98.50%. While it showed a lower test loss compared to some other models, it performed well on different data samples, indicating robust generalization.

On the other hand, simpler models, including conventional structures like VGG16, basic CNNs, as well as EfficientNetB2 and EfficientNetB3, also demonstrated solid performance with accuracy ranging from 90% to 95%. This range of results suggests that even models with lower complexity can deliver effective results when applied to moderately complex datasets.

Despite the promising performance of the Enhanced EfficientNetB3 model, there are still some limitations that need to be addressed in future research. One limitation is the model's dependency on a large amount of labeled training data, which may

not always be available, especially in regions with limited data for paddy disease classification. Additionally, the model's performance can be impacted by noise and variation in data quality, which may affect the accuracy in real-world applications. Future work could explore techniques such as semi-supervised learning or data augmentation to reduce the dependence on large labeled datasets and improve robustness (Ozdemir et al. 2024). Furthermore, incorporating domain-specific knowledge or hybrid models that combine deep learning with expert systems may help improve model accuracy and generalization in diverse field conditions. Another avenue for future research is exploring the deployment of these models on edge devices with limited computational resources. This could involve further optimization of the model to maintain high performance while reducing model size and computational requirements.

4.1. Detailed model performance comparison

Table 6- Comparison of Accuracy Rates of Paddy Disease Classification Models Using Deep Learning

Study & Reference	*Number of Images*	*Diseases Diagnosed*	*Models Used*	*Accuracy Rates (%)*
Shah et al. (2023)	2000	Blast, Brown spot, Bacterial blight	Inception V3, VGG16, VGG19, CNN, ResNet50	Inception V3: 92.4, VGG16: 90.2, VGG19: 91.5, CNN: 89.8, ResNet50: 93.7
Sun et al. (2023)	1500	Seed defects	Rice-VGG16	96.3
Liang et al. (2022)	1200	Multiple paddy diseases and pests	Improved CNN based on VGG16	94.6
Rahman et al. (2020)	3000	Brown spot, Leaf blast, Sheath blight	CNN	91.2
Yakkundimath et al. (2022)	2500	Blast, Sheath blight, Brown spot	Multiple CNN models	90.8
Dogra et al. (2023)	1800	Brown spot	Deep learning model	94.0
Razavi et al. (2024)	2200	Rice cultivar classification	ResNet models	95.8
Ganesan & Chinnappan (2022)	1400	Paddy leaf diseases	Hybrid ResNet-YOLO	97.0
Stephen et al. (2023)	1600	Paddy leaf diseases	Self-attention based ResNet	96.7
Liu et al. (2022)	2100	Paddy leaf diseases	Hybrid DenseNet-UNet	95.4
Li et al. (2022)	1300	Rice germ integrity	Improved EfficientNet	93.5
Bhujel & Shakya (2022)	1700	Paddy leaf diseases	EfficientNet	95.9
Deng et al. (2021)	2000	Multiple Paddy diseases	Deep learning models	93.2
Kaur & Sivia (2024)	1600	Leaf blast	Deep and machine learning convolutional networks	94.8
Latif et al. (2022)	1800	Paddy diseases	Improved CNN	94.2
Hukkeri et al. (2024)	2400	Various plant diseases	Pretrained CNN on ImageNet	92.9
Meena et al. (2024)	1700	Paddy diseases	Xception model	96.0
Proposed Work (2024)	**10407**	**10 Paddy diseases including normal leaves**	VGG16, VGG19, Inception v1, ResNet-50, Inception v3, DenseNet-121, Xception, EfficientNetB2 EfficientNetB3 **Enhanced EfficientNetB3**	93.88%, 94.12% 94.45% 94.80% 95.02% 95.23% 95.40% 94.85% 95.12% **98.50%**

In assessing the training performance of various models, including VGG16, VGG19, Inception v1, ResNet-50, Inception v3, DenseNet-121, Xception, EfficientNetB2, EfficientNetB3, and Enhanced EfficientNetB3, the Enhanced EfficientNetB3 model achieved the lowest training loss at 0.1385 and reached a training accuracy of 98.92%. The results indicate that the model has effectively learned the patterns from the training data, and the validation loss shows consistent performance, reflecting the model's ability to generalize well to new, unseen data.

The Enhanced EfficientNetB3 model showed a validation loss of 0.1450 and a test loss reaching 0.1505, both lower than those observed in other models. It attained a validation accuracy of 98.20% and a test accuracy of 98.50%, demonstrating strong generalization to new data. These observations suggest that the model demonstrates strong performance with new data, with the loss values staying within an optimal range.

Moreover, Enhanced EfficientNetB3 outperformed models such as Xception, DenseNet-121, EfficientNetB2, and EfficientNetB3 in validation accuracy. Its ability to maintain an effective balance between accuracy and loss highlights Enhanced EfficientNetB3 as a highly efficient model, making it an excellent choice for dataset classification.

Additionally, the Enhanced EfficientNetB3 model required only 68 minutes of training time, significantly faster than models such as Xception, which took 210 minutes, DenseNet-121, which took 200 minutes, and EfficientNetB2, which took 90 minutes. This efficiency highlights that Enhanced EfficientNetB3 is not only accurate but also computationally cost-effective compared to other architectures. This aspect makes Enhanced EfficientNetB3 a suitable choice when computational resources or training time are limited, while still maintaining high performance. Table 6 provides a comparison of accuracy rates among various deep learning models for paddy disease classification, including Enhanced EfficientNetB3. Given the lower computational cost and faster training time, Enhanced EfficientNetB3 is recommended when the task requires high accuracy but with limited time or computational resources.

5. Conclusions

The proposed Enhanced EfficientNetB3 model sets a new benchmark in paddy disease identification with its impressive performance, achieving a training accuracy of 98.92%, which exceeds the accuracy of previous models. It shows strong validation and test accuracies of 98.20% and 98.50%, respectively, indicating effective generalization to new data. While the model maintains excellent accuracy overall, it also achieves efficient training in just 68 minutes. The validation and test losses are consistent with the training loss, further emphasizing the model's strong performance. The Enhanced EfficientNetB3 model excels in precision, recall, and F1-scores, making it highly effective for classifying paddy diseases. It also supports real-time inference and resource optimization, providing significant advantages for precision agriculture and offering potential applications in managing diseases across various crops and climates.

Data availability: Indicates the availability of data upon request from the corresponding author.

Authorship Contributions:

Johnson B contributed to the study conception, design, methodology, conceptualization, and resources. Material preparation, investigation, and analysis were also conducted by Johnson B, along with drafting the initial manuscript. Chandrakumar Thangavel supervised the research and provided critical revisions to the manuscript. Both authors read and approved the final manuscript.

Conflict of Interest: The authors declare that they have no conflict of interest.

Acknowledgments

The authors express their gratitude to the Thiagarajar College of Engineering (TCE) for Supporting us to carry out this research work. Also, the financial support from TCE under Thiagarajar Research Fellowship scheme (File.no:TRF/Jan-2023/10) is gratefully acknowledged.

References

Bhujel S & Shakya S (2022). Rice leaf diseases classification using discriminative fine tuning and CLR on EfficientNet. *Journal of Soft Computing Paradigm* 4(3): 172-187. doi.org/10.30534/jscp/2022/05162022

Deb M, Dhal K G, Mondal R & Gálvez J (2021). Paddy disease classification study: A deep convolutional neural network approach. Optical Memory and Neural Networks 30: 338-357. doi.org/10.1134/S1063775821030077

Deng R, Tao M, Xing H, Yang X, Liu C, Liao K & Qi L (2021). Automatic diagnosis of rice diseases using deep learning. Frontiers in Plant Science 12: 701038. doi.org/10.3389/fpls.2021.701038

Dogra R, Rani S, Singh A, Albahar M A, Barrera A E & Alkhayyat A (2023). Deep learning model for detection of brown spot rice leaf disease with smart agriculture. Computers and Electrical Engineering 109: 108659. doi.org/10.1016/j.compeleceng.2023.108659

Dubey R K & Choubey D K (2024). Reliable detection of blast disease in rice plant using optimized artificial neural network. *Agronomy Journal* 116(3): 1099-1111

Ganesan G & Chinnappan J (2022). Hybridization of ResNet with YOLO classifier for automated paddy leaf disease recognition: An optimized model. *Journal of Field Robotics* 39(7): 1085-1109. doi.org/10.1002/rob.22085

Ganesan S, Sinha N & Sundararajan V (2023). A new hybrid deep learning model for classifying rice plant diseases. *Journal of Computational Biology and Bioinformatics* 17(2): 99-110. doi.org/10.1016/j.jcb.2023.103122

Gerdan D, Koç C & Vatandaş M (2023). Diagnosis of tomato plant diseases using pre-trained architectures and a proposed convolutional neural network model. *Journal of Agricultural Sciences* 29(2): 618-629

Hukkeri G S, Soundarya B C, Gururaj H L & Ravi V (2024). Classification of Various Plant Leaf Disease Using Pretrained Convolutional Neural Network on Imagenet. *The Open Agriculture Journal* 18(1). doi.org/10.2174/1874331502414010113

Kaur G & Sivia J S (2024). Development of deep and machine learning convolutional networks of variable spatial resolution for automatic detection of leaf blast disease of rice. Computers and Electronics in Agriculture 225: 109210. doi.org/10.1016/j.compag.2023.109210

Kiratiratanapruk K, Temniranrat P, Sinthupinyo W, Prempree P, Chaitavon K, Porntheeraphat S & Prasertsak A (2020). Development of paddy rice seed classification process using machine learning techniques for automatic grading machine. *Journal of Sensors* 2020(1): 7041310. doi.org/10.1155/2020/7041310

Kumar Y, Singh R, Moudgil M R & Kamini (2023). A systematic review of different categories of plant disease detection using deep learning-based approaches. Archives of Computational Methods in Engineering 30(8): 4757-4779. doi.org/10.1007/s11831-022-09783-x

Latif G, Abdelhamid S E, Mallouhy R E, Alghazo J & Kazimi Z A (2022). Deep learning utilization in agriculture: Detection of rice plant diseases using an improved CNN model. Plants 11(17): 2230. doi.org/10.3390/plants11172230

Li B, Liu B, Li S & Liu H (2022). An improved EfficientNet for rice germ integrity classification and recognition. Agriculture 12(6): 863. doi.org/10.3390/agriculture12060863

Liang K, Wang Y, Sun L, Xin D & Chang Z (2022). A lightweight-improved CNN based on VGG16 for identification and classification of rice diseases and pests. In The international conference on image, vision and intelligent systems (ICIVIS 2021) (pp. 195-207). Singapore: Springer Nature Singapore. doi.org/10.1007/978-981-16-7487-8_19

Liu W, Yu L & Luo J (2022). A hybrid attention-enhanced DenseNet neural network model based on improved U-Net for rice leaf disease identification. Frontiers in Plant Science 13: 922809. doi.org/10.3389/fpls.2022.922809

Malvade N N, Yakkundimath R, Saunshi G B & Elemmi M C (2023). Paddy variety identification from field crop images using deep learning techniques. *International Journal of Computational Vision and Robotics* 13(4): 405-419. doi.org/10.1504/IJCVR.2023.129934

Meena R, Joshi S & Raghuwanshi S (2024). Xception model for disease detection in rice plant. *Journal of Intelligent & Fuzzy Systems* (Preprint): 1-18. doi.org/10.3233/JIFS-230473

Ozdemir C, Dogan Y & Kaya Y (2024). RGB-Angle-Wheel: A new data augmentation method for deep learning models. Knowledge-Based Systems, 291: 111615

Ozdemir C (2024). Adapting transfer learning models to dataset through pruning and Avg-TopK pooling. Neural Computing and Applications 36(11): 6257-6270

Ozdemir C, Dogan Y & Kaya Y (2024). A new local pooling approach for convolutional neural network: local binary pattern. Multimedia Tools and Applications 83(12): 34137-34151

Razavi M, Mavaddati S & Koohi H (2024). ResNet deep models and transfer learning technique for classification and quality detection of rice cultivars. Expert Systems with Applications 247: 123276. doi.org/10.1016/j.eswa.2023.123276

Rahman C R, Arko P S, Ali M E, Khan M A I, Apon S H, Nowrin F & Wasif A (2020). Identification and recognition of rice diseases and pests using convolutional neural networks. Biosystems Engineering 194: 112-120. doi.org/10.1016/j.biosystemseng.2020.03.003

Shah S R, Qadri S, Bibi H, Shah S M W, Sharif M I & Marinello F (2023). Comparing Inception V3, VGG 16, VGG 19, CNN, and ResNet 50: A case study on early detection of a rice disease. Agronomy 13(6): 1633. doi.org/10.3390/agronomy13061633

Simhadri C G, Kondaveeti H K, Vatsavayi V K, Mitra A & Ananthachari P (2024). Deep learning for rice leaf disease detection: A systematic literature review on emerging trends, methodologies and techniques. Information Processing in Agriculture.

Sun J, Zhang Y, Zhu X & Zhang Y D (2023). Enhanced individual characteristics normalized lightweight rice-VGG16 method for rice seed defect recognition. Multimedia Tools and Applications 82(3): 3953-3972. doi.org/10.1007/s11042-022-12954-2

Verma S, Kumar P & Singh J P (2024). A unified lightweight CNN-based model for disease detection and identification in corn, rice, and wheat. *IETE Journal of Research* 70(3): 2481-2492

Yakkundimath R, Saunshi G, Anami B & Palaiah S (2022). Classification of rice diseases using convolutional neural network models. *Journal of The Institution of Engineers* (India): Series B 103(4): 1047-1059. doi.org/10.1007/s40031-022-00732-0

Journal of Agricultural Sciences (Tarim Bilimleri Dergisi) 2025, 31 (2) : 577 – 589 DOI: 10.15832/ankutbd.1486255

Journal of Agricultural Sciences
(Tarim Bilimleri Dergisi)

J Agr Sci-Tarim Bili
e-ISSN: 2148-9297
jas.ankara.edu.tr

How Does Cooperative Membership Affect Farm Efficiency? A Case Study of Dairy Farms in Izmir, Türkiye

Filiz Malkoc Kinikli[a,b*], Murat Yercan[a]

[a]*Department of Agricultural Economics, Faculty of Agriculture, Ege University, Izmir, TÜRKIYE*

[b]*Department of People and Society, Swedish University of Agricultural Sciences (SLU), SWEDEN*

ARTICLE INFO

Research Article
Corresponding Author: Filiz Malkoc Kinikli, E-mail: filiz.kinikli@slu.se
Received: 18 May 2024 / Revised: 10 December 2024 / Accepted: 23 December 2024 / Online: 25 March 2025

Cite this article

Kinikli F M, Yercan M (2025). How Does Cooperative Membership Affect Farm Efficiency? A Case Study of Dairy Farms in Izmir, Türkiye. *Journal of Agricultural Sciences (Tarim Bilimleri Dergisi),* 31(2):577-589. DOI: 10.15832/ankutbd.1486255

ABSTRACT

This study aims to measure the efficiency of dairy farms, both cooperative members and non-members, and to investigate the effect of farm size. To assess farm efficiency, we conducted Data Envelopment Analysis (DEA) and Tobit regression analysis to identify the factors that influence efficiency on farms. The study was carried out in Izmir, one of the most significant cities for dairy cooperatives and the dairy sector in Türkiye. The results showed that non-member dairy farms were more efficient than those of members. The study found that large-scale farms are more efficient than small-scale farms. It is also noteworthy that the majority of fully efficient small-scale farms are cooperative members. It can be concluded that cooperatives are more beneficial for small family farms in terms of efficiency; however, they have capacity limitations when compared to IOFs.

Keywords: Dairy farms, Data Envelopment Analysis, Tobit Regression, Efficiency, Agricultural Cooperatives

1. Introduction

The dairy industry plays a crucial role in agribusiness sector and ensuring food security in rural areas. The dairy processing sector is one of the largest subsectors of the EU's food processing industry. To sustain milk production, it is necessary to have a competitive and effective milk processing sector (Vlontzos & Theodoridis 2013; Zietek-Kwasniewska et al. 2022).

Türkiye is the eighth largest cow's milk producer in the world and third largest in the EU. The Turkish dairy industry has experienced substantial growth in export value, surging from over $167 million in 2009 to a noteworthy $371 million in 2020. This transformation has positioned Türkiye as a key supplier of dairy products in its region. Notably, this success can be attributed to the industry's strategic shift from a domestic market focus to a more internationally oriented approach (USK 2023).

Compared to crop production, dairy sector provides continuous farmer income covering the whole year. In Türkiye, farmers face numerous challenges in the process from production to marketing. These include small-scale farms, lack of financing, marketing issues, hygiene and quality concerns, high input prices, and inadequate use of information and technology. It is important to address these issues to improve the overall efficiency and profitability of the agricultural sector (Özüdoğru, 2010). Additionally, 40% of dairy farms in Türkiye consist of farms with 1-5 cows. Only 2.5% of farms have 50 or more cows. On average, each farm has approximately six dairy cows (MAF 2020). A comparison of EU countries to Türkiye revealed a notable difference in the yield of meat and milk. As reported by the FAO in the year 2022, Türkiye's yields in these two categories are considerably lower than the EU average (FAO 2022). In light of this, it is evident that the agricultural sector in Türkiye could benefit from the establishment of farmer cooperatives, which could serve to address the existing challenges faced by small family farms. Farmers' cooperatives play a crucial role in the vertical integration of dairy sector supply chains (Jansik et al. 2014). Their role is to bring smallholder farmers together and help them market their products collectively, negotiate better prices and access resources such as finance and technology. By promoting collaboration among farmers, cooperatives empower them with stronger bargaining power in the market, ensuring a fairer distribution of profits and reducing their vulnerability to price fluctuations. Cooperatives frequently offer training and support services to enhance the quality of dairy products, thereby improving the competitiveness of small-scale farmers in the industry (Inan et al. 2005). Given the conditions in Türkiye, the sustainability of dairy farms is at risk due to high input prices and low product prices. This is particularly the case for small-scale family farms, which constitutethe majority of the industry. Farmers gathered under the roof of cooperatives would be able to compete with their competitors both in production and product sales. Therefore, cooperatives are very important for the efficiency and sustainability of small-scale farms. In Türkiye, there are 11 754 agricultural cooperatives and 3 678 207 members. Agricultural

cooperatives operate under three different laws*: Law No. 1163, Law No. 1581, and Law No. 4572, with a total membership of 3 678 207 (MAF 2024).

Based on this background, the main research question here is: *How does cooperative membership affect farm efficiency?* Although there are many studies conducted about determining the efficiency of dairy farms in Türkiye (Nizam & Armagan 2006; Koyunbenbe & Candemir 2006; Uzmay et al. 2009; Gul et al. 2018; Kaygisiz et al. 2018; Aydemir 2019; Güler & Saner 2020), however, a limited study has been conducted to compare the performance of member and non-member dairy farms. In this context, the aim of this study is twofold: (1) to assess the efficiency of dairy farms by comparing cooperative members and non-members, and (2) to estimate the factors that significantly impact the efficiency levels of these farms.

2. Literature Review

Several studies have been carried out on the efficiency of the dairy sector at the farm level in Türkiye and worldwide (Heshmati & Kumbhakar 1997; Reinhard et al. 2000; Jaforullah & Whiteman 2001; Helfand & Levine 2004; Nizam & Armagan 2006;Koyunbenbe & Candemir 2006; Candemir & Koyunbenbe, 2006; Hansson & Öhlmér 2008; Uzmay et al. 2009; Aldeseit 2013; Chagwiza et al. 2016; Gül et al. 2018; Kumar et al. 2018; Kaygisiz et al. 2018; Priscilla & Chauhan 2019; Güler & Saner 2020; Luiz Beber at al. 2021; Onyango et al. 2023). These studies suggest that implementing various strategies can enhance the efficiency of dairy farms (Heshmati & Kumbhakar, 1994; Fraser & Cordina 1999). If all farms operate at the efficiency levels observed in the top-performing farms, there is significant potential for substantial profits within the dairy industry. According to the study conducted on Finnish farms, it was found that the farms could reduce their costs by 31% if they were as technically efficient as the best farms in the sample (Oude Lansink et al. 2002). Güler & Saner (2020) studied sample of Turkish dairy farms, using data envelopment analysis (DEA), and they found that farm income can be maintained even if the inputs used in production are reduced by 11.6%, which means that profits can be increased. Another study conducted in Türkiye showed similar results, indicating that dairy farms can reduce inputs by 24.8% while maintaining the same level of output (Sert, 2019). Mitsopoulos et al. (2021) conducted a study in Greece using the DEA method to estimate the efficiency of dairy farms for both CRS and VRS approaches. The results showed that dairy farms can achieve a 30.7% and 21.6% equaproportional decrease in inputs given the level of outputs and the production technology. Reinhard et al. (2000) conducted a study on Dutch dairy farms and found an average technical efficiency score of 78% using the DEA method. Hansson & Öhlmer (2008) reported technical output efficiency ranging from 86% to 89% in a sample of Swedish farms.

There is a limited literature comparing the efficiency of dairy cooperatives and IOFs, as well as the efficiency of cooperative member and non-member dairy farms. Kumar et al. (2018) assessed the impacts of cooperative membership on welfare in Bihar, India. The impact of membership on farm performance was measured using some indicators such as milk yield, net returns, and adaptation of food safety measures (FSM). For the comparison of members and non-members, the Endogenous Switching Regression (ESM) model was used. The results indicated that dairy cooperative membership positively and significantly affected certain variables, such as income. In contrast, a study conducted in a different state of India by Priscilla & Chauhan (2019) used the propensity score matching (PMS) approach to determine the impact of cooperative membership on yield, price, income and technical efficiency. The findings indicated that there is no significant impact of dairy cooperatives on the economic well-being of their members. However, there is a positive and significant impact on employment, indicating a beneficial influence on society. Luiz Beber at al. (2021) conducted their study in Brazil, focused on the efficiency and productivity differences between cooperatives and IOFs in Brazil's institutional set-up. The study analysed 243 milk processors in southern Brazil and used production frontier to estimate technical efficiency. The results indicate that, in general, cooperatives are more efficient than IOFs. Zietek-Kwasniewskaet al. (2022) conducted a study in Poland comparing the technical efficiency of cooperative and non-cooperative dairies using the DEA method. They estimated technical efficiency under both constant returns to scale (CRS) and variable returns to scale (VRS). They found that dairy cooperatives were less efficient than non-cooperatives, which contrasts with the findings of Luiz Beber et al. (2021). The authors recommended that inefficient dairies reduce labor costs and depreciation.

Our previous knowledge suggests that farmer cooperatives have the potential to significantly increase the efficiency and productivity of farm level. This knowledge is supported by the research conducted by Abate et al. (2014) in Ethiopia. The researchers used propensity score matching approach to examine the technical efficiency of cooperative members and non-members. Their findings show that cooperatives are very efficient in providing support services that make significant improvements to the technical efficiency of their members. The study conducted in Kenya assessed the impact of cooperatives on smallholder dairy farmers' income. The scholars found that cooperative market participation increased farmers' incomes by approximately 10% (Onyango, et al. 2023). Similarly, the study conducted in Ethiopia shows similar results as cooperative members' dairy income is higher than non-members (Chagwiza et al. 2016).

3. Material and Methods

* Under Law No. 1163, there are 9 780 cooperatives with 2 490 480 members.
Under Law No. 1581, there are 1 618 cooperatives with 853 869 members.
Under Law No. 4572, there are 338 cooperatives with 332 925 members.

3.1. Study area and data sources

The study was conducted in Izmir province, which is a significant city for dairy cooperatives and the dairy sector. The province is located in western Türkiye (Figure 1).

Figure 1- Research area

The region is distinguished by the prevalence of modern dairy farms and dairy processing industries, which are relatively uncommon in other agricultural regions of Türkiye. The production of cow milk in Türkiye has increased significantly in recent years, and the total rate of increase from 2004 to 2019 was approximately 116.24% (TurkStat 2023).

The majority of milk production is concentrated in the Aegean and Central Anatolia regions, although there are also dairy operations in other areas. The total milk production in Türkiye, the Aegean region, and Izmir was 20 782 374 tonnes, 3 751 147 tonnes, and 1 150 838 tonnes, respectively. Izmir has 30.68% of the milk production of the Aegean region and 5.54% of the milk production of Türkiye (TurkStat 2023).

Izmir is one of the most important provinces in Türkiye in terms of both dairy sector and dairy cooperatives competing with investor-owned firms (IOFs) in the market. There are significant cooperatives in the province that market products both locally and nationally under their own brands. Dairy cooperatives, in particular, are highly successful and powerful in this province's dairy industry. In Türkiye, a few successful dairy cooperatives dominate the majority of the market in Izmir. In Izmir, farmers often sell their raw milk to cooperatives or IOFs (dairy collectors, processors, etc.). Direct sales in streets or open bazaars are uncommon because food safety regulations state that such practices are prohibited (Notification No: 2017/20).

The selected province plays a significant role in agri-cooperatives, specifically in three types: agricultural development cooperatives, irrigation cooperatives, and fishery cooperatives. Currently, there are 163 agricultural development cooperatives with 19 641 members (Table 1).

Table 1- The number of cooperative members located in Izmir

	Number of cooperatives	*Number of members*
Agricultural development cooperatives (ADC)	163	19641
Irrigation cooperatives (IC)	82	13567
Fishery cooperatives (FC)	45	2519

Source: MAF 2020

Four well-known dairy cooperatives are involved in this study (Table 2). Because these cooperatives are vertically integrated and have their own processing facilities. Other dairy cooperatives in the region are just collecting milk from members and selling it to other cooperatives or investor-owned companies. The main aim of selected cooperatives is to help dairy farmers in the region develop both economically and socially while protecting both producers and consumers of their products.

Table 2- The number of members in selected cooperatives

	Number of members
Tire Milk ADC	1780
İğdeli ADC	2120
Bağarası-Yenibağarası ADC	170
Bademli Arboriculture ADC	275
Total	4345

Source: MAF 2020

The data for the empirical analysis was gathered from a sample of 200 dairy farms, which have cooperative members (100 dairy farms), and non-members (100 dairy farms). Member farms were randomly selected in cooperation with the selected cooperatives. Non-member farms were selected randomly from the same areas to ensure comparability. After identifying member farms, we asked for information about nearby non-member farms and conducted surveys with them. The sample size was determined by the proportional sampling method (95% for confidence interval and 10% for margin of error) (Newbold, 1995). The data was collected by using a structured questionnaire and personal interviews with the members and non-members during July-September 2021.

$$n = \frac{Np(1-p)}{(N-1)\sigma_{px^2}+p(1-p)} \quad (1)$$

Where: n, Sample size; N, The number of the dairy cooperative members in Izmir (Table 2); σ^2_{px},ratio variant

Dairy farms were divided into four groups according to the number of dairy cows, regardless of their membership status. While determining the distribution according to the scale of farms, the farms with five or more dairy cows were taken into consideration. While making the distribution of the groups, taking into account the studies conducted in the literature (Saner 1993; Talim et al. 1998; Armagan et al. 2004; Güler 2019; Sert 2019); dairy farms with 5-10 heads of cows formed group I, 11-25 heads formed group II, 26-50 heads formed group III, 51 heads and above formed group IV. The number and percentage of enterprises in each group are 64 (32.0%), 62 (31.0%), 43 (21.5%) and 31 (15.5%), respectively.

3.2. Data analysis

DEA, a nonparametric method of estimation, was used to measure the farm efficiency. DEA has been widely used in efficiency studies in the literature, including in the dairy sector (Jaforullah & Whiteman 2001; Heshmati & Kumbhakar 1997; Helfand & Levine 2004; Kumbar 2005; Nizam & Armagan 2006; Aldeseit 2013; Güler & Saner 2020; Von Hobe et al. 2021; Kaiser & Schaffer 2022). This method is based on comparing a group of homogeneous decision-making units (DMUs) with multiple inputs and outputs. In the method, which can be applied in cases where there are more than one input and output, the input and output combination is compared with others (Coelli 1995). DEA does not necessitate the specification of a specific functional form for the production frontier. This is important because specifying a functional form can potentially introduce bias into the results, as pointed out by Barnes (2006). The DEA method, originally proposed by Charnes et al. (1978), employs linear programming techniques to estimate the most efficient production frontier. In our present study, we chose to utilize this non-parametric DEA approach precisely because it eliminates the need for any prior specification of the functional form of the production function, thereby enhancing the robustness of our efficiency estimates.

This method, which is commonly used to establish efficient frontiers, uses linear programming methods to construct a nonparametric frontier. The efficient production frontier is constructed by utilizing all efficient and inefficient observations in the sample and the efficiency of each production unit is calculated according to this frontier. The frontier formed by efficient units also reveals the expected targets for other units (Günden & Miran 2001).

There are two methods used in Data Envelopment Analysis (DEA), namely CCR (Charnes, Cooper, Rhodes) and BCC (Banker, Charnes, Cooper).

The CCR Model, first proposed by Charnes et al. 1978, is a model based on the assumption of constant returns to scale and has a wide range of areas. This model, which is a radial model, is based on proportional changes in the levels of inputs or outputs, which means that an increase in its input levels leads to a proportional increase in its output levels. Therefore, the model is based on total factor productivity, which is the ratio of weighted total outputs to weighted total inputs (Cooper et al. 2000).

The representation of the constant returns to scale analysis is as follows (Charnes et al. 1978);

$$\begin{aligned} &\min \Phi,\lambda\theta, \\ \text{subject to.}\quad &-yi + Y\lambda \geq 0 \\ &\theta\, xi - X\lambda \geq 0 \\ &\lambda \geq 0 \end{aligned}$$

The BCC DEA model is a model of variable returns of scale. Banker et al. 1984 first propose this model constructed by adding a convexity constraint to the constant returns to scale model.

θ is a scale and λ is a vector of N x 1 constants. By adding the convexity constraint N1' λ=1 to the linear programming problem, a variable return to scale model is formed;

$$\begin{aligned} & \min \Phi,\lambda\theta, \\ \text{subject to.} \quad & -yi + Y\lambda \geq 0 \\ & \theta\, xi - X\lambda \geq 0 \\ & N1'\lambda = 1 \\ & \lambda \geq 0 \end{aligned}$$

Determining and understanding the factors that affect Technical Efficiency (TE) is critical for increasing efficiency and performance. Farrell (1957) defined TE in two ways: first, the ability of farms to produce the most feasible output with a given combination of inputs (output oriented); and second, the ability of farms to use the minimum inputs to produce a given level of outputs (input oriented). Input oriented models are used when there is little control over outputs. The aim of these models is to determine the extent to which the amount of inputs can be reduced proportionally without changing the current output. Output oriented models, on the other hand, seek to answer the question of how much output can be increased proportionally without any increase in the amount of inputs used.

We used both input oriented and output oriented models by considering the CCR model (Charnes et al. 1978) and BCC model (Banker et al. 1984). To conduct this, the DEAP Version 2.1 software of Coelli (1996) was used to measure the efficiency of dairy farms. A review of studies on the efficiency of dairy farms in the literature reveals that many of them employ only input-oriented models (Jaforullah & Whiteman 2001; Nizam & Armagan 2006; Gonçalves et al. 2008; Steeneveld et al. 2012; Gul et al. 2018; Lindsaar et al. 2019; Aydemir 2019; Güler & Saner 2020), while others use solely output-oriented models (Koyunbenbe & Candemir 2006; Theodoridis & Psychoudakis 2008; Uzmay et al. 2009; Huijps et al. 2010) and studies using both input and output oriented model together (Fraser & Cordina 1999; Kaygisiz et al. 2018; Sert 2019).

The input and output variables used in the efficiency analysis are given in Table 3. The model includes, as inputs, feed expenses, labour expenses (family and foreign labour), expenses of veterinary, medicine, vaccines and artificial insemination, other expenses (electricity, water, fuel oil, transportation, cleaning, etc.) and herd size (LSU) and the output was aggregated total annual animal production value (Table 3). We relied on previous research in the selection of the input variables (Kumbar 2005; Nizam & Armagan 2006; Gonçalves et al. 2008; Cabrera et al. 2010; Gelan & Muriithi 2012; Aldeseit 2013; Güler & Saner 2020; Koç & Uzmay 2022).

Table 3 presents descriptive statistics of output and inputs. The annual animal production value obtained by the farms varies between 82,982.00 TRY and 3,181,756.00 TRY, with an average of 655,229.88 TRY. Feed was the major expense on farms, at an average of 434,546.90 TL per farm. The average herd size is 43.00 LSU, with the largest farm having 191.00 LSU and the smallest farm having 3.90 LSU. When we examined the standard deviations of variables, it is remarked the sample heterogeneity and there is a large variation between the farms (Table 3).

Table 3- Summary statistics of variables used in the efficiency analysis

Output	*Mean*	*Std. Deviation*	*Min.*	*Max.*
Animal Production Value[a] (TRY)	655229.88	634038.50	82982.00	3181756.00
Inputs				
Feed expenses[b] (TRY)	434546.90	445042.30	41300.00	2345000.00
Labour expenses[c] (TRY)	44720.23	20935.82	10265.63	113562.50
Expenses of veterinary, medicine, vaccines and artificial insemination[d] (TRY)	13825.50	11638.86	2000.00	60000.00
Other expenses[e] (TRY)	29343.55	48703.82	2170.00	294500.00
Herd size[f] (LSU)	42.00	40.57	3.90	191.00

In 2021, 1 Euro was equal to an average of 10.47 TRY (Central Bank of the Republic of Türkiye, https://evds2.tcmb.gov.tr/index.php?/evds/serieMarket); [a],Total revenues of milk sales, livestock sales, carcass meat sales and fertilizer sales; [b], The sum of purchased and produced feed expenses; [c], The sum of the expenses of family and foreign labour; [d], The annual expenses of veterinary, medicine, vaccines and artificial insemination; [e], The sum of expenses such as electricity, water, fuel oil, transportation, cleaning etc; [f], Livestock Unit (LSU) is used in order to present the herd size of the farms examined homogeneously.

Tobit regression analysis was used to determine the factors of affect efficiency on farms. Instead of the classical ordinary least squares (OLS) method, the Tobit regression model was chosen since the scores of these factors vary between 0 and 1. The Tobit model is an extension of the Probit model developed by James Tobin. This model, in which the dependent variable is treated as limited, is also called censored (discrete) regression model (Gujarati 2004). The data set can be censored from top to bottom or within a certain range. The standard Tobit model equation can be showed as follows: (Ramanathan 1998).

$$u_i > -\beta_0 - \sum_{i=1}^{N} \beta_i X_i \qquad if \qquad Y_{ij} = \beta_0 + \sum_{i=1}^{N} \beta_i X_i + u_i \tag{2}$$

$$u_i \leq -\beta_0 - \sum_{i=1}^{N} \beta_i X_i \qquad if \qquad Y_{ij} = 0 \tag{3}$$

Where: Y_{ij}, dependent variable for i. farm; X_i, independent variables affecting the dependent variable; N, number of dependent variables; β, model parameter; u, error term.

The Tobit regression analysis was executed under the results of BCC DEA model. Thus, the Tobit model allows us to comment on the effects of the independent variables used in the model on the output-oriented efficiency of the farms. We used GRETL to perform tobit regression analysis for factors affecting the efficiency of farms. Efficiency values are censored between 0-1 in the tobit model.

We chose seven independent variables related to farms and farmers characteristics for tobit analyses. These are composed of years of farmer's age (AGE), years of farmer's education (EDUCATION), household size which means that number of family members (HSIZE), number of agricultural organizations that it is a member of (AGRORGANIZATION), provided agronomic services by firms (which by cooperatives or IOFs) (AGRONOMICSERVICES), having milk cooling tank (MCTANK) and whether to become a member of the cooperative (members sell milk to cooperatives, nonmembers sell milk to IOFs) (COOPMEMBERSHIP).

Multicollinearity among the independent variables was checked using the Variance Inflation Factor (VIF) test. It was shown that there is no multicollinearity problem, and the highest value is 4.79 which has COOPMEMBERSHIP variable.

4. Results and Discussion

4.1. Efficiency analysis

The efficiency scores of dairy farms were estimated both input-oriented and output-oriented models by considering the CCR and BCC model depicted in Table 4. As indicated in Table 4, in CCR model, input-oriented and output-oriented efficiency values are the same, whilst there is a slight difference in BCC model (Table 4).

Table 4- Distribution of efficiency scores of dairy farms (%)

Efficiency Score	*CCR Model*		*BCC Model*	
	Input oriented	*Output oriented*	*Input oriented*	*Output oriented*
1	26.50	26.50	38.00	37.50
0.999 - 0.901	14.00	14.00	21.00	15.00
0.900 – 0.801	18.00	18.00	15.00	16.50
0.800 – 0.701	17.00	17.00	17.50	15.50
0.700 – 0.601	14.50	14.50	6.50	9.00
< 0.600	10.00	10.00	2.00	6.50
Mean	0.832	0.832	0.894	0.874
Std. Deviation	0.155	0.155	0.121	0.141
Min.	0.527	0.527	0.529	0.537
Max.	1.000	1.000	1.000	1.000

When we examined the CCR model efficiency scores, the lowest efficiency score is 0.527, the highest is 1.000 and the mean is 0.832. When this situation is thought according to the input-oriented model, it shows that farms can obtain the same animal production value with 16.8% less inputs, and according to the output-oriented model, they can increase their animal production value by 16.8% provided that the inputs remain the same. 26.5% of farms are fully efficient in terms of the CCR model and 38% of farms are fully efficient under the BCC model. The input oriented scores estimated under the BCC model are higher than those calculated as output oriented under the BCC DEA model. In terms of the BCC model, the input oriented efficiency score was estimated at 0.894 and the output oriented efficiency score at 0.874 (Table 4).

Other studies, which were conducted in Aegean region, reported similar results to ours (Koyunbenbe & Candemir 2006; Nizam & Armagan 2006; Sert 2019; Güler & Saner 2020). In studies conducted in other regions of Türkiye reported less mean technical efficiency scores (Kumbar 2005; Aydemir 2019; Güneş & Güldal 2019). A review of studies conducted outside Türkiye reveals that the efficiency scores of dairy farms vary. The efficiency score was estimated as 94% in New Zealand (Jaforullah & Whiteman 2001), 78% in the Netherlands (Reinhard et al. 2002), 87% in the UK (Gerber & Franks 2001), 63% in Greece (Theodoridis & Psychoudakis, 2008), 79% in Austria and 78% in Ireland (Kelly et al. 2012). The study conducted in a sheep farm in Spain showed that the efficiency of low-technology farms was 70%, while that of high-technology farms was 83% (Morantes et al. 2022).

Summary of dairy farm efficiency scores according to marketing channels is contained in Table 5. The technical efficiency scores estimated under the CCR are equal both input and output-oriented models. It was depicted the CCR model, the efficiency score of dairy farms selling milk to cooperatives is 0.781 with a standard deviation of 0.165. The efficiency score of dairy farms selling milk to IOFs is 0.882 with a standard deviation of 0.126. The technical efficiency scores were calculated to be higher in the BCC model than predicted by the CCR model. Furthermore, both cooperatives and IOFs perform better under input-oriented than output-oriented conditions (Table 5).

Table 5- Summary of efficiency scores of dairy farms by marketing channels (Coop.-IOFs)

		Cooperative		*IOFs*	
		Mean	*Std. Deviation*	*Mean*	*Std. Deviation*
CCR Model	Input oriented	0.781	0.165	0.882	0.126
	Output oriented	0.781	0.165	0.882	0.126
BCC Model	Input oriented	0.883	0.128	0.905	0.113
	Output oriented	0.843	0.158	0.904	0.113

As indicated in Table 6, the CCR and BCC model results for dairy farms, classified into four groups based on scale size, are presented. When the efficiency scores are estimated under the CCR model, it is seen that the largest farms have the highest efficiency scores, while the smallest have the lowest. According to the BCC model, the farms with the highest efficiency scores for both input and output are the largest farms (Group IV).

Table 6- Summary statistics of dairy farms according to scale

		Scale of farms				
		I.Group (64) 5-10 heads	*II.Group (62) 11-25 heads*	*III.Group (43) 26-50 heads*	*IV.Group (31) ≥51 heads*	*p-value*
CCR Model	Input oriented	0.762	0.853	0.847	0.911	<0.001*
	Output oriented	0.762	0.853	0.847	0.911	<0.001*
BCC Model	Input oriented	0.903	0.891	0.859	0.928	0.003**
	Output oriented	0.855	0.872	0.852	0.945	0.003**

*: significant for p≤0.001; **: significant for p≤0.05

As shown in Figure 2, scatter of efficiency score of dairy farms according to scale is different to CCR models and BCC models. When the fully efficient farms are examined according to scale, 54.8% of the farms in Group IV are fully efficient, while the ratios of the farms in Group I, Group II, and Group III are 25.00%, 25.80%, and 11.60%, respectively.

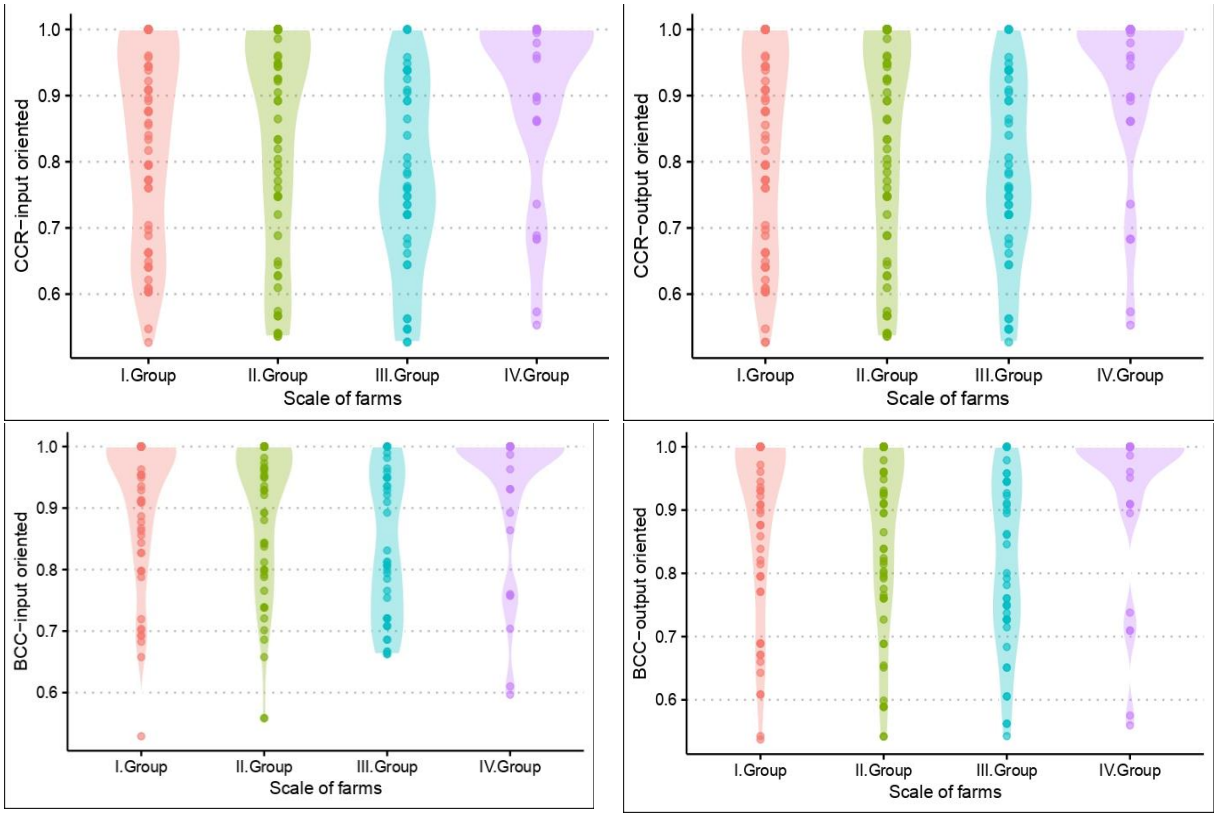

Figure 2- The scatter of efficiency scores of dairy farms according to scale

Figure 3 presents the distribution of fully efficient farms by scale and marketing channels. In comparison to non-member small-scale farms, small-scale member farms (Group I) are more prevalent among fully efficient farms under both the BCC and CCR models. In other words, cooperatives have a higher proportion of fully efficient small-scale farms compared to non-member alternatives. This indicates that cooperatives are better suited for small-scale farms and highlights the critical role of cooperatives in supporting small-scale farms compared to non-member alternatives.

In the study, a potential improvement analysis was conducted for dairy farms. With the potential improvement analysis, potential improvement ratios were determined according to the input target values for how inefficient farms can become efficient by using the combination of inputs and outputs of efficient farms in their reference cluster. When the potential improvement rates in the input-oriented model are examined, in order to achieve full efficiency in farms without much change in output; labor expenses should be reduced by 12.40%, other expenses (electricity, water, fuel oil, transportation, cleaning, etc.) by 13.44%, herd size (LSU) by 13.96%, feed expenses by 14.91%, and expenses of veterinary, medicine, vaccines, and artificial insemination by 15.64%. In terms of an output-oriented model, the value of animal production should be increased by 18.07% in order for the farms to achieve full efficiency. Upon examining the findings of both member and non-member dairy farms, it was determined that the members should aim to increase the value of animal production by 14.26%, whereas the nonmembers should aim for an increase of 11.42%.

We analysed constant returns to scale (CRS), decreasing returns to scale (DRS) and increasing returns to scale (IRS). CRS means that a proportional increase in the level of input occurs at the same rate at the output level. VRS means that a proportional increase in the level of inputs occurs at a different rate at the level of output. If the increase in output is greater than the proportional increase in all inputs, we have increasing returns to scale, and if it is less, we have decreasing returns to scale.

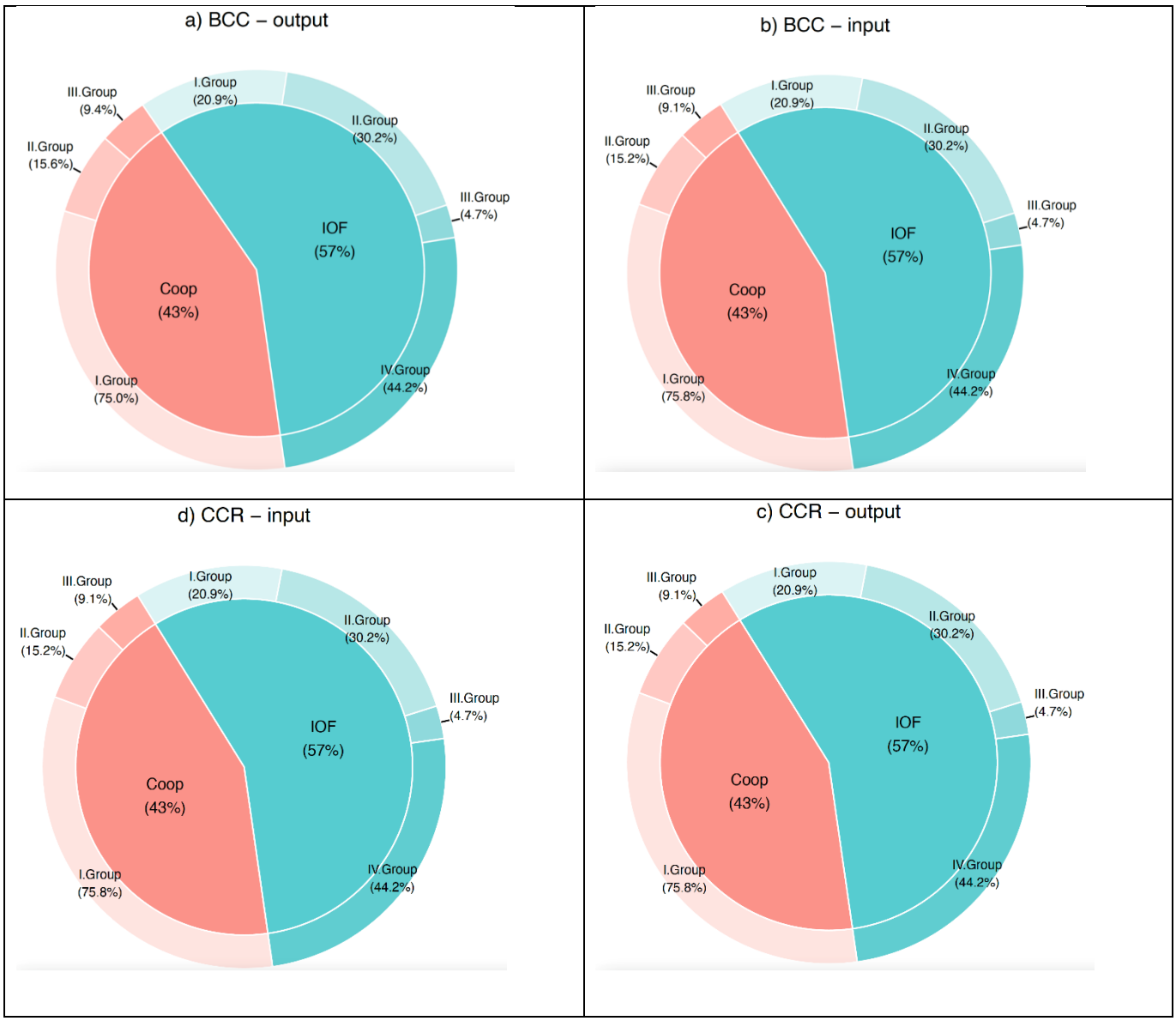

Figure 3- Distribution of fully efficient farms by scale and marketing channels (Coop – IOFs)

The results show that according to the input oriented model, 62.0% of farms (124 dairy farms) operate under increasing returns to scale. Of these 124 farms, 44 of the farms sell milk to IOFs and 80 of the farms to cooperatives. This is an expected result since the farms selling milk to cooperatives are smaller than the others. In terms of an output-oriented model, the results are similar. 50.5% of farms (101 dairy farms) operate under increasing returns to scale. In addition, these 69 farms sell milk to cooperatives and others sell to IOFs. As a result, they should be able to increase their efficiency by expanding.

In the study conducted in Izmir province, the scale efficiency of dairy farms was analyzed according to both input and output-oriented models. In the input and output-oriented model, 60% of the farms and 48% of them were found to have increasing returns to scale, respectively (Sert 2019). In another study conducted in the Thrace region, 82.3% of dairy farms were found to have increasing returns to scale (Kumbar 2005). According to Jaforullah & Whiteman (2001), 53% of farms in New Zealand and, according to Angon et al. (2021), 80% of farms in Argentina operate on an increasing returns scale.

4.2. Factors affecting efficiency of farms: Tobit analysis

Tobit estimates were analysed for efficiency measures (BCC output-oriented model) using 200 observations. The results of Tobit regression analysis are presented in Table 7. Most of the independent selected variables have significant effect on the efficiency measures. Among seven variables used in this study, only EDUCATION has not impact on the efficiencies, AGE and COOPMEMBERSHIP have a negative impact and others have a positive impact on the efficiencies.

Table 7- Tobit regression results

	Marginal Effect	*Coefficient*	*Std. Error*	*z-statistic*	*p-value*
Constant	-------	0.6667	0.0757	8.8021	<0.0001*
AGE	-0.0553	−0.0688	0.0186	−3.7057	0.0002*
EDUCATION	0.0018	0.0022	0.0034	0.6615	0.5083
HSIZE	0.0191	0.0238	0.0075	3.1699	0.0015*
MCTANK	0.0820	0.1020	0.0286	3.5670	0.0004*
COOPMEMBERSHIP	-0.1609	−0.2001	0.0574	−3.4853	0.0005*
AGRONOMICSERVICE	0.0466	0.0580	0.0137	4.2163	<0.0001*
AGRORGANIZATION	0.0290	0.0360	0.0117	3.0789	0.0021**
Log-likelihood 15.3980					
Test statistic: Chi-square(2) = 10.8784 with p-value = 0.0043					

*: significant for p≤0.001; **: significant for p≤0.01

Younger farmers are better educated and more cautious than older farmers. As expected, AGE has a statistically significant negative impact on technical efficiency, so a one-year increase in a farmer's age results in a 5.53% decrease in farm efficiency. Despite the fact that EDUCATION was not found to be statistically significant, its impact on farm efficiency is positive. The results suggest that an increase in the size of household by one person would lead to an increase in the efficiency of farms by 1.91%. Family labor is used intensively in dairy farms, so number of family members is an important factor in the efficiency of farms. Koç (2022) found similar results in a study conducted in the Thrace region of Türkiye: technical efficiency in dairy farms was negatively affected by age, positively affected by education.

The presence of milk cooling tank (MCTANK) in the farms has a positive and significant effect on the efficiency of farms. When compared to farms without one, having a milk cooling tank increases farm efficiency by 8.19%. Cooling tanks in dairy farms have an effect on both sales price and quality. There is a big difference in quality between the milk that reaches the cooling tank untouched and waits in the cooling tank until it reaches the buyer and the milk that is milked in barn conditions where milking hygiene is not paid enough attention and waits in unsuitable conditions for a long time until it reaches the buyer. There is also a difference between the sale prices of this milk. In other words, the presence of a cooling tank in farms (selling cold milk) is an important factor affecting the efficiency of farms. In addition, this situation shows that technology adaptation is higher in farms. This can be associated with technology. In this case, it would be appropriate to say that the use of technology increases efficiency.

COOPMEMBERSHIP has a statistically significant negative impact on efficiency of farms. Non-member farms sell milk to IOFs while member farms sell to cooperatives. The results showed that non-member farms were more efficient than member farms. This is related to size of farms, because nonmember farms are larger than member farms. However, when the small-scale and efficient farms are assessed, it is noted that member farms are quite high. In this case, it is possible to say that co-operatives are more suitable for small-scale farms and contribute positively to the efficiency of these farms. As was expected, AGRONOMICSERVICE has a statistically significant positive impact on efficiency. We know that cooperatives provide more agronomic services for members, so this increases the efficiency. AGRORGANIZATION has a statistically significant positive impact; farms with more agricultural organization memberships are more efficiency than farms with fewer memberships. This result agrees with the works of Kumbar (2005) in Thrace region, Türkiye.

5. Conclusions

An analysis of the efficiency results of dairy farms revealed that non-member farms were more efficient than member farms. According to scale of farms, it was determined that the efficiency of large-scale farms was higher. In addition, it is noteworthy that the majority of small-scale and efficient farms are cooperative members. This suggests that cooperatives are necessary, particularly for small-scale farms, and that they should be organizations dedicated to the sustainability of small farms. When the return to scale analysis was analyzed, as can be seen, the members' farms operate with increasing returns to scale. This means that the increase in output is greater than the increase in inputs. In general, it is recommended that the farms should reduce the expenses of veterinary, medicine, vaccines, and artificial insemination more than other inputs. Dairy farms of members need more improvements than others. At this point, it is important that members use the services provided by cooperatives effectively. For feed expenses, one of the most important expenses, cooperatives should not sell feed at higher prices to members who are already in debt. This situation forces members to work as debtors.

When the factors affecting the efficiency of farms were analyzed, it was observed that younger people worked more effectively than elders. It is believed that factors such as young people having greater awareness, adopting innovations, and planning for the future play a significant role. The presence of a cooling tank, which can be characterized as the use of technology, is a factor that increases efficiency in farms. The higher price of cold milk and the improved quality and hygiene of milk obtained

through automatic milking systems are factors that enhance efficiency. Although non-member farms exhibit higher overall efficiency, most efficient small-scale farms are cooperative members. This suggests that cooperatives contribute to improving the efficiency of small-scale farms. Additionally, cooperatives offer more agronomic services to their members. This has a positive effect on efficiency of farms. Membership in agricultural organizations is another factor that enhances efficiency. In addition to cooperatives, membership in producer unions and benefiting from the services of these organizations would increase the efficiency of farms.

This study concludes that cooperatives are better for small family farms; however, they have capacity issues when compared to IOFs. To increase their capacity and reach more farmers, cooperatives require support from municipalities and governments. Policymakers should consider providing assistance to cooperatives for their expansion, contributing to the sustainability of small-scale farms. In Türkiye conditions, there is a need for financial assistance to explore avenues for cooperatives to offer competitive prices on inputs and prevent members from working in debt. Cooperative managers should avoid showing opportunistic behavior and instead prioritise cooperative management in governance, avoiding self-interest and deception. In this context, it is necessary to implement training programs for cooperative management to ensure effective governance and prevent opportunistic behavior. If the main factors that distinguish cooperatives from IOFs are ignored, there will be no benefit to farmers from cooperatives. Small-scale farms will be condemned to closure and the sector will be monopolised under the management of large enterprises.

While this study contributes to the literature on the efficiency of dairy farms by comparing cooperative members and non-members, it is important to acknowledge certain limitations. Firstly, the research focuses on a specific region within Türkiye, which may limit the generalizability of the findings to the whole Turkish dairy industry. Future studies should address these limitations by expanding the geographical scope and incorporating a more comprehensive set of variables. Furthermore, different techniques can be used with different variables. Taking these limitations into account will contribute to the development of more robust and comprehensive insights in subsequent studies.

References

Abate G T, Francesconi G N & Getnet K (2014). Impact of agricultural cooperatives on smallholders' technical efficiency: Empirical evidence from Ethiopia. Annals of Public and Cooperative Economics 85(2): 257-286

Aldeseit B (2013). Measurement of scale efficiency in dairy farms: Data envelopment analysis (DEA) approach. *Journal of Agricultural Science* 5(9): 37-43. https://doi.org/10.5539/jas.v5n9p37

Angon E, Bragulat T, García A, Giorgis A & Perea J (2021). Key factors affecting the technical efficiency of bee farms in the province of La Pampa (Argentina): A two-stage DEA approach. Revista de la Facultad de Ciencias Agrarias UNCuyo 53(1): 150-163

Aydemir A (2019). Economical analysis of dairy operations: The case of Savsat town of Artvin Province (Master's thesis, Department of Agricultural Economics, Tokat Graduate School of Natural and Applied Sciences, Tokat, Turkey.

Banker R D, Charnes A & Cooper W W (1984). Some models for estimation of technical and scale inefficiencies in data envelopment analysis. Management Science 30(9): 1078-1092. https://doi.org/10.1287/mnsc.30.9.1078

Barnes A P (2006). Does multi-functionality affect technical efficiency? A non-parametric analysis of the Scottish dairy industry. *Journal of Environmental Management* 80: 287-294. https://doi.org/10.1016/j.jenvman.2005.09.020

Candemir M & Koyunbenbe N (2006). Efficiency analysis of dairy farms in the province of Izmir (Turkey): Data envelopment analysis (DEA). *Journal of Applied Animal Research* 29: 61-64. https://doi.org/10.1080/09712119.2006.9706572

Chagwiza C, Muradian R & Ruben R (2016). Cooperative membership and dairy performance among smallholders in Ethiopia. Food Policy 59(2016): 165-173. http://dx.doi.org/10.1016/j.foodpol.2016.01.008

Charnes A, Cooper W W & Rhodes E (1978). Measuring the efficiency of decision making units. *European Journal of Operational Research* 2(6): 8-11. https://doi.org/10.1016/0377-2217(78)90138-8

Coelli T A (1995). Multistage methodology for the solution of orientated DEA models. Operations Research Letters, 23: 143-149. https://doi.org/10.1016/S0167-6377(98)00036-4

Cooper W W, Seiford L M & Tone K (2000). Data envelopment analysis: A comprehensive text with models, application, references and DEA-Solver software. Kluwer Academic Publishers.

FAO (The Food and Agriculture Organization Corporate Statistical Database). (2022). Crops and livestock products statistics. Retrieved from https://www.fao.org/faostat/en/#data/QCL

Farrell M (1957). The measurement of productive efficiency. Journal of the Royal Statistical Society: Series A (General) 120(3): 253-290. https://doi.org/10.2307/2343100

Fraser I & Cordina D (1999). An application of data envelopment analysis to irrigated dairy farms in Northern Victoria, Australia. Agricultural Systems 59(3): 267-282. https://doi.org/10.1016/S0167-6377(98)00036-4

Gelan A & Muriithi B W (2012). Measuring and explaining technical efficiency of dairy farms: A case study of smallholder farms in Africa. Agrekon 51(2): 53-74

Gerber J & Franks J R (2001). Technical efficiency and benchmarking in dairy enterprises. *Journal of the Institute of Farm Management* 10(12): 715-728

Gonçalves R M L, Vieira W C, Lima J E & Gomes S T (2008). Analysis of technical efficiency of milk-producing farms in Minas Gerais. Economia Aplicada 12(2): 321-335. https://doi.org/10.1590/S1413-80502008000200007

Gujarati D N (2004). Basic Econometrics. McGraw-Hill Companies

Gül M, Yılmaz H, Parlakay O, Akkoyun S, Bilgili M E, Vurarak Y, Hızlı H & Kılıçalp N (2018). Technical efficiency of dairy cattle farms in East Mediterranean region of Turkey. Scientific Papers Series Management, Economic Engineering in Agriculture and Rural Development 18(2): 213-225

Güler D & Saner G (2020). The measurement of efficiency of dairy farms: The cases of Izmir and Manisa. *YYU Journal of Agricultural Science* 30(2): 386-397. https://doi.org/10.29133/yyutbd.715342

Günden C & Miran B (2001). Technical efficiency in cotton production: A case study. The Union of Turkish Chambers of Agriculture, Ankara, Turkey

Güneş E & Güldal H T (2019). Determination of economic efficiency of agricultural enterprises in Turkey: A DEA approach. New Medit, 18(4): 105-115. https://doi.org/10.30682/nm1904h

Hansson H & Öhlmér B (2008). The effect of operational managerial practices on economic, technical and allocative efficiency at Swedish dairy farms. Livestock Science 118(1-2): 34-43. https://doi.org/10.1016/j.livsci.2008.01.013

Helfand S M & Levine E S (2004). Farm size and the determinants of productive efficiency in the Brazilian Center-West. Agricultural Economics 31: 241-249. https://doi.org/10.1016/j.agecon.2004.09.021

Heshmati, A., & Kumbhakar, S. C. (1994). Farm heterogeneity and technical efficiency: Some results from Swedish dairy farms. *Journal of Productivity Analysis* 5(1): 45-61

Heshmati A & Kumbhakar S C (1997). Estimation of technical efficiency in Swedish crop farms: A pseudo panel data approach. *Journal of Agricultural Economics* 48(1): 22-37. https://doi.org/10.1111/j.1477-9552.1997.tb01128.x

Huijps K, Hogeveen H, Lam T J G M & Oude Lansink A G J M (2010). Costs and efficacy of management measures to improve udder health on Dutch dairy farms. *Journal of Dairy Science* 93: 115-124. https://doi.org/10.3168/jds.2009-2412

Inan I H, Direk M, Başaran B, Birinci S & Erkmen E (2005). Organisation in agriculture (Tarımda Örgütlenme). In Sixth Technical Congress of Agricultural Engineering (pp. 1133-1154)

Jaforullah M & Whiteman J (2001). Scale efficiency in the New Zealand dairy industry: A non-parametric approach. *The Australian Journal of Agricultural and Resource Economics* 43(4): 523-541. https://doi.org/10.1111/1467-8489.00093

Jansik C, Irz X & Kuosmanen N (2014). Competitiveness of Northern European dairy chains. MTT Economic Research, Agrifood Research Finland: Helsinki, Finland. ISBN 978-951-687-177-9.

Kaiser A & Schaffer A (2022). Considering environmental factors in technical efficiency analysis of European crop production. *German Journal of Agricultural Economics* 71(2): 92-106. https://doi.org/10.30430/gjae.2022.0222

Kaygısız F, Evren S, Koçak Ö, Aksel M & Tan T (2018). Efficiency analysis of dairy buffalo enterprises in Çatalca district of Istanbul. Ankara Univ Vet Fak Derg, 65, 291-296. https://doi.org/10.1501/Vetfak_0000002859

Kelly E, Shalloo L, Geary U, Kinsella A & Wallace M (2012). Application of data envelopment analysis to measure technical efficiency on a sample of Irish dairy farms. *Irish Journal of Agricultural and Food Research* 51: 63-77. https://doi.org/10.2307/41756846

Koç G (2022). A study on the development of a farm-level index for availability dimension of food security in Turkey: Case study of Thrace region. PhD Thesis, Ege University, Graduate School of Natural and Applied Sciences, Department of Agricultural Economics, Izmir, Turkey.

Koç G & Uzmay A (2022). Analyzing the effects of livestock policies on farm-level efficiency in Turkey: Thrace region case. *Journal of Tekirdag Agricultural Faculty* 19(3): 515-528. https://doi.org/10.33462/jotaf.978947

Koyunbenbe N & Candemir M (2006). Comparison of the technical efficiencies of dairy farms in Ödemiş, Tire, Bayındır and Torbalı districts the basin of Küçük Menderes. *Journal of Animal Production* 47(2): 9-20

Kumar A, Saroj S, Joshi P K & Takeshima H (2018). Does cooperative membership improve household welfare? Evidence from a panel data analysis of smallholder dairy farmers in Bihar, India. Food Policy 75(2018): 24-36. https://doi.org/10.1016/j.foodpol.2018.01.005

Kumbar N (2005). An efficiency analysis of breeding farm enterprises in Thrace region. PhD Thesis, Namık Kemal University Graduate School of Natural and Applied Sciences, Tekirdağ, Turkey.

Lindsaar H L, Põldaru R & Roots J (2019). Estonian dairy farms' technical efficiency and factors predicting it. Agronomy Research 17(2): 593-607. https://doi.org/10.15159/ar.19.067

Luiz Beber C, Lakner S & Skevas I (2021). Organizational forms and technical efficiency of the dairy processing industry in Southern Brazil. Agricultural and Food Economics 9(23): 2-22. https://doi.org/10.1186/s40100-021-00195-3

MAF (Republic of Türkiye Ministry of Agriculture and Forestry). (2020). Milk and meat sector report.https://www.esk.gov.tr/upload/Node/10255/files/2019_Yili_Sektor_Degerlendirme_Raporu.pdf

MAF (Republic of Türkiye Ministry of Agriculture and Forestry). (2024). Table of agricultural organization.https://www.tarimorman.gov.tr/TRGM/Belgeler/0TE%C5%9EK%C4%B0LATLANMA%20DA%C4%B0RE%20BA%C5%9EKANLI%C4%9EI/25.12.2023+Tarimsal_OrgutlenmeTablosu+(2)(1).xls

Mitsopoulos I, Tsiouni M, Pavloudi A, Gourdouvelis D & Aggelopoulos S (2021). Improving the technical efficiency and productivity of dairy farms in Greece. Studies in Agricultural Economics 123: 95-100. https://doi.org/10.7896/j.2154

Morantes M, Dios-Palomares R, Pablo D A L & Rivas J (2022). Efficiency and technology of dairy sheep production systems in Castilla-La Mancha, Spain: A metafrontier approach. New Medit 21(1): 33-52. https://doi.org/10.30682/nm2201c

Newbold P (1995). Statistics for Business and Economics. Prentice-Hall

Nizam S & Armağan G (2006). Determination of productivity of market-oriented dairy farms in Aydın province. *Journal of Adnan Menderes University Agricultural Faculty* 3(2): 530-560

Onyango V A, Owuor G, Rao E J & Otieno D J (2023). Impact of cooperatives on smallholder dairy farmers' income in Kenya. Cogent Food & Agriculture 9: 2291225, 1-13. https://doi.org/10.1080/23311932.2023.2291225

Özüdoğru T (2010). Analysis of economic impacts of Amasya cattle breeders association on the local farmers. PhD Thesis, Ankara University Graduate School of Natural and Applied Sciences, Department of Agricultural Economics, Ankara, Turkey.

Priscilla L & Chauhan A K (2019). Economic impact of cooperative membership on dairy farmers in Manipur: a propensity score matching approach. Agricultural Economics Research Review 32(1): 117-123. DOI: 10.5958/0974-0279.2019.00010.7

Ramanathan R (1998). Introductory Econometrics with Applications. Dryden Press, USA.

Reinhard S, Knox Lowell C A & Thijssen G J (2000). Environmental efficiency with multiple environmentally detrimental variables, estimated with SFA and DEAL. *European Journal of Operational Research* 121: 287-303

Reinhard S, Lovell C A & Thijssen G (2002). Analysis of environmental efficiency variation. *Journal of Agricultural Economics* 84(4): 1054-1065

Sert H (2019). Analysis of animal welfare economy in dairy cattle and evaluation in terms of agricultural policies: Izmir Province example. MSc Thesis, Ege University Graduate School of Natural and Applied Sciences, Department of Agricultural Economics, Izmir, Turkey

Steeneveld W, Tauer L W, Hogeveen H & Lansink A G J M (2012). Comparing technical efficiency of farms with an automatic milking system and a conventional milking system. *Journal of Dairy Science* 95: 7391-7398. https://doi.org/10.3168/jds.2012-5482

TurkStat (2023). Turkish Statistical Institute. https://www.tuik.gov.tr/Home/Index

USK (Ulusal Süt Konseyi) (2023). Discover Turkish dairy sector. https://ulusalsutkonseyi.org.tr/en/discover-turkish-dairy-sector/ (In Turkish)
Vlontzos G & Theodoridis A (2013). Efficiency and productivity change in the Greek dairy industry. Agricultural Economics Review 14: 14-28
Von Hobe C F, Michels M & Musshoff O (2021). Technical efficiency and productivity change in German large-scale arable farming. *German Journal of Agricultural Economics* 70(1): 36-48. https://doi.org/10.30430/70.2021.1.36-48
Zietek-Kwasniewska K, Zuba-Ciszewska M & Nucinska J (2022). Technical efficiency of cooperative and non-cooperative dairies in Poland: Toward the first link of the supply chain. Agriculture 12(52): 2-22. https://doi.org/10.3390/agriculture12010052